Structural Engineering Report No. ST-01-3.2

COLUMN STIFFENER DETAILING AND PANEL ZONE BEHAVIOR OF STEEL MOMENT FRAME CONNECTIONS

Daeyong Lee, Sean C. Cotton, Robert J. Dexter, Jerome F. Hajjar, Yanqun Ye, and Sara D. Ojard

June 2002

Department of Civil Engineering
Institute of Technology
University of Minnesota
Minneapolis, Minnesota 55455

Abstract

Extensive damage to steel moment connections has been reported since the 1994 Northridge earthquake. While low-toughness welds and notch-like discontinuities created by the bottom flange backing bars have been identified as primary causes of the fractures that occurred, other factors have also been linked to the failures. Column stiffening design practices, resulting in the design of weak panel zones and a lack of or insufficient use of continuity plates, have been speculated as potential contributors to the fractures. The concern associated with the role of column stiffener detailing in the Northridge damage has subsequently led to a tendency towards over-conservatism in stiffener design. However, the additional expense of larger stiffeners coupled with the potential for fabrication cracking due to larger, highly restrained welds required to attach such stiffeners is an undesirable consequence of this increased conservatism.

To study these column stiffener design issues, a research project was launched to reassess the AISC design criteria related to the limit states of Local Flange Bending (LFB), Local Web Yielding (LWY), and Panel Zone (PZ) strength, and to develop new, economical alternatives for the detailing of such stiffeners. The project contains three components: finite element analyses to investigate the performance of various column stiffener details and to corroborate the results of the experiments, monotonically-loaded pull-plate tests to evaluate the non-seismic LFB and LWY design criteria and to investigate non-seismic behavior of the alternative stiffener details, and cyclically-loaded cruciform tests to evaluate the seismic LFB, LWY, and PZ design criteria and to investigate the seismic behavior of the alternative stiffener details. This report focuses primarily on reporting the results of the cyclically-loaded cruciform tests.

A total of six cruciform girder-to-column joint subassemblages were fabricated and tested in this project. Five joint subassemblages were originally designed and fabricated for the investigation into the provisions for detailing of column stiffening. However, due to premature brittle girder fractures occurring in one of the five test

specimens, an additional cruciform specimen with similar detailing and improved notch-toughness in the weld metal was fabricated and tested. The column sizes selected in this project ranged from a W14x145 to a W14x283. The range of these column sizes permitted several stiffener details to be included in the test matrix, and for the limits of the LFB and PZ limit states to be explored. A W24x94 was used for all girders. The panel zones of the specimens were designed to be relatively weak in most specimens, such that the stiffening details would be thoroughly tested at large strains. The alternative stiffener details included two fillet-welded doubler plate details, one groove-welded offset doubler plate detail, and one fillet-welded continuity plate detail with a thickness of the continuity plate being approximately half the thickness of the girder flange. These details avoid placing highly restrained Complete Joint Penetration (CJP) groove welds in the potentially low-toughness k-area of the columns.

The connection detail tested in this project may be classified as a Welded Unreinforced Flange-Welded Web (WUF-W) connection detail, which is a prequalified connection within FEMA 350. This connection consisted of a CJP-welded girder web-to-column flange, an improved weld access hole detail in the girder, and girder flange-to-column flange CJP weld details outlined in FEMA 350 and FEMA 353. Welding included the use of E70T-6 consumables for the girder flange-to-column flange CJP welds and E71T-8 for the girder web-to-column flange CJP welds and the shear tab-to-girder web fillet welds. Shear tab-to-column flange and all stiffeners-to-column flange welds used E70T-1 consumables.

From the cruciform tests, the performance of the alternative stiffening details as well as the limit states of LFB and PZ strength were assessed. The five specimens, excluding the prematurely fractured specimen, completed the SAC loading history, each with several cycles at 4.0% interstory drift without noticeable strength degradation. The primary failure mode was Low-Cycle Fatigue (LCF) fracturing in one or more girder flanges. The test results showed that, when properly detailed and welded with notch-tough filler metal, the WUF-W moment connections can perform adequately under large quasi-static cyclic loads even though relatively weak panel zone strengths are chosen. In addition, the test results confirmed that satisfactory cyclic connection performance may

be achieved without continuity plates if the column flanges are sufficiently thick. The alternative column stiffener details in steel moment-resisting connections were also successfully verified.

The test results showed that the LFB strength equation included in the 1999 AISC LRFD Specification is adequate, if slightly conservative, for non-seismic detailing (in addition, related research on this project proposed alternative LFB and LWY strength equations that better match the test data). For seismic detailing, when coupled with the application of the seismic demand specified in the 1992 AISC Seismic Provisions and FEMA 350, the LFB strength equation is more clearly conservative. The panel zone strength equation included in the 1997 AISC Seismic Provisions was also evaluated based on the five successful test results, as well as on a comparison with the 44 past experimental tests. This equation was found to significantly overpredict the panel zone strength in many cases, particularly for specimens having larger columns. An alternate model (i.e., a modified Fielding and Huang model) estimating the panel zone post-elastic stiffness was developed from a newly assumed panel zone behavior at its ultimate state, and modified based on the five experimental results so as to more accurately capture the post-yield panel zone strength. This modified Fielding and Huang model was found to be more accurate in its prediction of the panel zone strength of W14 and larger columns, and was shown to be somewhat conservative for smaller columns.

In addition, it was determined that in order to provide a more accurate assessment of the panel zone strength corresponding to experimental results, the panel zone strength equation of the 1997 AISC Seismic Provisions, or that proposed in this research based upon the modified Fielding and Huang model, needs to be scaled. For this purpose, a new methodology, which also properly scales the corresponding panel zone design demand as well as the panel zone strength, is introduced. This methodology may be used to evaluate the selected panel zone equation based on experimental results, and can provide an appropriate demand for the selected panel zone strength equation.

The report concludes with a series of specific conclusions related to column stiffener design of steel moment-resisting connections. Conditions under which no stiffeners are required, both for non-seismic and seismic detailing, are clarified,

assessments of the alternative stiffener details are summarized, and issues related to the proposed design equations are highlighted.

Acknowledgements

This research was sponsored by the American Institute of Steel Construction, Inc. (AISC) and by the University of Minnesota. In-kind funding and materials were provided by LeJeune Steel Company, Minneapolis, Minnesota, Danny's Construction Company, Minneapolis, Minnesota, Braun Intertec, Minneapolis, Minnesota, and Edison Welding Institute, Columbus, Ohio. Special thanks are due to Lincoln Electric Company for donating an Idealarc DC-600 power supply and an LN-10 wire feed unit to the University of Minnesota Structures Laboratory. Supercomputing resources were provided by the Minnesota Supercomputing Institute. This support is gratefully acknowledged.

The authors wish to thank Professor Theodore V. Galambos of the University of Minnesota, Mr. Lawrence A. Kloiber of LeJeune Steel Company, and Dr. John C. Nelson of the University of Minnesota Institute of Technology Characterization Facility for their valuable assistance with the design, fabrication, and characterization of the experimental tests. A great deal of thanks is also extended to Mr. Paul M. Bergson of the University of Minnesota for his many hours of assistance and advice related to the experimental research. The authors also appreciate the efforts of a number of undergraduate and graduate students who assisted at various times throughout this project. Finally, the authors would like to thank the members of the external advisory group on this project for their advice and guidance, as well as others who have provided assistance throughout this research. These individuals include: T. Schlafly, AISC, C. Carter, AISC, W. Baker, Skidmore, Owings & Merrill, J. Barsom, Pennsylvania, R. Bjorhovde, The Bjorhovde Group, M. Engstrom, Nucor-Yamato Steel Company, J. Fisher, Lehigh University, M. Johnson, Edison Welding Institute, J. Malley, Degenkolb Engineers, D. Miller, Lincoln Electric Company, S. Rolfe, University of Kansas, and W. Thornton, Cives Engineering Corporation.

Table of Contents

Abstract i

Acknowledgements v

List of Figures x

List of Tables xxvii

1. Introduction 1

1.1 Research Objectives 3

1.2 Organization of the Report 5

2. Background of Design Provisions for Column Stiffening 7

2.1 History of Panel Zone Design Provisions 7

2.1.1 Panel Zone Shear Strength 8

2.1.2 Panel Zone Slenderness 15

2.2 Opinions Regarding Panel Zone Design and Behavior 16

2.3 Background of LFB and LWY Provisions 21

2.4 Economic Considerations of Column Stiffening 24

3. Specimen Selection and Design 28

3.1 Parametric Study of Panel Zone Stiffening Requirements 29

3.1.1 Definitions of Parameters 29

3.1.2 Results of Panel Zone Parameter Study 35

3.1.3 Conclusions 39

3.2 Specimen Selection 40

3.2.1 Cruciform Specimen Selection Procedure 40

3.2.2 Specimen Justification 55

3.2.2.1 Specimen Parameter Discussion 55
3.2.2.2 Individual Specimen Discussion 59
3.3 Specimen Design 62
3.3.1 Dimensions of Cruciform Specimens 62
3.3.2 Girder-to-Column Moment Connection Design 63
3.3.2.1 Welded Connection Details 64
3.3.2.2 Access Hole Details 66
3.3.3 Panel Zone and Column Stiffener Design 67
3.3.3.1 Panel Zone Design 67
3.3.3.2 Fillet-Welded Doubler Plate Design 69
3.3.3.3 Groove-Welded Offset (Box) Doubler Plate Design 72
3.3.3.4 Continuity Plate Design 72
3.4 Material Properties 74
3.4.1 Steel Material Properties 74
3.4.2 Weld Material Properties 76

4. Test Setup and Instrumentation 92
4.1 Test Setup 92
4.2 Loading History 94
4.3 Instrumentation 95
4.3.1 Strain Gages 95
4.3.2 Linear Variable Differential Transformers 97
4.3.3 Specimen Coordinate System and Gage Locations 99

5. Summary of Test Results 131
5.1 Applied Loading History 131
5.1.1 Loading History of Specimen CR1 131
5.1.2 Loading History of Specimen CR2 132
5.1.3 Loading History of Specimen CR3 132
5.1.4 Loading History of Specimen CR4 132

5.1.5 Loading History of Specimen CR4R 132
5.1.6 Loading History of Specimen CR5 133
5.2 Summary of Specimen Performance 133
5.2.1 Performance of Specimen CR1 133
5.2.2 Performance of Specimen CR2 135
5.2.3 Performance of Specimen CR3 137
5.2.4 Performance of Specimen CR4 139
5.2.5 Performance of Specimen CR4R 140
5.2.6 Performance of Specimen CR5 142

6. Analysis and Discussion of Test Results 198
6.1 Comparison of Experimental Behavior and Finite Element Analysis 199
6.2 Panel Zone Behavior 201
6.2.1 Progression of Panel Zone Yielding 201
6.2.2 Panel Zone Behavior in the Elastic Range 203
6.2.3 Effects of Large Panel Zone Deformation 205
6.2.4 AISC Panel Zone Provisions 207
6.3 Alternate Model for Post-Yield Panel Zone Strength 211
6.3.1 Modified Fielding and Huang Model 211
6.3.2 Verification of Modified Fielding and Huang Model (Equation 6.10) 215
6.3.3 Comparison of Panel Zone Thicknesses 218
6.3.4 Scaling of Panel Zone Design Capacity and Demand 222
6.4 Local Flange Bending 225
6.5 Stress Distribution in Girder Flange 233
6.6 Comparison of Results and Discussion of Continuity Plate and Doubler Plate Detailing 235

7. Summary and Conclusions 323
7.1 Research Summary 323
7.2 Conclusions and Recommendations 329

7.2.1 Conclusions.....329
7.2.2 Recommendations for Future Research.....334

Appendix A. Calculation of Specimen Deformation and Rotation Quantities.....336
A.1 Rotation and Deformation from Displacement Data.....336
A.2 Calculated Plastic Rotation and Deformation Quantities.....338
A.3 Plastic Rotations Relative to the Column Centerline.....340

Appendix B. Failure Analysis of Specimen CR4.....401

References.....427

List of Figures

2.1(a) Fielding and Huang Model for Post-Elastic Panel Zone Behavior 27
2.1(b) Krawinkler Model for Post-Elastic Panel Zone Behavior.....27

3.1 Seismic Girder-Column Combinations Meeting SCWB Criterion – 50 ksi Columns 81
3.2 Seismic Girder-Column Combinations Meeting SCWB Criterion – 65 ksi Columns 81
3.3 Seismic SCWB Girder-Column Combinations Requiring Doubler Plates – 50 ksi Columns 82
3.4 Seismic SCWB Girder-Column Combinations Requiring Doubler Plates – 65 ksi Columns 82
3.5(a) Beveled, Fillet-Welded Doubler Plate Detail (Detail I) 83
3.5(b) Square-Cut Fillet-Welded Doubler Plate Detail (Detail II) 83
3.5(c) Offset (Box) Doubler Plate Detail.....83
3.6 Typical Moment Frame Elevation Showing Interior Joint and Specimen Idealization.....83
3.7 Typical Cruciform Specimen With Basic Dimensions.....84
3.8 SAC WUF-W Moment Connection Details [after (FEMA, 2000a)].....84
3.9 Typical Welded Moment Connection Details.....85
3.10 Top Flange Weld With Reinforcing Fillets 86
3.11 Bottom Flange Reinforcing Fillet Weld 86
3.12 Access Hole and End of Web Groove Weld Showing Overlap of Shear Tab Into Access Hole.....87
3.13 Access Hole Dimensions 87
3.14 Specimen CR2 Fillet-Welded Doubler Plate Details.....88
3.15 Specimen CR3 Stiffening Details 89

3.16 Specimen CR5 Fillet-Welded Doubler Plate Details....90
3.17 Specimen CR4 Offset (Box) Doubler Plate Details....91

4.1 Load Frame Elevation With Specimen....107
4.2 Top View of Load Frame and Load Pin....108
4.3 Lateral-Torsional Buckling Bracing....108
4.4 Bottom Load Pin Assembly....109
4.5 Actuator Bracket Showing Connection to Girder and Top of Actuator....109
4.6 General Specimen Loading History: Drift Level vs. Cumulative Cycles....110
4.7 Panel Zone and Girder Web Instrumentation for Specimen CR1....111
4.8 Panel Zone and Girder Web Instrumentation for Specimen CR2....112
4.9 Doubler Plate Instrumentation for Specimen CR2....113
4.10 Panel Zone and Girder Web Instrumentation for Specimen CR3....114
4.11 Doubler Plate Instrumentation for Specimen CR3....115
4.12 Panel Zone and Girder Web Instrumentation for Specimen CR4....116
4.13 Doubler Plate Instrumentation for Specimen CR4....117
4.14 Panel Zone and Girder Web Instrumentation for Specimen CR4R....118
4.15 Doubler Plate Instrumentation for Specimen CR4R....119
4.16 Doubler Plate Instrumentation for Specimen CR5....120
4.17 Location and Labels of Girder Flange Strain Gages for All Specimens....121
4.18 Location of Column Flange Strain Gages for All Specimens....122
4.19 Strain Gage Labels for Girder and Column Flanges of All Specimens....123
4.20 CFN Group Strain Gages for Specimens CR1, CR2, and CR5....124
4.21 Continuity Plate Instrumentation for Specimen CR3....125
4.22 Girder and Panel Zone LVDT Placement for All Specimens....126
4.23 Column Flange LVDT Placement for Specimens CR1, CR2, and CR5....127
4.24 Column Flange LVDT Placement for Specimens CR4 and CR4R....128
4.25 Load Frame LVDT Placement....129
4.26 Specimen Coordinate System....130

5.1 Number of Completed 4.0% Interstory Drift Cycles without Significant Strength Degradation 157
5.2 Displacement History of Specimen CR1 158
5.3 Displacement History of Specimen CR2 158
5.4 Displacement History of Specimen CR3 159
5.5 Displacement History of Specimen CR4 159
5.6 Displacement History of Specimen CR4R 160
5.7 Displacement History of Specimen CR5 160
5.8 Moment vs. Interstory Drift for East Girder, CR1 161
5.9 Moment vs. Interstory Drift for West Girder, CR1 161
5.10 Plastic Rotation of East Connection, CR1 162
5.11 Plastic Rotation of West Connection, CR1 162
5.12 East Girder Plastic Rotation Relative to Column Centerline, CR1 163
5.13 West Girder Plastic Rotation Relative to Column Centerline, CR1 163
5.14 Panel Zone Plastic Shear Deformation, CR1 164
5.15 Panel Zone Plastic Rotation Relative to Column Centerline, CR1 164
5.16 Low-Cycle Fatigue Fracture of East Bottom Flange, CR1 165
5.17 East Bottom Flange Fracture Following Test, CR1 165
5.18 East Bottom Flange Fracture Surface After Testing, CR1 166
5.19 Typical Beam Web-to Column Weld Cracking, CR1 166
5.20 Typical Low-Cycle Fatigue Cracking of Access Hole 167
5.21 Moment vs. Interstory Drift for East Girder, CR2 168
5.22 Moment vs. Interstory Drift for West Girder, CR2 168
5.23 Plastic Rotation of East Connection, CR2 169
5.24 Plastic Rotation of West Connection, CR2 169
5.25 East Girder Plastic Rotation Relative to Column Centerline, CR2 170
5.26 West Girder Plastic Rotation Relative to Column Centerline, CR2 170
5.27 Panel Zone Plastic Shear Deformation, CR2 171
5.28 Panel Zone Plastic Rotation Relative to Column Centerline, CR2 171
5.29 Panel Zone Yielding and Column Local Flange Deformation, CR2 172

5.30 Significant Crack Opening in West Top Flange, CR2 172
5.31 Fracture in West Top Flange, CR2 173
5.32 Complete Failure of West Top Flange, CR2 173
5.33 Moment vs. Interstory Drift for East Girder, CR3 174
5.34 Moment vs. Interstory Drift for West Girder, CR3 174
5.35 Plastic Rotation of East Connection, CR3 175
5.36 Plastic Rotation of West Connection, CR3 175
5.37 East Girder Plastic Rotation Relative to Column Centerline, CR3 176
5.38 West Girder Plastic Rotation Relative to Column Centerline, CR3 176
5.39 Panel Zone Plastic Shear Deformation, CR3 177
5.40 Panel Zone Plastic Rotation Relative to Column Centerline, CR3 177
5.41 Panel Zone Yielding and Significant Column Deformation, CR3 178
5.42 Crack Opening in East Bottom Flange, CR3 178
5.43 Fracture in East Bottom Flange, CR3 179
5.44 Moment vs. Interstory Drift for East Girder, CR4 180
5.45 Moment vs. Interstory Drift for West Girder, CR4 180
5.46 Plastic Rotation of East Connection, CR4 181
5.47 Plastic Rotation of West Connection, CR4 181
5.48 East Girder Plastic Rotation Relative to Column Centerline, CR4 182
5.49 West Girder Plastic Rotation Relative to Column Centerline, CR4 182
5.50 Panel Zone Plastic Shear Deformation, CR4 183
5.51 Panel Zone Plastic Rotation Relative to Column Centerline, CR4 183
5.52 Fracture of East Top Flange, CR4 184
5.53 Fracture of West Top Flange, CR4 184
5.54 Fracture of West Bottom Flange, CR4 185
5.55 Moment vs. Interstory Drift for East Girder, CR4R 186
5.56 Moment vs. Interstory Drift for West Girder, CR4R 186
5.57 Plastic Rotation of East Connection, CR4R 187
5.58 Plastic Rotation of West Connection, CR4R 187
5.59 East Girder Plastic Rotation Relative to Column Centerline, CR4R 188

5.60 West Girder Plastic Rotation Relative to Column Centerline, CR4R 188
5.61 Panel Zone Plastic Shear Deformation, CR4R 189
5.62 Panel Zone Plastic Rotation Relative to Column Centerline, CR4R 189
5.63 Through-Width Line Crack on West Girder Top Flange, CR4R.....190
5.64 Fracture of East Girder Top Flange, CR4R 190
5.65 Crack following Bevel of the Base Metal at East Girder Top Flange, CR4R 191
5.66 Lateral-Tortional Buckling in the West Girder, CR4R.....191
5.67 Moment vs. Interstory Drift for East Girder, CR5.....192
5.68 Moment vs. Interstory Drift for West Girder, CR5 192
5.69 Plastic Rotation of East Connection, CR5 193
5.70 Plastic Rotation of West Connection, CR5.....193
5.71 East Girder Plastic Rotation Relative to Column Centerline, CR5 194
5.72 West Girder Plastic Rotation Relative to Column Centerline, CR5 194
5.73 Panel Zone Plastic Shear Deformation, CR5.....195
5.74 Panel Zone Plastic Rotation Relative to Column Centerline, CR5.....195
5.75 Panel Zone Yielding and Significant Column Deformation, CR5 196
5.76 Crack Opening in West Girder Top Flange, CR5.....196
5.77 Fracture in West Girder Top Flange, CR5.....197

6.1 Typical Cruciform Specimen Finite Element Model [after (Ye et al., 2000)].....251
6.2 Typical Cruciform Connection Region Modeling [after (Ye et al., 2000)] 251
6.3 Stress-Strain Curve for A992 Steel [after (Ye et al., 2000)].....252
6.4 Comparison of Experimental and FEA Load vs. Drift, Specimen CR1 252
6.5 Comparison of Experimental and FEA Load vs. Drift, Specimen CR2 253
6.6 Comparison of Experimental and FEA Load vs. Drift, Specimen CR3 253
6.7 Comparison of Experimental and FEA Load vs. Drift, Specimen CR4R 254
6.8 Comparison of Experimental and FEA Load vs. Drift, Specimen CR5 254
6.9 Comparison of Experimental and FEA Connection Plastic Rotation, Specimen CR1 255
6.10 Comparison of Experimental and FEA Connection Plastic Rotation,

Specimen CR2 255
6.11 Comparison of Experimental and FEA Connection Plastic Rotation, Specimen CR3 256
6.12 Comparison of Experimental and FEA Connection Plastic Rotation, Specimen CR4R....256
6.13 Comparison of Experimental and FEA Connection Plastic Rotation, Specimen CR5 257
6.14 Comparison of Experimental and FEA Panel Zone Deformation, Specimen CR1 257
6.15 Comparison of Experimental and FEA Panel Zone Deformation, Specimen CR2 258
6.16 Comparison of Experimental and FEA Panel Zone Deformation, Specimen CR3 258
6.17 Comparison of Experimental and FEA Panel Zone Deformation, Specimen CR4R....259
6.18 Comparison of Experimental and FEA Panel Zone Deformation, Specimen CR5 259
6.19 Specimen CR1 Panel Zone (1.0% Drift)....260
6.20 Specimen CR1 Panel Zone (1.5% Drift)....260
6.21 Specimen CR1 Panel Zone (2.0% Drift)....261
6.22 Specimen CR1 Panel Zone (3.0% Drift)....261
6.23 Specimen CR1 Panel Zone (Following Test) 262
6.24 Specimen CR2 Panel Zone (1.5% Drift)....263
6.25 Specimen CR2 Panel Zone (2.0% Drift)....263
6.26 Specimen CR2 Panel Zone (3.0% Drift)....264
6.27 Specimen CR2 Panel Zone (4.0% Drift)....264
6.28 Specimen CR3 Panel Zone (1.5% Drift)....265
6.29 Specimen CR3 Panel Zone (2.0% Drift)....265
6.30 Specimen CR3 Panel Zone (3.0% Drift)....266
6.31 Specimen CR3 Panel Zone (4.0% Drift)....266

6.32 Specimen CR4R Panel Zone (1.5% Drift) 267
6.33 Specimen CR4R Panel Zone (2.0% Drift) 267
6.34 Specimen CR4R Panel Zone (3.0% Drift) 268
6.35 Specimen CR4R Panel Zone (4.0% Drift) 268
6.36 Specimen CR5 Panel Zone (1.5% Drift) 269
6.37 Specimen CR5 Panel Zone (2.0% Drift) 269
6.38 Specimen CR5 Panel Zone (3.0% Drift) 270
6.39 Specimen CR5 Panel Zone (4.0% Drift) 270
6.40 Elastic Strain History of Specimen CR1 (Panel Zone Center) 271
6.41 Elastic Strain History of Specimen CR1 (Panel Zone Corner) 271
6.42 Elastic Strain History of Specimen CR2 (Panel Zone Center) 272
6.43 Elastic Strain History of Specimen CR2 (Panel Zone Corner) 272
6.44 Elastic Strain History of Specimen CR3 (Panel Zone Center) 273
6.45 Elastic Strain History of Specimen CR3 (Panel Zone Corner) 273
6.46 Elastic Strain History of Specimen CR4R (Panel Zone Center) 274
6.47 Elastic Strain History of Specimen CR4R (Panel Zone Corner) 274
6.48 Elastic Strain History of Specimen CR5 (Panel Zone Center) 275
6.49 Elastic Strain History of Specimen CR5 (Panel Zone Corner) 275
6.50(a) Elastic Panel Zone Shear Stress Contours at 0.375% Drift for Positive Loading Direction, Specimen CR1 276
6.50(b) Elastic Panel Zone Shear Stress Contours at 0.375% Drift for Negative Loading Direction, Specimen CR1 276
6.51(a) Elastic Panel Zone Shear Stress Contours at 0.5% Drift for Positive Loading Direction, Specimen CR1 276
6.51(b) Elastic Panel Zone Shear Stress Contours at 0.5% Drift for Negative Loading Direction, Specimen CR1 276
6.52 Close-up View of Column Flange Yielding and Kinking Due to the Concentrated Girder Flange Force (Specimen CR1) 277
6.53 Longitudinal Strains Profile in CR1 Column Flange (Bottom Girder Flange in Tension) 278

6.54 Longitudinal Strains Profile in CR1 Column Flange
(Bottom Girder Flange in Compression) 278
6.55 Longitudinal Strains Profile in CR2 Column Flange
(Bottom Girder Flange in Tension).....279
6.56 Longitudinal Strains Profile in CR2 Column Flange
(Bottom Girder Flange in Compression) 279
6.57 Longitudinal Strains Profile in CR3 Column Flange
(Bottom Girder Flange in Tension).....280
6.58 Longitudinal Strains Profile in CR3 Column Flange
(Bottom Girder Flange in Compression) 280
6.59 Longitudinal Strains Profile in CR4R Column Flange
(Bottom Girder Flange in Tension).....281
6.60 Longitudinal Strains Profile in CR4R Column Flange
(Bottom Girder Flange in Compression) 281
6.61 Longitudinal Strains Profile in CR5 Column Flange
(Bottom Girder Flange in Tension).....282
6.62 Longitudinal Strains Profile in CR5 Column Flange
(Bottom Girder Flange in Compression) 282
6.63 Panel Zone Behavior versus AISC Design Equation 2.1, CR1 283
6.64 Panel Zone Behavior versus AISC Design Equation 2.1, CR2 283
6.65 Panel Zone Behavior versus AISC Design Equation 2.1, CR3 284
6.66 Panel Zone Behavior versus AISC Design Equation 2.1, CR4R.....284
6.67 Panel Zone Behavior versus AISC Design Equation 2.1, CR5 285
6.68(a) Net Shear Forces Acting on Panel Zone Showing Deformed Shape 285
6.68(b) Modified Fielding and Huang Model for Post-Elastic Panel Zone Behavior 285
6.69 Comparison of Experimental Panel Zone Behavior to AISC (1997) and
Equation 6.9, CR1.....286
6.70 Comparison of Experimental Panel Zone Behavior to AISC (1997) and
Equation 6.9, CR2.....286
6.71 Comparison of Experimental Panel Zone Behavior to AISC (1997) and

Equation 6.9, CR3 287
6.72 Comparison of Experimental Panel Zone Behavior to AISC (1997) and Equation 6.9, CR4R 287
6.73 Comparison of Experimental Panel Zone Behavior to AISC (1997) and Equation 6.9, CR5 288
6.74 Comparison of Experimental Panel Zone Behavior to AISC (1997) and Modified Fielding and Huang Model (Equation 6.10), CR1 288
6.75 Comparison of Experimental Panel Zone Behavior to AISC (1997) and Modified Fielding and Huang Model (Equation 6.10), CR2 289
6.76 Comparison of Experimental Panel Zone Behavior to AISC (1997) and Modified Fielding and Huang Model (Equation 6.10), CR3 289
6.77 Comparison of Experimental Panel Zone Behavior to AISC (1997) and Modified Fielding and Huang Model (Equation 6.10), CR4R 290
6.78 Comparison of Experimental Panel Zone Behavior to AISC (1997) and Modified Fielding and Huang Model (Equation 6.10), CR5 290
6.79 Schematic Explanation for Scaling of Panel Zone Capacity, Specimen CR1 291
6.80 Longitudinal Strain on Inside Face of CR1 Column Flange Near Web (Bottom Girder Flange in Tension) 292
6.81 Longitudinal Strain on Inside Face of CR1 Column Flange Near Web (Bottom Girder Flange in Compression) 292
6.82 Longitudinal Strain on Inside Face of CR2 Column Flange Near Web (Bottom Girder Flange in Tension) 293
6.83 Longitudinal Strain on Inside Face of CR2 Column Flange Near Web (Bottom Girder Flange in Compression) 293
6.84 Longitudinal Strain on Inside Face of CR5 Column Flange Near Web (Bottom Girder Flange in Tension) 294
6.85 Longitudinal Strain on Inside Face of CR5 Column Flange Near Web (Bottom Girder Flange in Compression) 294
6.86 Transverse Strain on Inside Face of CR1 Column Flange at Location of Bottom Girder Flange (Bottom Girder Flange in Tension) 295

6.87 Transverse Strain on Inside Face of CR1 Column Flange at Location of Bottom Girder Flange (Bottom Girder Flange in Compression) 295
6.88 Transverse Strain on Inside Face of CR2 Column Flange at Location of Bottom Girder Flange (Bottom Girder Flange in Tension) 296
6.89 Transverse Strain on Inside Face of CR2 Column Flange at Location of Bottom Girder Flange (Bottom Girder Flange in Compression) 296
6.90 Transverse Strain on Inside Face of CR5 Column Flange at Location of Bottom Girder Flange (Bottom Girder Flange in Tension) 297
6.91 Transverse Strain on Inside Face of CR5 Column Flange at Location of Bottom Girder Flange (Bottom Girder Flange in Compression) 297
6.92 Longitudinal Strain in Transverse Direction on Inside Face of CR1 Column Flange (Bottom Girder Flange in Tension) 298
6.93 Longitudinal Strain in Transverse Direction on Inside Face of CR1 Column Flange (Bottom Girder Flange in Compression) 298
6.94 Longitudinal Strain in Transverse Direction on Inside Face of CR2 Column Flange (Bottom Girder Flange in Tension) 299
6.95 Longitudinal Strain in Transverse Direction on Inside Face of CR2 Column Flange (Bottom Girder Flange in Compression) 299
6.96 Longitudinal Strain in Transverse Direction on Inside Face of CR5 Column Flange (Bottom Girder Flange in Tension) 300
6.97 Longitudinal Strain in Transverse Direction on Inside Face of CR5 Column Flange (Bottom Girder Flange in Compression) 300
6.98 Specimen CR1 Column Flange Displacement Along Column Length (Bottom Girder Flange in Tension) 301
6.99 Specimen CR1 Column Flange Displacement Along Column Length (Bottom Girder Flange in Compression) 301
6.100 Specimen CR5 Column Flange Displacement Along Column Length (Bottom Girder Flange in Tension) 302
6.101 Specimen CR5 Column Flange Displacement Along Column Length (Bottom Girder Flange in Compression) 302

6.102 Specimen CR1 Column Flange Displacement Transverse to Column Length (Bottom Girder Flange in Tension).....303
6.103 Specimen CR1 Column Flange Displacement Transverse to Column Length (Bottom Girder Flange in Compression) 303
6.104 Specimen CR5 Column Flange Displacement Transverse to Column Length (Bottom Girder Flange in Tension).....304
6.105 Specimen CR5 Column Flange Displacement Transverse to Column Length (Bottom Girder Flange in Compression) 304
6.106 Assumed Yield Line Pattern in Column Flange Due to LFB 305
6.107 Longitudinal Strain on Specimen CR1 West Girder Top Flange near Column Flange (Girder Flange in Tension).....306
6.108 Longitudinal Strain on Specimen CR1 West Girder Top Flange near Column Flange (Girder Flange in Compression).....306
6.109 Longitudinal Strain on Specimen CR2 West Girder Top Flange near Column Flange (Girder Flange in Tension).....307
6.110 Longitudinal Strain on Specimen CR2 West Girder Top Flange near Column Flange (Girder Flange in Compression).....307
6.111 Longitudinal Strain on Specimen CR3 West Girder Top Flange near Column Flange (Girder Flange in Tension).....308
6.112 Longitudinal Strain on Specimen CR3 West Girder Top Flange near Column Flange (Girder Flange in Compression).....308
6.113 Longitudinal Strain on Specimen CR4R West Girder Top Flange near Column Flange (Girder Flange in Tension).....309
6.114 Longitudinal Strain on Specimen CR4R West Girder Top Flange near Column Flange (Girder Flange in Compression).....309
6.115 Longitudinal Strain on Specimen CR5 West Girder Top Flange near Column Flange (Girder Flange in Tension).....310
6.116 Longitudinal Strain on Specimen CR5 West Girder Top Flange near Column Flange (Girder Flange in Compression).....310
6.117 Longitudinal Strain on Specimen CR1 East Girder Bottom Flange near

Column Flange (Girder Flange in Tension).....311
6.118 Longitudinal Strain on Specimen CR1 East Girder Bottom Flange near Column Flange (Girder Flange in Compression).....311
6.119 Longitudinal Strain on Specimen CR2 East Girder Bottom Flange near Column Flange (Girder Flange in Tension).....312
6.120 Longitudinal Strain on Specimen CR2 East Girder Bottom Flange near Column Flange (Girder Flange in Compression).....312
6.121 Longitudinal Strain on Specimen CR3 East Girder Bottom Flange near Column Flange (Girder Flange in Tension).....313
6.122 Longitudinal Strain on Specimen CR3 East Girder Bottom Flange near Column Flange (Girder Flange in Compression).....313
6.123 Longitudinal Strain on Specimen CR4R East Girder Bottom Flange near Column Flange (Girder Flange in Tension).....314
6.124 Longitudinal Strain on Specimen CR4R East Girder Bottom Flange near Column Flange (Girder Flange in Compression).....314
6.125 Longitudinal Strain on Specimen CR5 East Girder Bottom Flange near Column Flange (Girder Flange in Tension).....315
6.126 Longitudinal Strain on Specimen CR5 East Girder Bottom Flange near Column Flange (Girder Flange in Compression).....315
6.127 Strain Distribution (Strains CP3 to CP1) in Specimen CR3 Continuity Plate (East Top Flange in Tension).....316
6.128 Strain Distribution (Strains CP3 to CP1) in Specimen CR3 Continuity Plate (East Top Flange in Compression) 316
6.129 Strain Distribution (Strains CP7 to CP4) in Specimen CR3 Continuity Plate (East Top Flange in Tension).....317
6.130 Strain Distribution (Strains CP7 to CP4) in Specimen CR3 Continuity Plate (East Top Flange in Compression) 317
6.131 Strain Distribution (Strains CP10 to CP8) in Specimen CR3 Continuity Plate (East Top Flange in Tension).....318
6.132 Strain Distribution (Strains CP10 to CP8) in Specimen CR3 Continuity Plate

(East Top Flange in Compression) 318
6.133 Strain Distribution (Strains CP12 to CP11) in Specimen CR3 Continuity Plate (East Top Flange in Tension).....319
6.134 Strain Distribution (Strains CP12 to CP11) in Specimen CR3 Continuity Plate (East Top Flange in Compression) 319
6.135 Strain Distribution (Strains CP13 to CP14) in Specimen CR3 Continuity Plate (East Top Flange in Tension).....320
6.136 Strain Distribution (Strains CP13 to CP14) in Specimen CR3 Continuity Plate (East Top Flange in Compression) 320
6.137 Strain Distribution (Strains CP15 to CP18) in Specimen CR3 Continuity Plate (East Top Flange in Tension).....321
6.138 Strain Distribution (Strains CP15 to CP18) in Specimen CR3 Continuity Plate (East Top Flange in Compression) 321
6.139 Shear Strain Variation in Specimen CR4R Panel Zone (East Bottom Flange in Tension) 322
6.140 Shear Strain Variation in Specimen CR4R Panel Zone (East Bottom Flange in Compression).....322

A.1 Load vs. Stroke for East Girder, CR1 342
A.2 Load vs. Stroke for West Girder, CR1.....342
A.3 Load vs. Stroke for East Girder, CR2 343
A.4 Load vs. Stroke for West Girder, CR2.....343
A.5 Load vs. Stroke for East Girder, CR3 344
A.6 Load vs. Stroke for West Girder, CR3.....344
A.7 Load vs. Stroke for East Girder, CR4 345
A.8 Load vs. Stroke for West Girder, CR4.....345
A.9 Load vs. Stroke for East Girder, CR4R 346
A.10 Load vs. Stroke for West Girder, CR4R 346
A.11 Load vs. Stroke for East Girder, CR5 347
A.12 Load vs. Stroke for West Girder, CR5.....347

A.13 Moment vs. Interstory Drift for East Girder, CR1 348
A.14 Moment vs. Interstory Drift for West Girder, CR1 348
A.15 Moment vs. Interstory Drift for East Girder, CR2 349
A.16 Moment vs. Interstory Drift for West Girder, CR2 349
A.17 Moment vs. Interstory Drift for East Girder, CR3 350
A.18 Moment vs. Interstory Drift for West Girder, CR3 350
A.19 Moment vs. Interstory Drift for East Girder, CR4 351
A.20 Moment vs. Interstory Drift for West Girder, CR4 351
A.21 Moment vs. Interstory Drift for East Girder, CR4R 352
A.22 Moment vs. Interstory Drift for West Girder, CR4R 352
A.23 Moment vs. Interstory Drift for East Girder, CR5 353
A.24 Moment vs. Interstory Drift for West Girder, CR5 353
A.25 Illustration of Girder LVDT Placement and Measurement of Rotation 354
A.26(a) East Girder Total Rotation, CR1 355
A.26(b) East Girder Total Rotation, CR1 (Re-scaled) 355
A.27 West Girder Total Rotation, CR1 356
A.28 East Girder Total Rotation, CR2 357
A.29 West Girder Total Rotation, CR2 357
A.30(a) East Girder Total Rotation, CR3 358
A.30(b) East Girder Total Rotation, CR3 (Re-scaled) 358
A.31 West Girder Total Rotation, CR3 359
A.32 East Girder Total Rotation, CR4 360
A.33 West Girder Total Rotation, CR4 360
A.34 East Girder Total Rotation, CR4R 361
A.35 West Girder Total Rotation, CR4R 361
A.36 East Girder Total Rotation, CR5 362
A.37(a) West Girder Total Rotation, CR5 363
A.37(b) West Girder Total Rotation, CR5 (Re-scaled) 363
A.38 Illustration of Panel Zone Shear Deformation Measurement
[after (Krawinkler et al., 1971)]of Flange 364

A.39(a) Panel Zone Total Shear Deformation, CR1 365
A.39(b) Panel Zone Total Shear Deformation, CR1 (Re-scaled) 365
A.40 Panel Zone Total Shear Deformation, CR2 366
A.41 Panel Zone Total Shear Deformation, CR3 367
A.42 Panel Zone Total Shear Deformation, CR4 367
A.43 Panel Zone Total Shear Deformation, CR4R 368
A.44 Panel Zone Total Shear Deformation, CR5 368
A.45 Total Plastic Rotation of East Connection, CR1 369
A.46 Total Plastic Rotation of West Connection, CR1 369
A.47 Total Plastic Rotation of East Connection, CR2 370
A.48 Total Plastic Rotation of West Connection, CR2 370
A.49 Total Plastic Rotation of East Connection, CR3 371
A.50 Total Plastic Rotation of West Connection, CR3 371
A.51 Total Plastic Rotation of East Connection, CR4 372
A.52 Total Plastic Rotation of West Connection, CR4 372
A.53 Total Plastic Rotation of East Connection, CR4R 373
A.54 Total Plastic Rotation of West Connection, CR4R 373
A.55 Total Plastic Rotation of East Connection, CR5 374
A.56 Total Plastic Rotation of West Connection, CR5 374
A.57(a) East Girder Plastic Rotation, CR1 375
A.57(b) East Girder Plastic Rotation, CR1 (Re-scaled) 375
A.58 West Girder Plastic Rotation, CR1 376
A.59 East Girder Plastic Rotation, CR2 377
A.60 West Girder Plastic Rotation, CR2 377
A.61(a) East Girder Plastic Rotation, CR3 378
A.61(b) East Girder Plastic Rotation, CR3 (Re-scaled) 378
A.62 West Girder Plastic Rotation, CR3 379
A.63 East Girder Plastic Rotation, CR4 380
A.64 West Girder Plastic Rotation, CR4 380
A.65 East Girder Plastic Rotation, CR4R 381

A.66 West Girder Plastic Rotation, CR4R.....381
A.67 East Girder Plastic Rotation, CR5.....382
A.68(a) West Girder Plastic Rotation, CR5.....383
A.68(b) West Girder Plastic Rotation, CR5 (Re-scaled).....383
A.69(a) Panel Zone Plastic Shear Deformation, CR1.....384
A.69(b) Panel Zone Plastic Shear Deformation, CR1 (Re-scaled).....384
A.70 Panel Zone Plastic Shear Deformation, CR2.....385
A.71 Panel Zone Plastic Shear Deformation, CR3.....386
A.72 Panel Zone Plastic Shear Deformation, CR4.....386
A.73 Panel Zone Plastic Shear Deformation, CR4R.....387
A.74 Panel Zone Plastic Shear Deformation, CR5.....387
A.75(a) East Girder Plastic Rotation Relative to Column Centerline, CR1.....388
A.75(b) East Girder Plastic Rotation Relative to Column Centerline, CR1 (Re-scaled).....388
A.76 West Girder Plastic Rotation Relative to Column Centerline, CR1.....389
A.77 East Girder Plastic Rotation Relative to Column Centerline, CR2.....390
A.78 West Girder Plastic Rotation Relative to Column Centerline, CR2.....390
A.79(a) East Girder Plastic Rotation Relative to Column Centerline, CR3.....391
A.79(b) East Girder Plastic Rotation Relative to Column Centerline, CR3 (Re-scaled).....391
A.80 West Girder Plastic Rotation Relative to Column Centerline, CR3.....392
A.81 East Girder Plastic Rotation Relative to Column Centerline, CR4.....393
A.82 West Girder Plastic Rotation Relative to Column Centerline, CR4.....393
A.83 East Girder Plastic Rotation Relative to Column Centerline, CR4R.....394
A.84 West Girder Plastic Rotation Relative to Column Centerline, CR4R.....394
A.85 East Girder Plastic Rotation Relative to Column Centerline, CR5.....395
A.86(a) West Girder Plastic Rotation Relative to Column Centerline, CR5.....396
A.86(b) West Girder Plastic Rotation Relative to Column Centerline, CR5 (Re-scaled).....396
A.87(a) Panel Zone Plastic Rotation Relative to Column Centerline, CR1.....397

A.87(b) Panel Zone Plastic Rotation Relative to Column Centerline, CR1 (Re-scaled) 397
A.88 Panel Zone Plastic Rotation Relative to Column Centerline, CR2 398
A.89 Panel Zone Plastic Rotation Relative to Column Centerline, CR3 399
A.90 Panel Zone Plastic Rotation Relative to Column Centerline, CR4 399
A.91 Panel Zone Plastic Rotation Relative to Column Centerline, CR4R 400
A.92 Panel Zone Plastic Rotation Relative to Column Centerline, CR5 400

B.1 Strain History of CR4 East Top Flange During 1.0% Drift Cycles 416
B.2 Strain History of CR4 West Top Flange During 1.0% Drift Cycles 416
B.3 Strain History of CR4 East Top Flange During 1.5%, 2.0% Cycles 417
B.4 Strain History of CR4 West Top Flange During 1.5%, 2.0% Cycles 417
B.5 Strain History of CR4 West Bottom Flange During 1.5%, 2.0% Cycles 418
B.6 West Top Flange Fracture Surface From Specimen CR4 418
B.7 West Top Flange Fracture Surface at Column Face from Specimen CR4 419
B.8 Close-up View of Specimen CR4 Fracture Surface Features Near Center of Flange 419
B.9 Typical Sectioning of Fracture Surfaces for Investigation 420
B.10 Fractured Weld Section From East Top Flange of Specimen CR4 420
B.11 Fractured Weld Section From West Top Flange of Specimen CR4 421
B.12 Fractured Weld Section From West Bottom Flange of Specimen CR4 421
B.13 Weld Section From East Bottom Flange of Specimen CR4 422
B.14 Weld Section From Top Flange of Specimen CR1 422
B.15 LOF and Slag Inclusions in Specimen CR4 West Top Flange 423
B.16 Slag Inclusions Above Backing Bar in Specimen CR4 West Top Flange 423
B.17 LOF in Center of Specimen CR4 West Bottom Flange 424
B.18 SEM Photo Showing Cleavage Planes on Fracture Surface of Specimen CR4 424
B.19 SEM Photo Showing Brittle Cleavage Behavior of Welds of Specimen CR4 425
B.20 SEM Photo Showing Ductile Fracture of E71T-8 Fillet Weld of Specimen CR4 425
B.21 Illustration of LEFM Application to Backing Bar Notch 426

List of Tables

3.1 Cruciform Test Specimen Matrix 77
3.2 Strength-to-Demand Ratios for PZ Yielding, LFB, and LWY Limit States 77
3.3 Panel Zone Strength Comparisons....77
3.4 Steel W-Shape Tensile Properties....78
3.5 Plate Material Tensile Properties....78
3.6 Weld Material Properties....79
3.7 Tested Weld Material Properties (E70T-6 Only)....79
3.8 Summary of Parameters used for CJP Welds....80

4.1 General Specimen Loading History....100
4.2 Definitions of Strain Gage Label Nomenclature....100
4.3 Specimen CR1 Strain Gage Locations....101
4.4 Specimen CR2 Strain Gage Locations....102
4.5 Specimen CR3 Strain Gage Locations....103
4.6 Specimen CR4 Strain Gage Locations....104
4.7 Specimen CR4R Strain Gage Locations....105
4.8 Specimen CR5 Strain Gage Locations....106

5.1 Summary of Peak Loads and Moments for Specimen CR1....145
5.2 Summary of Peak Loads and Moments for Specimen CR2....146
5.3 Summary of Peak Loads and Moments for Specimen CR3....147
5.4 Summary of Peak Loads and Moments for Specimen CR4....148
5.5 Summary of Peak Loads and Moments for Specimen CR4R....149
5.6 Summary of Peak Loads and Moments for Specimen CR5....150
5.7 Progression of Yielding and Fracture in Specimen CR1....151
5.8 Progression of Yielding and Fracture in Specimen CR2....152

5.9 Progression of Yielding and Fracture in Specimen CR3 153
5.10 Progression of Yielding and Fracture in Specimen CR4 154
5.11 Progression of Yielding and Fracture in Specimen CR4R 155
5.12 Progression of Yielding and Fracture in Specimen CR5 156

6.1 Panel Zone Strengths and Post-Elastic Strength Increases Using AISC (1997) and Modified Fielding and Huang (1971) Equations 241
6.2 Connection Member Sizes and Joint Type for Tests Used to Evaluate Panel Zone Provisions 242
6.3 Parameters For Tests Used to Evaluate Panel Zone Provisions 244
6.4 Panel Zone Strength Test-to-Predicted Ratios 246
6.5 Girder-Column Combinations for Panel Zone Thickness Calculations 248
6.6 Required Panel Zone Thicknesses 249
6.7 Comparison of Panel Zone Thicknesses 250
6.8 Scale Factor, α, for Panel Zone Capacity Corresponding to Test Results 250
6.9 Column Bending Stresses and Corresponding Strains in the Region 6 to 12 in. Below the Girder Flange 250

B.1 Comparison of Measured and Required CVN Toughness From Cruciform Tests 414
B.2 Comparison of AWS Test Plate and Strained Pull-Plate Specimen CVNs 414
B.3 E70T-6 Weld Chemistry From Specimens CR1 and CR4, and Consumable Producer's Typical Data 415
B.4 Welding Parameters From Specimens CR1 and CR4 415

Chapter 1

Introduction

Following the Northridge earthquake of January 17, 1994, damage was discovered in a number of steel moment frame structures. This damage most often consisted of brittle fractures of the bottom flange girder-to-column complete joint penetration (CJP) welds. The fractures caused were by a number of factors related to the use of low toughness welds; connection design and detailing that led to larger moment-frame members, less system redundancy, and higher strain demands on the connections; the use of higher strength girders leading to potential undermatching of the welds; and a number of other connection detailing and construction practices that were typical prior to the earthquake (FEMA, 2000a). Additionally, column stiffening practices have been cited as a possible contributor to the fractures, largely as a result of observations that many of the connections that fractured in the Northridge earthquake lacked continuity plates and that some had weak panel zones (Roeder, 1997; FEMA, 2000b). Finite element analysis also has showed an increase in stress or strain concentrations in the girder flange-to-column flange weld associated with excessively weak panel zones or insufficient continuity plates (El-Tawil et al., 1998; Ricles et al., 2000).

As a result of this, there has subsequently been a tendency to be overly conservative in the design and detailing of column stiffening. A wealth of research by the SAC program (FEMA, 2000b) and others has attempted to resolve many issues related to connection design and detailing, and has led to new guidelines for seismic construction (FEMA, 2000a). While there has also been some research on column stiffening issues, most has focused on the presence or absence of continuity plates and doubler plates, and not on the associated design equations and detailing. Without a

definitive verification of design procedures, the conservatism in stiffening design is understandable.

Design criteria for the limit states related to column stiffening are presented in Chapter K of the AISC Load and Resistance Factor Design (LRFD) Specification (AISC, 1993, 1999a). The limit states of primary importance for stiffening of connections include local flange bending (LFB), local web yielding (LWY), and panel zone yielding (PZ). Additional provisions for seismic design of doubler plates and continuity plates are included in the AISC Seismic Provisions (1992, 1997), however the 1997 AISC Seismic Provisions (AISC, 1997) removed all continuity plate design procedures, requiring instead that they be proportioned based on connection qualification tests. Continuity plate design equations were reestablished and new panel zone design equations were developed and included in the final SAC Recommended Seismic Design Criteria (FEMA, 2000a).

The current design equations for column stiffening included in the AISC LRFD Specification (1993, 1999a) and AISC Seismic Provisions (AISC, 1997) are largely based on bodies of research conducted several years ago. Work by Sherbourne and Jensen (1957) and Graham et al. (1960) established the provisions for LFB and LWY, while research by Krawinkler et al. (1971) and Bertero et al. (1973) led to the current PZ design equations. These provisions were derived from research conducted on older A7 and A36 steels, and on member sizes smaller than typically used in current moment frame construction.

A concern related to the tendency towards over-conservatism in stiffener design, and the various requirements for such stiffeners included in recent recommendations and codes, is the potential for fabrication problems. The SAC criteria (FEMA, 2000a) require continuity plates of equal thickness to girder flanges for interior connections. Thinner continuity plates are permitted for exterior connections. Furthermore, the connection of the continuity plates to the column flanges must be made with CJP welds, and must include reinforcing fillet welds under the backing bars, resulting in a condition of high restraint due to weld shrinkage. The new panel zone design equations may require moderately thicker doubler plates in the case of large columns. Often, these doublers are

connected to the column web by CJP welds in the k-area of the columns. Not only are excessive stiffeners economically undesirable, the associated welding of thick stiffeners as described above may cause fabrication cracking. The restraint imposed by CJP welds in the connection region has caused fabrication cracking in the k-area of the columns in the past (Tide, 2000).

1.1 Research Objectives

The research described herein is part of a larger research project sponsored by the American Institute of Steel Construction. The primary objectives of the project are to reassess the current provisions for column stiffening and to develop and test economical alternative details for such stiffeners. This includes an assessment of the LFB, LWY, and PZ provisions, as well as testing of various innovative doubler plate and continuity plate designs.

Three distinct components comprise the research in order to meet these objectives. The components include a computational study, monotonically-loaded pull-plate experiments, and cyclically-loaded cruciform connection experiments. The computational study included analyses of all experimental specimens as well as parametric studies to extend the results to member sizes and details not tested. Information on this work can be found in Ye et al. (2000). The pull-plate experiments investigated the limit states of LFB and LWY primarily for non-seismic design, and tested various doubler plate and continuity plate stiffener details. Information on these tests can be found in Prochnow et al. (2000a, 2000b) and Dexter et al. (2001). The final component of the research project is the subject of this report.

This report details the design and testing of the cyclically-loaded cruciform girder-to-column connection specimens. It was originally planned to test five cruciform specimens for this experimental study. Due to premature fracturing in three of the four complete joint penetration welds connecting the girder flanges to the column flanges in one of five specimens, one additional cruciform specimen was fabricated and tested.

The specimens were designed with the primary intent to assess the current PZ design provisions, to verify the results of the pull-plate experiments with respect to LFB

and continuity plate detailing for seismic design, and to test various innovative doubler plate details. A secondary focus of the experiments was an evaluation of the performance of new moment-frame connection details and weld metal notch-toughness requirements developed as a result of the Northridge earthquake.

The test specimens were selected following a parametric study of all practical girder-to-column combinations. The study identified the stiffening requirements of several potential test specimens. A range of dimensional and design parameters were considered in the selection of the final specimens. The member sizes and stiffening details of the five specimens were selected from the potential combinations to balance all primary objectives. These included the assessment of the panel zone design provisions, testing of various stiffener details, and verification of the LFB provisions. Additional consideration was given to specimens and details that could be correlated to the results of the pull-plate experiments conducted by Prochnow et al. (2000a). All specimens were fabricated from A992 wide-flange sections, and all detailing material was A572 grade 50 steel. Study of deep columns and members made of high strength steel is beyond the scope of this research.

One specimen included a large, unstiffened column section and no doubler plates. It was intended for investigation of the panel zone strength provisions of columns with thick flanges, as well as the LFB limit state behavior for large, heavy columns. Two additional specimens included one or two doubler plates but no continuity plates. These specimens were geared for testing the LFB limit states, as well as to investigate a panel zone detail that included a doubler plate fillet-welded to the column flanges. All three specimens were also intended to show that continuity plates are not necessarily required for all seismic moment-resisting connections. Another specimen investigated the use of a fillet-welded continuity plate detail similar to those tested in the pull-plate experiments of Prochnow et al. (2000a). Each of these specimens was designed with relatively weak panel zones to investigate the impact of the weak panel zone on the stress and strain concentrations in these new column-stiffening details. A final specimen featured an innovative offset doubler plate detail intended to act as both continuity plates and doubler plates.

1.2 Organization of the Report

This report consists of seven chapters. Chapter 2 provides background information on limit states pertaining to column stiffening, including LFB, LWY, and PZ yielding. A detailed history of the panel zone provisions is also presented, including opinions and recommendations from several research programs conducted both before and after the Northridge earthquake. The chapter concludes with a discussion of the economic issues related to column stiffening.

Chapter 3 describes the experimental procedure used for the cruciform tests. It begins with a presentation of the methods and results of the parametric study used to identify possible specimens, followed by a description of the specimen selection procedure. The selection procedure includes a discussion of several parameters related to the LFB, LWY, and PZ yielding limit states. Justification of the final test matrix is presented, and the features of each specimen are detailed. The design procedures for various specimen components are then presented, including the moment connections, panel zones, and all stiffeners (i.e., doubler plates and continuity plates). The material properties of the rolled sections, plate material, and welds are also given in this chapter, including test results, required properties, and manufacturer's data.

Chapter 4 illustrates the test setup used for the experimental study. This includes the configuration of load frame assembly. The loading protocol adopted in this test program is also described. Chapter 4 concludes with a presentation of the instrumentation plans for all specimens.

Chapter 5 summarizes the applied load histories and basic behavior of all of the test specimens. The first section details the actual load histories applied to each specimen. The behavior of each specimen is then individually discussed. Included are progressions of yielding and fracture, descriptions of the failure modes, and summaries of the rotation and deformation characteristics of each specimen.

Chapter 6 interprets and extends the basic results of the specimens presented in Chapter 5. A comparison is made between the finite element results from Ye et al. (2000) and the experimental results. The panel zone behavior of the specimens is then

discussed, including a comparison of results to the behavior predicted by the current AISC panel zone strength provisions. An alternate model of panel zone strength is also presented and compared to the experimental behavior. The LFB behavior of the specimens is also discussed, and comparisons are made to the results and recommendations given by Prochnow et al. (2000a).

Chapter 7 includes research summaries, conclusions and recommendations related to the cruciform testing. Based on the six cruciform specimens tested and analysis of these results, several conclusions and recommendations are made with respect to the panel zone strength provisions, the LFB limit state, and weld toughness requirements.

Appendix A documents the procedures used to calculate all rotation and deformation data from the actuator and linear variable differential transformer (LVDT) data. Additional plots not presented in Chapter 5 are also included in the appendix.

Appendix B summarizes the failure analysis of Specimen CR4, which exhibited premature brittle weld failure in three of the four complete joint penetration welds connecting the girder flanges to the column flanges. Forensic examination and material testing of the welds are used to explain the occurrence of the weld fractures.

Chapter 2

Background of Design Provisions for Column Stiffening

Both the AISC LRFD Specification (1993, 1999a) and the AISC Seismic Provisions (1997) contain design and detailing requirements for panel zones and doubler plates in moment-resisting connections. This chapter discusses the development of the present panel zone provisions, specifically focusing on the requirements in the Seismic Provisions. A collection of opinions from various researchers regarding panel zone design and behavior, both prior to and following the Northridge earthquake, is also presented. The provisions for local flange bending (LFB) and local web yielding (LWY), pertaining to the design of transverse stiffeners (continuity plates), are also outlined. The chapter concludes with a brief discussion of the economics of column stiffening alternatives.

2.1 History of Panel Zone Design Provisions

The 1997 AISC Seismic Provisions for panel zones in Special Moment Frames (SMF) and Intermediate Moment Frames (IMF) includes two design equations (AISC, 1997). The first specifies the shear strength of the joint panel and the second places a limitation on panel zone slenderness. The backgrounds of these provisions are presented below and include information on the research behind their development and on their adoption by other codes and specifications. These panel zone design criteria as given by the 1997 AISC Seismic Provisions (AISC, 1997) are:

$$\phi_v R_v = \phi_v 0.6 F_{yc} d_c t_p \left(1 + \frac{3 b_{cf} t_{cf}^2}{d_g d_c t_p}\right) \qquad \text{(Equation 9-1, 1997)} \qquad (2.1)$$

where:

R_v = nominal panel zone shear strength

ϕ_v = resistance factor = 1.0 [modified from 0.75 by AISC (2001)]

F_{yc} = minimum specified column yield stress

b_{cf} = column flange width

t_{cf} = column flange thickness

d_c = column depth

d_g = girder depth

t_p = panel zone thickness

$$t \geq (d_z + w_z)/90 \qquad \text{(Equation 9-2, 1997)} \qquad (2.2)$$

where:

t = column web or doubler plate thickness; or total thickness if doublers are plug welded

d_z = panel zone depth

w_z = panel zone width

2.1.1 Panel Zone Shear Strength

Prior to the development of the current design provisions used by AISC, panel zones were designed using either Allowable Stress Design (ASD) or Plastic Design (Krawinkler, 1978). The nominal panel zone shear capacity, V_n, for the ASD and Plastic Design methods (AISC, 1978) are, respectively:

$$V_n = 0.4F_{yc}d_g t_p \qquad (2.3)$$

$$V_n = 0.55F_{yc}d_g t_p \qquad (2.4)$$

The required shear strength was calculated as the shear produced by the unbalanced beam moments acting at the faces of the connection, less the column story shear. These shears due to gravity, wind, and/or seismic loads were calculated at service (unfactored) loads. However, SEAOC, in the 1975 Recommended Lateral Force Requirements ("Blue Book"), suggested designing the panel zones for the capacity of the members framing into the joint, thus assuring plastic hinges could form in the beams. In the case of seismic loading, ASD allowed a 33% increase in allowable stress, changing

the expression for the joint shear strength to $V_n = 0.53F_{yc}d_gt_p$, resulting in a value similar to plastic design. Both the plastic design equation and the latter ASD seismic expression have been observed to accurately predict the onset of inelastic behavior in the panel zone when column axial loads are small (Krawinkler, 1978).

Monotonic testing by Fielding and Huang (1971) revealed a large post-yield capacity in panel zones. An expression was derived for the post-yield stiffness assuming elastic-plastic behavior of the panel and treating the column flanges as elastic cantilevers in bending. This model is illustrated in Figure 2.1a. The expression for the post-yield stiffness is given by:

$$\frac{dV_f}{d\gamma} = \frac{24EI_f}{d_g^2} \tag{2.5}$$

where:

V_f = shear due to column flange contribution

γ = shear deformation

E = modulus of elasticity

I_f = moment of inertia of individual column flange

Their bi-linear model agreed well with the experimentally observed behavior during the initial stages of panel zone yielding.

Cyclic testing by Bertero, Krawinkler, and Popov in the early 1970's led to the development of an ultimate strength criterion for panel zones similar to that used today. It should be noted that this testing was conducted on very small member sizes (W8 sections used as columns, and W10, W12 and W14 sections used as girders). Krawinkler (1978) modeled the joint as an elastic-plastic shear panel bounded by rigid elements connected by rotational springs. Figure 2.1b illustrates this model. Based on an approximate expression for the spring stiffness from a finite element analysis (Krawinkler et al., 1971) and an assumed maximum allowable shear deformation of four times the nominal shear yield strain, $4\gamma_y$, to ensure controlled inelastic deformation, the following was derived:

$$V_n = 0.55 F_{yc} d_c t_p \left(1 + \frac{3.45 b_{cf} t_{cf}^2}{d_g d_c t_p} \right) \tag{2.6}$$

Equation 2.6 was adopted by SEAOC in the 1988 Blue Book, although the 3.45 factor was reduced to 3.0. UBC in 1988 also adopted the expression in this form. The AISC LRFD Specification (1993, 1999a) and the AISC Seismic Provisions (1992, 1997) further modified the equation by increasing the factor of 0.55 to 0.6, consistent with the assumed shear yield stress of $0.6F_y$ used in several equations by AISC.

Both SEAOC (1988) and UBC (1988) also defined the required strength of the panel zone as the shear originating from the connected girder bending moments due to gravity loads plus 1.85 times the seismic forces. However, this required shear strength was permitted to remain at or below that required to develop $0.8\Sigma M_s$, where M_s is the plastic moment strength of the connected girders. Prior to this, SEAOC had implied that panel zones should be designed to allow development of the full plastic capacity of the girders.

Depending on the basis for calculating the required shear strength, panel zones designed by Equation 2.1 can behave quite differently. If the panel zone is weak relative to the girder flexural strength, most of inelastic behavior may take place within the connection, while stronger panel zones will allow shared energy dissipation between the joint and the connected girders. More specifically, a weak panel zone will put relatively high stress and strain concentrations at the location of the kink in the column flange adjacent to the critical girder flange-to-column welds. This may increase the potential for low-cycle fatigue and brittle fracture at that location. On the other hand, a strong panel zone may increase the stress and strain concentrations in the girder, on the other side of the critical girder flange-to-column welds and at the critical weld access hole area. It is presently not clear whether a strong or weak panel zone is best for the overall resistance of the connection to low-cycle fatigue and brittle fracture. Such response may depend on a number of factors, including the fracture toughness of the welds, the detailing of the welds and access holes, and the particular girder and column section.

Following the adoption of this ultimate strength criterion, and prior to the 1994 Northridge earthquake, the capacity of panel zones had been infrequently questioned, the exception being the case of very thick column flanges. Krawinkler (1978) noted that Equation 2.6 would need verification for thick column flanges, and finite element analysis conducted by El-Tawil et al. (1998, 1999) showed the expression to be slightly unconservative for this case. However, one ongoing debate, especially in the wake of the Northridge earthquake, is over the determination of required shear in the joint.

Two common conclusions have generally been drawn from the analytical and experimental work on panel zone behavior:

- Panel zone yielding is a stable phenomenon under repeated cycles of large inelastic distortion and is thus an excellent dissipater of energy; however, excessive panel zone deformation can lead to localized kinking of the column flanges, which may increase the potential for low cycle-fatigue and brittle fracture of the girder flange-to-column welds.
- Panel zone stiffness can significantly influence global frame stiffness and must be considered in analysis; elastic drift is substantially greater in designs with weak panel zones.

The current expressions for panel zone strength, V_n, were adopted following repeated observations of this first conclusion and following additional testing on deeper sections by Popov et al. in 1986 (Roeder and Foutch, 1996). Since this time, a number of changes in panel zone design requirements have been due to changes in the specification of required shear strength, V_u [given as R_u in the 1997 AISC Seismic Provisions (AISC, 1997)]. Recent code provisions for required shear strength are summarized below.

- <u>1992 AISC Seismic Provisions:</u>

  V_u is determined from load combinations 3-5 and 3-6, which consider the full earthquake forces and overturning effects. However, V_u is not required to exceed the shear forces determined from $0.9\Sigma\phi_b M_p$, where $\phi_b = 0.9$, and M_p is the girder nominal plastic moment, $Z_x F_y$. These applicable load combinations, along with a reduced resistance factor for panel zone shear of $\phi_v = 0.75$, are intended to give

roughly the same level of safety as the 1991 UBC code, in which V_u is determined based on gravity loads plus 1.85 times the seismic forces (AISC, 1992). The 1994 NEHRP provisions also adopted this version of the Seismic Provisions (NEHRP, 1994).

- FEMA 267: Interim Guidelines (1995a)

  V_u is determined from the shear induced by girder bending moments due to gravity loads plus 1.85 times the seismic forces, but the required shear strength need not exceed that required to develop $0.8\Sigma M_f$, where M_f is the moment at the column face when a plastic mechanism forms. This is a slight modification of UBC 1994, which placed the ceiling at $0.8\Sigma M_s$, where M_s is the plastic moment capacity of the framing girders.

- 1997 AISC Seismic Provisions:

  R_u is determined from load combinations 4-1 and 4-2, but need not exceed the shear due to $0.8\Sigma R_y M_p$, where $R_y M_p$ is the expected plastic moment based on an assumed increase in yield strength beyond the nominal value. These combinations are similar to Equations 3-5 and 3-6 from the 1992 AISC Seismic Provisions (AISC, 1992), except for the amplification of earthquake forces by the structural overstrength factor, Ω_o, and the change in nominal earthquake loads included in ASCE 7-95 (ASCE, 1995) (note that the commentary to the Provisions contains an error in identifying the applicable load combinations as A4-5 and A4-6 from the 1993 AISC LRFD Specification). These provisions, however, are still intended to provide the same reliability as the 1991 UBC requirements (AISC, 1997). The 1997 NEHRP provisions also adopted this version of the Seismic Provisions (NEHRP, 1997).

- FEMA 267A: Advisory No. 1 (1997a)

  V_u is determined from the shear due to $0.8\Sigma M_f$. The load combination of gravity plus 1.85 times the seismic forces is no longer considered, and the maximum cap on the required shear previously specified instead constitutes the sole basis for calculating the required shear strength. This change is purportedly based on

experimental observations of kinking in the column flanges due to large panel zone deformations.

- AISC Seismic Provisions Supplement No. 1 (1999b)

  R_u is determined from load combinations 4-1 and 4-2, but need not exceed the shear due to $0.8\Sigma M^*_{pb}$, where $\Sigma M^*_{pb} = \Sigma(1.1R_yM_p + M_v)$, and M_v is the additional moment due to shear amplification. The change from R_yM_p to M^*_{pb} in the moment summation was made to be consistent with the definition of the expected girder moment capacity used for the strong column-weak beam (SCWB) check in the Provisions (AISC, 1999b).

- AISC Seismic Provisions Supplement No. 2 (2001)

  The use of load combinations 4-1 and 4-2 from the 1997 AISC Seismic Provisions (AISC, 1997) is no longer permitted, as it is recognized these combinations do not directly relate to achieving yielding of the girders. The thickness of the panel zone must be based on the method used to proportion tested (or prequalified) connections. However, as a minimum, R_u "shall be determined from the summation of the moments at the column faces as determined by projecting the expected moments at the plastic hinge points to the column faces" (AISC, 2001). One major change from Supplement No. 1 is the removal of the factor of 0.8 from the moment summation. A second major change in this supplement is an increase in the resistance factor used with the Equation 2.1, ϕ_v, from 0.75 to 1.0.

Observations of stable energy dissipation associated with inelastic panel zone behavior are what originally led to the desire for designs with weak panel zones. However, these same provisions may prevent the connected girders from ever reaching their plastic capacity except under extremely large panel zone deformations and significant strain hardening (i.e., deformations well beyond the maximum of $4\gamma_y$ assumed in Krawinkler's derivation). Although these extreme deformations may be stable in the panel zone, they may also lead to local kinking in the beam and column flanges. This kinking, observed by Krawinkler et al. (1971), Bertero et al. (1973), and Krawinkler

(1978), is considered one possible contributing factor to the Northridge fractures (Roeder and Foutch, 1996). The changes suggested in FEMA 267A (1997a) and the supplements to the 1997 AISC Seismic Provisions (1999b, 2001) - all of which increased the required shear strength - reflect this belief.

More recently, a new approach to panel zone design has been incorporated into the recommended design criteria put forth by SAC (FEMA, 2000a). The new method is in response to growing concern over the present provisions. Several recent investigations have shown that large panel zone deformations can occur even when they are designed as per Equation 2.1 (Choi et al., 2000; Ricles et al., 2000; FEMA, 2000b). Instead of incorporating the post-yield strength recognized in the current AISC provisions, and basing demand on the ultimate strength of the connected members, the method attempts to balance the onset of yielding between the panel zone and connected girders. It has been shown that this balance leads to better overall connection performance (Roeder, 2000). The panel zone demand associated with this method is essentially the shear due to flexural yielding of the beams, while the recognized shear strength of the panel zone is that at first yield. The required thickness, t_{req}, of the panel zone is determined as:

$$t_{req} = \frac{R_{yg} M_{yg} \dfrac{h - d_g}{h}}{(0.9)0.6 R_{yc} F_{yc} d_c \left(d_g - t_{gf}\right)} \tag{2.7}$$

$$M_{yg} = F_{yg} S_g \tag{2.8}$$

where:

h = height between girder centerlines of adjacent stories

R_{yg} = ratio of expected yield strength of girder to minimum specified value

M_{yg} = girder yield moment

R_{yc} = ratio of expected yield strength of column to minimum specified value

F_{yg} = minimum specified girder yield stress

S_g = elastic girder section modulus

If the required thickness determined by Equation 2.7 is greater than the column web thickness, doubler plates are required. As an alternative, the panel zone may be

proportioned based on a tested connection, similar to the provisions of AISC Supplement No. 2 (2001).

2.1.2 Panel Zone Slenderness

The empirical AISC panel zone slenderness provision given as $t \geq (d_z + w_z)/90$ first appeared in the 1988 SEAOC Blue Book. Since then, it has been adopted without change by the 1988 and subsequent UBC codes, as well as the 1992 and 1997 AISC Seismic Provisions (AISC, 1992, 1997). The equation appears in the Blue Book as Equation 4-2, Section 4F.2.b (SEAOC, 1988). The commentary to this section refers to a Krawinkler reference (1978) as the source, saying the equation is "based on tests" that show the buckling of panel zones meeting the criteria of Equation 4-2 will not reduce the shear capacity of the joint under repeated cyclic loading.

The referenced paper (Krawinkler, 1978), however, contains nothing pertaining to panel zone slenderness limitations and is not a report of experimental work. Rather it contains references to earlier experimental work by Bertero, Krawinkler, and Popov from the early 1970's. Data on these tests can be found in Krawinkler et al. (1971) and Bertero et al. (1973), and in abbreviated form in Bertero et al. (1972) and Krawinkler et al. (1975). None of the above references give specific slenderness criteria for panel zones, although all note that buckling of thin panel zones occurred at large inelastic distortions.

The actual development of the slenderness equation has been attributed to work performed by Teal as part of a SEAOC committee sometime in the early 1980's (Popov, 1999). However, no published records of the equation's development or any other background information appear to be available.

If, in fact, the data behind this provision is from the aforementioned tests (Bertero et al., 1973; Krawinkler et al., 1971), it is probably based on two test specimens, designated A1 and A2. These specimens consisted of W8x24 columns and W10x15 girders with unreinforced panel zones. The web thickness of a W8x24 is 0.245 inches. Using the dimensions of the resulting panel zone, an expression of $t \approx (d_z + w_z)/68$ can be derived. It was noted by Krawinkler et al. (1971) and Bertero et al. (1973) that when the panel zones of these specimens did buckle, there was no loss of strength observed. In

fact, the shear capacities of these panel zones continued to increase as the steel began to strain harden.

The question then arises as to whether the allowable value of $(d_z + w_z)/90$ was a liberalization of the tested slenderness limits based on the engineering judgement of Teal and the SEAOC committee. Although the test results from Krawinkler et al. (1971, 1975) and Bertero et al. (1972, 1973) are likely the basis for the panel zone slenderness provision, it is still unclear how the maximum value of $(d_z + w_z)/t = 90$ was arrived at.

2.2 Opinions Regarding Panel Zone Design and Behavior

Historically, the most common opinion regarding panel zone yielding has been that it is beneficial when limited, but undesirable when it becomes excessive. This desire to recognize the benefits of limited inelasticity in panel zone design is what led to the development of the present panel zone shear strength provision, allowing for "controlled inelastic deformations" (Krawinkler, 1978). This balanced approach to panel zone yielding is not universally accepted, however. Popov (1987) has discussed three major philosophies of panel zone design:

- *Rigid panel zone approach*: In this method, panel zones are designed to essentially remain elastic, forcing all yielding into the girders.
- *Flexible panel zone approach*: This method, previously advocated by Kawano (1984), confines most inelastic behavior to the panel zones, and was considered most suitable for low-rise structures.
- *Balanced approach*: This method allows for distributed inelasticity between the girders and panel zones, consistent with Krawinkler's "controlled inelastic deformation" assumption (Krawinkler, 1978).

Contained in these design philosophies are more than just panel zone strength calculations. Inherent in them are also methods of demand determination. As illustrated in Section 2.1, panel zone demands are either based on load combinations or are functions of the plastic capacity of the connected girders. Clearly, a design based on a

first-yield strength equation (e.g., Plastic Design), which intends that the panel zone remain essentially elastic, would still result in a flexible panel zone relative to the rest of the structural system if the demand was significantly underestimated. Thus, panel zone design is an issue of the relative strengths of the panel zone, girders, and columns. Summarized below are past opinions of researchers regarding panel zone strength and demand requirements:

- Krawinkler et al. (1971) advocated balanced inelasticity between girders and panel zones, even though extremely large, stable panel zone deformations were recorded in their tests. To ensure this balanced design, the researchers believed that a design method incorporating panel zone inelasticity would also have to be based on a demand from the full plastic capacity of the girders.
- Fielding and Huang (1971) noted the large post-yield capacity of panel zones, but felt that any changes to design provisions recognizing this strength would also have to take into account the required rigidity of the joint.
- Bertero et al. (1973) echoed the statements of Krawinkler et al. (1971) by proposing a design procedure for panel zone strength that allows for limited panel zone inelasticity based on a demand calculated from the full plastic capacity of the connected girders.
- Becker (1975) concluded that underdesigned panel zones can be the weak elements in a structure and can significantly reduce the structure's strength and stiffness.
- Popov et al. (1986) advocated designs incorporating balanced inelastic demands between the girders and panel zones. The researched cautioned against the design of weak panel zones, as they were considered potential contributors to some of the experimentally observed failures.
- Lee and Lu (1989) studied composite girder-to-column connections and concluded that the panel zones were still ductile in composite frames. Thus, they suggested designing panel zones for limited inelastic deformations.
- Ghobarah et al. (1992) advocated distributing the inelastic demands between the girders and panel zones, even though large recorded joint deformations were stable.

The researchers also recommended against designing overly stiff panel zones because of the large demands imposed on the girders.

- Schneider et al. (1993) concluded that weak panel zones are undesirable for weak column-strong beam (WCSB) frames. Even though the panel zone yielding was stable, large drifts and losses of stiffness were deemed unacceptable.

The 1994 Northridge earthquake caused the engineering community to question most aspects of connection design, including the design of panel zones. Generally, this has resulted in a trend of increased conservatism in the proportioning of doubler plates and other column reinforcement. While this has not resulted in a complete reversion to the rigid panel zone design approach, the trend towards stiffer joint designs are reflected by recent code changes and design guidelines. Opinions derived from recent testing and new design suggestions include:

- Tsai et al. (1995) proposed that panel zone demand be calculated as 80% of the flange ultimate moment, $Z_f F_u$, where Z_f is the plastic section modulus of the flanges. This suggestion was based on the distributed inelasticity in specimens designed in this manner. In addition, the researchers believed the post-yield strength criterion (e.g., AISC, 1992) should be replaced with a more conservative first-yield expression, even though it was noted that the current provisions satisfactorily predicted post-yield panel zone strengths in the specimens tested.
- The SAC Phase 1 testing (SAC, 1996) showed that designs based on UBC (1988) often resulted in panel zone rotations as large or larger than girder plastic rotations. While this panel zone deformation was stable, it was hypothesized to be a contributor to the Northridge fractures. Further study of the panel zone design provisions was suggested.
- Roeder and Foutch (1996) conducted a statistical analysis of past connection tests and concluded that panel zone yielding reduced the flexural ductility of the connected girders. The researchers hypothesized that the trend towards weaker panel zones in

recent pre-Northridge codes (e.g., UBC, 1988; AISC, 1992) may be correlated to the Northridge connection fractures.

- The AISC Seismic Provisions (AISC, 1997) retained the post-yield panel zone strength equation, but altered the load combinations used to calculate demand. The structural overstrength factor, with a value between two and three, replaced the 1.0 load factor on earthquake loads, which were adjusted accordingly in ASCE 7 (ASCE, 1995). Additionally, the demand cap was altered to reflect the expected strength properties of the girders instead of the nominal properties, resulting in a higher cap on required strength.
- The FEMA Interim Guidelines Advisory No. 1 (1997a) retained the post-yield panel zone strength equation, but eliminated the load combination method of demand calculation. Instead, demand was given by the expression previously specified as a demand cap in the original Interim Guidelines (FEMA, 1995a). The explicit intent of this change was designs with stronger panel zones.
- El-Tawil et al. (1998, 1999) conducted finite element analyses that showed the post-elastic panel zone strength to be reasonably accurate, except in cases of very thick column flanges. However, the researchers also showed that connections with very weak panel zones were more susceptible to brittle and/or ductile fractures, based on local stress conditions. The demand cap of 80% of the girder plastic moment capacities specified by the FEMA Interim Guidelines (1995a) was believed adequate for interior connections, but unconservative for exterior connections.
- Bjorhovde et al. (1999) conducted several tests on WCSB connections with weak panel zones to investigate the possibility of k-area fractures. Good plastic rotation was achieved in all specimens, and was dominated by panel zone yielding. Kinking of the column flanges was observed, and was hypothesized as a contributor to specimen failure. Several fractures propagated along the fillet region of the column, but none were found to originate in the k-area.
- Stojadinovic et al. (2000) observed similar connection plastic rotations regardless of panel zone strengths. One specimen with a weak panel zone and undersized fillet welds on the continuity plates failed by fracture of these welds and subsequent tearing

in the column k-line. While it was not concluded that a weak panel zone played a role in the fracture, it was not ruled out as a factor.

- Ricles et al. (2000) conducted full-scale tests and finite element analyses of connections, and concluded that stronger panel zones result in better overall performance. The finite-element work showed a 50% increase in ductile fracture potential at the end of the beam web groove welds for the weak panel zone case. A recommendation was made that panel zones be designed such that less than 50% of the total plastic rotation is due to panel zone deformation. Based on the experimental results, it was recommended that only the column web shear strength be considered in design, resulting in stronger panel zones. Cracking at the ends of the beam web groove welds in some specimens was attributed to effects of weaker panel zones.
- Choi et al. (2000) recommended designing panel zones for limited yielding (a ductility level of 3 or 4) based on tests of the free-flange connection detail. While good rotational performance was achieved in specimens with weak panel zones, the failure modes were different from those seen in the strong panel zone specimens. The column flange deformation associated with weak panel zones was thought to have led to low-cycle fatigue cracking in the beam flanges and the shear tab-to-column attachment. In contrast, lateral-torsional buckling was the failure mode observed in all specimens with strong panel zones.
- Chi et al. (2000) performed finite element analyses to investigate fracture toughness demands (K_I and CTOD) in the CJP welds of the beam flange to column. At large connection plastic rotations, weak panel zones resulted in toughness demands approximately double those of strong panel zones. The authors suggested a re-evaluation of current seismic panel zone design standards [e.g., AISC (1997)].
- Roeder (2000) analyzed over 100 past connection tests (including SAC testing) to identify trends related to panel zone behavior. Specimens that yielded in flexure first generally showed larger rotations than those with first yielding in the panel zone; however the largest rotations were achieved in tests where panel zone yielding initiated soon after beam yielding. Very stiff panel zones were shown to adversely

affect performance. The author recommended a balanced approach to design such that some panel zone yielding occurs following the onset of flexural yielding.

- FEMA (2000a) included a new approach to panel zone design based on the work of Roeder for the SAC program (FEMA, 2000b). The intent was to balance the onset of flexural and panel zone yielding. It is noted that the procedure will not result in dramatic differences from past design methods, except in cases of very thick column flanges. In this situation, moderately thicker doubler plates may be needed.

The research and recommendations discussed above clearly show the trend towards increased conservatism in the design of panel zones following the Northridge earthquake. However, with the exception of El-Tawil (1998, 1999), and to some extent Choi et al. (2000), none of the recent research has directly addressed the AISC design equations (Equations 2.1 and 2.2). Further evaluation of these provisions is necessary to bring the issue of appropriate panel zone design to a closure. The present research program is intended to contribute to this effort.

2.3 Background of LFB and LWY Provisions

The design of continuity plates in moment-resisting connections is primarily governed by local flange bending (LFB) and local web yielding (LWY) limit states. While the web crippling (WC) limit state is also applicable to moment connections, a study by Prochnow et al. (2000a) showed that it never governed the need for continuity plates in typical connection configurations. These LFB and LWY limit states are included in the AISC LRFD Specification (1993, 1999a) for non-seismic design, and additional requirements were provided in the 1992 AISC Seismic Provisions (AISC, 1992). The 1997 AISC Seismic Provisions (AISC, 1997), however, removed procedures for sizing continuity plates, requiring instead that they be proportioned based on tested connections. The SAC Recommended Seismic Design Criteria (FEMA, 2000a) restored equations for determining continuity plate requirements in seismic moment frames.

The AISC provisions for continuity plates are based primarily on the work of Sherbourne and Jensen (1957) and Graham et al. (1960). A detailed background on these

limit states can be found in Prochnow et al. (2000a). For the LFB limit state, continuity plates must be provided if the required strength, R_u, exceeds the resistance of the column flange, given by:

$$\phi R_n = \phi 6.25 t_{cf}^2 F_{yc} \qquad \text{(Equation K1-1, 1999a)} \qquad (2.9)$$

where:

ϕ = resistance factor = 0.9

For the LWY limit state, continuity plates are required if R_u exceeds the web resistance, given by:

$$\phi R_n = \phi(5k + N) F_{yc} t_{cw} \qquad \text{(interior)} \qquad \text{(Equation K1-2, 1999a)} \qquad (2.10)$$

$$\phi R_n = \phi(2.5k + N) F_{yc} t_{cw} \qquad \text{(exterior)} \qquad \text{(Equation K1-3, 1999a)} \qquad (2.11)$$

where:

ϕ = 1.0

k = distance from outer face of column flange to web toe of column fillet

N = length of bearing surface = t_{gf} for moment connections

The demand, R_u, for both limit states is based on the force delivered to the connection by the girder flanges. Several possibilities exist for calculation of this demand, including:

$$R_u = F_{yg} A_{gf} \qquad (2.12)$$

$$R_u = 1.8 F_{yg} A_{gf} \qquad (2.13)$$

$$R_u = 1.1 R_y F_{yg} A_{gf} \qquad (2.14)$$

where:

A_{gf} = area of girder flange

R_y = ratio of expected yield strength to minimum specified value

Equation 2.12 is typically used for non-seismic design, representing the nominal yield strength of the flange. Equation 2.13 was included in the 1992 AISC Seismic Provisions

(AISC, 1992). The 1.8 factor includes a strain-hardening factor of 1.3 on the yield strength, and assumes the full plastic capacity of the girder is carried by the flanges. Thus, the 1.3 factor is increased by the ratio of the plastic section modulus, Z_x, to the flange section modulus, Z_f. This ratio is typically at most about 1.4, resulting in the factor of 1.8 (1.4*1.3 ≈ 1.8) (Bruneau et al., 1998). Equation 2.13, however, predicts stresses in the flange well above the tensile strength of most structural steels. Equation 2.14 was presented by Prochnow et al. (2000a) and provided a more realistic flange force for the pull-plate experiments. The $1.1R_y$ factor is consistent with the SCWB check and panel zone demand calculations used by AISC (1997, 1999b).

The SAC Recommended Seismic Design Criteria (FEMA, 2000a) includes two equations for determining the need for continuity plates. Both are based on mitigating the LFB limit state. Continuity plates are required if:

$$t_{cf} < 0.4\sqrt{1.8 b_{gf} t_{gf} \frac{F_{yg} R_{yg}}{F_{yc} R_{yc}}} \tag{2.15}$$

$$t_{cf} < \frac{b_{gf}}{6} \tag{2.16}$$

where:

b_{gf} = girder flange width

R_{yg} = ratio of expected yield strength of girders to minimum specified value

R_{yc} = ratio of expected yield strength of column to minimum specified value

Equation 2.15 inherently includes a demand that is essentially given by Equation 2.13 and a capacity presented in Equation 2.9. Equation 2.16 is based on testing conducted by Ricles et al. (2000) for SAC.

The pull-plate tests recently conducted by Prochnow et al. (2000a) investigated the limit states of LFB and LWY. It was shown that the present AISC provisions (Equations 2.9 and 2.10) were reasonable and slightly conservative for non-seismic design (Prochnow et al., 2000a, 2000b; Dexter et al., 2001). New equations that better described the test results were presented for these limit states, however the calculated resistances are similar to the current AISC equations (Equations 2.9 and 2.10).

Furthermore, the test results showed that the demand given by Equation 2.13 was impossible to achieve in the pull-plate tests, and Equation 2.14 provided a more reasonable demand for these experiments.

2.4 Economic Considerations of Column Stiffening

The economics of column stiffening are an important aspect of design that must not be overlooked. It is well known that transverse stiffeners and doubler plates are expensive additions to the detailing of columns (Carter, 1999). While the material costs are low, the fabrication and installation costs are high. In a cost comparison of arbitrary column reinforcement details (i.e., continuity plates and doubler plates) it has been shown that the detailing (cutting, welding, etc.) governed the cost, and not the overall material thickness and dimensions (AISC, 1999c). Significant cost savings and increased simplicity can be achieved if column reinforcement can be fully or partially eliminated.

While eliminating transverse stiffeners and doubler plates generally requires larger column sections, the associated costs may often be fully offset by the savings associated with simplified detailing. The AISC study (1999c) and Troup (1999) showed that increasing the column size by up to 100 lb/ft to eliminate both continuity plates and doubler plates was often the more economical alternative. However, some recent seismic specifications (AISC, 1997) either require or suggest the use of transverse stiffeners in all high seismic applications. For these cases, eliminating the need for doubler plates alone may still prove the economical choice. These options are particularly attractive in non-seismic design.

One possible alternative to increasing the size of a column to avoid doubler plates would be to produce columns specifically designed to eliminate web stiffening (i.e., columns with thicker webs). This would lessen the need for doubler plates without adding unnecessary weight to the column flanges. Columns such as this have been available in the past. The fifth edition of the AISC Manual (AISC, 1959) included a "column core" section that was often used with flange cover plates to produce columns heavier than the largest available rolled sections. The column core section was a WF14x320 with a flange thickness of 2.093 in. and a web thickness of 1.89 in. This

flange thickness is very similar to currently produced W14x283 columns (t_{cf} = 2.07 in.), but the web thickness of the WF14x320 is similar to the much heavier W14x426 column (t_w = 1.875 in.).

Often, particularly in the case of interior moment-frame connections under lateral loading, the need for column stiffening will be governed by panel zone shear. For example, consider an interior connection consisting of a W14 column section and W36x150 girders. Using the 1992 AISC Seismic Provisions (AISC, 1992) for LFB, a W14x283 column is needed to avoid continuity plates in this connection. However, using the 1997 AISC Seismic Provisions (AISC, 1997) for panel zone strength, a W14x455 column is required to avoid doubler plates. Production of sections with thicker webs has been periodically discussed, but no mills presently roll such columns. By making columns available with thicker webs, the need for column stiffening may be reduced with only a minimal increase in steel weight.

In addition to increasing the column size, specifying a higher strength grade of steel may also lessen the need for stiffening. Specifying a minimum of grade 50 steel for columns is now standard. While grade 65 steel further strengthens a column, it is presently more expensive than other steels, and a more detailed cost assessment of the alternatives has to be made.

Not only can the elimination of column stiffening often lead to a lower cost structure, but other benefits can also be realized. The welding associated with transverse stiffeners and doubler plates can be highly constrained, leading to possible fabrication cracking and undesirable residual stress conditions. In addition to more favorable material conditions, eliminating stiffening simplifies the detailing and lessens the possibility of confusion between the designers and fabricators. Finally, the larger columns required to eliminate stiffening promote the strong column-weak beam condition required by the AISC Seismic Provisions (AISC, 1997) and FEMA (2000a).

In situations where stiffening cannot be fully or even partially eliminated, the AISC Steel Design Guide 13 (AISC, 1999c) provides suggestions on how to limit the economic impacts. The following are often applicable to both seismic and non-seismic applications:

- Increase the number of moment-resisting connections or frames, resulting in more economical stiffening details
- Use fillet welds instead of CJP welds where appropriate
- Specify a single doubler plate up to thicknesses around one-half inch; if greater, specify two doubler plates
- Select doubler plate thicknesses such that plug welding to the column web is not required
- Limit the number of different plate thicknesses for transverse stiffeners and doubler plates

This chapter has outlined the various design provisions for column stiffening related to the limit states of panel zone yielding, local flange bending, and local web yielding. The history behind the development of the present panel zone design equations was also presented. This revealed that a substantial body of past research directly and indirectly tied to column stiffening issues exists, including several programs conducted as a result of the 1994 Northridge earthquake. However, some issues remain unresolved or unaddressed. These include experimental evaluation of the current AISC Seismic Provisions (AISC, 1997) panel zone limit state, testing of alternative stiffening details that avoid welding in the potentially low-toughness k-line area of wide-flange shapes, and the reestablishment of definitive design criteria and details for continuity plates, especially in seismic moment frames. By addressing these issues, overly conservative stiffening designs can be avoided, resulting in more economical steel structures. The research described herein is intended to contribute to the resolution of such issues.

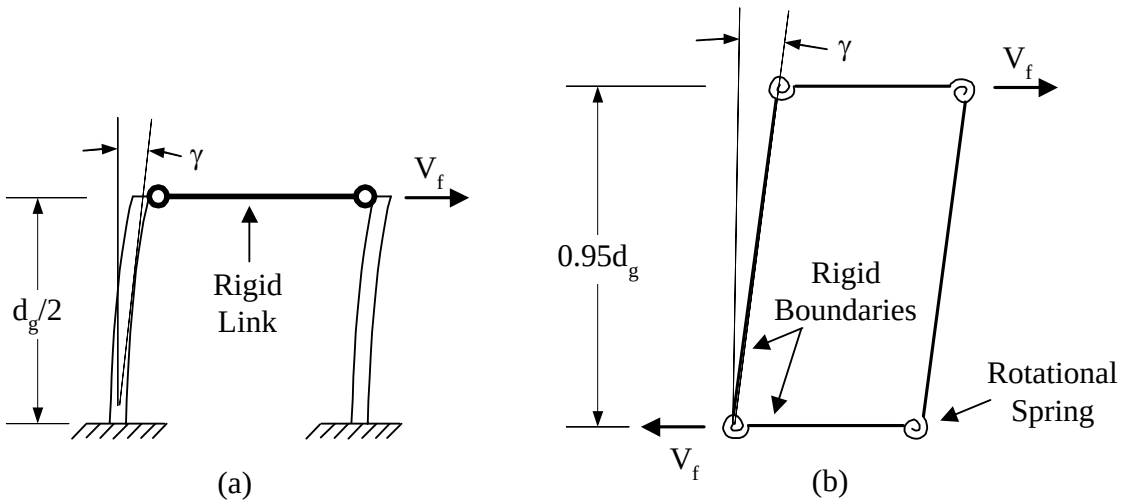


Figure 2.1: (a) Fielding and Huang, and (b) Krawinkler Models for Post-Elastic Panel Zone Behavior

Chapter 3

Specimen Selection and Design

This chapter describes the selection and design of the five cruciform specimens tested in this research. The selection of the five specimens was based partly on a parametric study of panel zone stiffening requirements, described in detail in this chapter. Other factors considered during the selection process included correlations with past research, testing equipment capacity, and a study of parameters relevant to moment frame connection design. A justification of the resulting test matrix is presented, outlining the key aspects of each specimen.

One of the five originally planned specimens resulted in an unexpected brittle fracture. As it turned out, the deposited weld metal did not meet the SAC minimum Charpy V-Notch (CVN) test (notch toughness) requirements (FEMA, 2000e). It is not believed that the fracture was related to the column stiffening details. Therefore, this result, although important, is tangential to the discussion of the effect of column stiffening, which presumes inherently that all welds meet the recommended SAC minimum CVN requirements. The behavior of this specimen and an analysis of the fracture are discussed in detail in Appendix B to this report. This specimen was replicated (with weld consumables that do meet the SAC CVN requirements) and was re-tested, creating a sixth specimen.

The specimen design section describes the basic dimensions of the total of six test specimens, the details of the girder-to-column moment connections common to all specimens, and the design of the various stiffening details. Also presented are the results of material testing, including the tensile properties of the steel, and properties of the weld metal.

3.1 Parametric Study of Panel Zone Stiffening Requirements

3.1.1 Definitions of Parameters

To aid the process of selecting sizes for the cruciform test specimens, and to identify general trends, a study was performed to compare various properties of and stiffening requirements for the panel zone. Initially, over 44,000 possible W-section girder and column combinations were considered, based on a list of over 200 available section sizes (AISC, 1995). However, the results discussed herein are limited to those girder-column combinations that can be defined as typical seismic moment frame configurations. For the purposes of this study, "typical seismic moment frame configurations" were defined as all W24 through W36 girders in combination with all W14x90 and larger W14 column sections (i.e., all W14 sections with a nominal flange width of 14 inches or greater). This resulted in an array of 1848 potential combinations.

Both 50 ksi and 65 ksi column material was considered, to include the possibility of grades A572/50, A572/65, A992, and A913 column steel. All girder steel was assumed to be grade 50. Plate material strength for all column stiffener material was assumed to be 50 ksi.

In addition to the parameters included in the study, a check of the strong column-weak beam (SCWB) condition was also implemented. The basic SCWB condition used was that specified in the AISC Seismic Provisions (AISC, 1997) for Special Moment Frame (SMF) and Intermediate Moment Frame (IMF) structures, and is given as:

$$\frac{\sum_{columns} M^*_{pc}}{\sum_{girders} M^*_{pg}} > 1.0 \tag{3.1}$$

where:

$$\sum_{columns} M^*_{pc} = \sum_{columns} Z_c \left(F_{yc} - P_{uc} / A_c \right) \tag{3.2}$$

$$\sum_{girders} M^*_{pg} = \sum_{girders} \left(1.1 R_y F_{yg} Z_g + M_v \right) \tag{3.3}$$

Z_c = column plastic section modulus

Z_g = girder plastic section modulus

F_{yc} = column yield strength

F_{yg} = girder yield strength

P_{uc}/A_c = column axial stress

R_y = ratio of expected yield strength to specified minimum yield strength

M_v = additional girder moment at column centerline due to shear amplification

This check included a variable column axial stress, P_{uc}/A_c, but no additional girder moment due to shear amplification from the location of the plastic hinge to the column centerline (i.e., $M_v = 0$). A range of axial stresses was considered, and included 0, 10, 20 and 40 ksi. Substituting Equations (3.2) and (3.3) into (3.1) yielded the SCWB relation used in the study. This is given as:

$$\frac{\sum_{columns} Z_c \left(F_{yc} - P_{uc}/A_c\right)}{\sum_{girders} 1.1 R_y Z_g F_{yg}} > 1.0 \qquad (3.4)$$

Girder-to-column configurations meeting this criterion for a particular axial load would be permitted for SMF and IMF applications, while those configurations failing this check, even at a column axial stress of zero, were considered permissible Ordinary Moment Frame (OMF) or non-seismic configurations. Five major parameters were then investigated for the study of panel zone stiffening requirements, including:

- Panel zone strength to demand ratio: $\phi R_v/R_u$
- Required doubler plate thickness: t_{req}
- Panel zone web slenderness: $(d_z+w_z)/t_w$
- Panel zone doubler plate slenderness: $(d_z+w_z)/t_{dp}$
- Panel zone aspect ratio: d_z/w_z

The development of the parametric study is discussed in the following sections. A similar parametric study for the LFB and LWY limit states was conducted and reported in Prochnow et al. (2000a). All development and results herein are applicable to general seismic design. No non-seismic design was explicitly considered in this study for two primary reasons. First, the cyclic testing plan does not represent the loading conditions of non-seismic moment frames, and would thus essentially give results applicable to non-seismic details under seismic loading. Second, panel zone demand in the AISC LRFD Specifications (1993, 1999a) is based on load combinations, which would require the design of prototype frames for a specified lateral load. There is no demand cap as is included in the AISC Seismic Provisions (AISC, 1997) that can be used to calculate the required shear strength. However, the test matrix presented in Section 3.2 includes some non-seismic (or OMF) details that will be tested cyclically. If these details can be shown to perform well under simulated seismic loading, it is almost assured that they would be adequate for static loading conditions. Non-seismic specimens and details were defined by girder-column combinations not meeting the SCWB requirement and/or column stiffeners sized for demands less than those given by the AISC Seismic Provisions (1992, 1997).

Panel Zone Strength to Demand Ratio

The basic formula used for the design strength of the panel zones, $\phi_v R_v$, was that given by the AISC Seismic Provisions (AISC, 1997), and modified by Supplements Nos. 1 and 2 to the Seismic Provisions (AISC, 1999b, 2001). It is also applicable to non-seismic applications when panel zone deformation is accounted for in the structural analysis (AISC, 1993, 1999a). This formula (using the Seismic Provisions notation) is given as:

$$\phi_v R_v = \phi_v 0.6 F_{yc} d_c t_p \left(1 + \frac{3 b_{cf} t_{cf}^2}{d_g d_c t_p} \right) \tag{3.5}$$

where:

$\phi_v R_v$ = panel zone design shear strength

F_{yc} = column yield strength

b_{cf} = column flange width

t_{cf} = column flange thickness

d_c = column depth

d_g = girder depth

t_p = panel zone thickness

As this section of the study only considered the strength of unreinforced panel zones, the total panel thickness, t_p, was taken as the column web thickness, t_w. The resistance factor, ϕ_v, was taken as 1.0, consistent with AISC Supplement No. 2 (2001).

The 1997 AISC Seismic Provisions (AISC, 1997) specified a panel zone demand based on load combinations, and included a cap on demand based on the capacity of the members framing into the joint. These load combinations were removed by Supplement No. 1 (AISC, 1999b). Instead of load combinations, the cap became the sole basis for calculation of demand. This general formula is given as:

$$R_u = C \sum_{girders} \frac{1.1 R_y M_p}{d_g} - V_c \tag{3.6}$$

where:

R_u = required panel zone strength

C = constant

R_y = overstrength factor; equal to 1.1 for grades 50 and 65 steel

M_p = nominal girder plastic moment capacity

V_c = column shear

The 1997 AISC Seismic Provisions (AISC, 1997) specified a value of the constant, C, equal to 0.8. This took into account the effect of gravity loading on interior spans offsetting a percentage of the moments due to lateral loading. However, because this assumption is unconservative for exterior connections, Supplement No. 2 (AISC, 2001) conservatively increased the value of the constant to 1.0 for all connections. Thus, the value of 1.0 was used for this study. The determination of column shear was based

on a statics analysis of the basic specimen dimensions (given in Section 3.3). If the resulting value of $\phi_v R_v/R_u$ for a particular combination of members was greater than or equal to one, no doubler plates were needed.

Required Doubler Plate Thickness

If the values of $\phi_v R_v/R_u$ given by the above study of strength to demand ratios were less than one, the need for doubler plates was indicated. The required thickness, t_{req}, was derived from the following:

$$R_{v,req} = \frac{R_u}{\phi_v} = 0.6 F_y d_c \left(t_w + t_{req}\right)\left(1 + \frac{3 b_{cf} t_{cf}^2}{d_g d_c \left(t_w + t_{req}\right)}\right) \tag{3.7}$$

where:

$R_{v,req}$ = required nominal panel zone shear strength

t_w = column web thickness

t_{req} = required doubler plate thickness

Solution of Equation (3.7) for t_{req} yielded the basic equation used for required doubler plate thickness in the study:

$$t_{req} = \frac{R_u}{\phi_v 0.6 F_y d_c} - t_w - \frac{3 b_{cf} t_{cf}^2}{d_g d_c} \tag{3.8}$$

This equation for the required thickness is based on a doubler plate yield strength equal to that of the column material. As the material used for the doubler plates was assumed to be grade 50, there is a potential discrepancy between the yield strengths of the columns and doubler plates if grade 65 columns are used. Thus, the final values of required thickness, t_{req}, were determined by scaling the value from Equation (3.8) by the ratio of the column yield strength to the doubler plate yield strength. While not correct, strictly speaking (as the equation for panel zone strength was derived based on a single

material strength), this method was considered satisfactory. A negative required thicknesses as per Equation (3.8) indicated doubler plates were not needed.

Panel Zone Web Slenderness

In addition to the panel zone strength equation given in the AISC Seismic Provisions, there is a slenderness limitation applicable to both the column web in the panel zone and any doubler plates, if needed (AISC, 1997). This requirement is given as:

$$t \geq (d_z + w_z)/90 \tag{3.9}$$

where:

t = column web, doubler plate, or total thickness (only if doublers are plug welded)

d_z = panel zone depth

w_z = panel zone width

The panel zone depth, d_z, is defined as the depth between continuity plates and was taken as the beam depth less twice the flange thickness. The width, w_z, is defined as the width of the panel zone between column flanges, and was thus taken as the column depth less twice the flange thickness. The thickness, t, can be either the web thickness or doubler plate thickness, depending on the component considered. In this section of the study, the column web thickness was considered. Equation (3.9) was then rearranged to give the expression used in the study:

$$(d_z + w_z)/t_w \leq 90 \tag{3.10}$$

If the value on the left side of Equation (3.10) was less than or equal to 90, the slenderness criterion was met. A value greater than 90 indicated that the column web thickness of the particular girder-column combination was insufficient.

Panel Zone Doubler Plate Slenderness

Similar to Equation (3.10) above, the slenderness criterion used in this section is given as:

$$\left(d_z + w_z\right)/t_{dp} \leq 90 \tag{3.11}$$

where:

t_{dp} = doubler plate thickness

The doubler plate thickness, t_{dp}, used in Equation (3.11) depends on whether a one- or two-sided doubler plate is assumed. All analyses discussed herein were conducted assuming a one-sided doubler plate, in which case t_{dp} equals the required doubler plate thickness, t_{req}, as calculated from Equation (3.8). As with the web slenderness investigation, a $(d_z + w_z)/t_{dp}$ value of 90 or less indicated that the slenderness criterion was met.

Panel Zone Aspect Ratio

The panel zone aspect ratio is given as d_z/w_z, where these variables are as defined previously. While there are no requirements pertaining to the aspect ratio in the current AISC Seismic Provisions (AISC, 1997), it has been investigated in the past (Krawinkler et al., 1971; Bertero et al., 1973), and has been targeted as a possible variable for further study in recent publications (El-Tawil et al., 1998, 1999). The concern stems from finite element studies that show significant bending deformations in thick panel zones with large aspect ratios (i.e., panel zones with large shear stiffness relative to panel zone bending stiffness). The strength equation given by Equation (3.5), however, is based on an assumption of pure shear deformation.

3.1.2 Results of Panel Zone Parameter Study

The following results are applicable to panel zones designed in accordance with the 1997 AISC Seismic Provisions (AISC, 1997) as modified by Supplement Nos. 1 and 2 (AISC, 1999b, 2001). All connections were assumed to be interior (i.e., girders

framing into both sides of the column), as these are the focus of the experimental investigation.

The SCWB check implemented in the study revealed that this requirement placed significant limitations on potential test specimens, if the SCWB criterion was strictly adhered to. For a column strength of 50 ksi and no column axial load, the number of possible girder-to-column combinations decreased from the total number of seismic combinations considered, 1848, to 575 when the SCWB criterion was applied. For axial loads of 10, 20, and 40 ksi, the number of SCWB combinations decreased to 436, 281, and 12, respectively. Similarly, for grade 65 column steel, the number of combinations meeting the SCWB requirement decreased from 766 to 645, 506, and 204 as the axial load was increased from zero to 40 ksi. Figures 3.1 and 3.2 illustrate these results. The results, as they apply to the parameters studied, are discussed further in the sections that follow.

Panel Zone Strength to Demand Ratio

Results from this section of the study indicated that, within a given nominal girder depth, as the girder sections get smaller (i.e., lower weight per foot), the number of girder-column combinations (for a particular girder) requiring panel zone reinforcement becomes smaller. That is, heavier girder sections within a given depth are more likely to require column reinforcement. Note that this result does not consider the effect of the SCWB requirement limiting the possible combinations. These results also indicated that large columns are generally needed, regardless of girder size, if an unreinforced panel zone is desired. For example, the smallest unreinforced grade 50 column section possible in combination with grade 50 W24x68 girders (the lightest girder section considered) was a W14x257. Similarly, a W14x211, grade 65 column was needed for W24x68 girders if the panel zone was to be unreinforced.

Required Doubler Plate Thickness

Regardless of the column yield strength or axial stress assumed in the SCWB check, this portion of the study yielded two general results applicable to all analyses of

required doubler plate thicknesses conducted. First, a majority of the girder-column combinations failed the SCWB check. Of the 1848 seismic combinations considered, over 50% failed this check even when grade 65 column steel was used with grade 50 girders, and no axial load was applied to the columns. At the other extreme, only 12 combinations met the SCWB requirement when grade 50 columns were used and a 40 ksi axial stress was applied.

The second general result was that, of the combinations meeting the SCWB criterion, fewer than half require doubler plates. Put another way, a majority of combinations that would have required doubler plates failed the SCWB check. For example, when a 40 ksi column axial stress was assumed, no configurations that met the SCWB criterion also required doubler plates for either grade of column steel. For grade 50 columns, assuming a column axial stress of 20 ksi (representing an upper bound of typical column loads), only 23 configurations requiring doubler plates also met the SCWB requirement. This number increased to 79 when grade 65 columns were considered. For a 10 ksi axial stress (representing a lower bound of typical column loads), the number of possible combinations requiring doubler plates increased further, but was still only 6.8% and 10.4% of the original 1848 seismic configurations for 50 ksi and 65 ksi columns, respectively. Figures 3.3 and 3.4 further illustrate these results. The figures show the number of combinations that both meet the SCWB condition and require doubler plates, as a function of assumed column axial stress. It is clear from these results that if both panel zone strength and SCWB requirements must be met, the possible choices of girder-to-column combinations requiring doubler plates are limited.

The actual required doubler plate thicknesses determined in this section of the study also revealed a general trend. Considering the analyses that assumed 10 and 20 ksi column axial stresses (i.e., those meant to represent the range of typical axial stresses), maximum required thicknesses above one inch were rare for configurations meeting the SCWB requirement. That is, once required doubler plate thicknesses became much larger than an inch, the combinations began failing the SCWB check.

Panel Zone Web Slenderness

The results of the panel zone web slenderness check indicated that this slenderness limitation would not be a controlling factor in any potential test specimens. While combinations of W14x90 and W14x99 columns with the W30 and larger girders often failed this check, these combinations also always failed the SCWB check. Furthermore, for potential combinations meeting the SCWB check, the value of $(d_z+w_z)/t_w$ was generally significantly less than the maximum allowable value of 90. In no case was this value greater than 73.

Panel Zone Doubler Plate Slenderness

The results of this second slenderness check indicated that, based on minimum required doubler plate thicknesses, the doubler plate slenderness limitation often controlled. Thus, the minimum doubler plate thickness of many potential test configurations was governed by this slenderness criterion.

To illustrate, in the case of grade 50 columns and a 10 ksi column axial stress, over 50% of those specimens both needing doubler plates and meeting the SCWB requirement failed this slenderness check. For grade 65 columns and a 10 ksi axial stress, this percentage dropped slightly below 50%. For both column grades, when a 20 ksi column axial stress was assumed, a large majority of specimens that both required doubler plates and met the SCWB check also failed the slenderness check.

Panel Zone Aspect Ratio

Results from the study of this parameter indicated that there is not a large amount of variability in the panel zone aspect ratio when the typical seismic configurations are considered. The range of aspect ratios calculated was 1.79 to 2.71. Previous analysis and testing has included aspect ratios ranging from approximately 1.0 (Krawinkler et al., 1971; Bertero et al., 1973; Popov et al., 1986) to approximately 2.7 (SAC, 1996; El-Tawil et al., 1998, Stojadinovic et al., 2000; Ricles et al., 2000). Using the testing equipment discussed in Section 3.2, the range of aspect ratios that can be tested becomes 1.79 to 2.25.

3.1.3 Conclusions

The major conclusions drawn from the results of the parametric study are summarized below:

- For seismic design, requiring that the SCWB criterion be met significantly limited the number of potential girder-column test specimen combinations. A majority of girder-column combinations failed the SCWB check even considering grade 65 columns with grade 50 girders and no column axial stress.
- Large columns are generally needed if an unreinforced panel zone is desired. Of all interior seismic combinations considered, the smallest column section needing no reinforcement was a W14x211. This assumed a grade 65 column, and W24x68 grade 50 girders.
- Most of the seismic girder-column configurations that required doubler plates failed the SCWB check. That is, of the combinations meeting the SCWB requirement, a majority required no doubler plates.
- Very thick doubler plates were rarely needed for those configurations that met the SCWB requirement. For typical column axial loads of 10 to 20 ksi, the computed total required thickness of doubler plates was rarely above 1.0 inches.
- The panel zone slenderness criterion, when applied to column webs, never controlled seismic girder-column configurations when the SCWB check was also applied.
- Of the configurations that both met the SCWB requirement and required doubler plates, many failed the panel zone slenderness limit. Thus, the minimum thickness of many doubler plates was controlled by this slenderness provision.
- The range of panel zone aspect ratios was relatively small, considering the seismic girder-column combinations. The values of the aspect ratios were large, however, when compared to a number of connections tested prior to the Northridge earthquake.

3.2 Specimen Selection

3.2.1 Cruciform Specimen Selection Procedure

As the entire range of W-section girder-column combinations includes over 40,000 possibilities, rational selection criteria were needed to limit the number of potential cruciform test configurations. A number of such criteria were applied to the range of possibilities, progressively narrowing the list of potential tests. These criteria fell into six general categories:

- Commonly used girder and column sizes
- SCWB condition
- Testing equipment capacity
- Recently tested sizes
- Width-thickness ratios
- Analysis of relevant parameters

The first five categories were used to eliminate a majority of the possible specimen configurations. The final category was then employed to rationally select potential combinations that could be used both to verify the panel zone design equations over a range of parameters and to test a variety of doubler plate and continuity plate details. A description follows of the above criteria and the resulting list of configurations.

Commonly Used Girder and Column Sizes

Generally, for seismic moment frame design, columns of W14 nominal size and girders of W24 to W36 nominal size are used. The columns considered in this category included W14x90 and larger. All combinations not within the above size range were thus eliminated from consideration as specimens. Thus, the study of deep column sections was not addressed in this research. The column and girder sizes were further limited by considering only sizes that are commonly made in the United States. This eliminated seven of the heaviest W14 column sizes. These two restrictions resulted in a list of 17

possible columns and 76 possible girders. The remaining selection criteria discussed below are limited to these seismic moment frame combinations.

SCWB Condition

As the experimental investigation is directed primarily at seismic moment frame detailing, and most moment frames in regions of high seismicity are either SMF or IMF [requiring the strong column-weak beam condition to be met as per the 1997 AISC Seismic Provisions (AISC, 1997)], a SCWB check was the next selection criterion applied to the list of potential combinations. This was described in the parametric study discussed previously in Section 3.1. Depending on the assumed column axial stress (0, 10, 20, or 40 ksi) and the column yield strength, the number of specimens eliminated by this check varied widely, but was always over 50% of the seismic moment frame combinations. An axial stress of 10 ksi was used as the standard for this selection criterion, representing an approximate lower bound of typical column axial loads.

The SCWB condition was not considered an absolute requirement, however. As discussed in the parametric study, some non-seismic detailing will be tested, including specimens not meeting the SCWB requirement. This served primarily to narrow the list to likely seismic girder-column combinations, from which the majority of the test specimens were selected.

Testing Equipment Capacity

The specimen configuration (discussed further in Section 3.3) consists of 11-foot girders attached to a 14.25-foot column section. The girder size and length is determined by the bolt hole locations in the floor, the actuator capacities, and the required girder rotations. Two 77-kip actuators are used on each girder, for a total capacity of 154 kips per girder. These actuators have a maximum stroke of plus or minus six inches. This results in a maximum moment of 1694 kip-feet and a maximum total rotation of 0.043 radians. This total rotation exceeds an interstory drift of 4.0%, required to qualify a connection as per FEMA design guidelines (FEMA, 2000a).

Using the maximum moment from an 11-foot girder length (1694 kip-feet), and an assumed stress of 60 ksi to account for strain hardening, an allowable plastic section modulus of 339 in^3 was calculated. This eliminated all W36 and W33 nominal depth girders, and limited the size of W30 sections to a W30x99. The heaviest W27 and W24 sections that could be tested were W27x102 and W24x117, respectively. This significantly reduced the number of girders that could be tested. Of the original 76 girder sizes in the W24 to W36 nominal size range, ten met the plastic section modulus requirement.

Recently Tested Sizes

A goal was established of using sections tested recently as a part of the SAC Steel Project or related research activities. This was done with the belief that it may help determine the reliability of post-Northridge connection designs while requiring limited extrapolations of results when comparing to previous testing. The list of most commonly tested sizes includes the following columns and girders: W14x120, W14x145, W14x176, W14x211, W14x257, W14x311, W14x398, W24x68, W27x94, W30x99, and W36x150 (SAC, 1996; Kaufmann et al., 1996; Xue et al., 1996; Leon et al., 1998; Dexter and Melendrez, 2000; Stojadinovic et al., 2000; Ricles et al., 2000).

Width-Thickness Ratios

While re-evaluation of the provisions for limiting width-thickness ratios, *b/t* and *h/t*, is beyond the scope of this project, consideration was given to these limiting values given by the AISC Seismic Provisions for SMF and IMF applications (AISC, 1997) when selecting specimens. The current limit on *b/t* for flanges in flexure of $52/\sqrt{F_y}$ yields a value of 8.7 for A36 steel, 7.4 for grade 50 steel, and 6.4 for grade 65 steel. These values are lower than the *b/t* values often used for the girders used in several previous relevant test results. Krawinkler et al. (1971) noted severe local flange buckling in A36 girders with a *b/t* of 15.4. The subsequent testing by Bertero et al. (1973) reduced the *b/t* ratios to 11.7 and 10.3 and noted much improved behavior through significant inelastic rotations. With the increasing use of higher strength steels, meeting the current *b/t* limits

becomes more difficult. This is especially true when grade 65 columns are considered. In this case, all W14 columns smaller than a W14x176 fail the *b/t* requirement. However, a relaxation of the current seismic limit on *b/t* of $52/\sqrt{F_y}$ to the non-seismic value of $65/\sqrt{F_y}$ is being considered (Iwankiw, 1999). At a minimum, all cruciform specimens were required to meet the non-seismic criteria of $65/\sqrt{F_y}$.

The limits on *h/t* imposed by AISC (1997) for seismic applications are much less restrictive, considering the typical seismic moment frame girders. If axial load is neglected in the girders, *h/t* is limited to 74 for grade 50 steel, based on the requirement that $h/t \leq 520/\sqrt{F_y}$ (AISC, 1997). The maximum *h/t* value of all typical girders considered was 54.5 (W33x118), and none of the W14 column sections considered approached this limit. Thus, the *h/t* limitation was not a governing factor in the cruciform specimen selection.

Analysis of Relevant Parameters

Both to verify the panel zone design equations and test new continuity plate and doubler plate details, a number of specimen parameters were considered. These included:

- Column flange thickness, t_{cf}
- Girder depth, d_g
- Post-elastic panel zone strength factor, $\left(\frac{3b_{cf}t_{cf}^2}{d_g d_c t_p}\right)$
- Column yield strength, F_{yc}
- Doubler plate effectiveness and detailing
- Axial load, P_u/P_y
- Panel zone demand, R_u
- Panel zone aspect ratio, d_z/w_z
- Panel zone slenderness parameter, $(d_z + w_z)/t$
- Column web thickness, t_{cw}
- Girder flange area, A_{gf}

- Continuity plate details (thickness and welding)

These parameters were used to find reasonable combinations of the remaining column and girder sections not eliminated by the other selection criteria. The first nine parameters relate primarily to the panel zone strength and buckling criteria. The remaining three relate to transverse stiffener design and have been discussed in detail by Prochnow et al. (2000a). They are discussed in Section 3.2.2 however, as they relate to the five cruciform tests. With only five specimens, not all parameters can be given detailed consideration without introducing too many variables in each test. A discussion, justification, and plan of investigation of each parameter to be tested are presented below. For those variables not included in the final test matrix, a justification is given.

- *Column Flange Thickness*

The contribution of panel zone boundary elements, namely the column flanges, to panel zone shear resistance has been recognized for over 30 years. Fielding and Huang (1971), Krawinkler et al. (1971), and Bertero et al. (1973) developed various models of panel zone shear behavior that incorporated the contributions of boundary elements into the inelastic range. One of the models proposed by Krawinkler et al. (1971) would eventually be used to formulate the panel zone shear strength equation that is used presently (Krawinkler, 1978). The post-elastic term in this panel zone shear strength equation is directly proportional to the square of the column flange thickness. Thus, the recognized post-yield strength of the panel zone is influenced most by the thickness of the column flange.

The experimental work behind the development of the panel zone strength provision involved specimens with column flange thicknesses of 0.40 inches (W8x24) and 0.935 inches (W8x67) (Krawinkler et al., 1971; Bertero et al., 1973). The larger thickness of 0.935 inches corresponds today with what would be considered a thin column flange for use in moment frame construction (roughly corresponding to the flange thickness of a W14x120). More typical column sections used presently have flange thicknesses of one to three inches or greater. In the concluding remarks of one

experimental report (Bertero et al., 1973), the reader is cautioned that careful extrapolation of the data must be made to cases of thick column flanges, and in the derivation of the current panel zone strength equation, Krawinkler (1978) encouraged further research into the verification of the provision for use with very thick column flanges.

Since 1978, a number of additional experimental investigations involving panel zone behavior have been conducted, but the tested column flange thicknesses remained relatively small until the most recent experiments following the Northridge earthquake. Popov et al. (1986) tested half-scale flange thicknesses of 0.625 and 1.25 inches, noting that they were relatively thin, but no comparisons to panel zone strength provisions were made. The investigators further speculated that the column stiffening requirements (continuity plates and doubler plates) would be reduced if thicker column flanges were used. Lee and Lu (1989) tested composite joint subassemblages with column flange thicknesses of 0.67 and 0.68 inches, and found reasonable agreement with the panel zone strength predictions developed by Krawinkler (1978). In fact, panel zone strength was significantly underestimated during positive bending due to the effects of the concrete slabs. Ghobarah et al. (1992) tested extended bolted end-plate joints with column flange thicknesses of 0.53 and 0.81 inches. The results indicated that predicted panel zone strengths were underestimated by 17-40%, due primarily to effects of the end-plates in the post-elastic range. Tsai et al. (1995) conducted full-scale tests using columns with a flange thickness of 1.19 inches and noted that the current provisions satisfactorily predict the post-yield strength of panel zones, but also suggested the adoption of simpler, more conservative strength and demand calculation procedures.

Phases 1 and 2 of the SAC program (SAC, 1996; Choi et al., 2000; Stojadinovic et al., 2000; Ricles et al., 2000; FEMA, 2000b) conducted tests with columns representative of those used in new construction. Column flange thicknesses from 0.94 to 2.845 inches were tested in these investigations. A general consensus of these investigations was that the panel zone design requirements prior to Northridge [e.g., UBC (1988) and AISC (1992)] needed re-evaluation. In other words, the panel zones of many experiments were considered weak in comparison to the girders. As noted in Chapter 2,

Ricles et al. (2000) recommended designing panel zones using only the column web contribution, neglecting the effects of the column flanges.

Recent analytical work by El-Tawil et al. (1998, 1999) focused on parameters affecting panel zone behavior. The three-dimensional, nonlinear, finite element analyses were performed on full-scale girder-to-column configurations, representative of member sizes typically used today. One variable was the column flange thickness, which was varied between 1.3 and 3.2 inches, while holding the girder to panel zone strength ratio essentially constant. The results indicated that, while the panel zone provisions accurately predicted the shear strength for most specimens, strength was slightly underestimated in the specimen with the thickest column flange.

The cruciform specimen test matrix attempts to further investigate the effects of column flange thickness on panel zone strength by incorporating a range of flange thicknesses.

- *Girder Depth*

While girder depth is only encountered in the panel zone strength provision as a variable in the denominator of the post-elastic term, it is still an important parameter in the design of panel zones and connections in general. In a study of past experiments by Roeder and Foutch (1996), it was shown that the flexural ductility ratio (FDR) of girders decreased significantly as the depths of the members increased. This can be partly explained by the finite element results from El-Tawil et al. (1998). As the girder depths were increased in their analyses, significantly larger inelastic strains were observed at plastic rotations of 0.03 radians. This indicated the potential for reduced ductility and low-cycle fatigue in those joints with the deepest girders.

Girder depth is also an important parameter when specifically considering panel zone strength and design. For those tests with significant panel zone yielding, Roeder and Foutch's results (1996) showed the same trend of reduced FDRs with increasing depth; however, the FDRs as a whole were much lower than those tests without significant panel zone deformation. This is important when considering that the depths of girders used in the experiments that formed the basis for the current panel zone

provisions (Krawinkler et al., 1971; Bertero et al., 1973) were small in comparison to common member sizes used today. In that work, W10, W12 and W14 nominal depth sections were tested, including W10x15, W10x29, W12x27, and W14x22 girders.

In fact, little full-scale testing related to panel zones occurred before 1994. Popov et al. (1986) conducted half-scale testing on 18- and 21-inch nominal depth girder and column sections, representing the largest cyclic tests of their kind at the time. Full-scale tests by Lee and Lu (1989) were conducted, but relatively small W18x35 girders were used, and experiments conducted by Ghobarah et al. (1992) tested 14- and 16-inch nominal depth girders. It was not until after the Northridge earthquake that full-scale tests, representative of member sizes currently used, became the norm. Tsai et al. (1995) tested W21 girders, ranging in size from 50 to 101 lb/ft, and W24, W30, and W36 girders have been tested as a part of the SAC experimental work (SAC, 1996; Choi et al., 2000; Stojadinovic et al., 2000; Ricles et al., 2000; FEMA, 2000b).

While the cruciform tests in the current research program represent realistic connection configurations presently used, girder depth was not varied. The range of depths possible taking testing equipment into consideration was not considered sufficient to warrant inclusion as a main parameter.

- *Post-Elastic Panel Zone Strength Factor*

The post-elastic term in the panel zone strength provisions (AISC, 1997) is given as:

$$\left(\frac{3 b_{cf} t_{cf}^2}{d_g d_c t_p} \right) \tag{3.12}$$

While the post-elastic strength of the panel zone is influenced most directly by the column flange thickness, this term takes into account more fully the contributions of the boundary elements than does t_{cf}^2 alone. This expression was developed by Krawinkler (1978) as a result of the panel zone behavior observed in earlier testing by Krawinkler et al. (1971) and Bertero et al. (1973), and was based on a finite element analysis of a joint by Krawinkler et al. (1971). Just as the results from El-Tawil et al. (1998, 1999) served to verify the panel zone strength provision for most cases, so too did they indirectly serve

to verify this post-elastic strength term. A similar argument can be made with respect to other tests that have investigated the panel zone strength equation (Lee and Lu, 1989; Ghobarah, et al., 1992).

An analysis of the post-elastic term revealed that values on the order of 0.10 to 0.40 are typical for common moment frame configurations. Thus, the post-elastic contribution to total panel zone strength is on the order of 10% to 40% of the elastic strength in most cases.

Because a range of column flange thicknesses was incorporated into the cruciform test matrix, the post-elastic strength factor is also varied in the current research program.

- *Column Yield Strength*

All current panel zone provisions were developed at a time when A36 steel was used almost exclusively as the structural framing material. Currently, A36 steel is being phased out for use in rolled wide-flange shapes, and what is still available generally has yield strengths similar to the grade 50 steels. While a trend towards grade 65 columns (e.g., A913 steel) will likely be seen, the current test program is limited to grade 50 (A992) column and girder sections.

- *Doubler Plate Effectiveness and Detailing*

There are two aspects of doubler plate effectiveness that must be considered as they relate to panel zone design. The first is concerned with the capacity of doubler plates to carry their proportionate share of the total shear demand. This is especially relevant for the case of Figure C-9.3 (c) now given in the commentary to the 1997 AISC Seismic Provisions (AISC, 1997). This detail consists of two doubler plates placed symmetrically at some distance from the column web, forming a box-type section. A similar detail has been investigated by Bertero et al. (1973), and found to be less than fully effective. In fact, the concept of an effectiveness factor was proposed for this detail, but not developed. Rather, further experimental study was suggested.

Other previous studies investigating doubler plate effectiveness have focused on configurations with doubler plates welded directly to the column webs. Results from

Becker (1975) indicated that the doubler plates were not fully effective until strains became high, after which the doubler plates did carry their share of the shear. The results from Ghobarah et al. (1992) showed the doubler plates to essentially be fully effective, as did additional results from Bertero et al. (1973) for doubler plates welded directly to the column web. Thus, there has been a general consensus that doubler plates, when welded to the column web, can be treated as fully effective in design.

The second aspect of doubler plate effectiveness is one of the relative strength between the column and doubler plate steels. Since doubler plates fabricated from modern, higher strength steels are uncommon, there will potentially be a discrepancy between the yield strength of the columns and the yield strength of the doubler plates. To meet strong column-weak beam requirements, columns may increasingly be fabricated with grade 65 steels, whereas plate material is most commonly specified grade 36 or 50. This raises a question of how to accurately determine required doubler plate thicknesses. Any required thickness determined from the current AISC panel zone strength equation (AISC, 1997) implicitly requires the same grade of steel as the column. It is unclear if scaling this calculated thickness by a ratio of the column to doubler plate yield strength is sufficient.

This issue of unequal yield strengths is beyond the scope of the present investigation. As all columns selected were A992, both column and stiffener detailing material are grade 50. The box detail, however, was included in the test matrix.

In addition to the box detail of Figure C-9.3 (c) in the Seismic Provisions (AISC, 1997), additional permitted doubler plate details are given, including fillet-welded and groove-welded configurations. As most recent tests have either omitted doubler plates or used the groove-welded detail, investigation into the fillet-welded detail is necessary. Thus, fillet-welded doubler plates were included in the present test matrix.

- *Column Axial Loads*

A wide range of column axial loads has been used in previous connection experiments. At one extreme, Peters and Driscoll (1968) performed tests with the axial compressive loads of P/P_y between 0.6 and 0.8. At the other extreme, most recent tests

have either used no axial load (e.g., Tsai et al., 1995; SAC, 1996, Stojadinovic et al., 2000; Ricles et al., 2000) or even placed the columns in tension (Leon et al., 1998). Most other past experiments, however, have used more typical axial loads of P/P_y between 0.1 and 0.5 (Fielding and Huang, 1971; Krawinkler et al., 1971; Bertero et al., 1973; Popov et al., 1986; Ghobarah et al., 1992; Schneider et al., 1993).

The question then arises whether axial loads would affect the results of the cruciform tests. Clearly, when P/P_y is as large as 0.8, axial-shear interaction is significant. This interaction becomes small, however, when P/P_y is reduced to a more typical 0.1 to 0.5 range. AISC only requires interaction be considered in the design of panel zones when P/P_y is greater than or equal to 0.75 (AISC, 1993, 1999a, 1997), implying minimal interaction effects below this level.

While the presence of axial load more closely replicates true conditions, the present experimental study does not involve the application of any column axial loads. Based on equipment capacity, axial loads, P/P_y, equal to 0.2 or less could be applied. The resulting axial stresses would be small in comparison to the triaxial stresses generated in the highly restrained regions of the connections, and consequently would not influence results to a measurable degree (Hajjar et al., 1998a). Furthermore, because recent SAC testing has also neglected axial loading, the results of the present tests are more directly comparable to this other ongoing research.

- *Panel Zone Demand*

The method used to calculate the shear demand on the panel zone can affect whether or not column flange kinking becomes a potential contributor to failure. This phenomenon of localized kinking of the column flanges at the level of the girder flanges has been seen experimentally (Krawinkler et al., 1971; Popov et al., 1986; Choi et al., 2000), reproduced computationally (El-Tawil et al., 1998; Ye et al., 2000), and has been speculated as a potential contributor to the failures in some tests following Northridge (SAC, 1996; Choi et al., 2000). It is caused by a panel zone, which is weak in comparison to the connected elements. Thus, it is an issue of relative strength. If the

method used to calculate panel zone demand underestimates the actual force delivered during a seismic event, the panel zone will be weak relative to the girders and columns.

As presented in Chapter 2, the method of calculating panel zone shear demand has changed numerous times since the current strength equation was adopted by SEAOC in 1988. Initially, demand was based on a working load combination of dead and live load plus 1.85 times the seismic forces (SEAOC, 1988; UBC, 1988). A demand cap of 80% of the plastic moment capacities of the connected girders was also specified. The FEMA Interim Guidelines (1995a) were initially similar to the UBC in their demand calculation procedure. However, the first advisory to these guidelines (FEMA, 1997a) removed the load combination from the calculation procedure. The former demand cap of 80% of the plastic moment capacity at the column face became the sole basis for shear demand calculation. The AISC Seismic Provisions (AISC, 1997) used factored load combinations with additional amplification of the earthquake loads. The intent was to provide similar reliability to the UBC provisions (AISC, 1997). A demand cap is also specified, based, in this case, on 80% of the expected girder plastic moment capacities, taking material overstrength and strain hardening into account. Supplement No. 1 to the AISC Seismic Provisions (AISC, 1999b) removed the load combinations, and Supplement No. 2 (AISC, 2001) changed the 80% factor on the expected girder plastic moment capacity to 100%.

It has been argued that basing required panel zone strength on a specified percentage of the girder plastic capacities is more logical than the use of load combinations when considering seismic design. From observations of the undesirable behavior of panel zones designed for working stresses, Krawinkler et al. (1971) concluded that structural elements must be designed relative to the other components, and weak links must be avoided. The assumption in seismic design of moment frames is that the girders will yield under the forces delivered by the design earthquake. Assuming the girders yield, then, it is logical to define ultimate panel zone strength relative to a fully plastic girder cross section instead of a comparatively arbitrary load combination.

The current research program does not include panel zone demand as a primary variable, as this would require specimens representing several different panel zone

strengths. Instead, as described in Section 3.2.2.1, the panel zones are designed with similar strengths such that the design deformation of $4\gamma_y$ recommended by Krawinkler (1978) is exceeded. For comparative purposes, however, the current research program calculates shear demand based on girder plastic moment capacities, and not load combinations. In other words, when comparing the relative strengths of the panel zones, (e.g., $\phi_v R_v / R_u$), the demand, R_u, is based on girder plastic capacity, consistent with AISC Supplement No. 2 (2001).

- *Panel Zone Aspect Ratio*

The derivation of the panel zone strength equation assumed that the panel zone deformed in pure shear (Krawinkler, 1978). Previous experimental and computational results, however, have shown that this is not generally a good assumption when the aspect ratio is high. Results presented by Krawinkler et al. (1971) and Bertero et al. (1973) showed large bending deformations of the panel zones tested with aspect ratios (depth to width) of approximately two. The finite element study by El-Tawil et al. (1998, 1999) showed significant reverse curvature bending in tests with large aspect ratios and high shear to bending stiffness (i.e., thick panel zones). A finite element analysis by Tsai and Popov (1988), however, showed that pure shear deformation was a reasonable assumption for aspect ratios near 1.0.

From the early 1970's until the 1994 Northridge earthquake, most of the investigations conducted to investigate panel zones have tested relatively low aspect ratios. The specimens tested by Popov et al. (1986) had aspect ratios of near 1.0, tests by Lee and Lu (1989) had aspect ratios of approximately 1.5 to 1.9, tests by Ghobarah et al. (1992) had aspect ratios of approximately 1.0 to 1.3, and specimens tested by Tsai et al. (1995) had aspect ratios of approximately 1.6. Much higher aspect ratios have been tested during the SAC program, however, ranging from approximately 1.8 to 2.7 (SAC, 1996; Leon et al., 1998; Choi et al., 2000; Stojadinovic et al., 2000; Ricles et al., 2000).

The fact that the observed deformations, in cases of large aspect ratios, were not in pure shear does not necessarily invalidate the panel zone strength provision. Results from El-Tawil et al. (1998, 1999) indicated that the strength provision was generally accurate over the range of parameters tested, including girder depth, column flange

thickness, and column web thickness. By changing the girder depth, the aspect ratio was varied, and by changing the column web thickness, the ratio of shear to bending stiffness was varied. Among these parameters, panel zone strength was only overestimated when the column web or column flange was very thick. The authors did suggest, however, that provisions for panel zones recognizing axial-shear-bending interaction may be warranted.

Because girder depth is not included as a parameter in the test matrix, the panel zone aspect ratio is held constant, and is similar to others tested in the SAC program.

- *Panel Zone Slenderness Parameter*

The current limitation placed on column web and doubler plate slenderness (AISC, 1997) is given by an empirical equation, yet relates to shear buckling:

$$t \geq \left(d_z + w_z\right)/90 \tag{3.9}$$

As discussed in Chapter 2, this expression was most likely developed by Teal in the early 1980's as a part of a SEAOC committee (Popov, 1999), and is likely based on test results from Krawinkler et al. (1971) and Bertero et al. (1973). No written record of its development has been uncovered, however. The provision is intended to ensure that, if a web or doubler plate meeting the requirement buckles, no loss of strength will occur under cyclic loading. Some of the column webs and doubler plates tested (Krawinkler et al. 1971; Bertero et al., 1973) did, in fact, buckle at large panel zone deformations. The value of 90 in the equation is apparently a liberalization of the tested web and doubler plate slendernesses (the tested thicknesses were approximately equal to $(d_z + w_z)/68$). A literature review uncovered no previous experiments that based doubler plate thicknesses on the minimum allowed by Equation (3.9). Thus, while the provision is empirical, it is clearly not overly conservative. However, no recent testing has addressed the provision.

An alternative to the slenderness provision given by Equation (3.9) could specifically incorporate shear buckling theory. One such possibility is the slenderness limitation given in the AISC LRFD Specifications (1993, 1999a) for stiffened members in shear. To avoid shear buckling, the following is required:

$$\frac{h}{t_w} \le 187\sqrt{\frac{k_v}{F_y}} \tag{3.13}$$

where:

$k_v = 5 + 5/(a/h)^2$ = shear buckling coefficient

h = clear distance between flanges less the fillet distances

t_w = web thickness

F_y = yield strength of steel

a = distance between stiffeners

Using the notation in the Seismic Provisions (AISC, 1997), h is approximately equal to w_z, a is equal to d_z, t_w becomes t (i.e., either the web or doubler plate thickness), and F_y is the column yield strength, F_{yc}. Using these substitutions and solving Equation (3.13) for the thickness, t, yields a slenderness provision based on AISC shear buckling criteria:

$$t \ge \frac{\sqrt{F_{yc}}}{418}\frac{d_z w_z}{\sqrt{d_z^2 + w_z^2}} \tag{3.14}$$

An analysis of the thicknesses given by Equation (3.14) revealed that required thicknesses were on the order of one-third to one-half those required by Equation (3.9), the current provision. Values given by Equation (3.14) for the common seismic girder-column combinations were always less than 0.25 inches. If it is again assumed that Equation (3.9) is not overly conservative, the limitation given by Equation (3.14) would clearly be unconservative for seismic design. Obviously, not all assumptions used in the development of Equation (3.13) are met when applied to panel zones, specifically doubler plates.

In summary, the slenderness provision given by AISC (1997) is investigated to some extent by the current research program. An alternative provision based on shear buckling would be more desirable, but current AISC LRFD (1993, 1999a) buckling equations do not appear to be appropriate.

3.2.2 Specimen Justification

Based on the above selection criteria and test parameters, the five cruciform specimens were selected. The test matrix is outlined in Table 3.1. Doubler plate details Fillet I and Fillet II represent the two fillet-welded details tested in this research program. Detail I is similar to the fillet-welded doubler plate detail given in Figure C-9.3 (b) of the AISC Seismic Provisions (AISC, 1997). Detail II is a fillet-welded detail developed as a part of the present research program. The box doubler detail is similar to that shown in Figure C-9.3 (c) of the Seismic Provisions. Figure 3.5 schematically illustrates the three doubler plate details. The design and detailing of these stiffening details are presented in Section 3.3.3. The continuity plate detail of Specimen CR3 is representative of transverse stiffeners used prior to the Northridge earthquake. The plate thickness is approximately equal to half the beam flange thickness, and fillet welds are used to connect the stiffeners to both the column flanges and web (or doubler plates). This detail has been shown to perform satisfactorily in recent monotonically loaded pull-plate tests (Prochnow et al., 2000a), and finite element analyses (Ye et al., 2000).

3.2.2.1 Specimen Parameter Discussion

- *Column Flange Thickness*

The four column sections represented by the five specimens exhibit a range of typical column flange thicknesses encountered in design. The section with the thinnest flange, a W14x145 (t_{cf} = 1.09 inches) is slightly larger than the thickest flange tested by Krawinkler et al. (1971) and Bertero et al. (1973) and would be used in relatively small moment frame connections. The largest section, a W14x283 (t_{cf} = 2.07 inches) represents a moderately thick flange, which will significantly increase the recognized post-elastic strength of the panel zone. While none of the column flanges are as thick as the 3.2 inch maximum thickness analyzed by El-Tawil et al. (1998, 1999), the range represented by the specimens is comparable to that tested in the SAC program (SAC, 1996; Leon et al., 1998; Choi et al., 2000; Stojadinovic et al., 2000; Ricles et al., 2000), and is sufficient to evaluate the panel zone strength provision for thin to moderately thick column flanges.

- *Girder Depth*

While girder depth is recognized as a parameter significantly contributing to the behavior of panel zones and connections in general (Roeder and Foutch, 1996; El-Tawil et al., 1998), it is not varied in the present test matrix. The single girder size of W24x94 was selected because it can deliver a larger flange force than other sections considered without exceeding the capacity of the available actuators.

- *Post-Elastic Panel Zone Strength Factor*

A range of post-elastic strength contributions is represented by the test specimens. This value ranges from under 10% for the thinnest column flanges to almost 40% for the unreinforced W14x283 specimen. The specimens are intended to help evaluate the reliability of the post-elastic panel zone strength contribution.

- *Doubler Plate Effectiveness*

Four of the five specimens include doubler plates, including three different details that will allow the evaluation of doubler plate effectiveness, in addition to verifying the suitability of the particular detailing. One specimen includes the box-type doubler plate configuration detail given by Figure C-9.3 (c) in the 1997 AISC Seismic Provisions (AISC, 1997), and three utilize doubler plates fillet welded to the column flange. While the effectiveness of doubler plates with a lower strength than the column is not investigated, effectiveness as it relates to the doubler plate detailing is a key parameter in the test matrix.

- *Panel Zone Demand*

The general philosophy of panel zone design for the test specimens (discussed in detail in Section 3.3.3.1) is based on testing stiffening details beyond expected levels of deformation. Thus, most specimens include weak panel zones [i.e., they do not meet the requirements of AISC (1997) or FEMA (2000a)]. However, the column web and doubler plate thicknesses were selected to ensure the panel zones exceed the design deformation of $4\gamma_y$ from Krawinkler (1978), and inherent in the AISC design provisions. Finite

element analyses by Ye et al. (2000) verified that deformations beyond this level should be reached in the tests. This design methodology also allows for further investigation of the present strength provisions and the effects of column flange kinking on connection performance. The strengths of the panel zones are quantified in Section 3.3.3.1 by comparing the relative strengths of the girders and panel zones.

- *Panel Zone Aspect Ratio*

Because the girder depth is not varied in the present research program, and column depth does not vary significantly, the aspect ratio is held constant. However, the W24 depth selected for the cruciform tests results in an aspect ratio of approximately 1.8, which is similar to many other recent tests. The specimens are intended to provide additional panel zone data for connections with realistic aspect ratios and varying shear to bending stiffness (i.e., a range of panel zone thicknesses). The effect of the expected deformation patterns of such panel zones on the performance and behavior of the welded moment connections will be studied.

- *Panel Zone Slenderness Parameter*

The present investigation includes testing of doubler plates with slenderness values approximately equivalent to those tested by Krawinkler et al. (1971) and Bertero et al. (1973), but none at the limiting value. The half-inch doubler plates of Specimen CR3 have a $(d_z + w_z)/t_{dp}$ value of 71, roughly equivalent to the value of 68 previously tested by Bertero et al. (1973). This specimen will help to confirm the validity of the slenderness provision. Testing of doubler plates with a $(d_z + w_z)/t_{dp}$ value of 90 or greater is desirable, but the plate thicknesses required for this were not compatible with the targeted strength of the panel zones.

- *Width-Thickness Ratios*

The selected columns cover a range of *b/t* values. The W14x145 represents the maximum value of 7.1, while the W14x283 has the minimum value at 3.9. The value of 7.1 for grade 50 steel is near the $52/\sqrt{F_y}$ limit of 7.4 (AISC, 1997). The single girder size

of W24x94 represents a *b/t* of 5.2. This section was chosen for its stockier flange (relative to the W30x99 and other sizes recently tested by the SAC program) to maximize the flange force delivered to the connection by delaying local buckling.

- *Column Web Thickness*

The test matrix represents a range of column web thicknesses between 0.68 inches (W14x145) and 1.29 inches (W14x283). When doubler plates are considered (as when evaluating the resistance to PZ yielding and LWY), the range of web thicknesses becomes the range of total panel zone thickness, t_p, of 1.29-2.33 inches. These ranges of thickness are significantly larger than those used to develop the current provisions for column stiffening (Sherbourne and Jensen, 1957; Graham et al., 1960; Krawinkler et al., 1971), and represent realistic values seen in current moment frame construction.

- *Girder Flange Area*

As with the recent pull-plate experiments (Prochnow et al., 2000a), a single girder size was selected, and girder flange area was not varied as a result. The girder section, a W24x94 (A_{gf} = 7.93 in^2), was chosen to deliver a large flange force without exceeding equipment capacity. The moderately thick flange of 0.875 in. (*b/t* = 5.2) was intended to ensure that early local buckling does not reduce the demand on the panel zone.

- *Continuity Plate Details*

To corroborate and extend the results from Prochnow et al. (2000a), a fillet-welded, half-thickness continuity plate detail is included in the test matrix. This detail was typically used prior to the Northridge earthquake, but has not been allowed subsequently (AISC, 1997; FEMA, 2000a). Some recent testing (Ricles et al., 2000) has addressed whether or not continuity plates are needed in all connections, but the issue of an appropriate thickness has not been thoroughly tested. Some recent finite element work, however, has been performed to investigate thickness and welding requirements (El-Tawil et al., 1998; Yee et al., 1998; Ye et al., 2000). These indicated that thinner, fillet-welded continuity plates may be adequate.

3.2.2.2 Individual Specimen Discussion

Discussed below are the key aspects of the five specimens, focusing on the details of the column stiffening, and the limit states targeted in each test. Table 3.2 presents the strength-to-demand ratios for the PZ yielding, LFB, and LWY limit states using various methods of demand calculation. Panel zone strengths are based on the AISC Seismic Provisions (1997, 2001), while LFB and LWY strengths are based on AISC LRFD Specifications (1993, 1999a).

SPECIMEN CR1

Girders: W24x94

Column: W14x283

Doubler Plates: None

Continuity Plates: None

Specimen CR1 represents a moderately large, unreinforced interior connection with a relatively weak panel zone. It is intended primarily to study the panel zone strength provision for thick column flanges. The relatively thick column flange of 2.07 inches coupled with the unreinforced panel zone results in a post-elastic strength contribution of approximately 40%, representing a high, yet typical value. This specimen meets the SCWB check as defined for this study at a column axial load of 20 ksi. No continuity plates are needed as per the 1992 AISC Seismic Provisions (AISC, 1992) and FEMA design guidelines (FEMA, 2000a) (i.e., Equations 2.9, 2.15 and 2.16). Specimen CR1 is also intended to show that continuity plates are not necessarily needed for all seismic applications.

SPECIMEN CR2

Girders: W24x94

Column: W14x193

Doubler Plates: 1 @ 0.625 in.

Continuity Plates: None

Specimen CR2 represents a moderate scale, reinforced interior connection with a single-sided doubler plate. It is intended primarily as a verification of the seismic AISC (1992) LFB criterion (Equations 2.9 and 2.13). This specimen requires continuity plates by calculation, but is on the cusp of needing them ($\phi R_n/R_u$ = 0.82, R_n/R_u = 0.91), and is intended to confirm that continuity plates are not always needed for seismic moment frame applications. A relatively weak panel zone, similar to Specimen CR1, is provided. An innovative fillet welded doubler plate detail is utilized (Detail II), the development of which is presented in Section 3.3.3. The SCWB condition is met for axial stresses up to approximately 5 ksi. The presence of the doubler plate and thinner column flanges reduces the value of the post-elastic panel zone strength contribution, but it is still of a moderate magnitude at approximately 17%. The single-sided doubler plate allows for comparisons in strain distributions between the column web and doubler plate.

SPECIMEN CR3

Girders: W24x94

Column: W14x176

Doubler Plates: 2 @ 0.5 in.

Continuity Plates: 0.5 in. thick, fillet-welded

Specimen CR3 represents a moderate scale, reinforcement with both doubler plates and continuity plates. It is intended primarily as a test of half-thickness, fillet-welded continuity plates. It is also a second test of doubler plate Detail II. This specimen requires continuity plates as per AISC (1992) seismic LFB equations (2.9 and 2.13), and is intended to show the fillet-welded continuity plate detail can perform adequately in cyclic loading applications. The provided panel zone strength is similar to Specimen CR1. The SCWB check is met for an axial load of zero. Because of the thinner column flanges and heavier panel zone reinforcement, the predicted post-elastic strength of the panel zone is reduced to approximately 12%.

SPECIMEN CR4

Girders: W24x94

Column: W14x176

Doubler Plates: 2 @ 0.75 in.

Continuity Plates: None

Specimen CR4 represents a moderate scale connection with innovative, heavy panel zone reinforcement (i.e., a total doubler plate thickness greater than the column web thickness), and no continuity plates in a situation in which they would be required by the 1992 AISC Seismic Provisions (AISC, 1992) (i.e., Equations 2.9 and 2.13). The offset doubler detail is used as the column stiffening of this specimen in order to investigate the feasibility of this detail to resist both panel zone shear and flange bending (by providing restraint to the column flanges). The design of this stiffening detail is presented in Section 3.3.3. Unlike the other specimens, a stronger panel zone is provided – based on the work of Bertero et al. (1973) on a similar stiffening detail – meeting the requirements of both AISC and SAC (Equations 2.1 and 2.7). Like Specimen CR3, this specimen meets the SCWB criterion for no axial load. The thick doubler plates result in a low post-elastic panel zone strength contribution, at just below 10%.

SPECIMEN CR5

Girders: W24x94

Column: W14x145

Doubler Plates: 2 @ 0.625 in.

Continuity Plates: None

Specimen CR5 represents the smallest column section tested (W14x145), with fillet-welded doubler plates and no continuity plates. It is primarily intended to verify the AISC (1993, 1999a) LFB provisions for non-seismic design (Equations 2.9 and 2.12). Also tested is doubler plate Detail I, the beveled fillet-welded design (presented in

Section 3.3.3). This specimen is on the cusp, but requires continuity plates as per the non-seismic design requirements ($\phi R_n/R_u = 0.84$, $R_n/R_u = 0.94$). While tested cyclically, the non-seismic details of this specimen (i.e., lack of continuity plates) are intended to verify the LFB requirements in the LRFD Specification (AISC, 1993, 1999a). The panel zone strength is again similar to Specimen CR1. Because a smaller column was needed to breach the non-seismic LFB limits, Specimen CR5 does not meet the SCWB criterion. A low post-elastic panel zone strength of approximately 8% is expected.

3.3 Specimen Design

As briefly mentioned earlier in this chapter, due to unexpected premature brittle fracture, one of the five originally selected specimens (i.e., Specimen CR4) was replicated with new weld consumables and re-tested. This new specimen was named as Specimen CR4R. This section describes the design of the total of six cruciform specimens, including Specimen CR4R. Specifically addressed are the general dimensions of the specimens, the moment connection design common to all tests, and the design of the panel zones and various stiffening details.

3.3.1 Dimensions of Cruciform Specimens

The cruciform specimens represent an interior moment frame joint from a structure in strong-axis bending (see Figure 3.6). When subjected to lateral loading, such a structure is expected to exhibit reverse curvature bending both in the columns and beams, with inflection points occurring near mid-span of the beams and mid-height of the columns. This assumption is reasonable when gravity loading is small in comparison to the seismic loads. The column inflection points were simulated with load pins at the top and bottom of the columns (discussed further in Chapter 4). The free end of the girders at the point of actuator attachment simulates the girder inflection points.

A typical cruciform specimen is illustrated in Figure 3.7. All wide-flange material was A992. The total length of column between inflection points is 171 inches, measured to the pin centerlines. The girder length, measured from the centerline of the column to the centerline of the actuator attachment, is 140 inches. Thus, the specimens

represent a moment frame structure with a 14.25-foot story height and 23.33-foot column spacing (resulting in an approximate girder clear span of 22 feet for typical W14 columns). The effective length of the girders measured from the face of the column to the point of load application is approximately 132 inches. This value varies slightly depending on column depth, as the 140-inch distance to the actuators is fixed. For the W24x94 girders, this effective length requires approximately 96 kips of load to reach the nominal plastic moment capacity of 12,700 kip-inches.

3.3.2 Girder-to-Column Moment Connection Design

The same moment connection details were used to join the girders to the columns in all specimens. The basic detail is similar to the Welded Unreinforced Flange – Welded Web connection (WUF-W) developed for the SAC program by Ricles et al. (2000) and prequalified for use in OMF and SMF structures (FEMA, 2000a). It is a fully welded connection consisting of complete joint penetration (CJP) welds of the beam flanges and web to the columns. Figure 3.8 illustrates the WUF-W connection recommended by SAC [after (FEMA, 2000a)].

A number of fundamental differences exist between this connection and the standard pre-Northridge moment connection. These differences are discussed in detail in the SAC State-of-the-Art Report on Connection Performance (FEMA, 2000b) and are briefly summarized here. First, improved welding materials and details are used to mitigate the brittle fracture problems seen following Northridge. Higher toughness electrodes (e.g., E70T-6 and E70TG-K2) are used in place of the E70T-4 electrode commonly specified prior to Northridge. Bottom backing bars are removed, and reinforcing fillet welds are placed below the bottom flange welds and top flange backing bars. A fully welded web connection, welding the shear tab to the girder web and the girder web to the column flange, is also required in place of bolted shear tabs. Another major difference in the WUF-W connection is the use of an improved access hole design. While the changes to welding materials and procedures mitigate the brittle fracture problem, low-cycle fatigue may occur in the access hole region if not properly detailed. Testing by Hajjar et al. (1998a) and Stojadinovic et al. (2000) clearly illustrated the

problem of low-cycle fatigue in the access hole region. The access hole design is based on a computational parametric study (Mao et al., 2001) and experimental testing by Ricles et al. (2000).

3.3.2.1 Welded Connection Details

Figure 3.9 illustrates the typical welded connection details used to fabricate the specimens. This connection is essentially the prequalified WUF-W connection discussed above with minor differences, primarily in the attachment and detailing of the shear tab. These differences arose from the fact that the specimens were detailed prior to the publication of the final SAC design recommendations. The connections tested by Ricles et al. (2000) formed the basis for the detailing of the present specimens.

All girder flanges were groove-welded using the self-shielded, flux cored arc welding process (FCAW-s). The bottom backing bars were removed, and the weld roots were backgouged using an air-arc process.

For the first two specimens that were fabricated, Specimens CR1 and CR4, 5/64 in. diameter E70T-6 (Lincoln Innershield NR-305) wire was used. The weld procedures are summarized in Section 3.4.2. This wire and the weld procedures were subsequently found to produce weld metal that did not meet the SAC recommended minimum notch toughness requirements. The SAC guidelines (FEMA, 2000e) recommend that weld metal be used that meets two Charpy V-Notch test requirements: 1) 40 ft-lbs at 70ºF; and 2) 20 ft-lbs at 0ºF. The low temperature requirement is a relaxation of the AWS classification requirements of 20 ft-lbs at –20ºF.

Details of these fractures and the reasons for the low CVN of the weld metal are discussed in Appendix B since they are not related to column reinforcing details. The fact that low notch toughness can be obtained in some consumables that are supposed to have adequate toughness according to their classification is very important and should be investigated further. However, it is the intent of this study to investigate the effect of column stiffening details on the performance of connections that do meet the SAC minimum requirements for weld metal. It would ordinarily be best to purchase the consumables on the market and thereby get weld metal with representative material

properties. However, these tests are expensive to perform and the chance of further low toughness welds could not be tolerated. Therefore, while the consumable manufacturers continue to investigate the reasons for the variation in notch toughness, it was decided to use consumables that were previously characterized by the Edison Welding Institute (EWI) in past SAC research and are known to have good notch toughness for the remaining specimens. This 3/32 in. diameter E70T-6 (Lincoln Innershield NR-305) wire was used for the girder flange-to-column CJP welds in Specimens CR2, CR3, CR4R, and CR5. As noted in Section 3.4.2, different welding equipment was also used for these remaining specimens.

The CJP welds connecting the girder web to the column flange and all reinforcing fillet welds were placed using 0.068 in. diameter E71T-8 (Lincoln Innershield NR-203MP) wire for Specimens CR1 and CR4, and using 5/64 in. diameter E71T-8 (Lincoln Innershield NR-232) wire for the other specimens. Both of these E71T-8 weld wires are notch-tough FCAW-s electrodes capable of all-position welding. These reinforcing welds were placed under the top flange backing bar and below the backgouged region under the bottom flange. The ends of the bottom flange welds were ground to a smooth transition between the beam flanges and column face. Figures 3.10 and 3.11 show typical as-welded flanges.

The shear tab acted as the backing bar for the CJP weld of the girder web to the column flange, and was designed to extend approximately 0.25 inches into the top and bottom access holes. This extension acts as a short runoff tab, allowing the weld to extend the full depth of the girder web (see Figure 3.12). For the specimens fabricated for this research, the ends of the CJP weld of the girder web to the column flange were not ground smooth, in contrast to the recommendations of FEMA (2000a), so as to investigate whether this economy of labor was detrimental to the connection performance. Note that the shear tabs were located on the north side of the specimen for Specimens CR1 and CR4, and on the south side for the remaining specimens.

The gas-shielded, flux cored process (FCAW-g) and notch-tough E70T-1 was used for all shop welds, including the shear tab welding. The shear tab was welded to the column in the fabrication shop using 1/4 in. fillet welds on each side of the plate although

this deviated from the prequalified WUF-W connections of FEMA (2000a), which requires partial joint penetration (PJP) welds for this detail. Two 7/8 in. A325 bolts were used on each connection for erection purposes. These were placed far enough from the access holes to allow ultrasonic (UT) inspection of the web weld terminations, and they were snug tight.

Supplemental fillet welding was also provided between the shear tab and girder web. A 5/16 in. fillet weld was placed along the full height of the shear tab between it and the girder web using E71T-8 wire. This weld cannot be wrapped around to the top and bottom of the shear tab due to interference with the access holes. This was addressed by the final SAC WUF-W recommendations (FEMA, 2000a), which require a beveled shear tab (see Figure 3.8), allowing both for overlap into the access holes and the wrap-around of the fillet welds.

All field welding was conducted in the Structures Laboratory at the University of Minnesota by an experienced field welder. The complete penetration welds (both flanges and webs) were ultrasonically tested by a certified inspector in conformance with AWS D1.1-00, Table 6.3 for cyclically loaded joints (AWS, 2000).

3.3.2.2 Access Hole Details

As stated previously, the access holes for the test specimens were designed based on the work of Ricles et al. (2000) and Mao et al. (2001). Figure 3.13 illustrates the dimensions of the access holes in the present experiments. This design is required for many of the SAC prequalified connections (FEMA, 2000a), including the WUF-W. The key parameter in this type of access hole is the slope of the flat transition region between the girder flange and drilled hole. The depth of the access hole and the size and location of the drilled hole are selected to ensure this transition slope does not exceed 25°. A shallow slope reduces the plastic strain demand at the toe of the transition, delaying the onset of low-cycle fatigue cracks. Using the dimensions of the access hole shown in Figure 3.13, a slope of 15° was provided for the current specimens. Figure 3.12 illustrates a typical access hole as fabricated.

3.3.3 Panel Zone and Column Stiffener Design

As the primary focus of the cruciform tests is to investigate the design provisions for panel zones and column stiffening, and to test new stiffening alternatives, a significant effort was put into the design of the specimen panel zones and column stiffeners. The panel zones were designed with the intent to exceed the limit state shear deformation of $4\gamma_y$, where γ_y is the shear yield strain. As discussed in Chapter 2, this deformation level of $4\gamma_y$ is based on the panel zone design equation developed by Krawinkler (1978). This ensures that the strength provision (Equation 3.5) can be investigated, and subjects the panel zones and stiffeners to upper-bound strain demands. Column stiffening was designed to both mitigate LFB and increase the panel zone strength. A number of stiffening alternatives are explored by the six test specimens in the current research.

3.3.3.1 Panel Zone Design

As mentioned in Section 3.2.2, the design of the panel zones was based on providing a panel zone weak enough to exceed the typical design deformation of $4\gamma_y$. This ensures that all column stiffening details are rigorously tested through large strain cycles, and provides a means for evaluating the strength of the panel zone at the design deformation. It was also desirable, however, to ensure the panel zones were strong enough to allow for development of the plastic moment strength of the girders. This is necessary to develop large flange forces, thereby placing high force demands on the column details.

To meet this balance of girder and panel zone strength, a method of estimating the relative strengths was used. Nominal strength ratios provide a convenient method to evaluate the relative strength of the components. The quantity of most interest for the purpose of panel zone design was the ratio of nominal panel zone strength (P_z) to girder strength (P_g). These strengths were calculated as the total girder tip loads required to reach the nominal strength under consideration, and are given by:

$$P_z = \frac{0.6F_{yc}d_c t_p\left(1+\dfrac{3b_{cf}t_{cf}^2}{d_g d_c t_p}\right)}{\left(\dfrac{L_g}{d_g}-\dfrac{L_g+d_c/2}{L_c}\right)} \tag{3.15}$$

$$P_g = \frac{2Z_g F_{yg}}{L_g} \tag{3.16}$$

where:

L_g = girder length to face of column

L_c = column length between top and bottom load pins

Z_g = girder plastic section modulus

F_{yg} = minimum specified yield strength of girders

These equations are similar to those used by El-Tawil et al. (1998) to make strength ratio comparisons in their parametric finite element studies. The nominal strength of the panel zone is based on the AISC provision (Equation 3.5) with a resistance factor, ϕ_v, of 1.0. The nominal girder strength is calculated from the summation of the girder plastic moment strengths.

A baseline value of P_z/P_g equal to approximately 1.0 was targeted for the specimens. This implies that the nominal strength of the panel zone (at an average shear distortion of $4\gamma_y$) is achieved at the same time the girders reach their plastic moment strength. By selecting this ratio, the intent is to achieve the goals of exceeding both M_p in the girders and $4\gamma_y$ in the panel zones.

Table 3.3 expresses the panel zone strengths of the six specimens in terms of the P_z/P_g ratio (using both the nominal material strengths and the mill report values), $\phi_v R_v/R_u$ [from AISC (1997, 2001)], and t_p/t_{req} [using the SAC procedure (FEMA, 2000a)]. Significant deviations from the target P_z/P_g were made for Specimens CR4 and CR4R. These specimens feature the box doubler plate detail. As described in Section 3.2.1, it was expected that this type of detail would be less than fully effective, based on the

results of Bertero et al. (1973). Thus, the doubler plates provided were 50% thicker than Specimen CR3, which has the same W14x176 column section. The strength to demand ratios given in Table 3.3 for the AISC and SAC procedures reveal that the panel zones of most specimens are weak or borderline satisfactory as per current design standards, so as to impart high strains to the stiffening details. Again the exception is Specimen CR4, which meets the requirements of both methods.

3.3.3.2 Fillet-Welded Doubler Plate Design

As was shown in Figure 3.5, two fillet-welded doubler plate details are included in the test matrix. The first (Detail I) is essentially the detail shown in Figure C-9.3 (b) of the AISC Seismic Provisions (AISC, 1997). It consists of doubler plates beveled at 45° to avoid interference with the column radius region. The plates are placed flush against the column web and fillet-welded to the column flanges. A minimum fillet weld is also required across the top and bottom of the plate as per AISC Seismic Provisions (AISC, 1997). This procedure avoids placing highly restrained CJP welds in the column k-area, a situation that has caused fabrication cracking in some instances (Tide, 2000), especially as the welds become larger.

This detail has its limitations, however, one of which led to the development of the second fillet-welded design (Detail II). For practical fillet weld sizes (approximately 1 in. or less), plate thicknesses are limited to about 3/4 in. This may not be practical for some connections, and larger fillet welds needed for thicker plates may make the detail less economical. A second, more critical issue was discovered during fabrication of this detail. Using nominal *k* dimensions and maximum permissible fillet encroachments from the AISC Manual (1995), a minimum bevel size (and thus minimum plate thickness) of 7/16 in. was calculated. A practical minimum doubler thickness using this detail of 1/2 in. was thus selected. As revealed in a recent AISC Dimension Advisory (2001), the actual *k* values for many shapes currently rolled – including the columns selected for the cruciform specimens – have become significantly larger. The large fillet radii of the columns used for the specimens made proper fit-up of 1/2 in. and 5/8 in. beveled doubler plates impossible. Forcing these doubler plates flush against the column web would have

required gaps between the doublers and column flanges of greater than 1/16 in.. Fillet welds are not prequalified for gaps exceeding 1/16 in. Using the new *k* dimensions given for detailing, minimum plate thickness for proper fit-up increases to approximately 1 in. This is larger than the thicknesses of the doubler plates intended for the specimens, and would require 1.25 in. fillet welds.

Fillet Detail II was developed as an alternative to the beveled detail. Instead of beveling the plate to fit against the column web, the doublers are simply cut square to the width between column flanges (approximately 12.5 in. for W14 columns) and placed in the column until they interfere with the column radius. As with Detail I, the plates are then fillet-welded to the column flanges. By cutting the plates just narrower than the width between flanges, the gap between the doublers and column flanges remains below the 1/16 in. A result of this detail, however, is a gap between the column web and doubler plate of approximately 7/8 in. This does not allow for welding across the top and bottom of the plate. According to the AISC Steel Design Guide 13, however, there is theoretically no force transfer at these welds if the doublers are extended above and below the level of the beam flanges (AISC, 1999c). This same situation arises with the use of the offset (box) doubler plates (discussed in Section 3.3.3.3). Detail II is considered an economical alternative because it requires no beveling, and is fillet-welded as opposed to CJP-welded.

The size of the fillet welds needed for both details were calculated using procedures given in the AISC Design Guide 13 (AISC, 1999c). It is required that the fillet welds be able to develop the full shear strength of the doubler plates (AISC, 1997). Two equations are given in the AISC Design Guide:

$$w_{\min} = \frac{\phi_s 0.6 F_{ydp} t_{dp}}{\phi_w 0.6 F_{EXX}} \left(\frac{\sqrt{2}}{2} \right) = \frac{1.70 F_{ydp} t_{dp}}{F_{EXX}} \tag{3.17}$$

$$w_{\min} = t_{dp}\sqrt{2} - \left(t_{dp} - bevel \right) \tag{3.18}$$

where:

w_{min} = minimum required fillet weld size

ϕ_s = resistance factor for shear = 0.9

ϕ_w = resistance factor for weld = 0.75

F_{ydp} = minimum specified yield strength of doubler plate

t_{dp} = thickness of doubler plate

F_{EXX} = minimum specified strength of weld electrode

bevel = beveled width of doubler plate

Equation 3.17 yields the weld size necessary to develop the shear strength of the full plate thickness, while Equation 3.18 satisfies the geometric requirements, ensuring the effective throat in the beveled and welded region is at least equal to the plate thickness. Only Equation 3.17 is applicable to Detail II.

All doubler plates were extended 6 in. above and below the beam flanges. This corresponds to approximately ($2.5k + N$), the extension necessary for the doublers to be considered effective in resisting LWY. Although LWY was not the controlling limit state expected in any specimen, this was done to be consistent with the doubler plate placement used in the pull-plate experiments conducted by Prochnow et al. (2000a) that investigated the LWY provisions.

Doubler plate Detail II was used for Specimens CR2 and CR3, while Detail I was used for Specimen CR5. Strictly speaking, proper fit-up of the 5/8 in. plates could not be achieved in Specimen CR5 with Detail I due to the large column radii, however this specimen has member sizes similar to some of the pull-plate specimens tested by Prochnow et al. (2000a). It was desired to replicate the doubler plate details tested on the pull-plates for the best correlation between the tests. A gap between the web and doubler plate of approximately 1/4 in. still resulted using the beveled plates, but this was considered sufficiently similar to the pull-plate doubler configuration. This gap did not allow for welding across the top and bottom of the doublers, however. The thickness of all doubler plates was based on the procedures outlined in Section 3.3.3.1.

Figures 3.14 to 3.16 show the details of the fillet welded doubler plates for the three specimens incorporating them. The FCAW-g process with E70T-1 notch-tough consumables was used for all shop welding of the doubler plates.

3.3.3.3 Groove-Welded Offset (Box) Doubler Plate Design

The final doubler plate detail tested by the present research is an offset stiffener similar to that given in Figure C-9.3 (c) of the AISC Seismic Provisions (AISC, 1997). It differs from this detail, however, because it does not include continuity plates in addition to the offset doublers. This detail is economically desirable if the plates can be shown to be effective both as doublers and continuity plates (i.e., mitigating PZ yielding, LFB, and LWY). In addition to carrying shear, the offset plates act to stiffen the column flanges. Like both fillet-welded details (i.e., Detail I and Detail II), the box detail also avoids welding in the column k-area. Complete joint penetration (CJP) welds are used to join the plates to the column flanges.

The location of the plates (i.e., the amount of offset from the column web) was based on the parametric finite element study conducted by Ye et al. (2000). This study showed that the doublers were most effective when placed between 1/3 and 2/3 of the half-flange width from the web. In this location, the strain concentrations in the center of the girder flanges were reduced without an excessive increase towards the flange tips. A second result of the finite element study was that the expected loss of effectiveness of the offset doublers did not occur in the models. The shear strains carried by the offset doublers were very similar to the strains in the doublers placed directly against the web. A location corresponding to an offset of 2/3 of the half-flange width was selected for the experiments. For a W24x94 girder, this equates to a gap of 2 in. between the column web and doubler plate.

The offset stiffener detail was used on Specimens CR4 and CR4R. The placement and welding details are shown in Figure 3.17. The welds to the column flanges were made using a prequalified, single-bevel CJP groove weld. The FCAW-g process with an E70T-1 consumable was used, and the welds were ultrasonically tested.

3.3.3.4 Continuity Plate Design

The design of the continuity plates on Specimen CR3 was an extension of the testing conducted by Prochnow et al. (2000a) on pull-plate specimens. The basic detail consists of continuity plates with a thickness equal to half the beam flange thickness,

fillet-welded to both the doubler plates and column flanges. These half-thickness, fillet-welded continuity plates were shown to perform adequately in the monotonically loaded tests. This detail is included in the present testing to investigate the suitability for cyclically loaded seismic applications, and is considered an economical alternative to the full-thickness, CJP-welded continuity plates typically specified following Northridge.

Sizing of the continuity plates and welds was predominantly based on the AISC Steel Design Guide 13 (AISC, 1999c) for wind or low-seismic applications. The requirements for high-seismic design require full-thickness continuity plates (i.e., equal to the beam flange thickness) that are CJP-welded to the column flanges. Figure 3.15 illustrates the continuity plate details of Specimen CR3. Note that this detail is used in conjunction with fillet-welded doubler plate Detail II. The 1/2 in. thickness of the continuity plates is approximately half the thickness of the W24x94 flange. A 5 in. width was selected in compliance with the requirement of $b/t \le 95/\sqrt{F_y}$ contained in the LRFD Specifications (AISC, 1993, 1999a). 1 in. clips were provided to avoid interference with the fillet welds between the doubler plates and column flanges. Using the seismic LFB demand (Equation 2.13) and the LFB resistance of the W14x176 column (Equation 2.9), the continuity plate demand is 231 kips per pair, equal to the difference between the demand and resistance. The area of the provided continuity plates must resist this force. The 5 in. wide, 1/2 in. thick continuity plates have a design resistance of 225 kips based on tensile yielding of the full width, essentially equal to the demand of 231 kips.

The fillet weld sizes were based on developing the tensile yield strength of the plate at the connection to the column flanges, and developing the shear strength of the plate along the connection to the doubler plates. The equations for these criteria, based on the AISC Design Guide (AISC, 1999c), are:

$$w_{\min} = \frac{\phi_t F_{ycp} t_{cp}}{\phi_w 1.5(0.6F_{EXX})\sqrt{2}} = \frac{0.943 F_{ycp} t_{cp}}{F_{EXX}} \tag{3.19}$$

$$w_{\min} = \frac{\phi_s 0.6 F_{ycp} t_{cp}}{\phi_w 0.6 F_{EXX} \sqrt{2}} = \frac{0.849 F_{ycp} t_{cp}}{F_{EXX}} \tag{3.20}$$

where:

ϕ_t = resistance factor for tension = 0.9

F_{ycp} = minimum specified yield strength of continuity plate

t_{cp} = thickness of continuity plate

Equation 3.19 determines the weld size to the column flange, while Equation 3.20 determines the weld size needed along the doubler plates. Note that both equations assume double-sided fillet welds. As with the doubler plate details, the continuity plates were welded with the FCAW-g process and E70T-1 electrodes.

3.4 Material Properties

Material testing was performed on all wide-flange shapes and available stiffening plates used for the test specimens. Tensile testing was conducted to characterize the stress-strain behavior of the steel. Results of the coupon tests are compared to reported mill values and requirements for the A992 steel sections. Typical weld properties from the E70T-6 and E71T-8 consumables supplied by the producer are compared to SAC and AWS requirements (FEMA, 2000a, 2000d; AWS, 1995). Four sets of tested material properties of the E70T-6 wire are also presented.

3.4.1 Steel Material Properties

Tensile testing was performed on all structural wide-flange shapes included in the test matrix. The Structural Stability Research Council (SSRC) Technical Memorandum No. 7 (SSRC, 1998) was followed as the testing procedure. Tensile properties of the plate material used for the stiffening details were either determined from testing or mill certificate data (when available). All W-shapes of the same size were produced from the same heat, and all plate material of a given thickness was produced from the same heat. For each W-section, two coupons were taken from the flanges and two from the web. The edge of web coupons was taken no closer than 2 in. from the k-line, as recommended in the SAC Phase 2 testing protocol (SAC, 1997). Full-thickness specimens were used, with a gage length and width of 8 in. and 1.5 in., respectively. When material was available, at least two coupons from each plate thickness were tested. Full-thickness

coupons with a gage length and width of 2 inches and 0.5 inches, respectively, were used for the plate material tests.

Several quantities were obtained for each wide-flange section coupon, including the dynamic yield stress, $F_{y,dyn}$, (at a 0.2% offset), static yield stress, $F_{y,st}$, modulus of elasticity, E, strain hardening modulus, E_{sh}, ultimate strength, F_u, yield-to-tensile ratio (using $F_{y,dyn}$), Y/T, and percent elongation. Table 3.4 summarizes the tensile test results and mill certificate values for the W-shapes. The test results represent the average of the two coupons cut from each location. Table 3.5 reports the tensile properties of the plate material. When coupons were tested, the results are the average of the two or three samples taken from each thickness. The strain hardening modulus of the W-shapes was calculated using the procedure recommended in the SAC Protocol (SAC, 1997).

As shown in Table 3.4, the web material generally exhibited higher yield strengths, higher yield-to-tensile ratios, lower strain hardening moduli, and lower total elongation. These trends are characteristic of work-hardened steel, and would typically be expected in the thinner web material of rolled W-shapes. Although all dynamic yield points exceeded the required 50 ksi for A992 shapes, note that several of the static yield stresses are below this value. It is also noted that the mill test values generally corresponded more closely with the dynamic yield stress measurements. This was expected, as mill tests do not report static yield points. The ASTM specification for A992 steel (ASTM, 1998a) specifies the yield strength between 50 and 65 ksi, a minimum tensile strength of 65 ksi, a maximum Y/T of 0.85 and a minimum elongation of 18%. Referring to Table 3.4, all shapes met these requirements of this specification when the dynamic (0.2% offset) yield strength values are used. If static yield strengths are used, the flange of the W24x94, and both the W14x193 and W14x283 column sections do not meet the minimum yield strength requirements. The measured values of the strain hardening modulus, E_{sh}, ranged between 272 and 636 ksi, with an average value of 512 ksi. In a recent study of wide-flange shapes, Frank (FEMA, 2000c) reported an average strain hardening modulus of 380 ksi.

3.4.2 Weld Material Properties

Table 3.6 lists the typical as-welded properties of the E70T-6 and E71T-8 consumables used for fabrication of the girder-to-column moment connections. Data was obtained from the manufacturer's literature for 2000. Also included in the table are the SAC and AWS minimum requirements for the electrodes (FEMA, 2000a, 2000d; AWS, 1995). Based on SAC testing, E70T-6 has been recommended for use in girder-to-column welds for new seismic construction (FEMA, 2000d), as it has been shown to typically meet the minimum toughness requirements.

In order to verify the material properties of the CJP welds, one weld test plate was made for Specimens CR2, CR3, CR4R, and CR5 in the Structures Laboratory at the time of the welding. Basic dimensions of the weld test plate can be found in Figure 2A in AWS A5.20-95 (AWS, 1995). These test results, which followed ASTM E23 (ASTM, 1994b) for the Charpy V-Notch impact test and ASTM E8 (ASTM, 1994a) for the tensile coupon test, are presented in Table 3.7, while the weld procedures for these girder flange-to-column CJP welds are summarized in Table 3.8. Table 3.7 also shows the CVN test results for Specimens CR1 and CR4. These CVN specimens were machined from one of the groove welds in the cruciform joint specimen after the test. The strain from the cyclic testing could have strain hardened the weld and adversely affected the weld notch toughness. However, the weld is supposed to be overmatched (i.e., having a higher yield strength than the base metal) and therefore should not experience significant plastic strain during loading, particularly for Specimen CR4, which failed early in the testing history, so this effect is not thought to significantly affect the CVN results of that specimen. Unfortunately, weld test plates were not prepared at the time of the welding for Specimens CR1 and CR4.

Table 3.1: Cruciform Test Specimen Matrix

Specimen	CR1	CR2	CR3	CR4	CR5
Girder	W24x94	W24x94	W24x94	W24x94	W24x94
Column	W14x283	W14x193	W14x176	W14x176	W14x145
Doubler Plate	None	Fillet II	Fillet II	Box	Fillet I
DP Thickness	NA	0.625 in.	2 @ 0.5 in.	2 @ 0.75 in.	2 @ 0.625 in.
Continuity Pl.	None	None	Fillet	None (box)	None
CP Thickness	NA	NA	0.5 in.	NA	NA

Table 3.2: Strength-to-Demand Ratios for PZ Yielding, LFB and LWY Limit States

Specimen	PZ $\phi_v R_v/R_u$	LFB $\phi R_n/R_u$			LWY $\phi R_n/R_u$		
		(2.12)*	(2.13)*	(2.14)*	(2.12)*	(2.13)*	(2.14)*
CR1	0.83	3.04	1.69	2.51	2.38	1.32	1.97
CR2	0.76	1.47	0.82	1.22	2.20	1.22	1.82
CR3	0.86	1.22	0.68	1.01	2.51	1.39	2.07
CR4	1.07	1.22	0.68	1.01	3.19	1.77	2.64
CR5	0.85	0.84	0.47	0.70	2.34	1.30	1.94

*Numbers in parentheses represent the equations used to calculate demand, R_u

Table 3.3: Panel Zone Strength Comparisons

Specimen	P_z/P_g (nominal)	P_z/P_g (mill reports)	$\phi_v R_v/R_u$ (AISC)	t_p/t_{req} (SAC)
CR1	1.02	1.10	0.83	0.72
CR2	0.93	1.01	0.76	0.78
CR3	1.05	1.20	0.86	0.92
CR4, CR4R	1.31	1.49	1.07	1.18
CR5	1.04	1.20	0.85	0.95

Table 3.4: Steel W-Shape Tensile Properties

	W24x94 flange (All Girders Except CR3)	W24x94 web (All Girders Except CR3)	W24x94 flange (CR3 Girder)	W24x94 web (CR3 Girder)	W14x283 flange (CR1 Column)	W14x283 web (CR1 Column)	W14x193 flange (CR2 Column)	W14x193 web (CR2 Column)	W14x176 flange (CR3 & CR4 Column)	W14x176 web (CR3 & CR4 Column)	W14x176 flange (CR4R Column)	W14x176 web (CR4R Column)	W14x145 flange (CR5 Column)	W14x145 web (CR5 Column)
Coupon Test Results														
$F_{y,dyn}$ (ksi)	50.6	59.7	54.3	60.0	50.7	52.3	50.1	54.0	55.2	57.5	54.3	56.8	56.6	58.7
$F_{y,st}$ (ksi)	46.4	55.0	NA	NA	47.8	48.8	46.4	49.8	51.8	53.6	NA	NA	52.9	54.8
F_u (ksi)	69.2	74.1	72.3	76.0	73.1	72.6	72.2	72.4	76.6	76.1	73.8	74.3	77.2	77.2
E (ksi)	28300	29500	NA	NA	28200	29850	29800	29650	29500	29750	NA	NA	29100	29350
E_{sh} (ksi)	535	272	NA	NA	636	572	572	479	564	486	NA	NA	507	500
Y/T (%)	73.1	80.6	75.1	78.9	69.1	72.0	69.4	74.6	72.1	75.5	73.6	76.4	73.3	76.1
% Elong	30.7	25.0	34.5	83.5	31.3	29.7	31.8	28.0	29.0	27.1	34.0	34.0	27.0	26.1
Mill Test Results														
F_y (ksi)	50.0		NA*		54.0		54.5		57.0		55.0		57.5	
F_u (ksi)	68.5		NA*		73.5		74.0		76.0		72.0		76.5	
% Elong	27.5		NA*		22.0		25.5		25.0		27.0		21.5	

*NA = Not available

Table 3.5: Plate Material Tensile Properties

Plate Thickness	F_y (ksi)	F_u (ksi)	% Elongation
½ in. (CR3)	NA	NA	NA
5/8 in.* (CR2 & CR5)	62.0	81.0	34.0
5/8 in.** (CR2 & CR5)	57.8	81.0	80.5
3/4 in.** (CR4)	48.8	73.2	33.8
3/4 in.** (CR4R)	57.5	77.3	31.0

*Properties obtained from mill test report
**Properties obtained from coupon tests

Table 3.6: Weld Material Properties

	E70T-6 Typical	E70T-6 Required	E71T-8 Typical	E71T-8 Required
CVN @ 0°F (ft-lbs)	21 – 54	20 min.*	NR	20 min.*
CVN @ -20°F (ft-lbs)	21 – 35	20 min.**	50 – 200	20 min.**
F_y (ksi)	62.0 – 76.0	58.0 min.**	60.0 – 65.0	58.0 min.**
F_u (ksi)	72.0 – 89.0	70.0 min.**	72.0 – 80.0	70.0 min.**
% Elongation	23 – 32	22 min.**	28 – 31	22 min.**

*Requirement as per SAC Recommended Specifications (FEMA, 2000e)
**Requirement as per AWS A5.20-95 (AWS, 1995)

Table 3.7: Tested Weld Material Properties (E70T-6 Only)

	E70T-6* 5/64 in. wire		E70T-6 3/32 in. wire			
	CR1	CR4	CR2	CR3	CR4R	CR5
CVN @ 0°F (ft-lbs)	2.6	2.0	34.3	44.3	33.0	33.0
CVN @ 70°F (ft-lbs)	19.3	2.3	54.3	73.3	58.7	53.7
F_y (ksi)	NA	NA	59.5	50.0	56.0	53.5
F_u (ksi)	NA	NA	79.5	72.5	78.2	75.5
% Elongation	NA	NA	25.0	23.0	27.5	26.0

*These CVN tests were performed on specimens machined after the experiment from the welds that did not fracture in these cruciform joints. Specimen CR1 was subjected to 20 cycles at strains reaching 3 to 4% strain at nearby girder flange strain gages, and Specimen CR4 was subjected to 2 cycles at strains reaching 1 to 2% strain at nearby girder flange strain gages, although the welds are presumed to be overmatched and therefore should only be strained in the elastic range.

Table 3.8: Summary of Parameters used for CJP Welds

	CR1	CR4	CR2	CR3	CR4R	CR5
Electrode Manufacturer	Lincoln	Lincoln	Lincoln	Lincoln	Lincoln	Lincoln
Trade Name	NR-305	NR-305	NR-305	NR-305	NR-305	NR-305
AWS Designation	E70T-6	E70T-6	E70T-6	E70T-6	E70T-6	E70T-6
Electrode Type	FCAW-s	FCAW-s	FCAW-s	FCAW-s	FCAW-s	FCAW-s
Electrode Diameter (in.)	5/64	5/64	3/32	3/32	3/32	3/32
Power Supply	Miller Maxtron 450	Miller Inverter	Lincoln DC-600	Lincoln DC-600	Lincoln DC-600	Lincoln DC-600
Wire Feeder	Miller S-64	Lincoln LN-25	Lincoln LN-10	Lincoln LN-10	Lincoln LN-10	Lincoln LN-10
Voltage (V)	28.5 - 29.5	29 - 30	26 - 28	26 - 28	26 - 28	26 - 28
WFS (ipm)	380	380	280	280	280	280
Current (A)	430 - 460	330 - 380	470 - 500	470 - 500	470 - 500	470 - 500
Preheat (°F)	150 min	150 min	50 min	50 min	50 min	50 min
Interpass (°F)	150 min	150 min	50 min	50 min	50 min	50 min
Electrode Extension (in.)	1	1	1	1	1	1
Travel Speed (ipm)	10 - 15	10 - 15	10 - 15	10 - 15	10 - 15	10 - 15

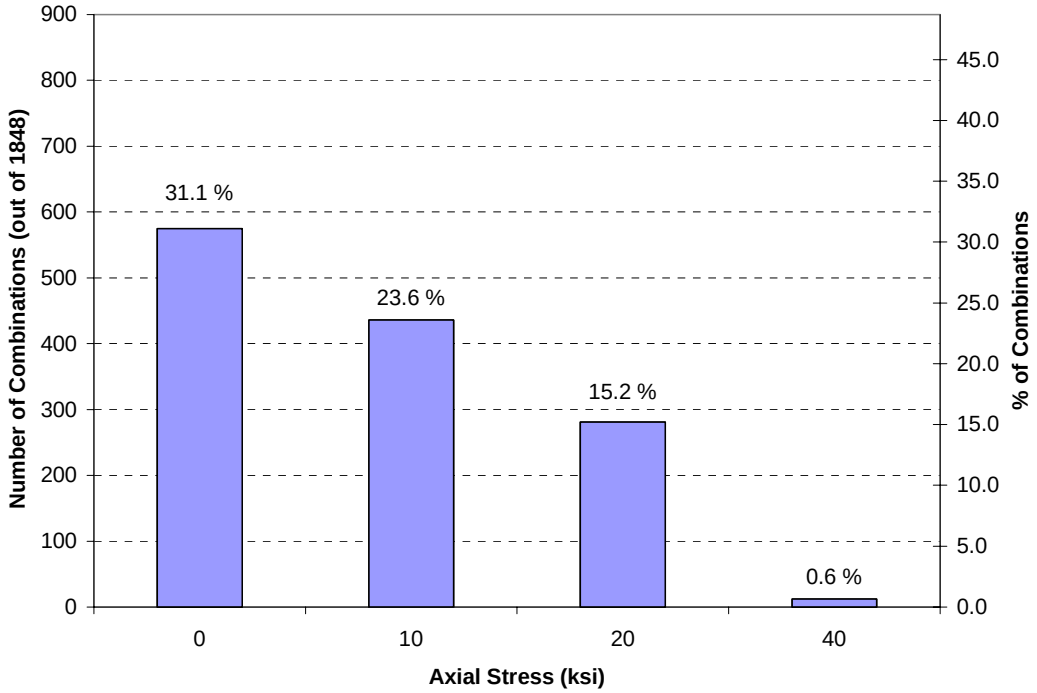


Figure 3.1: Seismic Girder-Column Combinations Meeting SCWB Criterion - 50 ksi Columns

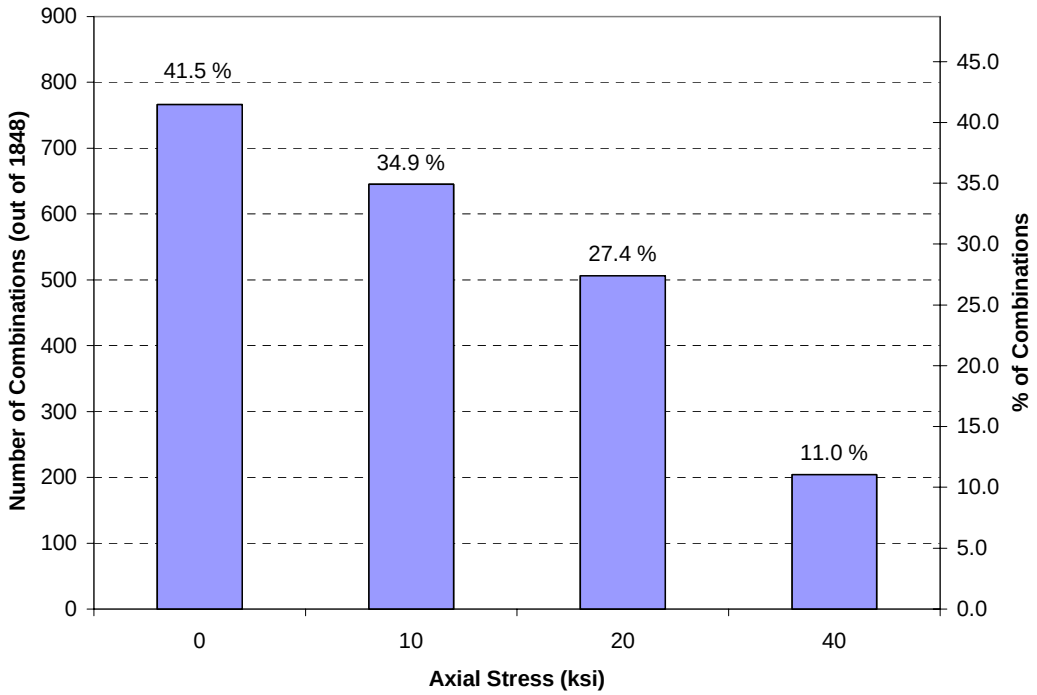


Figure 3.2: Seismic Girder-Column Combinations Meeting SCWB Criterion - 65 ksi Columns

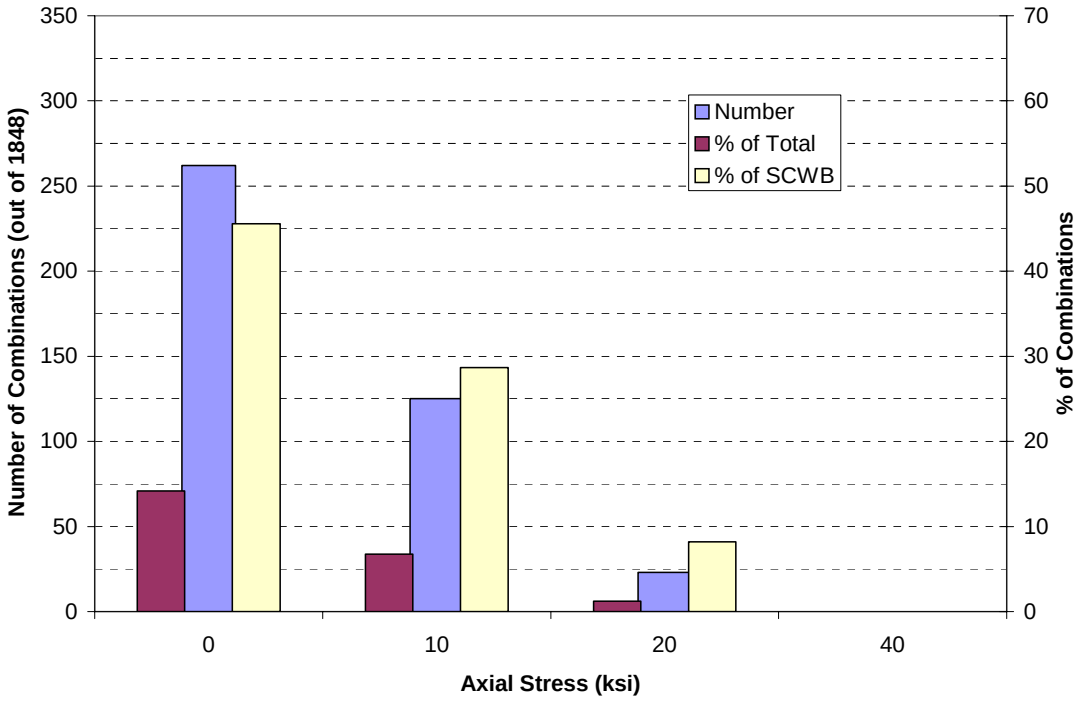


Figure 3.3: Seismic SCWB Girder-Column Combinations Requiring Doubler Plates – 50 ksi Columns

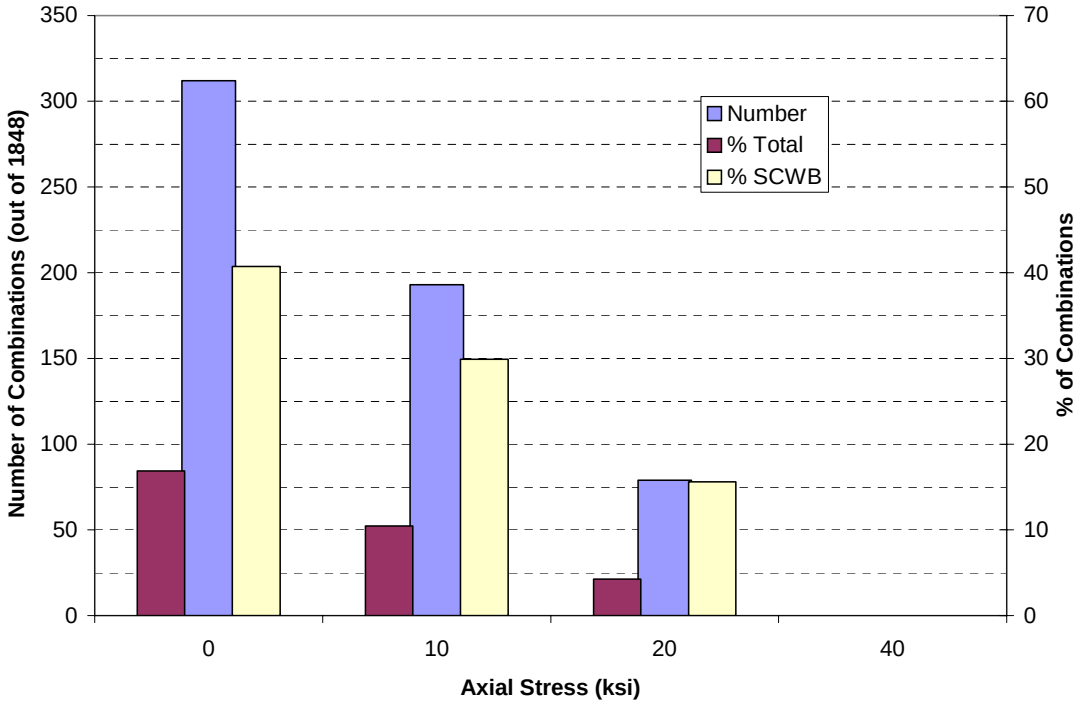


Figure 3.4: Seismic SCWB Girder-Column Combinations Requiring Doubler Plates – 65 ksi Columns

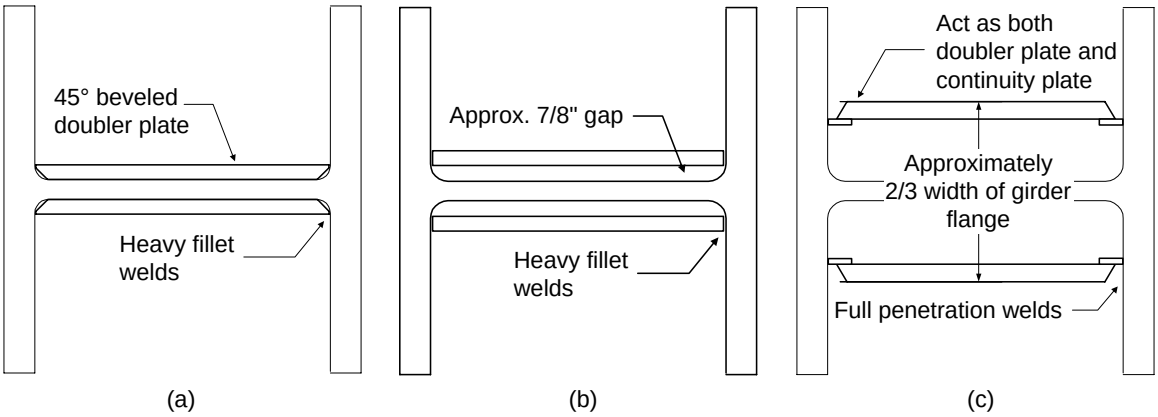


Figure 3.5: Doubler Plate Details: (a) Beveled, Fillet-Welded Doubler (Detail I), (b) Square-Cut Fillet-Welded Doubler (Detail II), (c) Offset (Box) Detail

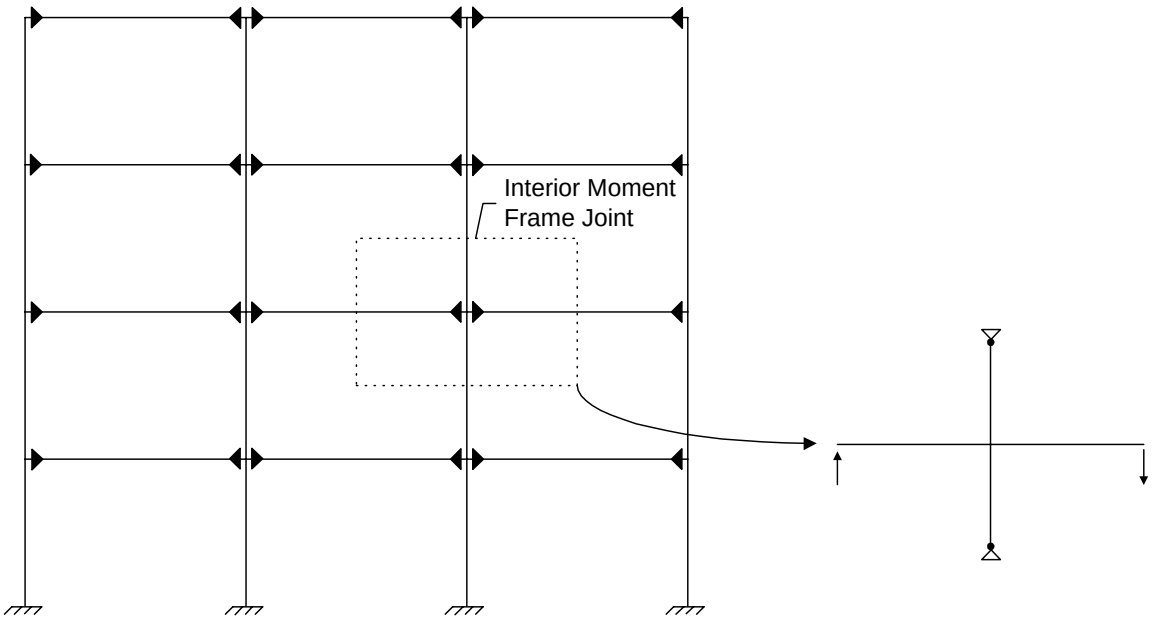


Figure 3.6: Typical Moment Frame Elevation Showing Interior Joint and Specimen Idealization

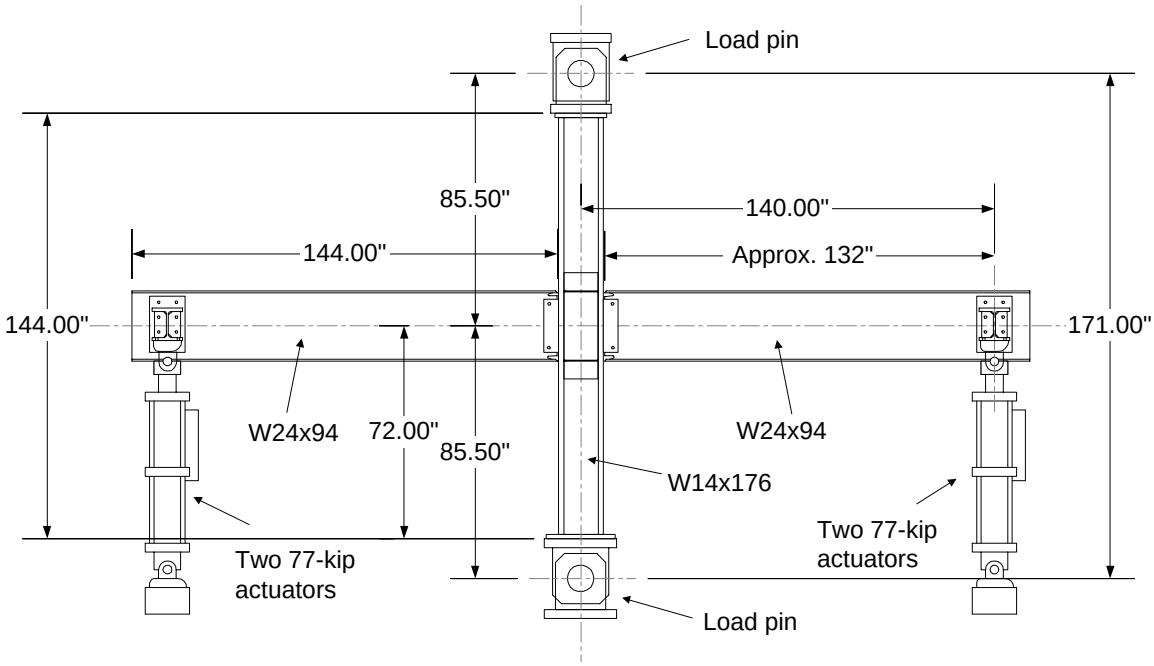


Figure 3.7: Typical Cruciform Specimen With Basic Dimensions

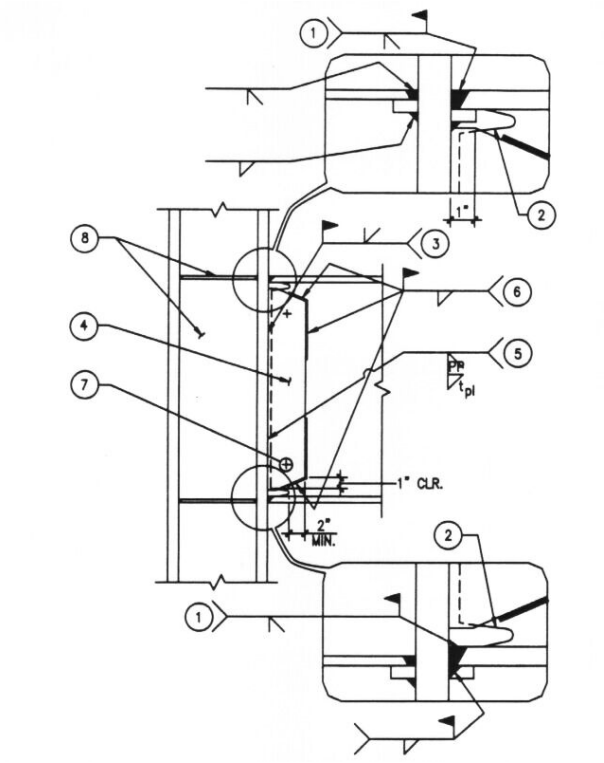


Figure 3.8: SAC WUF-W Moment Connection Details [after (FEMA, 2000a)]

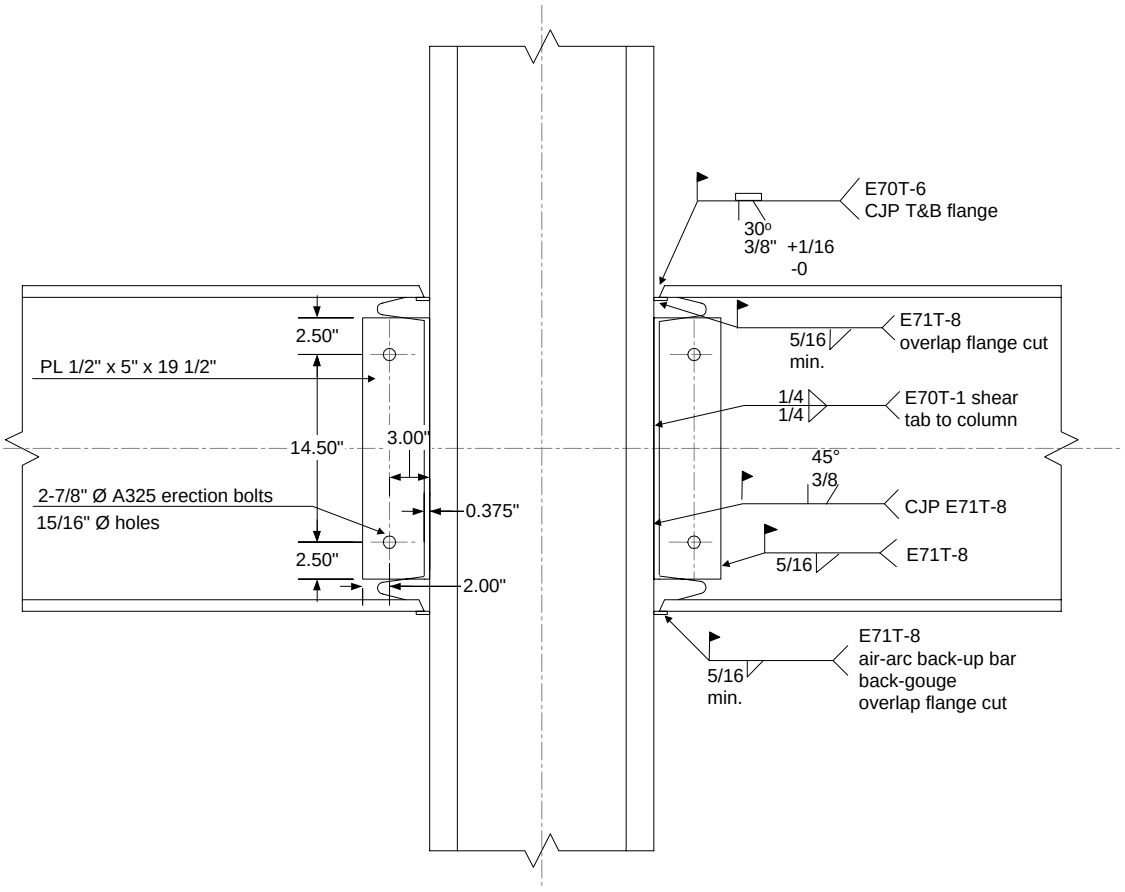


Figure 3.9: Typical Welded Moment Connection Details



Figure 3.10: Top Flange Weld With Reinforcing Fillets



Figure 3.11: Bottom Flange Reinforcing Fillet Weld



Figure 3.12: Access Hole and End of Web Groove Weld Showing Overlap of Shear Tab Into Access Hole

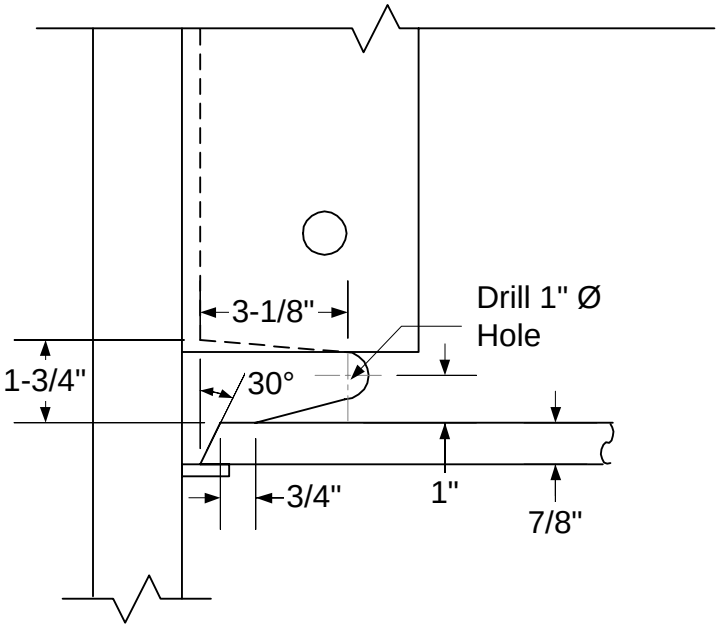


Figure 3.13: Access Hole Dimensions

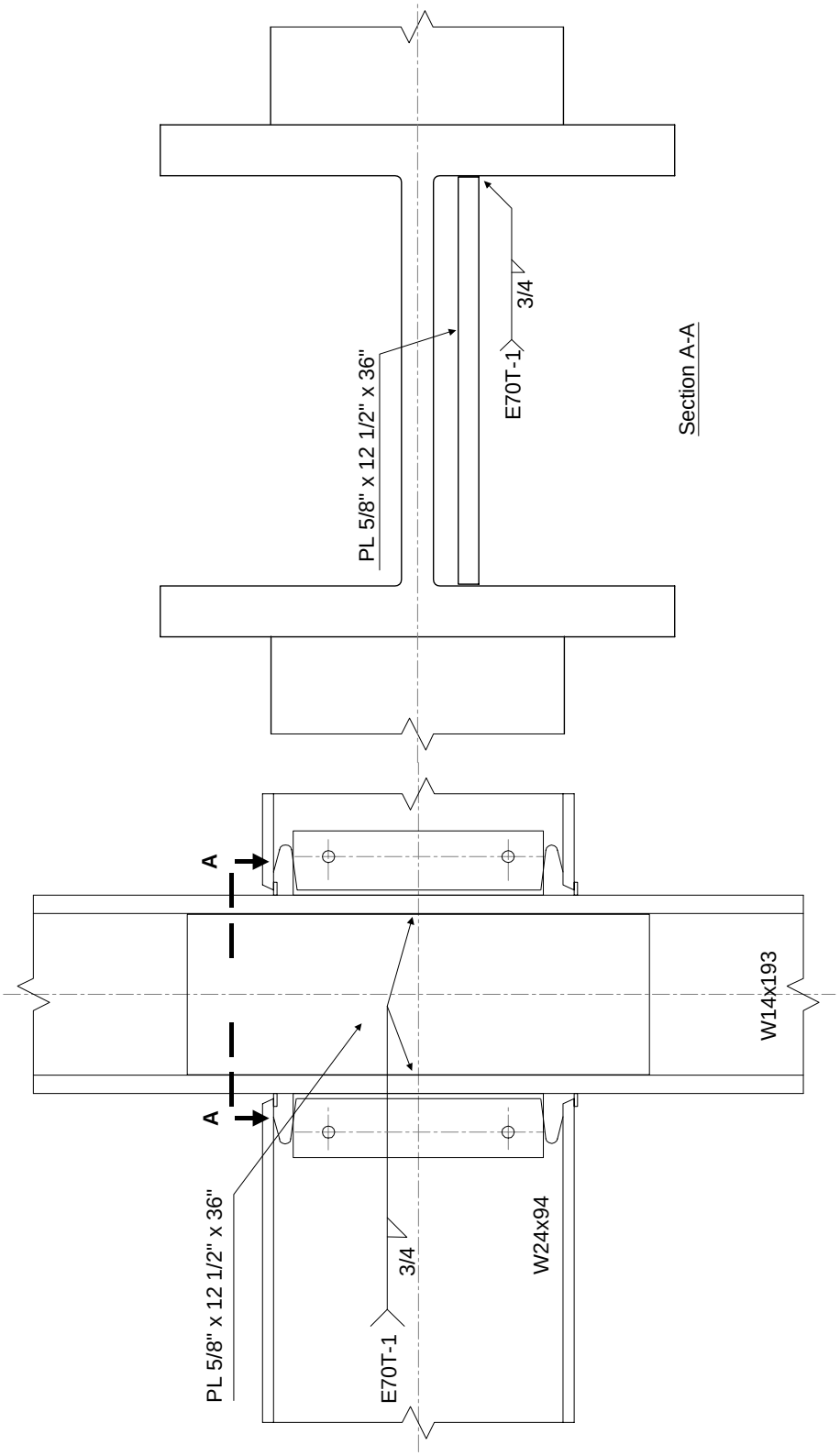


Figure 3.14: Specimen CR2 Fillet-Welded Doubler Plate Details

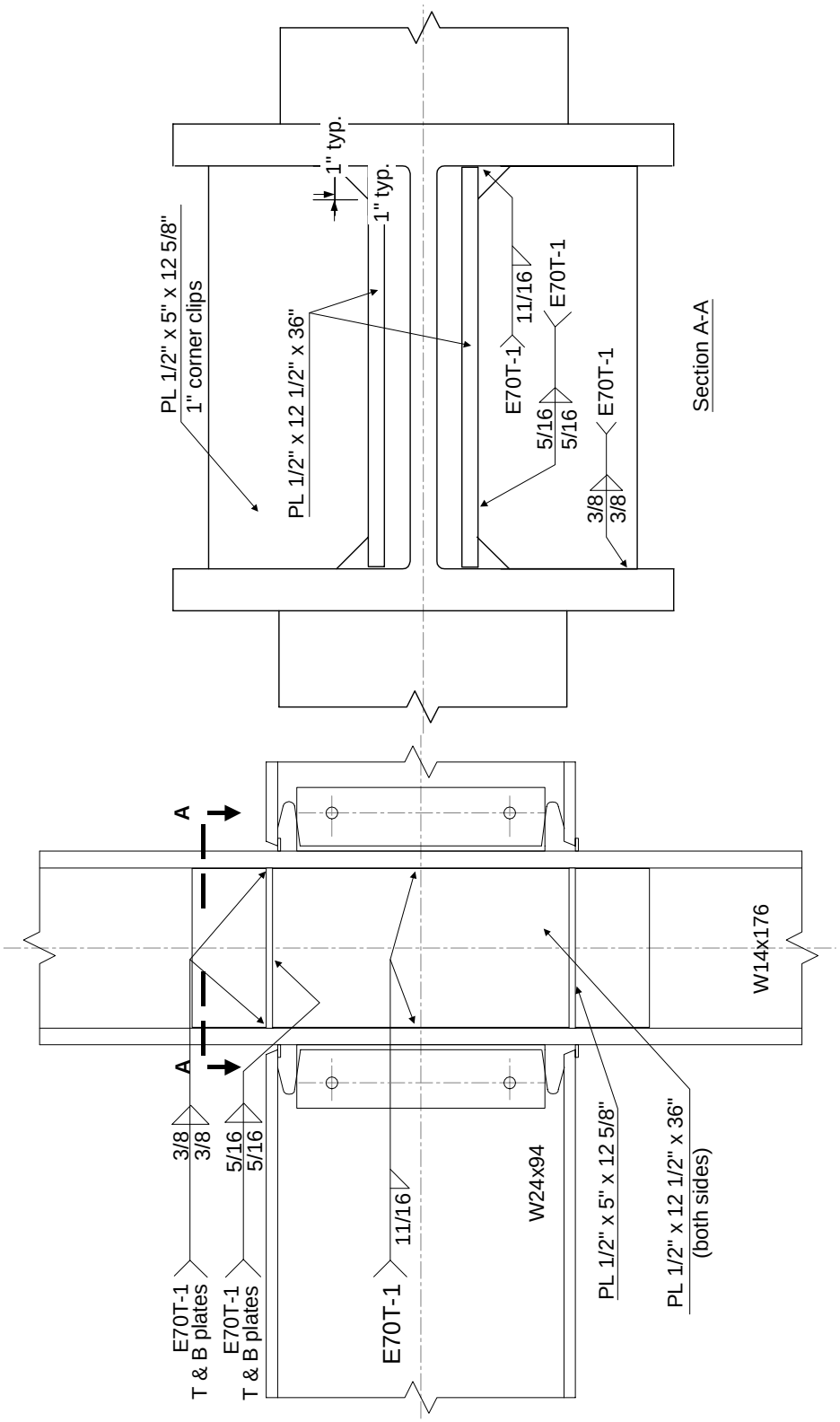


Figure 3.15: Specimen CR3 Stiffening Details

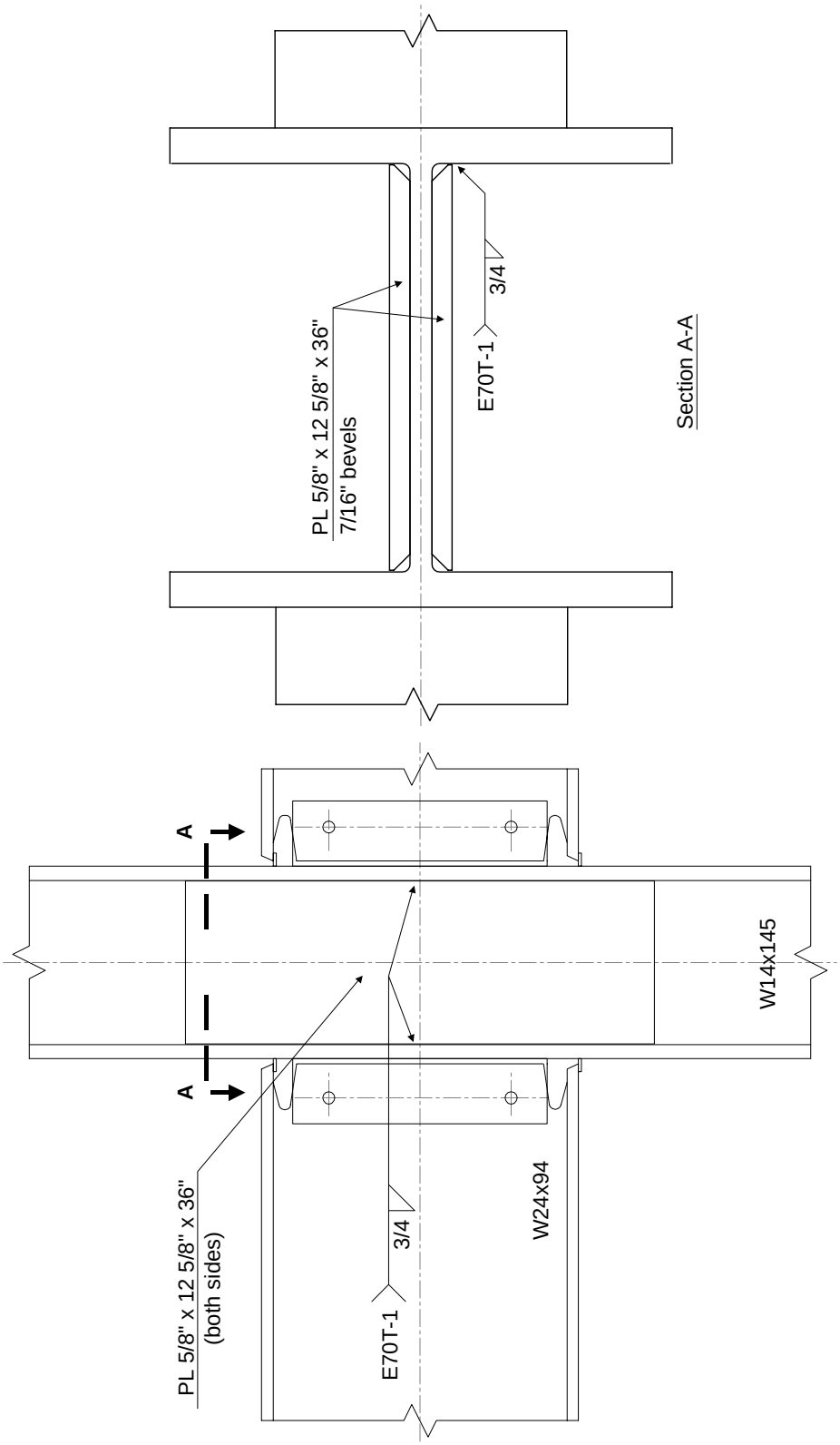


Figure 3.16: Specimen CR5 Fillet-Welded Doubler Plate Details

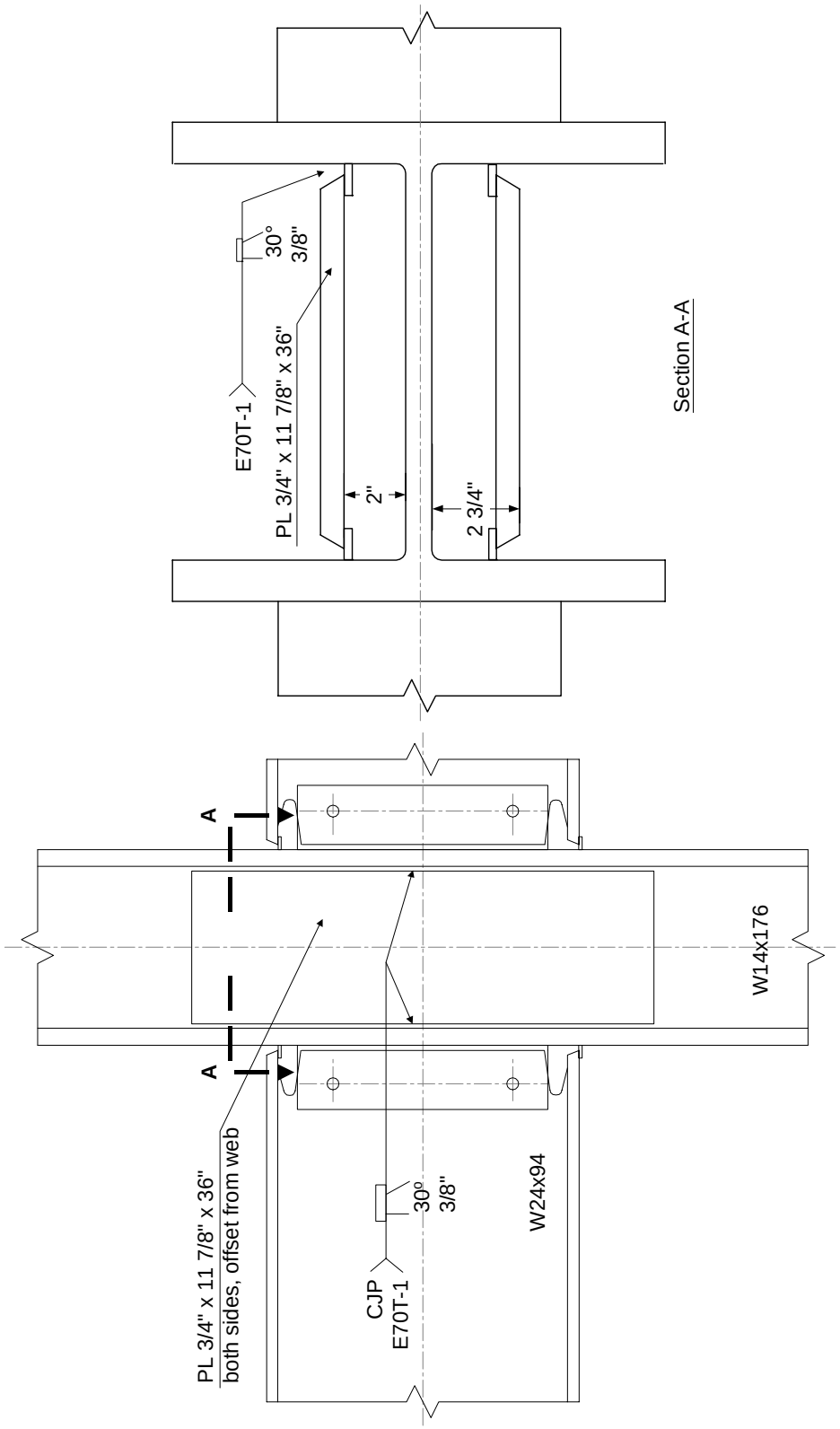


Figure 3.17: Specimen CR4 Offset (Box) Doubler Plate Details

Chapter 4

Test Setup and Instrumentation

This chapter is composed of three parts; test setup, loading history, and instrumentation. For test setup, the configuration of load frame assembly is described, followed by a description of the loading system using four MTS hydraulic actuators. The loading history used for SAC Phase 2 was adopted in this test program and is explained in this chapter. The description of the instrumentation includes a discussion of the various groupings of strain gages and their intended functions, and the locations of the linear variable differential transformers (LVDTs). A detailed list of strain gage locations, based on a defined coordinate system, is included for reproducibility of the instrumentation.

4.1 Test Setup

The load frame assembly used for the present research was previously designed for testing conducted at the University of Minnesota during Phase 1 of the SAC program (Hajjar et al., 1998b, Leon et al., 1998). It consists of a system of members designed to transfer the shear forces from the top column pin to the laboratory strong floor. A second major component of the system is the 600 kip MTS hydraulic testing machine, to which the top pin is connected. While the MTS system was not used to apply axial loads to the columns in these experiments, this configuration was re-used to avoid additional design and fabrication. Figures 4.1 and 4.2 show the features of the load frame. Shear is transferred from the load pin in bearing against C15x40 channel sections, which, in turn, transfer the forces through the system of W24x104 sections to the W30x99 columns. The W8x31 diagonal members carry the forces from the columns to floor beams attached to the concrete lab floor. Each pair of 2 in. holes on the strong floor is rated for 100 kips of

load. High-strength threaded steel rod (grade B2), 1.5 in. diameter, was used to attach all components to the floor. All rods were fully pre-tensioned to prevent slip in the system. The load frame was designed to carry 300 kips of horizontal shear with a maximum horizontal deflection of 0.25 in. at the top (Hajjar et al., 1998b).

Braces were also attached to the diagonal load frame members to restrict the out-of-plane movement of the girders due to lateral-torsional buckling (see Figure 4.3). These braces were placed approximately 95 in. from the column face. This is in accordance with the AISC Seismic Provisions (AISC, 1997), Section 9.8, which limits the unbraced length of beams in steel moment-resisting frames to $2500r_y/F_y$. For the W24x94 section, this limiting unbraced length is 99 inches.

The large load pins placed at the top and bottom of the column sections were designed to allow free rotation of the column ends during loading, simulating inflection points at the mid-height of the columns of each story. The pins (see Figure 4.4) were fabricated from 3 in. thick plate material and solid 9 in. steel dowels. A previous analysis of the pin assemblies showed the effects of load pin friction to be negligible (Hajjar et al., 1998b).

Loading was applied to the girder tips by four MTS hydraulic actuators. Each actuator is capable of 77 kips at a stroke of +/- 6.0 in. The actuators were attached to the girders by brackets consisting of a W10x100 stub welded to a bolted end plate (see Figure 4.5). The brackets were designed as slip-critical, extended end-plate moment connections. The bottoms of the actuators were attached to beams tied to the laboratory strong floor.

Quasi-static, anti-symmetric, cyclic loads were applied to the girder tips. Section 4.2 details the applied load histories. A displacement controlled, master/slave loading control system was used. One actuator on the East girder received the master displacement signal, which sent an inverted master signal to one of the West actuators. The second actuator on each girder was slaved off the first using displacement control to avoid twisting of the beams. Loading rates of 0.01 in/sec were used through the 3.0% interstory drift cycles and were increased to 0.02 in/sec for the first two cycles of 4.0%.

Increased rates of up to 0.16 in/sec were used for any remaining cycles to expedite testing.

4.2 Loading History

The SAC Phase 2 loading history (SAC, 1997) was used to ensure results could be compared to numerous other tests conducted during the SAC investigations. This load history differs from that specified in the 1997 AISC Seismic Provisions (AISC, 1997), Appendix S, which includes the requirements for qualifying cyclic beam-to-column tests. The AISC load history is based on the ATC-24 protocol (ATC, 1992), commonly used prior to the Northridge earthquake. Other load histories are permitted, however, if they can be shown to induce demands of equal severity on the tested connection. Supplement No. 1 to the Seismic Provisions (AISC, 1999b) states that the SAC loading protocol is considered an acceptable alternative to the ATC-24 protocol. The SAC Phase 2 load history differs from previous loading protocols (e.g., ATC-24) in that it is based on the interstory drift angle instead of plastic rotation levels. This is consistent with recent FEMA guidelines for seismic construction (FEMA, 2000a), which now qualify connections based on required interstory drift as opposed to required plastic rotation.

The loading history adopted in this test program is based on specified levels of interstory drift. The drift angle, θ, is defined as the lateral story displacement, Δ_{story}, divided by the story height, h_{story}. As discussed in the previous Section 4.1, however, the specimens are loaded by applying displacements to the tips of the girders. Thus, the interstory drift angle is related to the applied beam tip displacement, Δ_{tip}, by the following relation:

$$\theta = \frac{\Delta_{tip}}{\left(L_g + d_c / 2 \right)} \tag{4.1}$$

where:

L_g = girder length between loading point and column face

d_c = column depth

Table 4.1 and Figure 4.6 give the prescribed loading history. The length ($L_g + d_c/2$) is 140 in. for all specimens. This value is used to calculate the prescribed tip displacements at each drift level in Table 4.1. As an alternative to increasing the drift level to 5.0% following the two cycles at 4.0%, the SAC protocol allows for additional cycles at 4.0% until failure of the specimen or significant strength degradation occurs (SAC, 1997). This alternative was adopted for the present investigation. Anti-symmetric loading was applied to the cruciform specimens to simulate the effects of lateral loading on an interior connection. Thus, the tip displacements given in Table 4.1 were applied in equal magnitudes and opposite directions to the two girders of each specimen. Prior to the 0.375% cycles, elastic cycles of 0.1% and 0.25% drift were conducted to verify instrumentation.

4.3 Instrumentation

Extensive instrumentation, including strain gages and linear variable differential transformers (LVDTs), was used to gather information about specimen behavior in critical regions. The majority of the instrumentation was concentrated in and around the connection region of the specimens. Specific targeted regions included the panel zones (both the doubler plates and column webs, if accessible), girder flanges near the CJP welds, column flanges (both the interior and exterior faces), continuity plates, and girder webs near the bottom access holes. The instrumentation plan satisfies the minimum requirements of the SAC Protocol (SAC, 1997), and augments it in most cases.

4.3.1 Strain Gages

The strain gages were divided into six categories to identify the particular functions of the gages. These categories included: panel zone (PZ group), girder flange (GF group), column flange (CF group), column flanges for specimens without continuity plates (CFN group), continuity plate (CP group), and girder web (GW group). Depending on the specimen and data acquisition channel limitations, not all groups were used on every specimen. For example, specimen CR3, with continuity plates, does not have any CFN group gages, and is the only specimen with CP group gages.

Both uniaxial strain gages and three-element rosettes (45°/90° configuration) were used. High elongation uniaxial gages and rosettes were used wherever strains were expected to exceed 1% based on preliminary finite element analyses (Ye et al., 2000). Integral lead wire gages, manufactured by Tokyo Sokki Kenkyujo Co., Ltd., were used for both high elongation and general purpose.

Figures 4.7 through 4.21 illustrate the locations of all gages. The naming scheme for the gages identifies the location of the gage relative to the laboratory (in terms of four quadrants: Northeast, Northwest, Southeast and Southwest), the gage group to which it belongs, the type of gage, and a unique gage number. Table 4.2 outlines this nomenclature. For example, a designation of *ne_1gf_h* indicates a high-elongation gage in the Northeast quadrant of the specimen, which is part of the girder flange group.

The PZ group gages include all strain gage rosettes in the panel zones. The basic panel zone gage layout consists of eight strain gage rosettes distributed in the panel zone (e.g., see Figure 4.7). Additional rosettes are provided on the stiffened specimens, consisting of three rosettes oriented diagonally in the panel zone (e.g., see Figure 4.13) as per SAC minimum panel zone instrumentation requirements (SAC, 1997). An exception is Specimen CR3, which has two sets of the three diagonal rosettes, and no eight-rosette configuration. This was necessary to fulfill the channel requirements of the continuity plate gages on this specimen. The panel zone gages are used primarily to capture the strain distribution in the column web and doubler plates as loading progresses, and to capture the high shear strains observed at the center of panel zones.

The GF gage group includes a number of uniaxial gages placed near the toe of the girder-to-column CJP welds, as well as gages located away from the column face. Four gages are placed at the extreme fiber of each girder flange to measure the high strains expected in the connection region (see Figures 4.17 and 4.19). Three additional gages are placed on the inside face of one bottom flange near the weld to measure differences in strain through the girder flange thickness. Gages located 13 in. from the column at the center of the beam flange are used to calculate strain-based moments for verification of the load-based moments (see Figure 4.17).

The CF group consists of uniaxial gages placed on the outside face of the column near the beam flanges, as well as gages placed 12 in. above and below the connections (see Figures 4.18 and 4.19). The gages near the girder flanges are intended to capture high strains associated with localized kinking of the column flanges in this area, and to illustrate the distribution of strain along the height of the column near a girder-to-column weld. Those gages placed above and below the connections are used for calculation of strain-based column moments. These values are for comparison to load moments determined by a statics analysis of the specimen and actuator loads.

The CFN gage group is intended to investigate LFB behavior by characterizing the strain distribution on the inside face of columns near the concentrated forces delivered by the girder flanges. It consists of rosettes and uniaxial gages located along theoretical and predicted yield lines (from finite element analyses). Figure 4.20 illustrates the typical gage pattern used on Specimens CR1, CR2, and CR5. This layout is similar to those used in the pull-plate experiments (Prochnow et al., 2000a). Note that the diagonal "b" channel of the rosettes is not used in this gage group.

The CP group of Specimen CR3 consists of 21 uniaxial gages placed on one pair of continuity plates (see Figure 4.21). These gages provide a picture of the strain distribution along the length and width of the continuity plates, and are used to determine whether the plates have yielded across the full, unclipped width. This criterion was used by Prochnow et al. (2000a) to define a continuity plate limit state.

The GW group present on Specimens CR1, CR3, and CR4 (and CR4R) consists of three rosettes placed on the East girder web (e.g., Figure 4.7). These gages attempt to characterize the flow of shear force in the connection boundary region and identify localized strain concentrations near the access hole. It is known that the shear stress distribution does not follow traditional beam theory near the connection (Lee et al., 1997; Hajjar et al., 1998b; Leon et al., 1998; Ye et al., 2000).

4.3.2 Linear Variable Differential Transformers

Several Linear Variable Differential Transformers (LVDTs) were used for displacement measurements on the specimens. These were grouped similar to the strain

gages, based on location and function. Four LVDTs are used to measure the rotation of the girders, denoted as the GR group. Two are used to measure panel zone deformation (PZR group). Up to five LVDTs are used to measure column flange bending near the bottom flange of one girder (LFB group). Finally, two are used to measure lateral deflection at the top of the load frame. All LVDTs were manufactured by Schaevitz and have displacement ranges of +/- 0.1 in., +/-0.5 in., and +/- 1.0 in. Figures 4.22 through 4.24 illustrate the LVDT locations.

The four LVDTs in the GR group are placed in the center of each beam flange to measure rotation in the plastic hinge regions of the girders (see Figure 4.22). Each is attached to the face of the column and to the beam flange at a distance of 12 in. from the column face, representing a plastic hinge length of $d_g/2$. Small threaded steel blocks are tack-welded to the column flange and beam flange to facilitate attachment of the LVDTs.

The two panel zone LVDTs in the PZR group are placed diagonally in the panel zone, and are attached at the corners (see Figure 4.22). These LVDTs measure the average shear distortion of the panel zone. They are attached to the specimen by small threaded blocks tack-welded to the column web.

The LFB group LVDTs are placed on the column flange near the bottom girder flanges to measure column flange deformations relative to the column web centerline. For Specimens CR1, CR2, and CR5, five LVDTs are placed as shown in Figure 4.23. For Specimens CR4 and CR4R, however, only four LVDTs are placed. The illustration of the LVDT placement for Specimens CR4 and CR4R is presented in Figure 4.24. The LFB group LVDTs were anchored to the web centerline as opposed to the other column flange because the compressive force on the opposite flange offsets some of the displacement produced by the tensile force on the flange of interest.

Two LVDTs are also used to measure the lateral deflection of the load frame assembly (see Figure 4.25). The first is attached to the center of a W24x104 crossbeam at a height corresponding to the centerline of the top pin. This LVDT measures the overall deflection of the load frame. A second LVDT is placed between the crossbeam and the top pin to measure any relative displacement between the top pin and the load

frame. The summation of the two LVDT measurements represents the total lateral displacement of the top of the test specimen relative to the laboratory floor.

4.3.3 Specimen Coordinate System and Gage Locations

A coordinate system was established to define the position of all strain gages in terms of an *x*-*y*-*z* coordinate space. Five axes were used to identify the gage locations based on the orientation of the specimens in the laboratory (see Figure 4.26). The two *x*-axes (x_{north} and x_{south}) run perpendicular to the girders of the specimens. The *z*-axes (z_{east} and z_{west}) run parallel to the girders. The *y*-axis is parallel to the column. The origin of this coordinate system is the centroid of the column cross section at the level of the extreme fiber of the girder bottom flanges. Three of the five axes are needed to identify each unique gage location.

Tables 4.3 through 4.8 show the coordinates of all strain gages on the tested six specimens. All values are in inches.

Table 4.1: General Specimen Loading History

Load Level	θ	No. Cycles	Δ_{tip} (in.)
1	0.00375	6	0.53
2	0.005	6	0.70
3	0.0075	6	1.05
4	0.01	4	1.40
5	0.015	2	2.10
6	0.02	2	2.80
7	0.03	2	4.20
8	0.04	2	5.60

Table 4.2: Definitions of Strain Gage Label Nomenclature

Gage Location	Gage Group	Gage Type
ne = Northeast	*cf* = column flange	*g* = general purpose gage
se = Southeast	*cfn* = column flange (unstiffened)	*gr* = general purpose rosette
nw = Northwest	*cp* = continuity plate	*h* = high-elongation gage
sw = Southwest	*gf* = girder flange	*hr* = high-elongation rosette
	gw = girder web	
	pz = panel zone	

Table 4.3: Specimen CR1 Strain Gage Locations

GF Gages	x_{north}	y	z_{east}
ne_1gf_h	0.00	0.00	9.87
ne_2gf_h	2.25	0.00	9.87
ne_3gf_h	3.50	0.00	9.87
ne_4gf_h	0.00	0.88	9.87
ne_5gf_h	2.25	0.88	9.87
ne_6gf_h	3.50	0.88	9.87
ne_7gf_h	0.00	24.31	9.87
ne_8gf_h	2.25	24.31	9.87
ne_9gf_h	3.50	24.31	9.87
ne_10gf_g	0.00	0.00	21.37
ne_11gf_g	0.00	24.31	21.37

GF Gages	x_{south}	y	z_{west}
sw_1gf_h	0.00	0.00	9.87
sw_2gf_h	2.25	0.00	9.87
sw_3gf_h	3.50	0.00	9.87
sw_4gf_h	0.00	24.31	9.87
sw_5gf_h	2.25	24.31	9.87
sw_6gf_h	3.50	24.31	9.87
sw_7gf_g	0.00	0.00	21.27
sw_8gf_g	0.00	24.31	21.37

GF Gages	x_{north}	y	z_{west}
nw_1gf_h	3.50	0.00	9.87
nw_2gf_h	3.50	24.31	9.87

GF Gages	x_{south}	y	z_{east}
se_1gf_h	3.50	0.00	9.87
se_2gf_h	3.50	24.31	9.87

CFN Gages	x_{north}	y	z_{east}
ne_1cfn_g	2.50	-11.56	6.30
ne_2cfn_gr	2.50	-5.56	6.30
ne_3cfn_gr	2.50	-1.56	6.30
ne_4cfn_gr	2.50	0.44	6.30
ne_5cfn_gr	3.75	0.44	6.30
ne_6cfn_gr	5.00	0.44	6.30
ne_7cfn_g	5.81	-7.56	6.30
ne_8cfn_g	3.56	-3.56	6.30

PZ Gages	x_{north}	y	z_{east}
ne_1pz_gr	0.65	2.15	5.00
ne_2pz_hr	0.65	7.15	2.50
ne_3pz_hr	0.65	12.15	0.00
ne_4pz_hr	0.65	17.15	0.00
ne_5pz_gr	0.65	22.15	0.00

PZ Gages	x_{north}	y	z_{west}
nw_1pz_hr	0.65	12.15	2.50
nw_2pz_hr	0.65	12.15	5.00
nw_3pz_gr	0.65	22.15	5.00

CF Gages	x_{north}	y	z_{east}
ne_1cf_g	6.56	-11.56	8.37
ne_2cf_g	6.56	-5.56	8.37
ne_3cf_g	6.56	-1.56	8.37
ne_4cf_h	6.56	0.44	8.37
ne_5cf_g	6.56	2.44	8.37
ne_6cf_g	6.56	6.44	8.37
ne_7cf_g	6.56	35.87	8.37

CF Gages	x_{north}	y	z_{west}
nw_1cf_g	6.56	-11.56	8.37
nw_2cf_g	6.56	35.87	8.37

CF Gages	x_{south}	y	z_{east}
se_1cf_g	6.56	-11.56	8.37
se_2cf_h	6.56	0.44	8.37
se_3cf_g	6.56	35.87	8.37

CF Gages	x_{south}	y	z_{west}
sw_1cf_g	6.56	-11.56	8.37
sw_2cf_g	6.56	35.87	8.37

GW Gages	x_{south}	y	z_{east}
se_1gw_hr	0.26	1.88	12.87
se_2gw_hr	0.26	3.25	9.62
se_3gw_gr	0.26	12.15	9.62

Table 4.4: Specimen CR2 Strain Gage Locations

GF Gages	x_{north}	y	z_{east}
ne_1gf_h	0.00	0.00	9.24
ne_2gf_h	2.25	0.00	9.24
ne_3gf_h	3.50	0.00	9.24
ne_4gf_h	0.00	0.88	9.24
ne_5gf_h	2.25	0.88	9.24
ne_6gf_h	3.50	0.88	9.24
ne_7gf_h	0.00	24.31	9.24
ne_8gf_h	2.25	24.31	9.24
ne_9gf_h	3.50	24.31	9.24
ne_10gf_g	0.00	0.00	20.74
ne_11gf_g	0.00	24.31	20.74

GF Gages	x_{south}	y	z_{west}
sw_1gf_h	0.00	0.00	9.24
sw_2gf_h	2.25	0.00	9.24
sw_3gf_h	3.50	0.00	9.24
sw_4gf_h	0.00	24.31	9.24
sw_5gf_h	2.25	24.31	9.24
sw_6gf_h	3.50	24.31	9.24
sw_7gf_g	0.00	0.00	20.74
sw_8gf_g	0.00	24.31	20.74

GF Gages	x_{north}	y	z_{west}
nw_1gf_h	3.50	0.00	9.24
nw_2gf_h	3.50	24.31	9.24

GF Gages	x_{south}	y	z_{east}
se_1gf_h	3.50	0.00	9.24
se_2gf_h	3.50	24.31	9.24

CFN Gages	x_{north}	y	z_{east}
ne_1cfn_g	2.50	-11.56	6.30
ne_2cfn_gr	2.50	-5.56	6.30
ne_3cfn_gr	2.50	-1.56	6.30
ne_4cfn_gr	2.50	0.44	6.30
ne_5cfn_gr	3.75	0.44	6.30
ne_6cfn_gr	5.00	0.44	6.30
ne_7cfn_g	5.61	-7.56	6.30
ne_8cfn_g	3.36	-3.56	6.30

PZ Gages	x_{north}	y	z_{east}
ne_apz_gr	0.45	22.15	5.00
ne_bpz_hr	0.45	12.15	0.00

PZ Gages	x_{north}	y	z_{west}
nw_cpz_gr	0.45	2.15	5.00

PZ Gages	x_{south}	y	z_{east}
se_1pz_gr	1.95	2.15	5.00
se_2pz_hr	1.95	7.15	2.50

PZ Gages	x_{south}	y	z_{west}
sw_1pz_hr	1.95	12.15	2.50
sw_2pz_hr	1.95	12.15	5.00
sw_3pz_gr	1.95	22.15	5.00
sw_3pz_hr	1.95	12.15	0.00
sw_4pz_hr	1.95	17.15	0.00
sw_5pz_gr	1.95	22.15	0.00

CF Gages	x_{north}	y	z_{east}
ne_1cf_g	6.36	-11.56	7.74
ne_2cf_g	6.36	-5.56	7.74
ne_3cf_g	6.36	-1.56	7.74
ne_4cf_h	6.36	0.44	7.74
ne_5cf_g	6.36	2.44	7.74
ne_6cf_g	6.36	6.44	7.74
ne_7cf_g	NA	NA	NA

CF Gages	x_{north}	y	z_{west}
nw_1cf_g	6.36	-11.56	7.74
nw_2cf_g	NA	NA	NA

CF Gages	x_{south}	y	z_{east}
se_1cf_g	6.36	-11.56	7.74
se_2cf_h	6.36	0.44	7.74
se_3cf_g	NA	NA	NA

CF Gages	x_{south}	y	z_{west}
sw_1cf_g	6.36	-11.56	7.74
sw_2cf_g	NA	NA	NA

GW Gages	x_{north}	y	z_{west}
nw_1gw_hr	0.26	1.88	12.24

Table 4.5: Specimen CR3 Strain Gage Locations

GF Gages	x_{north}	y	z_{east}
ne_1gf_h	0.00	0.00	9.11
ne_2gf_h	2.25	0.00	9.11
ne_3gf_h	3.50	0.00	9.11
ne_4gf_h	0.00	0.88	9.11
ne_5gf_h	2.25	0.88	9.11
ne_6gf_h	3.50	0.88	9.11
ne_7gf_h	0.00	24.31	9.11
ne_8gf_h	2.25	24.31	9.11
ne_9gf_h	3.50	24.31	9.11
ne_10gf_g	0.00	0.00	20.61
ne_11gf_g	0.00	24.31	20.61

GF Gages	x_{south}	y	z_{west}
sw_1gf_h	0.00	0.00	9.11
sw_2gf_h	2.25	0.00	9.11
sw_3gf_h	3.50	0.00	9.11
sw_4gf_h	0.00	24.31	9.11
sw_5gf_h	2.25	24.31	9.11
sw_6gf_h	3.50	24.31	9.11
sw_7gf_g	0.00	0.00	20.61
sw_8gf_g	0.00	24.31	20.61

GF Gages	x_{north}	y	z_{west}
nw_1gf_h	3.50	0.00	9.11
nw_2gf_h	3.50	24.31	9.11

GF Gages	x_{south}	y	z_{east}
se_1gf_h	3.50	0.00	9.11
se_2gf_h	3.50	24.31	9.11

PZ Gages	x_{north}	y	z_{east}
ne_1pz_gr	1.79	22.15	5.00
ne_2pz_hr	1.79	12.15	0.00

PZ Gages	x_{north}	y	z_{west}
nw_1pz_gr	1.79	2.15	5.00

PZ Gages	x_{south}	y	z_{east}
se_1pz_gr	1.79	2.15	5.00

PZ Gages	x_{south}	y	z_{west}
sw_3pz_gr	1.79	22.15	5.00
sw_3pz_hr	1.79	12.15	0.00

CF Gages	x_{north}	y	z_{east}
ne_1cf_g	6.33	-11.56	7.61
ne_2cf_g	6.33	-5.56	7.61
ne_3cf_g	6.33	-1.56	7.61
ne_4cf_h	6.33	0.44	7.61
ne_5cf_g	6.33	2.44	7.61
ne_6cf_g	6.33	6.44	7.61
ne_7cf_g	NA	NA	NA

CF Gages	x_{north}	y	z_{west}
nw_1cf_g	6.33	-11.56	7.61
nw_2cf_g	NA	NA	NA

CF Gages	x_{south}	y	z_{east}
se_1cf_g	6.33	-11.56	7.61
se_2cf_h	6.33	0.44	7.61
se_3cf_g	NA	NA	NA

CF Gages	x_{south}	y	z_{west}
sw_1cf_g	6.33	-11.56	7.61
sw_2cf_g	NA	NA	NA

GW Gages	x_{north}	y	z_{east}
ne_1gw_hr	0.26	1.88	12.11
ne_2gw_hr	0.26	3.25	8.86
ne_3gw_gr	0.26	12.15	8.86

CP Gages	x_{north}	y	z_{east}
cp1	5.75	24.31	5.55
cp2	4.50	24.31	5.55
cp3	3.50	24.31	5.55
cp4	5.75	24.31	4.80
cp5	4.50	24.31	4.80
cp6	3.50	24.31	4.80
cp7	2.25	24.31	4.80
cp8	5.75	24.31	1.50
cp9	3.50	24.31	1.50
cp10	2.25	24.31	1.50
cp11	5.75	24.31	-5.55
cp12	3.50	24.31	-5.55
cp13	-3.50	24.31	5.55
cp14	-5.75	24.31	5.55
cp15	-2.25	24.31	-4.80
cp16	-3.50	24.31	-4.80
cp17	-4.50	24.31	-4.80
cp18	-5.75	24.31	-4.80

Table 4.6: Specimen CR4 Strain Gage Locations

GF Gages	x_{north}	y	z_{east}
ne_1gf_h	0.00	0.00	9.11
ne_2gf_h	2.25	0.00	9.11
ne_3gf_h	3.50	0.00	9.11
ne_4gf_h	0.00	0.88	9.11
ne_5gf_h	2.25	0.88	9.11
ne_6gf_h	3.50	0.88	9.11
ne_7gf_h	0.00	24.31	9.11
ne_8gf_h	2.25	24.31	9.11
ne_9gf_h	3.50	24.31	9.11
ne_10gf_g	0.00	0.00	20.61
ne_11gf_g	0.00	24.31	20.61

GF Gages	x_{south}	y	z_{west}
sw_1gf_h	0.00	0.00	9.11
sw_2gf_h	2.25	0.00	9.11
sw_3gf_h	3.50	0.00	9.11
sw_4gf_h	0.00	24.31	9.11
sw_5gf_h	2.25	24.31	9.11
sw_6gf_h	3.50	24.31	9.11
sw_7gf_g	0.00	0.00	20.61
sw_8gf_g	0.00	24.31	20.61

GF Gages	x_{north}	y	z_{west}
nw_1gf_h	3.50	0.00	9.11
nw_2gf_h	3.50	24.31	9.11

GF Gages	x_{south}	y	z_{east}
se_1gf_h	3.50	0.00	9.11
se_2gf_h	3.50	24.31	9.11

PZ Gages	x_{north}	y	z_{east}
ne_1pz_gr	3.17	2.15	5.00
ne_2pz_hr	3.17	7.15	2.50
ne_3pz_hr	3.17	12.15	0.00
ne_4pz_hr	3.17	17.15	0.00
ne_5pz_gr	3.17	22.15	0.00
ne_6pz_gr	0.42	2.15	5.00
ne_7pz_hr	0.42	12.15	0.00

PZ Gages	x_{north}	y	z_{west}
nw_1pz_hr	3.17	12.15	2.50
nw_2pz_hr	3.17	12.15	5.00
nw_3pz_gr	3.17	22.15	5.00
nw_4pz_gr	0.42	22.15	5.00

PZ Gages	x_{south}	y	z_{east}
se_1pz_gr	3.17	2.15	5.00
se_2pz_hr	3.17	12.15	0.00
se_3pz_gr	0.42	2.15	5.00
se_4pz_hr	0.42	12.15	0.00

PZ Gages	x_{south}	y	z_{west}
sw_1pz_gr	3.17	22.15	5.00
sw_2pz_gr	0.42	22.15	5.00

CF Gages	x_{north}	y	z_{east}
ne_1cf_g	6.33	-11.56	7.61
ne_2cf_g	6.33	-5.56	7.61
ne_3cf_g	6.33	-1.56	7.61
ne_4cf_h	6.33	0.44	7.61
ne_5cf_g	6.33	2.44	7.61
ne_6cf_g	6.33	6.44	7.61
ne_7cf_g	6.33	35.87	7.61

CF Gages	x_{north}	y	z_{west}
nw_1cf_g	6.33	-11.56	7.61
nw_2cf_g	6.33	35.87	7.61

CF Gages	x_{south}	y	z_{east}
se_1cf_g	6.33	-11.56	7.61
se_2cf_h	6.33	0.44	7.61
se_3cf_g	6.33	35.87	7.61

CF Gages	x_{south}	y	z_{west}
sw_1cf_g	6.33	-11.56	7.61
sw_2cf_g	6.33	35.87	7.61

GW Gages	x_{south}	y	z_{east}
se_1gw_hr	0.26	1.88	12.11
se_2gw_hr	0.26	3.25	8.86
se_3gw_gr	0.26	12.15	8.86

Table 4.7: Specimen CR4R Strain Gage Locations

GF Gages	x_{north}	y	z_{east}
ne_1gf_h	0.00	0.00	9.11
ne_2gf_h	2.25	0.00	9.11
ne_3gf_h	3.50	0.00	9.11
ne_4gf_h	0.00	0.88	9.11
ne_5gf_h	2.25	0.88	9.11
ne_6gf_h	3.50	0.88	9.11
ne_7gf_h	0.00	24.31	9.11
ne_8gf_h	2.25	24.31	9.11
ne_9gf_h	3.50	24.31	9.11
ne_10gf_g	0.00	0.00	20.61
ne_11gf_g	0.00	24.31	20.61

GF Gages	x_{south}	y	z_{west}
sw_1gf_h	0.00	0.00	9.11
sw_2gf_h	2.25	0.00	9.11
sw_3gf_h	3.50	0.00	9.11
sw_4gf_h	0.00	24.31	9.11
sw_5gf_h	2.25	24.31	9.11
sw_6gf_h	3.50	24.31	9.11
sw_7gf_g	0.00	0.00	20.61
sw_8gf_g	0.00	24.31	20.61

GF Gages	x_{north}	y	z_{west}
nw_1gf_h	3.50	0.00	9.11
nw_2gf_h	3.50	24.31	9.11

GF Gages	x_{south}	y	z_{east}
se_1gf_h	3.50	0.00	9.11
se_2gf_h	3.50	24.31	9.11

PZ Gages	x_{north}	y	z_{east}
ne_1pz_gr	3.17	22.15	5.00
ne_2pz_hr	3.17	12.15	0.00
ne_apz_gr	0.42	22.15	5.00
ne_bpz_hr	0.42	12.15	0.00

PZ Gages	x_{north}	y	z_{west}
nw_1pz_gr	3.17	2.15	5.00
nw_cpz_gr	0.42	2.15	5.00

PZ Gages	x_{south}	y	z_{east}
se_1pz_gr	3.17	2.15	5.00
se_2pz_hr	3.17	7.15	2.50
se_bpz_hr	0.42	12.15	0.00
se_cpz_gr	0.42	2.15	5.00

PZ Gages	x_{south}	y	z_{west}
sw_1pz_hr	3.17	12.15	2.50
sw_2pz_hr	3.17	12.15	5.00
sw_3pz_gr	3.17	22.15	5.00
sw_3pz_hr	3.17	12.15	0.00
sw_4pz_hr	3.17	17.15	0.00
sw_5pz_gr	3.17	22.15	0.00
sw_apz_gr	0.42	22.15	5.00

CF Gages	x_{north}	y	z_{east}
ne_1cf_g	6.33	-11.56	7.61
ne_2cf_g	6.33	-5.56	7.61
ne_3cf_g	6.33	-1.56	7.61
ne_4cf_h	6.33	0.44	7.61
ne_5cf_g	6.33	2.44	7.61
ne_6cf_g	6.33	6.44	7.61
ne_7cf_g	NA	NA	NA

CF Gages	x_{north}	y	z_{west}
nw_1cf_g	6.33	-11.56	7.61
nw_2cf_g	NA	NA	NA

CF Gages	x_{south}	y	z_{east}
se_1cf_g	6.33	-11.56	7.61
se_2cf_h	6.33	0.44	7.61
se_3cf_g	NA	NA	NA

CF Gages	x_{south}	y	z_{west}
sw_1cf_g	6.33	-11.56	7.61
sw_2cf_g	NA	NA	NA

GW Gages	x_{north}	y	z_{east}
ne_1gw_hr	0.26	1.88	12.11
ne_2gw_hr	0.26	3.25	8.86
ne_3gw_gr	0.26	12.15	8.86

Table 4.8: Specimen CR5 Strain Gage Locations

GF Gages	x_{north}	y	z_{east}
ne_1gf_h	0.00	0.00	8.89
ne_2gf_h	2.25	0.00	8.89
ne_3gf_h	3.50	0.00	8.89
ne_4gf_h	0.00	0.88	8.89
ne_5gf_h	2.25	0.88	8.89
ne_6gf_h	3.50	0.88	8.89
ne_7gf_h	0.00	24.31	8.89
ne_8gf_h	2.25	24.31	8.89
ne_9gf_h	3.50	24.31	8.89
ne_10gf_g	0.00	0.00	20.39
ne_11gf_g	0.00	24.31	20.39

GF Gages	x_{south}	y	z_{west}
sw_1gf_h	0.00	0.00	8.89
sw_2gf_h	2.25	0.00	8.89
sw_3gf_h	3.50	0.00	8.89
sw_4gf_h	0.00	24.31	8.89
sw_5gf_h	2.25	24.31	8.89
sw_6gf_h	3.50	24.31	8.89
sw_7gf_g	0.00	0.00	20.39
sw_8gf_g	0.00	24.31	20.39

GF Gages	x_{north}	y	z_{west}
nw_1gf_h	3.50	0.00	8.89
nw_2gf_h	3.50	24.31	8.89

GF Gages	x_{south}	y	z_{east}
se_1gf_h	3.50	0.00	8.89
se_2gf_h	3.50	24.31	8.89

CFN Gages	x_{north}	y	z_{east}
ne_1cfn_g	2.50	-11.56	6.66
ne_2cfn_gr	2.50	-5.56	6.66
ne_3cfn_gr	2.50	-1.56	6.66
ne_4cfn_gr	2.50	0.44	6.66
ne_5cfn_gr	3.75	0.44	6.66
ne_6cfn_gr	5.00	0.44	6.66
ne_7cfn_g	5.50	-7.56	6.66
ne_8cfn_g	3.25	-3.56	6.66

PZ Gages	x_{north}	y	z_{east}
ne_1pz_gr	1.22	22.15	5.00
ne_2pz_hr	1.22	12.15	0.00

PZ Gages	x_{north}	y	z_{west}
nw_1pz_gr	1.22	2.15	5.00

PZ Gages	x_{south}	y	z_{east}
se_1pz_gr	1.22	2.15	5.00
se_2pz_hr	1.22	7.15	2.50

PZ Gages	x_{south}	y	z_{west}
sw_1pz_hr	1.22	12.15	2.50
sw_2pz_hr	1.22	12.15	5.00
sw_3pz_gr	1.22	22.15	5.00
sw_3pz_hr	1.22	12.15	0.00
sw_4pz_hr	1.22	17.15	0.00
sw_5pz_gr	1.22	22.15	0.00

CF Gages	x_{north}	y	z_{east}
ne_1cf_g	6.25	-11.56	7.39
ne_2cf_g	6.25	-5.56	7.39
ne_3cf_g	6.25	-1.56	7.39
ne_4cf_h	6.25	0.44	7.39
ne_5cf_g	6.25	2.44	7.39
ne_6cf_g	6.25	6.44	7.39
ne_7cf_g	NA	NA	NA

CF Gages	x_{north}	y	z_{west}
nw_1cf_g	6.25	-11.56	7.39
nw_2cf_g	NA	NA	NA

CF Gages	x_{south}	y	z_{east}
se_1cf_g	6.25	-11.56	7.39
se_2cf_h	6.25	0.44	7.39
se_3cf_g	NA	NA	NA

CF Gages	x_{south}	y	z_{west}
sw_1cf_g	6.25	-11.56	7.39
sw_2cf_g	NA	NA	NA

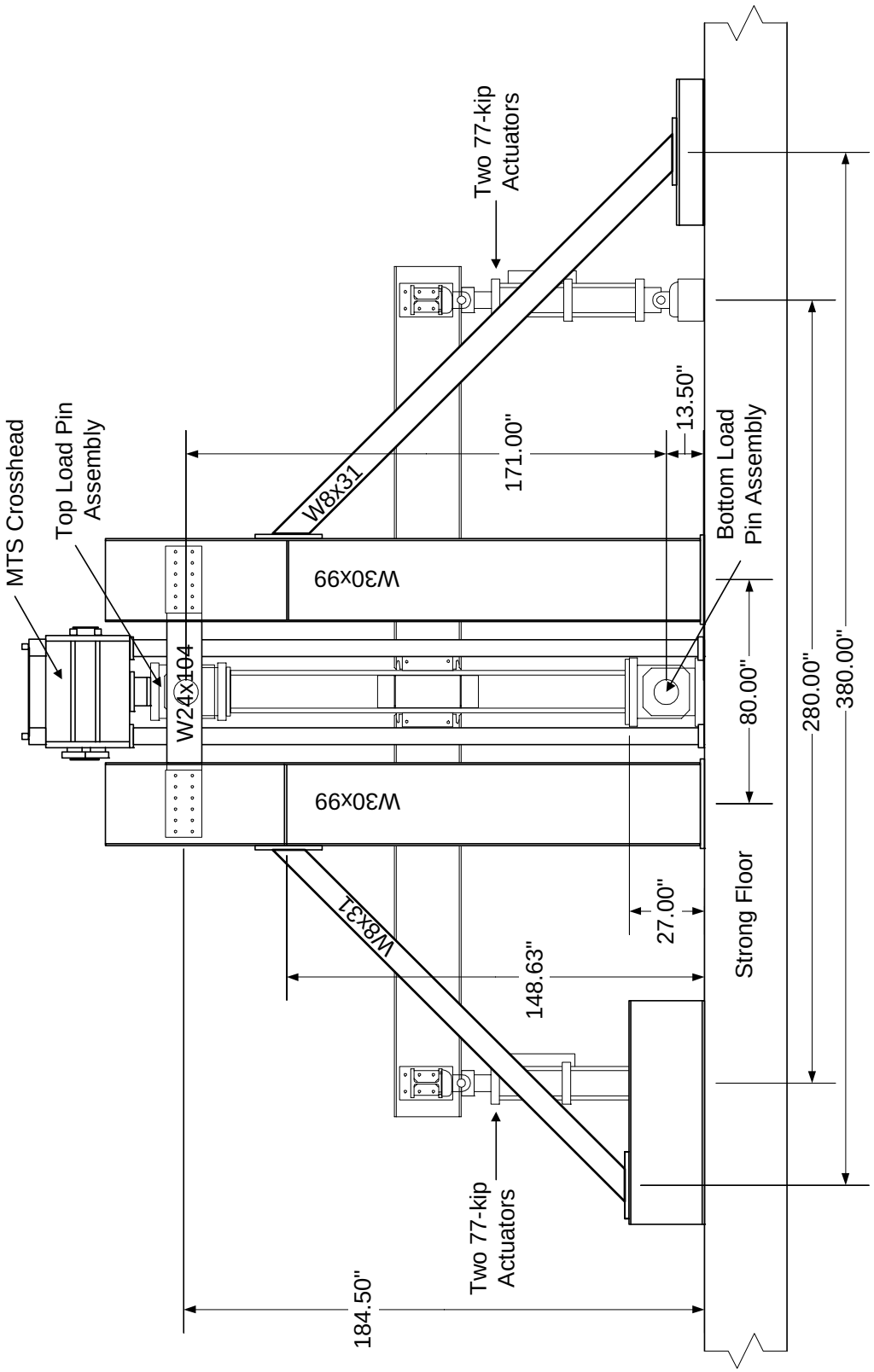


Figure 4.1: Load Frame Elevation With Specimen

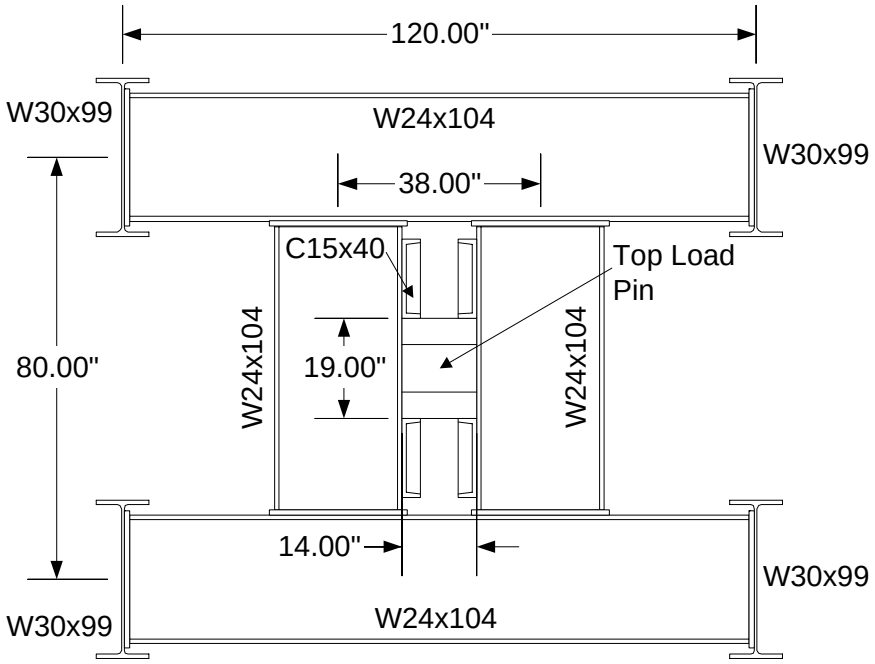


Figure 4.2: Top View of Load Frame and Load Pin



Figure 4.3: Lateral-Torsional Buckling Bracing



Figure 4.4: Bottom Load Pin Assembly

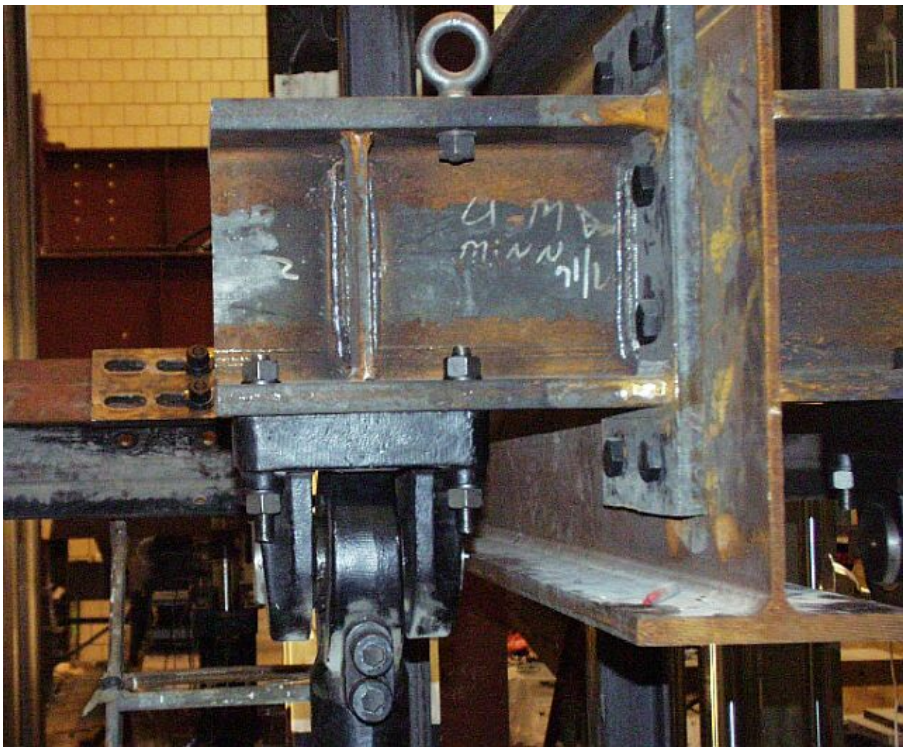


Figure 4.5: Actuator Bracket Showing Connection to Girder and Top of Actuator

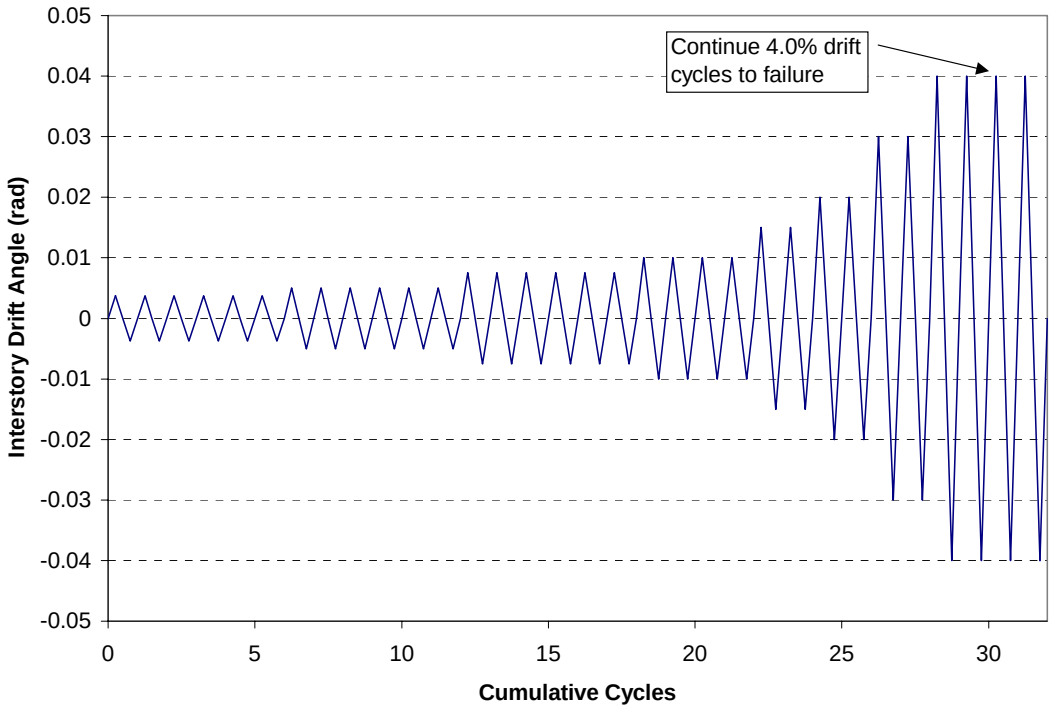


Figure 4.6: General Specimen Loading History: Drift Level vs. Cumulative Cycles

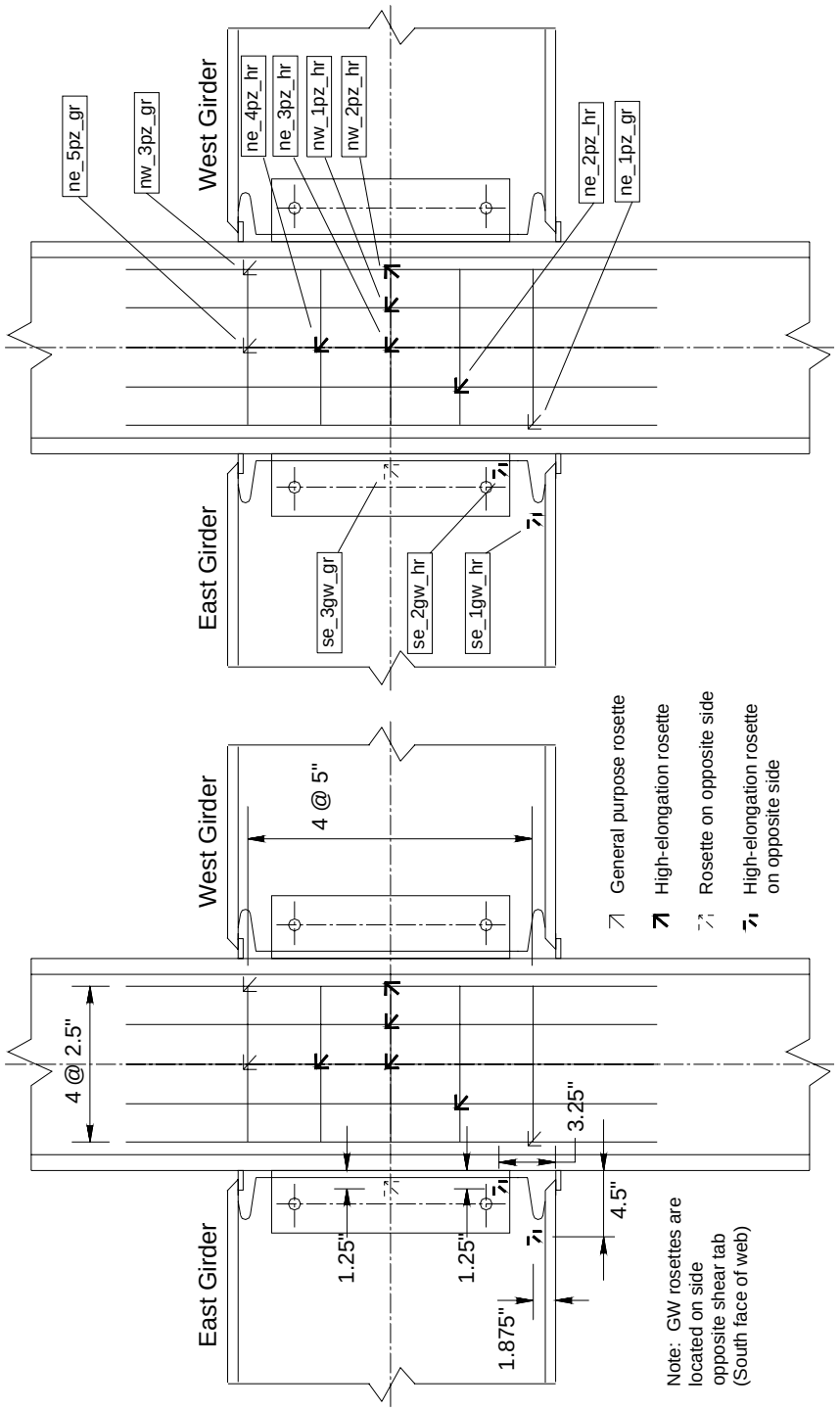


Figure 4.7: Panel Zone and Girder Web Instrumentation for Specimen CR1

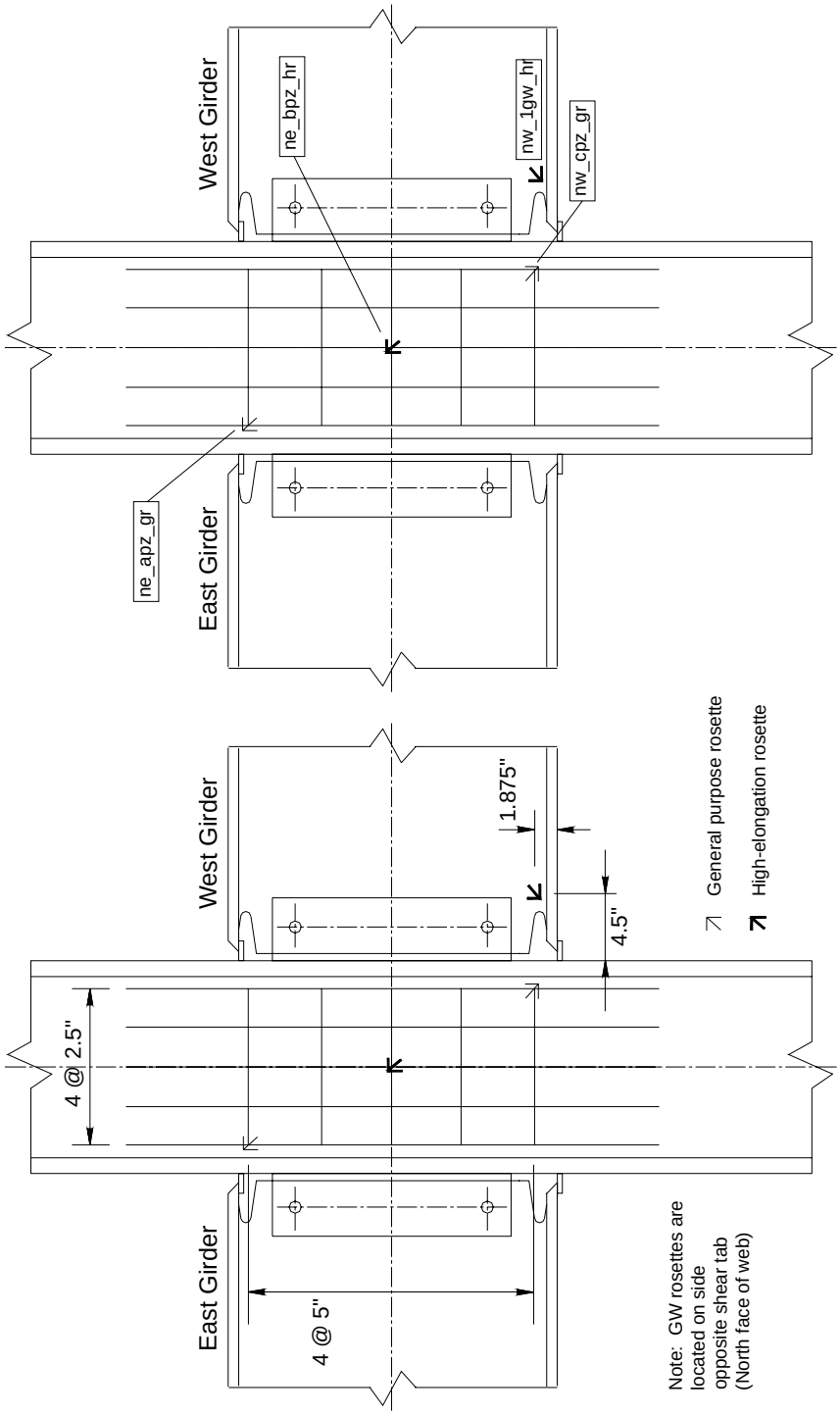


Figure 4.8: Panel Zone and Girder Web Instrumentation for Specimen CR2

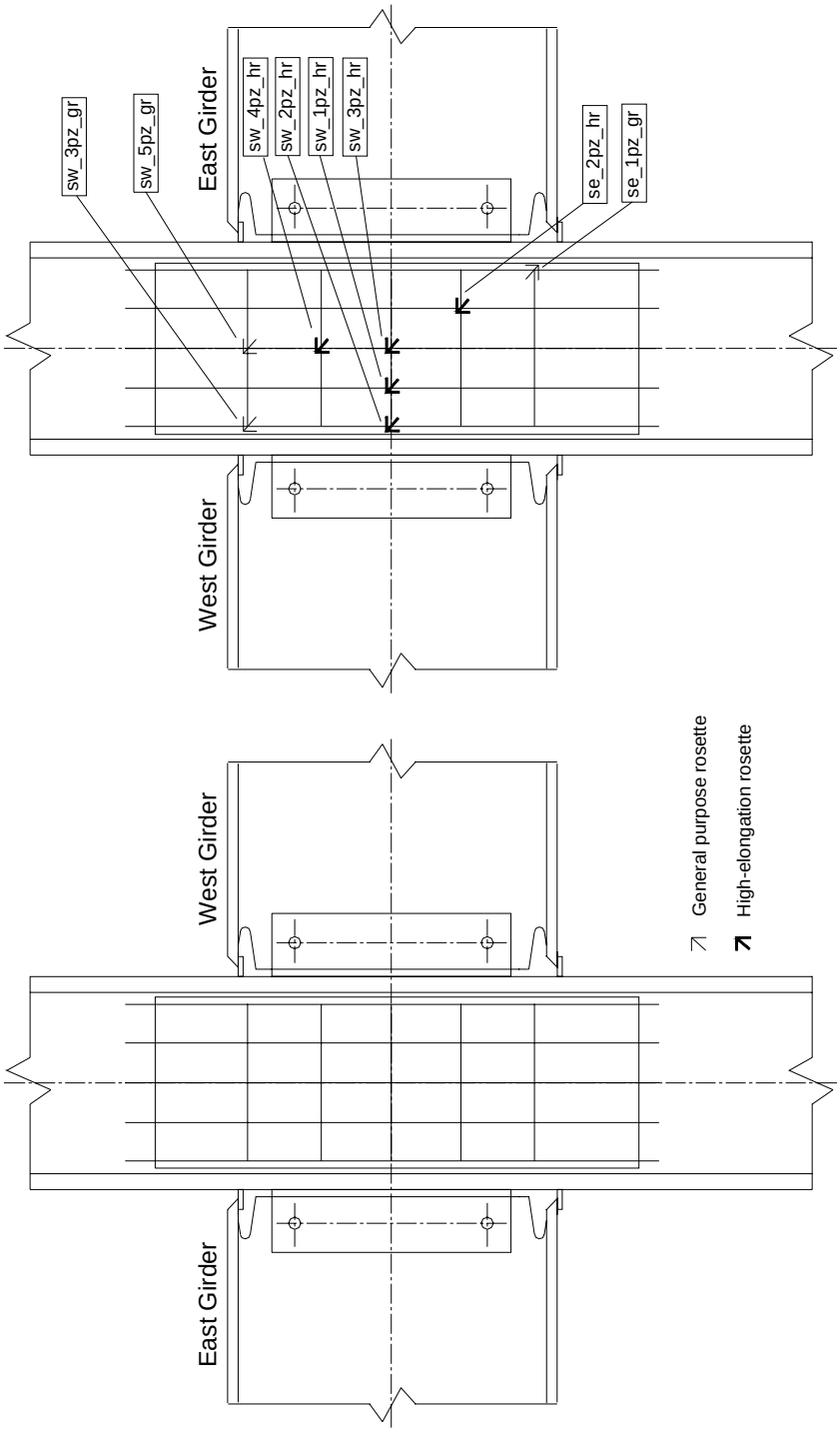


Figure 4.9: Doubler Plate Instrumentation for Specimen CR2

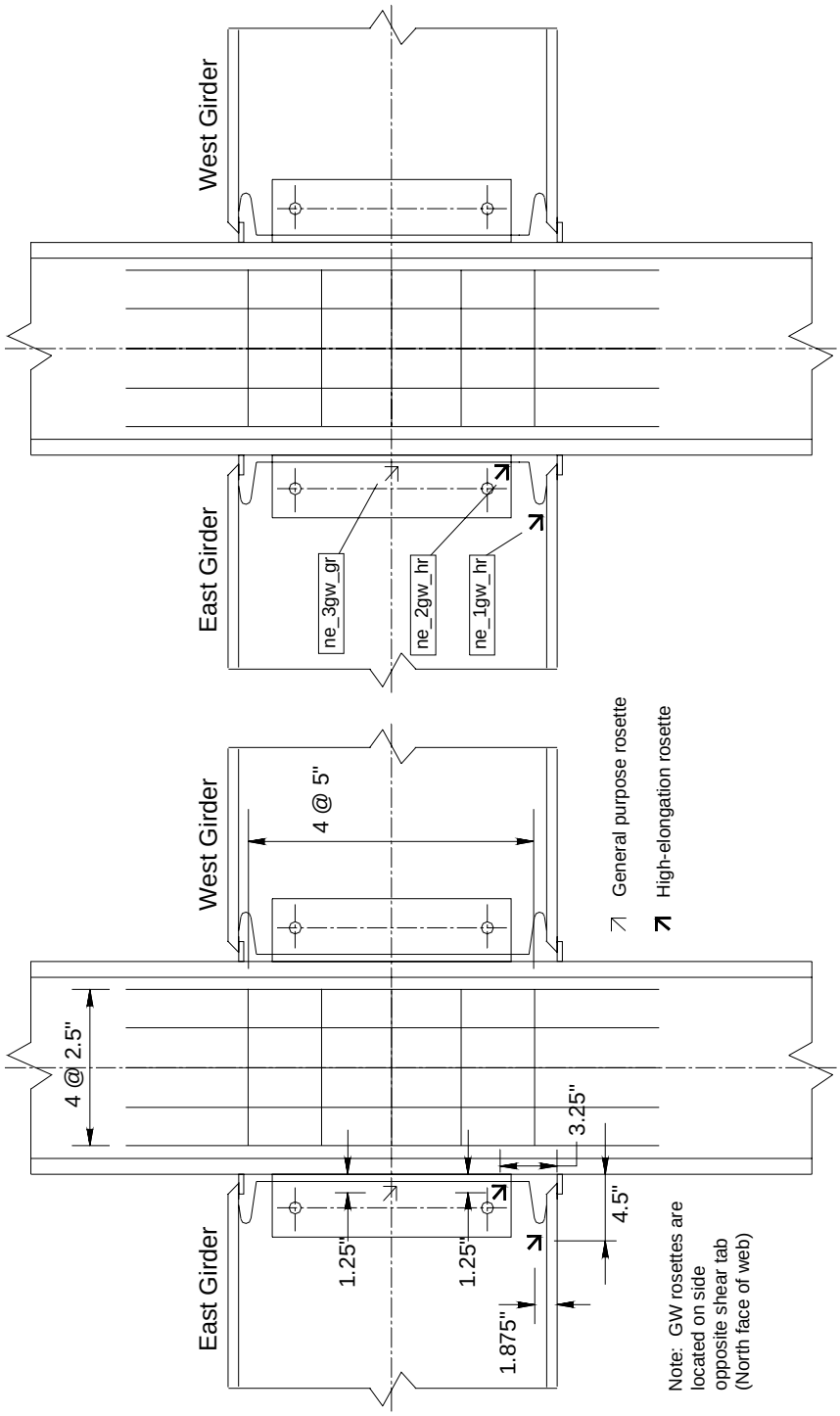


Figure 4.10: Panel Zone and Girder Web Instrumentation for Specimen CR3

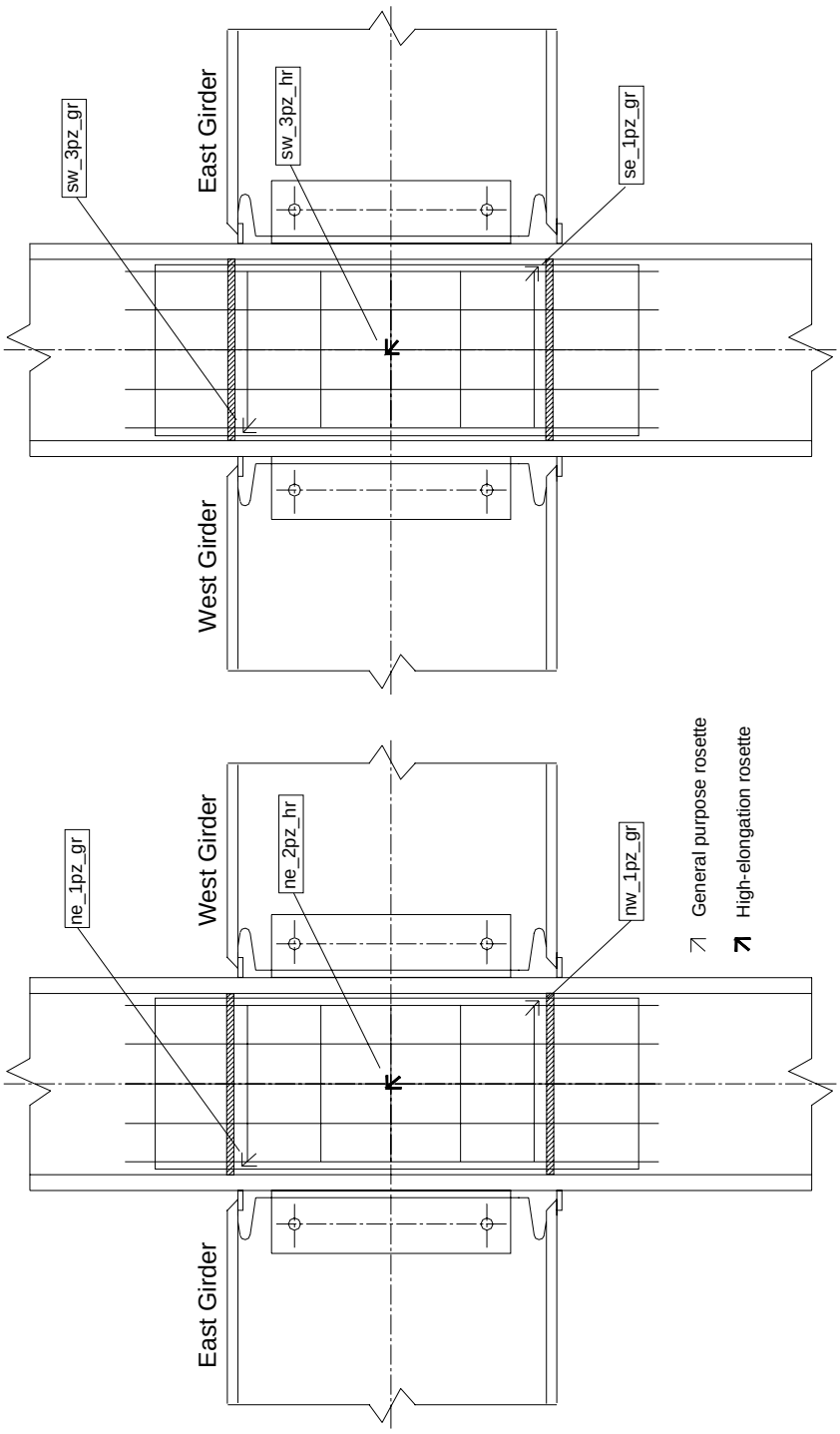


Figure 4.11: Doubler Plate Instrumentation for Specimen CR3

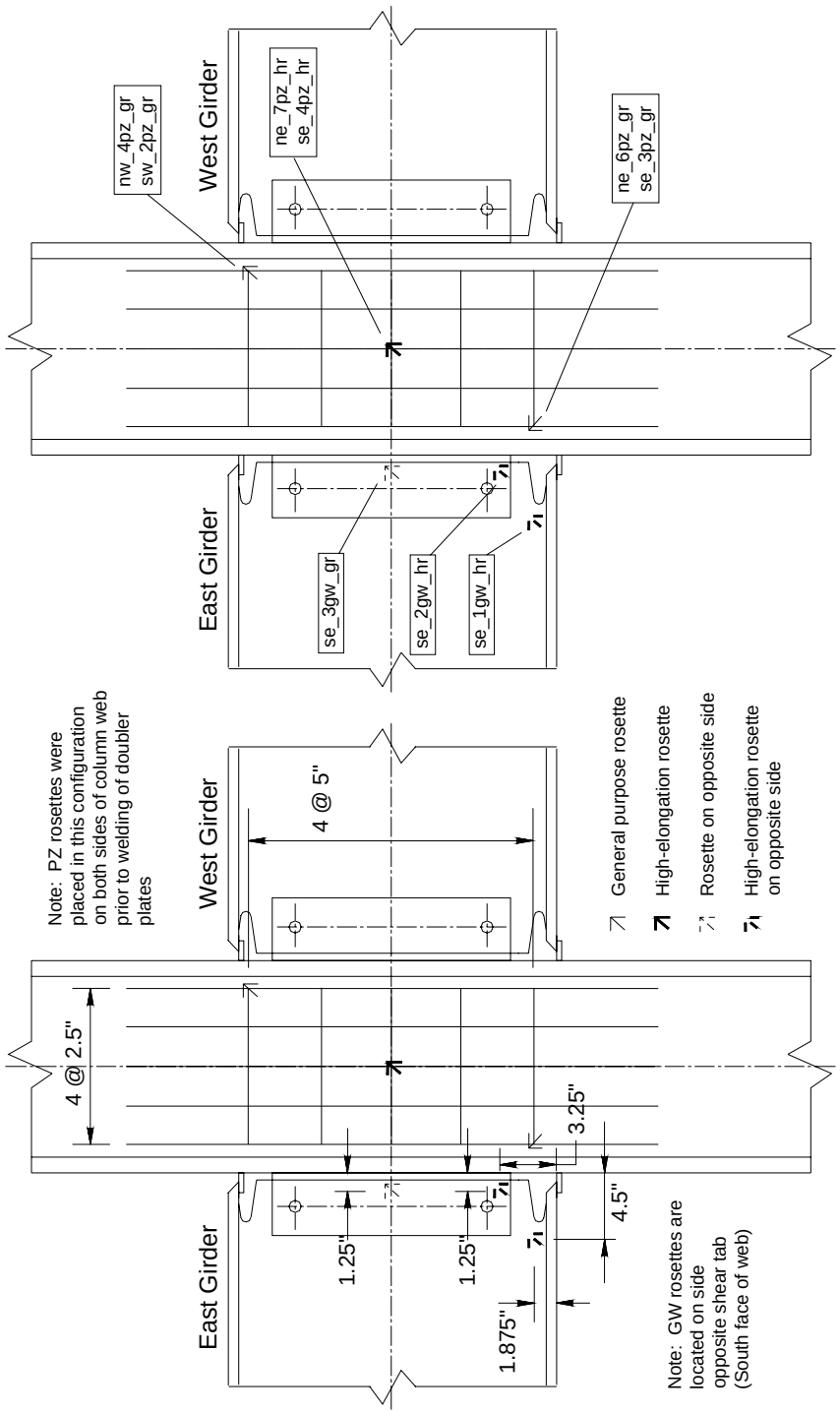


Figure 4.12: Panel Zone and Girder Web Instrumentation for Specimen CR4

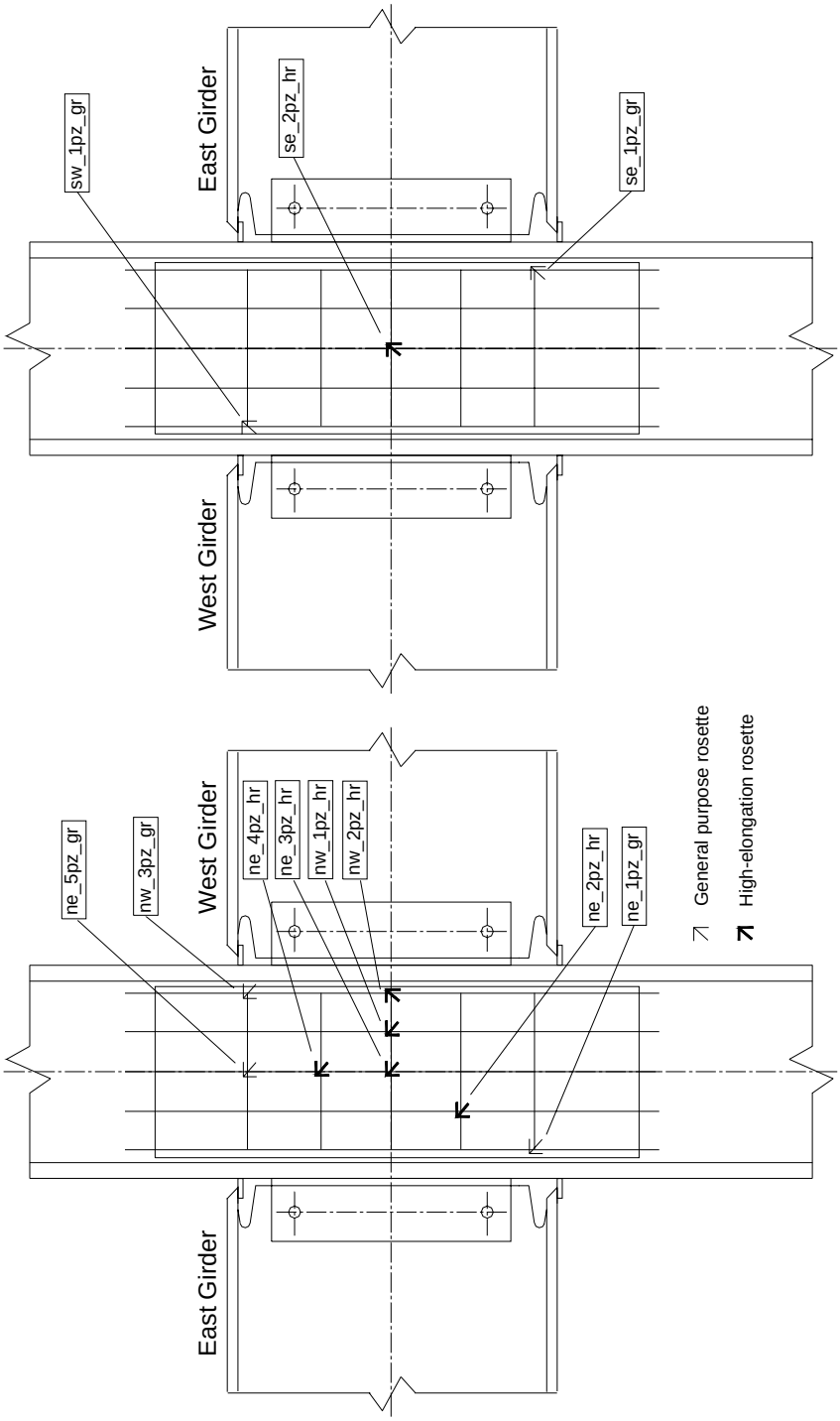


Figure 4.13: Doubler Plate Instrumentation for Specimen CR4

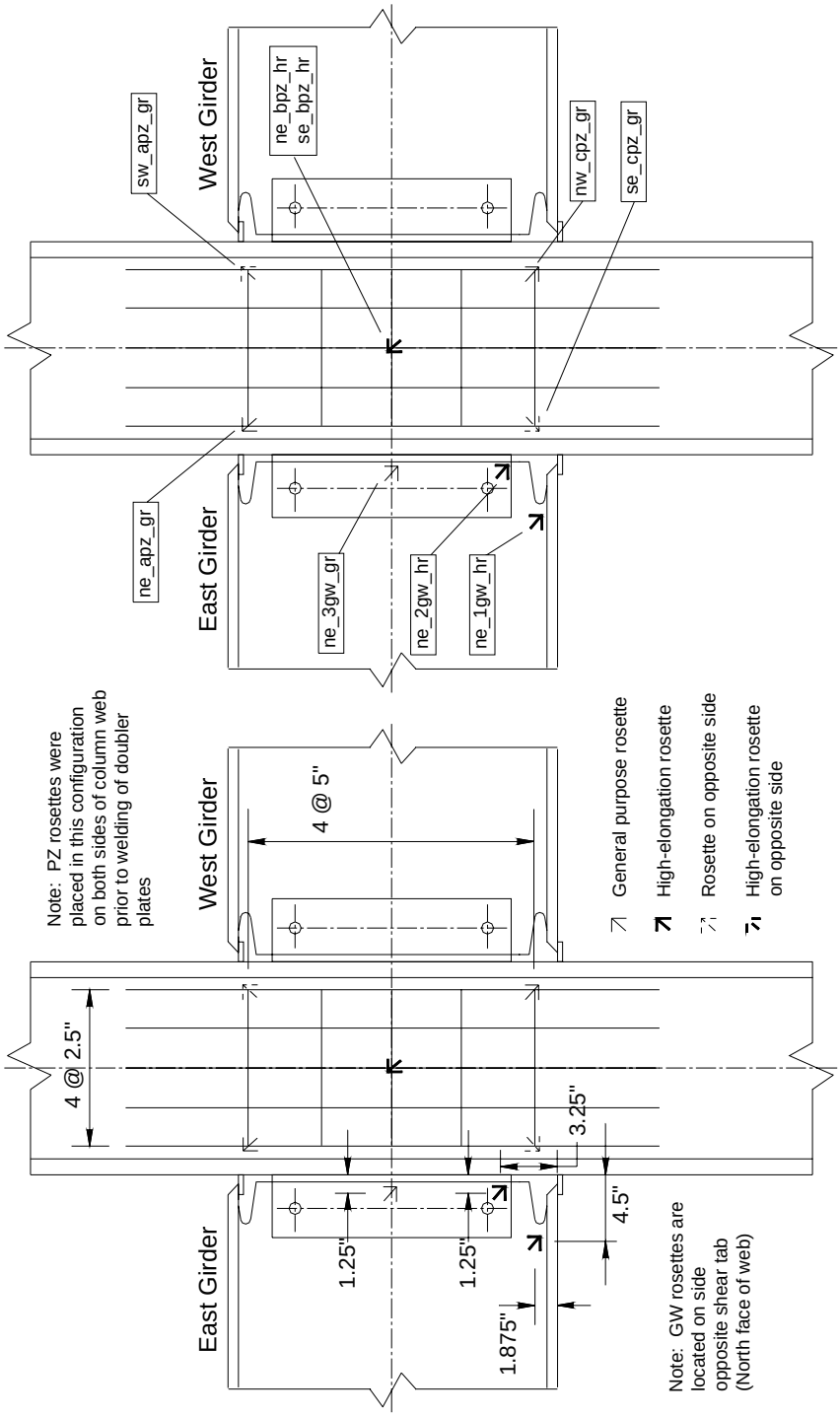


Figure 4.14: Panel Zone and Girder Web Instrumentation for Specimen CR4R

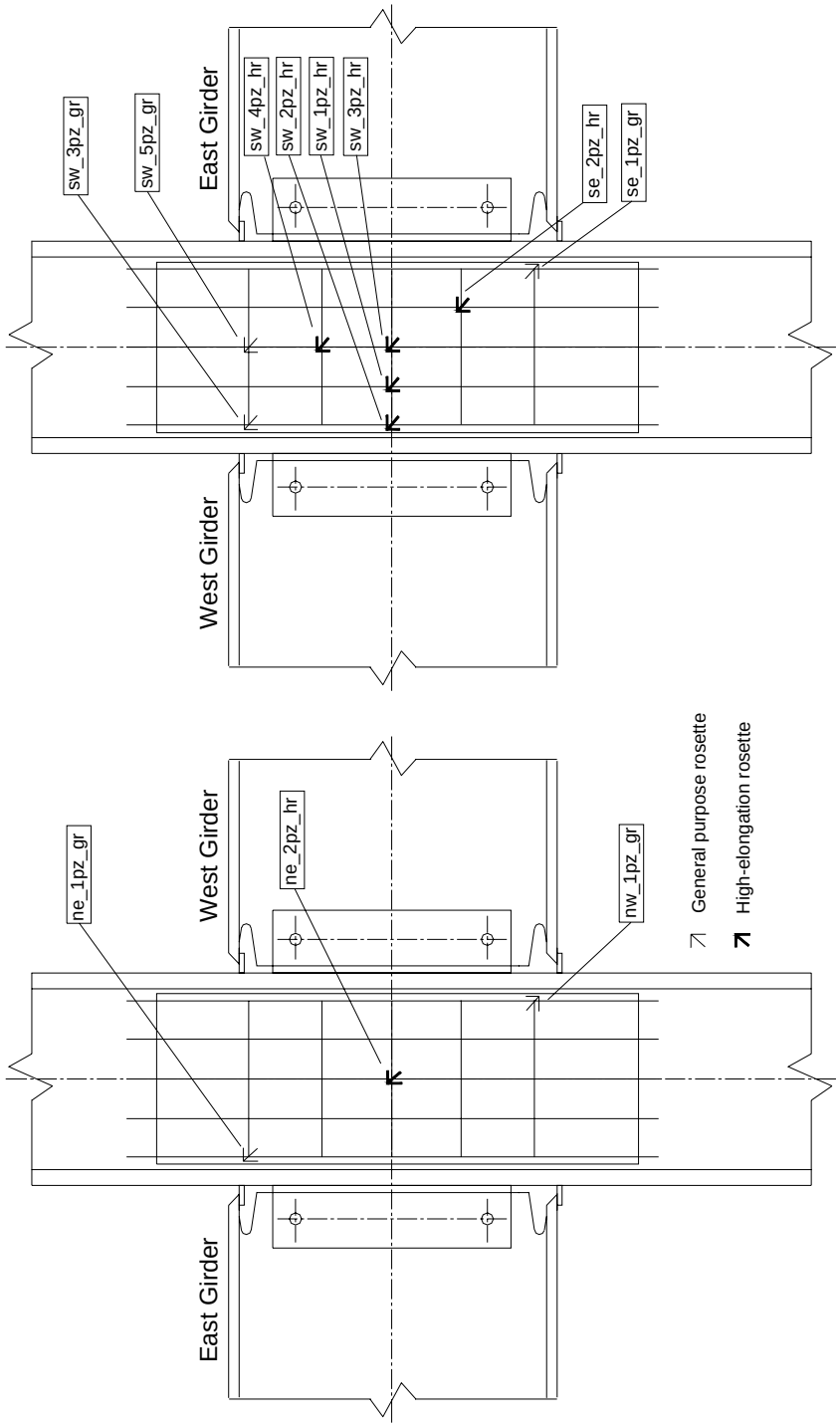


Figure 4.15: Doubler Plate Instrumentation for Specimen CR4R

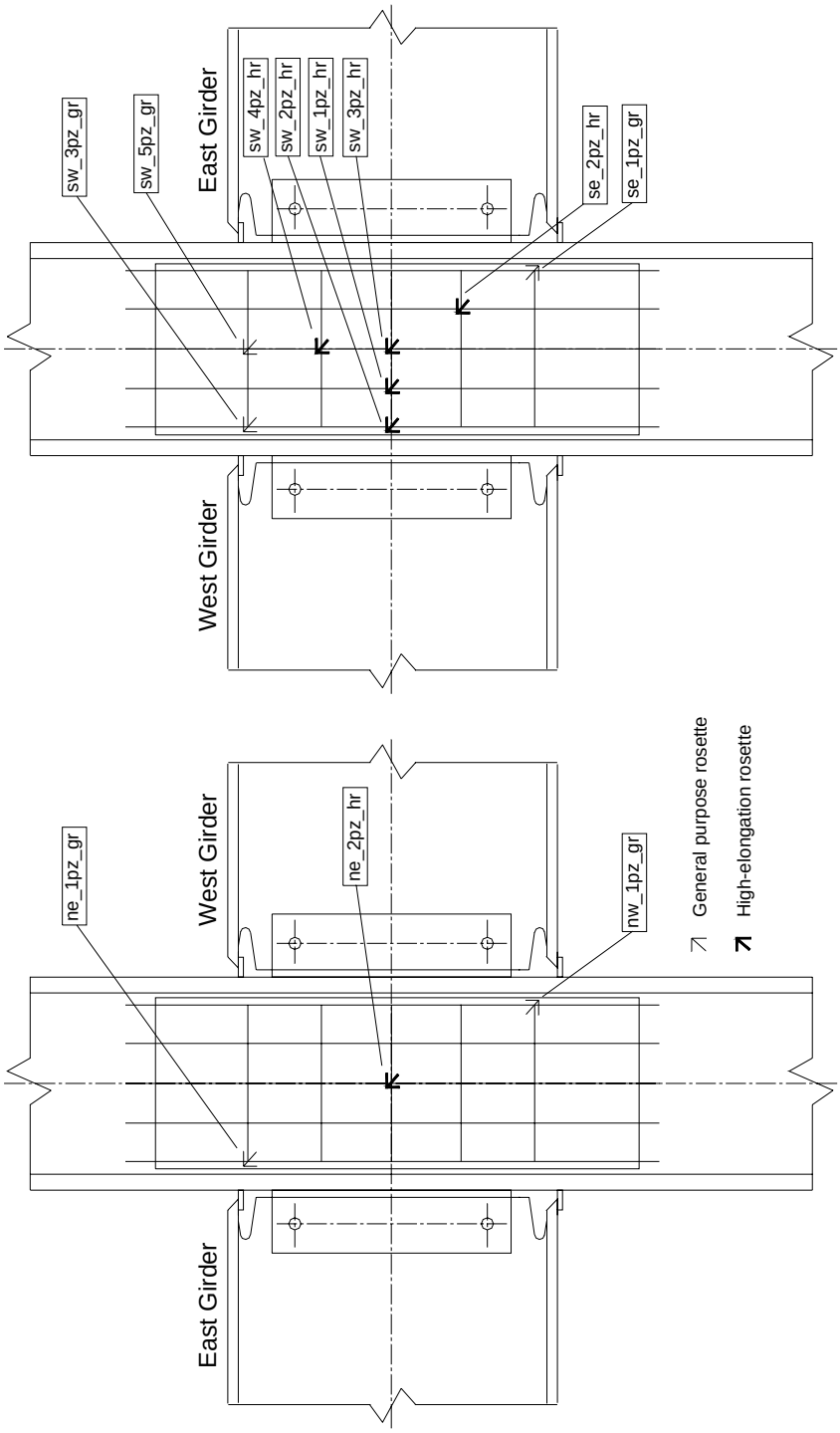


Figure 4.16: Doubler Plate Instrumentation for Specimen CR5

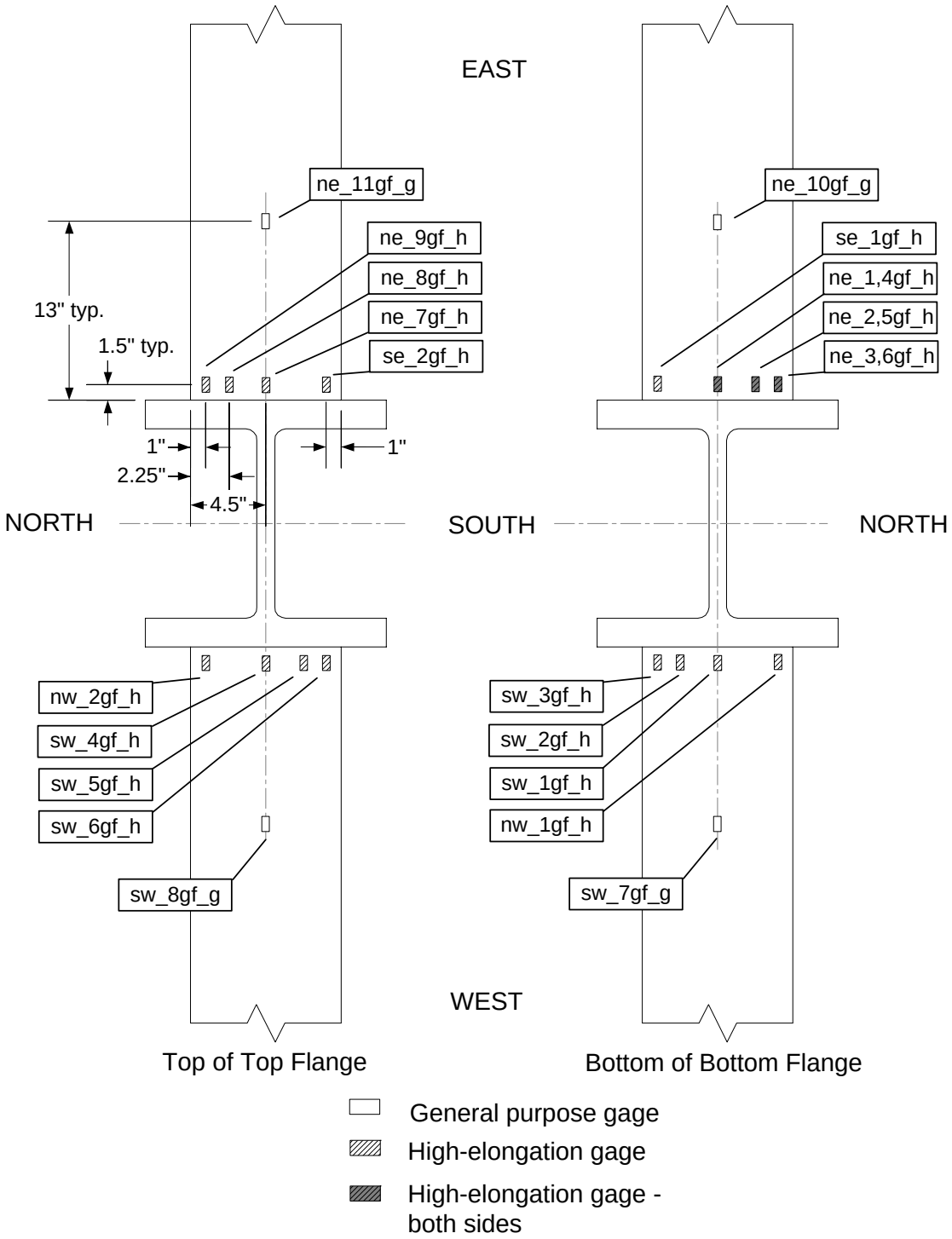


Figure 4.17: Location and Labels of Girder Flange Strain Gages for All Specimens

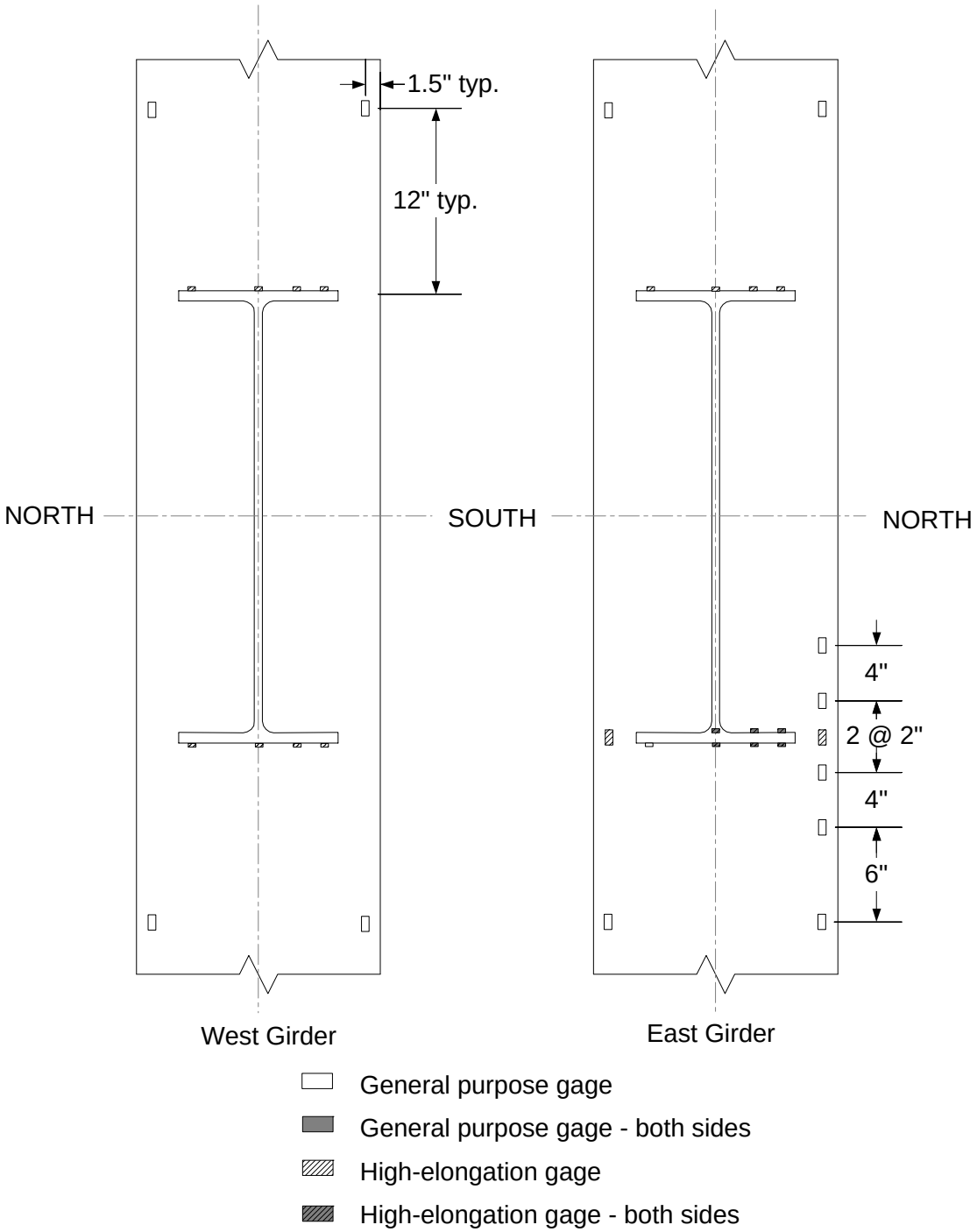


Figure 4.18: Location of Column Flange Strain Gages for All Specimens

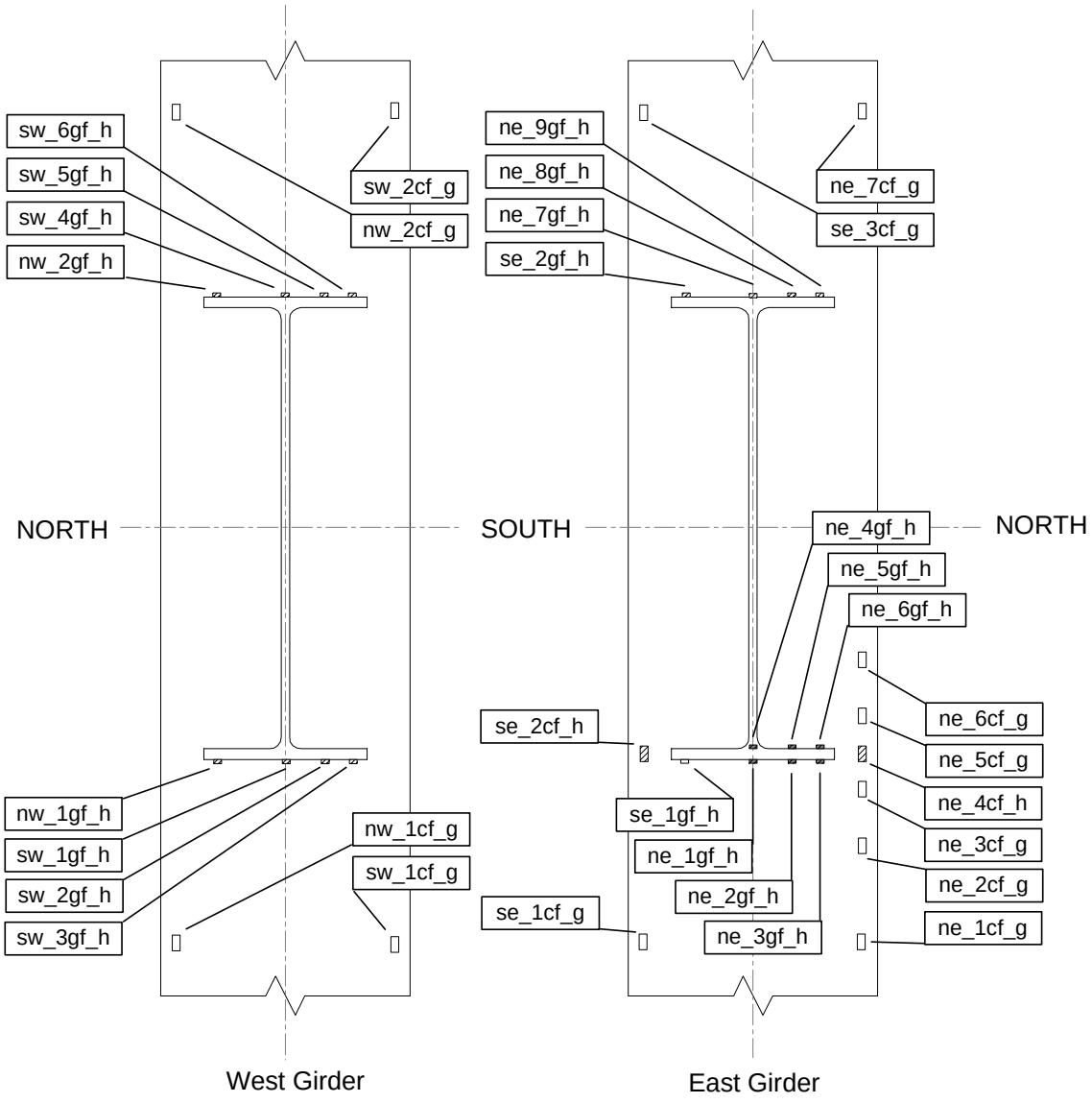


Figure 4.19: Strain Gage Labels for Girder and Column Flanges of All Specimens

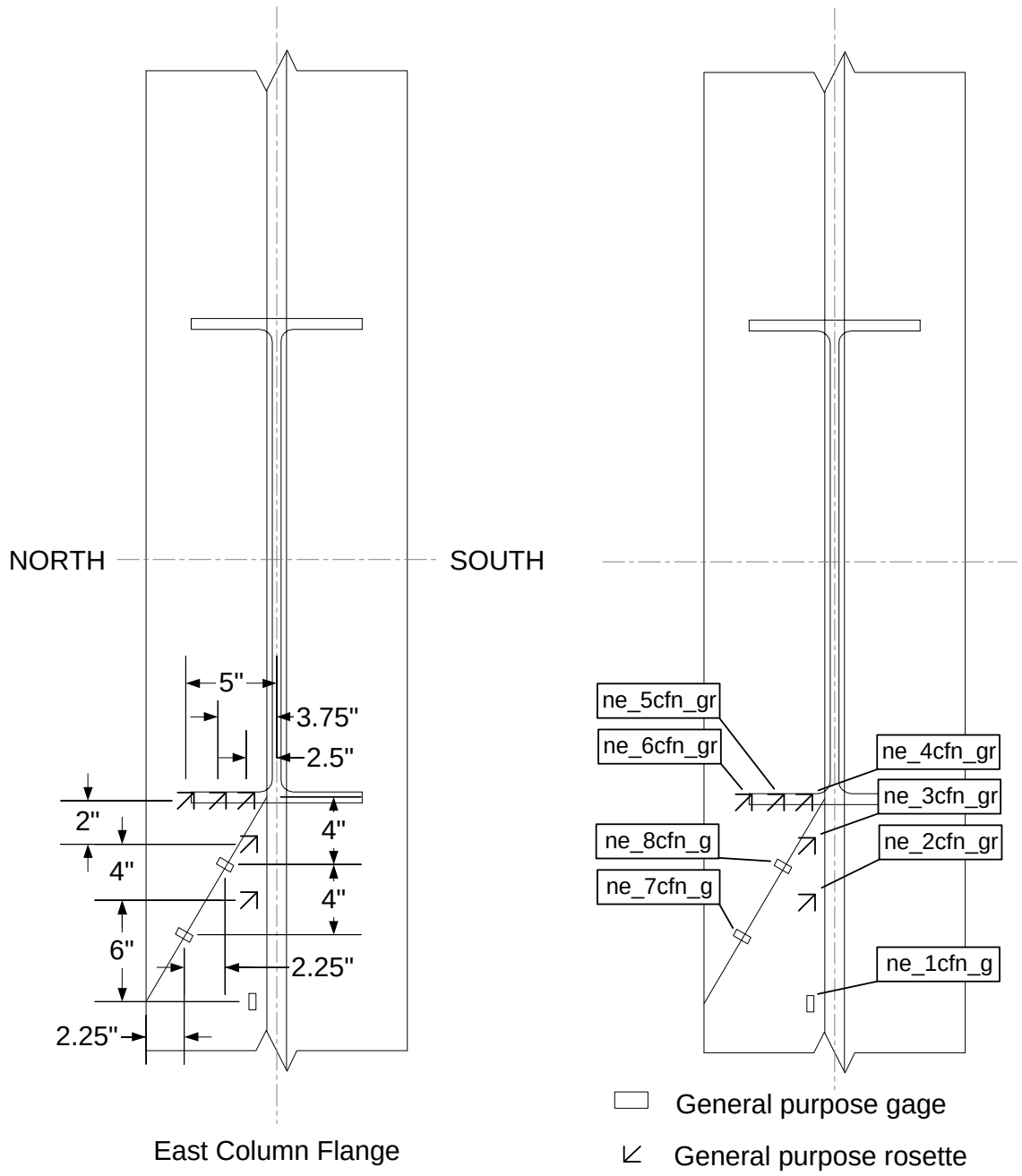


Figure 4.20: CFN Group Strain Gages for Specimens CR1, CR2, and CR5

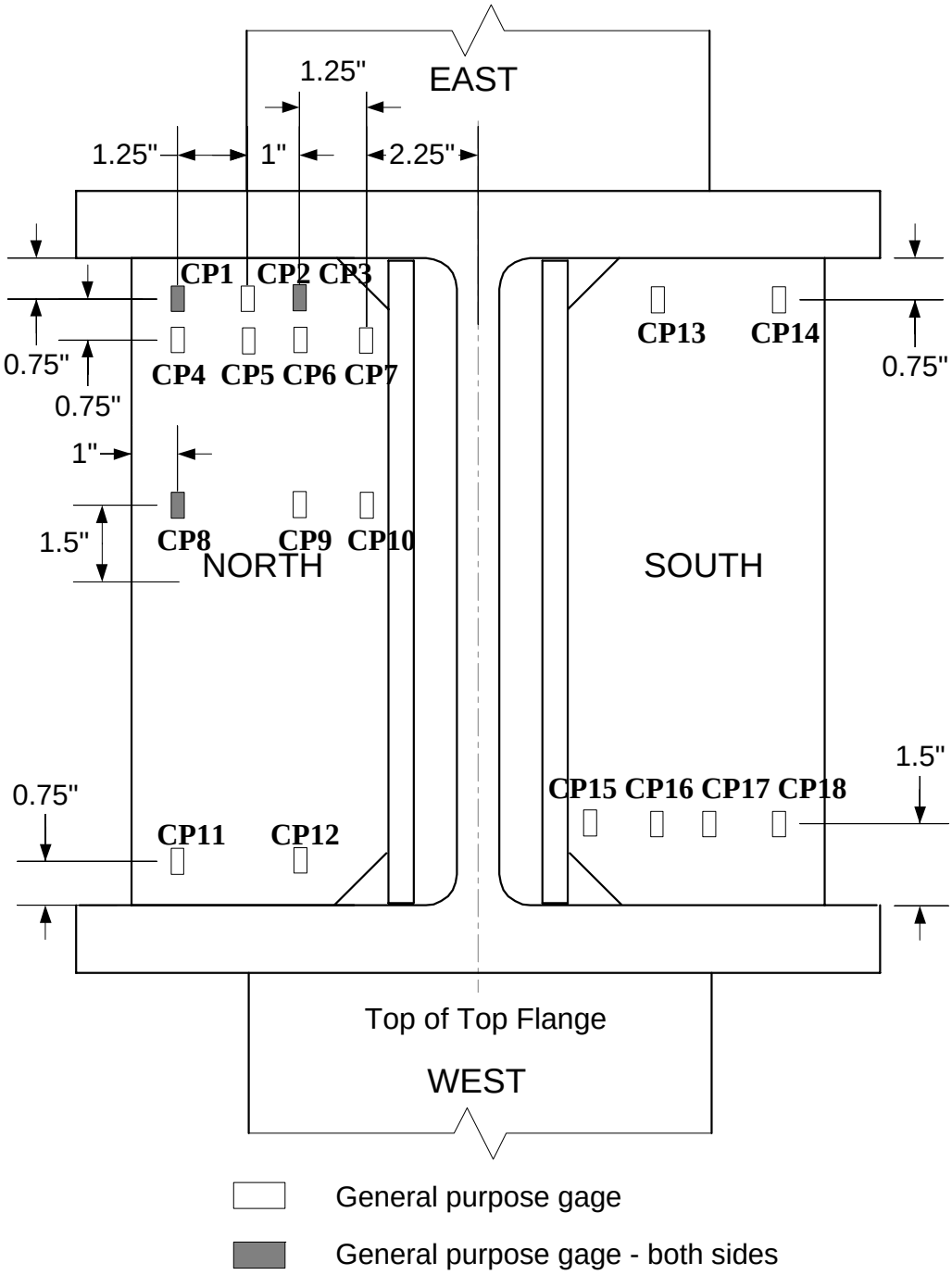


Figure 4.21: Continuity Plate Instrumentation for Specimen CR3

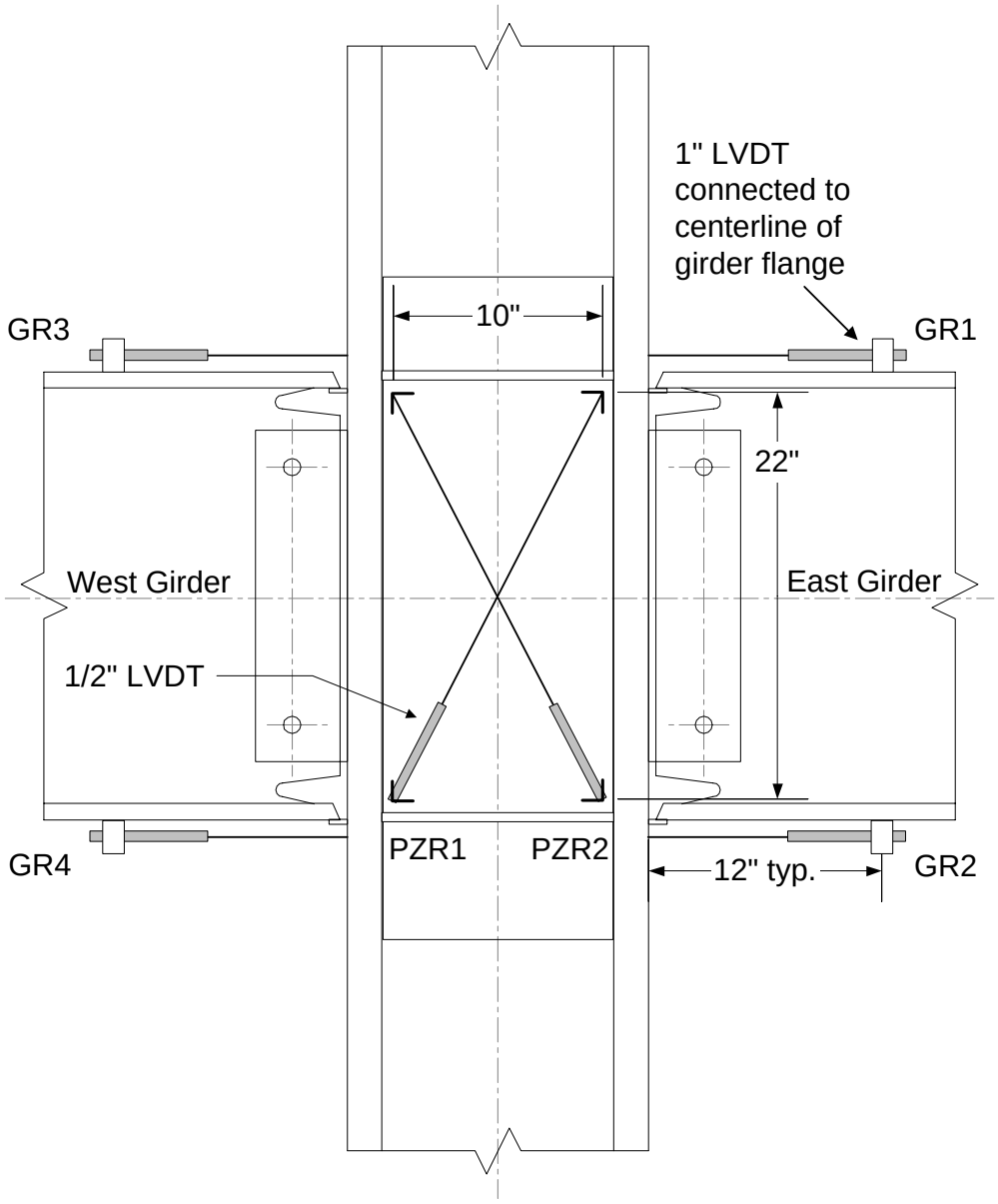


Figure 4.22: Girder and Panel Zone LVDT Placement for All Specimens

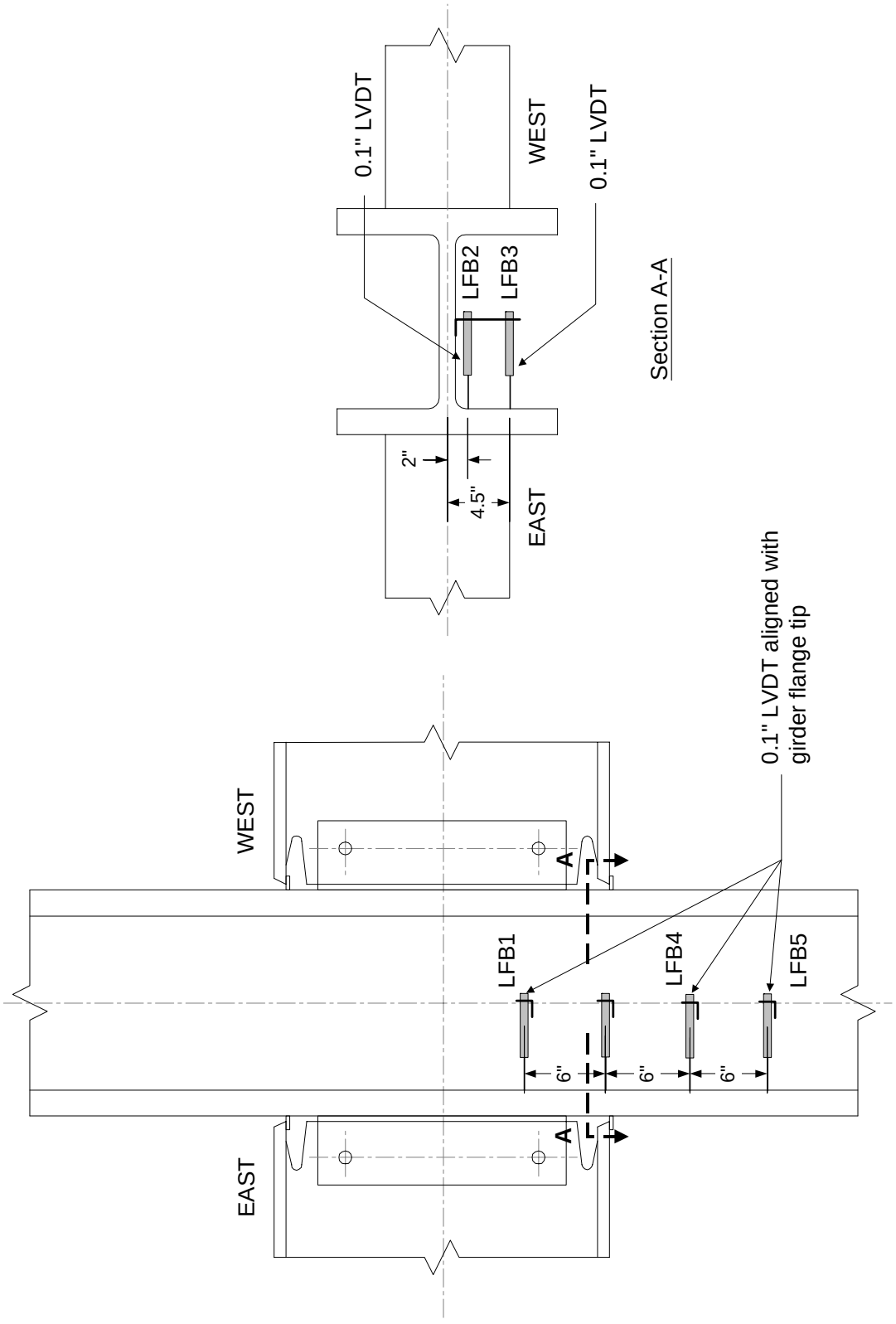


Figure 4.23: Column Flange LVDT Placement for Specimens CR1, CR2, and CR5

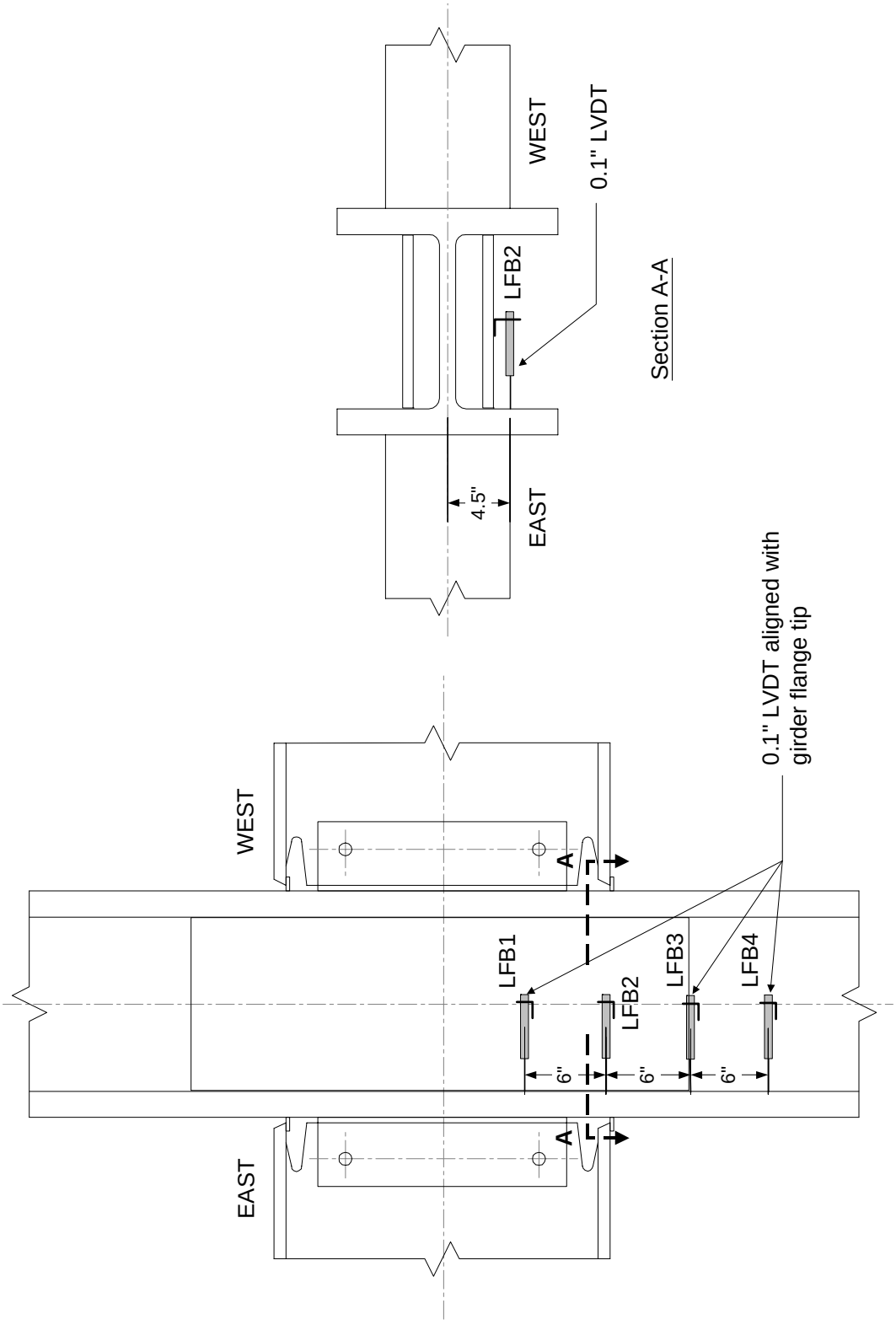


Figure 4.24: Column Flange LVDT Placement for Specimens CR4 and CR4R

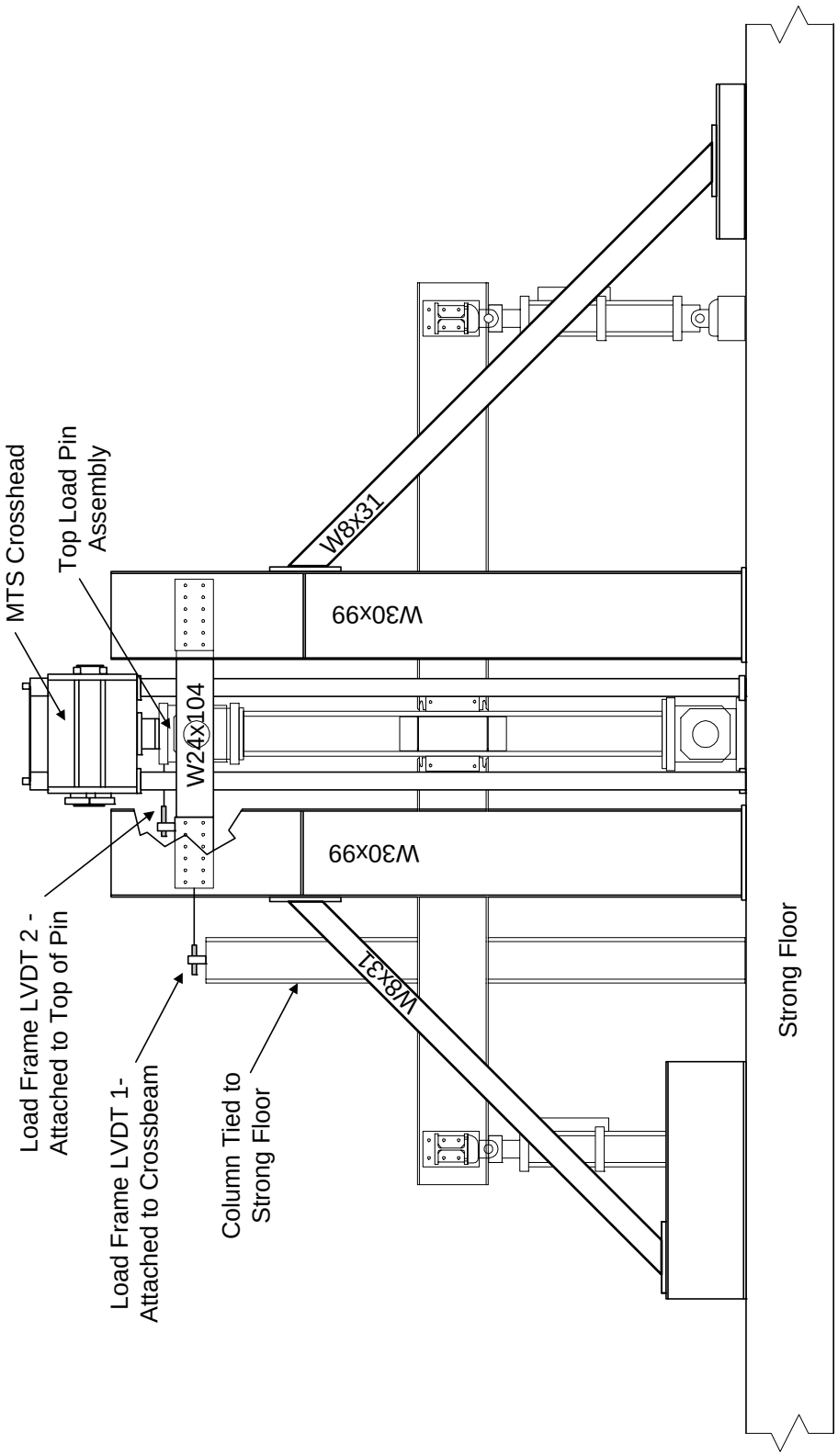


Figure 4.25: Load Frame LVDT Placement

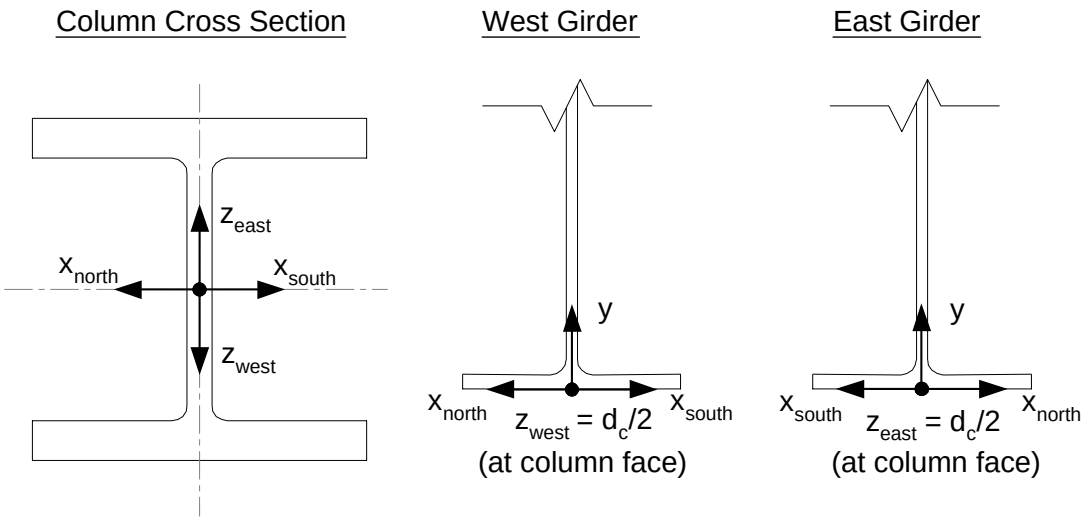


Figure 4.26: Specimen Coordinate System

Chapter 5

Summary of Test Results

Tests of six cruciform specimens, including one repeated test of Specimen CR4 (i.e., Specimen CR4R), have been completed. This chapter describes the loading histories applied to each specimen and the global cyclic performance of the specimens. Test results presented in this chapter include the plots of load vs. stroke and moment vs. all rotation components. The failure mechanisms of each specimen are also discussed.

5.1 Applied Loading History

As discussed in Chapter 4, an anti-symmetric loading pattern was applied to the six cruciform specimens to simulate the effects of lateral loading on an interior steel moment-resisting connection. These specimens were loaded by applying displacements following the SAC Phase 2 cyclic loading protocol (SAC, 1997) to the tip of each girder. After completing the two cycles at 4.0% interstory drift outlined in SAC (1997), as discussed in Chapter 4, additional cycles at the same interstory drift level were applied until the specimen failed or until the specimen showed a significant degradation in strength. In this section, the complete loading histories directly applied to the East girder of each specimen are described. In Figure 5.1, the number of 4.0% interstory drift cycles that were completed before the specimen failing or achieving significant strength degradation are compared.

5.1.1 Loading History of Specimen CR1

A total of 50.5 cycles were applied to Specimen CR1, including initial elastic cycles. One elastic cycle at 0.1% drift and one at 0.25% drift were first conducted to check instrumentation. A second elastic cycle was then conducted at 0.1% drift after

some instrumentation adjustments. Figure 5.2 shows the applied displacement history of the East girder of Specimen CR1 in terms of the interstory drift angle.

5.1.2 Loading History of Specimen CR2

A total of 50 cycles were applied to Specimen CR2, including initial elastic cycles. Two elastic cycles at 0.1% drift and two at 0.25% drift were first conducted to check instrumentation. Figure 5.3 shows the applied displacement history of the East girder of Specimen CR2 in terms of the interstory drift angle.

5.1.3 Loading History of Specimen CR3

A total of 46 cycles were applied to Specimen CR3, including initial elastic cycles. One elastic cycle at 0.1% drift and one at 0.25% drift were first conducted to check instrumentation. Figure 5.4 shows the applied displacement history of the East girder of Specimen CR3 in terms of the interstory drift angle.

5.1.4 Loading History of Specimen CR4

Due to premature CJP weld fracturing, the test of Specimen CR4 was terminated after one-half cycle at the 2.0% interstory drift level. A total of 26.5 cycles, including initial elastic cycles, were applied to this specimen. One elastic cycle at 0.1% drift and one at 0.25% drift were conducted prior to beginning the prescribed loading history. Figure 5.5 shows the applied displacement history of the East girder of Specimen CR4 in terms of the interstory drift angle.

5.1.5 Loading History of Specimen CR4R

A total of 46 cycles were applied to Specimen CR4R, including initial elastic cycles. One elastic cycle at 0.1% drift and two at 0.25% drift were first conducted to check instrumentation. One more elastic cycle at 0.375% was applied between 3.0 % drift and 4.0% drift to check the four MTS hydraulic actuators. Figure 5.6 shows the applied displacement history of the East girder of Specimen CR4R in terms of the interstory drift angle.

5.1.6 Loading History of Specimen CR5

A total of 41 cycles were applied to Specimen CR5, including initial elastic cycles. One elastic cycle at 0.1% drift and one at 0.25% drift were first conducted to check instrumentation. Figure 5.7 shows the applied displacement history of the East girder of Specimen CR5 in terms of the interstory drift angle.

5.2 Summary of Specimen Performance

The general behavior of six specimens may be summarized in terms of various load and deformation parameters. Tables 5.1 through 5.6 list the peak loads and moments of the East and West girders at each drift level for the six specimens. The peaks during the first cycle of each drift level are used for consistency. Positive loading is defined as tension in the East girder actuators and compression in the West actuators, i.e., downward displacement of the East girder tip and upward displacement of the West girder tip. In Tables 5.1 through 5.6, the moments are also normalized by the nominal plastic moment strength, M_p, of the W24x94 girder section (M_p = 254 in^3 x 50 ksi = 12,700 kip-in.).

The deformation components of primary interest include connection rotation (total and plastic), girder rotation (total and plastic), and panel zone rotation (total and plastic). The calculation of these quantities from the actuator and LVDT data is described in Appendix A. Additional plots of specimen behavior not included in this chapter may be found in this appendix.

5.2.1 Performance of Specimen CR1

Specimen CR1 was distinguished by the use of no column stiffeners (i.e., doubler plates and continuity plates). Based on experimental research conducted by Ricles et al. (2000b) and computational research by Mao et al. (2001), a strong correlation between panel zone strength and resistance to the development of low cycle fatigue fracture in steel moment connections has been reported. Thus, in order to investigate the effects of a weak panel zone on seismic connection behavior and ductility, the panel zone of this

specimen was designed to be relatively weak, i.e., $\phi_v R_v / R_u = 0.83$ for the panel zone yielding limit state according to the 1997 AISC Seismic Provisions (AISC, 1997).

Specimen CR1 completed the SAC loading history (SAC, 1997) up to 4.0% drift without noticeable strength degradation. After completing the two cycles at 4.0% drift required by the SAC protocol (SAC, 1997), additional 4.0% drift cycles were applied until the specimen failed. Figures 5.8 and 5.9 show the moment vs. interstory drift for the East and West girders of Specimen CR1, respectively. Figures 5.10 through 5.15 illustrate the performance of Specimen CR1 in terms of the various plastic rotation components. The test was stopped during the 20th cycle at 4.0% drift due to excessive strength degradation in the East girder following fracture. Table 5.7 documents the key events observed during testing of Specimen CR1, including the progression of yielding and fracture.

Prior to any cracking in this specimen, substantial yielding of the panel zone and beam flanges occurred, first initiating during the 0.75% drift cycles. Moderate yielding in the column flanges was also evident due to kinking of the column flanges at the level of the girder flanges. Some girder web yielding occurred, but full-depth plastic hinges did not form. Refer to Table 5.7 for the progression of yielding.

The East girder sustained a low-cycle fatigue (LCF) rupture in the bottom flange during the 15th cycle at 4.0% drift. This LCF rupture first became visible during the 11th cycle at 4.0% drift. It originated in the center of the flange base metal at the toe of the girder-to-column reinforcing fillet weld, and was visible across approximately 2/3 of the flange width before becoming unstable. Figures 5.16 through 5.18 illustrate the flange fracture. Low-cycle fatigue cracking also became visible in the West girder bottom flange at the toe of the reinforcing fillet weld during the 11th cycle at 4.0% drift, but did not become unstable prior to the end of the test. This rupture was of a similar size to the East bottom flange crack when the East flange ruptured completely, and continued to grow in a stable manner during the final five cycles at 4.0% drift. Following testing, LCF cracking was also discovered in the top flanges of both girders. Cracks existed both in the girder flanges at the CJP weld toes and at the faces of the column flanges.

First cracking was noted during the 4th cycle at 4.0% drift. It consisted of a small crack originating at the bottom edge of the West shear tab. The top edge of the East shear tab was the next to crack during the 8th cycle at 4.0% drift. The top edge of the West shear tab also began to crack during the latter half of this cycle. By the time the East girder bottom flange fractured, all four ends of the shear tab welds (top and bottom corners of both girder webs) had developed cracks that reached lengths of approximately 1 in. Following the LCF rupture in the East bottom flange, the shear tab weld crack in this location propagated to approximately half the girder depth by the 18th cycle at 4.0% drift. LCF cracking also occurred in the access holes during the last several cycles at 4.0% drift. It was first noted during the 16th cycle at 4.0% drift in both West girder access holes. Following the test, a LCF crack was also noted in the East top access hole. Figures 5.19 and 5.20 illustrate typical web weld and access hole cracking.

Specimen CR1 exhibited excellent energy dissipation capacity, as is evident from the hysteresis loops of connection plastic rotation shown in Figures 5.10 and 5.11. A comparison of Figures 5.12 and 5.13 with Figure 5.15 reveals that plastic rotation was dominated by panel zone yielding. This was expected based on the weak panel zone philosophy adopted for design of this specimen discussed in Section 3.3.3.1. The panel zone behavior is discussed in detail in Chapter 6. Both girders slightly exceeded their nominal plastic moment capacities, as shown in Table 5.1.

5.2.2 Performance of Specimen CR2

Specimen CR2 was distinguished by the use of a one-sided fillet-welded doubler plate and by the use of no continuity plates as shown in Figure 3.14 in Chapter 3. The panel zone of this specimen was also designed to be relatively weak, i.e., $\phi_v R_v / R_u = 0.76$ including the doubler plate, calculated according to the 1997 AISC Seismic Provisions (AISC, 1997). In addition to the effects of a weak panel zone on seismic connection behavior and ductility, potential adverse effects of the doubler plate detail on the unstiffened column flange deformation were investigated in this test.

Specimen CR2 completed the SAC loading history up to 4.0% drift without noticeable strength degradation. Figures 5.21 and 5.22 show the moment vs. interstory

drift for the East and West girders of Specimen CR2, respectively. Figures 5.23 through 5.28 illustrate the performance of Specimen CR2 in terms of the various plastic rotation components. The test was stopped after completion of the 18th cycle at 4.0% drift due to excessive strength degradation in the West girder following fracture. Table 5.8 documents the key events observed during testing of Specimen CR2, including the progression of yielding and fracture.

Due to the weak panel zone, Specimen CR2 exhibited yielding in the panel zone at an early stage of the loading history. The panel zone started to yield during the 1st cycle at 1.5% drift, and was fully yielded at 3.0% drift, as shown in Figure 5.29. This relatively weak panel zone coupled with moderately thin column flanges also caused relatively large local flange deformation in the column. However, in spite of large inelastic cyclic deformation of the doubler plate and column flanges, no clear damage was observed in the fillet welds connecting the doubler plate to the column flange by the completion of the test at the 18th cycle of 4.0% drift.

The primary failure mode of Specimen CR2 was low-cycle fatigue fracturing in the West girder top flange. The crack located in the West girder top flange was observed on the girder-flange-side toe of the CJP weld. The initial visual indication of this crack occurred during the 2nd cycle at 3.0% drift. This crack began to propagate significantly around the center of the girder flange during the 11th cycle at 4.0% drift as shown in Figure 5.30. However, the first cycle where this crack had a discernable effect on the moment-interstory drift curves was the 14th cycle. The crack became unstable and a brittle fracture occurred during the 17th cycle, as shown in Figures 5.31 and 5.32. On the other hand, a visual indication of a possible crack in the East girder top flange was observed at the girder-flange-side toe of the CJP weld during the 1st cycle at 4.0% drift. However, this crack did not propagate significantly prior to the West girder top flange fracturing at the 17th cycle of 4.0% drift.

During the application of the 4.0% drift cycles, other cracks were also observed at the top and bottom edges of the fillet welds connecting the shear tab to the column flange and of the CJP welds connecting the girder web to the column flange. The cracks in the shear tab occurred first at the top and bottom edges of the fillet welds on the East shear

tab during the 5th cycle at 4.0% drift, while the top and bottom edge cracks on the West shear tab were observed during the 7th cycle and 9th cycles, respectively. The maximum initial crack length was approximately 1.0 in. at the top edge of the East shear tab. In spite of the repeated large column flange local deformation originated by the relatively weak panel zone strength, the cracks in both shear tabs did not extend significantly prior to the West girder top flange fracturing at the 17th cycle of 4.0% drift.

Specimen CR2 exhibited excellent energy dissipation capacity, as is evident from the hysteresis loops of connection plastic rotation shown in Figures 5.23 and 5.24. A comparison of Figures 5.25 and 5.26 with Figure 5.28 reveals that plastic rotation was dominated by panel zone yielding. The panel zone behavior is discussed in detail in Chapter 6. Due to the large panel zone deformations, both girders had peak moments just below their nominal plastic moment capacities during the 1st cycle of 4.0% drift, as shown in Table 5.2.

5.2.3 Performance of Specimen CR3

Specimen CR3 was distinguished by the use of fillet-welded doubler plates and by the use of fillet-welded 1/2 in. thick continuity plates as shown in Figure 3.15 in Chapter 3. This test was intended primarily to show that a fillet-welded continuity plate detail can perform adequately in cyclic loading applications. In addition, the effects of a weak panel zone on seismic connection behavior and ductility were investigated. For this purpose, the panel zone of this specimen was designed to have a capacity-to-demand ratio of $\phi_v R_v / R_u = 0.86$, including the doubler plate, calculated according to the 1997 AISC Seismic Provisions (AISC, 1997).

Specimen CR3 completed the SAC loading history up to 4.0% drift without noticeable strength degradation. Figures 5.33 and 5.34 show the moment vs. interstory drift for the East and West girders of Specimen CR3, respectively. Figures 5.35 through 5.40 illustrate the performance of Specimen CR3 in terms of the various plastic rotation components. The test was stopped after completion of the 16th cycle at 4.0% drift due to excessive strength degradation in the East girder following fracture. Table 5.9 documents

the key events observed during testing of Specimen CR3, including the progression of yielding and fracture.

Specimen CR3 exhibited yielding in the panel zone at an early stage of the loading history. The panel zone started to yield during the 1st cycle at 1.5% drift, and fully yielded before achieving 3.0% drift. This weak panel zone, coupled with moderately thin column flanges, caused significant column deformations around panel zone area, as shown in Figure 5.41. However, through the completion of the test at the 16th cycle of 4.0% drift, no clear damage was observed in the fillet welds connecting the doubler plate to the column flange and in the fillet welds of the continuity plates.

The primary failure mode of Specimen CR3 was low-cycle fatigue fracturing in the East girder bottom flange. The crack located in the East girder bottom flange was observed on the girder-flange-side toe of the CJP weld. The initial visual indication of this crack occurred during the 2nd cycle at 3.0% drift. This crack began to propagate significantly around the center of the girder flange during the 9th cycle at 4.0% drift and a visible significant crack opening was observed during the 11th cycle as shown in Figure 5.42. This crack grew steadily and the girder flange fractured through its whole flange width during the 15th cycle at 4.0% drift as shown in Figure 5.43. On the other hand, visual indications of possible cracks in the East and West girder top flanges were observed at the girder-flange-side toe of the CJP weld during the 2nd cycle at 3.0% drift and 1st cycle of 4.0% drift, respectively. These cracks opened significantly during the 13th cycle at 4.0% drift. However, no fracturing in the top girder flanges occurred by the end of the test.

Other cracks were also observed at the top and bottom edges of the shear tab during the application of the 4.0% drift cycles. The cracks in the shear tab occurred first at the East shear tab bottom edge and at the West shear tab top edge during the 2nd cycle at 4.0% drift. Cracks at the top edge of the East shear tab and at the bottom edge of the West shear tab were also observed in the following cycle (i.e., 3rd cycle at 4.0% interstory drift). Due to the repeated large column deformation, the cracks in the West shear tab propagated up to 2 in. through both the fillet and the CJP welds during the 9th cycle at

4.0% drift. The maximum crack length in the East shear tab was 1 in. after completing the 10th cycle. However, these cracks did not extend significantly prior to the East girder bottom flange fracturing at the 15th cycle of 4.0% drift.

Specimen CR3 exhibited excellent energy dissipation capacity, as is evident from the hysteresis loops of connection plastic rotation shown in Figures 5.35 and 5.36. A comparison of Figures 5.37 and 5.38 with Figure 5.40 reveals that plastic rotation was dominated by panel zone yielding. Both girders slightly exceed their nominal plastic moment capacities during the 1st cycle of 4.0% drift, as shown in Table 5.3. The panel zone behavior is discussed in detail in Chapter 6.

5.2.4 Performance of Specimen CR4

Specimen CR4 was distinguished by the use of a detail in which two doubler plates were welded to the column flange using CJP welds, with each plate offset away from the column web by a distance equal to two-thirds of the half-flange width of the girder. This stiffening detail, shown in Figure 3.17 in Chapter 3, is similar to the web doubler plate detail shown in Figure C-9.3 (c) of the 1997 AISC Seismic Provisions (AISC, 1997). Unlike the other specimens, a relatively strong panel zone is provided meeting the requirements of the 1997 AISC Seismic Provisions (AISC, 1997). i.e., a capacity-to-demand ratio of $\phi_v R_v / R_u = 1.07$, including the doubler plates.

The test of Specimen CR4 was stopped after one-half cycle at 2.0% due to brittle fracture of three girder flange welds. Table 5.10 documents the key events observed during testing of Specimen CR4, including the progression of yielding and fracture. Figures 5.44 and 5.45 show the moment vs. interstory drift for the East and West girders of Specimen CR4, respectively. Figures 5.46 through 5.51 illustrate the performance of Specimen CR3 in terms of the various plastic rotation components.

The top flange of the West girder was completely severed at the end of the 1.5% drift cycles. The top flange of the East girder and bottom flange of the West girder completely fractured during the first quarter-cycle at 2.0% drift. These weld fractures, however, initiated as early as the 1.0% drift cycles, based on analysis of strain gages near

the girder flange welds. The East top flange was the first to show indications of cracking in the strain gage data during the first quarter cycle of the second cycle at 1.0% drift. The West top flange first showed indications of cracking in the strain gage data during the third quarter-cycle of the third cycle at 1.0%. The bottom flange of the West girder gave no indications of cracking prior to the first quarter-cycle at 2.0%. However, first visible cracking was discovered in both flanges of the West girder after the 1st cycle at 1.5%. The three flange fractures are shown in Figures 5.52 through 5.54.

Some yielding had occurred prior to the flange fractures. Moderate yielding of the girder flanges was visible, initiating during the 0.75% drift cycles. Some yielding of the panel zone occurred as well, first visible during the 1.0% cycles. Minor web yielding and cracking at the edges of shear tabs also occurred, but was a result of deformation induced by the flange weld fractures near the end of testing.

Specimen CR4 exhibited poor ductility and energy dissipation due to the premature fractures of the flange CJP welds. Very limited connection plastic rotation is evident in Figures 5.46 and 5.47. The girders accounted for most of the inelastic deformation in this specimen (see Figures 5.48 and 5.49). As shown in Figures 5.50 and 5.51, the panel zone of Specimen CR4 showed little inelasticity. Both girders did not reach their nominal plastic moment capacities prior to fracture, as shown in Table 5.4. The investigation of the premature weld fractures is described in detail in Appendix B.

5.2.5 Performance of Specimen CR4R

Specimen CR4 had three of its four complete joint penetration (CJP) weld fracturing in a brittle manner at an early stage of the SAC loading history. As shown in Table 3.7 in Chapter 3, Charpy V-Notch tests performed after the experiment on the as-deposited E70T-6 weld metal in Specimen CR4 had an average fracture energy of 2 ft-lbs at 0°F and 2.3 ft-lbs at 70°F, substantially less than recommended in FEMA 350 (2000a).

In order to investigate the performance of this connection detail and the importance of weld toughness, a new specimen, CR4R, was constructed having identical detailing and girders generated from the same heat as those in Specimen CR4. However, a new lot of E70T-6 weld wire was used. As discussed in Chapter 3, this lot of weld wire

was obtained from Edison Welding Institute (EWI) and was a lot of wire that they had previously characterized for the SAC project. The Charpy V-Notch test results from as-deposited weld metal for this new E70T-6 weld wire was 33 ft-lb at 0°F and 58.7 ft-lb at 70°F, as shown in Table 3.7.

Specimen CR4R completed the SAC loading history up to 4.0% interstory drift without noticeable strength degradation. After completing two cycles at 4.0% interstory drift, additional 4.0% drift cycles were applied until the specimen failed. Figures 5.55 and 5.56 show the moment vs. interstory drift for the East and West girders of Specimen CR4R, respectively. Figures 5.57 through 5.62 illustrate the performance of Specimen CR4R in terms of the various plastic rotation components. Table 5.11 documents the key events observed during testing of Specimen CR4R, including the progression of yielding and fracture.

Low-cycle fatigue cracks began to form during the 4.0% drift cycles, including: (1) shallow surface cracks along the weld toes of the girder flange welds; and (2) an edge crack at the East girder flange tip. The first surface crack, shown in Figure 5.63, was clearly observed during the 2nd cycle of 4.0% drift along the toe of the CJP weld in the West girder top flange. The second surface crack was observed during the 5th cycle of 4.0% drift at the toe of the CJP weld in the East girder top flange. Fortunately, the depths of these two surface cracks were very shallow and so the connection strength was not significantly decreased by these cracks. The edge crack appeared at the north tip of East girder top flange during the 2nd cycle at 4.0% drift. This edge crack grew dramatically during the 12th cycle and finally fractured the girder flange during the 13th cycle. The shapes of the fracture in the East girder top flange are shown in Figures 5.64 and 5.65.

The West girder top flange and East girder top flange buckled locally during the 9th cycle at 4.0% drift, whereas local buckling on the East girder bottom flange was observed during the 10th cycle. The connection strength was not affected significantly by this local flange buckling.

The test was terminated at the beginning of the 13th cycle at 4.0% interstory drift due to the fracture in the East girder top flange and to extensive lateral-torsional buckling

in the West girder, as shown in Figure 5.66. While the West girder exhibited some mild lateral bending and buckling throughout the experiment, particularly during the 4.0% drift cycles, the lateral-torsional buckling did not become significant until the 12th cycle at 4.0% drift. A preliminary assessment of the better performance of this test relative to the original CR4 specimen would seem to indicate the importance of weld toughness in connection performance, as well as rule out the geometry of this detail as a causal factor in the fracture of the original CR4 test.

Specimen CR4R exhibited excellent energy dissipation capacity, as is evident from the hysteresis loops of connection plastic rotation shown in Figures 5.57 and 5.58. A comparison of Figures 5.59 and 5.60 with Figure 5.62 reveals that the contribution of panel zone yielding in connection plastic rotation was less significant as compared with the other specimens. This is because a relatively strong panel zone was designed for Specimen CR4R, i.e., a capacity-to-demand ratio of $\phi_v R_v / R_u = 1.07$, including the doubler plates, as per the 1997 AISC Seismic Provisions (AISC, 1997). The panel zone behavior is discussed in detail in Chapter 6. Both girders exceeded their nominal plastic moment capacities by approximately 20%, as shown in Table 5.5.

5.2.6 Performance of Specimen CR5

Specimen CR5 was distinguished by the use of the smallest column section and doubler plates that were 7/16 in. backside-beveled and fillet-welded to the column flanges, as shown in Figure 3.16 in Chapter 3. This stiffening detail follows the web doubler plate detail (b) shown in Figure C-9.3 of the 1997 AISC Seismic Provisions (AISC, 1997). This test was intended primarily to verify the AISC local flange bending (LFB) limit state for non-seismic and seismic design applications. Thus, continuity plates (transverse stiffeners) were eliminated from Specimen CR5, even though they are required as per the non-seismic AISC LRFD Specification (AISC, 1999), i.e., $\phi R_n / R_u = 0.84$. Note that this ratio is even smaller, i.e., $\phi R_n / R_u = 0.47$, when using the demand outlined in the 1992 AISC Seismic Provisions (AISC, 1992) for the LFB limit state. Because a smaller column section was intentionally chosen for the study of the LFB

limits, Specimen CR5 does not meet the Strong Column-Weak Beam criterion as per the 1997 AISC Seismic Provisions (AISC, 1997). This test was also intended to show how the connection detailed with a relatively weak panel zone strength and relatively thin flanges coupled with the omission of continuity plates could perform in cyclic loading applications. For this purpose, the panel zone of this specimen was designed to have a capacity-to-demand ratio of $\phi_v R_v / R_u = 0.85$, including the doubler plates, calculated according to the 1997 AISC Seismic Provisions (AISC, 1997).

Specimen CR5 completed the SAC loading history up to 4.0% drift without noticeable strength degradation. Figures 5.67 and 5.68 show the moment vs. interstory drift for the East and West girders of Specimen CR5, respectively. Figures 5.69 through 5.74 illustrate the performance of Specimen CR5 in terms of the various plastic rotation components. The test was stopped after completion of the 11th cycle at 4.0% drift due to excessive strength degradation in the West girder following fracture. Table 5.12 documents the key events observed during testing of Specimen CR5, including the progression of yielding and fracture.

Due to the weak panel zone, Specimen CR5 exhibited yielding in the panel zone at an early stage of the loading history. The panel zone started to yield during the 1st cycle at 1.5% drift, and fully yielded during the application of 3.0% drift cycles. In addition, due to the smaller section of the column coupled with the weak panel zone, relatively large column deformations were observed around the joint area as shown in Figure 5.75.

The primary failure mode of Specimen CR5 was low-cycle fatigue fracture in the West girder top flange. The crack located in the West girder top flange was observed in the middle of the CJP weld instead of the toe of the CJP weld, where initial cracks of the other specimens were usually observed. The initial visual indication of this crack occurred during the 1st cycle at 4.0% drift. This crack began to propagate significantly around the center of the girder flange CJP weld during the 5th cycle at 4.0% drift as shown in Figure 5.76. With the increasing number of interstory drift cycles, this crack grew significantly, and finally the girder flange fractured through the whole flange width during the 7th cycle at 4.0% drift as shown in Figure 5.77. Visual indications of possible

cracks in the other three girder flanges were observed at the toe of the CJP weld during the 2nd cycle at 3.0% drift. However, no significant crack opening and fracturing in these girder flanges occurred prior to the fracturing in the West girder top flange during the 7th cycle at 4.0% drift.

Cracks at the top and bottom edges of the shear tab were observed at earlier stages of the interstory drift cycles. The cracks occurred first at the top and bottom edges of the West shear tab during the application of 2.0% drift. The initial cracks in the East shear tab were observed at its top edge during the application of 3.0% drift. However, these cracks did not extend significantly prior to the West girder top flange fracturing at the 7th cycle of 4.0% drift. After completion of the 4th cycle of 4.0% interstory drift, the maximum crack lengths were 3/4 in. at the bottom edge of the East shear tab and 1/2 in. at the bottom edge of the West shear tab.

Specimen CR5 exhibited good energy dissipation capacity, as is evident from the hysteresis loops of connection plastic rotation shown in Figures 5.69 and 5.70. A comparison of Figures 5.71 and 5.72 with Figure 5.74 reveals that plastic rotation was dominated by panel zone yielding. The panel zone behavior is discussed in detail in Chapter 6. Both girders exceeded their nominal plastic moment capacities by approximately 10% during the 1st cycle of 4.0% drift, as shown in Table 5.6.

Table 5.1: Summary of Peak Loads and Moments for Specimen CR1

Drift Cycle (%)	East Girder			West Girder		
	Load (kips)	**Moment (kip-in)**	M/M_p	**Load (kips)**	**Moment (kip-in)**	M/M_p
0.375^+	24.9	3281	0.26	-24.3	-3204	-0.25
0.375^-	-25.1	-3313	-0.26	25.2	3329	0.26
0.5^+	33.4	4406	0.35	-32.5	-4286	-0.34
0.5^-	-33.2	-4381	-0.35	33.8	4464	0.35
0.75^+	50.2	6629	0.52	-48.0	-6339	-0.50
0.75^-	-48.9	-6454	-0.51	50.9	6712	0.53
1.0^+	61.6	8134	0.64	-58.0	-7653	-0.60
1.0^-	-59.0	-7784	-0.61	61.6	8130	0.64
1.5^+	72.5	9567	0.75	-66.3	-8757	-0.69
1.5^-	-68.9	-9088	-0.72	73.0	9636	0.76
2.0^+	82.4	10882	0.86	-77.3	-10201	-0.80
2.0^-	-80.1	-10579	-0.83	81.9	10816	0.85
3.0^+	89.3	11789	0.93	-86.0	-11345	-0.89
3.0^-	-92.1	-12156	-0.96	92.6	12219	0.96
4.0^+	99.3	13109	1.03	-96.9	-12794	-1.01
4.0^-	-100.9	-13322	-1.05	99.6	13147	1.04

Table 5.2: Summary of Peak Loads and Moments for Specimen CR2

Drift Cycle (%)	East Girder			West Girder		
	Load (kips)	**Moment (kip-in)**	M/M_p	**Load (kips)**	**Moment (kip-in)**	M/M_p
0.375^+	21.3	2809	0.22	-21.3	-2813	-0.22
0.375^-	-22.3	-2945	-0.23	21.4	2828	0.22
0.5^+	28.4	3748	0.30	-28.5	-3761	-0.30
0.5^-	-29.6	-3904	-0.31	28.5	3767	0.30
0.75^+	42.3	5578	0.44	-42.5	-5607	-0.44
0.75^-	-44.5	-5874	-0.46	43.1	5695	0.45
1.0^+	54.6	7213	0.58	-54.7	-7221	-0.57
1.0^-	-58.1	-7668	-0.60	56.5	7459	0.59
1.5^+	68.6	9053	0.71	-68.2	-9005	-0.71
1.5^-	-70.9	-9365	-0.74	69.2	9129	0.72
2.0^+	74.3	9806	0.77	-74.2	-9794	-0.77
2.0^-	-79.6	-10504	-0.83	77.0	10160	0.80
3.0^+	84.8	11198	0.88	-85.5	-11285	-0.89
3.0^-	-86.9	-11474	-0.90	85.0	11223	0.88
4.0^+	91.1	12023	0.95	-91.4	-12068	-0.95
4.0^-	-95.4	-12598	-0.99	92.6	12228	0.96

Table 5.3: Summary of Peak Loads and Moments for Specimen CR3

Drift Cycle (%)	East Girder			West Girder		
	Load (kips)	**Moment (kip-in)**	M/M_p	**Load (kips)**	**Moment (kip-in)**	M/M_p
0.375^{+}	21.6	2847	0.22	-20.9	-2754	-0.22
0.375^{-}	-22.4	-2954	-0.23	21.2	2794	0.22
0.5^{+}	28.8	3806	0.30	-28.3	-3734	-0.29
0.5^{-}	-30.0	-3954	-0.31	28.1	3707	0.29
0.75^{+}	42.8	5652	0.45	-41.9	-5528	-0.44
0.75^{-}	-44.7	-5898	-0.46	42.3	5579	0.44
1.0^{+}	56.8	7498	0.59	-54.3	-7173	-0.57
1.0^{-}	-58.8	-7760	-0.61	57.3	7564	0.60
1.5^{+}	74.4	9818	0.77	-71.6	-9447	-0.74
1.5^{-}	-78.3	-10333	-0.81	75.7	9987	0.79
2.0^{+}	80.8	10659	0.84	-78.6	-10370	-0.82
2.0^{-}	-86.1	-11364	-0.89	83.4	11013	0.87
3.0^{+}	92.7	12241	0.96	-93.1	-12293	-0.97
3.0^{-}	-95.7	-12627	-0.99	94.2	12431	0.98
4.0^{+}	101.5	13391	1.05	-102.5	-13531	-1.07
4.0^{-}	-104.9	-13849	-1.09	105.2	13880	1.09

Table 5.4: Summary of Peak Loads and Moments for Specimen CR4

Drift Cycle (%)	East Girder			West Girder		
	Load (kips)	**Moment (kip-in)**	M/M_p	**Load (kips)**	**Moment (kip-in)**	M/M_p
0.375^+	23.1	3045	0.24	-22.3	-2949	-0.23
0.375^-	-22.5	-2967	-0.23	22.7	2998	0.24
0.5^+	30.8	4071	0.32	-29.9	-3952	-0.31
0.5^-	-30.0	-3962	-0.31	30.2	4001	0.32
0.75^+	46.2	6103	0.48	-44.7	-5910	-0.47
0.75^-	-44.9	-5927	-0.47	45.7	6052	0.48
1.0^+	61.6	8135	0.64	-58.9	-7794	-0.61
1.0^-	-59.3	-7829	-0.62	61.0	8076	0.64
1.5^+	82.6	10909	0.86	-81.1	-10679	-0.84
1.5^-	-84.1	-11103	-0.87	76.6	10231	0.81
2.0^+	57.2	7552	0.59	-57.6	-7611	-0.60

Table 5.5: Summary of Peak Loads and Moments for Specimen CR4R

Drift Cycle (%)	East Girder			West Girder		
	Load (kips)	**Moment (kip-in)**	M/M_p	**Load (kips)**	**Moment (kip-in)**	M/M_p
0.375^+	23.1	3054	0.24	-22.4	-2960	-0.23
0.375^-	-23.9	-3154	-0.25	22.4	2959	0.23
0.5^+	30.7	4049	0.32	-30.2	-3991	-0.31
0.5^-	-31.7	-4190	-0.33	29.8	3939	0.31
0.75^+	45.8	6045	0.48	-45.4	-5987	-0.47
0.75^-	-47.8	-6305	-0.50	45.1	5950	0.47
1.0^+	60.5	7983	0.63	-59.8	-7900	-0.62
1.0^-	-63.7	-8408	-0.66	60.3	7956	0.63
1.5^+	84.4	11144	0.88	-83.2	-10989	-0.87
1.5^-	-89.3	-11791	-0.93	86.8	11462	0.90
2.0^+	96.5	12737	1.00	-94.5	-12479	-0.98
2.0^-	-98.1	-12946	-1.02	95.2	12570	0.99
3.0^+	104.4	13784	1.09	-104.6	-13804	-1.09
3.0^-	-107.8	-14235	-1.12	105.6	13942	1.10
4.0^+	114.3	15089	1.19	-114.7	-15139	-1.19
4.0^-	-117.3	-15478	-1.22	114.3	15087	1.19

Table 5.6: Summary of Peak Loads and Moments for Specimen CR5

Drift Cycle (%)	East Girder			West Girder		
	Load (kips)	**Moment (kip-in)**	M/M_p	**Load (kips)**	**Moment (kip-in)**	M/M_p
0.375^+	20.4	2691.047	0.211893	-19.2	-2537	-0.20
0.375^-	-20.8	-2743.64	-0.21603	19.5	2568	0.20
0.5^+	26.9	3552.141	0.279696	-26.4	-3491	-0.27
0.5^-	-27.9	-3682.08	-0.28993	25.8	3408	0.27
0.75^+	40.1	5289.797	0.416519	-39.4	-5203	-0.41
0.75^-	-42.1	-5553.8	-0.43731	38.6	5089	0.40
1.0^+	52.8	6970.734	0.548877	-52.6	-6945	-0.55
1.0^-	-56.6	-7466.77	-0.58793	51.6	6806	0.54
1.5^+	74.7	9863.391	0.776645	-74.6	-9848	-0.78
1.5^-	-77.5	-10230.5	-0.80555	73.5	9704	0.76
2.0^+	84.9	11204.02	0.882206	-84.9	-11205	-0.88
2.0^-	-84.5	-11148.3	-0.87782	80.4	10606	0.84
3.0^+	93.7	12364.17	0.973557	-93.0	-12277	-0.97
3.0^-	-98.8	-13040.7	-1.02682	94.9	12525	0.99
4.0^+	103.9	13720.27	1.080336	-103.0	-13592	-1.07
4.0^-	-107.7	-14216.3	-1.11939	105.0	13824	1.09

Table 5.7: Progression of Yielding and Fracture in Specimen CR1

Drift Cycle	Location/Description
1st @ 0.75%	Minor yielding in all girder flanges beyond CJP weld toes; minor panel zone yielding in center of North side of web
1st @ 1.0%	Moderate panel zone yielding in both sides of column web
1st @ 1.5%	Moderate girder flange yielding; minor local yielding on outer face of column flanges at level of girder flanges
1st @ 4.0%	Complete panel zone yielding; significant column and girder flange yielding, minor local yielding at edges of shear tabs
4th @ 4.0%	Initial fracture at bottom edge of West shear tab (length < 0.5 in.)
8th @ 4.0%	Remaining three shear tab edges cracked
11th @ 4.0%	Visible LCF crack at toe of reinforcing fillet welds in center of East and West bottom flanges
15th @ 4.0%	Complete fracture of East bottom flange, LCF crack in West bottom flange continues to grow in stable manner
17th @ 4.0%	Crack at bottom edge of East shear tab growing following flange fracture, moderate local buckling of West bottom flange
18th @ 4.0%	Crack length at bottom edge of East shear tab reached approximately half the girder depth
20th @ 4.0%	Test stopped due to excessive strength degradation in East Girder

Table 5.8: Progression of Yielding and Fracture in Specimen CR2

Drift Cycle	Location/Description
1st @ 0.75%	Minor yielding in all girder flanges beyond CJP weld toes
1st @ 1.0%	Moderate yielding in all girder flanges beyond CJP weld toes
1st @ 1.5%	Moderate panel zone yielding in doubler plate (South) and column web (North); minor local yielding on outer face of column flanges at level of girder flanges
1st @ 2.0%	Moderate local yielding on outer face of column flanges at level of girder flanges
1st @ 3.0%	Complete panel zone yielding
2nd @ 3.0%	Visible indication of an initial LCF crack at toe of CJP welds in center of West top flange; minor local flange buckling at East bottom flange
1st @ 4.0%	Visible indication of an initial LCF crack at toe of CJP welds in center of East top flange; visible indication of an initial LCF crack at toe of reinforcing fillet welds in center of West bottom flange
3rd @ 4.0%	Visible indication of an initial LCF crack at toe of reinforcing fillet welds in center of East bottom flange
5th @ 4.0%	Initial crack at top edge of East shear tab (length < 1.0 in.); initial crack at bottom edge of East shear tab (length < 0.5 in.); moderate local flange buckling at all girder flanges
7th @ 4.0%	Initial crack at top edge of West shear tab (length < 1.0 in.)
9th @ 4.0%	Initial crack at bottom edge of West shear tab (length < 0.5 in.)
11th @ 4.0%	Significant LCF crack opening at toe of CJP welds in center of West top flange
17th @ 4.0%	Complete fracture of West top flange
18th @ 4.0%	Test stopped due to excessive strength degradation in West girder

Table 5.9: Progression of Yielding and Fracture in Specimen CR3

Drift Cycle	Location/Description
1st @ 0.75%	Minor yielding in all girder flanges beyond CJP weld toes
1st @ 1.0%	Moderate yielding in all girder flanges beyond CJP weld toes
1st @ 1.5%	Moderate panel zone yielding in both doubler plates; minor local yielding on outer face of column flanges at level of girder flanges
1st @ 2.0%	Significant panel zone yielding in both doubler plates; moderate local yielding on outer face of column flanges at level of girder flanges
1st @ 3.0%	Complete panel zone yielding; minor local flange buckling at East top flange and West bottom flange
2nd @ 3.0%	Visible indication of an initial LCF crack at toe of reinforcing fillet welds in center of East bottom flange; Visible indication of an initial LCF crack at toe of CJP welds in center of East top flange
1st @ 4.0%	Visible indication of an initial LCF crack at toe of CJP welds in center of East top flange; minor local flange buckling at East bottom flange; moderate local flange buckling at East top flange and West bottom flange
2nd @ 4.0%	Initial crack at bottom edge of East shear tab; Initial crack at top edge of West shear tab
3rd @ 4.0%	Initial crack at top edge of East shear tab; Initial crack at bottom edge of West shear tab
9th @ 4.0%	Significant LCF crack opening at toe of reinforcing fillet welds in center of East bottom flange; maximum crack lengths at top and bottom edges of West shear tab (2 and 1.5 in., respectively)
10th @ 4.0%	Maximum crack lengths at top and bottom edges of East shear tab (0.25 and 1 in., respectively)
15th @ 4.0%	Complete fracture of East bottom flange
16th @ 4.0%	Test stopped due to excessive strength degradation in East girder

Table 5.10: Progression of Yielding and Fracture in Specimen CR4

Drift Cycle	Location/Description
1st @ 0.75%	Minor yielding in girder flanges beyond CJP weld toes
1st @ 1.0%	Minor panel zone yielding visible near center of North doubler plate
2nd @ 1.0%	Initial cracking in center of East top flange weld (from strain data)
3rd @ 1.0%	Initial cracking across width of West top flange weld (from strain data)
1st @ 1.5%	Moderate beam flange yielding; visible yielding in both doubler plates; cracks visible in East and West top flanges across entire flange width
2nd @ 1.5%	Complete fracture of West top flange
1st @ 2.0%	Complete fracture of East top flange; complete fracture of West bottom flange; test stopped after half-cycle

Table 5.11: Progression of Yielding and Fracture in Specimen CR4R

Drift Cycle	Location/Description
1st @ 0.75%	Minor yielding in all girder flanges beyond CJP weld toes
1st @ 1.0%	Moderate yielding in all girder flanges beyond CJP weld toes
1st @ 1.5%	Minor panel zone yielding in both doubler plates
1st @ 3.0%	Moderate panel zone yielding in both doubler plates; minor local yielding on outer face of column flanges at level of girder flanges
1st @ 4.0%	Significant panel zone yielding; moderate local yielding on outer face of column flanges at level of girder flanges
2nd @ 4.0%	Initial LCF crack along toe of CJP welds in West top flange; Initial edge crack at the North tip of East top flange
3rd @ 4.0%	Initial crack at bottom edge of East shear tab (length < 0.25 in.)
5th @ 4.0%	Initial LCF crack along toe of CJP welds in East top flange
9th @ 4.0%	Moderate local flange buckling at East top flange and West top flange
10th @ 4.0%	Moderate local flange buckling at East bottom flange
12th @ 4.0%	Significant edge crack opening at the North tip of East top flange
13th @ 4.0%	Test stopped due to the fracture of East top flange and to the extensive lateral-torsional buckling of West girder

Table 5.12: Progression of Yielding and Fracture in Specimen CR5

Drift Cycle	Location/Description
1st @ 0.75%	Minor yielding in all girder flanges beyond CJP weld toes
1st @ 1.0%	Moderate yielding in all girder flanges beyond CJP weld toes
1st @ 1.5%	Minor panel zone yielding in doubler plates; minor local yielding on outer face of column flanges at level of girder flanges
1st @ 2.0%	Moderate panel zone yielding in doubler plates; moderate local yielding on outer face of column flanges at level of girder flanges; initial crack at top edge of West shear tab (length < 1/8 in.)
2nd @ 2.0%	Initial crack at bottom edge of West shear tab (length < 1/8 in.)
1st @ 3.0%	Significant local yielding on outer face of column flanges at level of girder flanges; initial crack at top edge of East shear tab (length < 1/16 in.); Complete panel zone yielding
2nd @ 3.0%	Visible indication of an initial LCF crack at toe of CJP welds in center of East top flange; visible indication of an initial LCF crack at toe of reinforcing fillet welds in center of East bottom flange and West bottom flange
1st @ 4.0%	Visible indication of an initial LCF crack in the middle of CJP welds in West top flange
3rd @ 4.0%	Initial crack at bottom edge of East shear tab (length < 1/2 in.)
4th @ 4.0%	Crack length at bottom edge of East shear tab (< 3/4 in.); crack length at bottom edge of West shear tab (< 1/2 in.)
5th @ 4.0%	Significant crack opening in the middle of CJP welds in West top flange
7th @ 4.0%	Complete fracture of West top flange
11th @ 4.0%	Test stopped due to excessive strength degradation in West girder

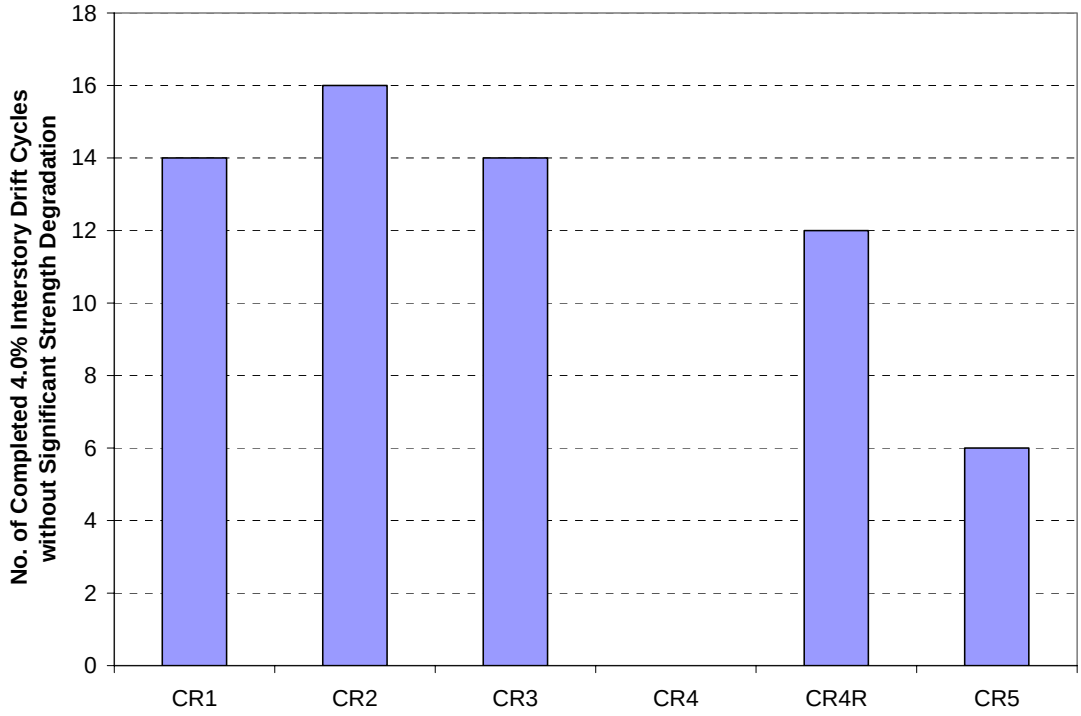


Figure 5.1: Number of Completed 4.0% Interstory Drift Cycles without Significant Strength Degradation

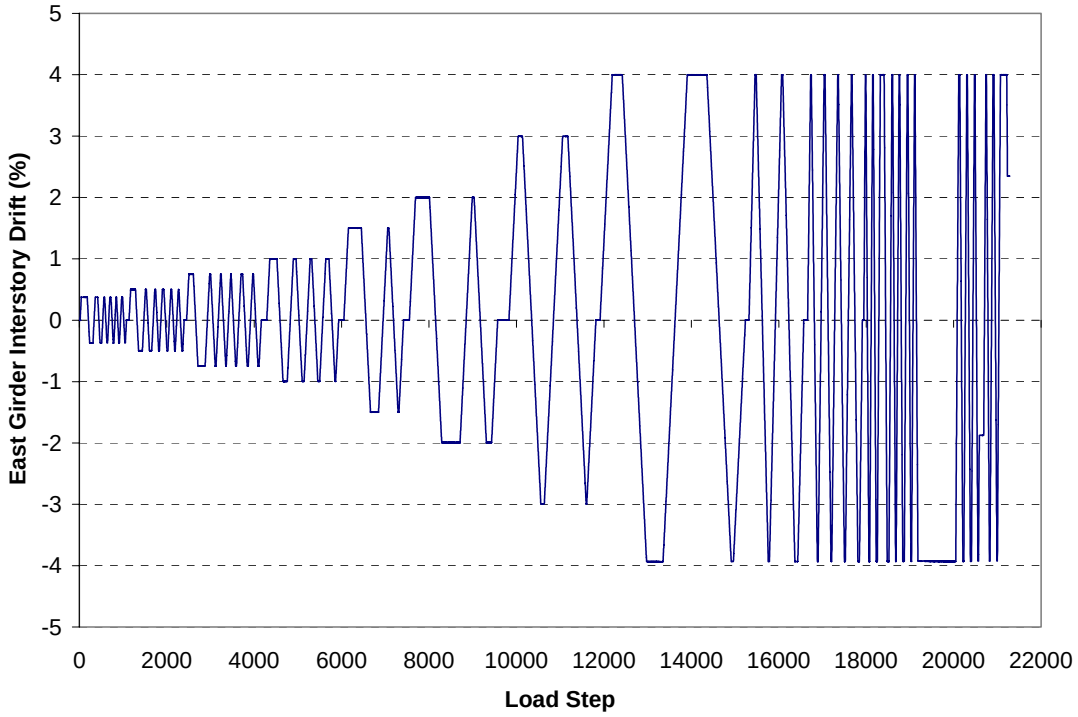


Figure 5.2: Displacement History of Specimen CR1

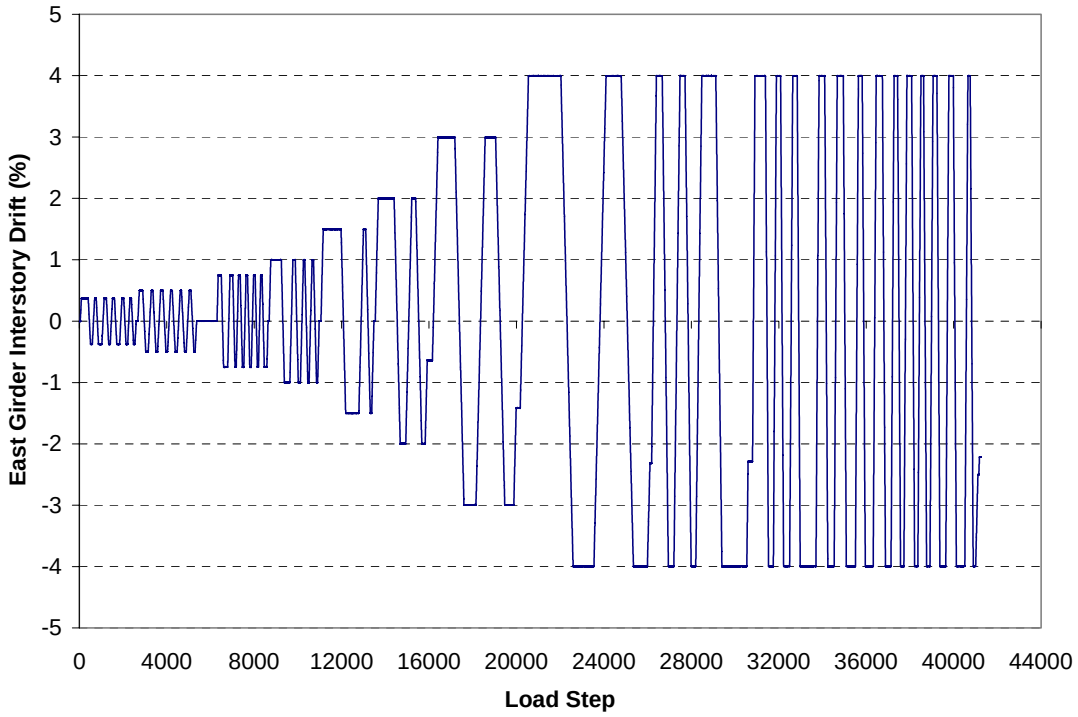


Figure 5.3: Displacement History of Specimen CR2

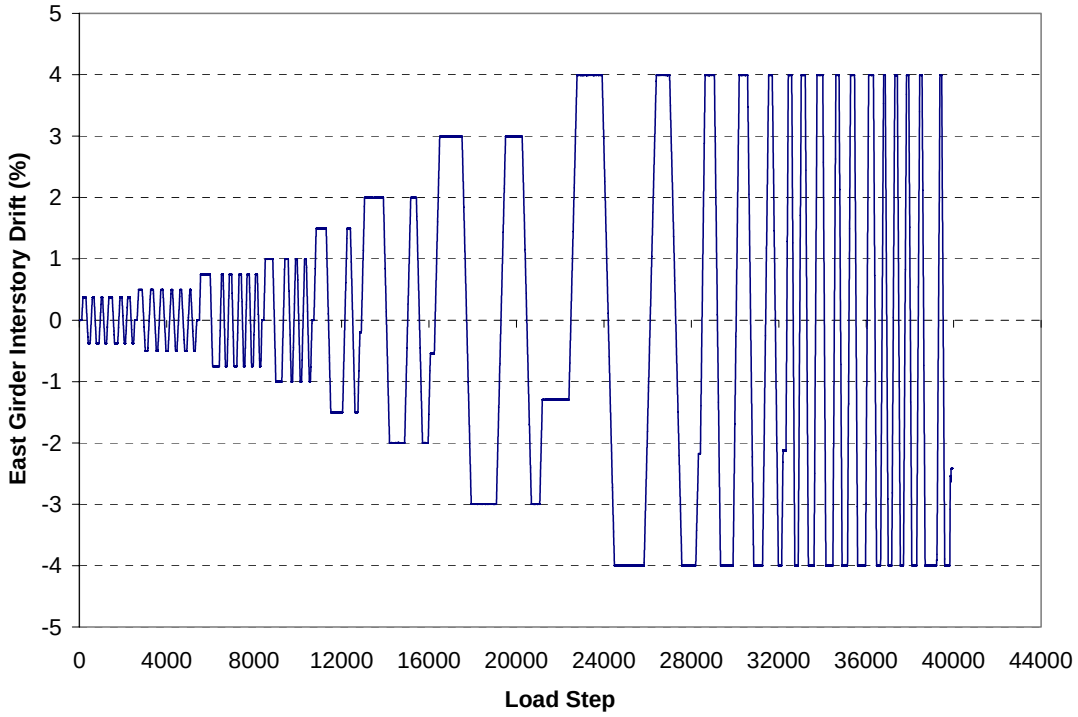


Figure 5.4: Displacement History of Specimen CR3

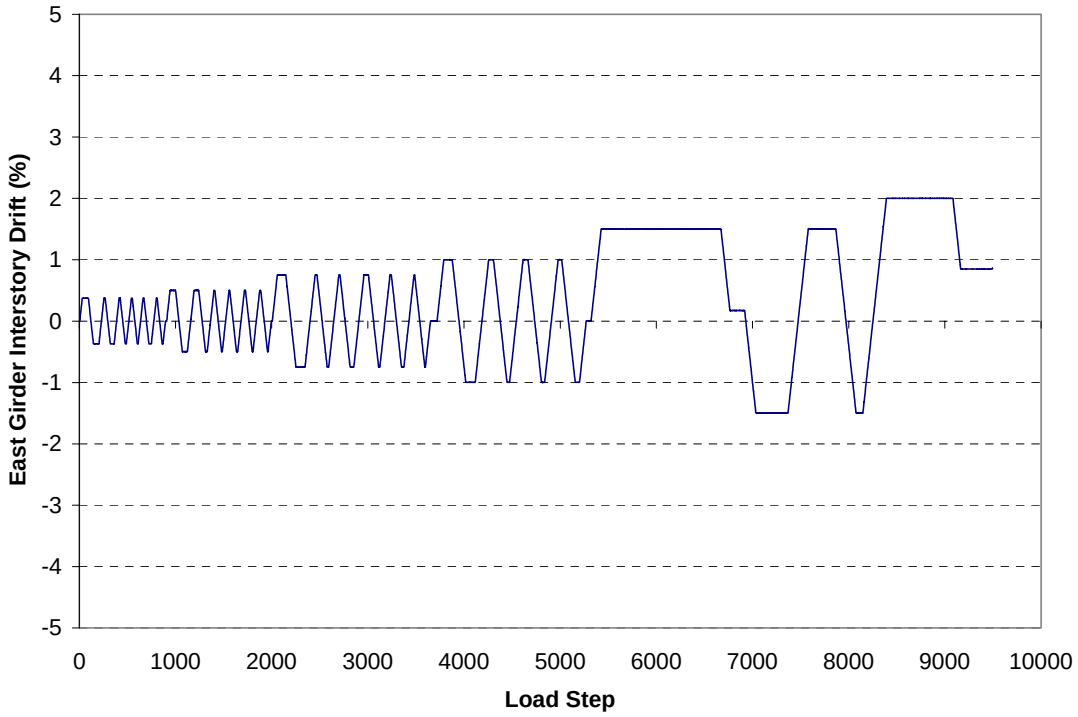


Figure 5.5: Displacement History of Specimen CR4

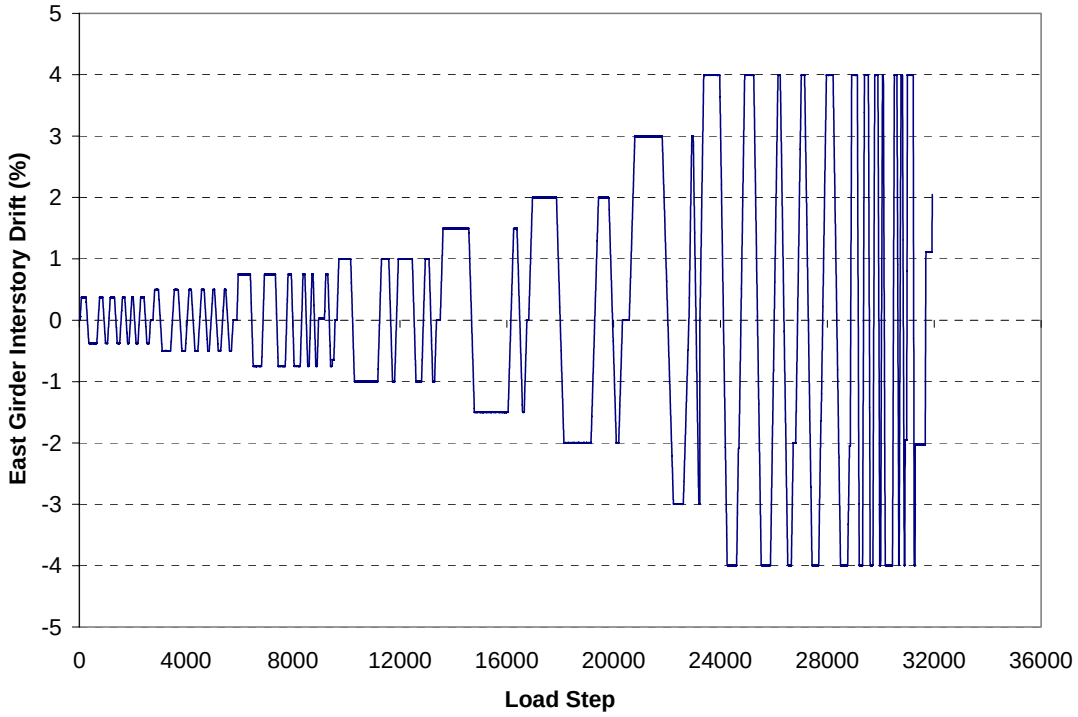


Figure 5.6: Displacement History of Specimen CR4R

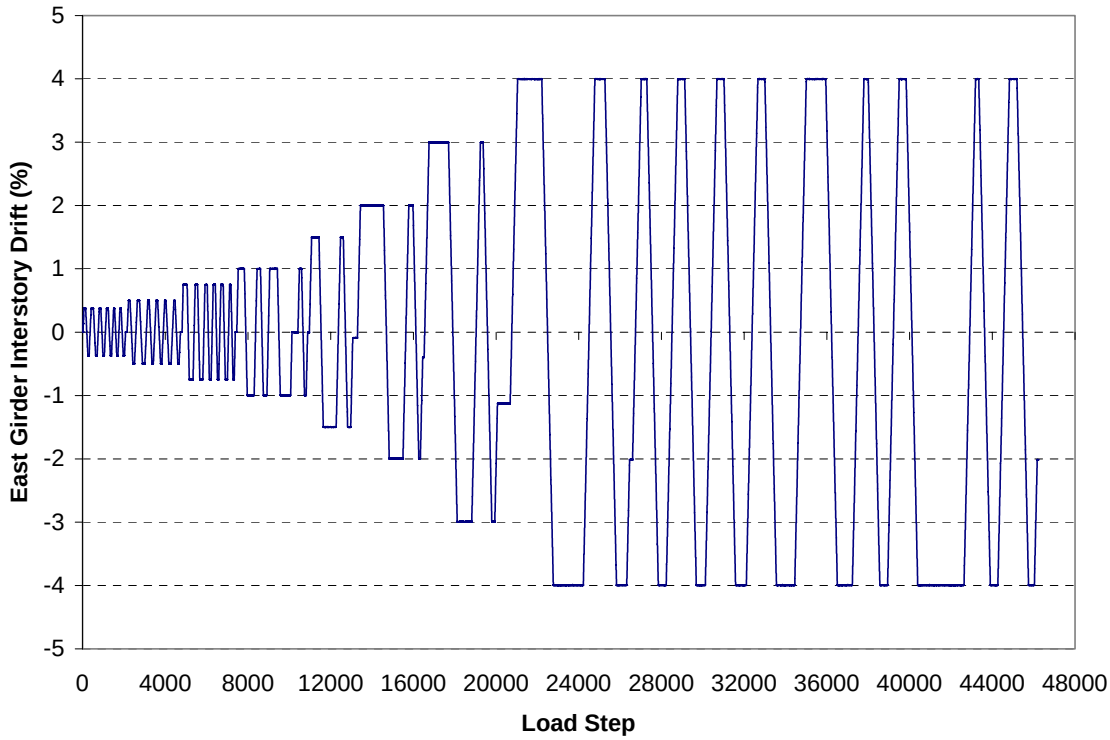


Figure 5.7: Displacement History of Specimen CR5

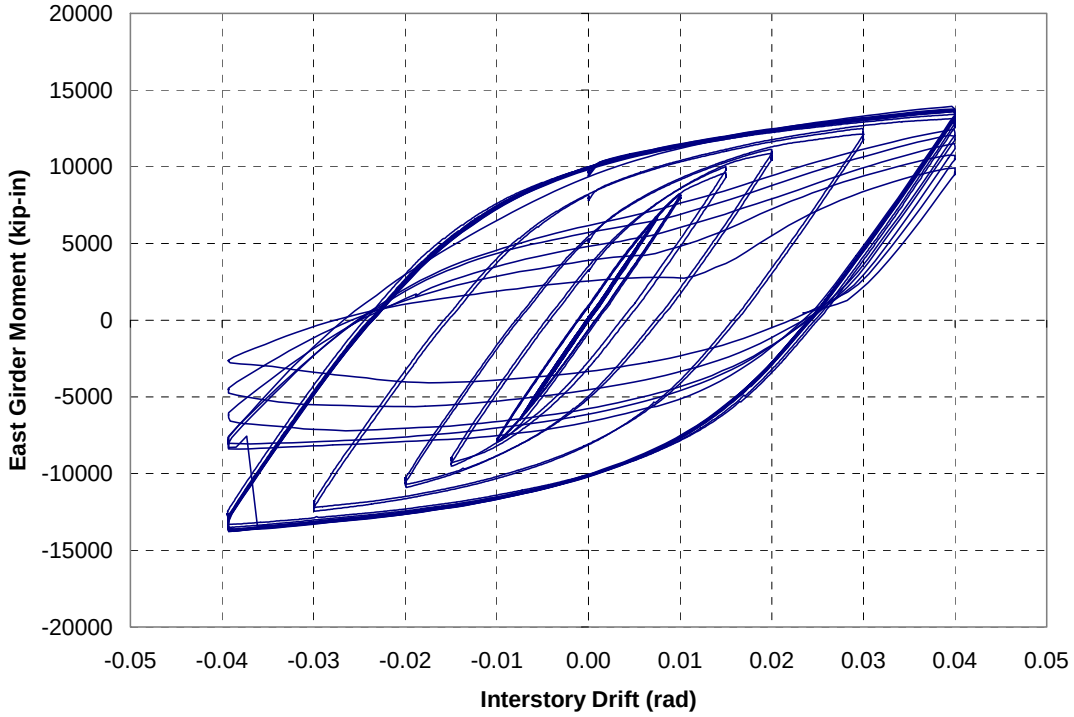


Figure 5.8: Moment vs. Interstory Drift for East Girder, CR1

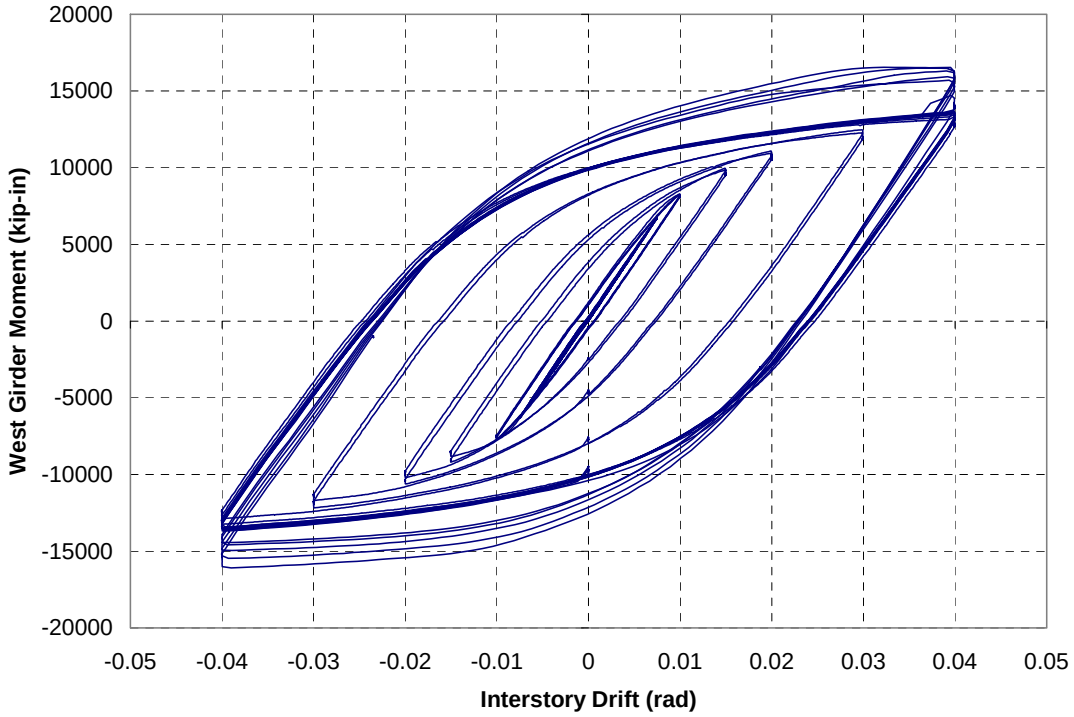


Figure 5.9: Moment vs. Interstory Drift for West Girder, CR1

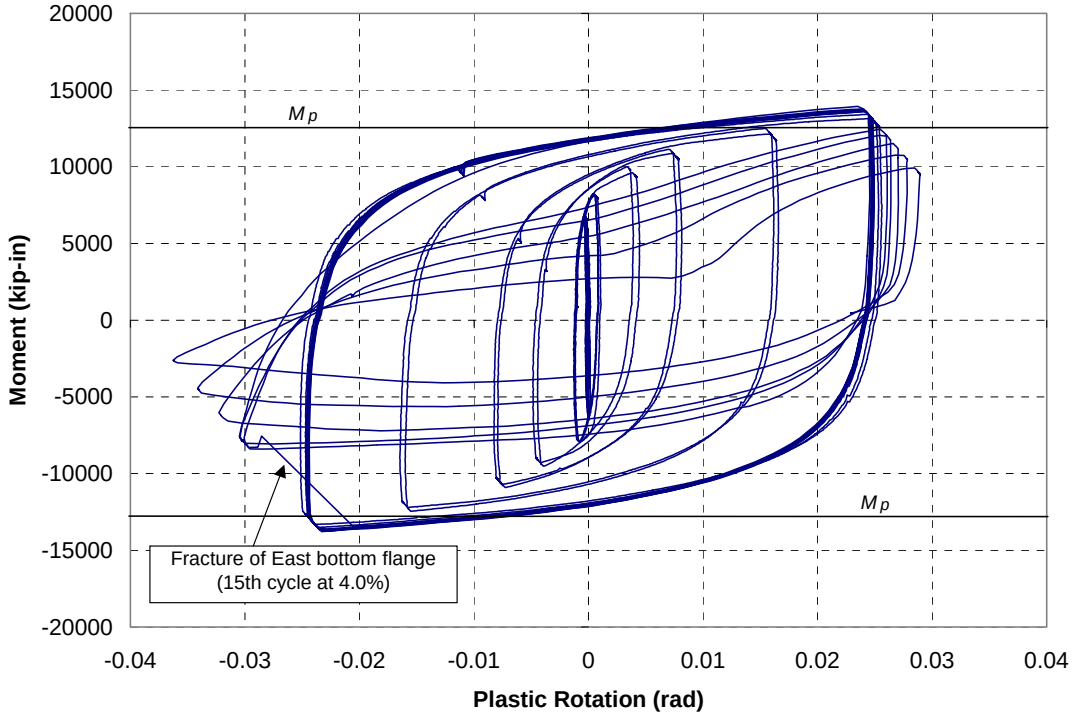


Figure 5.10: Plastic Rotation of East Connection, CR1

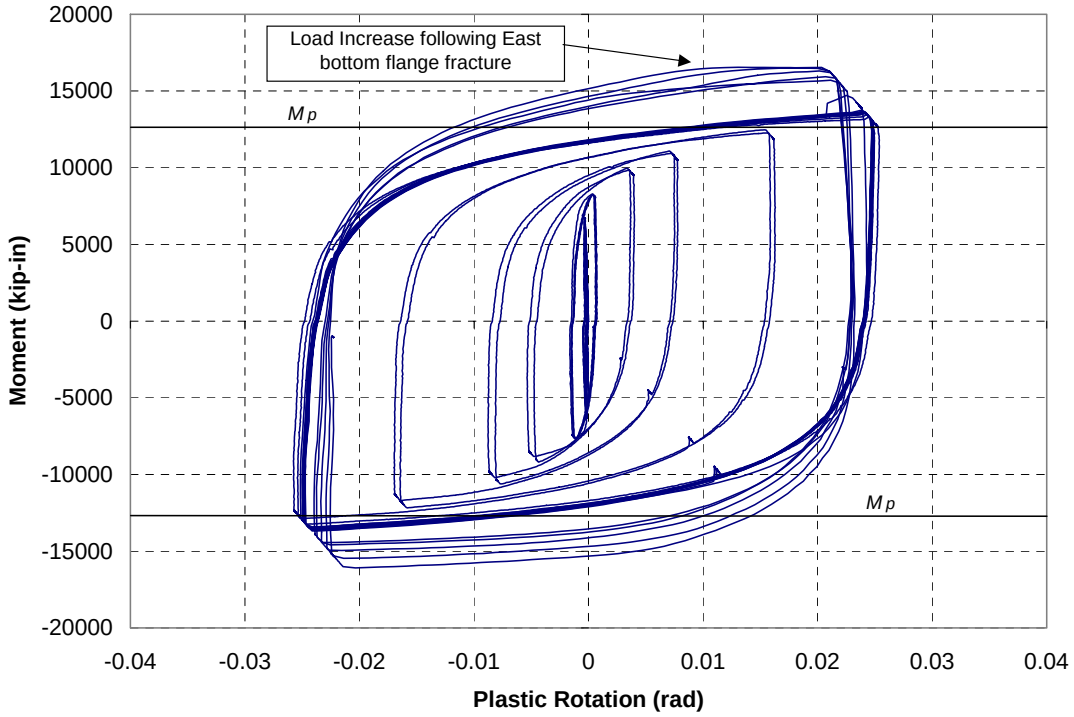


Figure 5.11: Plastic Rotation of West Connection, CR1

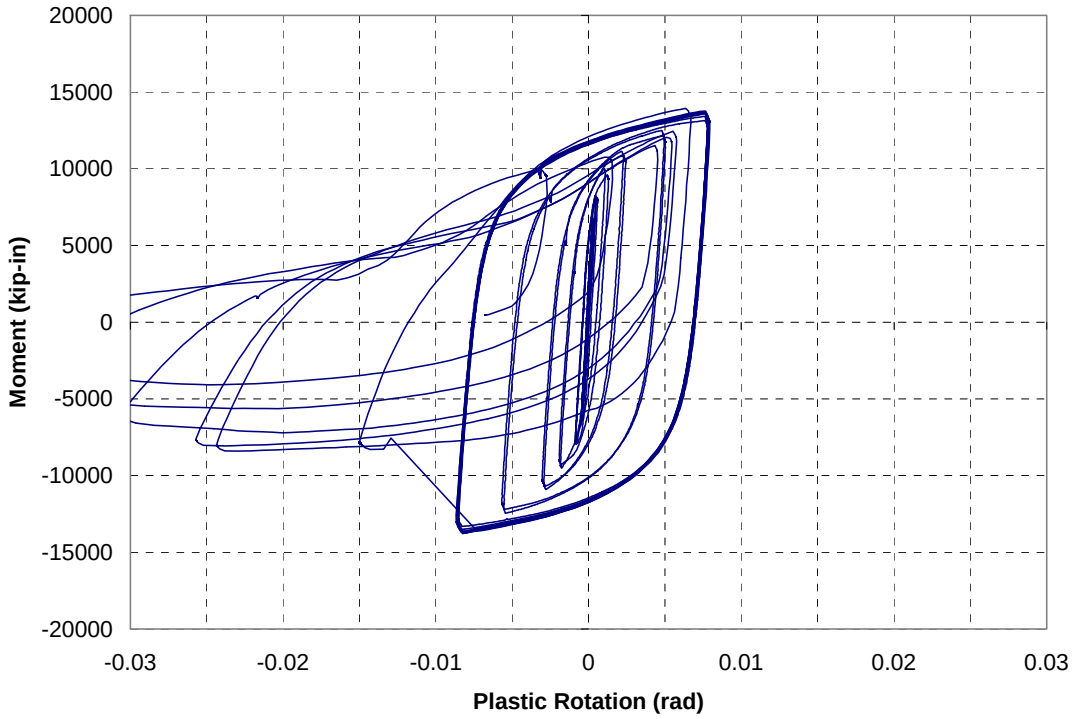


Figure 5.12: East Girder Plastic Rotation Relative to Column Centerline, CR1

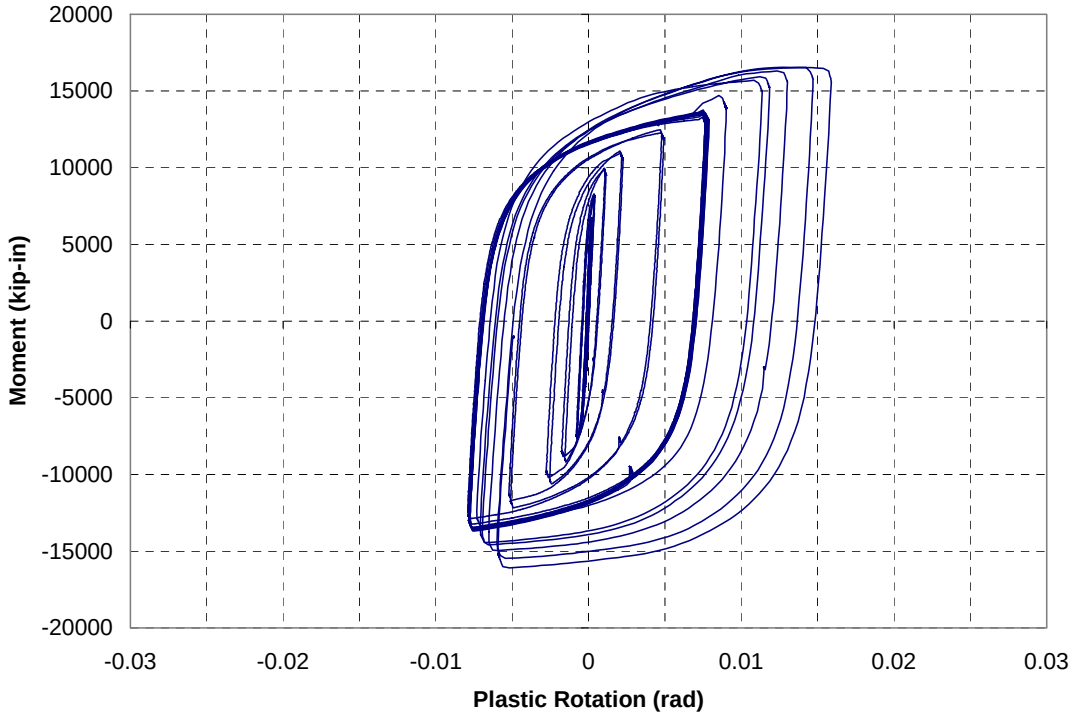


Figure 5.13: West Girder Plastic Rotation Relative to Column Centerline, CR1

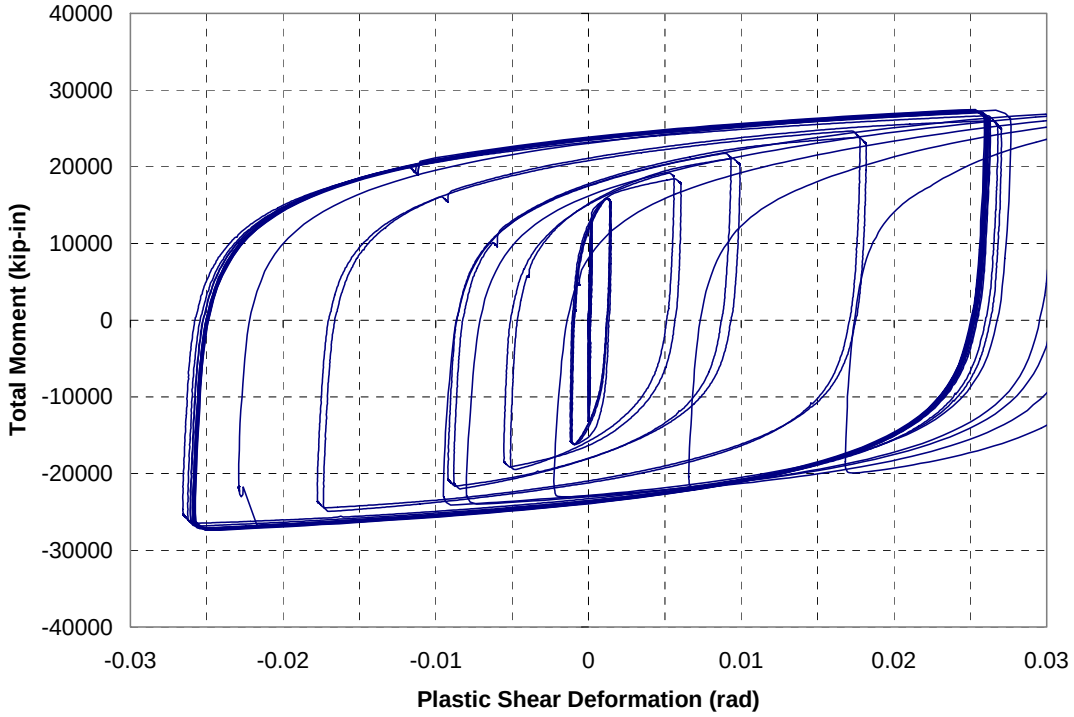


Figure 5.14: Panel Zone Plastic Shear Deformation, CR1

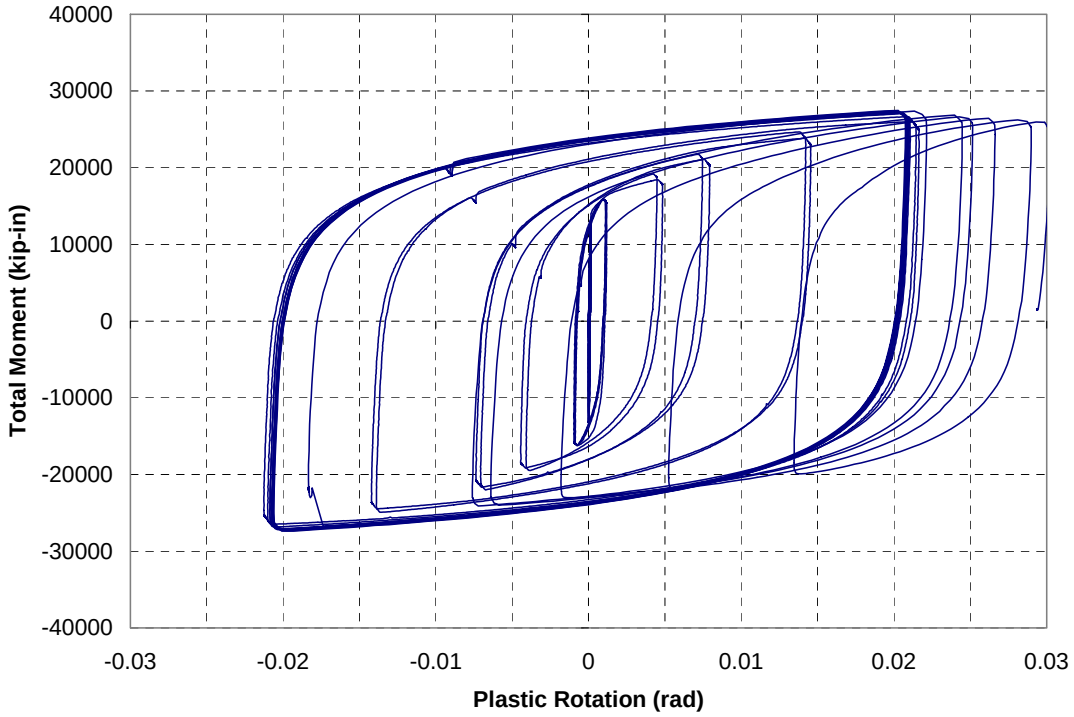


Figure 5.15: Panel Zone Plastic Rotation Relative to Column Centerline, CR1

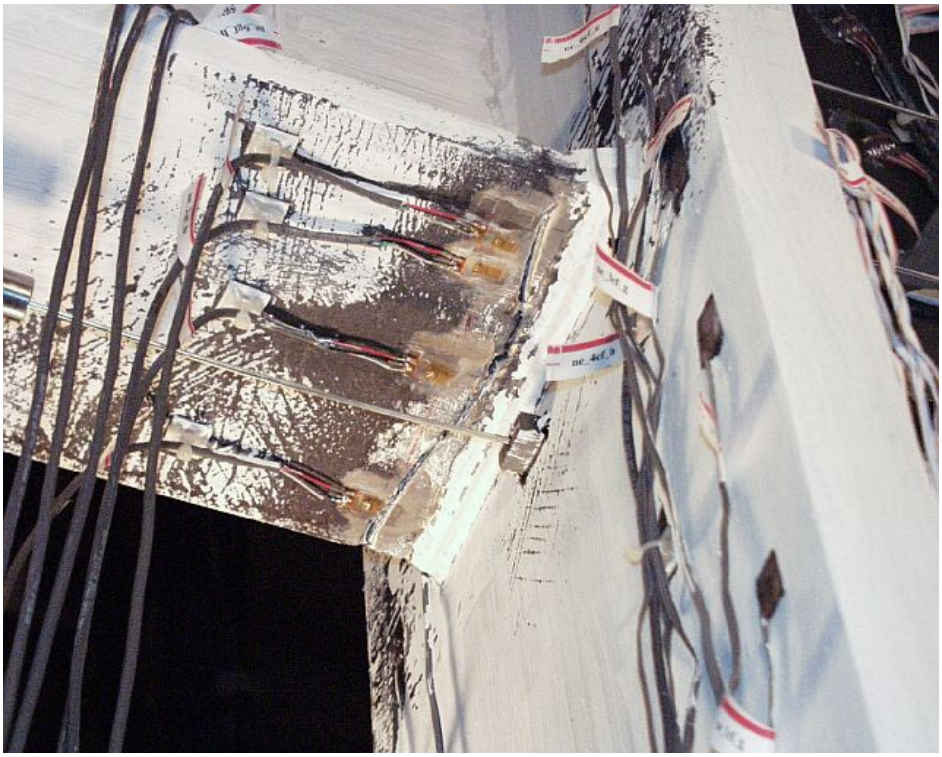


Figure 5.16: Low-Cycle Fatigue Fracture of East Bottom Flange, CR1



Figure 5.17: East Bottom Flange Fracture Following Test, CR1

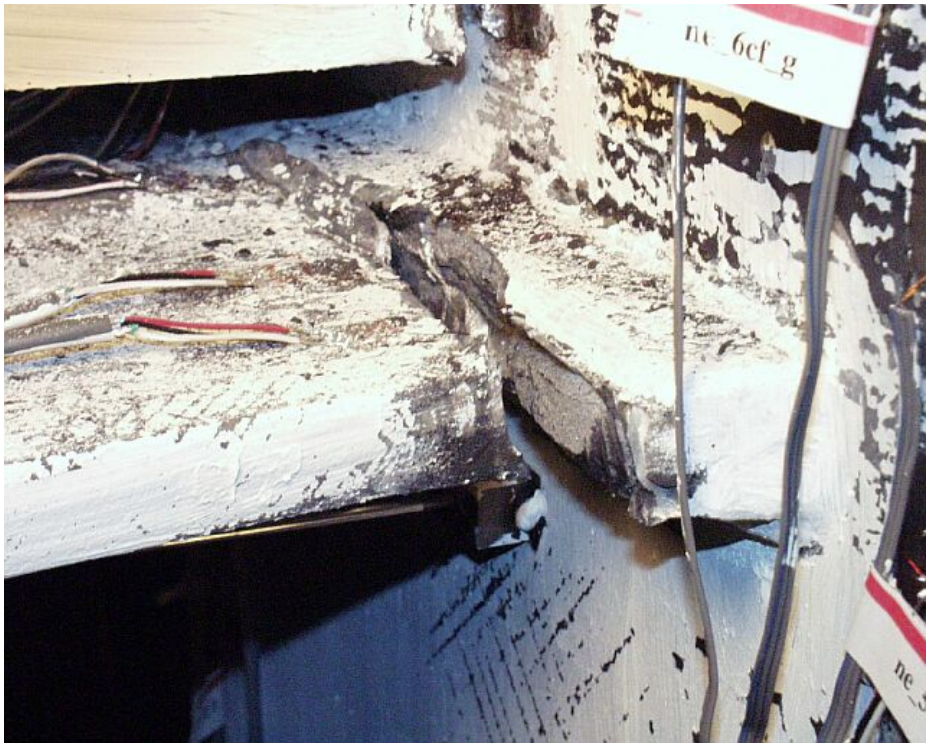


Figure 5.18: East Bottom Flange Fracture Surface After Testing, CR1



Figure 5.19: Typical Beam Web-to-Column Weld Cracking, CR1

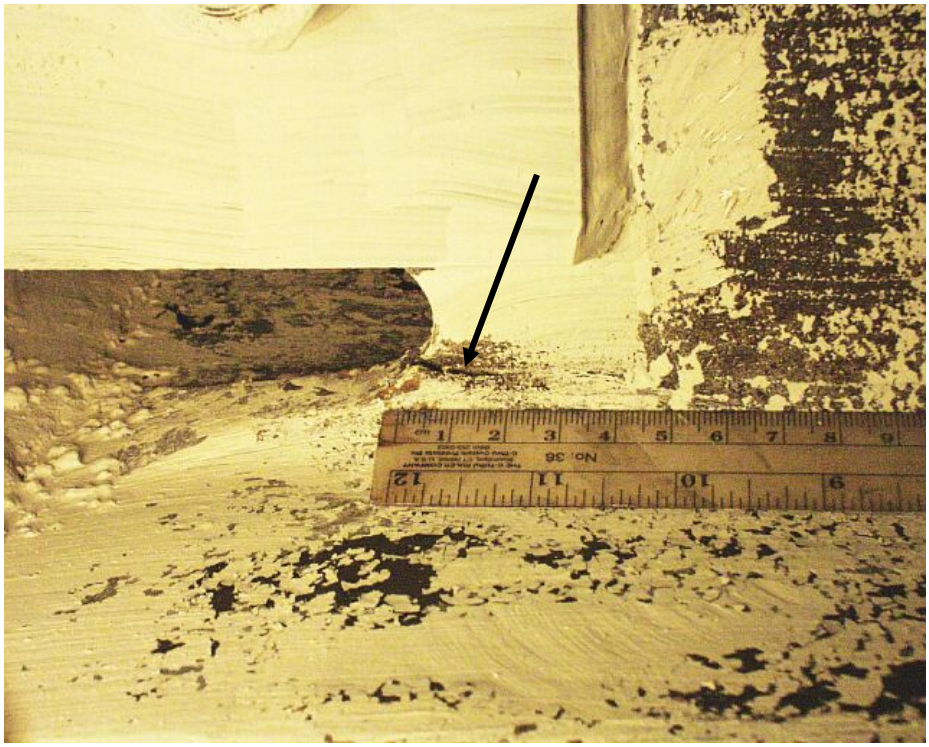


Figure 5.20: Typical Low-Cycle Fatigue Cracking of Access Hole

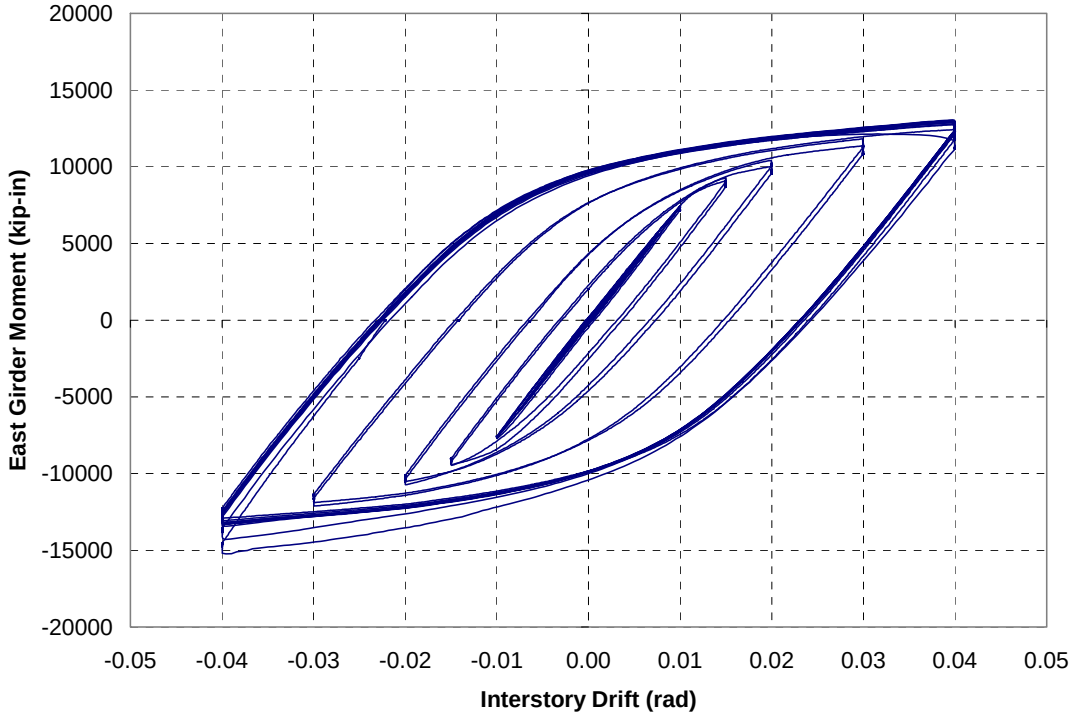


Figure 5.21: Moment vs. Interstory Drift for East Girder, CR2

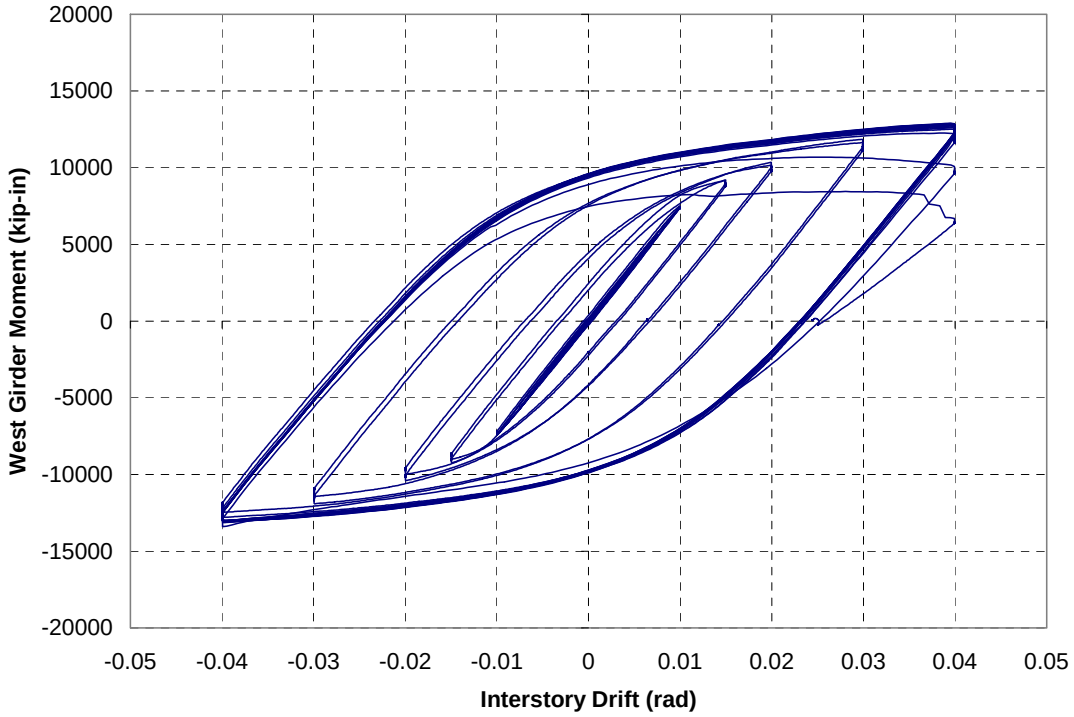


Figure 5.22: Moment vs. Interstory Drift for West Girder, CR2

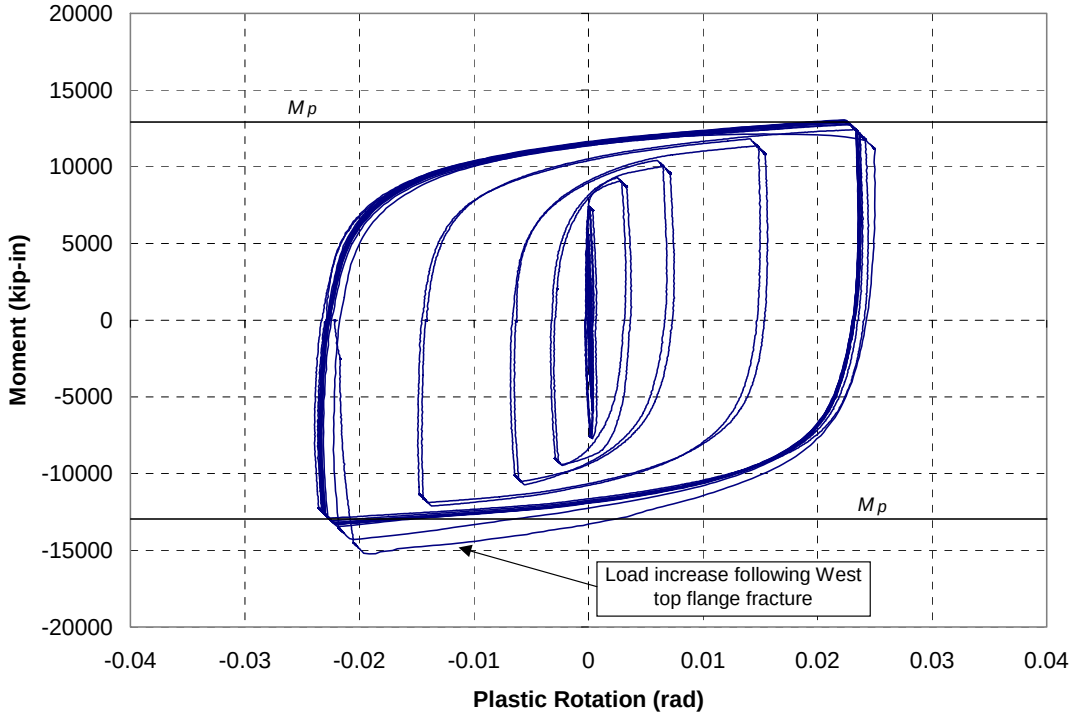


Figure 5.23: Plastic Rotation of East Connection, CR2

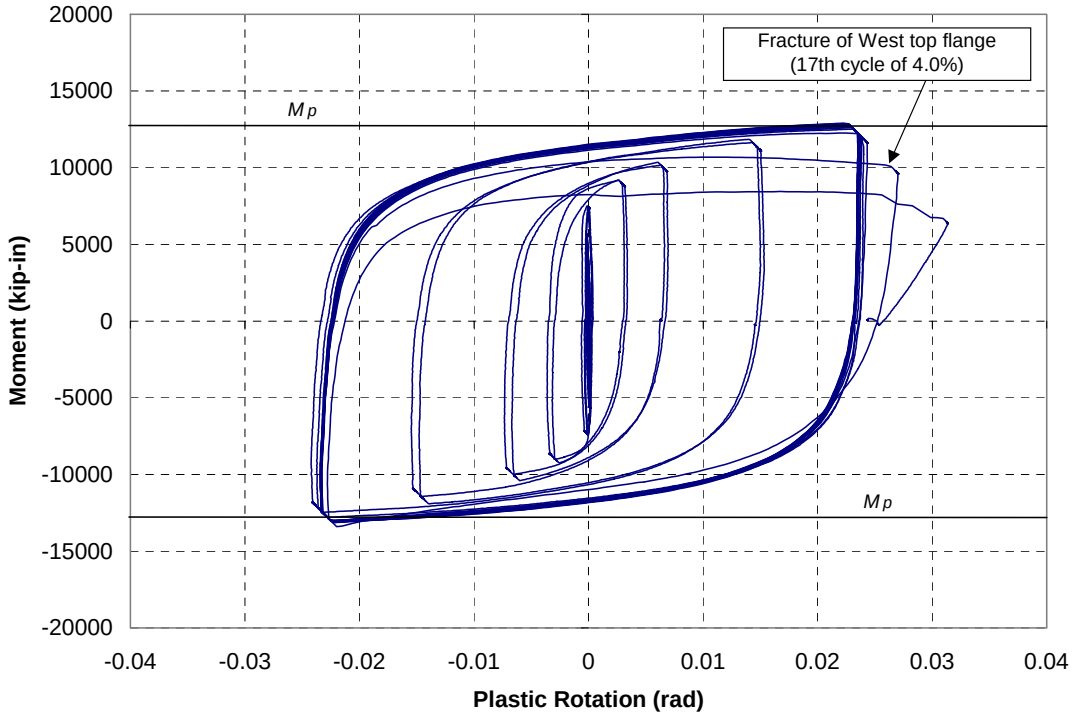


Figure 5.24: Plastic Rotation of West Connection, CR2

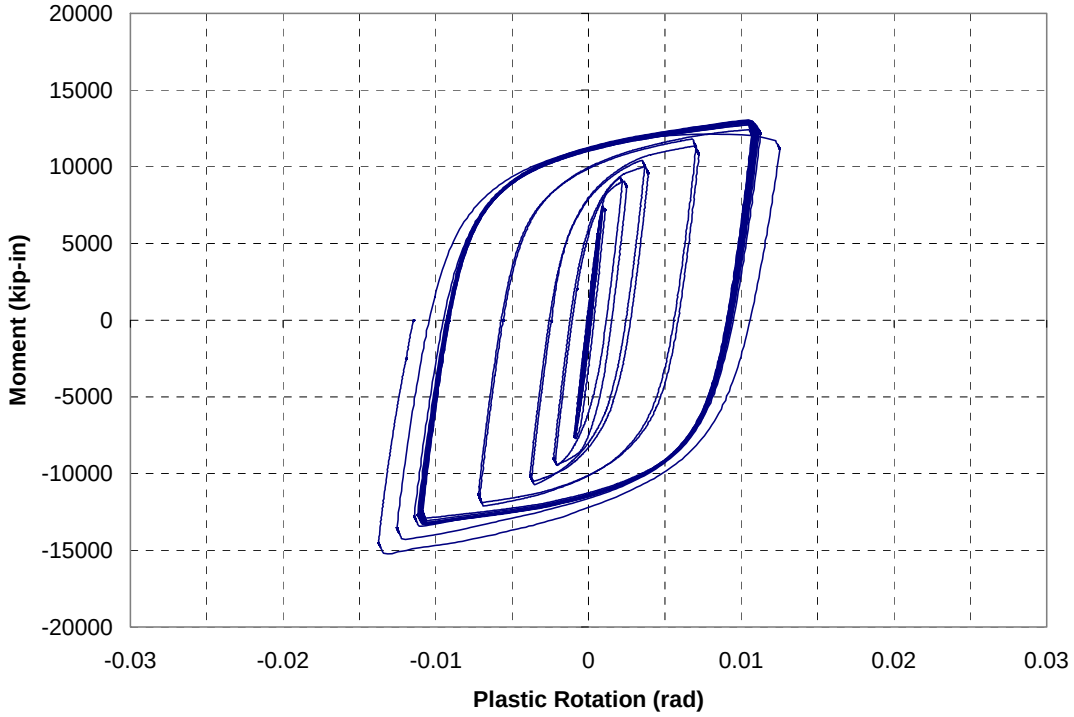


Figure 5.25: East Girder Plastic Rotation Relative to Column Centerline, CR2

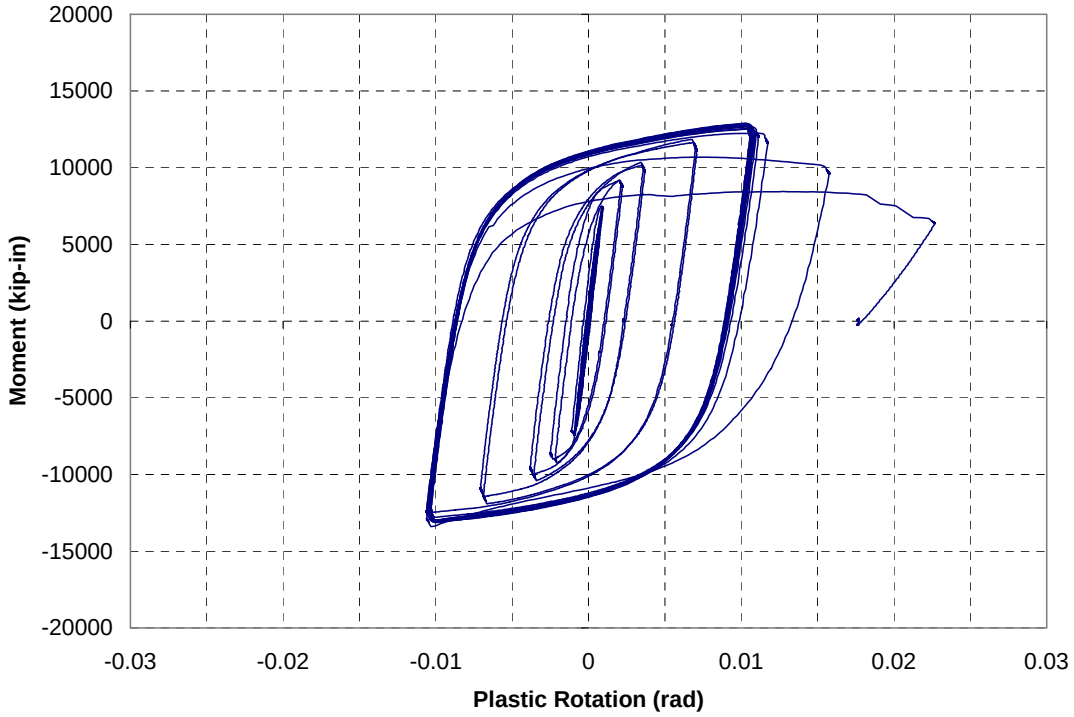


Figure 5.26: West Girder Plastic Rotation Relative to Column Centerline, CR2

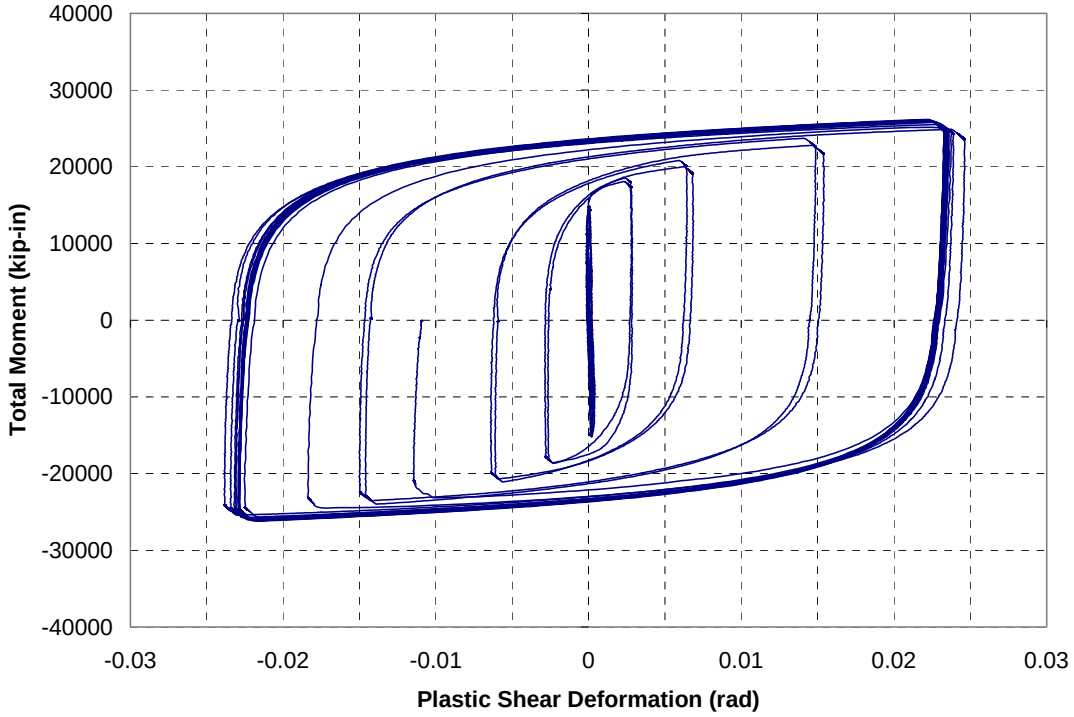


Figure 5.27: Panel Zone Plastic Shear Deformation, CR2

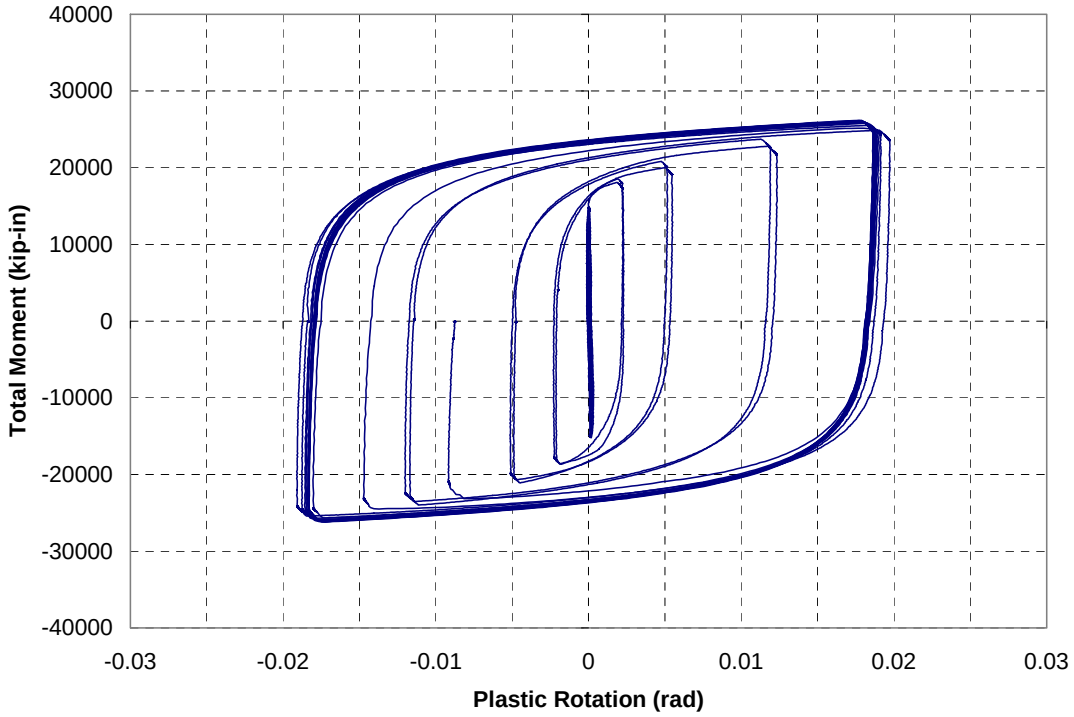


Figure 5.28: Panel Zone Plastic Rotation Relative to Column Centerline, CR2



Figure 5.29: Panel Zone Yielding and Column Local Flange Deformation, CR2



Figure 5.30: Significant Crack Opening in West Top Flange, CR2



Figure 5.31: Fracture in West Top Flange, CR2



Figure 5.32: Complete Failure of West Top Flange, CR2

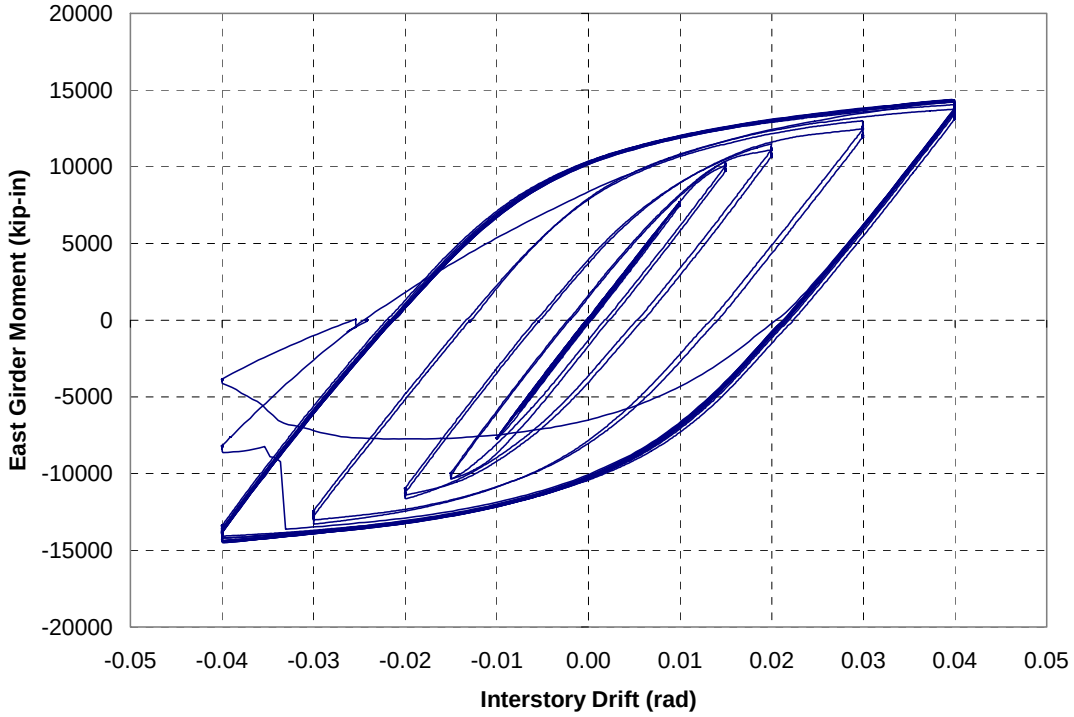


Figure 5.33: Moment vs. Interstory Drift for East Girder, CR3

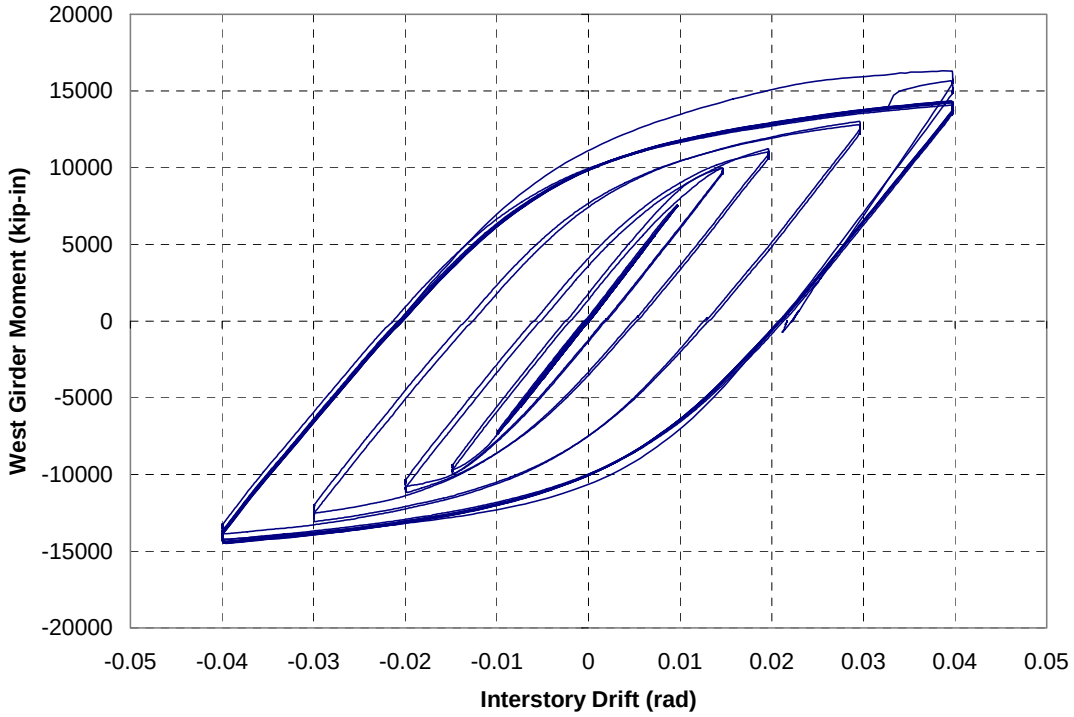


Figure 5.34: Moment vs. Interstory Drift for West Girder, CR3

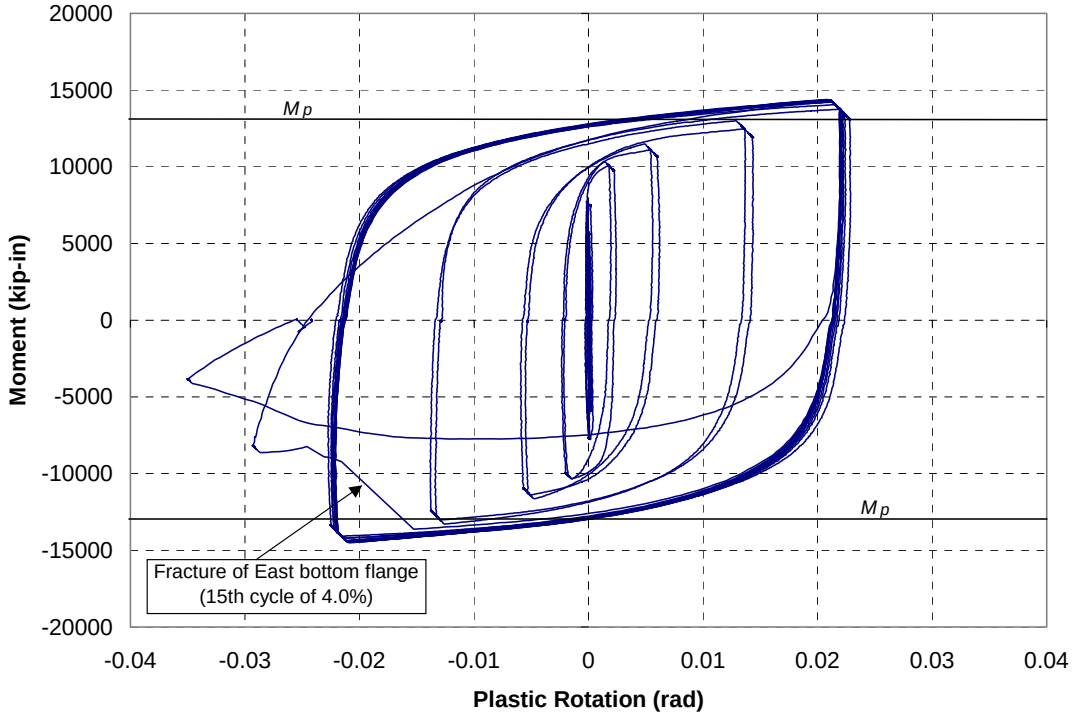


Figure 5.35: Plastic Rotation of East Girder, CR3

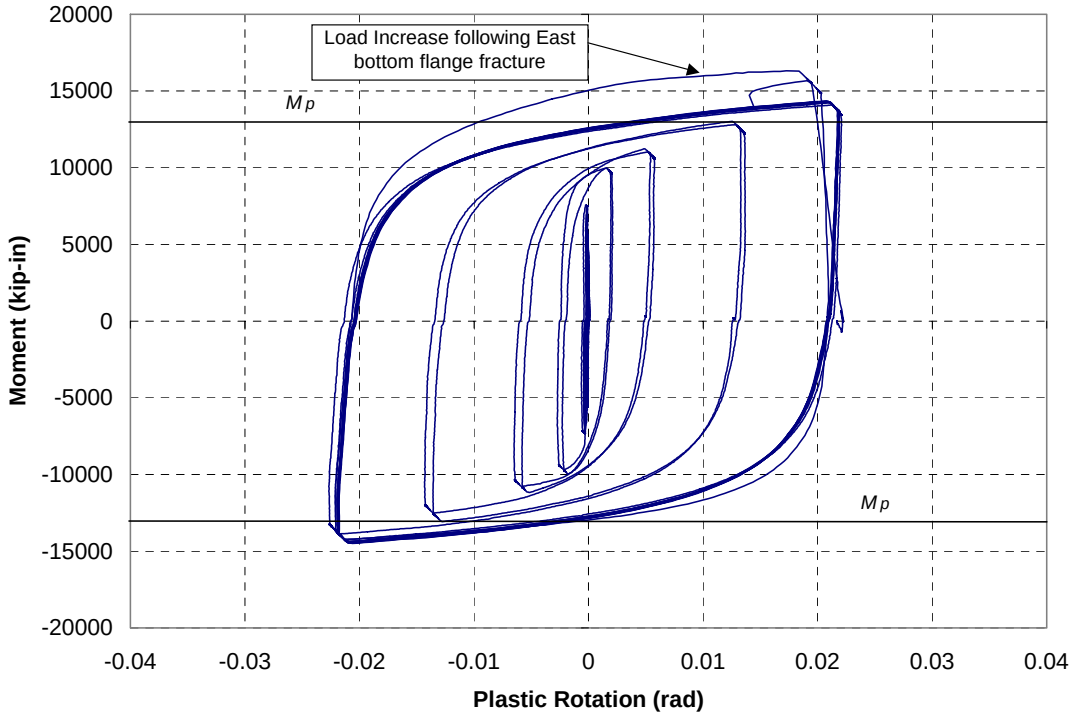


Figure 5.36: Plastic Rotation of West Girder, CR3

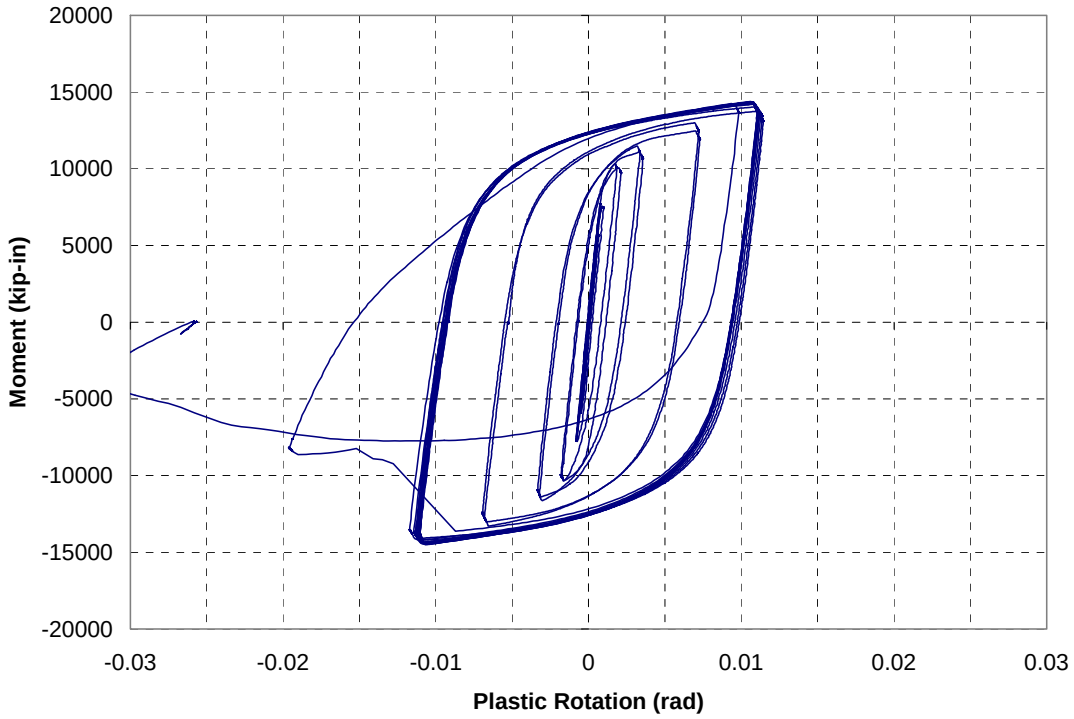


Figure 5.37: East Girder Plastic Rotation Relative to Column Centerline, CR3

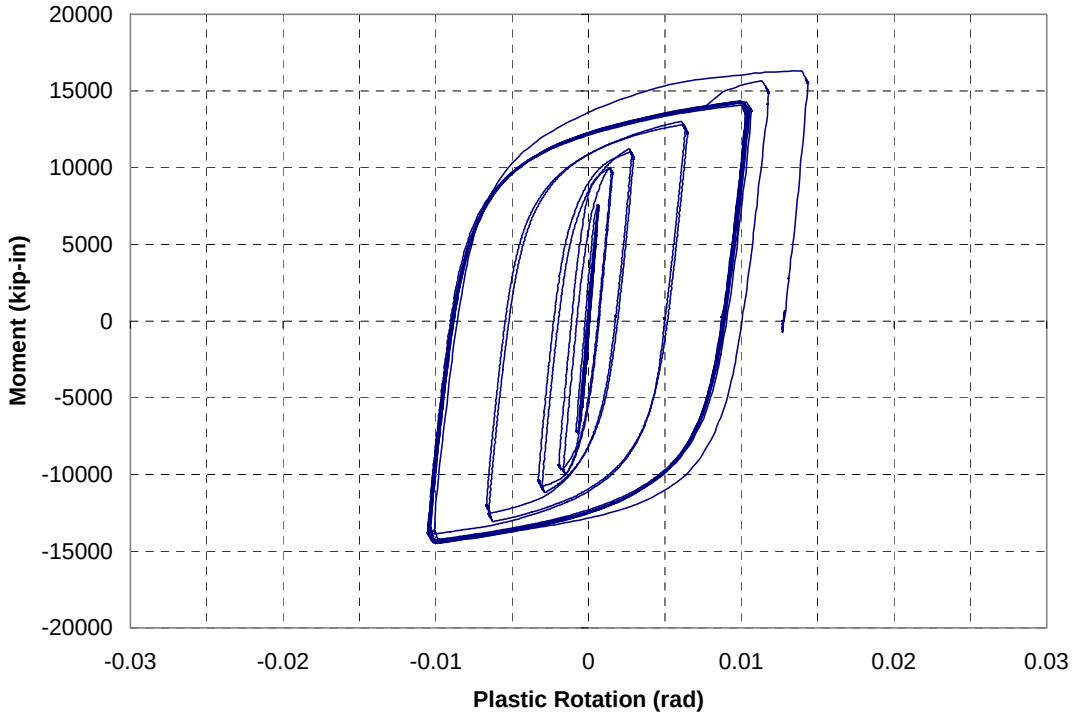


Figure 5.38: West Girder Plastic Rotation Relative to Column Centerline, CR3

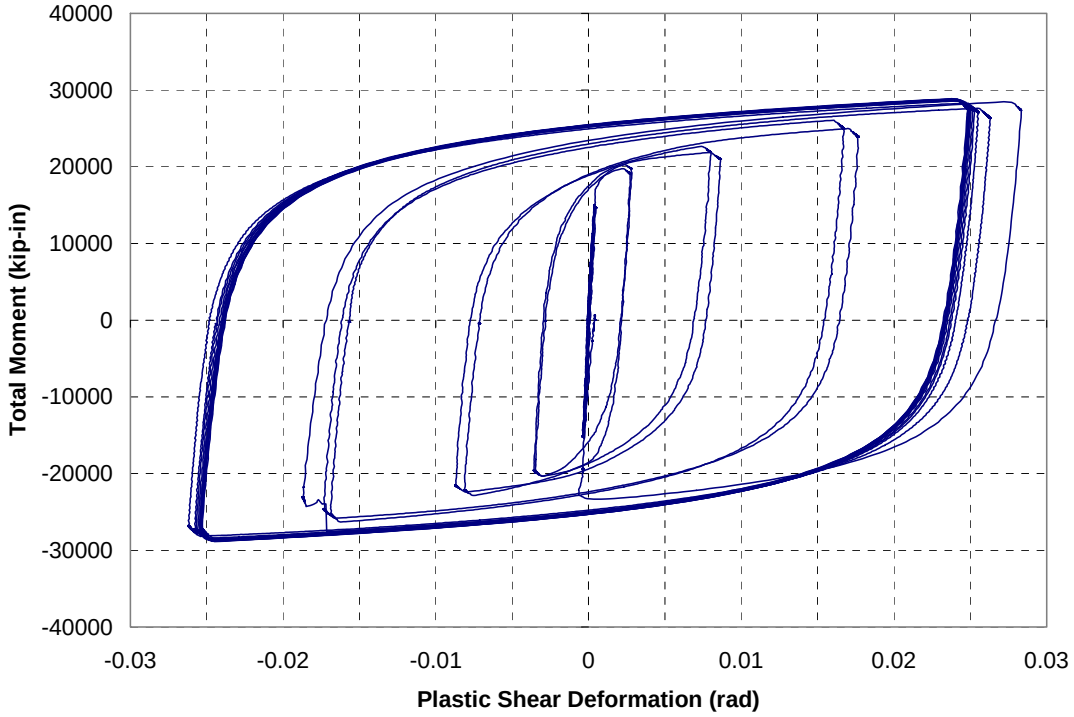


Figure 5.39: Panel Zone Plastic Shear Deformation, CR3

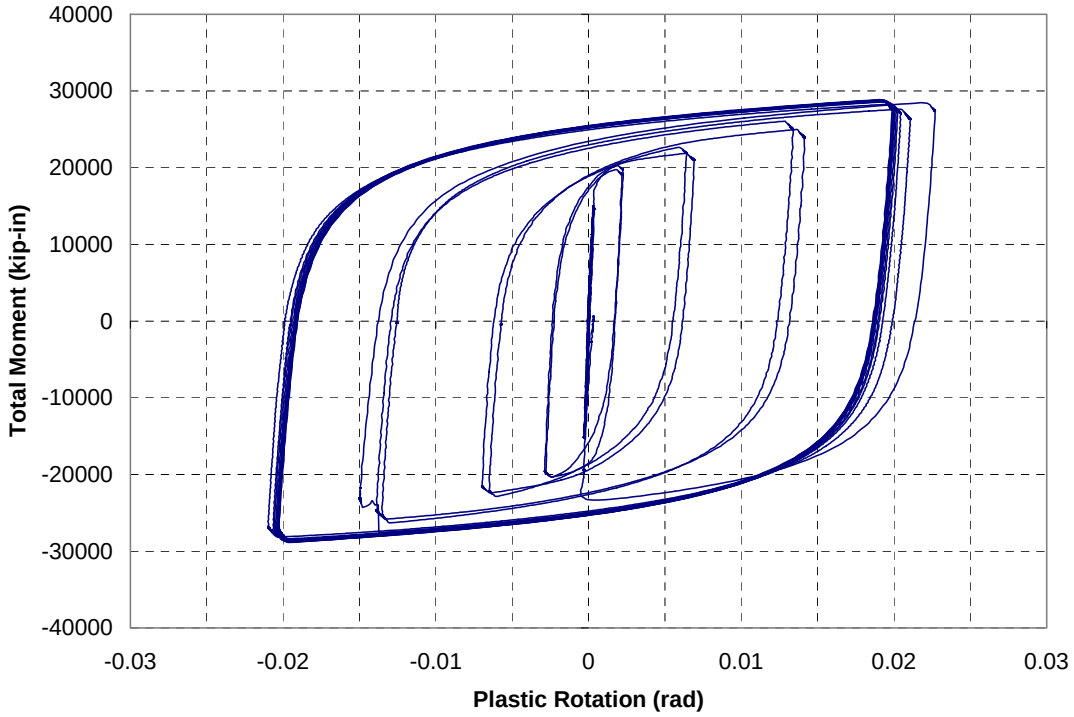


Figure 5.40: Panel Zone Plastic Rotation Relative to Column Centerline, CR3

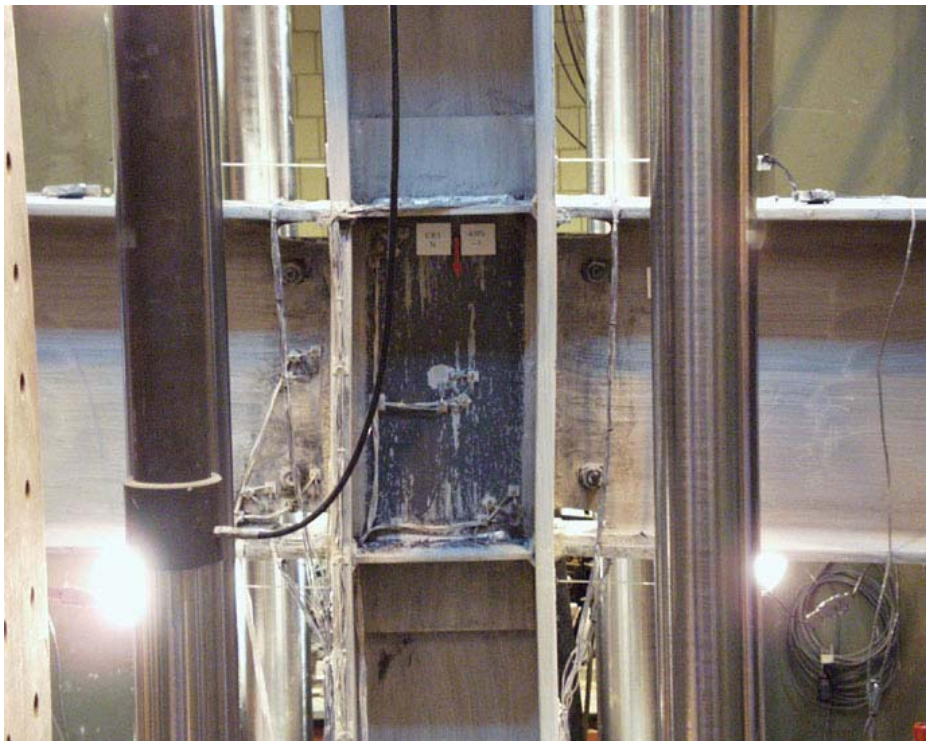


Figure 5.41: Panel Zone Yielding and Significant Column Deformation, CR3

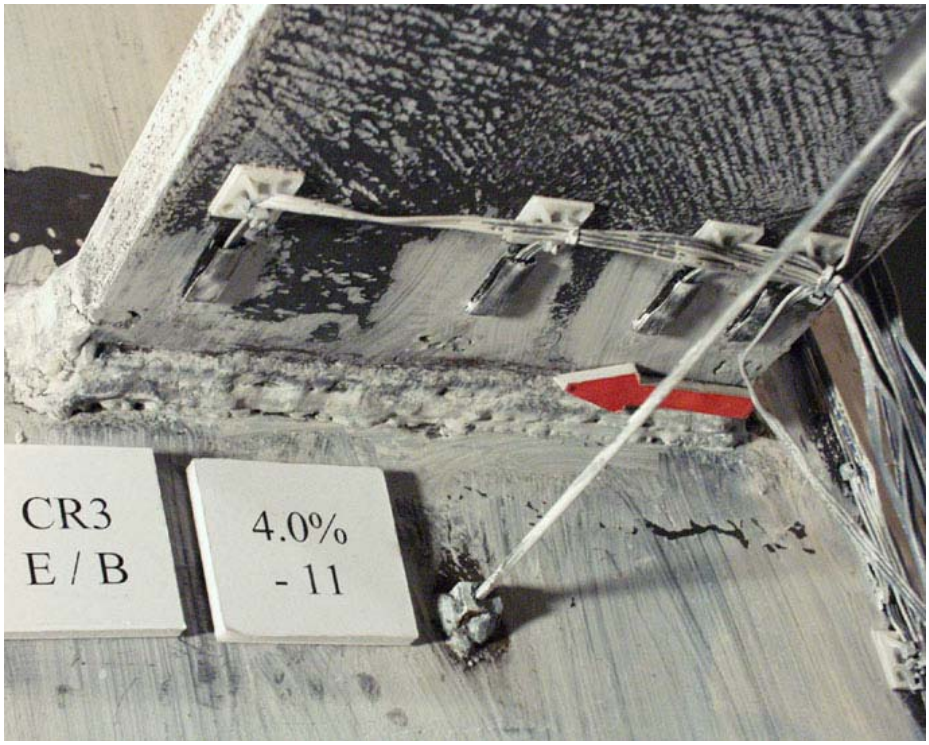


Figure 5.42: Crack Opening in East Bottom Flange, CR3

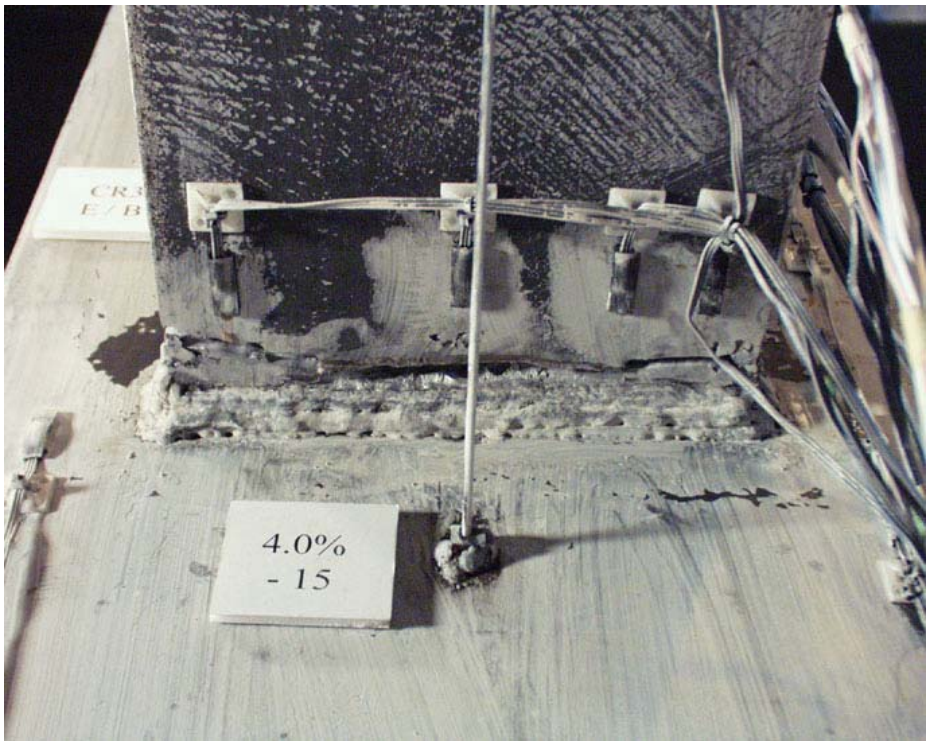


Figure 5.43: Fracture in East Bottom Flange, CR3

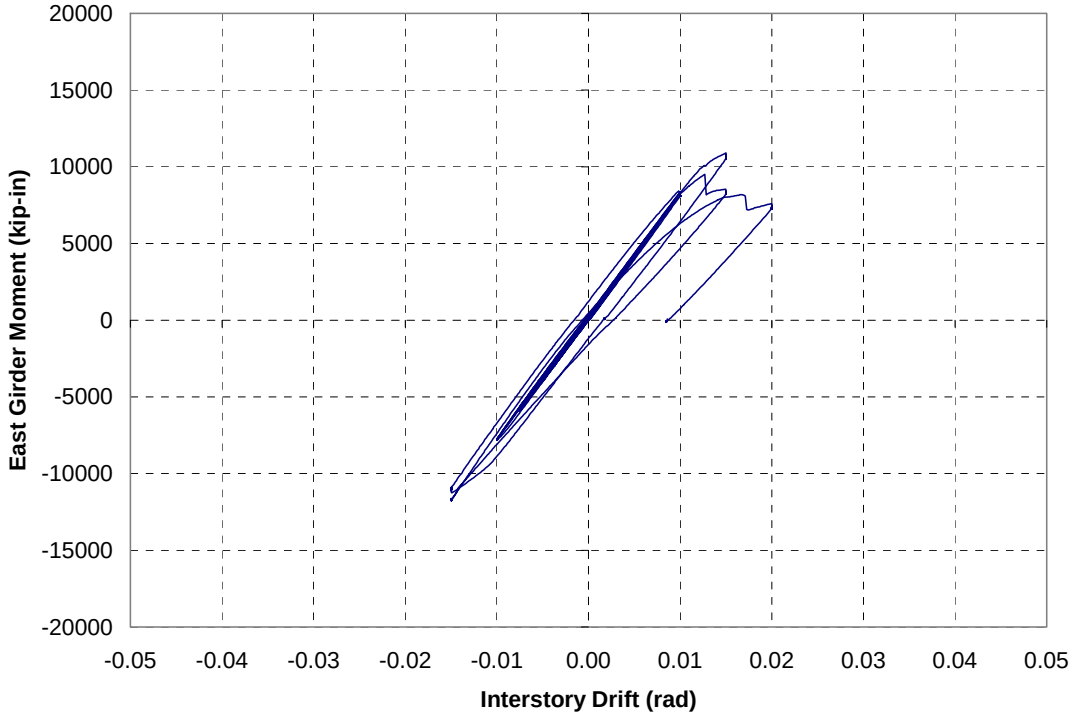


Figure 5.44: Moment vs. Interstory Drift for East Girder, CR4

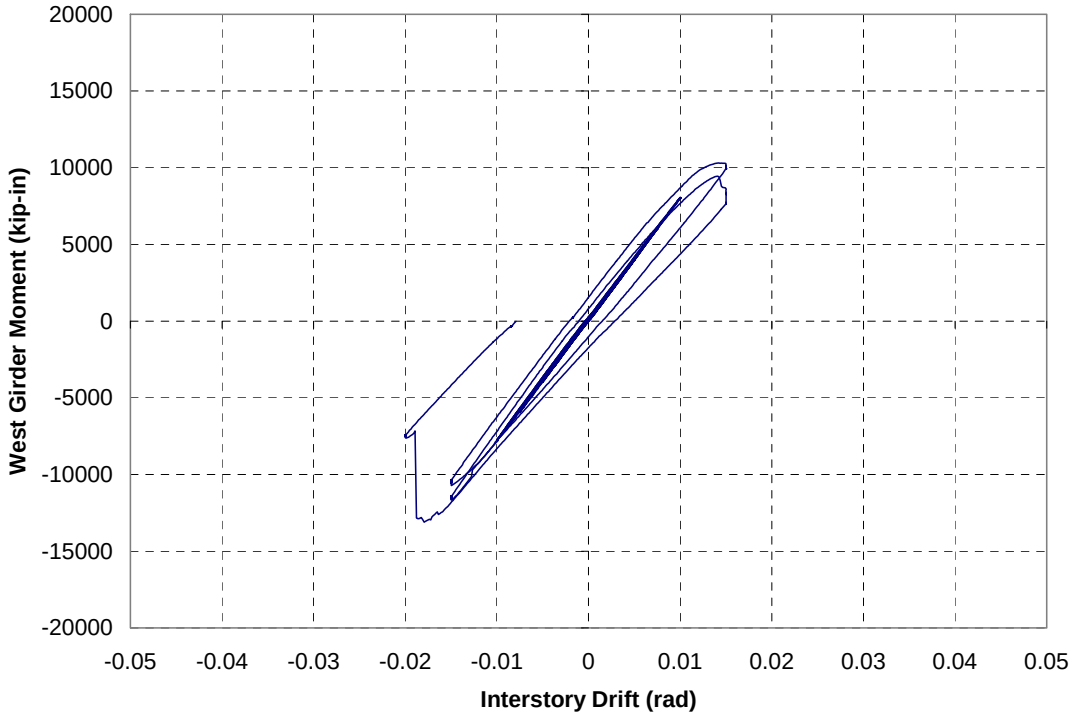


Figure 5.45: Moment vs. Interstory Drift for West Girder, CR4

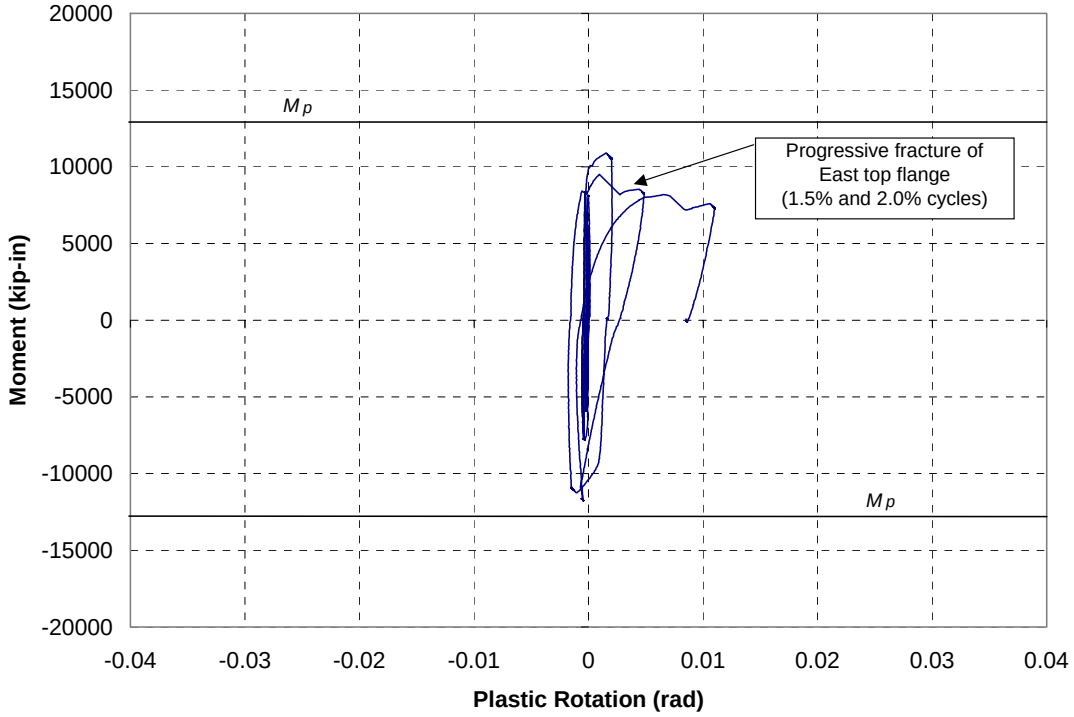


Figure 5.46: Plastic Rotation of East Connection, CR4

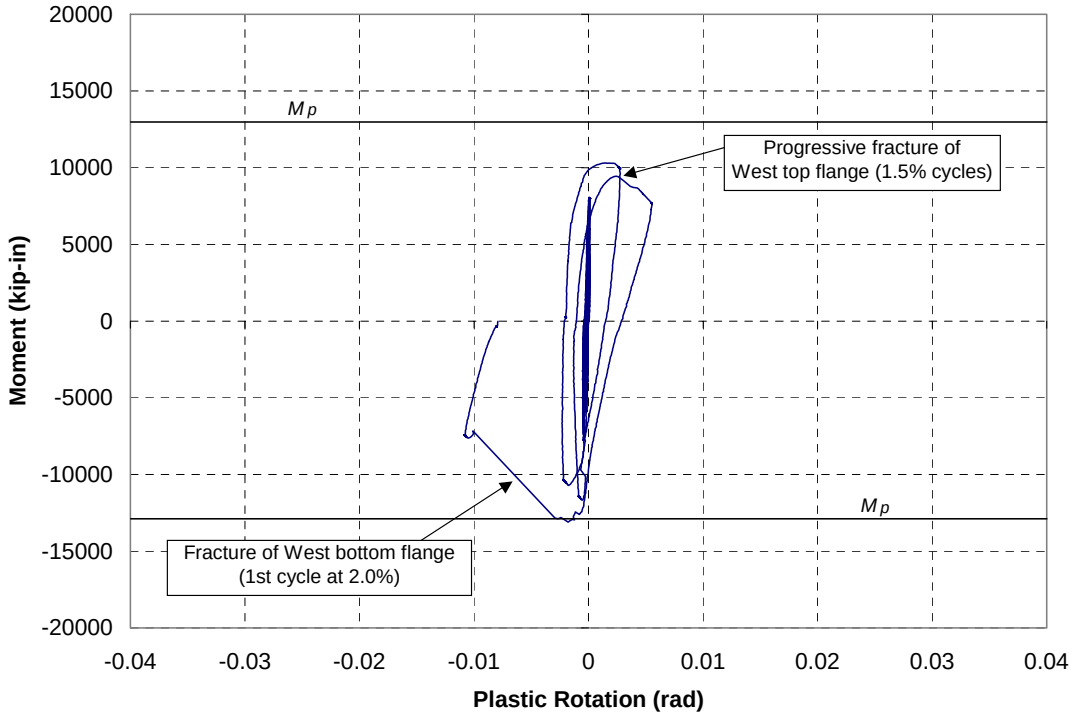


Figure 5.47: Plastic Rotation of West Connection, CR4

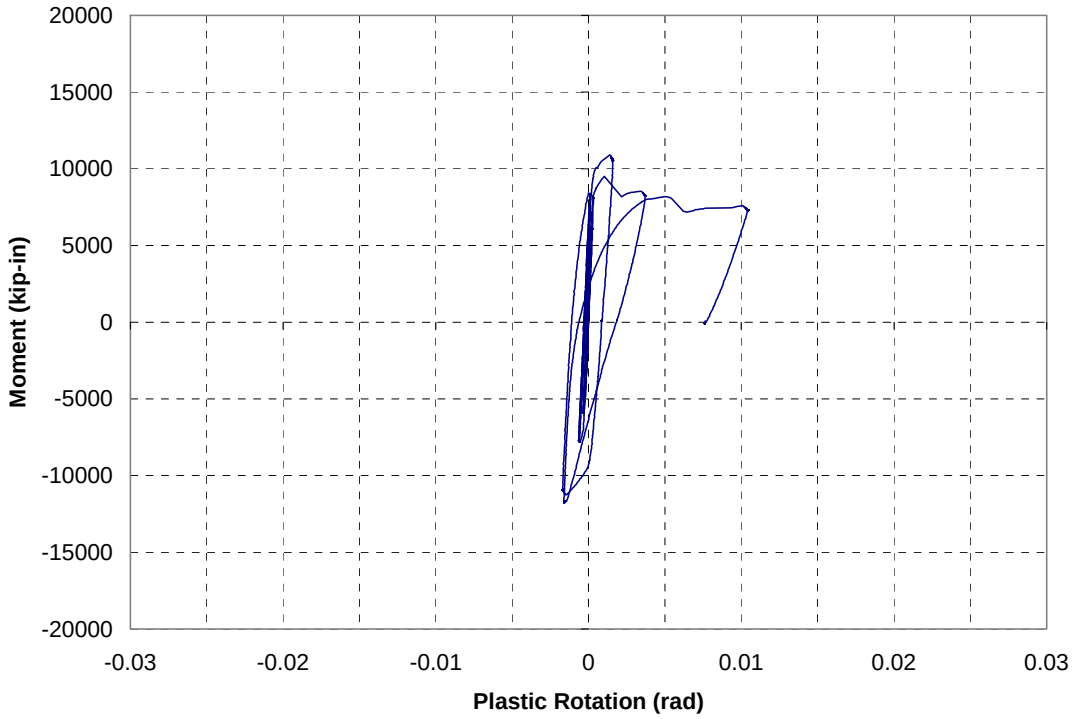


Figure 5.48: East Girder Plastic Rotation Relative to Column Centerline, CR4

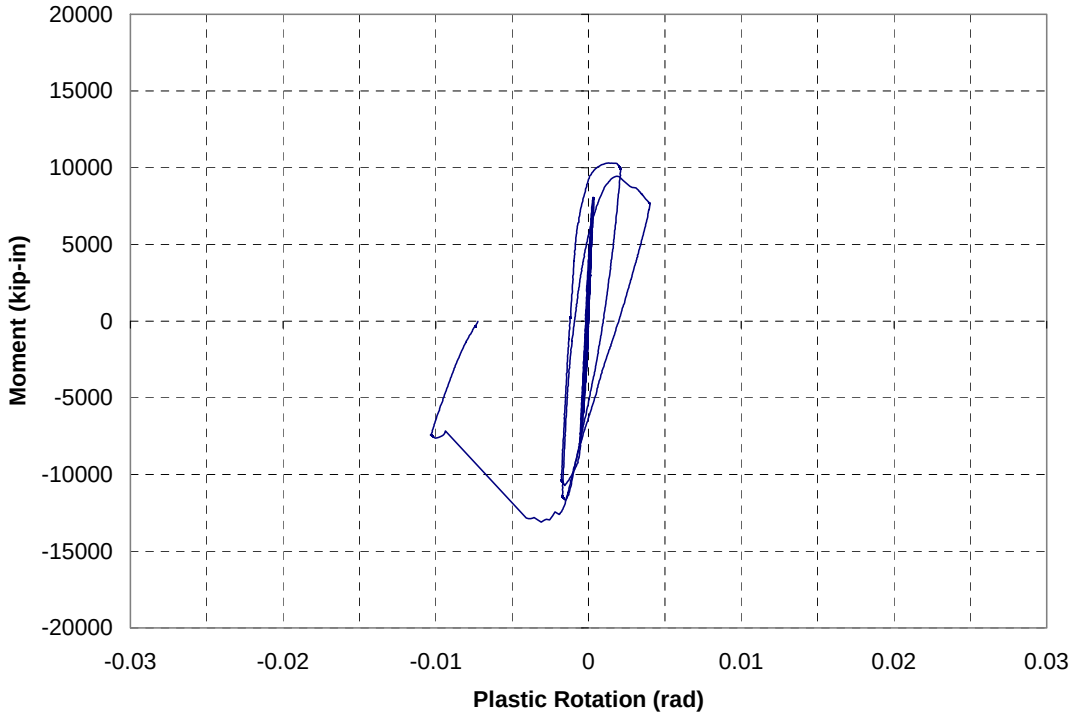


Figure 5.49: West Girder Plastic Rotation Relative to Column Centerline, CR4

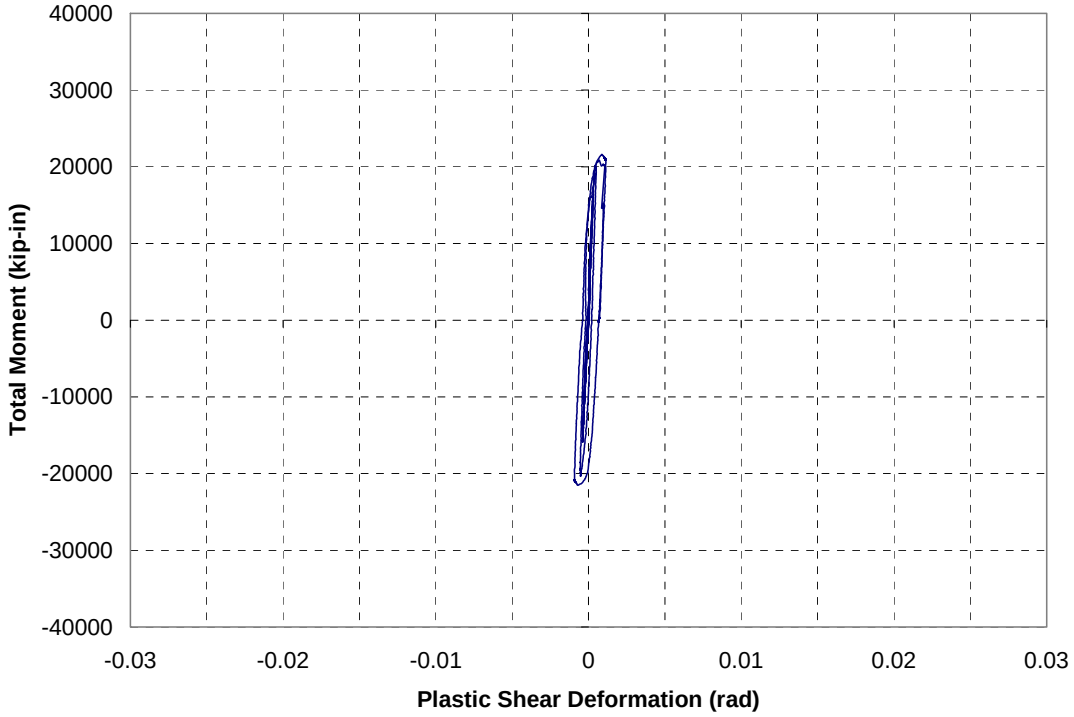


Figure 5.50: Panel Zone Plastic Shear Deformation, CR4

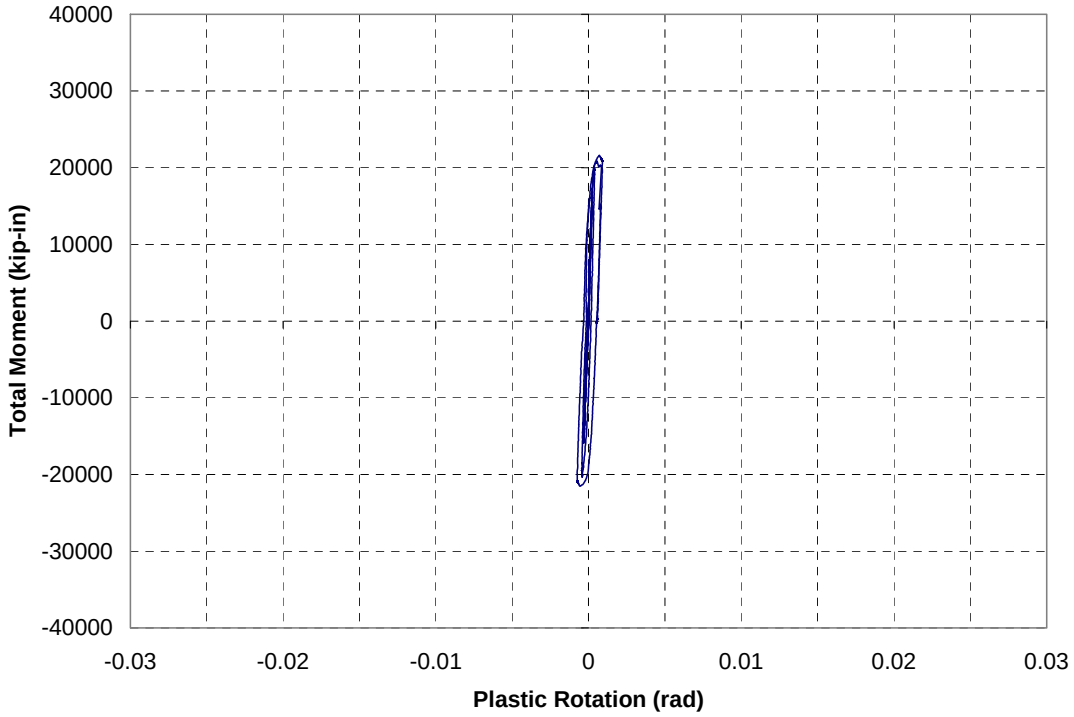


Figure 5.51: Panel Zone Plastic Rotation Relative to Column Centerline, CR4

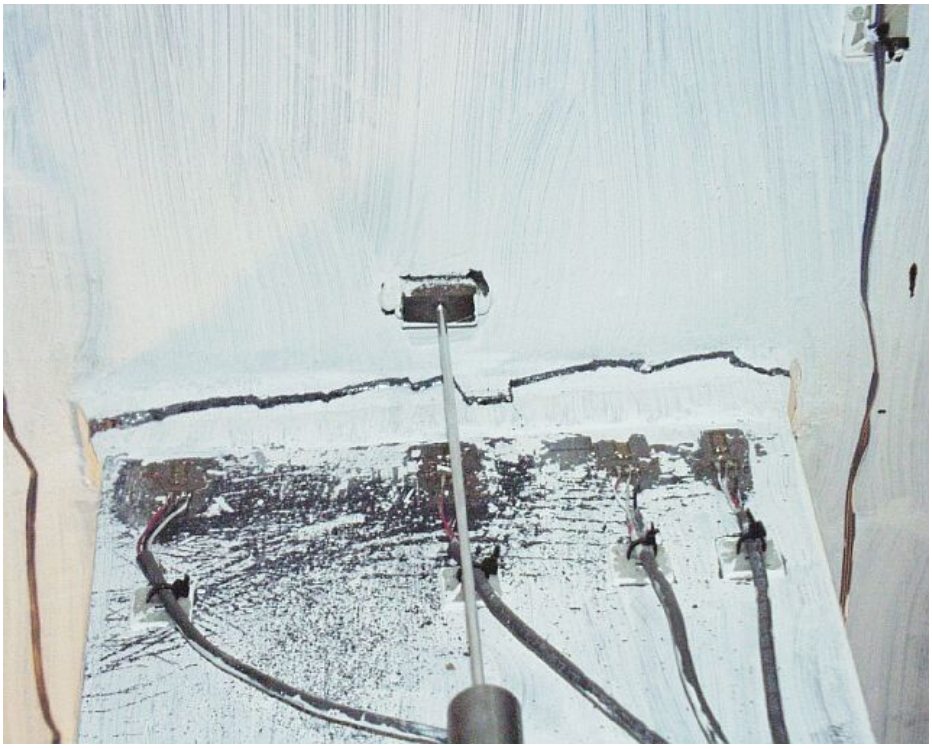


Figure 5.52: Fracture of East Top Flange, CR4

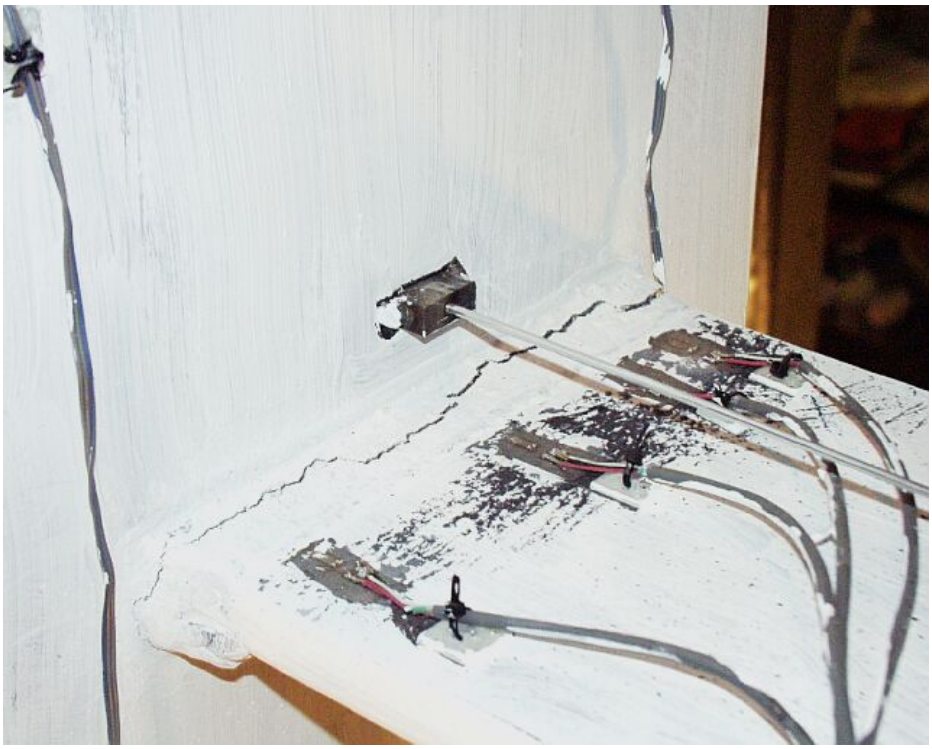


Figure 5.53: Fracture of West Top Flange, CR4

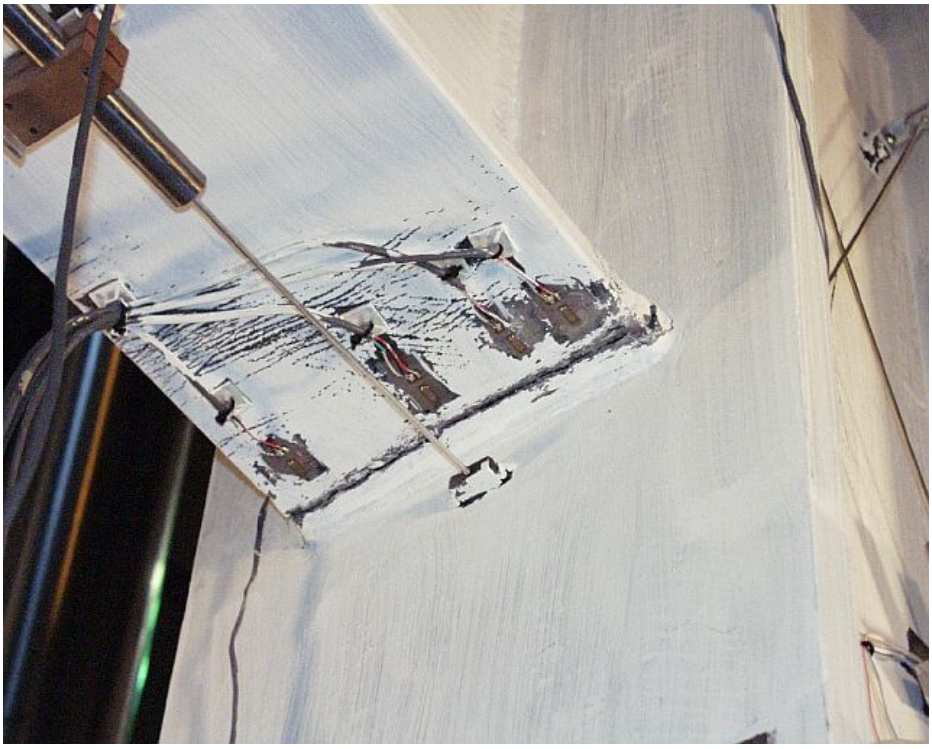


Figure 5.54: Fracture of West Bottom Flange, CR4

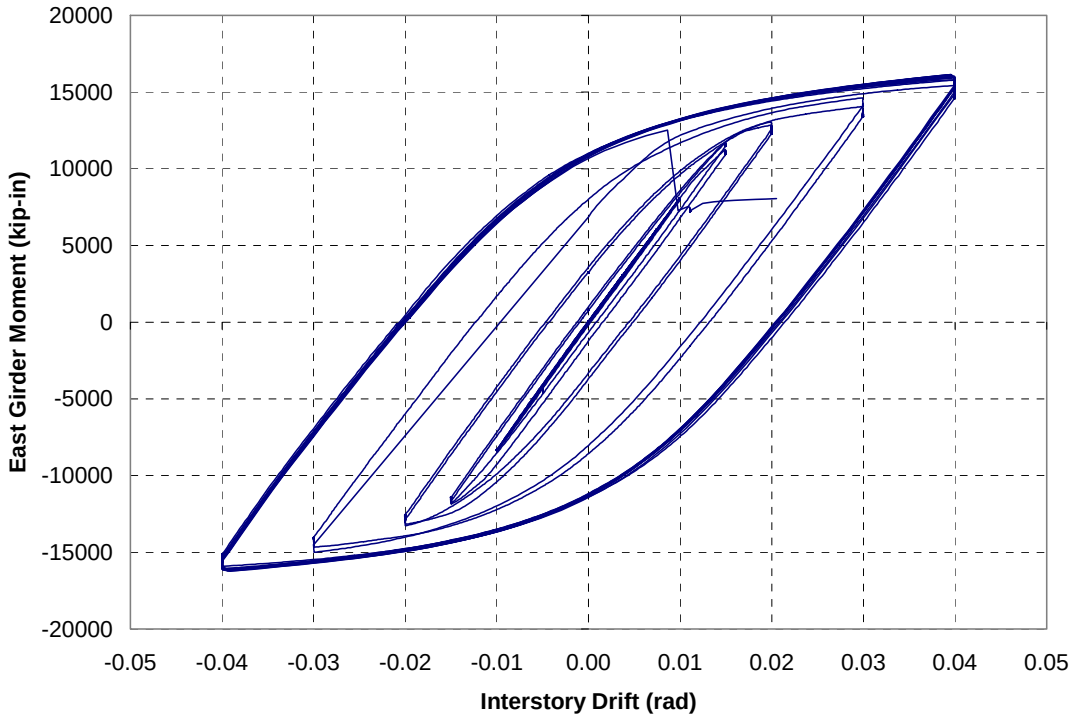


Figure 5.55: Moment vs. Interstory Drift for East Girder, CR4R

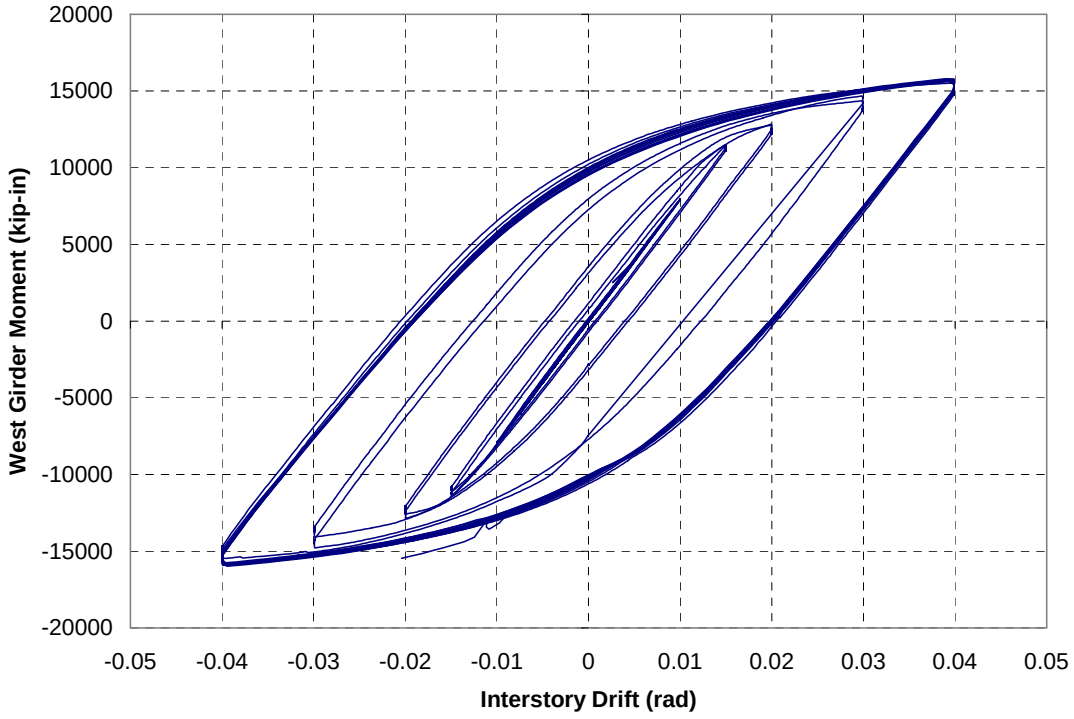


Figure 5.56: Moment vs. Interstory Drift for West Girder, CR4R

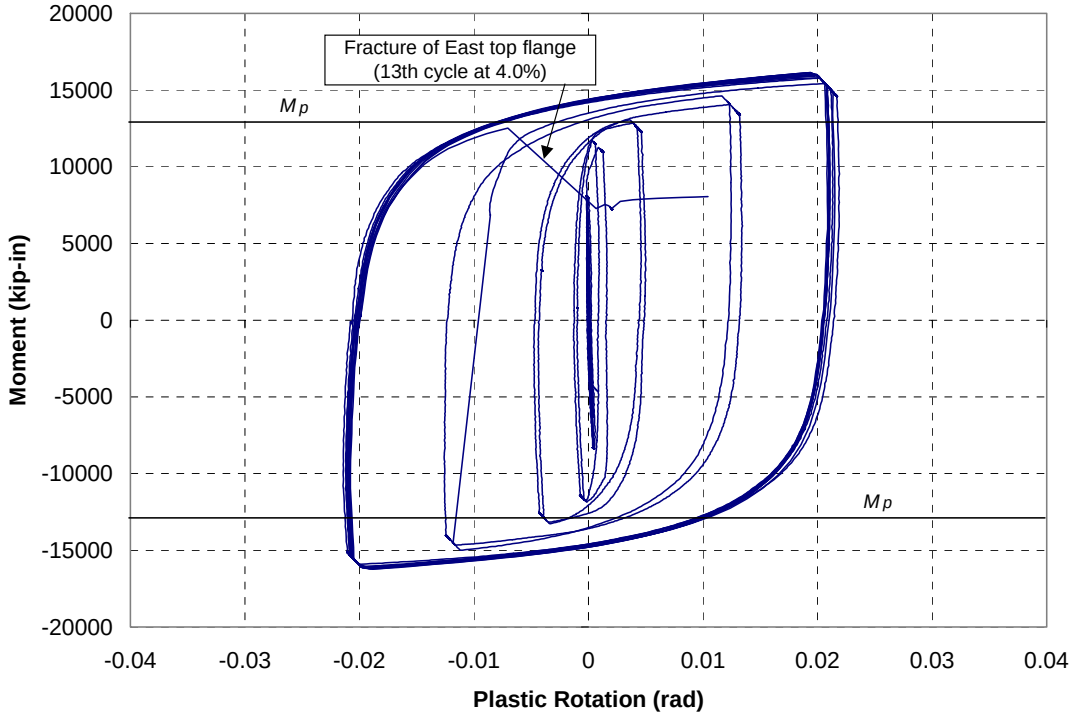


Figure 5.57: Plastic Rotation of East Connection, CR4R

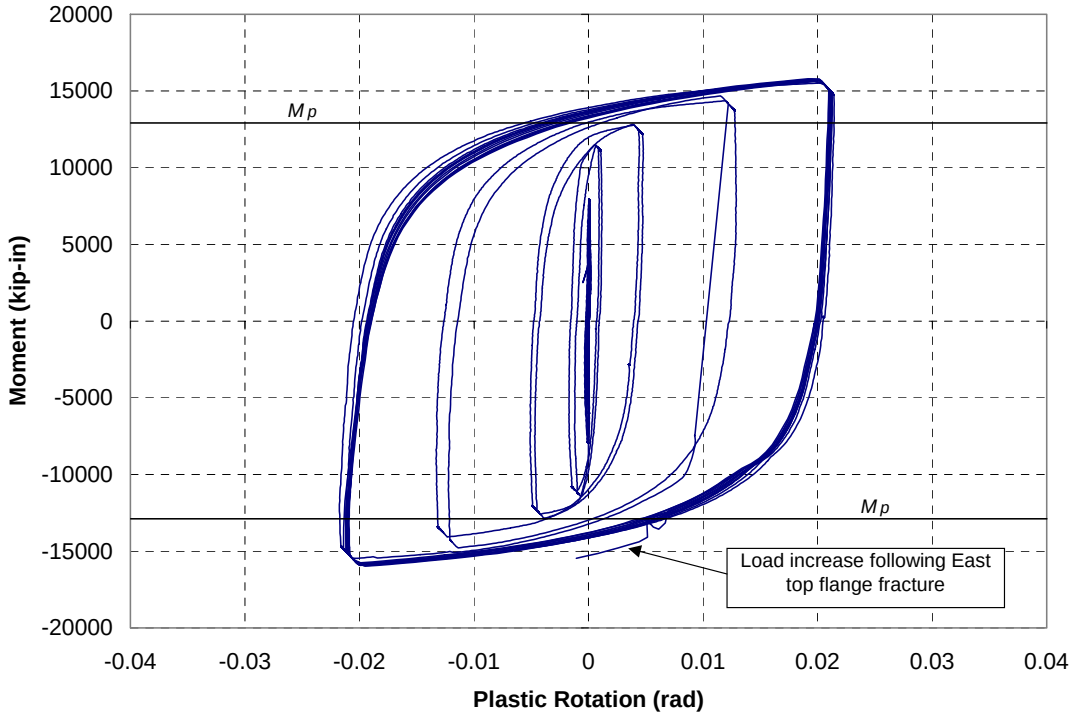


Figure 5.58: Plastic Rotation of West Connection, CR4R

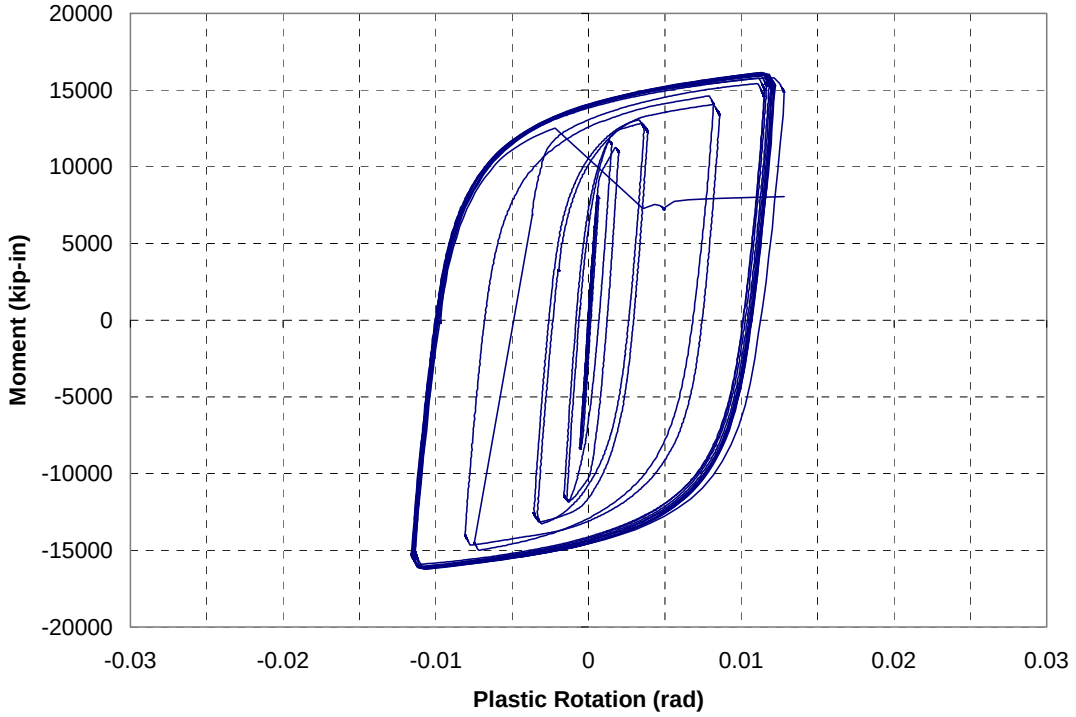


Figure 5.59: East Girder Plastic Rotation Relative to Column Centerline, CR4R

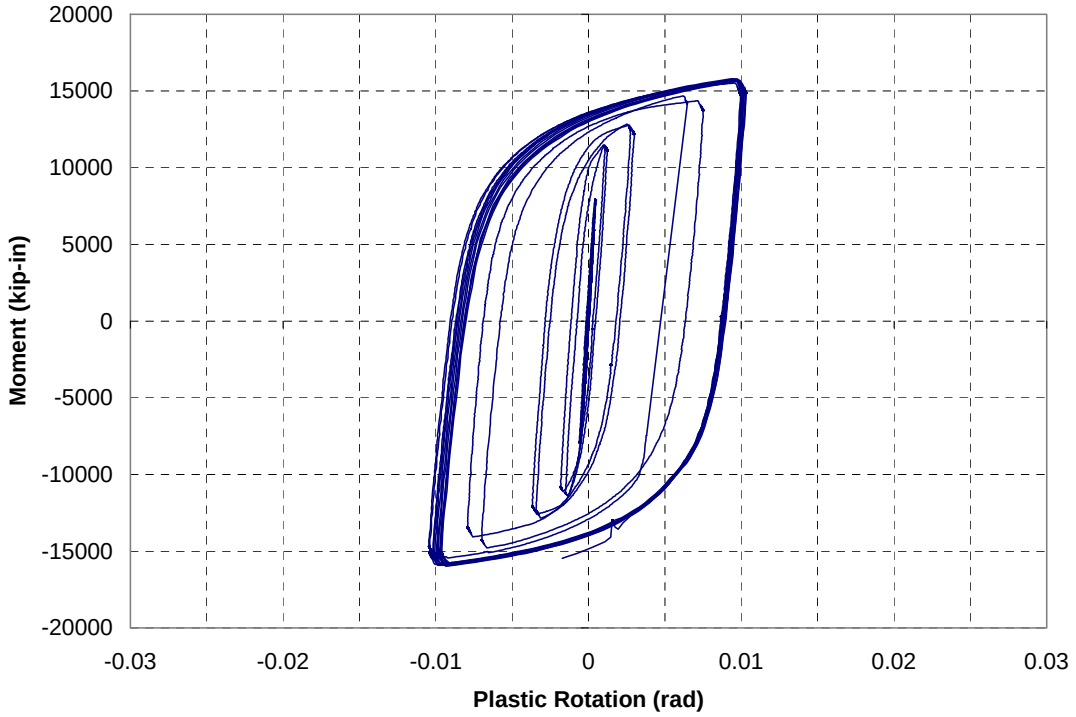


Figure 5.60: West Girder Plastic Rotation Relative to Column Centerline, CR4R

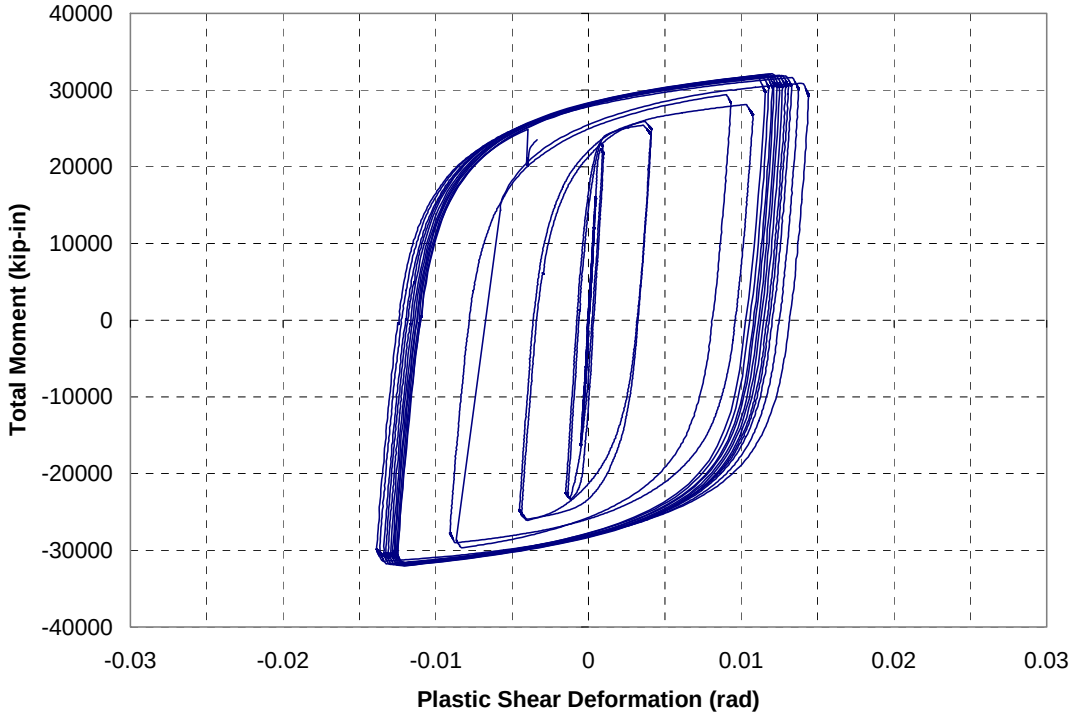


Figure 5.61: Panel Zone Plastic Shear Deformation, CR4R

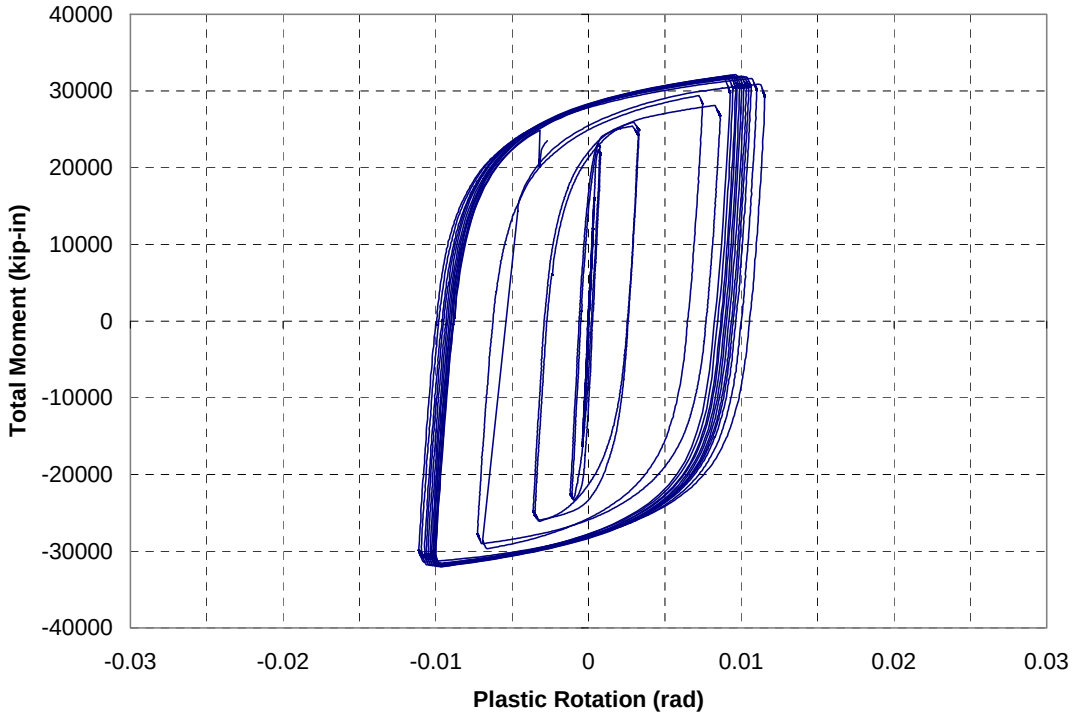


Figure 5.62: Panel Zone Plastic Rotation Relative to Column Centerline, CR4R

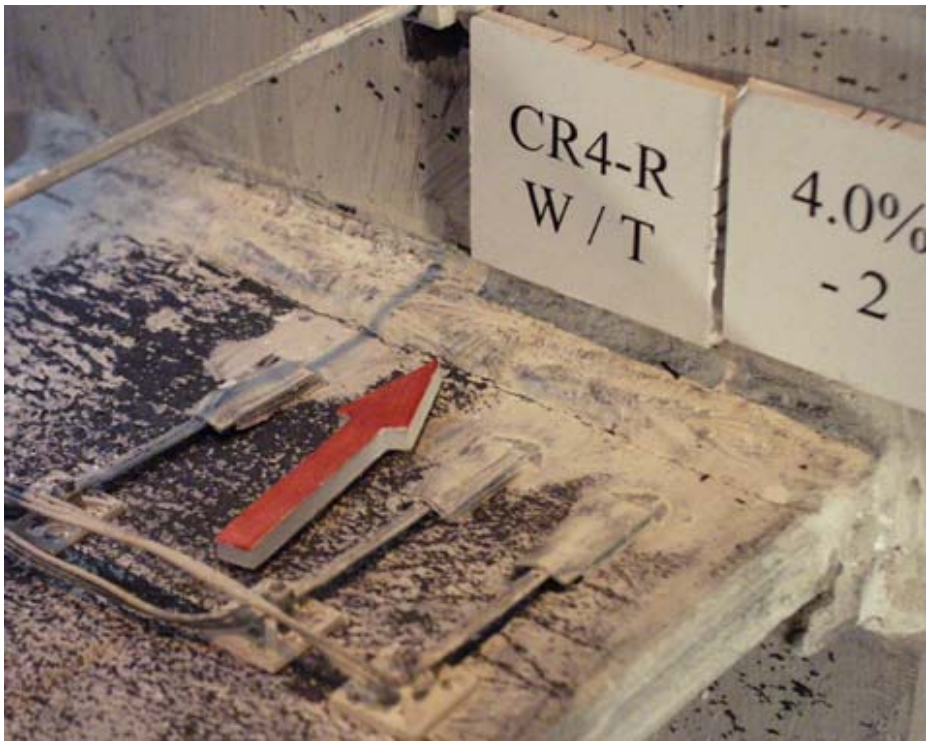


Figure 5.63: Through-Width Line Crack on West Girder Top Flange, CR4R



Figure 5.64: Fracture of East Girder Top Flange, CR4R



Figure 5.65: Crack following Bevel of the Base Metal at East Girder Top Flange. CR4R

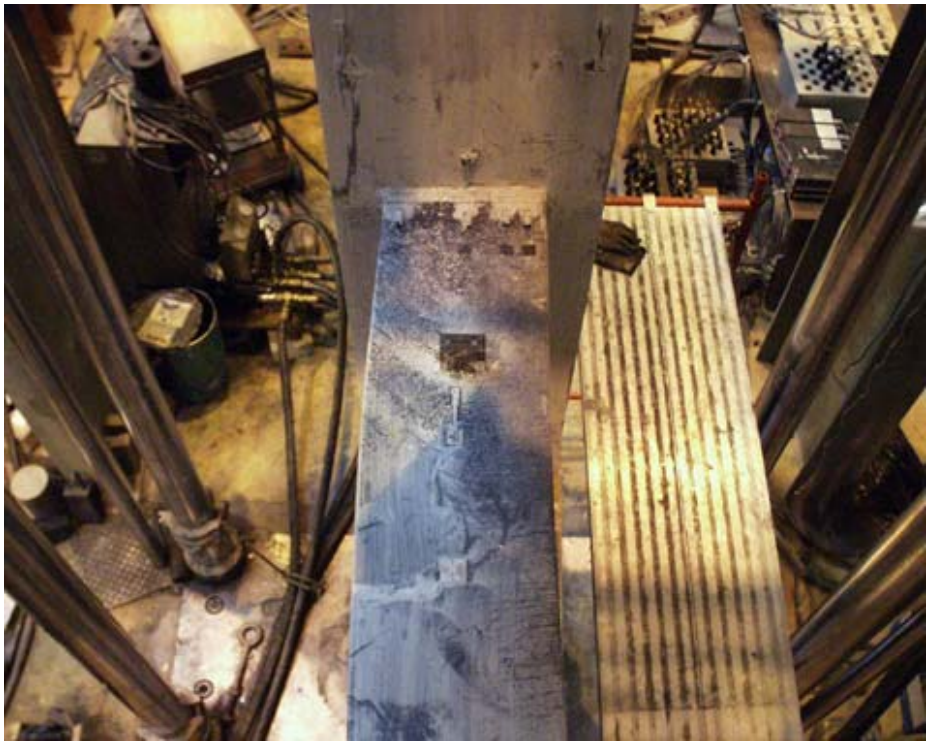


Figure 5.66: Lateral-Torsional Buckling in the West Girder, CR4R

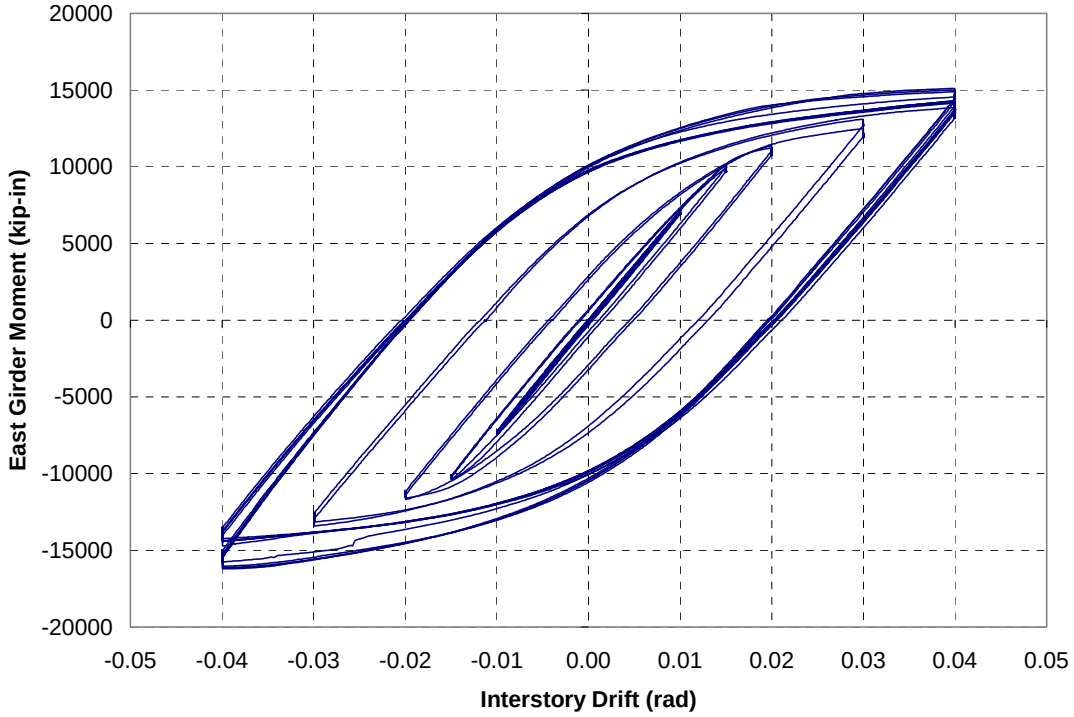


Figure 5.67: Moment vs. Interstory Drift for East Girder, CR5

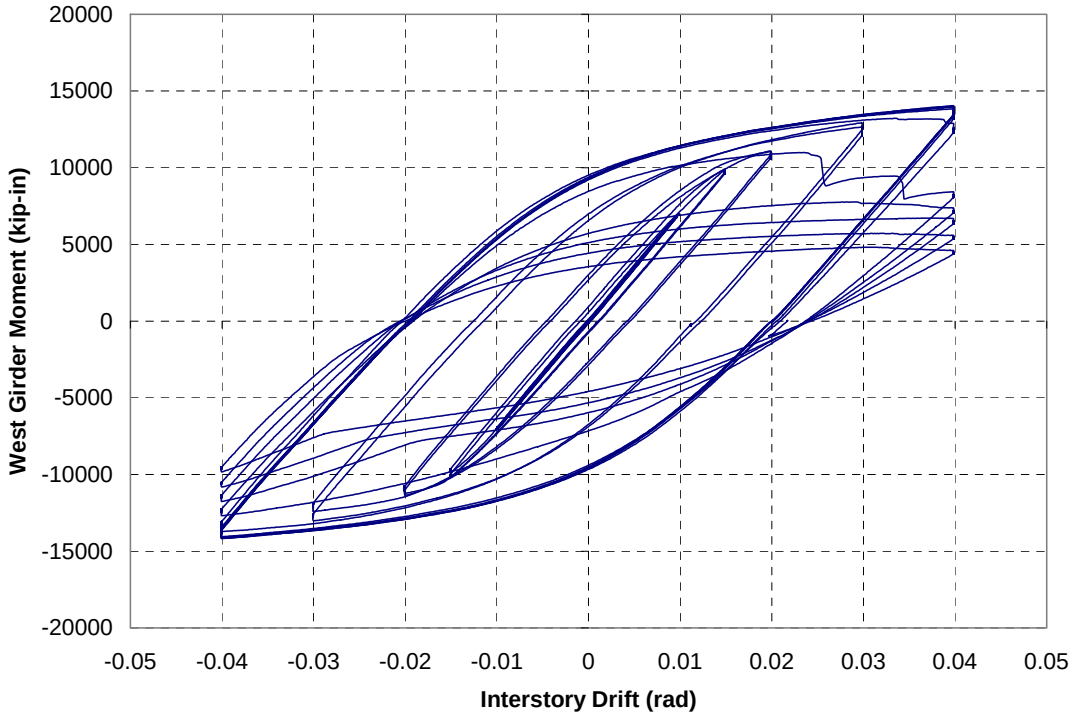


Figure 5.68: Moment vs. Interstory Drift for West Girder, CR5

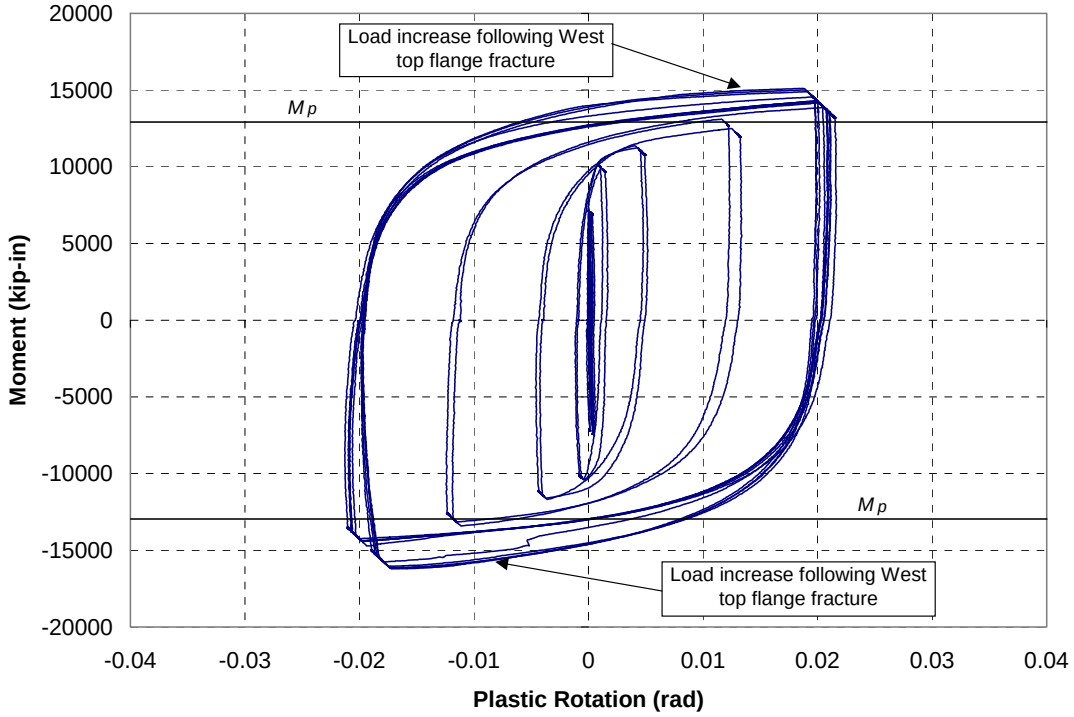


Figure 5.69: Plastic Rotation of East Connection, CR5

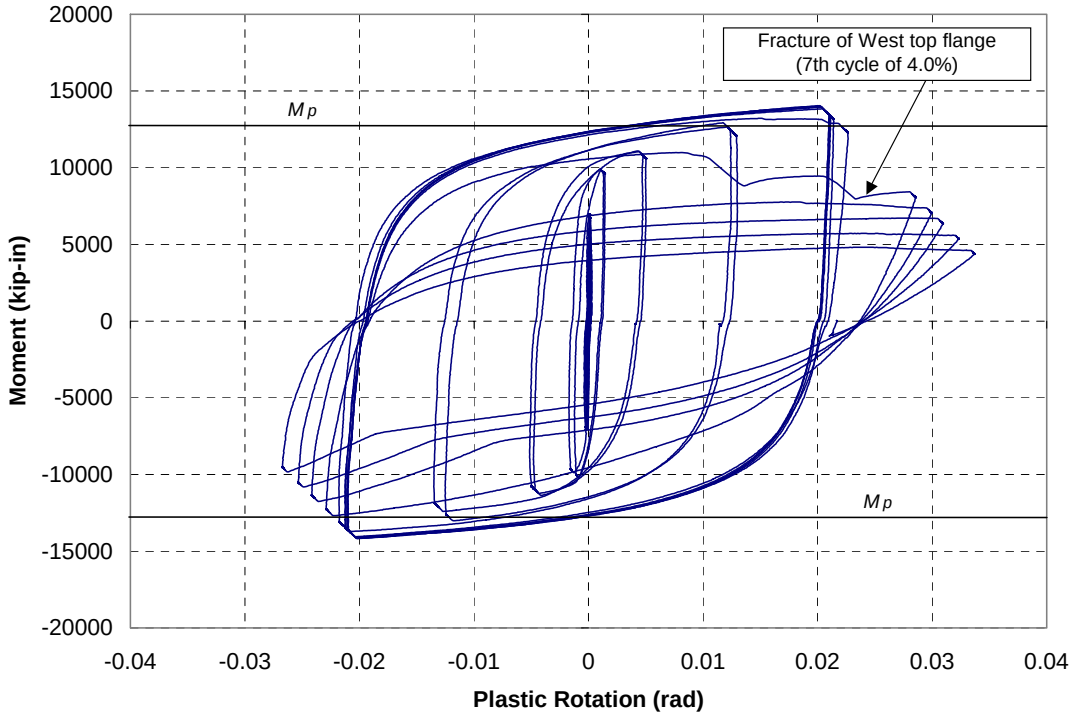


Figure 5.70: Plastic Rotation of West Connection, CR5

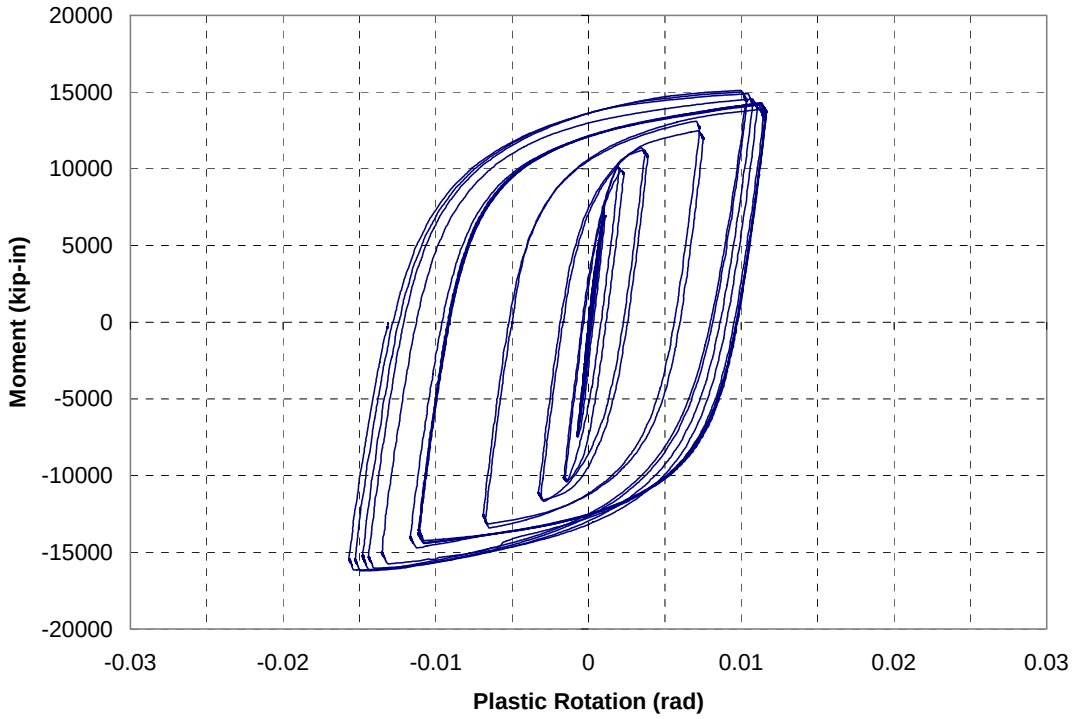


Figure 5.71: East Girder Plastic Rotation Relative to Column Centerline, CR5

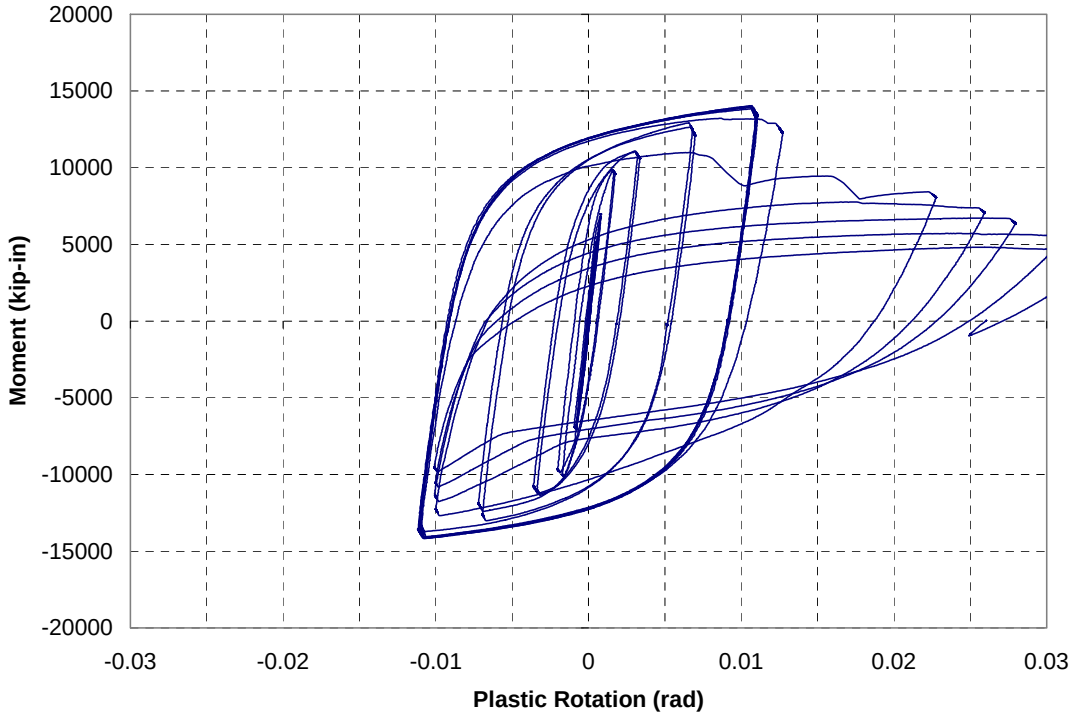


Figure 5.72: West Girder Plastic Rotation Relative to Column Centerline, CR5

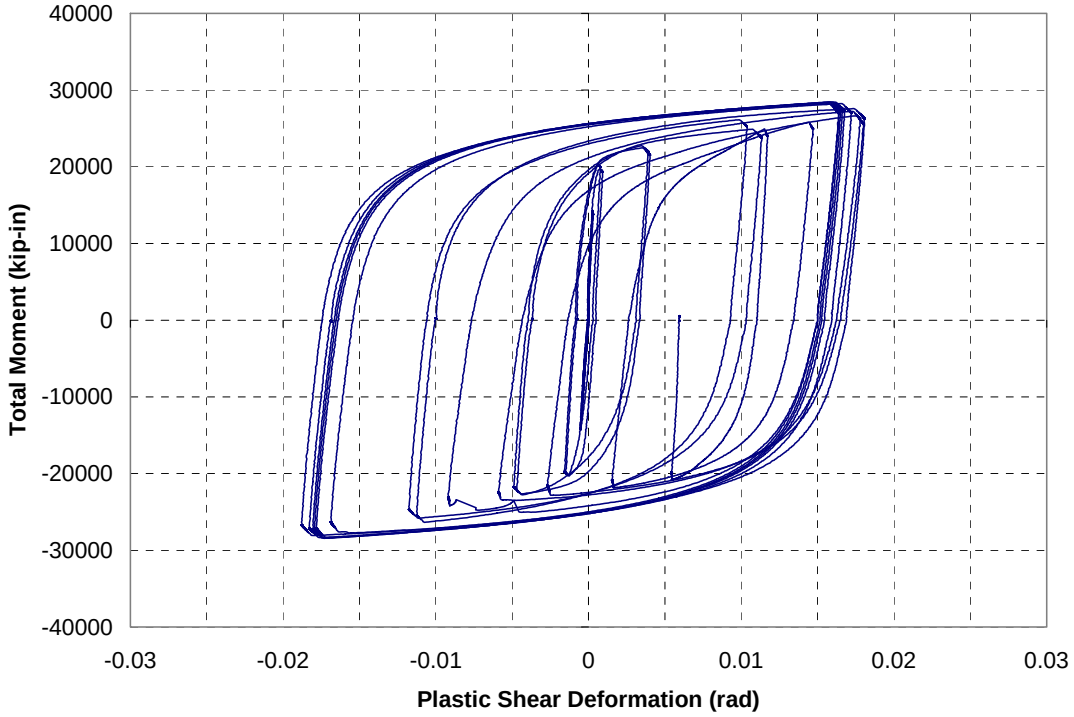


Figure 5.73: Panel Zone Plastic Shear Deformation, CR5

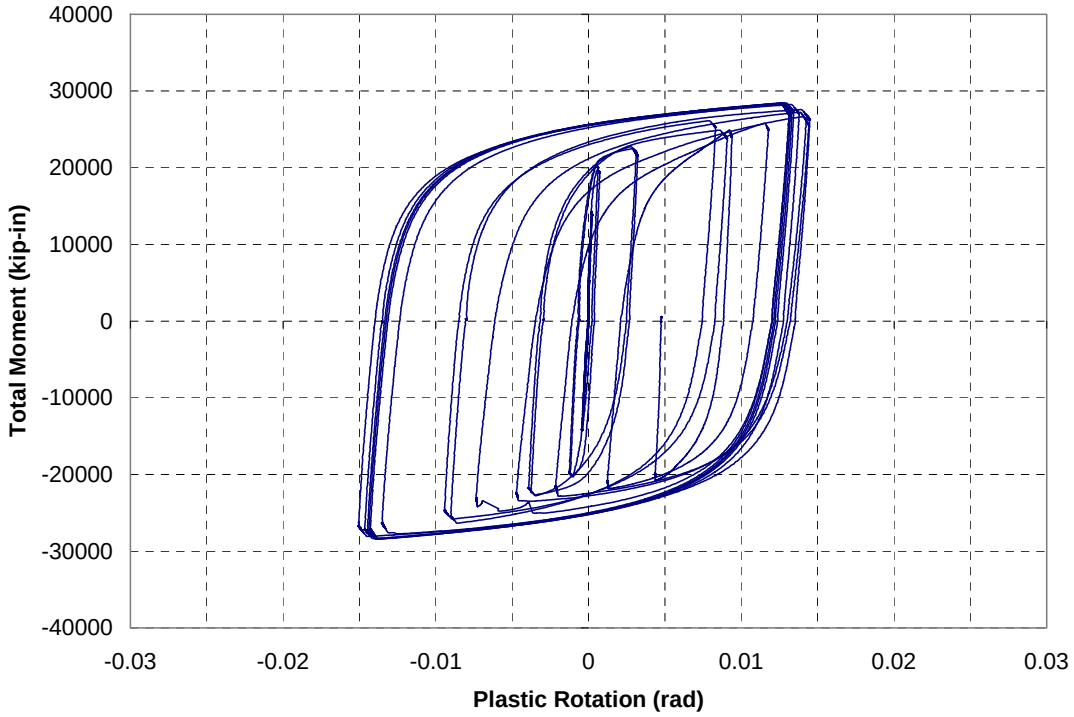


Figure 5.74: Panel Zone Plastic Rotation Relative to Column Centerline, CR5

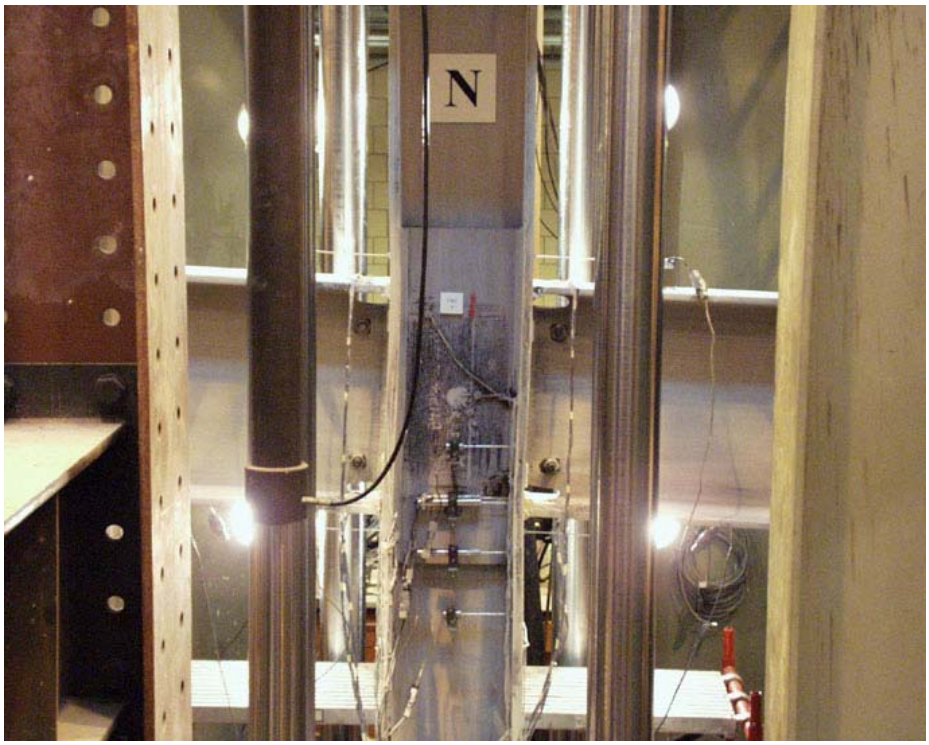


Figure 5.75: Panel Zone Yielding and Significant Column Deformation, CR5

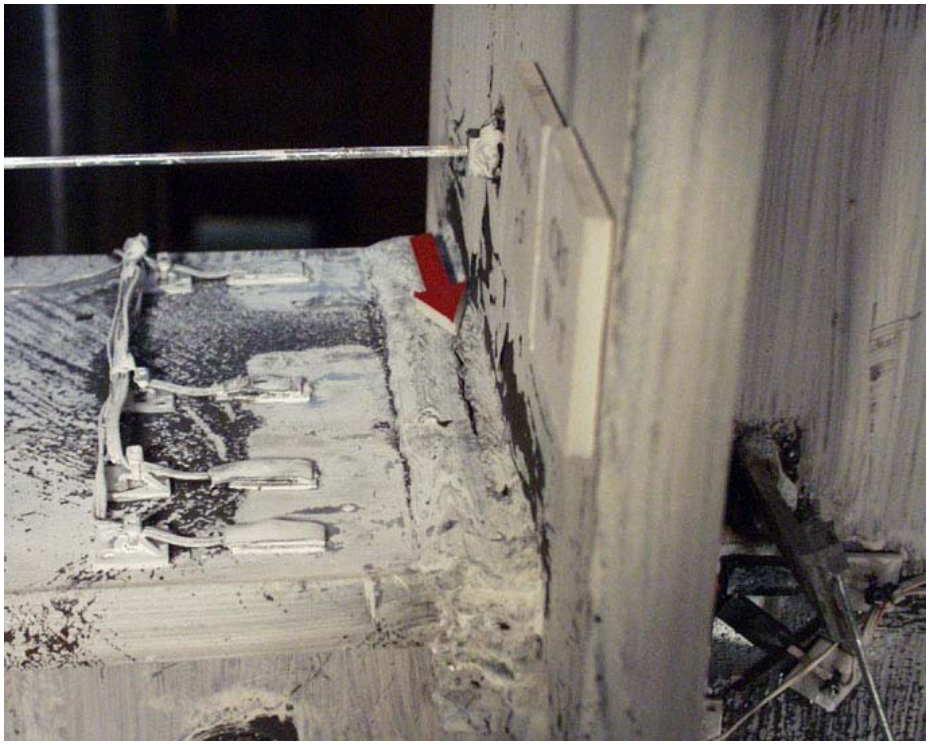


Figure 5.76: Crack Opening in West Girder Top Flange, CR5



Figure 5.77: Fracture in West Girder Top Flange, CR5

Chapter 6

Analysis and Discussion of Test Results

The results of the cruciform tests are compared and further analyzed in this chapter. A description of the finite element modeling of these specimens conducted by Ye et al. (2000) is presented, followed by a comparison of the global computational results to the experimental results of the five specimens. The panel zone behavior of these specimens is analyzed in terms of the average shear deformation and localized strain responses. Progression of panel zone yielding is further analyzed for each specimen based on the measured strain and LVDT readings. Panel zone behavior in its elastic range and effects of large panel zone deformation on connection performance are also discussed. The shear force vs. deformation responses of the panel zone are compared to the current AISC Seismic Provisions for panel zones (AISC, 1997).

A second model of post-elastic panel zone behavior is then developed from the original Fielding and Huang model (1971) and modified based on the experimental results. The application of this modified Fielding and Huang model is evaluated through comparisons with the selected 49 past test results, including the five cruciform specimens tested in the present research. Required panel zone thicknesses determined from the AISC Provisions (1992, 1997), the modified Fielding and Huang model, and the SAC Recommended Seismic Design Criteria (FEMA, 2000a) are also compared and the differences are discussed.

In order to provide a panel zone design strength corresponding to the experimental results, it is proposed that the AISC (1997) panel zone equation should be scaled down. To investigate this recommendation, a new methodology for scaling the panel zone design strength and associated demand based on the experimental results is

explored. The results presented in this chapter call into question several aspects of the AISC (1997) panel zone design criteria.

The LFB behavior of the five specimens (other than CR4) is discussed in detail in Section 6.4, and the results are compared to the yield mechanism limit state criteria developed by Prochnow et al. (2000a). In order to investigate the effects of column stiffening detail on the strain distributions in girder flanges, strains in the longitudinal direction of the girder were also compared among the five specimens in Section 6.5. Finally, Section 6.6 provides a summary comparison of the relative performance of the six cruciform experiments.

6.1 Comparison of Experimental Behavior and Finite Element Analysis

Finite element analysis (FEA) was conducted on the five cruciform specimens for comparison to the experimental results. A detailed discussion of the models and results can be found in Ye et al. (2000). For computational efficiency, half of each specimen was modeled, using the mid-plane of the girder and column webs as a plane of symmetry. The nominal dimensions of all shapes were used to construct the models.

Eight-node solid elements were used in the connection region, while two-node beam elements were used for the portions of girders and columns expected to remain elastic. Figures 6.1 and 6.2 illustrate features of a typical model. Four layers of solid elements were used through the thickness of the girder flanges, girder webs, and column webs. Three layers were used through the thickness of the column flanges. Smaller element sizes were used in the connection regions in areas of expected high stress and strain gradients. The welds connecting the girder flanges and web to the column, as well as all stiffener welds, were explicitly modeled. Meshes were refined until convergence was seen in the results (Ye et al., 2000). A typical mesh consisted of 24,310 elements and 88,342 nodes.

The boundary conditions and loading of the models represented those used in the experiments. The column was pinned at the bottom and roller-supported at the top, allowing for vertical translation. A displacement controlled, anti-symmetric load history

was applied to the ends of the girders. For computational efficiency, monotonic displacements were applied to the girders at the same drift increments as used in the experiments and specified by the SAC Protocol (1997). The quasi-static, cyclic loading of the tests was not modeled.

The yield and tensile strength properties used in the models from Ye et al. (2000) were taken from mill report data. The shape of the stress-strain curve was based on a study by Frank (FEMA, 2000c), and is shown in Figure 6.3. Referring to this figure, the actual mill yield and tensile strengths, F_y and F_u, were used in place of the statistical values of $1.09F_{yn}$ and $1.45F_{yn}$, where F_{yn} is the nominal yield strength of the steel (i.e., 50 ksi). The static, nonlinear analyses were conducted accounting for both material and geometric nonlinearity. The results from the FEA are plotted for comparison to the experimental behavior. In this section, only global quantities are compared. These include load vs. interstory drift, moment vs. connection plastic rotation, and load vs. panel zone shear deformation.

Figures 6.4 through 6.8 show comparisons between the experimental and computational load vs. interstory drift for the five specimens. The experimental curve is a skeleton curve based on the peak positive loads in the East girder. The peak loads from the first cycle at each drift level are used. In all cases, the FEA results are plotted to an interstory drift level of 4.0%, corresponding to the maximum experimental drift. These plots reveal a good correlation between the experimental and computational results. Nonlinearity was observed earlier in the tests than predicted by the numerical analysis, possibly due to residual stress effects, which were not modeled in the FEA. The loads from the FEA are also somewhat under-predicted at larger drift levels (i.e., 3.0 and 4.0% drift). This is primarily due to the effects of cyclic strain hardening which were also not modeled in the monotonic analyses.

Figures 6.9 through 6.13 show comparisons of experimental and computational moment vs. connection plastic rotation for the five specimens. Experimental skeleton curves were determined in the manner described above. All specimens show a reasonable correlation between the experiment and FEA results. At 4.0% drift, the total

connection plastic rotation is predicted within a maximum error range of 15% (CR1), 14% (CR2), 15% (CR3), 16% (CR4R), and 17% (CR5), respectively.

Figures 6.14 through 6.18 compare the experimental and computational panel zone shear deformation for the five specimens. These plots show girder load vs. panel zone shear deformation. Experimental skeleton curve loads were determined from the average of the East and West girder end loads at the drift peaks. Again, data from the first peak at each drift level is used to construct the curves. These five figures show that the elastic stiffness of the panel zone was underpredicted by the FEA in all cases. Despite the differences in elastic behavior, Figures 6.14 through 6.18 show that the finite element model predicted the inelastic panel zone behavior of the five specimens well, with the exception of Specimen CR5. At 4.0% drift, the panel zone deformations were predicted within a maximum error range of 2% (CR1), 10% (CR2), 3% (CR3), 12% (CR4R), and 25% (CR5), respectively. Only two specimens (i.e., Specimens CR3 and CR4R) slightly passed the predicted panel zone shear deformation at 4.0% drift.

6.2 Panel Zone Behavior

Chapter 5 presented the general behavior of the five specimens (other than CR4). This section further discusses the observed behavior of the panel zone in terms of stress and strain distributions, global and local deformation characteristics, and their potential effects on connection performance. The behavior presented is useful in providing insight into the pros and cons of the present AISC design procedures available for panel zones. The panel zone instrumentation was discussed in Section 4.3.

6.2.1 Progression of Panel Zone Yielding

Figures 5.14, 5.27, 5.39, 5.61, and 5.73 showed the global moment vs. panel zone shear deformation responses of the five specimens. As discussed in Section 3.3.3.1, this weak panel zone design philosophy was adopted for all tests to allow for investigation of the design criteria, and to thoroughly test the column stiffening details. The associated deformations also allow for an investigation into the effects of large panel zone

distortions on moment connection performance, and provide further information on general panel zone behavior.

Figures 6.19 through 6.23 show the progression of panel zone yielding in Specimen CR1 through the 4.0% drift cycles. As discussed in Chapter 5, the first visible yielding initiated during the 0.75% drift cycles, but the yielding was very localized. Widespread yielding was first visible during the 1.0% drift cycles (See Figure 6.19). The panel zone was essentially fully yielded during the 3.0% drift level (See Figure 6.22). Figure 6.23 shows the panel zone following the test.

Figures 6.24 through 6.27 show the progression of panel zone yielding in Specimen CR2 through the 4.0% drift cycles. The first visible yielding initiated in the column web during the 1.0% drift cycles, and widespread yielding was first visible in both column web and doubler plate during the 1.5% drift cycles (See Figure 6.24). The panel zone significantly yielded during the 2.0% drift cycles (See Figure 6.25) and finally, was fully yielded during the 3.0% drift level (See Figure 6.26). Figure 6.27 shows the panel zone yielding during the 1st cycle of 4.0% drift.

Figures 6.28 through 6.31 show the progression of panel zone yielding in Specimen CR3 through the 4.0% drift cycles. The panel zone behavior of Specimen CR3 was similar to that of Specimen CR2. The first visible yielding initiated in the panel zone during the 1.0% drift cycles, and widespread yielding was first visible in doubler plates during the 1.5% drift cycles (See Figure 6.28). The panel zone was fully yielded during the 3.0% drift cycles (See Figure 6.30). Figure 6.31 shows the panel zone yielding during the 1st cycle of 4.0% drift.

Figures 6.32 through 6.35 show the progression of panel zone yielding in Specimen CR4R through the 4.0% drift cycles. Due to the relatively stronger panel zone, the first visible yielding in the panel zone initiated later than the other four specimens. The panel zone slightly yielded in the doubler plates during the 1.5% drift cycles (See Figure 6.32). Significant yielding was observed during the 3.0% drift cycles (See Figure 6.34), but the panel zone was not fully yielded. Figure 6.35 shows the panel zone yielding during the 1st cycle of 4.0% drift.

Figures 6.36 through 6.39 show the progression of panel zone yielding in Specimen CR5 through the 4.0% drift cycles. Moderate yielding was observed in the doubler plates during the 2.0% drift cycles (See Figure 6.37). This panel zone significantly yielded during the 3.0% drift cycles (See Figure 6.38) and fully yielded during the 4.0% drift cycles. Figure 6.39 shows the panel zone yielding during the 1st cycle of 4.0% drift.

6.2.2 Panel Zone Behavior in the Elastic Range

As panel zone deformation is a shearing phenomenon, the present AISC (1993, 1997, 1999a, 2001) provisions for panel zone strength (Equation 2.1) are based on an assumption of pure, uniform shear deformation. While the shear is not truly uniform in the panel zone region, this approach has been believed to be sufficient in predicting the onset of global panel zone behavior, especially in the elastic range.

The assumption of pure shear in the panel zone is investigated by comparing the strain histories of the two rosettes in the elastic range, as shown in Figures 6.40 through 6.49. Figures 6.40, 6.42, 6.44, 6.46, and 6.48 show the strain history of the rosette located in the center of the panel zone (gage *ne_3pz_hr*, see Figure 4.7), while Figures 6.41, 6.43, 6.45, 6.47, and 6.49 show the strain history for the rosette in the bottom East corner of the panel zone (gage *ne_1pz_gr*, see Figure 4.7). All of these plots are presenting data through the 0.75% drift cycles. The 45° diagonal gages on the rosettes are designated the "b" channels (e.g. *ne_1pz_grb*). If pure shear exists at the strain gage location, only this diagonal channel will read a strain. The horizontal and vertical components of strain are zero in a location of pure panel zone shear. Note that "horizontal" refers to the direction along the girder length, and "vertical" refers to the direction along the column height. The "a" gages (e.g., *ne_1pz_gra*) denote the horizontal channel of the rosettes, and the "c" gages (e.g., *ne_1pz_grc*) denote the vertical rosette channels.

As Figures 6.40, 6.42, 6.44, 6.46, and 6.48 show, it can be assumed that the center of the panel zone is under a state of nearly pure shear stress. Only the diagonal gages show significant cyclic strain variations through the 0.75% drift cycles. Specimens CR2

and CR3 show some strain variations in the horizontal and vertical gages, but the variations are very small and thus negligible. Figures 6.41, 6.43, 6.45, 6.47, and 6.49, on the other hand, show very different behavior at the corner of the panel zone. Clearly shown by the plots are the effects of the concentrated girder flange force delivered to the panel zone near the gage location. The horizontal component of strain is approximately equal in magnitude to the diagonal component in most of the five specimens. This horizontal strain is due to the concentrated girder flange force, and represents the effects of LWY near the girder flange. As shown by Prochnow et al. (2000a) and Ye et al. (2000), however, the LWY strains drop off rapidly from the point of load application.

Figures 6.50 and 6.51 show the elastic shear stress contours in the panel zone of Specimen CR1 at the 0.375% and 0.5% drift levels, respectively. The rosettes, placed as shown in Figure 4.7, with symmetry assumed about the column and girder centerlines, were used to map the stresses over the entire panel zone. The figures show that shear stresses are fairly uniform over most of the panel zone, but decrease substantially at the corners.

In summary, the stress and strain state within the panel zone was dominated by shear. In the elastic range, fairly uniform shear stresses existed throughout most of the panel zone, with a rapid drop towards the corners. Most of the panel zone also experienced an essentially pure state of shear, with one exception to this observation occurring at the corners of the panel zone near the concentrated girder flange forces. Significant horizontal strains were induced by these flange forces, representing the strains governing the LWY limit state. These horizontal strains became negligible by the mid-height location of the panel zone, and did not affect the global shearing behavior. An important finding from this research is that this pattern of stress was consistently exhibited in panel zones of a specimen having no doubler plates, in specimens with one-sided and two-sided fillet-welded doubler plates, and in a specimen with an offset doubler plate detail. This behavior is consistent with and corroborates similar findings reported in past experimental and computational research, e.g., Krawinkler et al. (1971), Ye et al. (2000).

6.2.3 Effects of Large Panel Zone Deformation

One effect of the large panel zone distortions evident in Figure 6.23 is the kinking that occurs in the column flanges at the level of the girder flanges. As discussed in Chapters 2 and 3, this phenomenon has been repeatedly observed (Krawinkler et al., 1971; Popov et al., 1986; El-Tawil et al., 1998; Choi et al., 2000; Ye et al., 2000) and hypothesized to affect connection performance (Roeder and Foutch, 1996; SAC, 1996; Choi et al., 2000; Ricles et al., 2000a). Figure 6.23 showed the deformed profile of the column following testing of Specimen CR1. The kinks in the column flanges near the corners of the panel zone are clearly visible. Figure 6.52 shows a closer view of the column flanges near one of the Specimen CR1 girder flanges following testing. Note the concentrated yielding in the column flange at this location. Yielding through the thickness of the column flanges indicates evidence of plastic hinge formation. The formation of this plastic hinge was accounted for in the post-yield panel zone strength models discussed in Chapter 2. The Fielding and Huang (1971) model explicitly incorporates the plastic capacity of the column flanges, while the Krawinkler model (1978) was based on a rotational spring representation of these hinge locations.

The strain gages placed along the column height near the East girder bottom flange further illustrate the concentrated deformation at this location. Figures 6.53 through 6.62 show the longitudinal strain profiles in the column flange near the East girder bottom flange under tensile and compressive girder flange loading, respectively. Refer to Figures 4.14 and 4.15 for the names and locations of the strain gages. Figures 6.53 through 6.62 show very large strain gradients in the vicinity of the girder flange. Strains near the girder flange due to the large panel zone deformation are several times larger than the nominal flexural strains in the column. At 4.0% drift, strains of approximately 7000 με exist at the level of the girder flange and drop to approximately 600 με at a location 12 in. below the bottom flange in Specimens CR1 and CR2. The other specimens also show similar strain patterns following the column flanges, but the variation is somewhat smaller. This is particularly true when the bottom girder flange is in tension for Specimen CR3, which has a continuity plate, and Specimen CR4, with the offset box detail, although the strain gradients in these columns pick up again when the

girder flange goes into compression. These strains due to kinking of the column flanges are further discussed in the context of local flange bending in Section 6.4.

The potential detrimental effects of these kinking deformations in the panel zone are due to the demands such deformations place on the moment connections. Large panel zone deformations are a stable energy dissipation mechanism. However, this mode of deformation becomes undesirable if it reduces the performance of the moment connections. The moment connections are also relied upon to provide substantial energy dissipation through girder plastic hinge formation. Not only can a weak panel zone prevent development of the full plastic capacity of the girders, but the resulting deformations have also been thought to accelerate failure of the girder-to-column connection.

Experiments by Krawinkler et al. (1971) revealed the effects of excessive panel zone distortion. The kinks in the column flanges caused local deformations in the girder flanges, which led to low-cycle fatigue cracking of the copes and girder flange-to-column flange welds. Analyses by Lee et al. (1997) showed the effects of panel zone deformation on the elastic stress state at the girder-to-column connection. The column bending (i.e., kinking) associated with panel zone deformation caused an increase in local deformation of the girder flanges, and focused a significant portion of the girder shear force into the flanges. Furthermore, because shear deformations in the panel zone are opposite those in the girder web at a location removed from the connection, a restraint condition at the column face is created that further increases the redistribution of forces into the girder flanges. Computational studies by Chi et al. (2000) and Mao et al. (2001) also predicted the effects of large panel zone deformations. Chi et al. (2000) showed that flange weld toughness demands dramatically increased for the case of weak panel zones, this being at least partially attributable to kinking of the column flanges adjacent to the welds. The study by Mao et al. (2000) showed that the deformations in a weak panel zone increase the potential for ductile fracture at the ends of girder web-to-column groove welds and cause a local prying effect in the girder flange welds. Experiments by Ricles et al. (2000a) confirmed the earlier onset of cracking in the web groove welds of specimens with weak panel zones.

Test results of the five specimens were consistent with the observations above. As presented in Chapter 5, first cracking often occurred at the top or bottom edges of the shear tab in most of the specimens, although ultimately low-cycle fatigue cracking in the girder flanges was the prevalent mode of connection failure. It may be reasonable to assume then, that the large panel zone deformation and the associated kinking of the column flange did contribute to the failure of the specimen. However, because significant cracking associated with strength degradation did not initiate until the 4.0% drift cycles in most specimens, it cannot be concluded that the weak panel zone caused premature failure of the connection. To the contrary, the test results clearly show that, when properly detailed, good connection performance can be achieved even in the presence of the demands due to a weak panel zone. The onset of low-cycle fatigue may have been delayed further, however, had a stronger panel zone been provided.

6.2.4 AISC Panel Zone Provisions

This section further explores the issue of panel zone yielding in the context of AISC design provisions. The current AISC strength provisions for seismic panel zone design (AISC, 1997) recognize a significant post-elastic strength contributed by the boundary elements of the panel zone. This is primarily governed by the thickness of the column flanges. To restate, the design shear strength is given by:

$$\phi_v R_v = \phi_v 0.6 F_{yc} d_c t_p \left(1 + \frac{3 b_{cf} t_{cf}^2}{d_g d_c t_p} \right) \tag{2.1}$$

where:

R_v = nominal panel zone shear strength

ϕ_v = resistance factor = 1.0 [modified from 0.75 by AISC (2001)]

F_{yc} = minimum specified column yield stress

b_{cf} = column flange width

t_{cf} = column flange thickness

d_c = column depth

d_g = girder depth

t_p = panel zone thickness

The post-elastic contribution (given by the second term in parentheses) increases with the square of the column flange thickness. Thus, this term becomes large for heavier columns, especially those without panel zone reinforcement. This results in an increase in recognized strength for the five specimens beyond the AISC nominal shear yield panel zone strength of $0.6F_{yc}d_ct_p$ of 39.4% (CR1), 17.1% (CR2), 11.9% (CR3), 9.3% (CR4R), and 8.0% (CR5) . Note that t_p includes the thickness of doubler plates. The above post-elastic contributions result in design strengths (i.e., $\phi_v R_v$) of 903 kips (CR1), 824 kips (CR2), 935 kips (CR3), 1163 kips (CR4R), and 924 kips (CR5), using the minimum specified yield strength of 50 ksi. These strengths increase to 945 kips (CR1), 890 kips (CR2), 1075 kips (CR3), 1322 kips (CR4), and 1085 kips (CR5) when the measured yield strengths (See Table 3.4) are used. (The measured yield strengths used throughout Chapter 6 are the dynamic yield strengths, i.e., the 0.2% offset yield strengths.) In contrast, the nominal yield strengths ($0.6F_{yc}d_ct_p$) were 648 kips (CR1), 704 kips (CR2), 836 kips (CR3), 1064 kips (CR4R), and 856 kips (CR5), respectively, using nominal material properties.

As discussed in Section 3.3.3.1, the panel zones of the cruciform specimens were not designed such that $\phi_v R_v \geq R_u$. Rather, a weak panel zone design approach was used to ensure all panel zones exceeded the design deformation of $4\gamma_y$ implied by Equation 2.1. As such, a comparison of the five specimen's behavior to the AISC provisions involves comparing the experimental shear forces carried by the panel zones to the predicted forces (i.e., $\phi_v R_v$ = 945 kips in the case of Specimen CR1 when the measured yield strength is used) at the deformation level of $4\gamma_y$. The experimental panel zone shear forces were calculated from the following:

$$V_{pz} = \frac{M_{tot}}{d_g} - V_c \tag{6.1}$$

where:

V_{pz} = experimental panel zone shear

M_{tot} = total moment at the column face = $P_{tot}L_g$

P_{tot} = absolute value of the sum of actuator loads

L_g = girder length to column face

V_c = column shear

The first term of Equation 6.1 is the sum of the girder flange forces delivered to the connection region, and the second is the column shear. The column shear, V_c, is calculated from statics on the specimen dimensions of Figure 3.7, resulting in the expression:

$$V_c = \frac{P_{tot}\left(L_g + d_c/2\right)}{L_c} \tag{6.2}$$

where:

L_c = column height measured between load pin centerlines

Combining Equations 6.1 and 6.2 yields the final expression for calculating the experimental panel zone shear force:

$$V_{pz} = P_{tot}\left(\frac{L_g}{d_g} - \frac{\left(L_g + d_c/2\right)}{L_c}\right) \tag{6.3}$$

Skeleton curves of panel zone shear forces in the five specimens were developed using Equation 6.3, and the actuator load data from each interstory drift level. The first positive and negative peak at each drift level was used to generate the curve data. Figures 6.63 through 6.67 show the skeleton curves, along with the experimental data and the AISC (1997) shear capacities from Equation 2.1 using both nominal and measured material properties (see Table 3.4). The measured yield strengths of the column web are used. The horizontal axis is normalized by the shear yield deformation, γ_y, equal to $F_y/\sqrt{3}G$. Measured yield strength values are used for the normalization. Positive shear corresponds to positive loading, defined previously as downward displacement of the East girder tip.

A predicted curve can be generated from Equation 2.1, using the same bi-linear approximation adopted by Krawinkler (1978). The first portion of the curve is defined by

the elastic stiffness, and is valid to general shear yielding of the panel zone (V_y = $0.6F_{yc}d_ct_p$):

$$K_e = \frac{dV}{d\gamma} = d_c t_p G \qquad (0 < \gamma \leq \gamma_y) \qquad (6.4)$$

where:

K_e = elastic panel zone stiffness

G = shear modulus of elasticity = 11,150 ksi

The second portion of the curve is defined by the post-elastic stiffness, and is valid to a shear deformation of $4\gamma_y$. This deformation level was selected by Krawinkler (1978) as a limit to avoid excessive panel zone deformation. The shear force at this point (i.e., $4\gamma_y$) is that given by Equation 2.1. This post-elastic stiffness, K_p, is:

$$K_p = \frac{dV}{d\gamma} = \frac{b_{cf} t_{cf}^2 G}{d_g} \qquad (\gamma_y < \gamma \leq 4\gamma_y) \qquad (6.5)$$

Potential shortcomings of the current design methodology have been discussed in other research, dating back to the original publication of the model by Krawinkler (1978). The small member sizes from the tests used to develop Equation 2.1 were noted, and caution was suggested when extrapolating the results to larger columns. The finite element study by El-Tawil et al. (1998) indicated the present provisions underestimate the panel zone shear strength when the column flanges are very thick. The finite element models of the five specimens in the present research yielded predicted panel zone strengths at a deformation of $4\gamma_y$ averaging approximately 80% of the shear given by Equation 2.1 (Ye et al., 2000). This is consistent with the experimental results of the five specimens.

In order to evaluate the current AISC (1997) panel zone provisions, the curves developed by Equations 6.4 and 6.5 are plotted for each specimen and compared with the experimental data in Figures 6.63 through 6.67. Both the nominal and measured yield strengths of the column web are used in the equations. It is evident from these figures that the panel zone design shear strength given by Equation 2.1 is significantly

overestimated. For example, at $4\gamma_y$, the shear carried by the panel zone in Specimen CR1, the specimen with the thickest column flanges, was approximately 700 kips even though Equation 2.1 predicted 903 kips for the W14x283 column (See Figure 6.63) using nominal material properties; the discrepancy is more severe using the measured yield strength for the strength prediction. While the AISC (1997) nominal shear capacity of 903 kips was eventually reached in this specimen, it did not occur until a deformation of over $11\gamma_y$, corresponding to the 4.0% interstory drift cycles. This suggests that a re-evaluation of the present design provisions for panel zone is warranted. Thus, in the following section, an alternate model for predicting the post-elastic strength of the panel zone is developed.

6.3 Alternate Model for Post-Yield Panel Zone Strength

As discussed in Chapter 2, significant strength beyond general yielding of panel zones was also noted by Fielding and Huang (1971). Using symmetry at the mid-height of the panel zone, a frame consisting of two fixed-base cantilevers (representing the column flanges) connected by a rigid link at the top was used by Fielding and Huang (1971) to model the post-elastic stiffness of the joint region (See Figure 2.1a). In this section, in order to develop an alternative design equation to the present AISC provisions (1997) for panel zones, the Fielding and Huang (1971) model is modified to better model the panel zone post-elastic behavior. Design application of this modified Fielding and Huang (1971) model are verified through comparisons with the experiments from the present research and with results of other tests that exceeded the deformation of $4\gamma_y$ in the panel zones.

6.3.1 Modified Fielding and Huang Model

While modeling the effect of the column flanges in the original Fielding and Huang (1971) model is reasonable, the boundary conditions do not reflect the behavior observed in numerous tests. Figure 2.1a implies hinging of the column flanges at mid-height of the panel zone, and bending deformations of the flanges with curvatures opposite of the typically observed deformations. In the revised model, shown in Figure

6.68, the fixed bases of Figure 2.1a are replaced with pin supports, and the rigid link is replaced with an infinitely rigid member. The pinned ends represent the inflection points seen at mid-height of deformed panel zones, and the infinitely rigid girder represents the restraint imposed on the panel zone by the columns above and below the panel zone. This revised model is essentially a restatement of the Fielding and Huang (1971) model, and gives the same stiffness, as will be shown below. Plastic hinges are assumed to form at the tops of the flange cantilevers (i.e., at the corners of the panel zone), consistent with experimental observations. The model also predicts the reverse curvature bending deformation typically exhibited by panel zones.

The elastic lateral deflection of the frame shown in Figure 6.68 is expressed as:

$$\Delta = \frac{1}{2}\left(\frac{dV_f l^3}{3EI_f}\right) \tag{6.6}$$

where:

Δ = lateral deflection = $l*d\gamma$

dV_f = incremental panel zone shear force carried by column flanges

l = height of frame model = $d_g/2$

E = modulus of elasticity

I_f = moment of inertia of individual column flange

Substituting ($l*d\gamma$) for the deflection, Δ, $d_g/2$ for the height, l, and $b_{cf}t_{cf}^3/12$ for the column flange moment of inertia, I_f, into Equation (6.6) and rearranging results in the post-yield panel zone stiffness of the modified Fielding and Huang model:

$$K_p = \frac{dV_f}{d\gamma} = \frac{2Eb_{cf}t_{cf}^3}{d_g^2} \tag{6.7}$$

The stiffness given by Equation 6.7 implies that the additional shear force carried by the panel zone following the shear yielding is resisted entirely by elastic bending of the column flanges.

Equation 6.7 is equivalent to the original Fielding and Huang (1971) post-yield stiffness given previously by Equation 2.5, following substitution of the expression for

the flange moment of inertia. Like Krawinkler (1978), this model is assumed herein to be valid up to a shear deformation of $4\gamma_y$. Beyond this deformation level, significant inelasticity will develop in the column flanges (i.e., column flange kinking), and Equation 6.6 is no longer valid. Assuming a maximum deformation of $4\gamma_y$, the ultimate shear strength of the panel zone can be expressed by the following (from Krawinkler, 1978):

$$R_v = V_y\left(1+\frac{3K_p}{K_e}\right) \tag{6.8}$$

In the proposed new panel zone strength model, the elastic stiffness (See Equation 6.4) is used without any change. Substituting Equations 6.4 and 6.7 into Equation 6.8, and replacing E with $2.6G$ yields a new ultimate strength criterion for panel zones:

$$R_v = 0.6F_{yc}d_c t_p\left(1+\frac{15.6b_{cf}t_{cf}^3}{d_g^2 d_c t_p}\right) \tag{6.9}$$

Equation 6.9 is similar in form to the AISC panel zone provisions (Equation 2.1), and can also be plotted as a bi-linear curve. In Figures 6.69 through 6.73, the panel zone strength curve developed by Equation 6.9 is plotted along with the AISC model (Equation 2.1, developed from Equations 6.4 and 6.5) and the experimental data for each specimen. Both the nominal and measured yield strengths of the column web are used in Equations 2.1 and 6.9. These figures reveal that Equation 6.9 more accurately captures the post-yield strength at $4\gamma_y$ than does the current AISC equation. Compared to the predicted post-yield strength increase of 39.4% (CR1), 17.1% (CR2), 11.9% (CR3), 9.3% (CR4R), and 8.0% (CR5) in Equation 2.1, Equation 6.9 predicts an increase of 17.5% (CR1), 5.3% (CR2), 3.3% (CR3), 2.6% (CR4R), and 1.9% (CR5), respectively.

Despite the improvement, Equation 6.9 still over-predicts the panel zone shear strength at the design deformation of $4\gamma_y$, especially for Specimens CR3 and CR4R. It is clear that part of the discrepancy is the assumed yield strength of the panel zone ($V_y = 0.6F_{yc}d_c t_p$), i.e. the panel zone shear force at $1\gamma_y$ in Figures 6.69 through 6.73. These figures show that yielding of the panel zone begins at loads below this value ($V_y = 0.6F_{yc}d_c t_p$). The SAC State of the Art Report on Connection Performance (FEMA,

2000b) discussed the differences between the AISC Seismic Provisions (1997) and the Krawinkler (1978) derivation (Equation 2.6). The use of the 0.6 factor on shear yield strength as opposed to 0.55 results in a 9% difference between the nominal panel zone yield strengths. While the use of $0.6F_y$ can be reasonably argued for other shear applications, this appears unconservative when applied to panel zones. The use of $0.55F_y$ may be more appropriate in this case (FEMA, 2000b).

Two modifications to Equation 5.9 are now presented. First, $0.6F_{yc}$ is replaced with $0.55F_{yc}$ to more accurately reflect the onset of yielding in the panel zone. Second, the 15.6 factor in the post-yield term is conservatively rounded down to 15. This was also done upon adoption of the Krawinkler formula (Equation 2.6) by the UBC code (1988), which rounded the factor of 3.45 to 3. The revised model is now given as:

$$R_v = 0.55F_{yc}d_c t_p\left(1+\frac{15b_{cf}t_{cf}^3}{d_g^2 d_c t_p}\right) \tag{6.10}$$

Figures 6.74 through 6.78 compare the experimental data to Equation 6.10 and the AISC model (Equation 2.1) using both the nominal and measured yield strengths of the column web. The post-yield strengths at $4\gamma_y$ are slightly underpredicted in Specimens CR1, CR2, and CR5 when the nominal yield strengths are used, but the differences are very small and negligible. The shear strength at the onset of panel zone yielding is still overpredicted in all cases when the measured yield strengths of the column webs are used, but is more closely approximated than using Equation 2.1. Thus, the modified Fielding and Huang (1971) model of Equation 6.10 may be a more rational procedure for determining the design strength of panel zones for seismic applications.

Table 6.1 summarizes the predicted strengths of the panel zones of the five cruciform tests using the AISC (1997) provisions (Equation 2.1) and Equation 6.10 using both the specified minimum yield strengths and the coupon tensile test results. Also tabulated are the percent increases beyond yield incorporated in each equation. In all cases, Equation 6.10 results in a smaller panel zone resistance. For those specimens with thinner column flanges and column web reinforcement (e.g., Specimen CR5), Equation 6.10 predicts very low post-yield strengths. Evaluation of the post-yield strength term in Equation 6.10 is evaluated further below.

6.3.2 Verification of Modified Fielding and Huang Model (Equation 6.10)

An analysis of past connection test data was conducted to evaluate Equation 6.10 relative to the current AISC provisions (Equation 2.1). Test data from the following sources are included in this analysis: Fielding and Huang (1971), Krawinkler et al. (1971), Bertero et al. (1973), Becker (1975), Popov et al. (1986), Ghobarah et al. (1992), Tsai et al. (1995), FEMA (1997b), Choi et al. (2000), Lee et al. (2000), and Ricles et al. (2000a). A total of 49 tests, including the five cruciform specimens tested in the present research, that exceeded the design deformation of $4\gamma_y$ in the panel zones were included, as the experimental shear force at this deformation level is required for the comparison. Tables 6.2 and 6.3 tabulate the relevant parameters from all tests included in the following analysis. The reported yield stress is the coupon yield stress, or otherwise the dynamic yield stress from the mill reports.

The collection of tests represents a wide range of parameters. Nominal steel yield strengths of 36 ksi and 50 ksi are included, with a range of measured column yield strengths from 31.4 ksi to 60.0 ksi. Column sizes range from W8 sections to W21 sections, while girder sizes range from W10 sections to W36 sections. Several tests were stiffened with doubler plates and/or continuity plates, and some haunched, cover-plated, and end-plate connections are also included. Panel zone thicknesses range from 0.245 in. to 3.27 in., and column flange thicknesses range from 0.398 in. to 2.845 in. Most tests conducted prior to the Northridge earthquake included compressive column axial loads, while none of the post-Northridge tests were axially loaded. With the exception of the tests by Fielding and Huang (1971) and Becker (1975), the girders of the specimens were cyclically loaded.

To determine the experimental shear force in the panel zones at $4\gamma_y$, the girder loads or moments at this deformation level were first required. Most test results reported panel zone behavior in one of two forms. Moments and loads were generally either plotted against total panel zone deformation, γ_{pz}, or against panel zone plastic rotation, $\theta_{p,pz}$. If the total panel zone deformation was reported, the loads or moments at $4\gamma_y$ could be obtained directly. If panel zone plastic rotation was reported, the plastic rotation

corresponding to a total deformation of $4\gamma_y$ had to first be computed. The panel zone shear yield deformation, γ_y, was calculated as $F_{y,web}/\sqrt{3}G$, where $F_{y,web}$ is the column web yield strength taken from mill reports, or coupon tests when available (Table 6.3). The equation relating $4\gamma_y$ to an equivalent $\theta_{p,pz}$ was adapted from Hajjar et al. (1998b) and Leon (1983). This equation is given as:

$$\theta_{p,pz} = \frac{1}{\left(L_g + d_c/2\right)}\left[\frac{3\gamma_y L_g\left(L_c - d_g\right)}{L_c} - \frac{3\gamma_y d_g d_c}{2L_c}\right] \tag{6.11}$$

Equation 6.11 converts a shear deformation into an equivalent connection rotation due to panel zone shear deformation. By using $3\gamma_y$ in the equation, the plastic rotation due to a shear deformation of $4\gamma_y$ is computed (i.e., $3\gamma_y$ is the plastic shear deformation associated with the total deformation of $4\gamma_y$).

From the design deformation of $4\gamma_y$ or the associated $\theta_{p,pz}$, the moments or loads were scaled off of the appropriate plots of moment or load vs. panel zone deformation or rotation. For those cyclic tests exceeding $4\gamma_y$ in both loading directions, the average moment or load was used. The values of moments or loads during the first excursion to $4\gamma_y$ were recorded. When $4\gamma_y$ occurred between loading peaks, an equivalent skeleton curve was constructed between peaks, and the moments or loads were interpolated. Thus, this method does not account for cyclic strain hardening which often occurs in subsequent cycles to deformations beyond $4\gamma_y$. One exception to this procedure was the testing by Fielding and Huang (1971). In this case, panel zone shear stress, τ_{pz}, was directly reported.

From the known moment or load at a panel zone deformation of $4\gamma_y$, the experimental panel zone shear force, V_{pz}, at this deformation was calculated. The same procedure used to calculate the experimental shear forces for the five specimens tested in the present research was used for the analysis of past test data. Recall Equation 6.1:

$$V_{pz} = \frac{M_{tot}}{d_g} - V_c \tag{6.1}$$

Column shear was calculated from the dimensions of the test specimens. In terms of loads and moments, Equation 6.1 can be transformed, respectively, in:

$$V_{pz} = P_{tot}\left(\frac{L_g}{d_g} - \frac{\left(L_g + d_c/2\right)}{L_c}\right) \tag{6.3}$$

$$V_{pz} = M_{tot}\left(\frac{1}{d_g} - \frac{\left(L_g + d_c/2\right)}{L_g L_c}\right) \tag{6.12}$$

Equation 6.3 was also used in Section 6.2.4 to determine the experimental panel zone shear force of the five cruciform specimens tested in the present research.

For haunched or cover-plated connections, the depth of the haunches and thickness of the cover plates were included in the effective girder depth. Because Fielding and Huang (1971) directly reported panel zone shear stress, the experimental shear force was calculated as $\tau_{pz}A_{cw}$, where A_{cw} is the column web area. The reported shear stress took the effects of column shear into account. No column shear was present in the tests by Becker (1975) because the test configuration modeled corner joints.

Predicted panel zone strengths, R_v, were calculated using Equation 2.1 (AISC, 1997) and the proposed Equation 6.10. No resistance factors were included ($\phi = 1.0$). For the calculation of panel zone strengths, measured material properties were used (mill reports, or coupon tests when available), instead of the specified minimum yield strengths. Table 6.4 presents the test-to-predicted ratios (V_{pz}/R_v) for the selected tests using both Equations 2.1 and 6.10. Also tabulated are the increases beyond yield incorporated in each equation. These post-yield contributions are defined in each equation by the second term in parentheses, and represent the effects of the panel zone boundary elements (primarily column flanges) following panel zone yielding. As Table 6.4 shows, the modified Fielding and Huang model of Equation 6.10 better predicted the panel zone shear strength for the group of tests analyzed. The mean test-to-predicted ratio was 1.060, as compared to a mean of 0.856 for the AISC provisions (Equation 2.1). The standard deviations for both methods were comparable. In all cases, however, a lower strength increase beyond yielding is predicted by Equation 6.10.

An important observation arises when comparing the test-to-predicted ratios of tests with W14 and larger columns to those with W12 and smaller columns. For those tests with W14 and larger columns, the mean test-to-predicted ratio is 0.812 for Equation 2.1 and 1.012 for Equation 6.10. When tests with W12 and smaller columns are considered, the mean test-to-predicted ratio increases to 1.005 for Equation 2.1 and 1.226 for Equation 6.10. This suggests that the AISC provisions (Equation 2.1) are satisfactory for smaller columns and somewhat unsatisfactory for larger columns. Recall that these provisions were developed from the results of testing by Krawinkler et al. (1971) and Bertero et al. (1973) on W8 column sections. Equation 6.10, on the other hand, was more accurate in its prediction of the panel zone strength of larger columns and appears somewhat conservative for smaller columns. These results suggest that the modified Fielding and Huang model of Equation 6.10 better predicts panel zone behavior in joints with member sizes commonly used in current seismic moment frame construction.

A resistance factor was also calculated for Equation 6.10 using the data from the group of 49 tests and the procedure given by Equation C-A5-4 in the Commentary to the AISC LRFD Specification (AISC, 1999a). The referenced equation computes an approximate resistance factor based on the mean and nominal resistances, the coefficient of variation of the resistance, and a reliability index. A reliability index of 2.6 was selected, consistent with the typical value specified for members (AISC, 1999a). Using the mean test-to-predicted ratio of 1.060 and corresponding coefficient of variation equal to 0.160, a resistance factor of 0.86 was calculated.

6.3.3 Comparison of Panel Zone Thicknesses

To compare the panel zone design criteria as determined by the AISC provisions (Equation 2.1), Equation 6.10, and the SAC panel zone design procedure (Equation 2.7), required panel zone thicknesses based upon nominal material properties were calculated for several girder-to-column connection configurations using the three methods. These girder-to-column combinations include the five connections tested in the present research.

The SAC panel zone design procedure (FEMA, 2000a) was outlined in Chapter 2 (See Equation 2.7). Rather than consisting of a computation of the design strength, this method attempts to balance the onset of yielding in the girders and panel zone. The panel zone deformation at the ultimate strength of the girders is not explicitly addressed. According to the SAC Recommended Seismic Design Criteria (FEMA, 2000a), the SAC method may require moderately thicker doubler plates for connections with thick column flanges when compared to the current AISC (1997) panel zone requirements (Equation 2.1).

In the previous two sections, the comparison of AISC (1997) and the modified Fielding and Huang model (Equation 6.10) was independent of any demand calculations. However, for the Equation 6.10 to be compared to the AISC provisions (AISC, 1992, 1997, 2001) and to the SAC procedure, the panel zone demand had to be incorporated so as to calculate its required thickness. For this purpose, the demand given by AISC (1997) and modified by Supplement Nos. 1 and 2 (AISC, 1999b, 2001) was adopted for the calculation of the required panel zone thickness for the application of AISC (1997), Equation 6.10, and SAC (Equation 2.7). This demand is presented in Equation 3.6. Additionally, the demand cap specified in the 1992 AISC Seismic Provisions (AISC, 1992) was used with Equation 2.1 for comparison of all results to a pre-Northridge specification. The AISC (1992) demand cap is given as:

$$R_u = \frac{0.9\sum \phi_b M_p}{d_g} - V_c \tag{6.13}$$

where:

R_u = panel zone demand

ϕ_b = resistance factor for bending = 0.9

M_p = nominal girder plastic moment capacity

The resistance factor on panel zone shear strength in the 1992 AISC Seismic Provisions was specified as 0.75. Thus, this value was substituted in place of ϕ_v = 1.0 in Equation 2.1 for calculations of required panel zone thicknesses according to the 1992 Seismic Provisions (AISC, 1992).

In Table 6.5, three distinct groups of girder-to-column connection configurations are included. The first group consists of the five cruciform (i.e., interior joint) specimens described in this work, while the second group includes three typical exterior joint combinations tested in both phases of the SAC program (FEMA, 1997b; Lee et al., 2000). The final group consists of ten interior and ten exterior combinations. Within each group of ten, five girder sizes are included – one from each nominal depth between W24 and W36, inclusive. The chosen girders represent the smallest size in each depth category that meets the seismic flange compactness criteria of $52/\sqrt{F_y}$ (AISC, 1997). For each girder, two column sections were chosen. The first was selected to represent a large column requiring little or no panel zone reinforcement (i.e., no doubler plates), while the second column was selected such that relatively thick doubler plates were required. With the exception of cruciform Specimen CR5, all combinations meet the SCWB criterion presented in Chapter 3 for an axial load of zero. Column shear, V_c, was calculated from statics based on the specimen dimensions and the development of the maximum girder moment corresponding to the specified demand. For the final group of combinations, calculation of column shear was based on the dimensions of the cruciform specimens in this work.

In the case of the SAC panel zone provisions (Equation 2.7), the required thickness was directly computed. For the 1992 and 1997 AISC seismic provisions, and Equation 6.10, the required panel zone thickness was computed by setting $\phi_v R_v = R_u$ for the respective cases and solving the resulting expression for the thickness, t_p. The resistance factor, ϕ_v, was taken as 1.0 for Equation 6.10. While a resistance factor of 0.86 was previously calculated for this equation, a value of 1.0 was used for these panel zone thickness calculations to be consistent with AISC (1997). As discussed in Chapter 2, Supplement No. 2 to the 1997 AISC Seismic Provisions (AISC, 2001) increased the resistance factor from 0.75 to 1.0. The commentary to Supplement No. 2 (AISC, 2001) states that the resistance factor was set to 1.0 "because ϕ is typically applied to systems to assure that they remain elastic. In this case [seismic panel zone design], it is known that yielding will occur."

Table 6.6 presents the results in terms of the required panel zone thicknesses determined by each of the four cases. The table reveals that the panel zone strength model proposed herein (Equation 6.10) requires thicker panel zones than the 1997 AISC Seismic Provisions [using the demand specified by Supplement No. 2 (AISC, 2001)], the SAC procedure (FEMA, 2000a), and the 1992 AISC Seismic Provisions [using the demand cap specified by Equation 6.13]. This is because the panel zone yield strength and post-yield stiffness were decreased in Equation 6.10 as compared with Equation 2.1 even though the demand, presented in Equation 3.6, remained without any change. The decrease of panel zone yield strength and post-yield stiffness in Equation 6.10 can be clearly observed in Figures 6.74 through 6.78 for the five specimens tested in the present research. The relationship between demand and capacity in the panel zone design will be further discussed in the following section. In addition, in the following section, the panel zone demand and capacity of the five cruciform specimens tested in the present research will be scaled for the design application of the modified Fielding and Huang model of Equation 6.10.

In addition to the above findings for Equation 6.10, it should be noted that the SAC and 1997 AISC required thicknesses that were generally similar, even for columns with thick flanges. In fact, the AISC (1997) thicknesses are often higher than the SAC requirements. The required thicknesses as determined by the 1992 AISC Seismic Provisions are generally lower than the AISC (1997) and SAC values. While the resistance factor of 0.75 included in AISC (1992) is lower than the resistance factor of 1.0 specified in Supplement No. 2 of the 1997 AISC Seismic Provisions (AISC, 2001), the demand cap given by Equation 6.13 is lower than the demand given in the Supplement No. 2 (AISC, 2001). However, while the 1992 AISC provisions yield thinner panel zones, the thicknesses are sufficiently close to suggest that weak panel zones designed prior to the Northridge earthquake were generally not a result of the demand cap given by Equation 6.13. It is likely then, that the applicable load combinations used with AISC (1992) resulted in significantly lower demands, and thus weaker panel zones, than did the cap (Equation 6.13). As discussed in Chapter 2, the 1992 AISC Seismic Provisions were intended to provide the same level of safety as the

1991 UBC code (See Section 2.1.1). It was the UBC code that first adopted the Krawinkler panel zone model (based on Equation 2.6) in 1988 (UBC, 1988).

The results shown in Table 6.6 have several implications. Considering the modified Fielding and Huang model (Equation 6.10), it was previously shown that this procedure better predicts panel zone shear strength at the design deformation of $4\gamma_y$ than does the current AISC provisions (AISC, 1997) for a wide range of experiments. This analysis was independent of a specified demand. When calculating required panel zone thickness (which necessitates specifying a demand), however, Equation 6.10 is more conservative than both AISC (1997) and SAC (FEMA, 2000a) for the same demand. If it is assumed that the AISC (1997) and SAC (FEMA, 2000a) procedures result in adequate panel zone designs, Equation 6.10 would require a lower demand to yield similar panel zone thicknesses. While Equation 6.10 appears to better model the shear-deformation behavior of panel zones, further study is needed to identify an appropriate combination of capacity and demand for panel zones in seismic application.

6.3.4 Scaling of Panel Zone Design Capacity and Demand

To further consider the interrelationship of capacity and demand in panel zone design, panel zone thicknesses for the five cruciform specimens tested in the present research were re-designed using the modified Fielding and Huang model (Equation 6.10) and nominal material properties, and these are compared in Table 6.7 with the values selected for the experimental study. The demand from AISC (1997) and modified by AISC (2001) was used for these calculations. The re-designed panel zone thicknesses clearly show larger values in all cases.

There were two primary reasons for these differences. First, as described in Section 3.3.3.1, a P_z / P_g of 1.0 was targeted for the panel zone design of the cruciform specimens tested in the present research instead of strictly satisfying the 1997 AISC provisions (Equation 2.1). This design approach resulted in a panel zone capacity-to-demand ratio equal to 0.83 (with the application of Equation 2.1) for Specimen CR1, as shown in Table 3.3. In other words, for a given panel zone demand, the panel zone capacity would have increased by 1/0.83 = 1.205 times the original capacity calculated if

Equation 2.1 had been used for the design of the Specimen CR1 panel zone. Had Equation 2.1 been used for the panel zone design of Specimen CR1 without any changes in the demand, a thickness of t_p = 1.63 in. would have been recommended given the configuration of Specimen CR1, as shown in Table 6.6

The second reason causing the differences between the panel zone thicknesses selected for the tests and those re-designed using Equation 6.10 is the use of the different equation of panel zone strength (i.e., Equation 6.10 versus Equation 2.1). For the panel zone design of the five cruciform specimens tested in the present research, as shown in Equation 3.15, the panel zone strength equation from the AISC (1997) provisions (Equation 2.1) was partially incorporated into the calculation, while the re-designed panel zone thicknesses in Table 6.7 were obtained exclusively from the application of Equation 6.10 in conjunction with the seismic demand of AISC (1997, 2001). The differences in panel zone capacity between Equation 2.1 and Equation 6.10 can be clearly observed in Figures 6.74 through 6.78 for the case of the five specimens tested in the present research. The differences between these two equations is partially from the different coefficient related to nominal yielding of the panel zone (0.55 for Equation 6.10 versus 0.6 for Equation 2.1), but even more so to the magnitude of the post-yield strength term, as shown in Table 6.4. The difference in the post-yield strength term is exhibited by the difference in the post-elastic slope between the two equations.

The results shown in Figure 6.74 to 6.78 show first that the slope of Equation 6.10 tends to be more appropriate for columns with thicker flanges (e.g., Specimen CR1), while the slope of Equation 2.1 tends to be more appropriate for columns with thinner flanges (e.g., Specimen CR5), although other parameters of the column and girder may also influence this difference. Rectifying this difference would increase the complexity of the resulting equation, but would refine the strength estimates such as those outlined in Table 6.4. However, Figures 6.74 to 6.78 exhibit that a more substantial increase in accuracy of the panel zone strength may be obtained through a scaling of the nominal panel zone yield strength, i.e., the strength at which the elastic zone terminates. Scaling down the panel zone capacity and demand is thus investigated here so as to formulate a

new panel zone equation corresponding to the behavior of the five cruciform specimens tested in the present research.

Using the modified Fielding and Huang model (Equation 6.10), a method scaling panel zone capacity corresponding to the actual test results is introduced. This methodology is schematically explained in Figure 6.79 for the case of Specimen CR1. In this figure, the panel zone shear capacity in Equation 6.10 corresponding to $4\gamma_y$ ($\phi_v R_v$ = 1073 kips) is scaled down by the scale factor of (α = 711/1073 = 0.663), where 711 kips is the panel zone strength obtained in the experiment at a panel zone deformation of $4\gamma_y$ (with nominal material properties used to compute $4\gamma_y$). The general form of scaled panel zone capacity is then:

$$\alpha R_v = \alpha 0.55 F_{yc} d_c t_p \left(1 + \frac{15 b_{cf} t_{cf}^3}{d_g^2 d_c t_p}\right) \tag{6.14}$$

where:

α = panel zone capacity scale factor

This scale factor was also computed for the other four specimens; these values are shown in Table 6.8. This scale factor varies from 0.652 (Specimen CR2) to 0.858 (Specimen CR4R). It should be noted that the test specimen designed using the larger $\phi_v R_v / R_u$ value results in a larger scale factor.

In order to apply Equation 6.14 for the panel zone design of other new girder-to-column connections, the demand (R_u) should also be scaled by using the same factor, α, if it is assumed that the column thickness resulting from Equation 6.10 are appropriate as shown in Table 6.6 (as discussed in the prior section, the demand may need to be further modified given the thicker panel zones already being required from Equation 6.10 and, therefore, Equation 6.14). If the demand is not scaled, the decreased capacity (Equation 6.14) combined with the original demand (R_u) will result in thicker panel zones that are not justified based upon the test results in this research. Using a scaled panel zone capacity (Equation 6.14) and a corresponding scaled demand, the panel zone capacity curve more closely corresponds to the experimental results, and the panel zone thickness

would be the same as the t_p as Table 6.6. The methodology introduced above can similarly be used to evaluate the current panel zone design provisions (AISC, 1997, 2001) based on the experimental results and to estimate the appropriate demand for the selected panel zone capacity. As discussed above, a scaled version of Equation 6.10 for columns with relatively thin flanges coupled with a scaled version of Equation 2.1, all coupled with an appropriate demand assessment, would result in the most reliable and accurate prediction of panel zone size.

6.4 Local Flange Bending

The pull-plate tests conducted by Prochnow et al. (2000a) extensively studied the local flange bending (LFB) limit state. As discussed in Chapter 2, this research concluded that the present AISC provisions for LFB are satisfactory for non-seismic design. Extension of this conclusion to seismic design was one focus of the five cruciform specimens tested in the present research. This section discusses the LFB yield mechanism defined by Prochnow et al. (2000a), and compares the results of the five specimens to this yield mechanism and the pull-plate experimental results.

In the pull-plate tests, the LFB yield mechanism was defined by a limiting column flange separation, measured between the column flanges at the edges of the pull-plates (representing girder flanges). For the limit, flange separation of ¼ in. was chosen. This value was chosen based on the allowable variation in member cross sections as per ASTM A6 (1998b). These provisions allow the flanges of wide-flange sections to be out of square by a maximum of ¼ in. (Prochnow et al., 2000a).

For purposes of the cruciform experiments, however, the above yield mechanism is modified slightly. Due to the reverse cyclic loading in girders, one column flange is in tension while the other is in compression at the same girder flange level (i.e., top or bottom girder flange level). The compressive force tends to offset some of the flange separation caused by the tensile force on the opposite column flange. As discussed in Section 4.3.2, the LVDTs used to measure the column flange deformation were anchored to the column web centerline to avoid the offsetting effects of the compressive flange forces (See Figures 4.19 and 4.20). For the cruciform experiments, then, the limiting

flange separation is redefined as a limiting flange deformation. This limiting deformation is taken as one-half the pull-plate separation value of 1/4 in, as the deformation of only one flange is measured. Thus, the LFB yield mechanism for the present experiments is defined as a column flange deformation of 1/8 in at the location of the girder flanges.

In the pull-plate tests (Prochnow et al., 2000a), three demand levels were considered to analyze the LFB yield mechanism, representing non-seismic and seismic demands. These were presented in Chapter 2:

$$R_u = F_{yg} A_{gf} \quad \text{(non-seismic)} \quad (2.12)$$

$$R_u = 1.8 F_{yg} A_{gf} \quad \text{(seismic)} \quad (2.13)$$

$$R_u = 1.1 R_y F_{yg} A_{gf} \quad \text{(seismic)} \quad (2.14)$$

where:

F_{yg} = minimum specified yield strength of girder flange

A_{gf} = girder flange area

R_y = ratio of expected yield strength to minimum specified value = 1.1 for A992 steel

In this experimental study, however, only Equations 2.13 and 2.14 were considered for the seismic application.

Using the measured yield strength of the W24x94 girder (See Table 3.4), the seismic demand from Equation 2.14 is approximately 486 kips for Specimens CR1, CR2, CR4R, and CR5, and is approximately 521 kips for Specimens CR3. Using the nominal strength of 50 ksi for A992 steel, these demands become 480 kips for all specimens, i.e., 55 ksi on the gross area. This stress is reasonable in comparison to typical yield strengths. For example, a survey of more than 20,000 mill reports from 1998 (Dexter, 2000; Bartlett et al., 2001; Dexter et al., 2001) showed that A992 steel has a mean yield strength of 55.8 ksi. The 97.5 percentile yield strength was 62.3 ksi, and the maximum value reported was 65 ksi.

Equation 2.13 yields a demand of 722 kips for Specimens CR1, CR2, CR4R, and CR5 and a demand of 775 kips for Specimen CR3 using measured material properties. Using nominal properties, Equation 2.13 yields a demand of 714 kips in all cases, i.e., 90

ksi on the gross area. This value is clearly greater than any yield strength value. In fact, the mean ultimate strength in the 1998 data was 73.3 ksi, with a 97.5 percentile ultimate strength was 80.0 ksi, and the maximum ever reported was 88 ksi. Therefore, an A992 girder flange is incapable of producing a demand as high as Equation 2.13.

However, assuming all the moment in the girder is carried by these flange forces, the demand of 480 kips corresponds to a moment of approximately 11,700 kip-in (or approximately 92% of the nominal plastic capacity of the girder section) and the demand of 714 kips corresponds to a moment of approximately 17,350 kip-in (or approximately 137% of the nominal plastic capacity of the girder section). The assumption that the full moment is carried by only girder flanges is thus somewhat conservative. The true moment at the development of the 480 kip flange force is likely at or above the nominal plastic capacity of the section.

For purposes of comparing LFB data from the five specimens to the yield mechanism limit deformations, flange deformations at the 4.0% drift level are examined since this drift level represents the maximum moment demand on the columns. At this drift level, the corresponding girder moments were approximately 103% (CR1), 95% (CR2), 105% (CR3), 119% (CR4R), and 108% (CR5) of M_p. The moment resulting from development of the demand given by Equation 2.13 was not reached in the five tests. However, it is also recognized that the derivation of Equation 2.13 (Bruneau et al., 1998) is partially accounting for the multi-axial stress state that may be entering the column flange from the girder flange.

In addition, assuming all the moment in the girder is carried by the flange forces, the range of flange forces at the 4.0% interstory drift level would be between approximately 500 to 600 kips. The actual forces in the girder flanges would be somewhat lower, as some moment is transferred through the welded web. Nevertheless, these forces correspond well with the 450 kip nominal pull-plate force that was often used as the target demand (from Equation 2.13) for assessing the results of the pull-plate experiments, and facilitates comparison between the two sets of experiments used in this research.

Figures 6.80 through 6.85 show the strain distributions on the inside face of the column flange near its web in the longitudinal direction, for the case of the specimens with no continuity plates or offset doubler plate detail, i.e., Specimens CR1, CR2, and CR5. The strains for the tensile and compressive load peaks are plotted from the first cycle at each interstory drift levels as a function of position on the column flange. Refer to Figure 4.20 for the location of the strain gages. From Figures 6.80 through 6.85, it is clear that a complex state of stress exists inside face of the column flange near its web due to a concentrated girder flange force.

Considering tensile flange loading (Figures 6.80, 6.82, and 6.84), the longitudinal strain changes rapidly from compression directly underneath the girder flange to a nearly uniform tensile strain beginning 6 in. below the flange, indicating a high, localized strain gradient. Strains due to LFB dominate the observed behavior near the concentrated girder flange loading, especially for Specimens CR1 and CR2, even though these strains are superimposed with the column flange strains due to the bending of the column and the deformation of the panel zone.

The column flexural strains are of a larger magnitude than the strain due to local flange bending beyond the gage 6 in. below the girder flange, and can explain the relatively constant strain in this region. Specimen CR5 (Figure 6.84) showed relatively large flexural strain distribution beyond the gage 6 in. below the girder flange. This was expected since it was the weakest column member among the five specimens. In spite of the large flexural bending in the column flange, localized strain distributions due to LFB having even larger strains were also observed around the girder flange levels in Specimen CR5.

Using the elastic section properties of the column and statics on the test configuration for the applied actuator loads at 4.0% interstory drift, bending stresses in the region 12 to 6 in. below the girder flanges were calculated for the comparison with the measured strain readings. These calculated column bending stresses and the corresponding strains are summarized in Table 6.9. For Specimen CR1, the bending stress range of 22 to 24ksi existed in the region 12 to 6 in. below the girder flanges. This corresponds to the strain range of 750 to 820 $\mu\varepsilon$. This value is comparable to the

measured strains of approximately 600 με in the case of Specimen CR1. The corresponding strain ranges of 1020 to 1120 με and 1550 to 1700 με were provided for Specimens CR2 and CR5, respectively, as compared to measured values of 680 to 1060 με in Specimen CR2 and 1310 to 2200 με in Specimen CR5.

As shown in figures 6.80, 6.82, and 6.84, local flange bending had little influence on the column flange beyond approximately 6 in. from the girder flanges. Strains obtained in the pull-plate tests (Prochnow et al., 2000a) exhibited similar behavior, with the exception that no flexural stresses were present in the column stubs. Instead of approaching the flexural strain levels, longitudinal strains in the pull-plate tests approached zero between 4 and 12 in. from the concentrated force, depending on the specimen. However, since this is relatively far from the girder flange, it is not believed to significantly influence the outcome of the pull-plate test. The similarity between the strain distributions near the girder flanges of the pull-plate test and the cruciform test supports the use of pull-plate tests for investigation of local flange bending and other localized phenomena.

The peak longitudinal strain in the column flange was variable between the specimens, and no consistent trend was observed between the magnitudes of the peak longitudinal strain (other than being opposite in sign) when the girder flanges were in compression versus in tension. However, the results clearly indicate that, at least on the level of localized strain, local flange bending may be induced both by tensile and compressive concentrated girder flange forces.

Figures 6.86 through 6.91 show the strain distributions in the transverse direction of the inside face of the column flange at the location directly opposite of the East girder bottom flange. Refer to Figure 4.20 for the location of the strain gages. Not only are the strains smaller in the transverse direction than the longitudinal direction, they also do not exhibit any well-defined trends. This indicates that transverse column flange bending due to LFB could not be well captured by strain data.

More significant at this location are the longitudinal strains along the transverse direction of the column flange (See Figures 6.92 through 6.97). These strains are often relatively uniform, especially for Specimen CR1, in both tensile and compression loading

cases, and approximately one order of magnitude larger than the transverse strains. The high strains at this location are due primarily to localized bending of the column flange due to panel zone deformation, and are offset somewhat by the column flexural strains. Section 6.2 discussed this kinking phenomenon resulting from the large panel zone distortions. The measured strain data indicates that the longitudinal column flange deformations due to panel zone yielding, coupled with the concentrated girder flange forces, dominated the strain behavior in the transverse direction for Specimens CR1 and CR2. For Specimen CR5 (See Figures 6.96 and 6.97), no significant strain variation was observed when increasing the interstory drift level for both the tensile and compressive loading cases. This is because the bending in the column flange occurred about a point approximately 2 in. below the girder flange level, instead of at the girder flange level, as already shown in Figures 6.84 and 6.85.

The complexity of the strain distributions discussed above does not lend itself well to any strain-based yield mechanism criteria for LFB. Prochnow et al. (2000a) reached similar conclusions with respect to the pull-plate tests. Interactions between the strains due to the two-way local flange bending deformations, strain due to high panel zone deformation, and strain due to column flexure create a state of stress that is difficult to interpret. The displacement-based criteria presented below is thus much more useful in capturing the limitation of LFB.

For Specimen CR1 and CR5, column flange out-of-plane displacements are shown as a function of distance in the longitudinal and transverse directions in Figures 6.98 through 6.101 (longitudinal) and Figures 102 through 105 (transverse), respectively. In these figures, displacements under both tensile and compressive girder flange loading are shown. The displacements were measured by LVDTs placed as shown in Figure 4.23. The figures show the flange deformation profiles from the peak of the first cycle at each interstory drift level peak.

The flange displacement data indicates that only slight local flange bending occurred in Specimen CR1 and CR5 (unfortunately, the corresponding LVDTs on Specimen CR2 did not produce reliable results and are not discussed here). At the location of the girder flange level, the maximum column flange displacements at 4.0%

interstory drift were 0.032 in. in Specimen CR1 and 0.061 in. in Specimen CR5. Specimen CR5 is analogous to the pull-plate specimen 2-LFB, having the same column size and detailing and rough equivalence between the girder flange and the pull-plate, as well as between the materials used. The maximum out-of-plane displacement of the column flange in the pull-plate specimen 2-LFB was 0.055 in., which is reasonably close to the 0.061 in. measured in cruciform Specimen CR5. It is recognized that there are numerous differences in the loading and stress distributions between these two types of test specimens. For example, as explained above, the two values compared above were not assessed at precisely the same demand level. In addition, in the pull-plate specimens, a relatively greater share of the out-of-plane displacement resulted from stretching in the web, which is not subjected to uniform tension in the cruciform tests. Nevertheless, the demand levels corresponded fairly well, and the favorable comparison in the measured out-of-plane displacement between the two types of specimens further supports the use of pull-plate experiments to study local phenomena like local flange bending.

The measured displacements in cruciform Specimens CR1 and CR5 correspond to just 26% of the assumed yield mechanism limit of 1/8 in. flange displacement in case of Specimen CR1 and to 49% of the limit in case of Specimen CR5. While Specimen CR1 meets the seismic criteria for not requiring continuity plates, Specimen CR5 does not even meet the non-seismic criteria (the non-seismic strength to demand ratio was approximately 0.84). Yet the flange displacements in Specimen CR5 are not significant. This conclusion further supports the conclusion from the pull-plate testing that the present AISC non-seismic design criteria for continuity plates are reasonable but conservative. The fact that the displacement did not increase after cyclic loading in the cruciform test indicates that these non-seismic criteria are sufficient for seismic loading as well, as far as local flange bending is concerned.

Column flange displacements as a function of distance in the transverse directions at the girder flange level (See Figures 102 through 105) also showed similar comparisons observed above between Specimen CR1 and Specimen CR5. In summary, both specimens did not reach the yield mechanism limit defined in this research. A fairly sharp displacement gradient is evident in both Specimen CR1 (See Figures 6.98 and 6.99)

and Specimen CR5 (See Figures 6.100 and 6.101), as the displacements approach zero at a location of approximately 12 in. from the concentrated flange force. This is consistent with the assumed yield line mechanism presented by Graham et al. (1960) and discussed by Prochnow et al. (2000a).

Figure 6.106 illustrates the assumed yield line pattern from Graham et al. (1960). Fixed boundaries (i.e., edges with zero displacement) are assumed at a location of $6t_{cf}$ from the concentrated force, corresponding to 12.42 in. for the W14x283 column (t_{cf} = 2.07 in.) and 6.54 in. for the W14x145 column (t_{cf} = 1.09 in.). The displacement gradients seen in both the longitudinal and transverse directions are evidence of the two-way column flange bending occurring.

The displacement profiles for Specimen CR1 (Figures 9.98, 9.99, 9.102, and 9.103) show a similar shape to those obtained in a pull-plate experiment (Prochnow et al., 2000a). In addition, the displacement magnitudes in Specimen CR1 closely match the values obtained in the stiffened pull-plate specimen (Specimen 1-LFB). Thus, the large, unstiffened W14x283 column of Specimen CR1 behaved similarly to the much smaller W14x132 stiffened specimen [Specimen 1-LFB tested as a part of the pull-plate research (Prochnow et al., 2000a)]. The figures also reveal that transverse and longitudinal deformations under tensile and compressive flange loading were similar. This is further evidence that LFB may be caused by compressive concentrated forces in addition to tensile forces.

The LVDT column flange displacement data from 6 in. above the girder flange (LFB1 from Figure 4.23) are not shown in Figures 6.98 through 6.101 because it is believed this location is influenced strongly by panel zone yielding. In other words, a significant portion of the displacement measured at this location is believed to be due to shear deformation of the column web to which the LVDT is attached.

Using the present AISC (1993, 1999a) LFB formula given by Equation 2.9, the resistance, R_n, of the W14x283 column flange is 1205 kips for Specimen CR1 and 334 kips for Specimen CR5, using nominal material properties. This is far larger than the seismic demands given by both Equation 2.13 (714 kips using nominal properties) and Equation 2.14 (480 kips using nominal properties) for the case of Specimen CR1. For

Specimen CR5, however, the capacity is only 47% of the seismic demand given by Equation 2.13 and 70% of the Equation 2.14, using nominal properties. It should be noted that both specimens showed good seismic performance over the 2nd cycle at 4.0% drift, as explained in Chapter 5. The test results of the five cruciform specimens tested in the present research thus indicate that the seismic demand given by Equation 2.14 may be more appropriate for the LFB design using the capacity presented in Equation 2.9.

What can also be stated based on the five cruciform specimens tested in the present research is that it is possible to achieve a desired connection behavior with a completely unstiffened column. Specimen CR3, which was stiffened with 1/2 in. thick (about half of girder flange thickness) continuity plates, completed 14 cycles of 4.0% drift without significant strength degradation in the connection. This test results are in agreement with other recently conducted tests (Ricles et al., 2000a), and supports the reestablishment by SAC (FEMA, 2000a) of design criteria for continuity plates, as opposed to a proscriptive requirement that continuity plates be used in all connections.

6.5 Stress Distribution in Girder Flange

Since the 1994 Northridge earthquake, the fracture of welded components in steel moment-resisting connections has left many questions about the correlation between the quality assurance and notch toughness of the girder flange groove welds and the performance of these connections. Stress and strain concentrations near the column web, and stress triaxiality in the girder flange, are often cited as potential causes of the poor performance of the steel moment connections. Extensive finite element analyses have been carried out in order to understand the complex stress distribution in the middle of the girder flange near the column flange face.

In this experimental study, the distributions of strains in the longitudinal direction in the girder flanges were investigated. In Figures 6.107 through 6.116, longitudinal strain distributions on the top side of the West girder top flange near the column flange face are presented. Similar strains are presented in Figures 6.117 to 6.126 for the bottom side of the East girder bottom flange. The strains for the tensile and compressive load peaks are plotted at the peak of the first cycle at each interstory drift levels as a function

of position on the girder flange. Refer to Figure 4.17 for the location of the strain gages. In Figures 6.107 through 6.126, strain data from only one side of the girder flange are reflected about the centerline of the girder to increase the clarity of the plots.

In all five specimens, the maximum longitudinal tensile strains in the middle of West girder top flange are within the range of 20,000 to 27,500 με at the 1st cycle of 4.0% drift. Similarly, the maximum longitudinal tensile strains in the middle of the East girder bottom flange are within the range of 10,000 to 33,000 at the 1st cycle at 4.0% drift. Significant strain gradients along the girder flange width were not observed up to the 0.75% drift cycle in the specimens.

When considering the West girder top flange, Specimens CR3 and CR4R showed relatively low strain gradients up to the 4.0% drift cycle as compared with the other three specimens. The strain gradients of the East girder bottom flange for Specimens CR3 and CR4R were either lower or comparable to the other three specimens. It is believed that the trend towards having lower strain gradients in Specimens CR3 and CR4R girder flange are primarily due to the column stiffening provided by those details. As shown in Figures 3.15 and 3.17, Specimen CR3 column was reinforced by including doubler plates and continuity plates, and Specimen CR4R column was reinforced by two doubler plates located 2 in. away from the column web. These results reaffirm that the half-thickness continuity plates and the offset doubler plate detail performed well as column stiffeners to mitigate local flange bending.

Specimens CR1, CR2, and CR5 on the other hand did not have continuity plates, which could explain the greater girder flange strain gradients in these specimens, both with the girder flange in tension and compression. This would lend some support to the use of continuity plates. However, there is no evidence that these high strain gradients were detrimental to the performance of the connection. For example, as indicated in Chapters 3 and 5, Specimen CR1 had low notch toughness [far less than the FEMA (2000a) requirements], yet the high strain gradient did not cause a brittle fracture. The strain gradient was worse in the West girder top flange of Specimen CR1 than in Specimen CR2, whereas Specimen CR1 did not require continuity plates and Specimen CR2 did, based upon the seismic girder demand. Therefore some of the variation in the

strain gradient among the different specimens may be somewhat random, based upon local residual stresses, etc.

6.6 Comparison of Results and Discussion of Continuity Plate and Doubler Plate Detailing

This section provides a summary comparison of the results between the six cruciform experiments conducted in this research. These specimens had a full range of column stiffening details and yet all performed comparably. Specimen CR1 had no stiffening at all. Specimen CR2 had no continuity plates [although they were required to satisfy seismic demand criteria as per AISC (1992)] and featured an innovative doubler plate detail, with a single-sided doubler plate in which a square cut (rather than beveled) doubler plate rested on the column fillets, slightly offset from the column web, and was fillet-welded to the column flanges. Specimen CR3 also featured this doubler plate detail, but had two doubler-plates as well as continuity plates, although these were only approximately half the thickness of the girder flange and were fillet-welded to the column flanges and the doubler plates. The recommended seismic design criteria from FEMA (2000a) require continuity plates having the full thickness of the girder flange in case of interior moment connections, and that are groove-welded connections to the column flanges. Specimen CR4R included the offset doubler plate detail. Specimen CR5 contained fillet-welded doubler plates, similar in detail to Specimen CR2 but with beveled sides, on both sides of the web. While it contained no continuity plates, continuity plates were required even as per non-seismic design criteria (AISC, 1993, 1999a).

Figure 5.1 compared the cycles at 4.0% interstory drift before achieving significant strength degradation for the six specimens. Specimens CR1, CR2, CR3, and CR4R were subjected to 14, 16, 14, and 12 cycles, respectively, before significant strength degradation occurred. Because of the small sample size, it cannot be determined that there is any significance to the variation in number of cycles in the range from 12 to 16 cycles, so it is assumed that these specimens performed approximately equally well.

The fact that Specimen CR2 and CR3 performed approximately equally well indicates that the continuity plates in specimen CR3 did not noticeably improve the performance relative to Specimen CR2. Consequently, the seismic criteria for continuity plates for the limit state of local flange bending (AISC, 1992, 1997) are somewhat conservative. As discussed further in Section 2.4 and Section 6.4, the girder flange demand typically used for assessment of seismic demand for local flange bending may be excessive. The fact that Specimen CR3 performed well also indicates that if continuity plates are used, it is not necessary to use full thickness continuity plates that are groove-welded to the column flanges. Also, the comparable performance of Specimen CR4R relative to Specimen CR3 shows that the box detail is equally effective as continuity plates in providing column flange bending resistance. These findings were also indicated by the pull-plate tests (Prochnow et al., 2000a), and it is now verified that cyclic loading does not affect these conclusions.

The fact that thinner continuity plates are recommended also means that smaller fillet welds are required to attach the continuity plates to the column, as compared to using thicker continuity plates. For example only 3/8 inch fillet welds were required for Specimen CR3. The smaller welds pose a much less significant risk of causing k-line cracking.

In fact, it is not clear if the continuity plates must be fully developed. The stretching of the continuity plate in the girder flange direction must remain compatible with the stretching of the column web, so even if there was yielding of the fillet welds, the displacement would be limited. Furthermore, only localized yielding was observed in the continuity plates only at their corners near k-area of the column. This is shown in Figures 6.127 to 6.138, which show the strains oriented along the length of the two continuity plates. The strain gage locations are shown in Figure 4.21, and in each plot the strains are shown across the width of the continuity plate at specific locations along the length of the continuity plate. The largest strains have peak magnitudes less than twice the magnitude of the yield strain. In addition, these peak strains are occurring only in the very late loading stages and are generally only near the column web in the lines of gages that are closest to the column flanges.

These specimens also featured a range of doubler plate details. Yet these variations had no significant impact on the performance of the connections in these tests. Therefore it cannot be concluded that any of these details are advantageous, and the most economical details should be recommended. This was also supported by the pull-plate tests.

Specimen CR5 was the most substantially underdesigned cruciform specimen with respect to local flange bending – the resistance-to-demand ratio was only 0.84 for non-seismic demand as per AISC (1993, 1999a), and it equaled 0.47 for seismic demand as per AISC (1992). Specimen CR5 completed the SAC loading history (SAC, 1997) with more than two cycles at 4.0% interstory drift; therefore it is possible that the non-seismic demand criteria are sufficient even for seismic loading., although there is insufficient evidence to support this conclusion.

Although the performance of Specimen CR5 was adequate, the number of cycles before significant strength degradation in this specimen was distinctly smaller than for the other specimens (except Specimen CR4). This could be an adverse effect of the small column or the lack of continuity plates. On the other hand, it cannot be concluded that this distinction is significant because it is not known how much variability is expected for low-cycle fatigue failures such as these. Furthermore, Specimen CR5 met the FEMA performance requirement of two cycles at 4% interstory drift, therefore this potential adverse effect may not be significant with respect to the ability to meet the minimum performance requirements.

Specimen CR5 was analogous to the pull-plate test 2-LFB in Prochnow et al. (2000a, 2000b) and Hajjar et al. (2002). These two different types of tests exhibited similar column flange displacement, and similarities in the strain distributions. These findings support the use of pull-plate tests to investigate local flange bending and other localized phenomena.

All specimens except Specimens CR4 and CR4R had inadequate panel zone strengths as per the current AISC panel zone provisions (1997), yet showed very good energy dissipation capacities. The weak panel zones and associated kinking of the column flange did nothing noticeable to harm the performance of the connection in these

tests. Also it is not clear whether these doubler plate welds need to develop the shear capacity of the doubler plates. There must be compatibility between the shear deformation of the doubler plate and the web of the column. Therefore, even if the doubler plate welds were to begin yielding in shear, their distortion would be limited.

With respect to the primary mode of failure, all specimens exhibited ductile response, failing by low-cycle fatigue (LCF) in the girder flanges, with the exception of Specimen CR4, which exhibited premature brittle fractures in the girder flange-to-column welds. As explained in detail in Appendix B, Specimen CR4 was unintentionally prepared with very low toughness weld metal, having an average of 2.0 ft lbs at 0°F and 2.3 ft lbs at 70°F. In contrast, the FEMA guidelines (FEMA, 2000a), require 20 ft lbs at 0°F and 40 ft lbs at 70°F. This was the only test that did not satisfy the connection prequalification requirement of completing two cycles at 4.0% interstory drift without significant strength degradation (FEMA, 2000a).

Specimen CR4R was essentially a replicate test except that the batch of weld metal used met the FEMA guidelines (FEMA, 2000e). In contrast to the performance of Specimen CR4, Specimen CR4R not only performed acceptably according to the FEMA requirements, it performed as well as any of the specimens. This result is an example of the importance of weld metal notch toughness in achieving good performance of groove-welded connections.

Specimens CR4 and CR4R both had the unique offset doubler detail given by Figure C-9.3 (c) in the 1997 AISC Seismic Provisions (AISC, 1997). This detail was intended to resist both panel zone shear and local flange bending, and these specimens would normally require continuity plates in addition to web doubler plates. The fact that this detail performed well in Specimen CR4R indicates that the detail itself was probably not a factor in the fracture that occurred in Specimen CR4.

Specimens CR4 and CR4R also had a relatively stiff panel zone, considering the two 3/4-in. thick doubler plates in addition to the column web. This was done to assure that the panel zone stiffness and strength would be adequate, because it was felt [based upon reports in the literature (Bertero et al., 1973)] that this detail may not be as effective as a doubler plate that was not offset from the column web. The test results do not

support this conclusion. Figures 6.139 and 6.140 show the shear strain at the center of both sides of the column web and on each doubler plate in Specimen CR4R at the peak of the first cycle at each interstory drift level (see Figures 4.14 and 4.15 for the rosette locations). The shear strain compatibility is excellent during the loading stages in which the connection response is approximately linear. This indicates that the column flange on the W14x176 was able to transfer the girder flange force uniformly to both the column web and the doubler plates, as also evidenced by the relatively uniform strains seen in the results for Specimen CR4R in the prior section. After significant yielding occurs during the 1.5% interstory drift cycles, the shear strains deviate on either side of the column web due to a variety of complex behavioral phenomena. However, the shear strains on the doubler plates remain bounded by the column web strains, and continue to increase well into the yielding region. Thus, the results show that the doubler plates were engaged and effective throughout the experiment. In addition, like the detail itself, the relatively high stiffness of the panel zone in these specimens was also not likely to have been a factor in the fracture of Specimen CR4.

Following the fracture in Specimen CR4, it was found that the previously tested Specimen CR1 also had relatively low notch toughness, an average of 2.7 ft lbs at 0°F and 19.3 ft lbs at 70°F. This is interesting because Specimen CR1 performed well, experiencing 14 cycles of 4.0% drift before significant strength degradation. Specimen CR1 had no column stiffening at all. Continuity plates would not be required, even for seismic design. However, doubler plates would be required since the capacity of the column web was approximately 20 to 25% less than the demand provided by the girder, depending on the design equations used.

If the difference in the column stiffening between Specimens CR1 and CR4 is not a factor in the fracture of Specimen CR4, then the better performance of Specimen CR1 shows that the marginal difference in notch toughness between this specimen and Specimen CR4 is sufficient to resist fracture. Thus these two experiments have potentially closely bounded the actual minimum notch toughness required for good groove weld performance. Also, the feasibility of using no column stiffening at all in appropriate circumstances has been tested under a likely worst-case susceptibility to

brittle fracture through Specimen CR1. Therefore, it is not necessarily true that continuity plates are necessary for good performance under all circumstances.

Table 6.1: Panel Zone Strengths and Post-Elastic Strength Increases Using AISC (1997) and Modified Fielding and Huang (1971) Equations

Test Specimen	Equation 2.1 R_v (kips)*	Equation 6.10 R_v (kips)	Equation 2.1 Post-Elastic (%)	Equation 6.10 Post-Elastic (%)
CR1	903 (945)	694 (725)	39.4 (39.4)	16.8 (16.8)
CR2	824 (890)	678 (732)	17.1 (17.1)	5.1 (5.1)
CR3	935 (1075)	790 (909)	11.9 (11.9)	3.2 (3.2)
CR4R	1163 (1322)	1000 (1136)	9.3 (9.3)	2.5 (2.5)
CR5	924 (1085)	798 (937)	8.0 (8.0)	1.8 (1.8)

* Numbers in parenthesis are calculated from coupon tensile test results.

Table 6.2: Connection Member Sizes and Joint Type for Tests Used to Evaluate Panel Zone Provisions

Test Designation	Column	Girder(s)	Joint Type
Fielding and Huang	W14x184	W24x160	Exterior
Krawinkler et al.: A-1	8 WF 24	10 B 15	Interior
Krawinkler et al.: A-2	8 WF 24	10 B 15	Interior
Krawinkler et al.: B-2	8 WF 67	14 B 22	Interior
Bertero et al.: A-3	8 WF 24	10 B 15	Interior
Bertero et al.: B-3	8 WF 67	12 WF 27	Interior
Bertero et al.: B-4	8 WF 67	10 WF 29	Interior
Becker: 1	W14x61	W14x61	Exterior
Becker: 2	W14x61	W14x61	Exterior
Popov et al.: 2	18" built-up	W18x40	Interior
Popov et al.: 3	19" built-up	18" built-up	Interior
Popov et al.: 4	19" built-up	18" built-up	Interior
Popov et al.: 6	19" built-up	18" built-up	Interior
Popov et al.: 7	W21x93	W18x71	Interior
Popov et al.: 8	W21x93	W18x71	Interior
Ghobarah et al.: CB-1	W14x43	W14x38	Exterior
Ghobarah et al.: CC-3	W12x87	W16x40	Exterior
Tsai et al.: TH2	W14x159	W21x83	Exterior
FEMA: EERC-PN1	W14x176	W30x99	Exterior
FEMA: EERC-PN2	W14x176	W30x99	Exterior
FEMA: EERC-PN3	W14x176	W30x99	Exterior
FEMA: EERC-AN1	W14x176	W30x99	Exterior
FEMA: USCD-1	W14x176	W30x99	Exterior
FEMA: USCD-2	W14x176	W30x99	Exterior
FEMA: USCD-3	W14x176	W30x99	Exterior
FEMA: UCB-PN1	W14x257	W36x150	Exterior
FEMA: UCB-RN2	W14x257	W36x150	Exterior
FEMA: UCB-RN3	W14x257	W36x150	Exterior

Table 6.2 (continued): Connection Member Sizes and Joint Type for Tests Used to Evaluate Panel Zone Provisions

Test Designation	Column	Girder(s)	Joint Type
FEMA: UCB-AN1	W14x257	W36x150	Exterior
FEMA: UTA-4	W14x257	W36x150	Exterior
Choi et al.: SP-9.1	W14x176	W30x99	Exterior
Choi et al.: SP-10.1	W14x257	W30x124	Exterior
Choi et al.: SP-10.2	W14x257	W30x124	Exterior
Lee et al.: SP-3.1	W14x120	W24x68	Exterior
Lee et al.: SP-3.2	W14x120	W24x68	Exterior
Lee et al.: SP-4.1	W14x145	W30x99	Exterior
Lee et al.: SP-4.2	W14x145	W30x99	Exterior
Lee et al.: SP-5.1	W14x176	W30x99	Exterior
Lee et al.: SP-7.2	W14x257	W36x150	Exterior
Ricles et al.: LU-T1	W14x311	W36x150	Exterior
Ricles et al.: LU-T2	W14x311	W36x150	Exterior
Ricles et al.: LU-T4	W14x311	W36x150	Exterior
Ricles et al.: LU-C1	W14x398	W36x150	Interior
Ricles et al.: LU-C2	W14x398	W36x150	Interior
U. of Minnesota: CR1	W14x283	W24x94	Interior
U. of Minnesota: CR2	W14x193	W24x94	Interior
U. of Minnesota: CR3	W14x176	W24x94	Interior
U. of Minnesota: CR4R	W14x176	W24x94	Interior
U. of Minnesota: CR5	W14x145	W24x94	Interior

Table 6.3: Parameters for Tests Used to Evaluate Panel Zone Provisions

Test Designation	$F_{y,web}$ (ksi)	t_p (in)	t_{cf} (in)	b_{cf} (in)	d_g (in)	d_c (in)	Axial (Y/N)
Fielding and Huang	31.4	0.84	1.378	15.66	24.72	15.38	Y
Krawinkler et al.: A-1	41.0	0.245	0.398	5.82	10.0	7.93	Y
Krawinkler et al.: A-2	41.0	0.245	0.398	5.82	10.0	7.93	Y
Krawinkler et al.: B-2	47.0	0.575	0.933	8.29	13.72	9.0	Y
Bertero et al.: A-3	44.7	0.495	0.398	5.82	10.0	7.93	Y
Bertero et al.: B-3	47.0	0.575	0.933	8.29	11.96	9.0	Y
Bertero et al.: B-4	47.0	0.575	0.933	8.29	10.22	9.0	Y
Becker: 1	40.6	0.875	0.645	9.995	13.89	13.89	N
Becker: 2	40.6	0.375	0.645	9.995	13.89	13.89	N
Popov et al.: 2	49.0	0.5625	0.625	8.25	17.9	18.0	Y
Popov et al.: 3	49.0	1.0625	1.25	8.5	18.75	19.125	Y
Popov et al.: 4	49.0	1.0625	1.25	8.5	18.75	19.125	Y
Popov et al.: 6	49.0	0.6875	1.25	8.5	18.75	19.125	Y
Popov et al.: 7	60.0	0.955	0.93	8.42	18.47	21.62	Y
Popov et al.: 8	60.0	0.955	0.93	8.42	18.47	21.62	Y
Ghobarah et al.: CB-1	52.2	0.305	0.53	7.995	14.1	13.66	Y
Ghobarah et al.: CC-3	47.3	0.515	0.81	12.125	16.01	12.53	Y
Tsai et al.: TH2	56.6	0.745	1.19	15.565	21.43	14.98	N
FEMA: EERC-PN1	49.5	0.83	1.31	15.65	29.65	15.22	N
FEMA: EERC-PN2	53.5	0.83	1.31	15.65	29.65	15.22	N
FEMA: EERC-PN3	56.0	0.83	1.31	15.65	29.65	15.22	N
FEMA: EERC-AN1	56.0	0.83	1.31	15.65	31.275	15.22	N
FEMA: USCD-1	51.2	0.83	1.31	15.65	29.65	15.22	N
FEMA: USCD-2	51.2	0.83	1.31	15.65	29.65	15.22	N
FEMA: USCD-3	51.2	0.83	1.31	15.65	29.65	15.22	N
FEMA: UCB-PN1	53.5	1.175	1.89	15.995	35.85	16.38	N
FEMA: UCB-RN2	53.5	1.175	1.89	15.995	45.6	16.38	N

Table 6.3 (continued): Parameters for Tests Used to Evaluate Panel Zone Provisions

Test Designation	F_{yc} (ksi)	t_p (in)	t_{cf} (in)	b_{cf} (in)	d_g (in)	d_c (in)	Axial (Y/N)
FEMA: UCB-RN3	53.5	1.175	1.89	15.995	35.85	16.38	N
FEMA: UCB-AN1	50.0	1.175	1.89	15.995	44.85	16.38	N
FEMA: UTA-4	53.5	1.175	1.89	15.995	37.85	16.38	N
Choi et al.: SP-9.1	57.0	0.83	1.31	15.65	29.65	15.22	N
Choi et al.: SP-10.1	59.0	1.175	1.89	15.995	30.17	16.38	N
Choi et al.: SP-10.2	59.0	1.675	1.89	15.995	30.17	16.38	N
Lee et al.: SP-3.1	49.8	0.59	0.94	14.67	23.73	14.48	N
Lee et al.: SP-3.2	49.8	0.59	0.94	14.67	23.73	14.48	N
Lee et al.: SP-4.1	48.3	0.68	1.09	15.5	29.65	14.78	N
Lee et al.: SP-4.2	48.3	0.68	1.09	15.5	29.65	14.78	N
Lee et al.: SP-5.1	51.3	0.83	1.31	15.65	29.65	15.22	N
Lee et al.: SP-7.2	44.2	1.175	1.89	15.995	35.85	16.38	N
Ricles et al.: LU-T1	49.2	1.41	2.26	16.23	35.85	17.12	N
Ricles et al.: LU-T2	49.2	1.41	2.26	16.23	35.85	17.12	N
Ricles et al.: LU-T4	49.2	1.41	2.26	16.23	35.85	17.12	N
Ricles et al.: LU-C1	54.0	3.27	2.845	16.59	35.85	18.29	N
Ricles et al.: LU-C2	54.0	3.27	2.845	16.59	35.85	18.29	N
U. of Minnesota: CR1	52.3	1.29	2.07	16.11	24.31	16.74	N
U. of Minnesota: CR2	54	1.515	1.44	15.71	24.31	15.48	N
U. of Minnesota: CR3	57.5	1.83	1.31	15.65	24.31	15.22	N
U. of Minnesota: CR4R	56.8	2.33	1.31	15.65	24.31	15.22	N
U. of Minnesota: CR5	58.7	1.93	1.09	15.5	24.31	14.78	N

Table 6.4: Panel Zone Strength Test-to-Predicted Ratios

Test Designation	V_{pz}/R_v (Eqn. 2.1)	V_{pz}/R_v (Eqn. 6.10)	Post-Elastic (Eqn. 2.1)	Post-Elastic (Eqn. 6.10)
Fielding and Huang	0.781	1.011	0.279	0.078
Krawinkler et al.: A-1	0.996	1.208	0.142	0.028
Krawinkler et al.: A-2	0.904	1.095	0.142	0.028
Krawinkler et al.: B-2	0.946	1.220	0.305	0.104
Bertero et al.: A-3	0.913	1.051	0.070	0.014
Bertero et al.: B-3	1.020	1.322	0.350	0.136
Bertero et al.: B-4	1.091	1.413	0.409	0.187
Becker: 1	0.645	0.743	0.074	0.017
Becker: 2	0.740	0.911	0.172	0.040
Popov et al.: 2	1.090	1.241	0.053	0.009
Popov et al.: 3	0.929	1.082	0.105	0.035
Popov et al.: 4	0.923	1.075	0.105	0.035
Popov et al.: 6	1.106	1.330	0.162	0.054
Popov et al.: 7	0.708	0.805	0.057	0.014
Popov et al.: 8	0.713	0.811	0.057	0.014
Ghobarah et al.: CB-1	1.062	1.264	0.115	0.022
Ghobarah et al.: CC-3	1.142	1.450	0.231	0.058
Tsai et al.: TH2	0.835	1.080	0.276	0.077
FEMA: EERC-PN1	0.803	1.016	0.215	0.048
FEMA: EERC-PN2	0.790	1.000	0.215	0.048
FEMA: EERC-PN3	0.740	0.936	0.215	0.048
FEMA: EERC-AN1	0.715	0.901	0.204	0.043
FEMA: USCD-1	0.776	0.982	0.215	0.043
FEMA: USCD-2	0.826	1.045	0.215	0.043
FEMA: USCD-3	0.809	1.024	0.215	0.043
FEMA: UCB-PN1	0.789	1.008	0.248	0.065
FEMA: UCB-RN2	0.783	0.981	0.195	0.040

Table 6.4 (continued): Panel Zone Strength Test-to-Predicted Ratios

Test Designation	V_{pz}/R_v (Eqn. 2.1)	V_{pz}/R_v (Eqn. 6.10)	Post-Elastic (Eqn. 2.1)	Post-Elastic (Eqn. 6.10)
FEMA: UCB-RN3	0.789	1.008	0.248	0.065
FEMA: UCB-AN1	0.832	1.044	0.199	0.042
FEMA: UTA-4	0.781	0.994	0.235	0.059
Choi et al.: SP-9.1	0.844	1.069	0.215	0.048
Choi et al.: SP-10.1	0.748	0.967	0.295	0.092
Choi et al.: SP-10.2	0.688	0.851	0.207	0.065
Lee et al.: SP-3.1	1.068	1.338	0.192	0.038
Lee et al.: SP-3.2	1.090	1.365	0.192	0.038
Lee et al.: SP-4.1	1.017	1.272	0.185	0.034
Lee et al.: SP-4.2	0.986	1.234	0.185	0.034
Lee et al.: SP-5.1	0.910	1.152	0.215	0.048
Lee et al.: SP-7.2	0.921	1.178	0.248	0.065
Ricles et al.: LU-T1	0.807	1.040	0.287	0.091
Ricles et al.: LU-T2	0.798	1.028	0.287	0.091
Ricles et al.: LU-T4	0.851	1.096	0.287	0.091
Ricles et al.: LU-C1	0.729	0.879	0.188	0.075
Ricles et al.: LU-C2	0.783	0.944	0.188	0.075
U. of Minnesota: CR1	0.752	0.981	0.394	0.168
U. of Minnesota: CR2	0.787	0.956	0.171	0.051
U. of Minnesota: CR3	0.711	0.840	0.119	0.032
U. of Minnesota: CR4R	0.697	0.812	0.093	0.025
U. of Minnesota: CR5	0.764	0.885	0.080	0.018
Mean	**0.856**	**1.060**		
Standard Deviation	**0.132**	**0.170**		

Table 6.5: Girder-Column Combinations for Panel Zone Thickness Calculations

Identification	Interior/Exterior	Column	Girder(s)
CR1	Interior	W14x283	W24x94
CR2	Interior	W14x193	W24x94
CR3, CR4R	Interior	W14x176	W24x94
CR5	Interior	W14x145	W24x94
SAC-1	Exterior	W14x120	W24x68
SAC-2	Exterior	W14x176	W30x99
SAC-3	Exterior	W14x257	W36x150
I-1	Interior	W14x257	W24x76
I-2	Interior	W14x176	W24x76
I-3	Interior	W14x311	W27x94
I-4	Interior	W14x211	W27x94
I-5	Interior	W14x342	W30x108
I-6	Interior	W14x257	W30x108
I-7	Interior	W14x398	W33x130
I-8	Interior	W14x311	W33x130
I-9	Interior	W14x426	W36x150
I-10	Interior	W14x370	W36x150
E-1	Exterior	W14x159	W24x76
E-2	Exterior	W14x109	W24x76
E-3	Exterior	W14x176	W27x94
E-4	Exterior	W14x120	W27x94
E-5	Exterior	W14x211	W30x108
E-6	Exterior	W14x132	W30x108
E-7	Exterior	W14x233	W33x130
E-8	Exterior	W14x159	W33x130
E-9	Exterior	W14x257	W36x150
E-10	Exterior	W14x193	W36x150

Table 6.6: Required Panel Zone Thicknesses

Identification	Required Panel Zone Thickness, t_p (in.)			
	Equation 6.10	AISC (1997)	SAC (Eqn. 2.7)	AISC (1992)
CR1	2.11	1.63	1.80	1.42
CR2	2.45	2.05	1.94	1.82
CR3, CR4R	2.51	2.13	1.98	1.90
CR5	2.61	2.27	2.04	2.03
SAC-1	0.92	0.75	0.71	0.66
SAC-2	1.17	0.93	0.90	0.81
SAC-3	1.56	1.21	1.23	1.05
I-1	1.76	1.33	1.47	1.14
I-2	2.02	1.68	1.59	1.48
I-3	2.01	1.51	1.69	1.29
I-4	2.36	1.96	1.84	1.72
I-5	2.17	1.63	1.79	1.39
I-6	2.46	2.01	1.92	1.75
I-7	2.45	1.84	2.06	1.57
I-8	2.78	2.24	2.20	1.95
I-9	2.73	2.08	2.26	1.78
I-10	2.94	2.34	2.36	2.03
E-1	1.01	0.78	0.81	0.68
E-2	1.09	0.92	0.84	0.81
E-3	1.21	0.96	0.95	0.83
E-4	1.30	1.11	1.00	0.98
E-5	1.28	0.98	1.00	0.85
E-6	1.42	1.21	1.07	1.07
E-7	1.49	1.17	1.17	1.01
E-8	1.65	1.40	1.26	1.23
E-9	1.64	1.29	1.29	1.12
E-10	1.78	1.49	1.37	1.31

Table 6.7: Comparison of Panel Zone Thicknesses

	Panel Zone Thickness, t_p (in.)				
	CR1	**CR2**	**CR3**	**CR4R**	**CR5**
Used for Experimental Study	1.29	1.515	1.83	2.33	1.93
Re-designed Using Equation 6.10	2.11	2.45	2.51	2.51	2.61

Table 6.8: Scale Factor, α, for Panel Zone Capacity Corresponding to Test Results

	Specimens				
	CR1	**CR2**	**CR3**	**CR4R**	**CR5**
Predicted Panel Zone Capacity at $4\gamma_y$ = Panel Zone Demand (kips)	1073	1074	1074	1074	1075
Target Panel Zone Capacity at $4\gamma_y$ Based on Experiments (kips)	711	700	764	922	829
Scale Factor, α	0.663	0.652	0.711	0.858	0.771

Table 6.9: Column Bending Stresses and Corresponding Strains in the Region 6 to 12 in. Below the Girder Flange

	Specimens		
	CR1	**CR2**	**CR5**
Range of Stress (ksi)	22 - 24	30 - 32	45 - 49
Range of Strain ($\mu\varepsilon$)	750 - 820	1020 - 1120	1550 - 1700

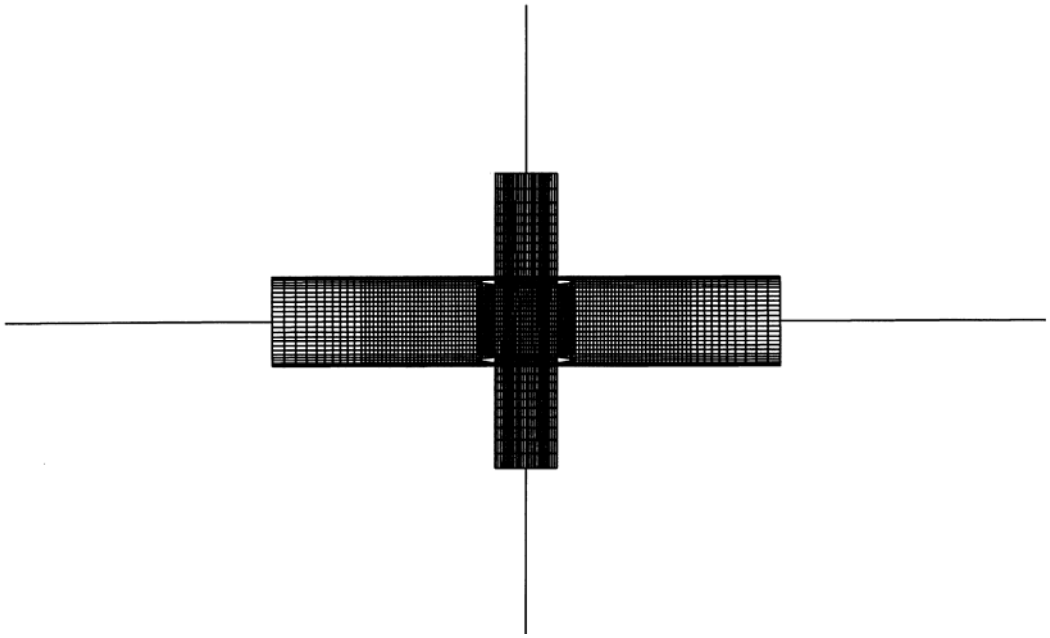


Figure 6.1: Typical Cruciform Specimen Finite Element Model [after (Ye et al., 2000)]

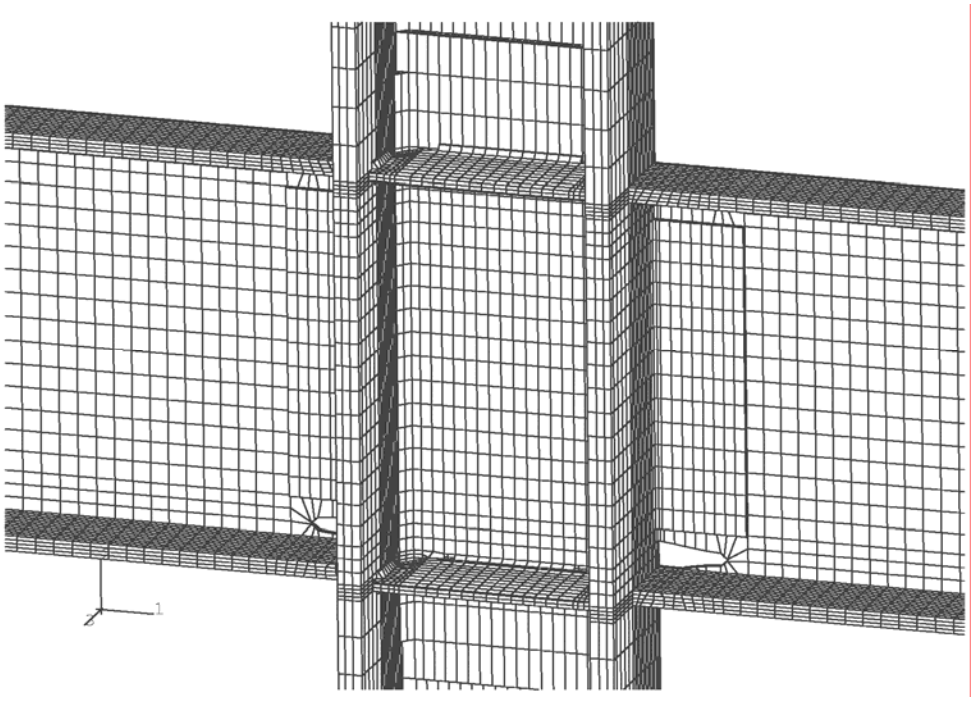


Figure 6.2: Typical Cruciform Connection Region Modeling [after (Ye et al., 2000)]

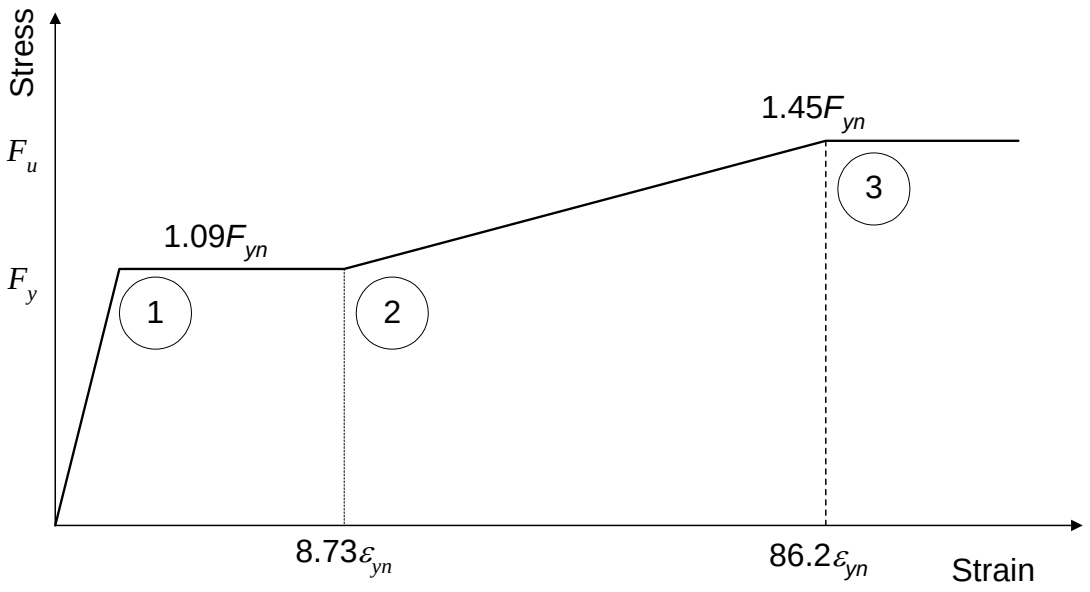


Figure 6.3: Stress-Strain Curve for A992 Steel [after (Ye et al., 2000)]

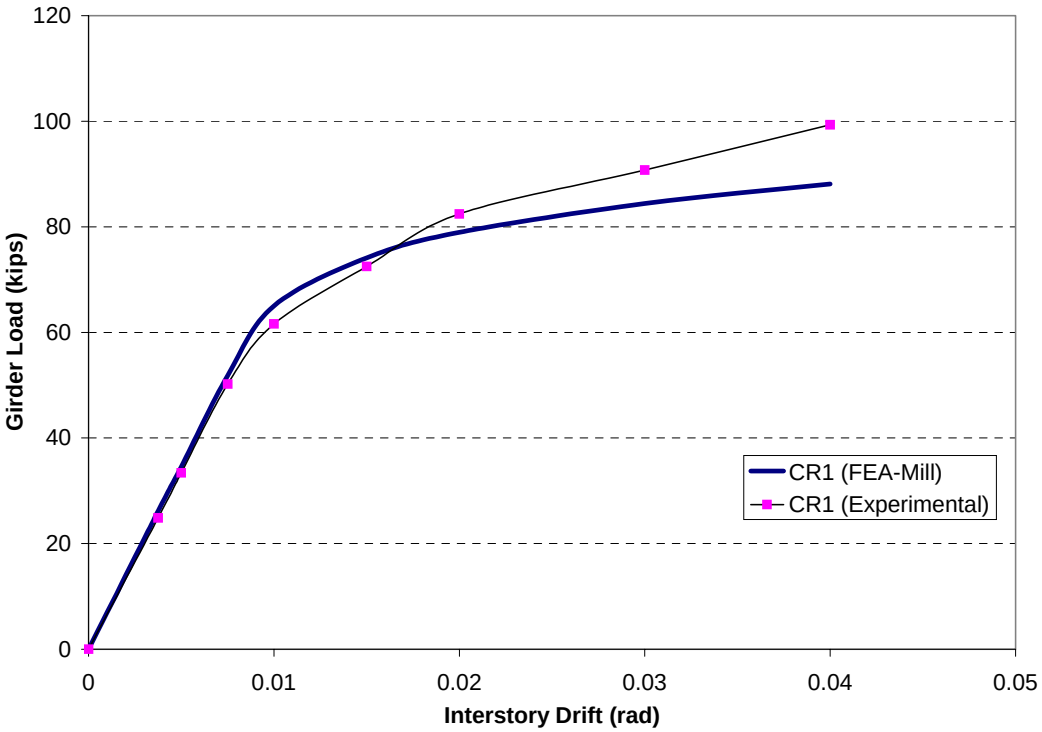


Figure 6.4: Comparison of Experimental and FEA Load vs. Drift, Specimen CR1

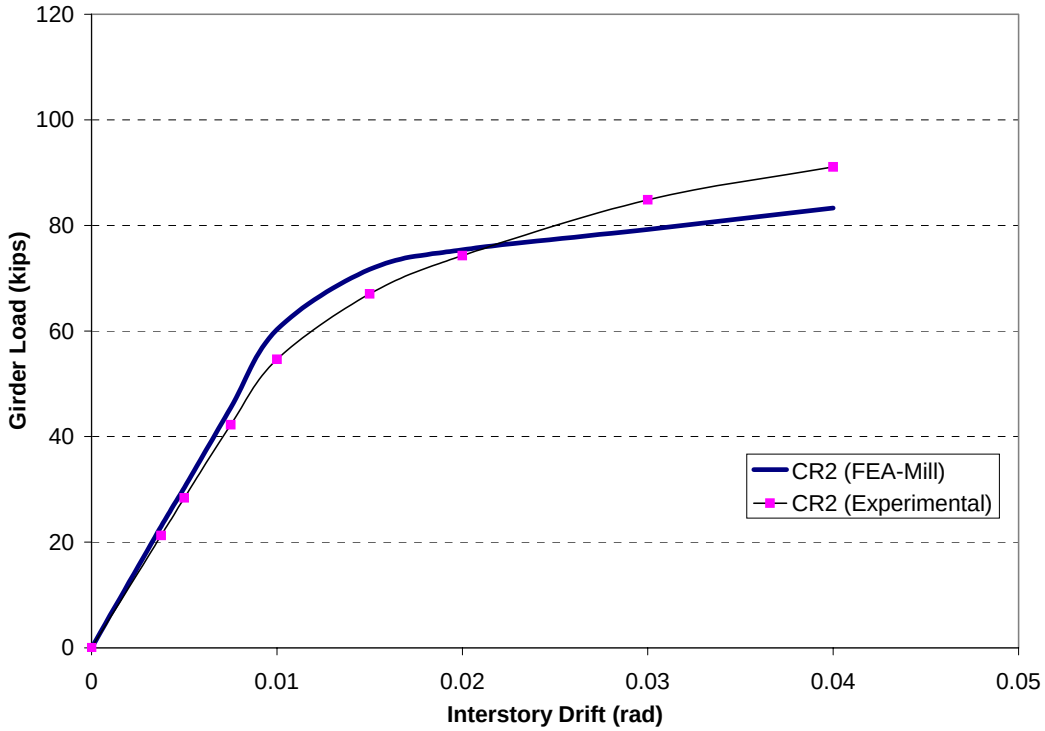


Figure 6.5: Comparison of Experimental and FEA Load vs. Drift, Specimen CR2

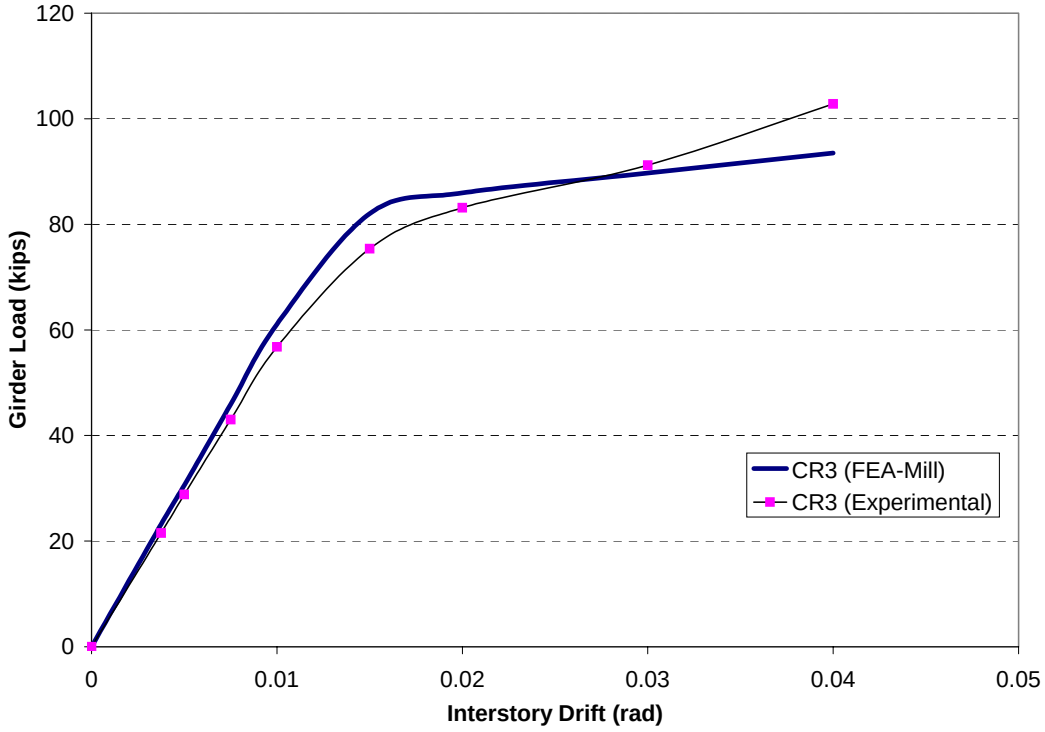


Figure 6.6: Comparison of Experimental and FEA Load vs. Drift, Specimen CR3

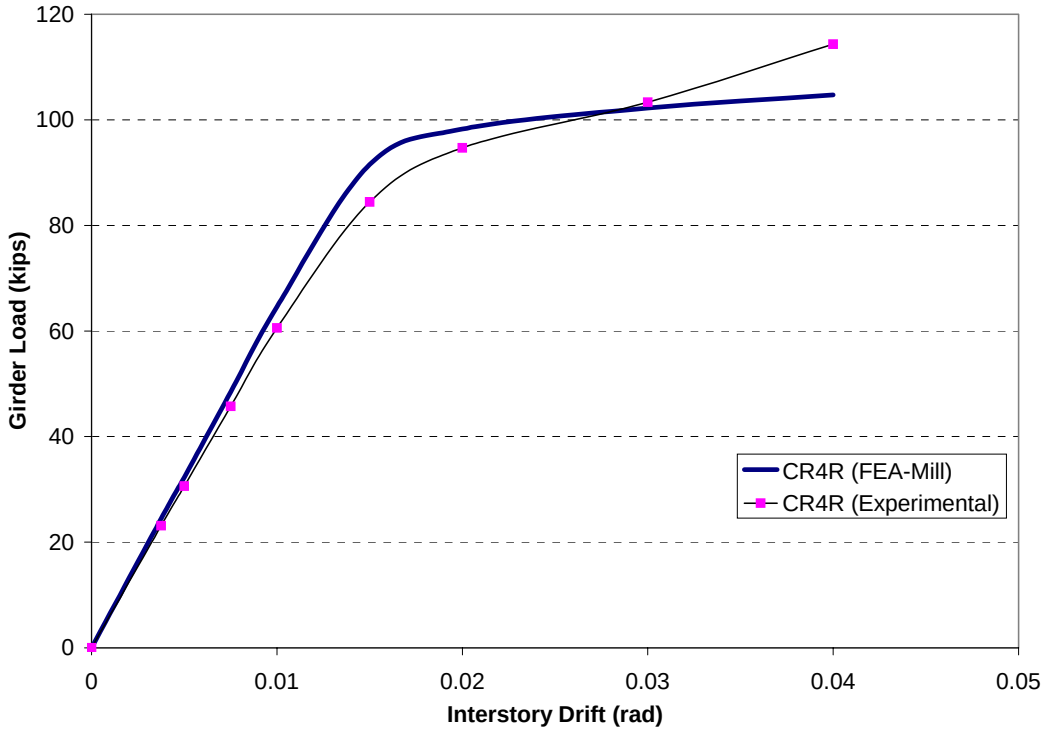


Figure 6.7: Comparison of Experimental and FEA Load vs. Drift, Specimen CR4R

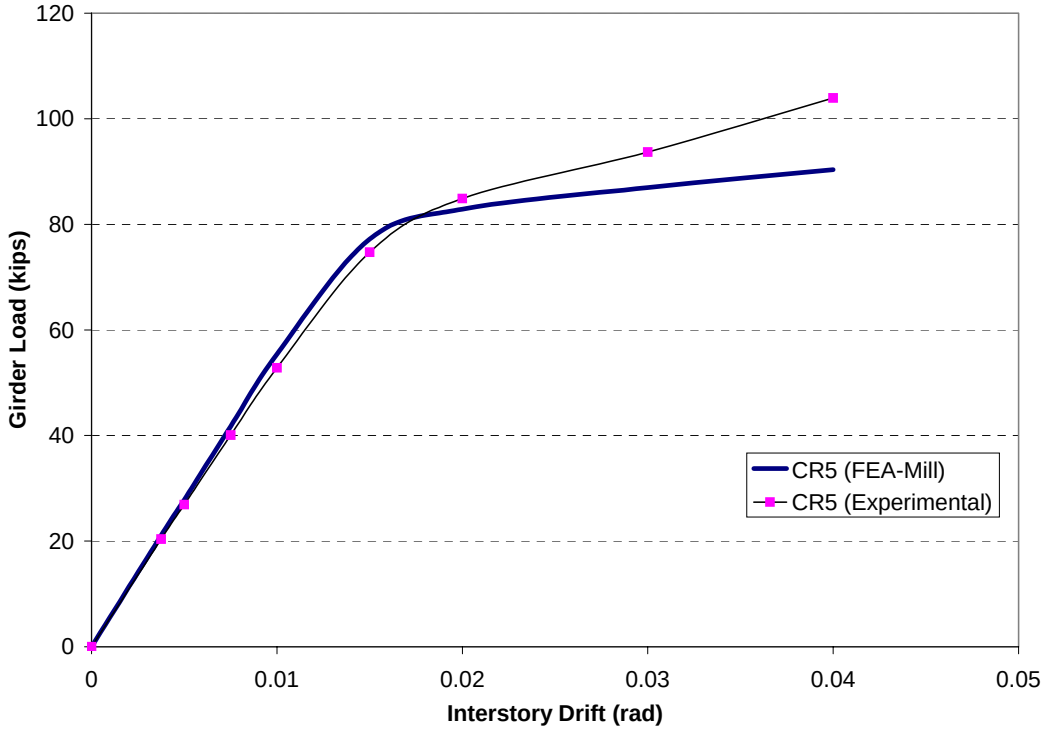


Figure 6.8: Comparison of Experimental and FEA Load vs. Drift, Specimen CR5

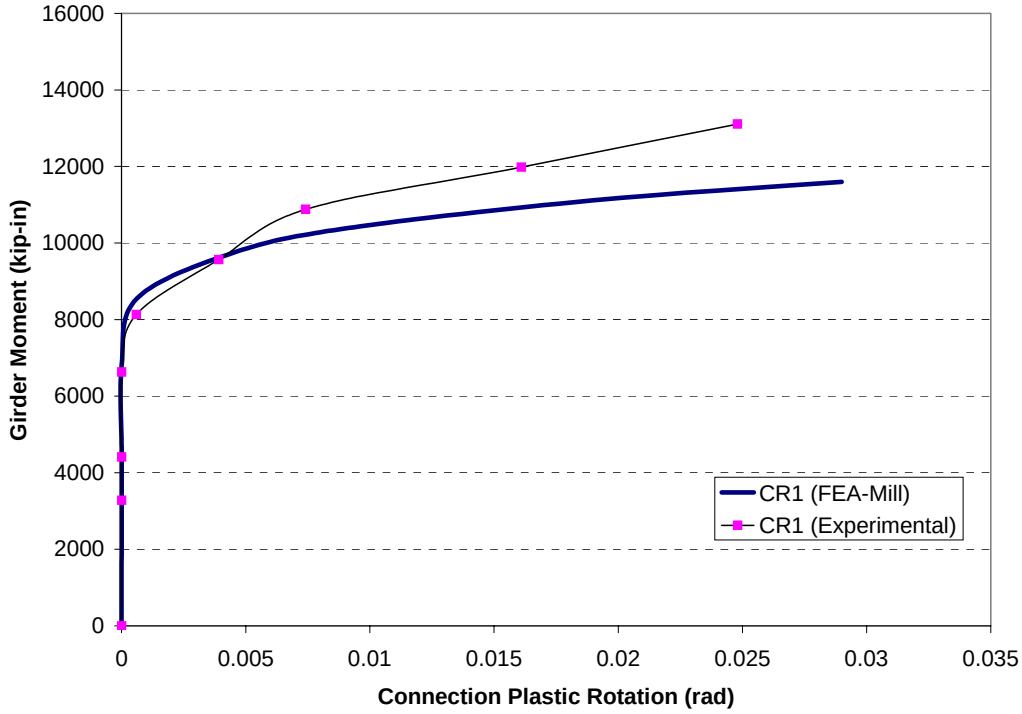


Figure 6.9: Comparison of Experimental and FEA Connection Plastic Rotation, Specimen CR1

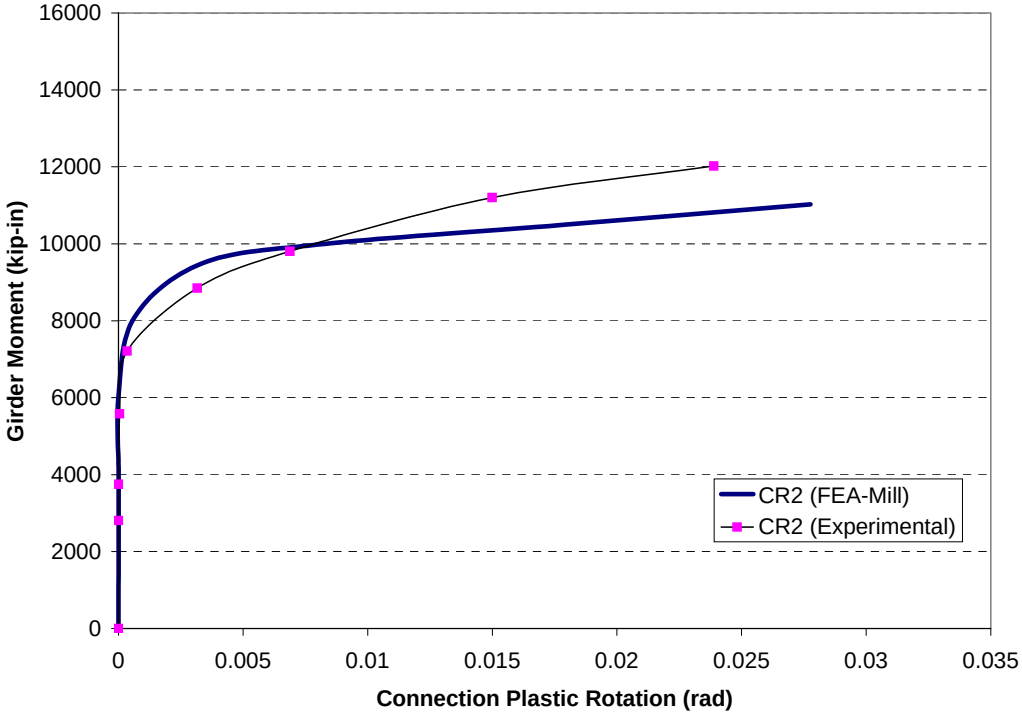


Figure 6.10: Comparison of Experimental and FEA Connection Plastic Rotation, Specimen CR2

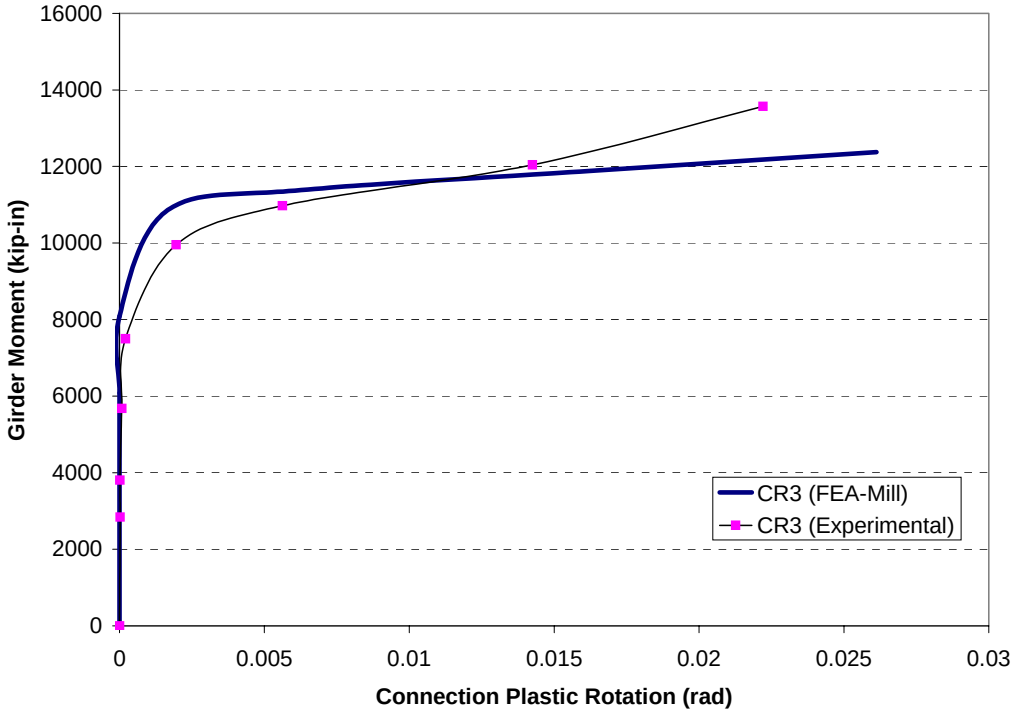


Figure 6.11: Comparison of Experimental and FEA Connection Plastic Rotation, Specimen CR3

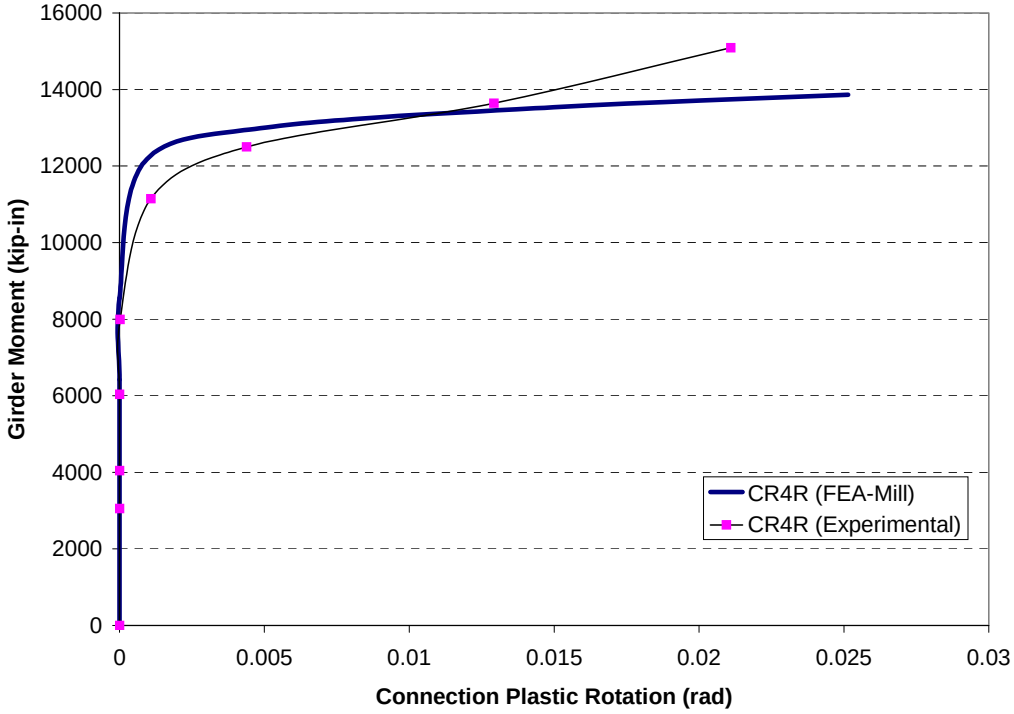


Figure 6.12: Comparison of Experimental and FEA Connection Plastic Rotation, Specimen CR4R

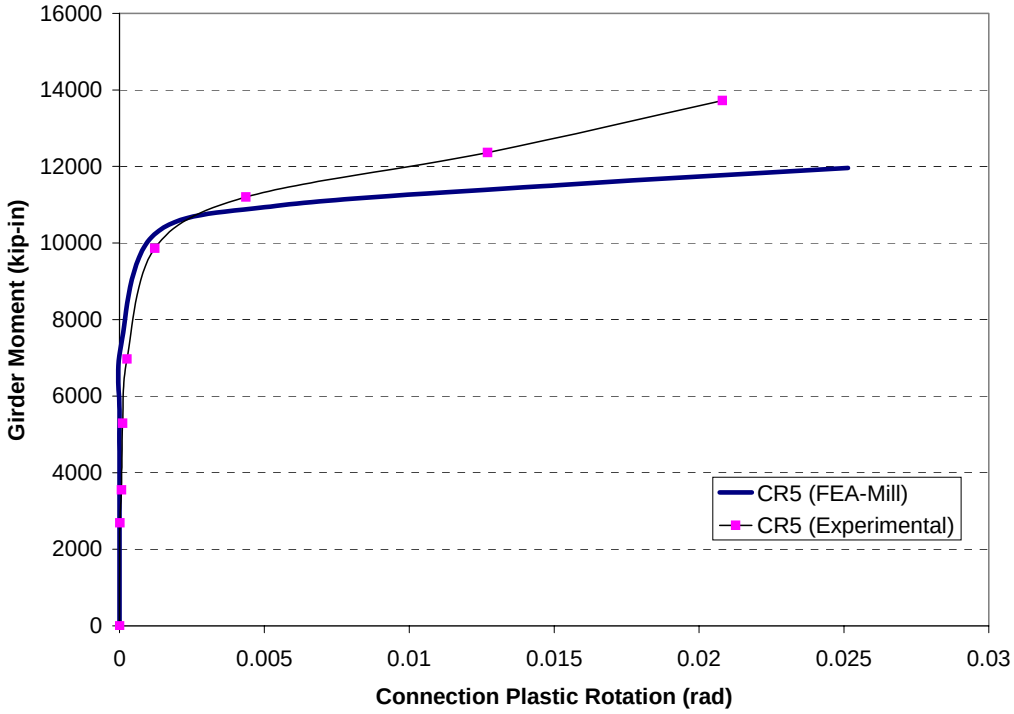


Figure 6.13: Comparison of Experimental and FEA Connection Plastic Rotation, Specimen CR5

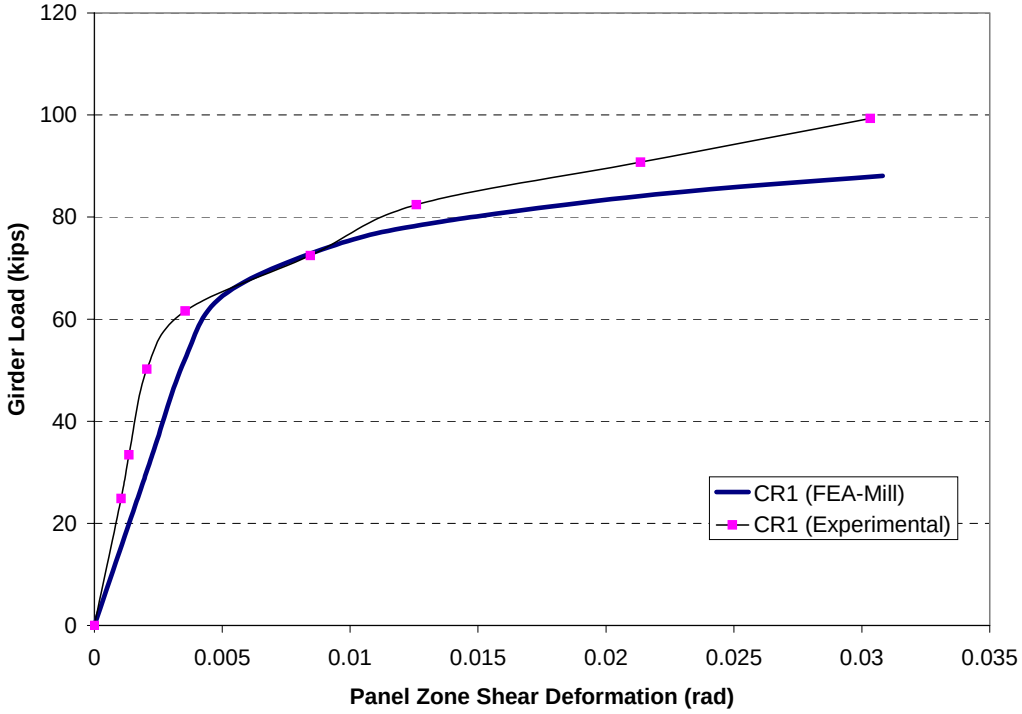


Figure 6.14: Comparison of Experimental and FEA Panel Zone Deformation, Specimen CR1

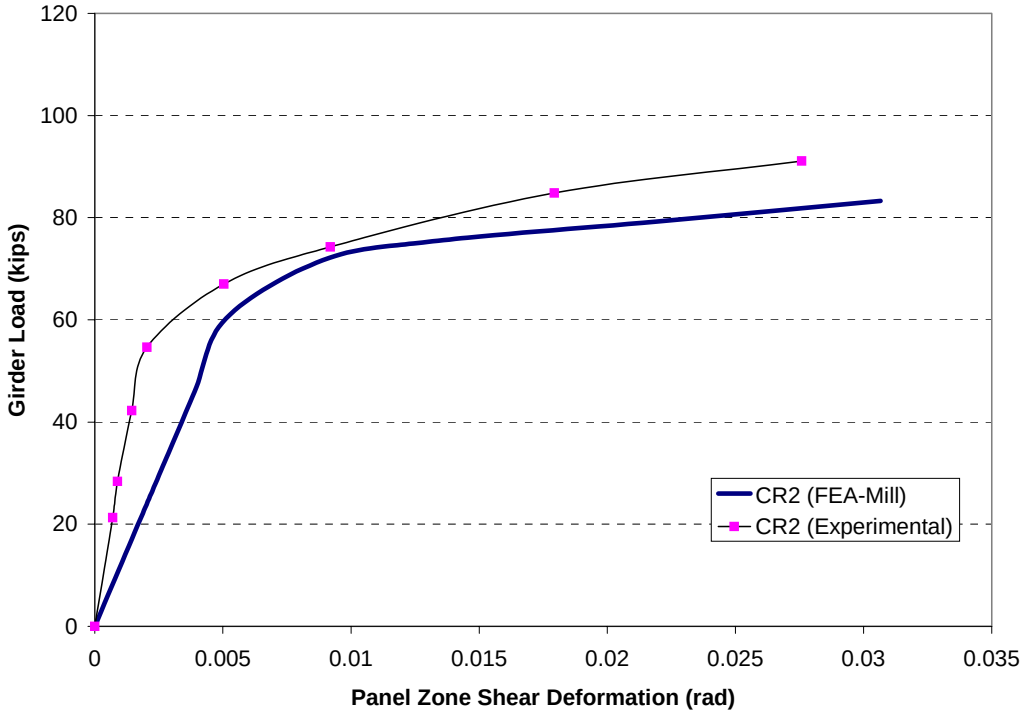


Figure 6.15: Comparison of Experimental and FEA Panel Zone Deformation, Specimen CR2

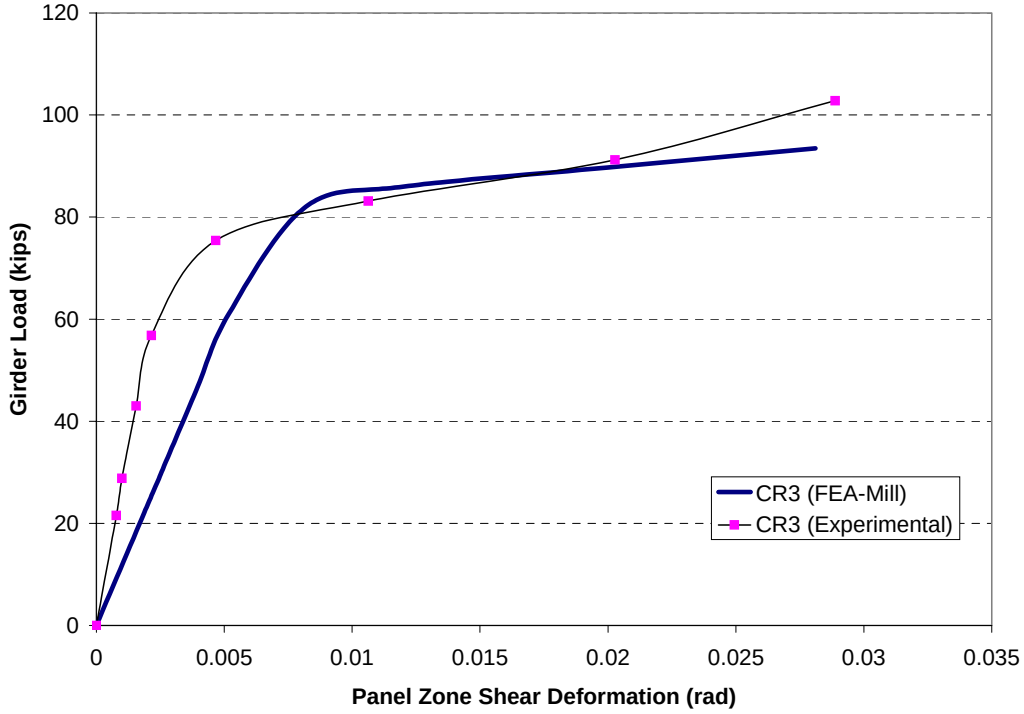


Figure 6.16: Comparison of Experimental and FEA Panel Zone Deformation, Specimen CR3

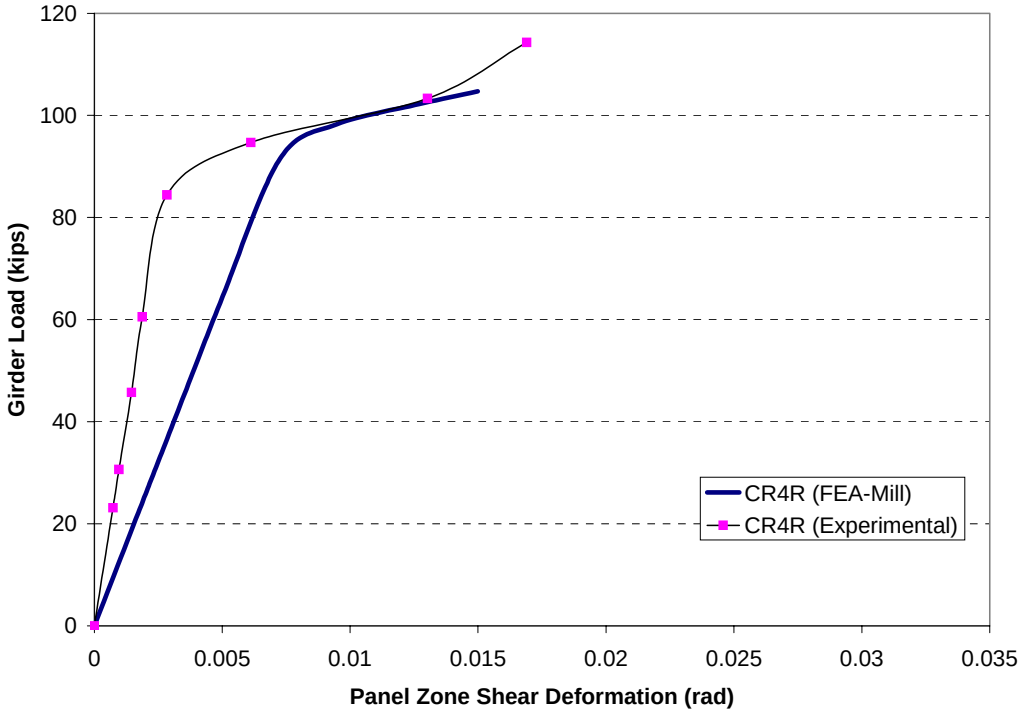


Figure 6.17: Comparison of Experimental and FEA Panel Zone Deformation, Specimen CR4R

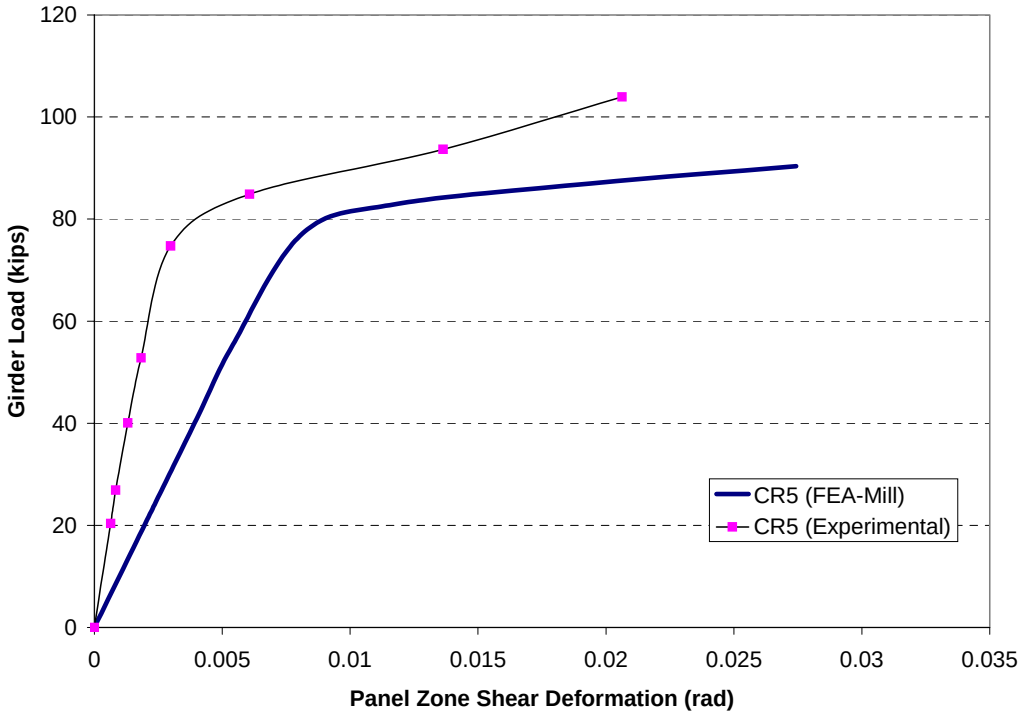


Figure 6.18: Comparison of Experimental and FEA Panel Zone Deformation, Specimen CR5

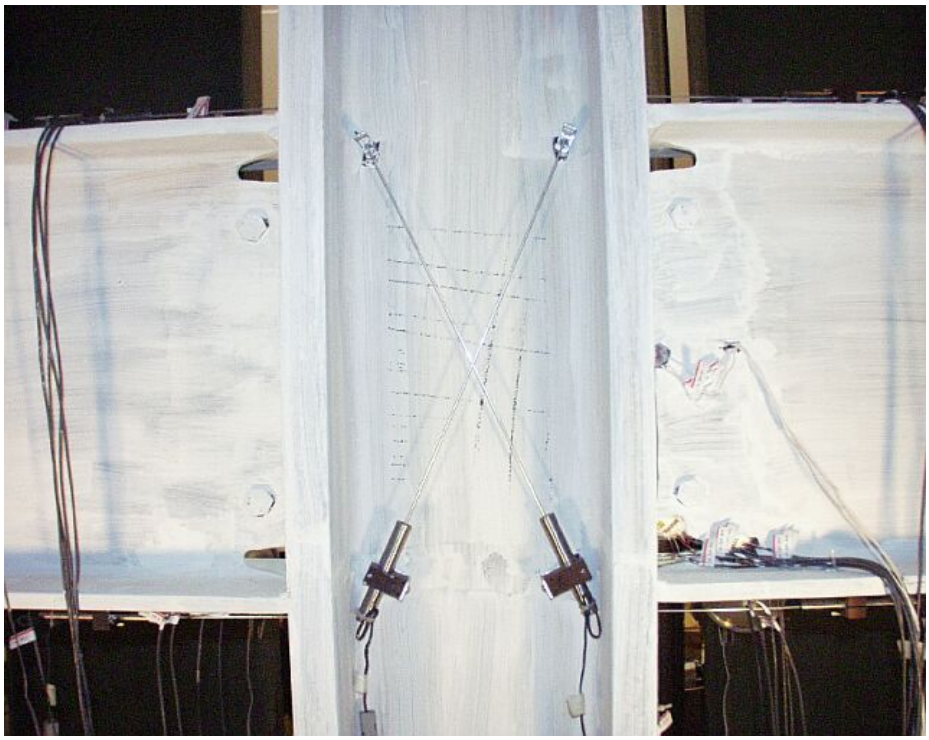


Figure 6.19: Specimen CR1 Panel Zone (1.0% Drift)



Figure 6.20: Specimen CR1 Panel Zone (1.5% Drift)

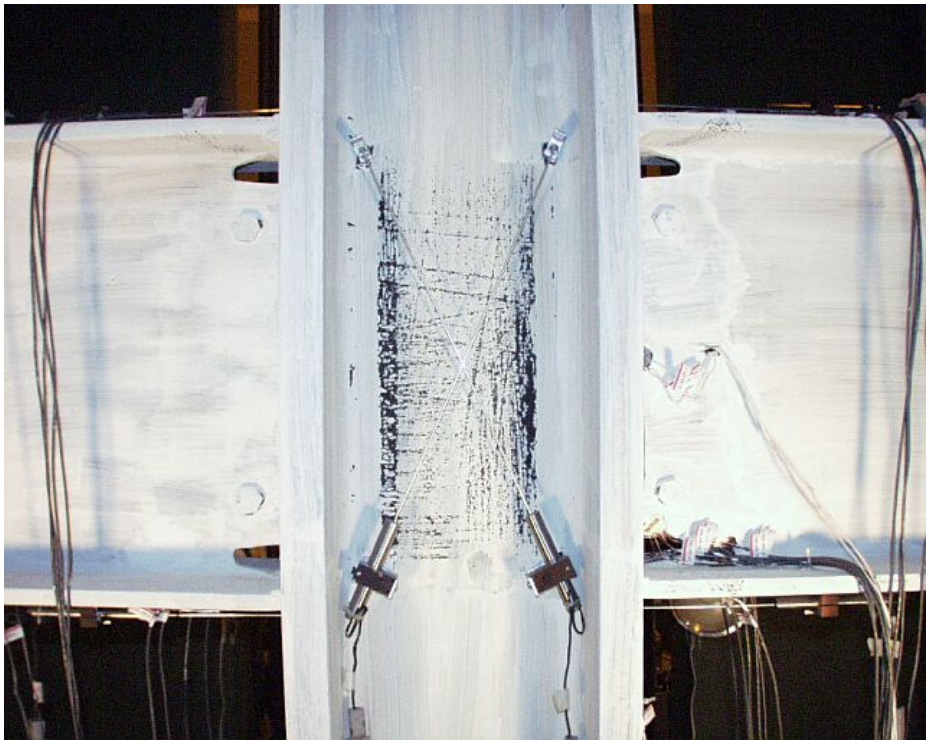


Figure 6.21: Specimen CR1 Panel Zone (2.0% Drift)

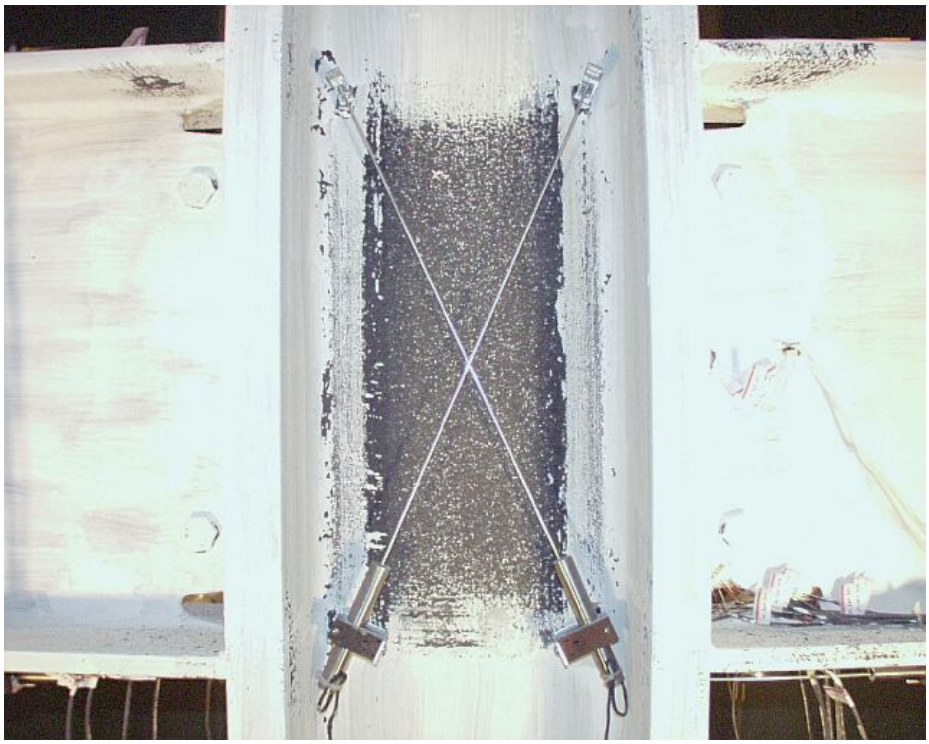


Figure 6.22: Specimen CR1 Panel Zone (3.0% Drift)

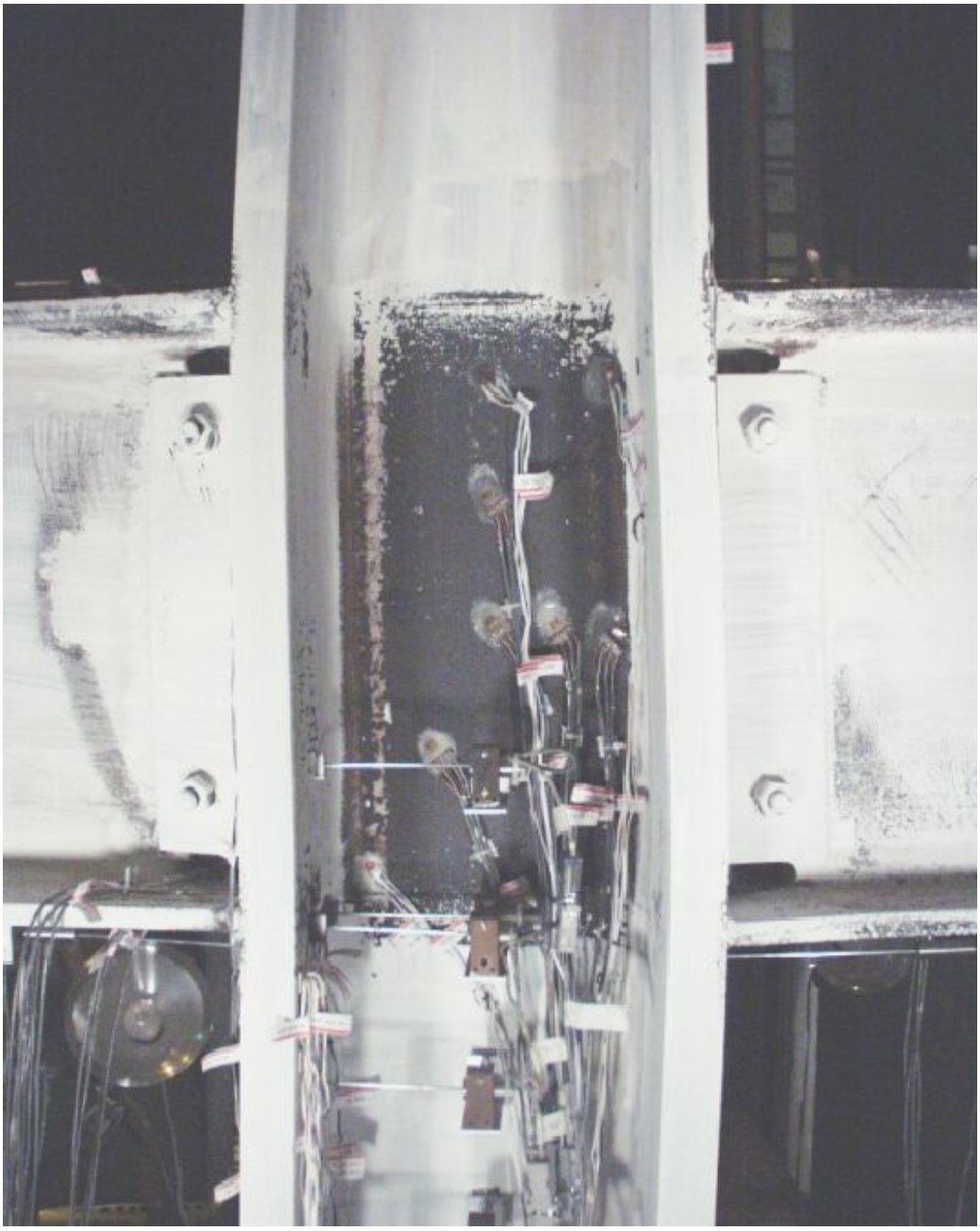


Figure 6.23: Specimen CR1 Panel Zone (Following Test)

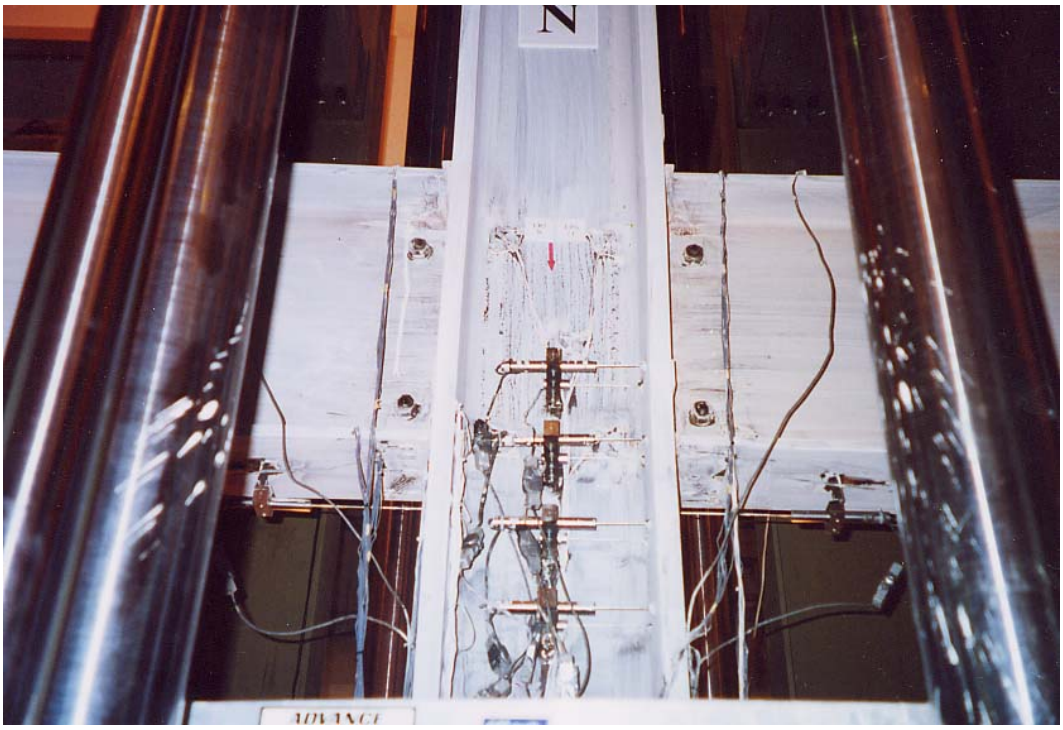


Figure 6.24: Specimen CR2 Panel Zone (1.5% Drift)

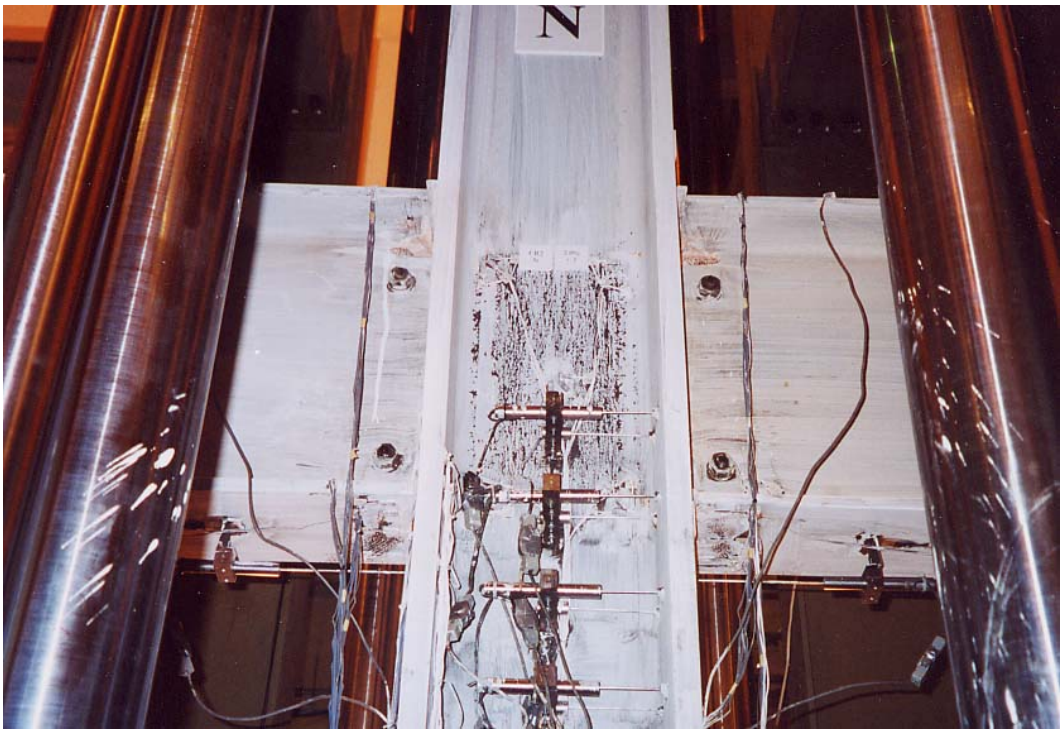


Figure 6.25: Specimen CR2 Panel Zone (2.0% Drift)

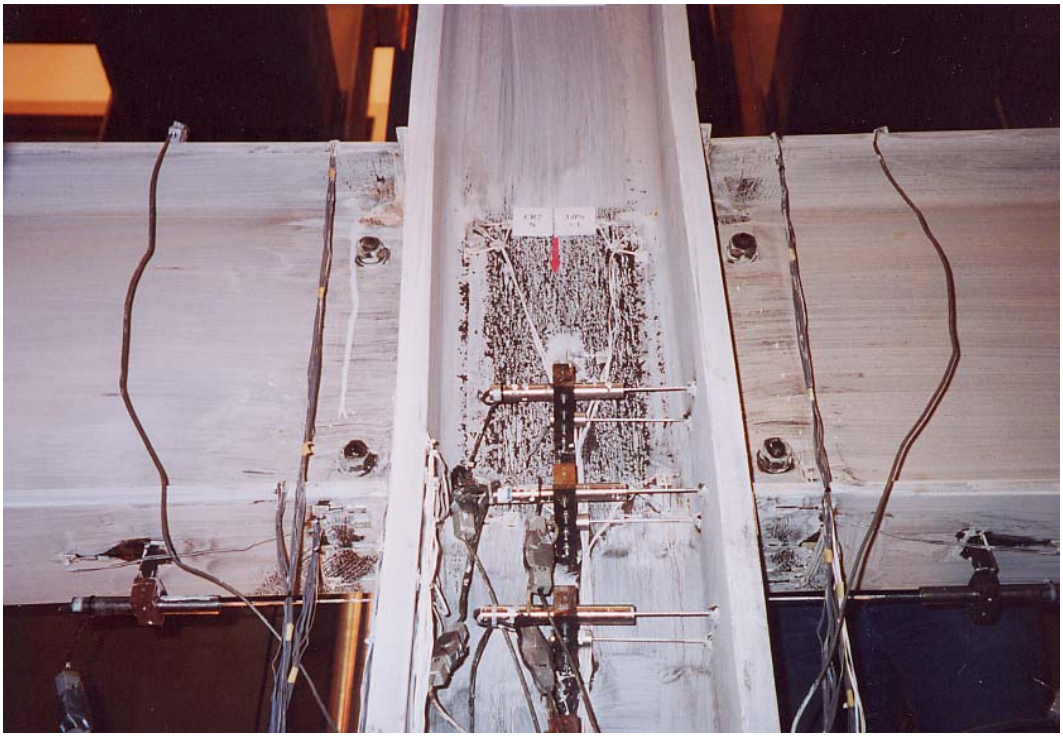


Figure 6.26: Specimen CR2 Panel Zone (3.0% Drift)

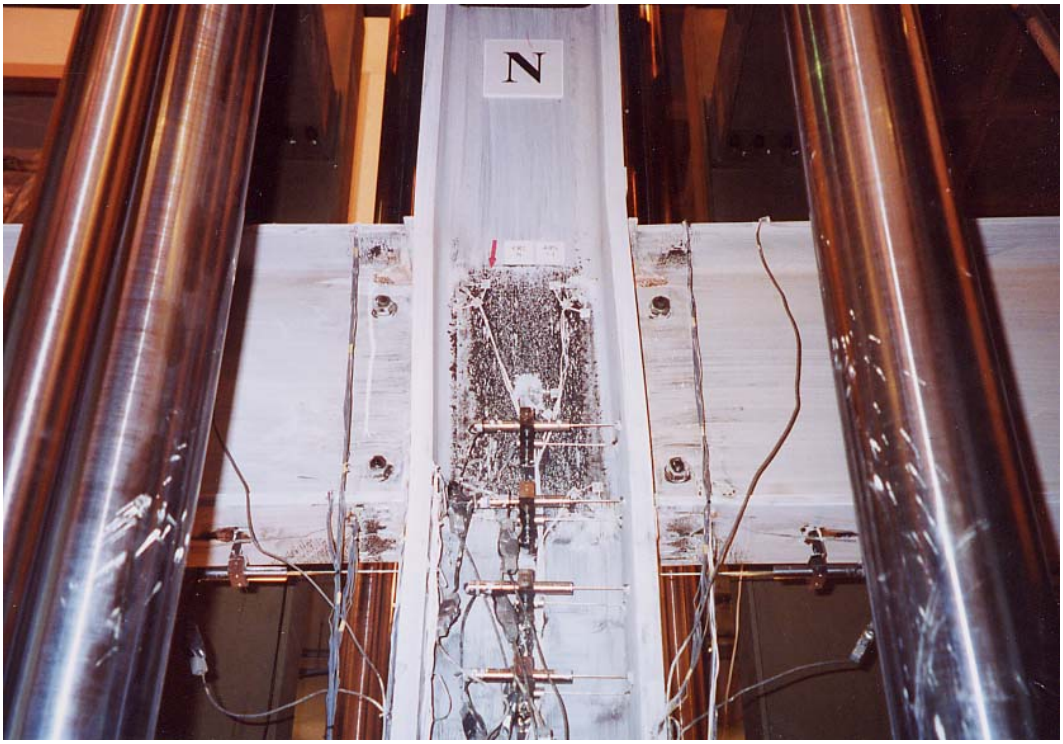


Figure 6.27: Specimen CR2 Panel Zone (4.0% Drift)

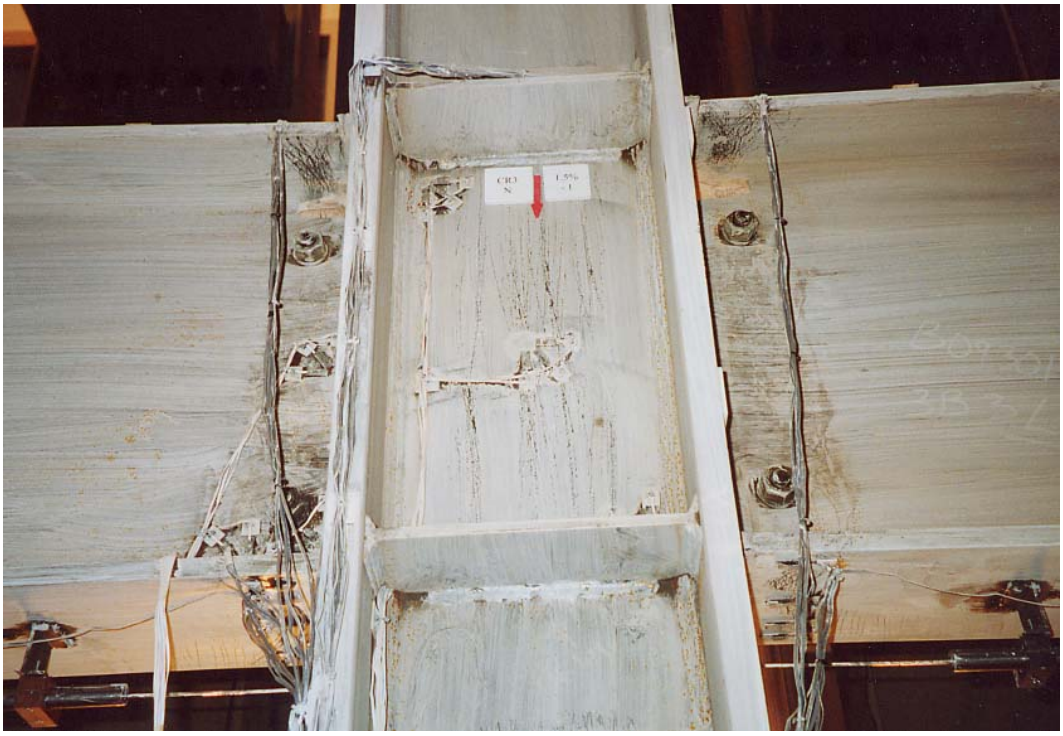


Figure 6.28: Specimen CR3 Panel Zone (1.5% Drift)



Figure 6.29: Specimen CR3 Panel Zone (2.0% Drift)

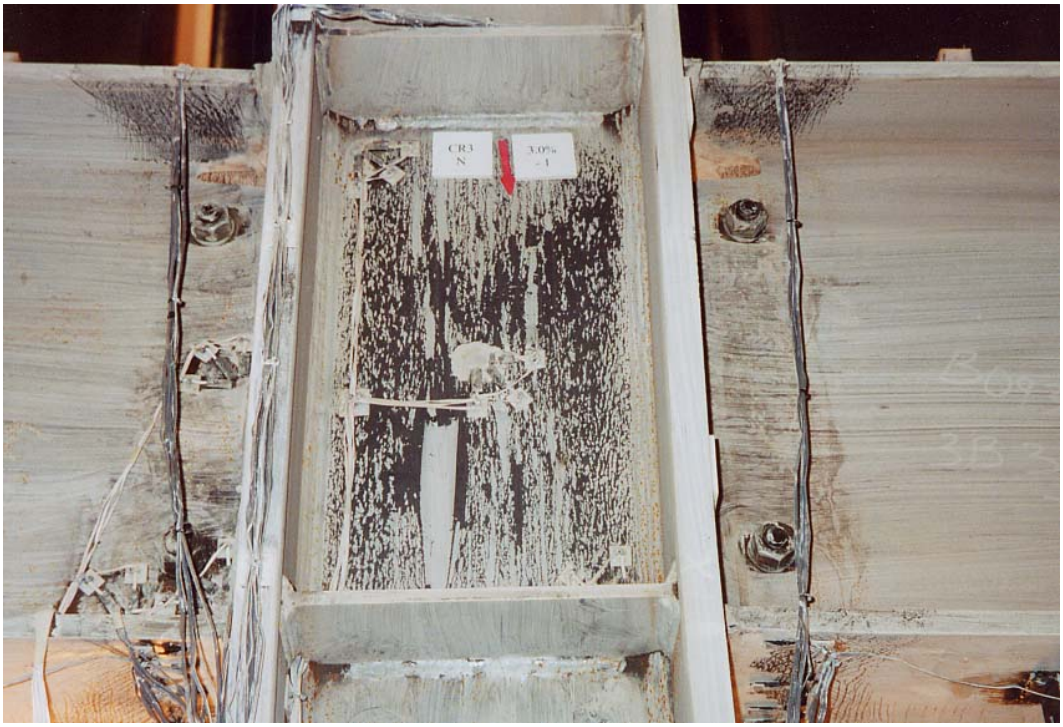


Figure 6.30: Specimen CR3 Panel Zone (3.0% Drift)

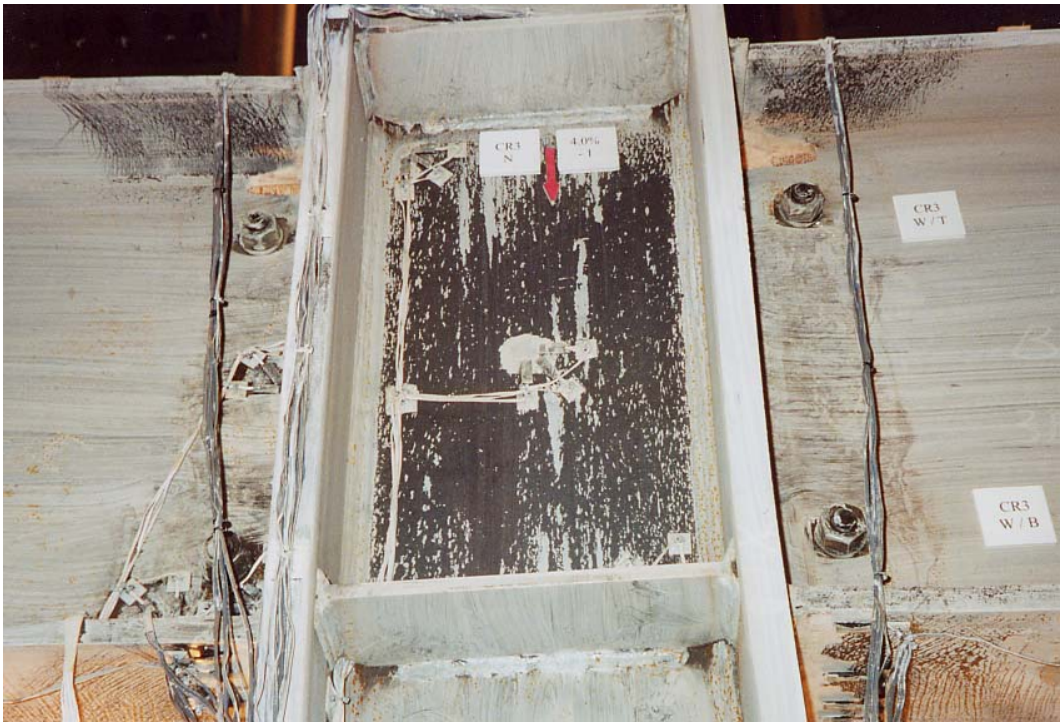


Figure 6.31: Specimen CR3 Panel Zone (4.0% Drift)



Figure 6.32: Specimen CR4R Panel Zone (1.5% Drift)

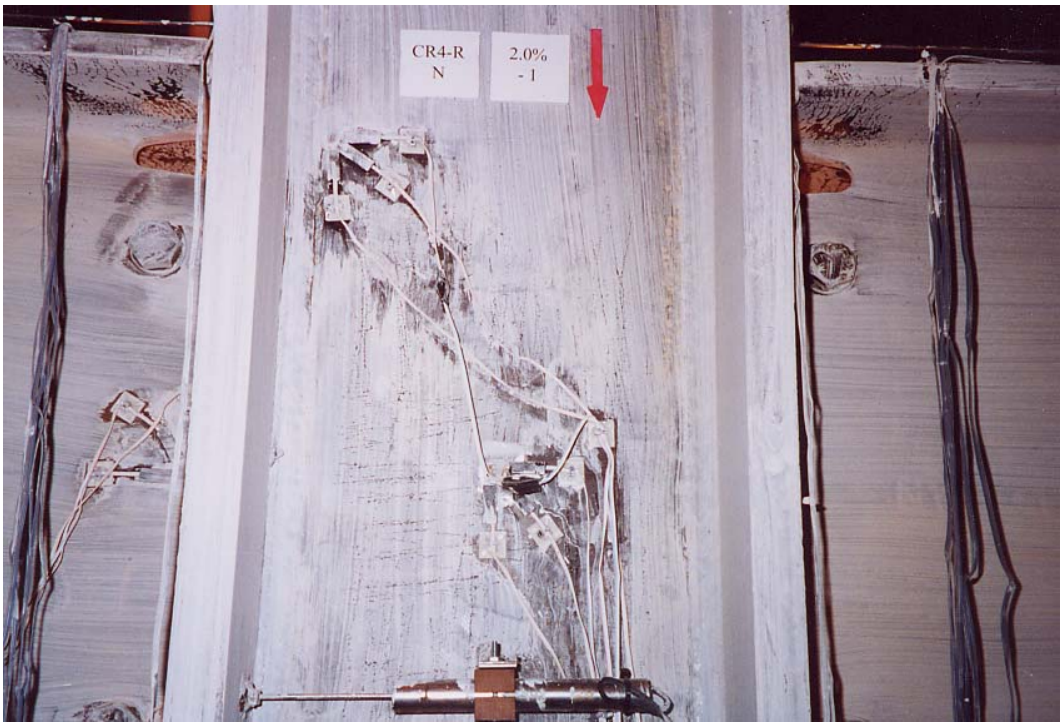


Figure 6.33: Specimen CR4R Panel Zone (2.0% Drift)



Figure 6.34: Specimen CR4R Panel Zone (3.0% Drift)

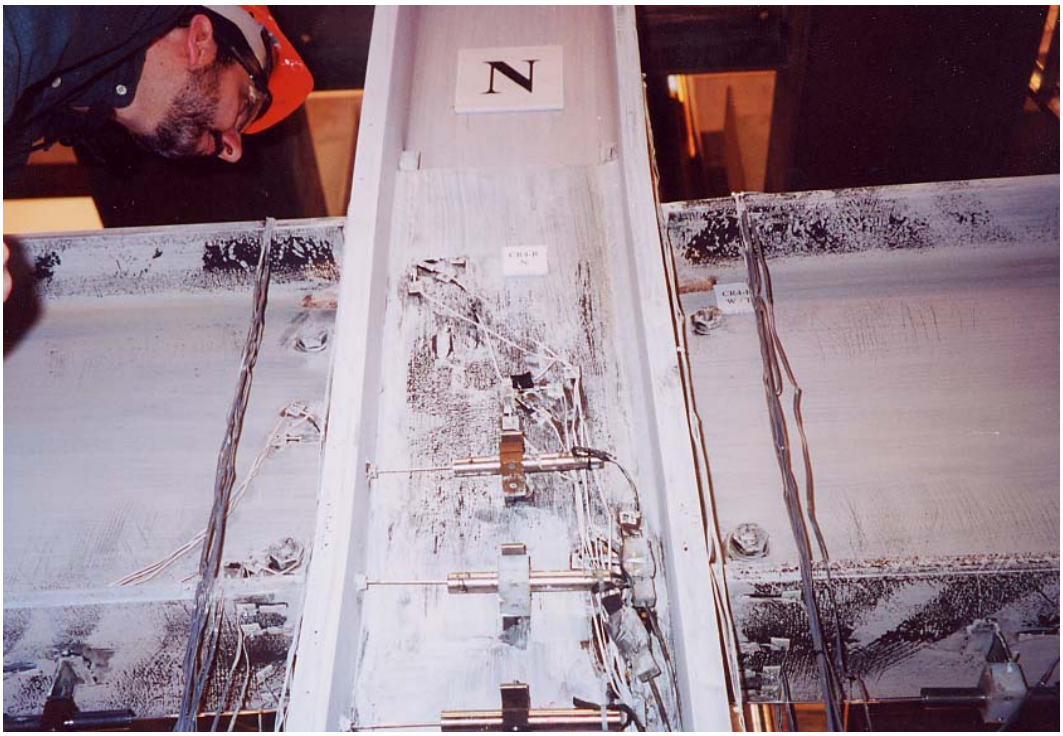


Figure 6.35: Specimen CR4R Panel Zone (4.0% Drift)



Figure 6.36: Specimen CR5 Panel Zone (1.5% Drift)

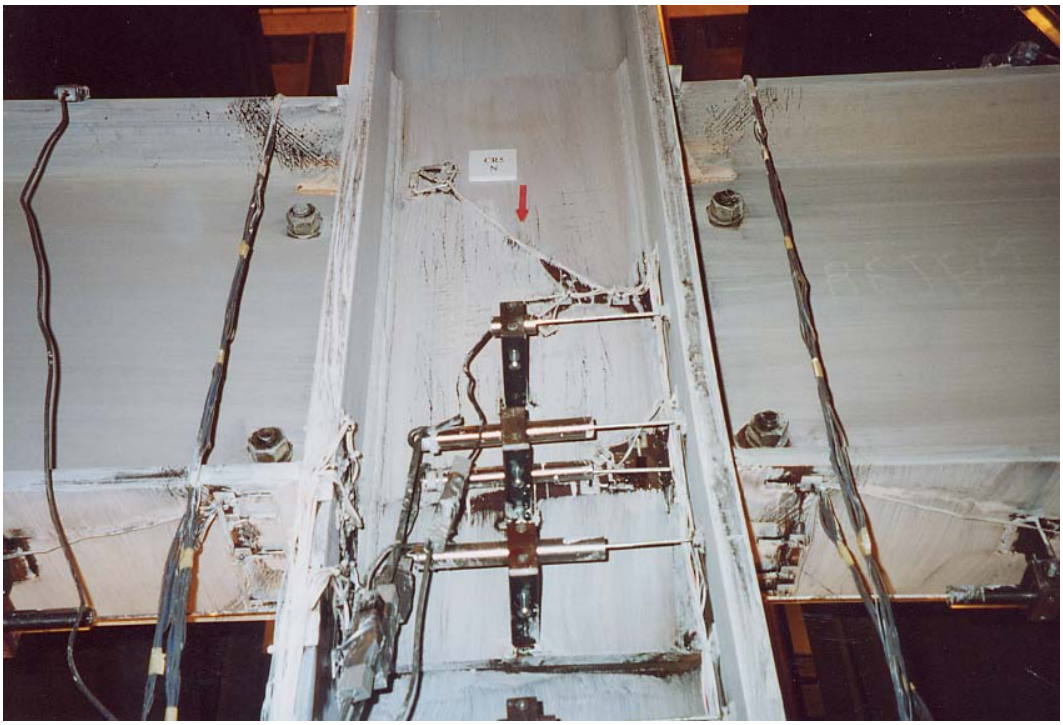


Figure 6.37: Specimen CR5 Panel Zone (2.0% Drift)

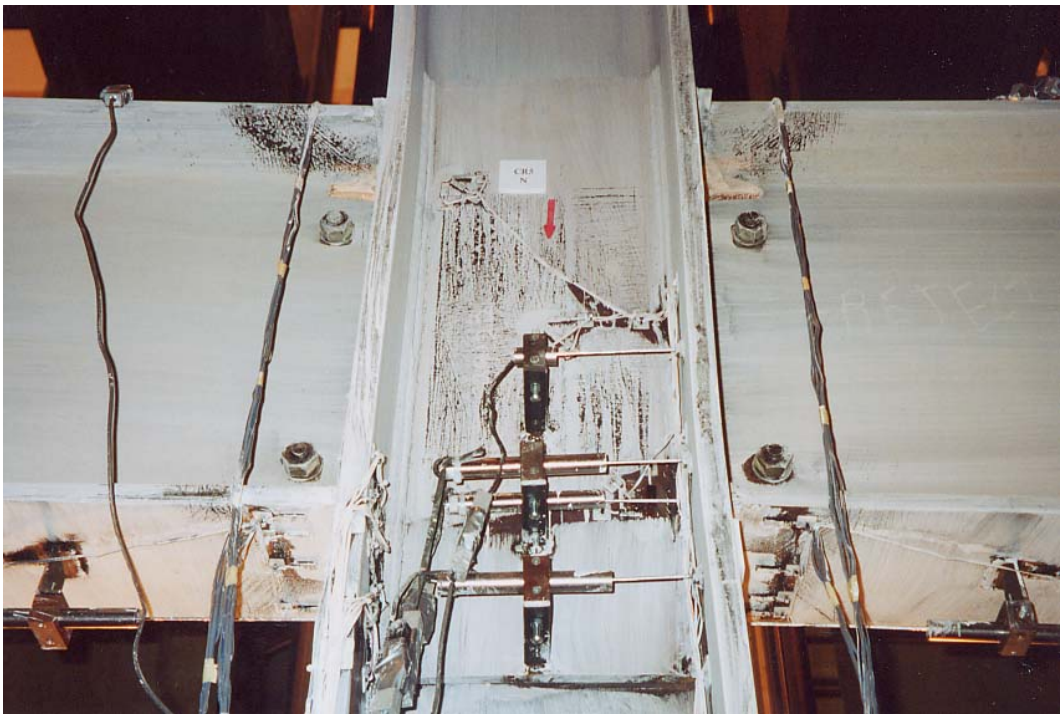


Figure 6.38: Specimen CR5 Panel Zone (3.0% Drift)

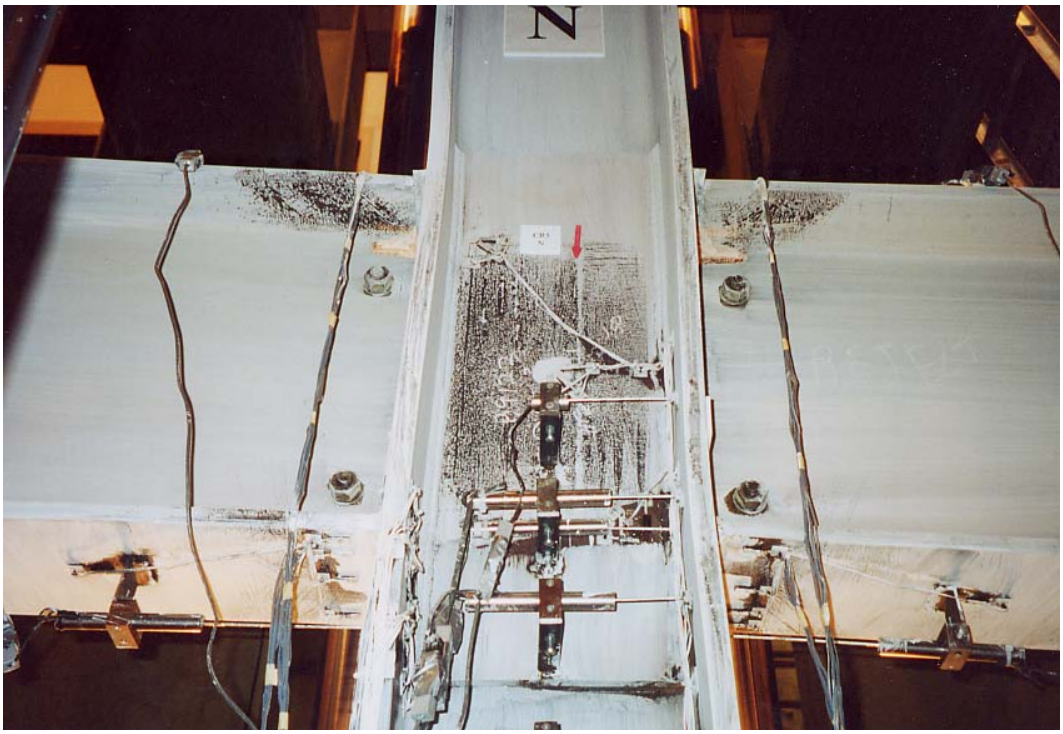


Figure 6.39: Specimen CR5 Panel Zone (4.0% Drift)

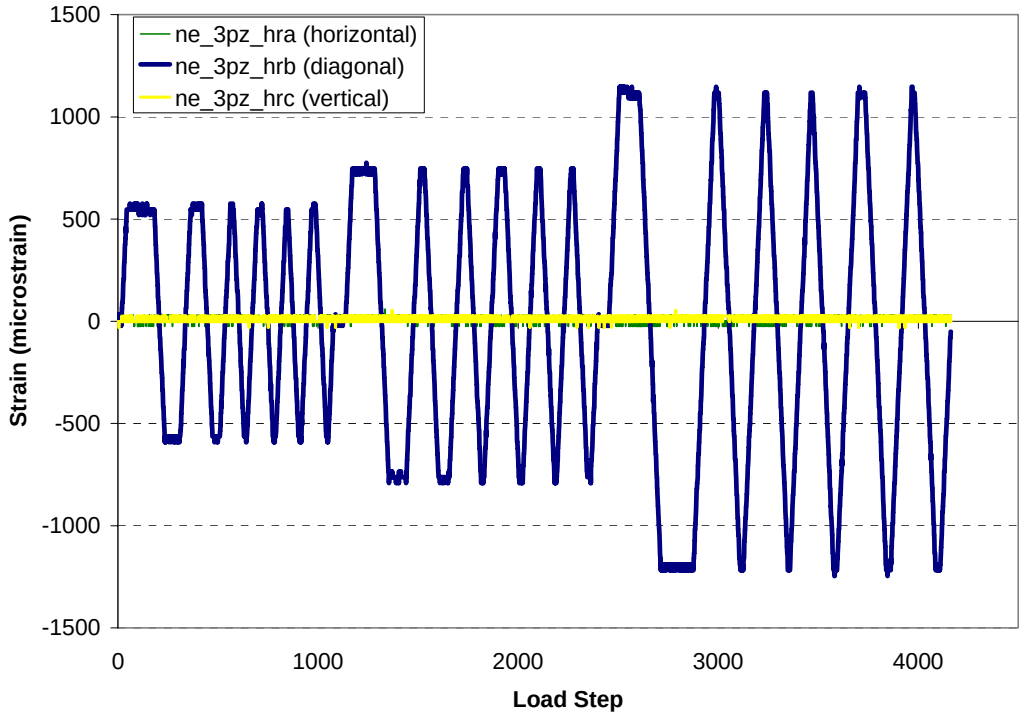


Figure 6.40: Elastic Strain History of Specimen CR1 (Panel Zone Center)

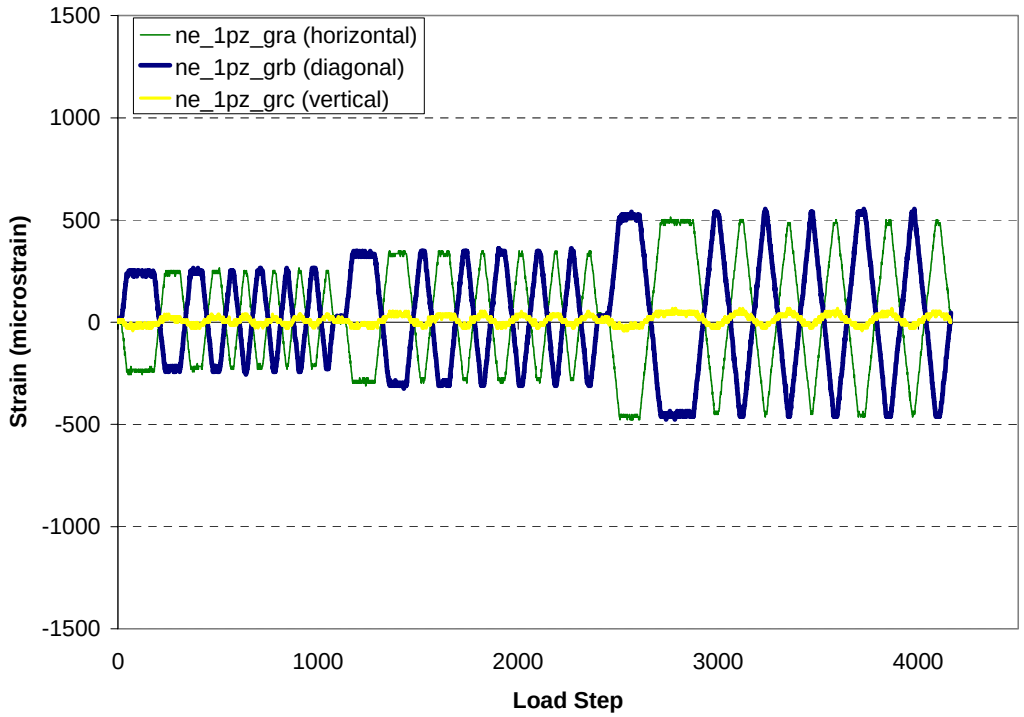


Figure 6.41: Elastic Strain History of Specimen CR1 (Panel Zone Corner)

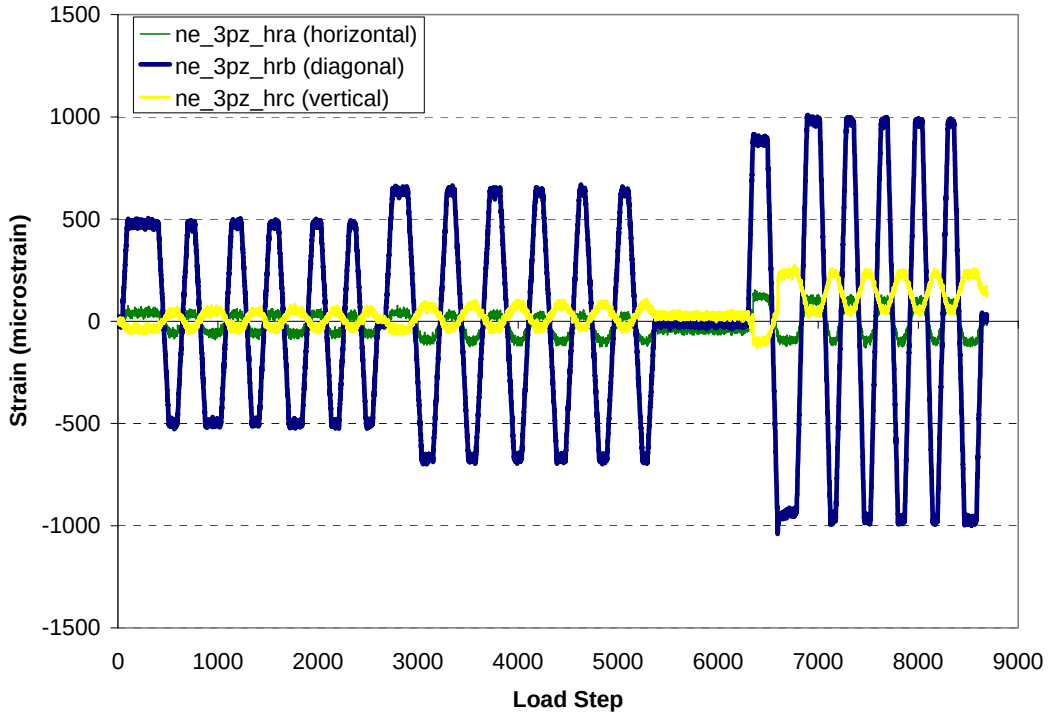


Figure 6.42: Elastic Strain History of Specimen CR2 (Panel Zone Center)

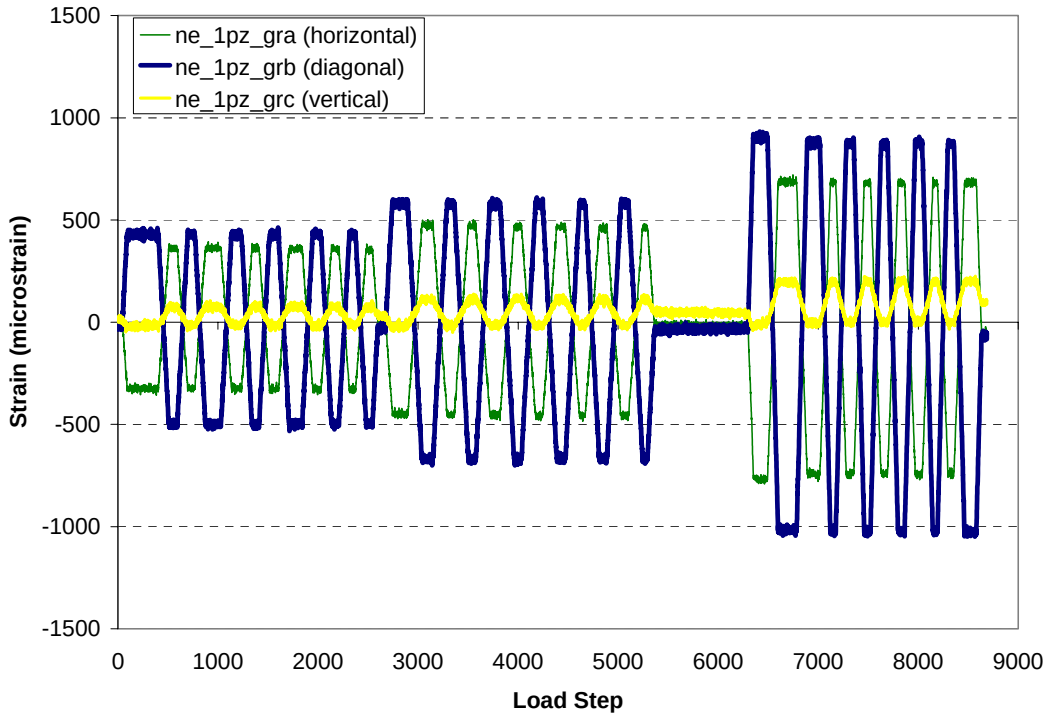


Figure 6.43: Elastic Strain History of Specimen CR2 (Panel Zone Corner)

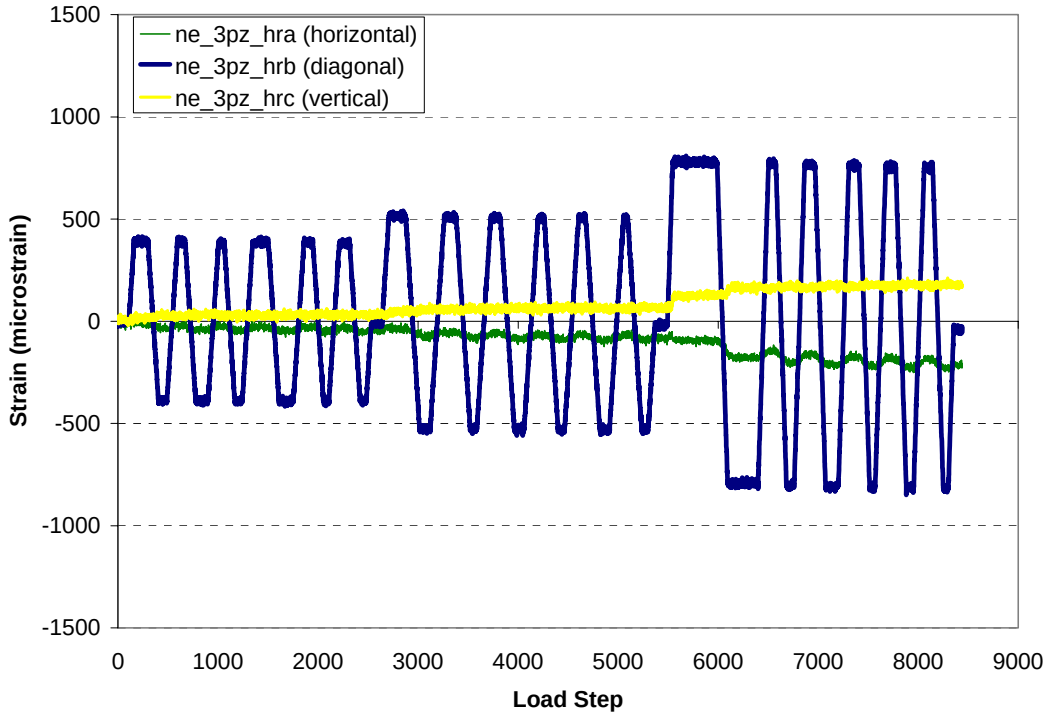


Figure 6.44: Elastic Strain History of Specimen CR3 (Panel Zone Center)

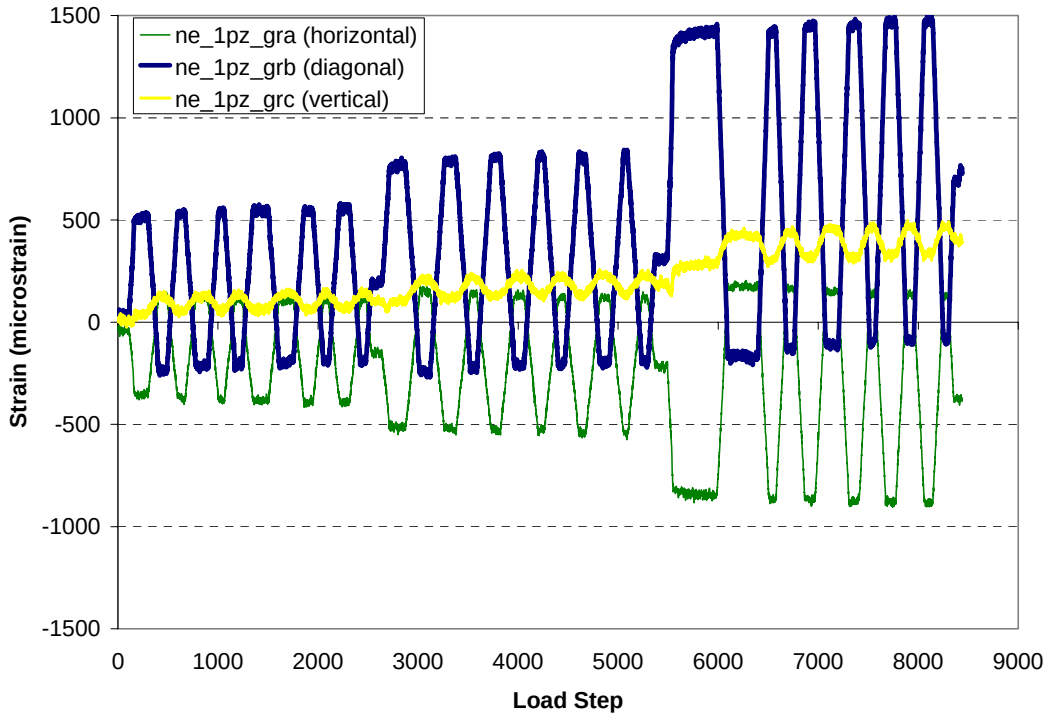


Figure 6.45: Elastic Strain History of Specimen CR3 (Panel Zone Corner)

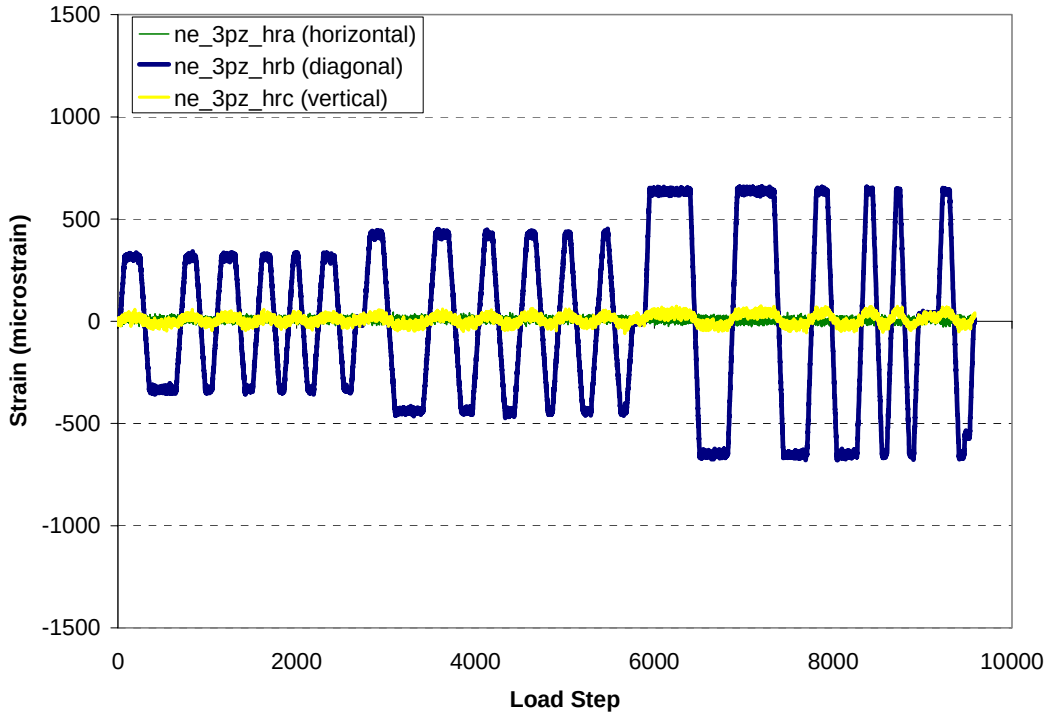


Figure 6.46: Elastic Strain History of Specimen CR4R (Panel Zone Center)

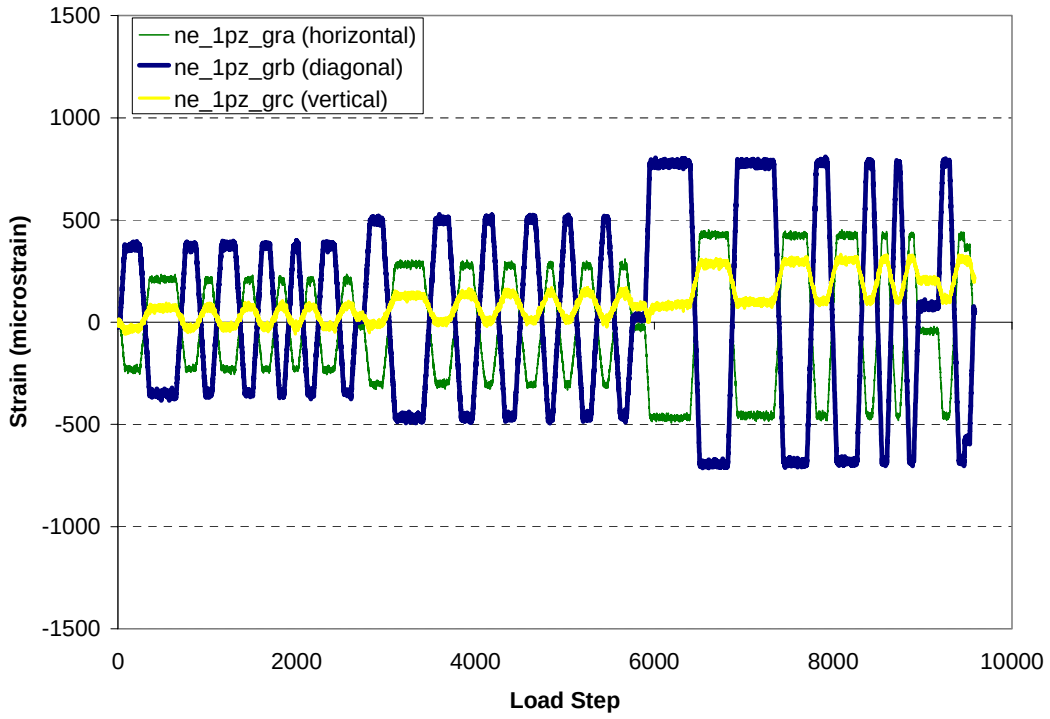


Figure 6.47: Elastic Strain History of Specimen CR4R (Panel Zone Corner)

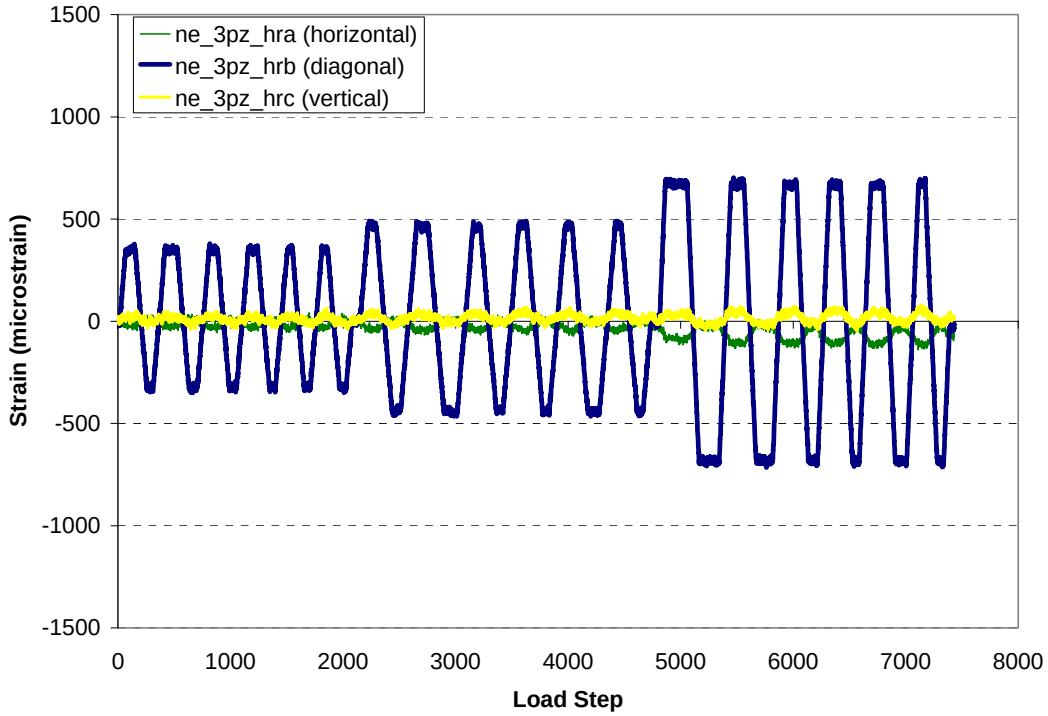


Figure 6.48: Elastic Strain History of Specimen CR5 (Panel Zone Center)

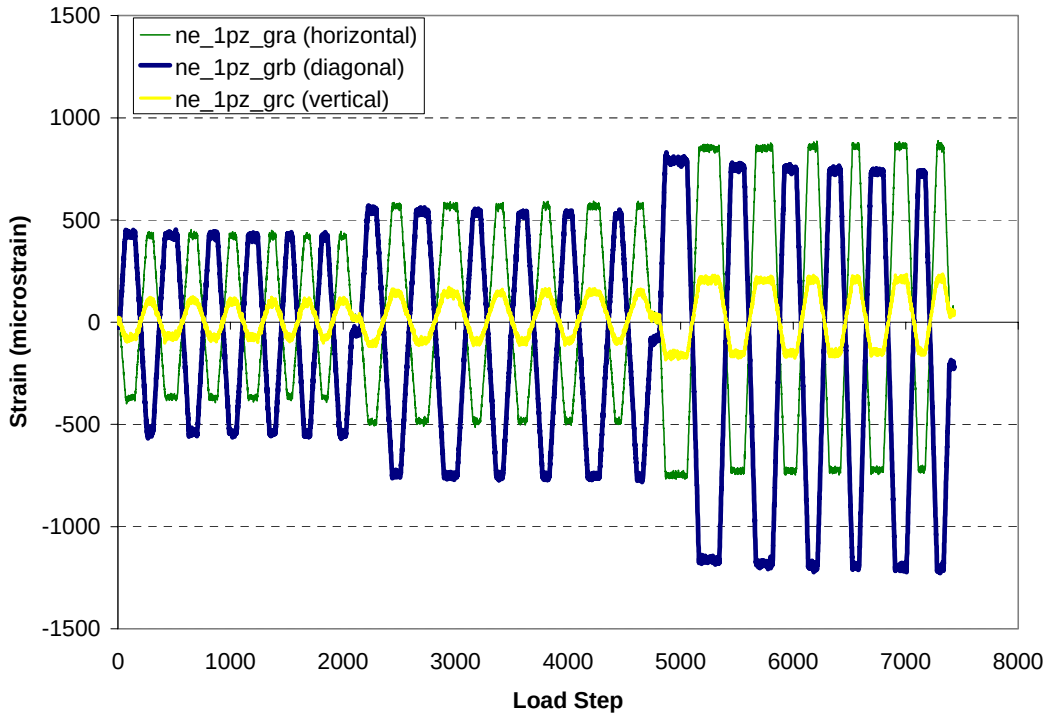
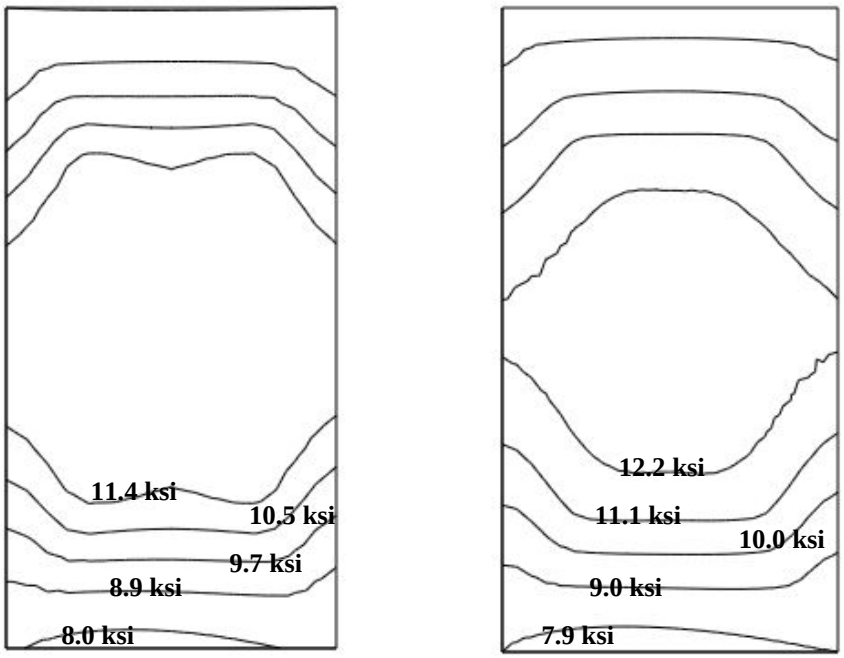
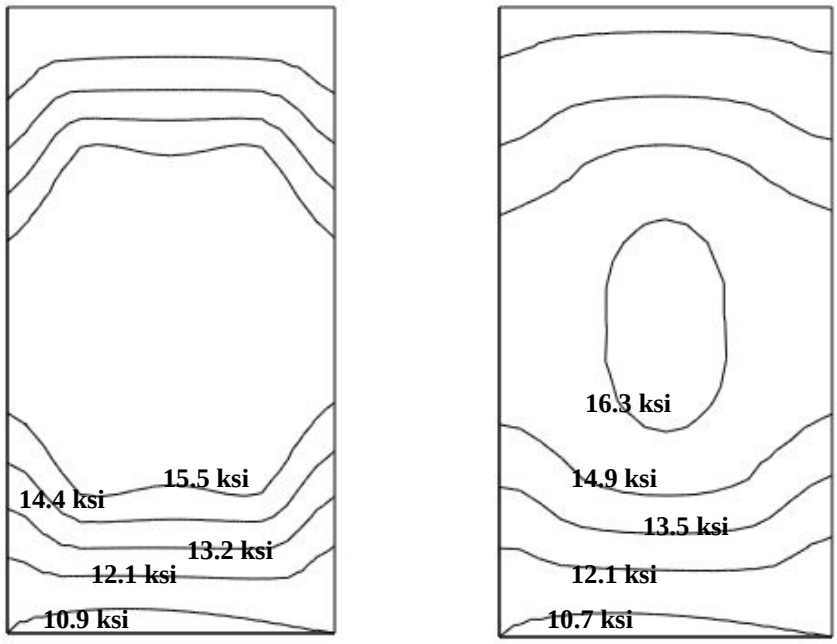


Figure 6.49: Elastic Strain History of Specimen CR5 (Panel Zone Corner)



(a) (b)

Figure 6.50: Elastic Panel Zone Shear Stress Contours at 0.375% Drift in Specimen CR1 for (a) Positive Loading Direction, and (b) Negative Loading Direction



(a) (b)

Figure 6.51: Elastic Panel Zone Shear Stress Contours at 0.5% Drift in Specimen CR1 for (a) Positive Loading Direction, and (b) Negative Loading Direction



Figure 6.52: Close-up View of Column Flange Yielding and Kinking due to the Concentrated Girder Flange Force (Specimen CR1)

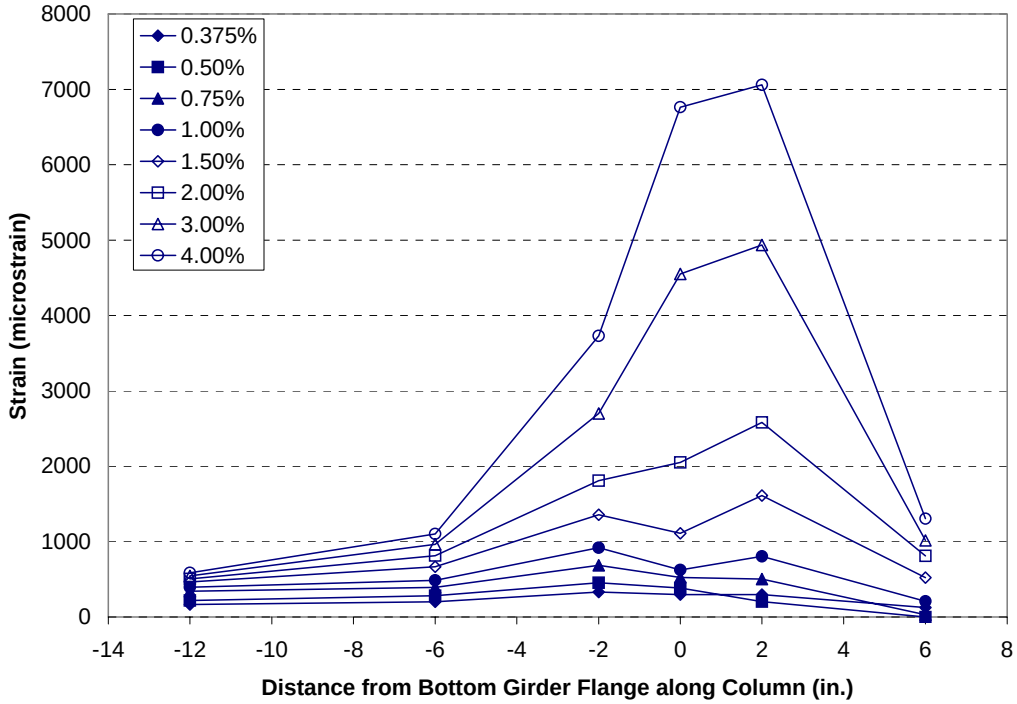


Figure 6.53: Longitudinal Strains in CR1 Column Flange (Bottom Girder Flange in Tension)

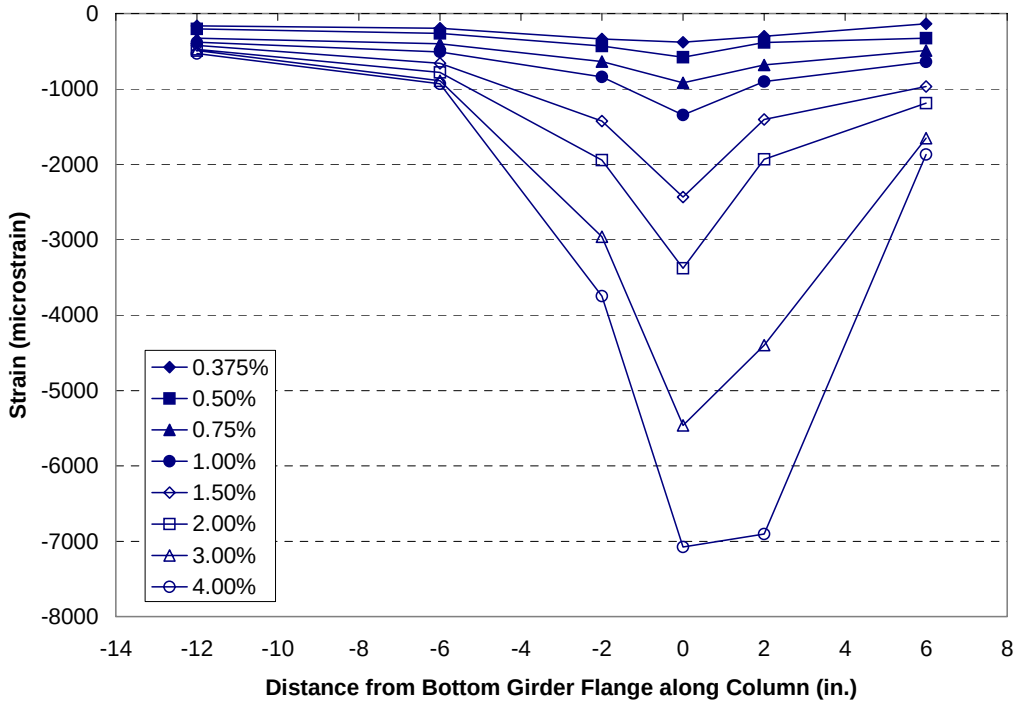


Figure 6.54: Longitudinal Strains in CR1 Column Flange (Bottom Girder Flange in Compression)

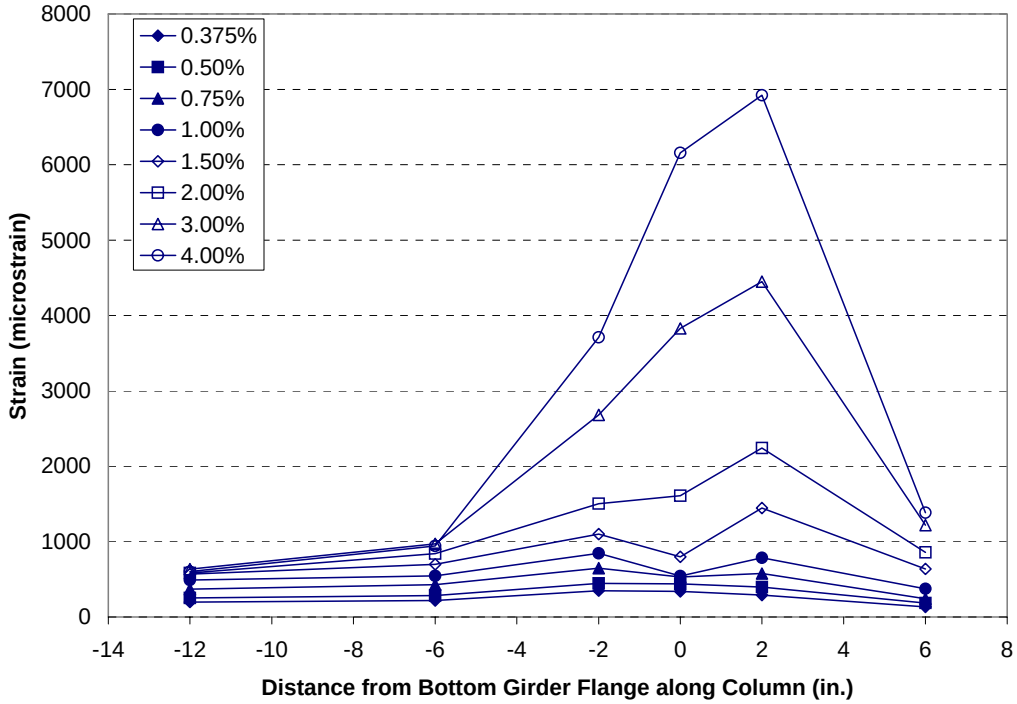


Figure 6.55: Longitudinal Strains in CR2 Column Flange (Bottom Girder Flange in Tension)

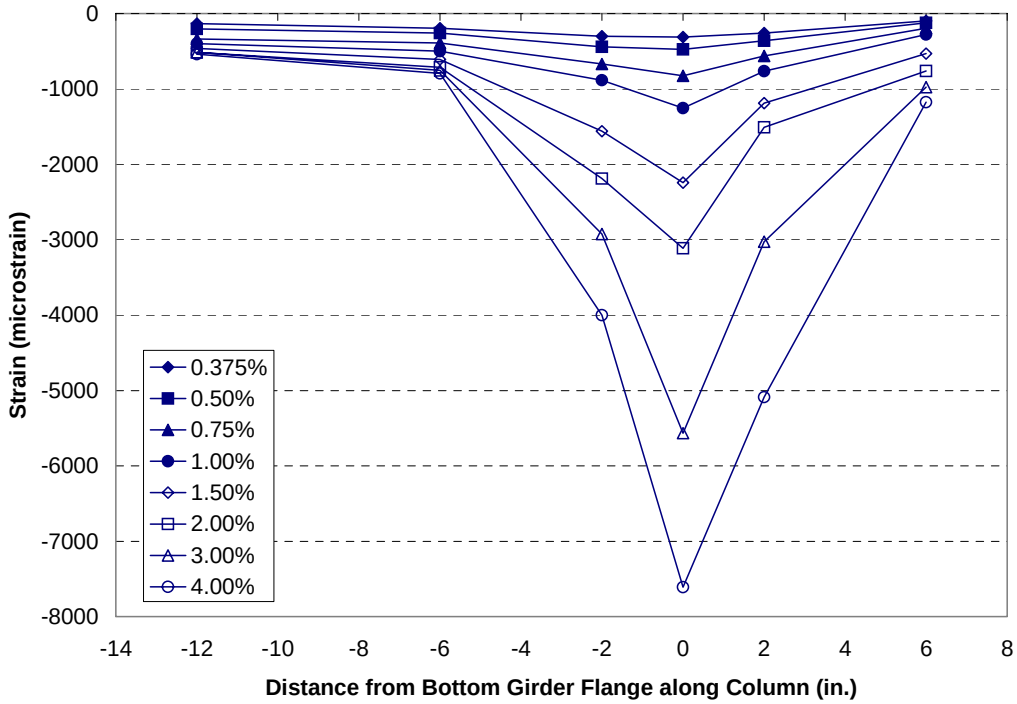


Figure 6.56: Longitudinal Strains in CR2 Column Flange (Bottom Girder Flange in Compression)

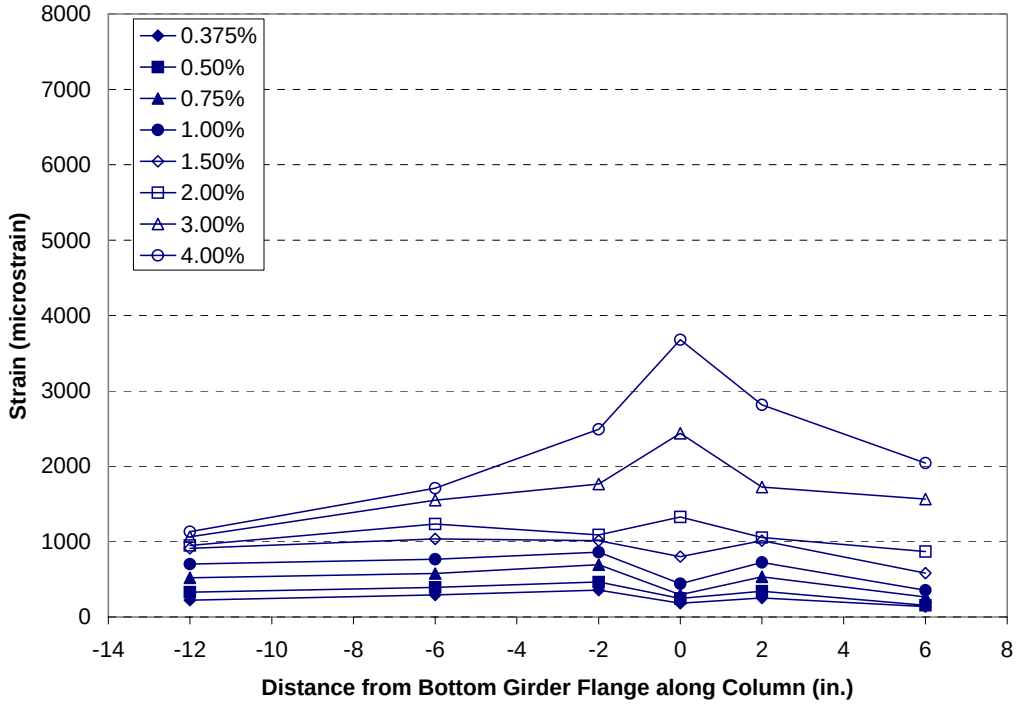


Figure 6.57: Longitudinal Strains in CR3 Column Flange (Bottom Girder Flange in Tension)

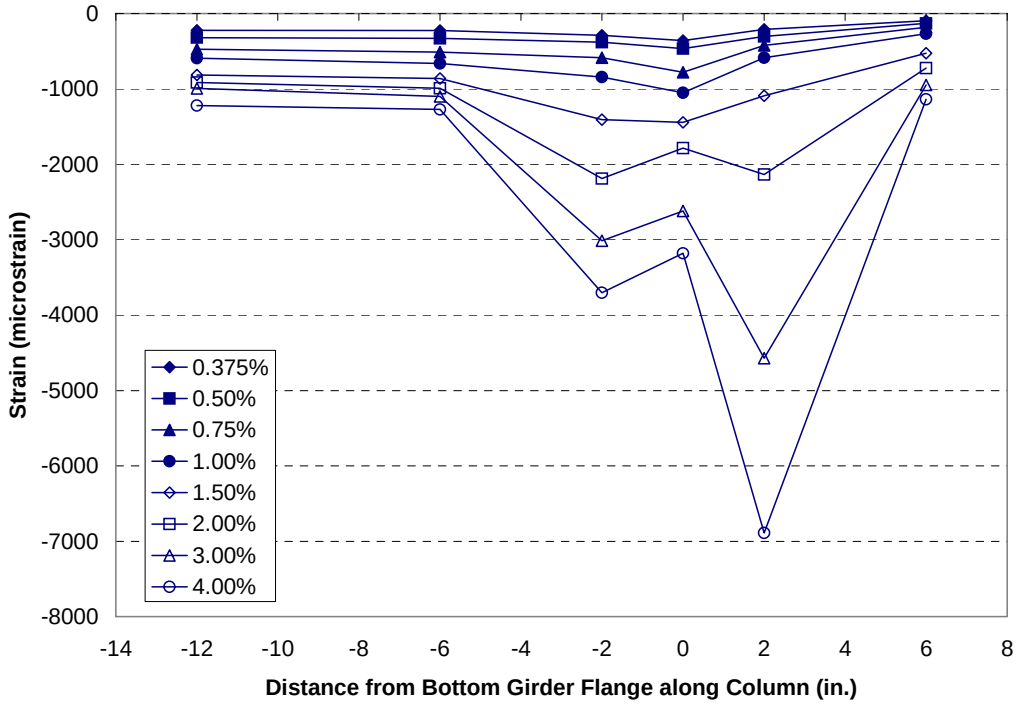


Figure 6.58: Longitudinal Strains in CR3 Column Flange (Bottom Girder Flange in Compression)

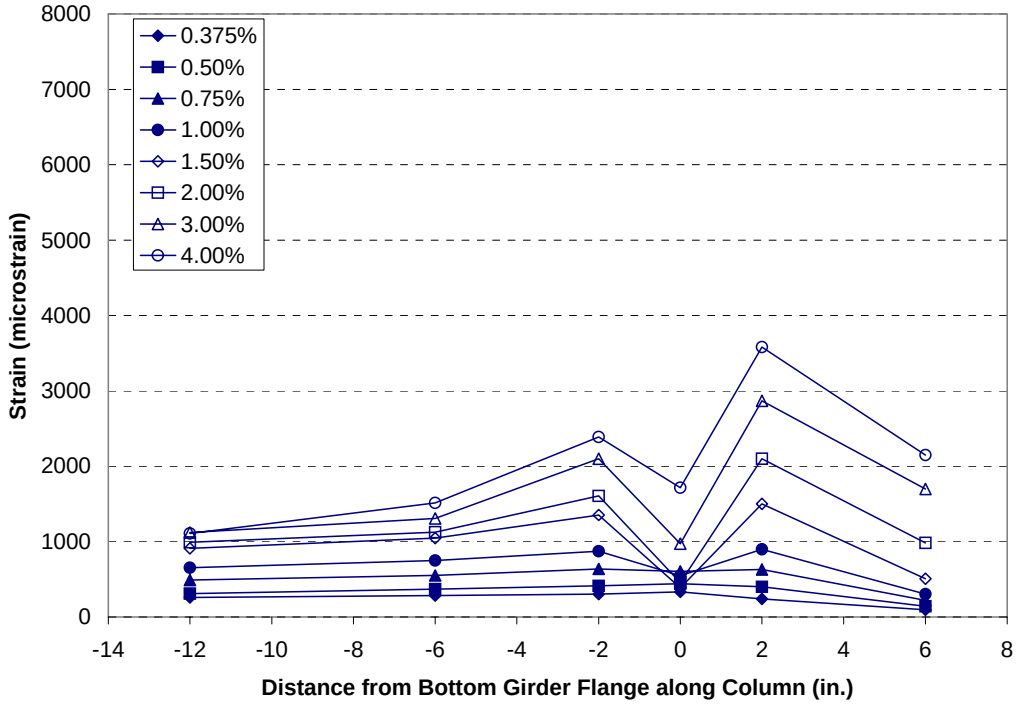


Figure 6.59: Longitudinal Strains in CR4R Column Flange (Bottom Girder Flange in Tension)

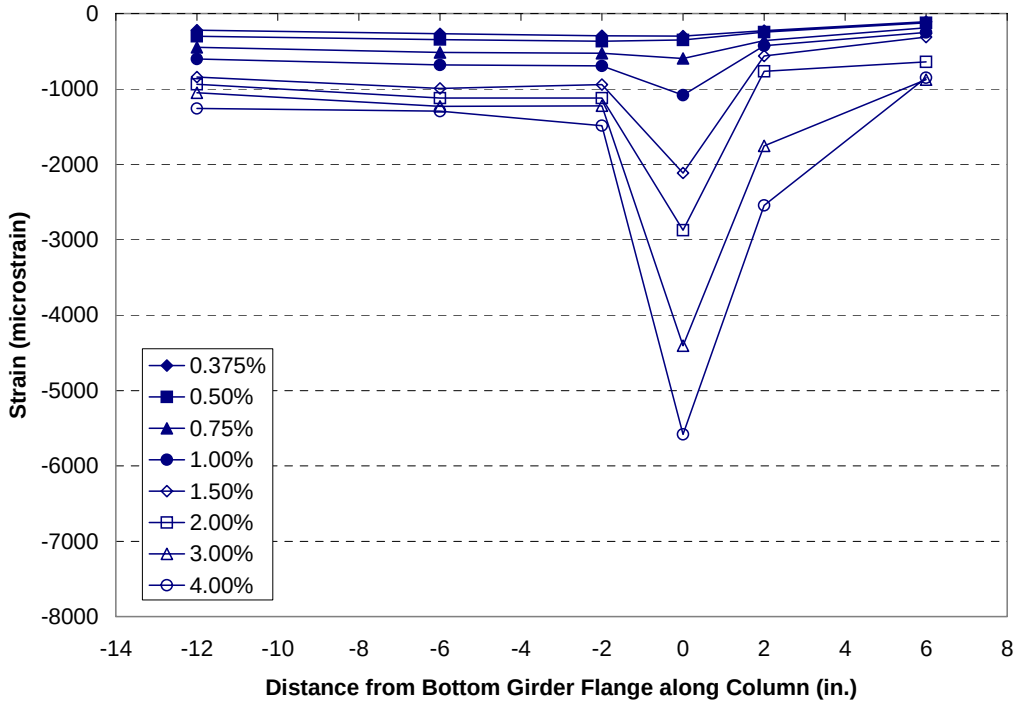


Figure 6.60: Longitudinal Strains in CR4R Column Flange (Bottom Girder Flange in Compression)

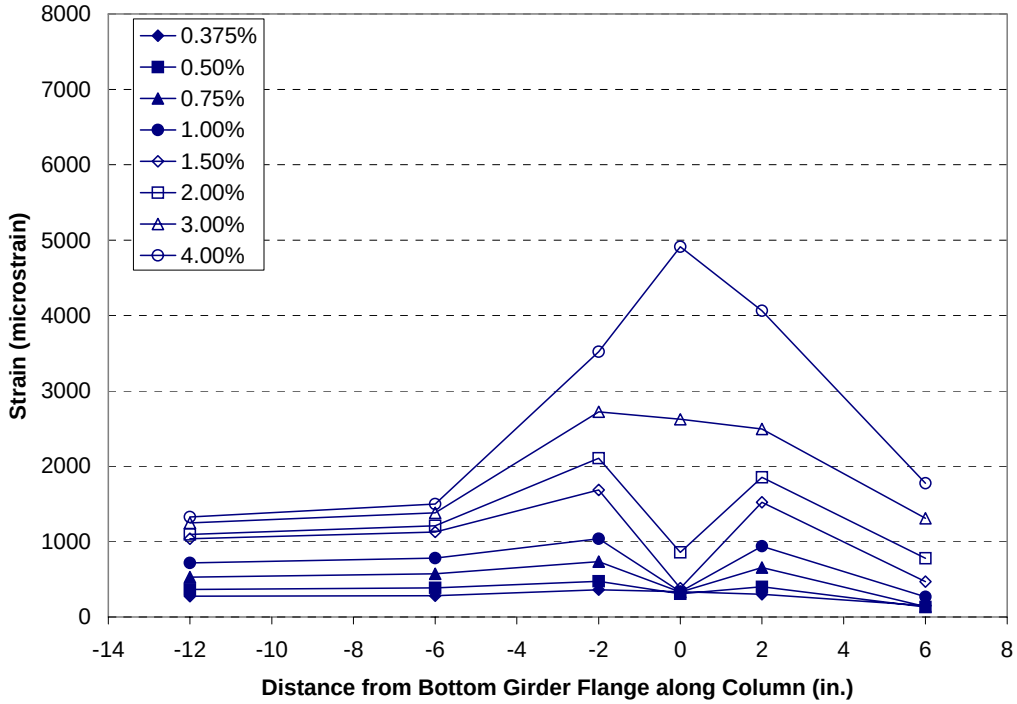


Figure 6.61: Longitudinal Strains in CR5 Column Flange (Bottom Girder Flange in Tension)

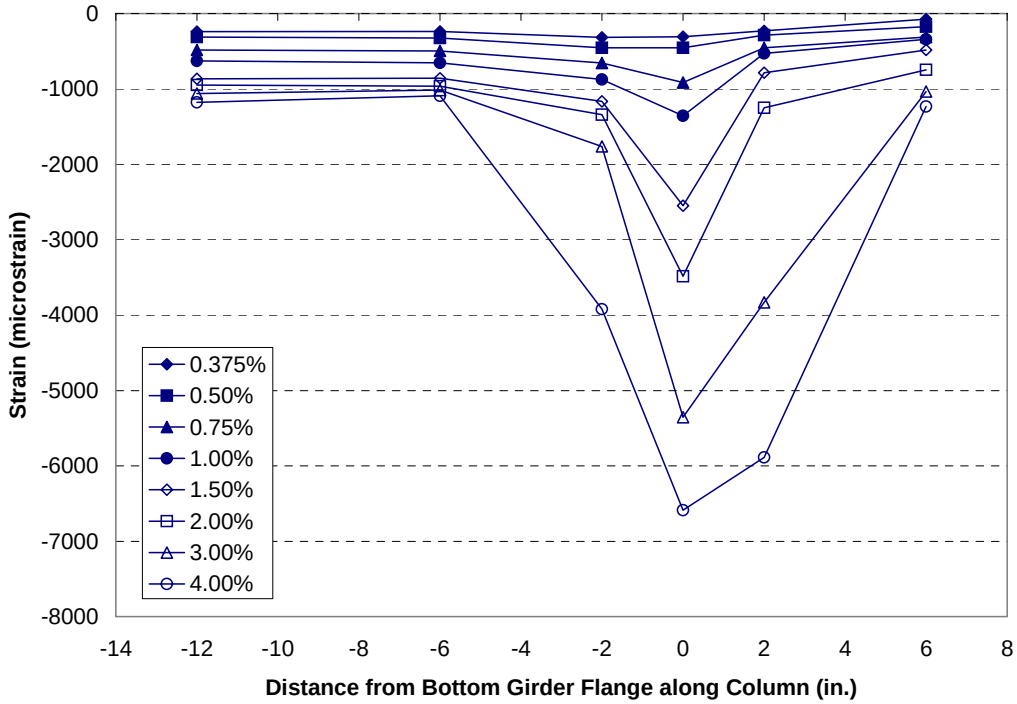


Figure 6.62: Longitudinal Strains in CR5 Column Flange (Bottom Girder Flange in Compression)

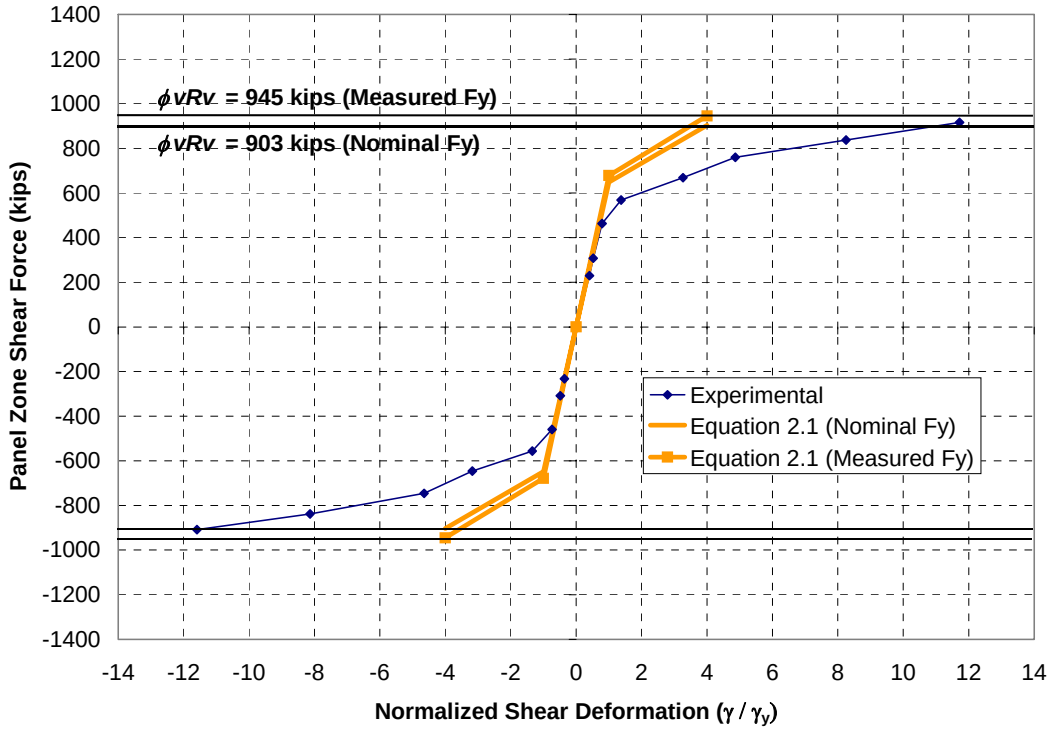


Figure 6.63: Panel Zone Behavior versus AISC Design Equation 2.1, CR1

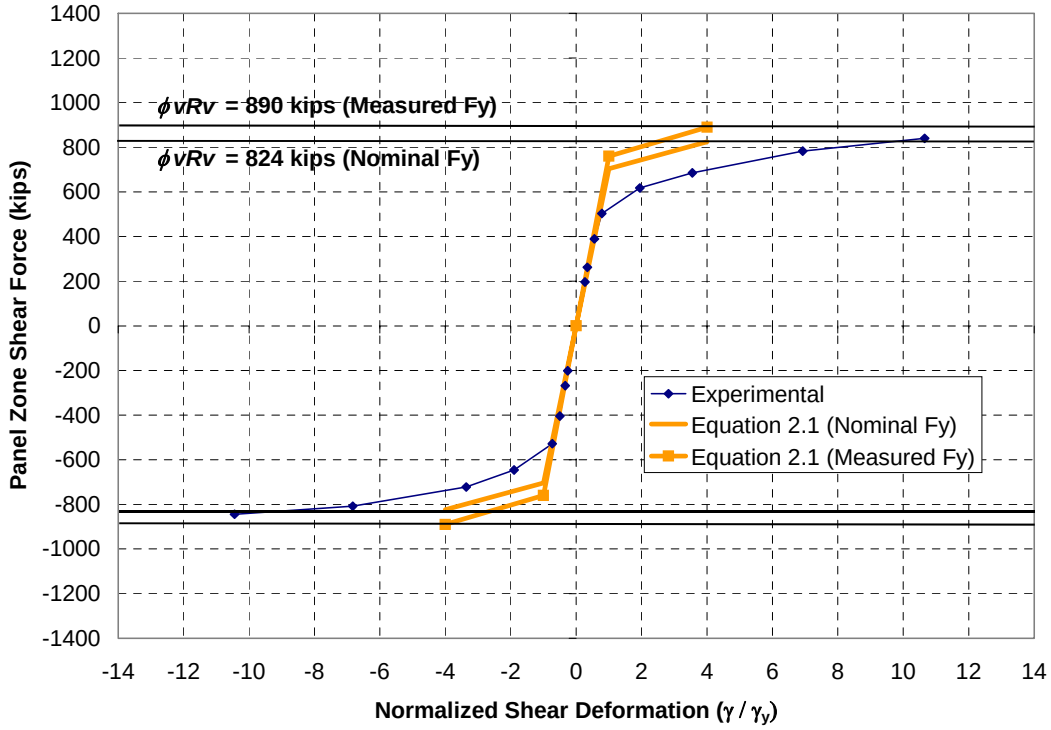


Figure 6.64: Panel Zone Behavior versus AISC Design Equation 2.1, CR2

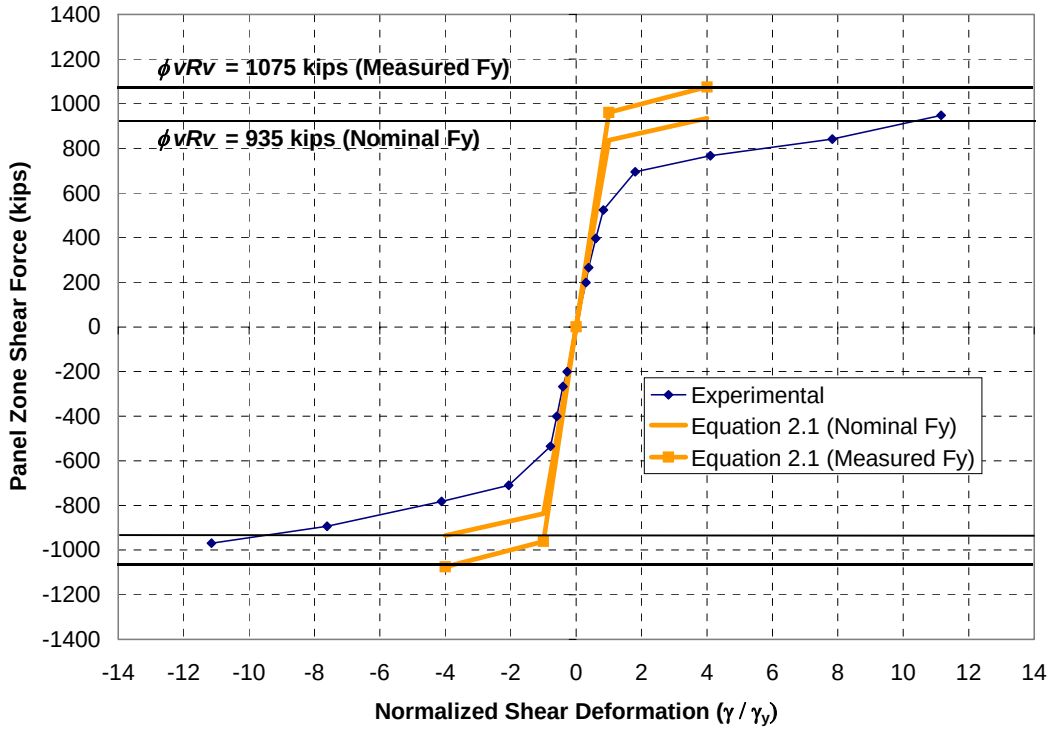


Figure 6.65: Panel Zone Behavior versus AISC Design Equation 2.1, CR3

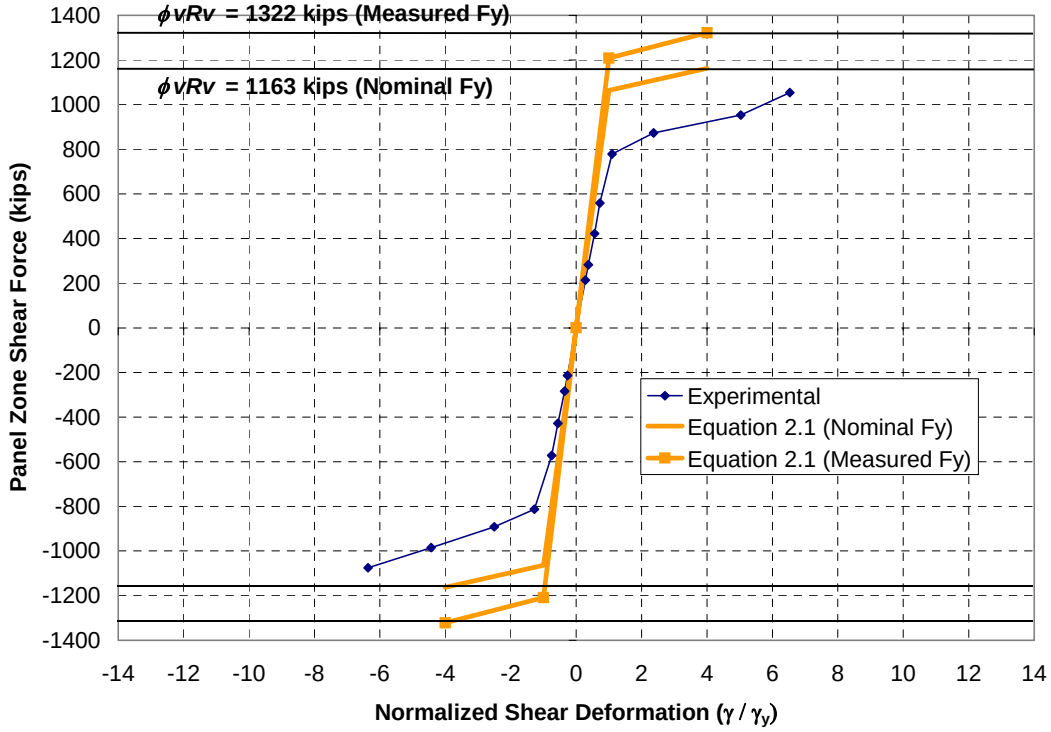


Figure 6.66: Panel Zone Behavior versus AISC Design Equation 2.1, CR4R

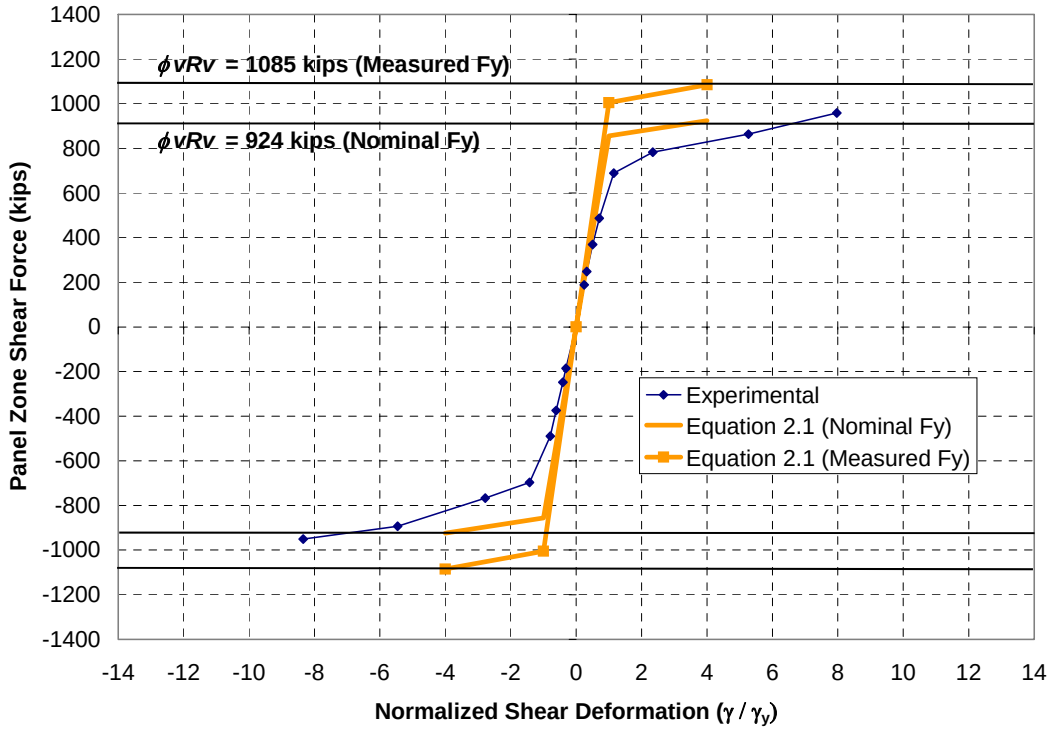
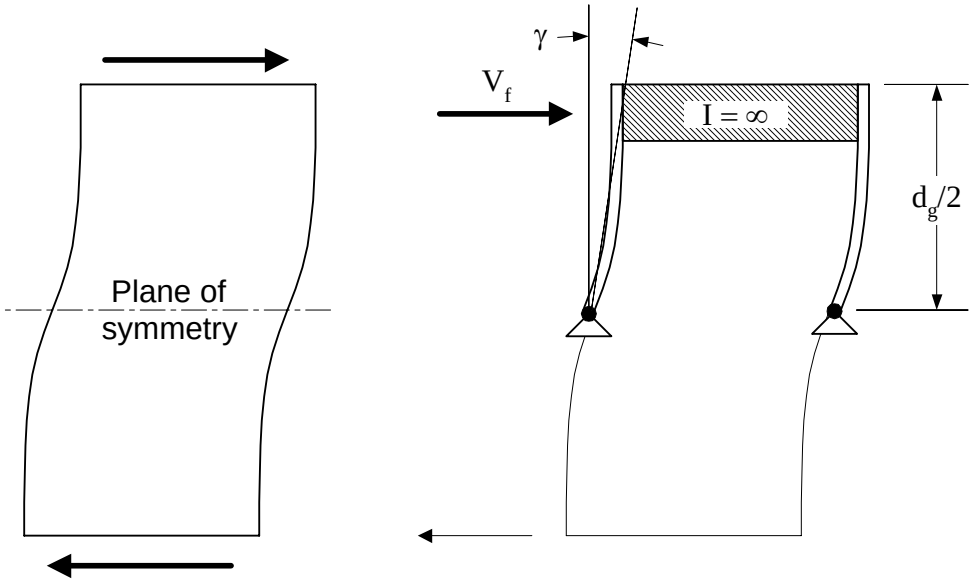


Figure 6.67: Panel Zone Behavior versus AISC Design Equation 2.1, CR5



(a) (b)

Figure 6.68: (a) Net Shear Forces Acting on Panel Zone Showing Deformed Shape, and (b) Modified Fielding and Huang Model for Post-Elastic Panel Zone Behavior

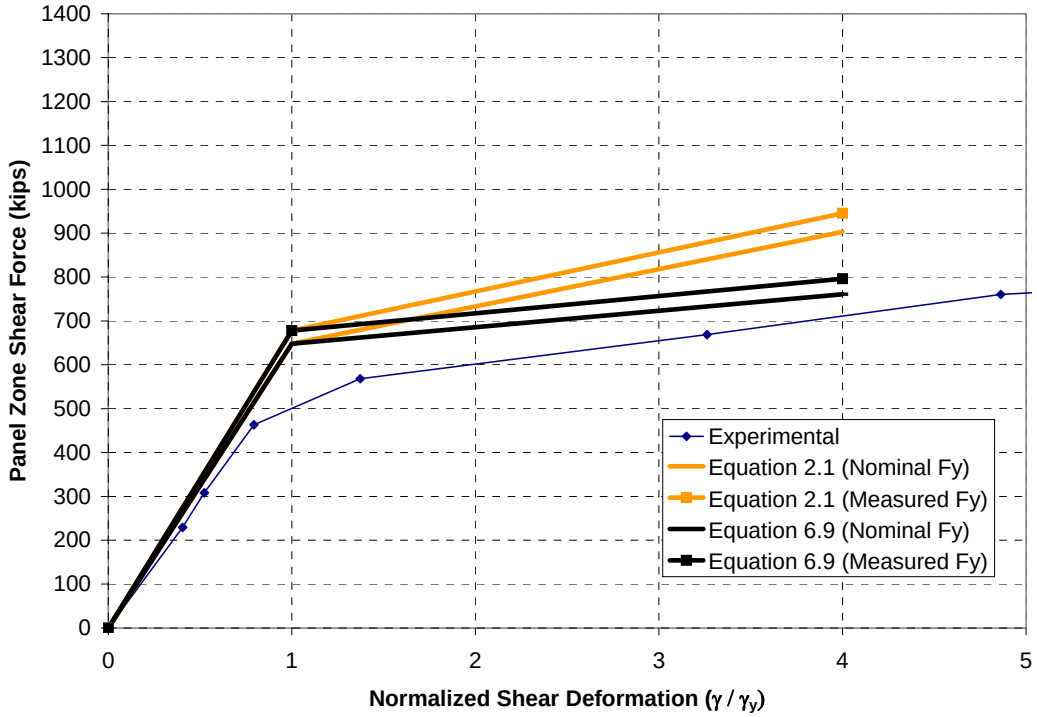


Figure 6.69: Comparison of Experimental Panel Zone Behavior to AISC (1997) and Equation 6.9, CR1

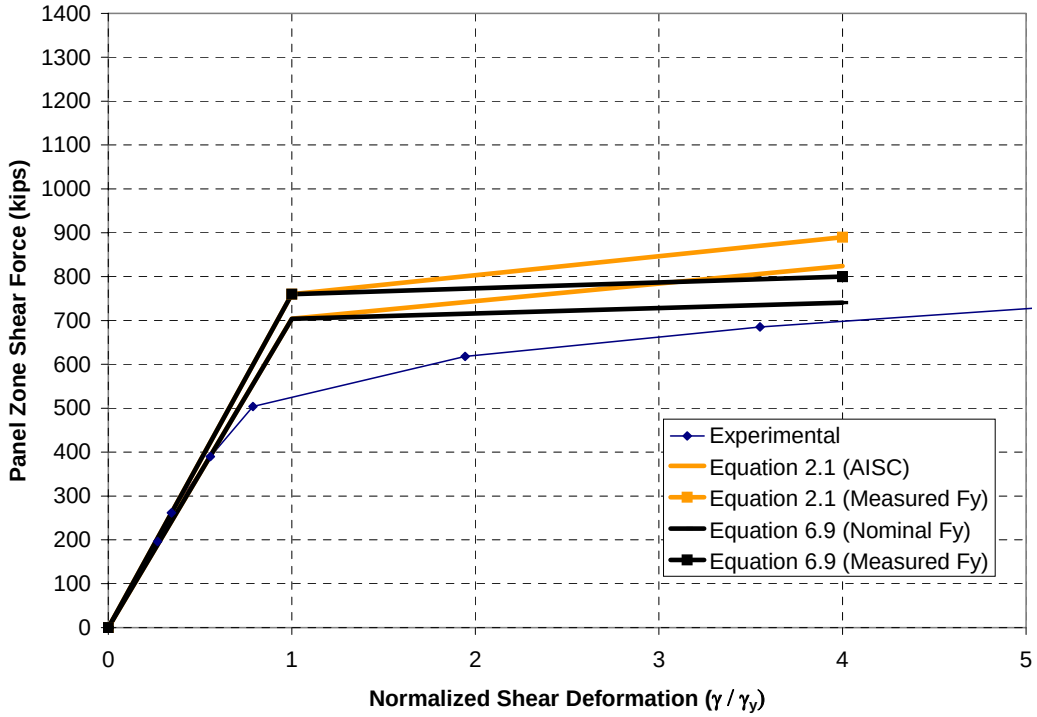


Figure 6.70: Comparison of Experimental Panel Zone Behavior to AISC (1997) and Equation 6.9, CR2

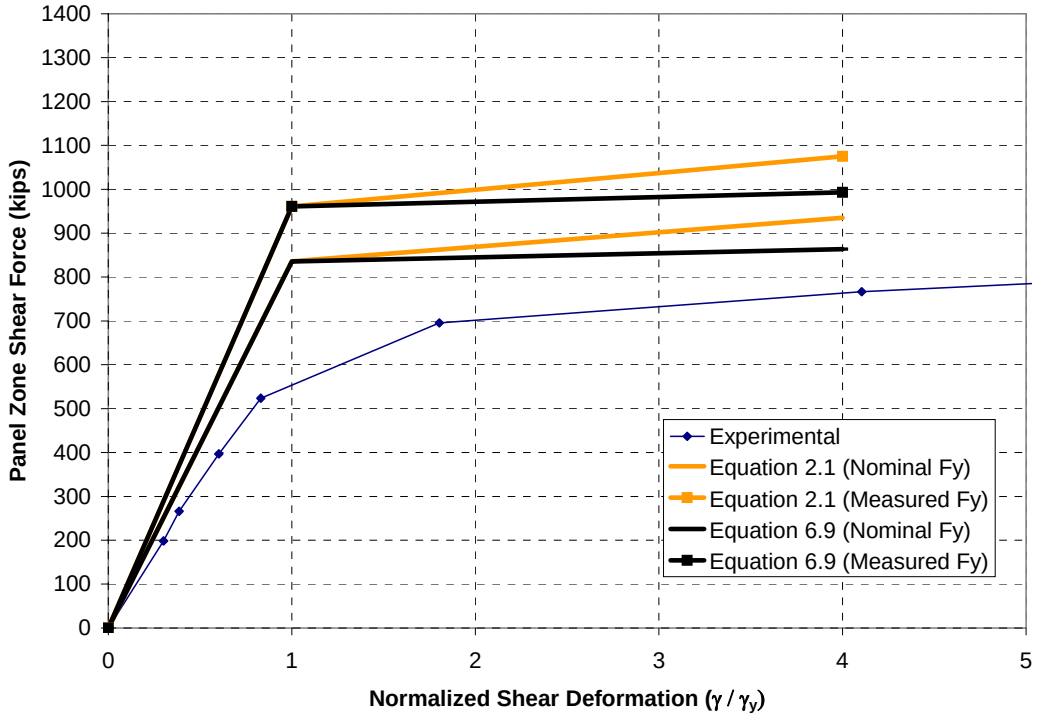


Figure 6.71: Comparison of Experimental Panel Zone Behavior to AISC (1997) and Equation 6.9, CR3

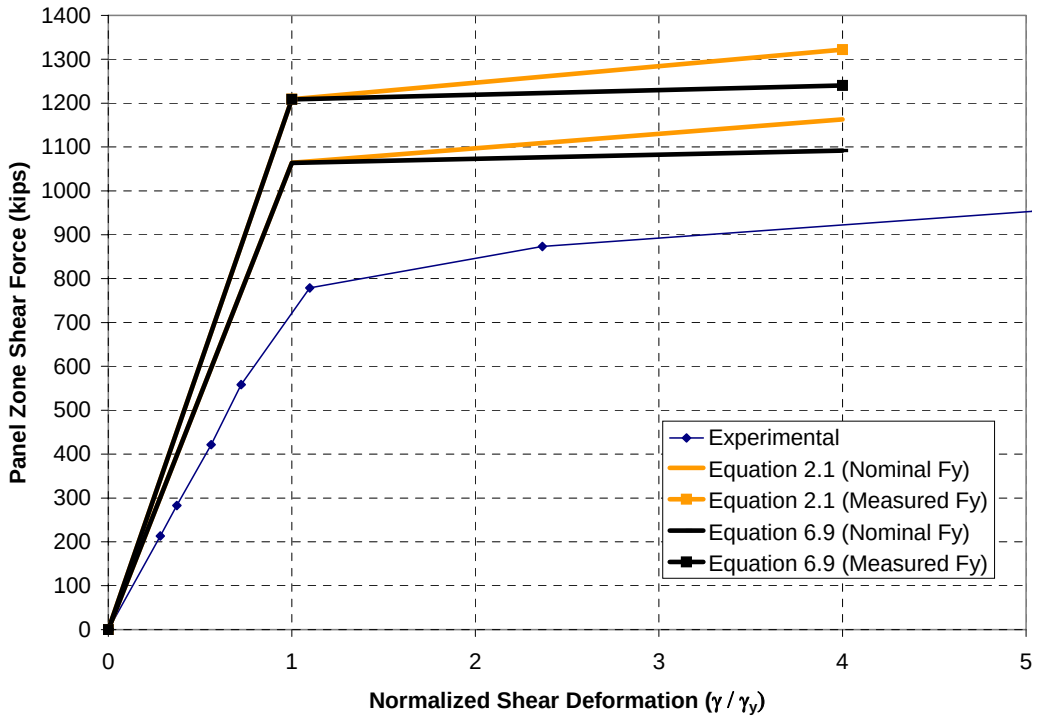


Figure 6.72: Comparison of Experimental Panel Zone Behavior to AISC (1997) and Equation 6.9, CR4R

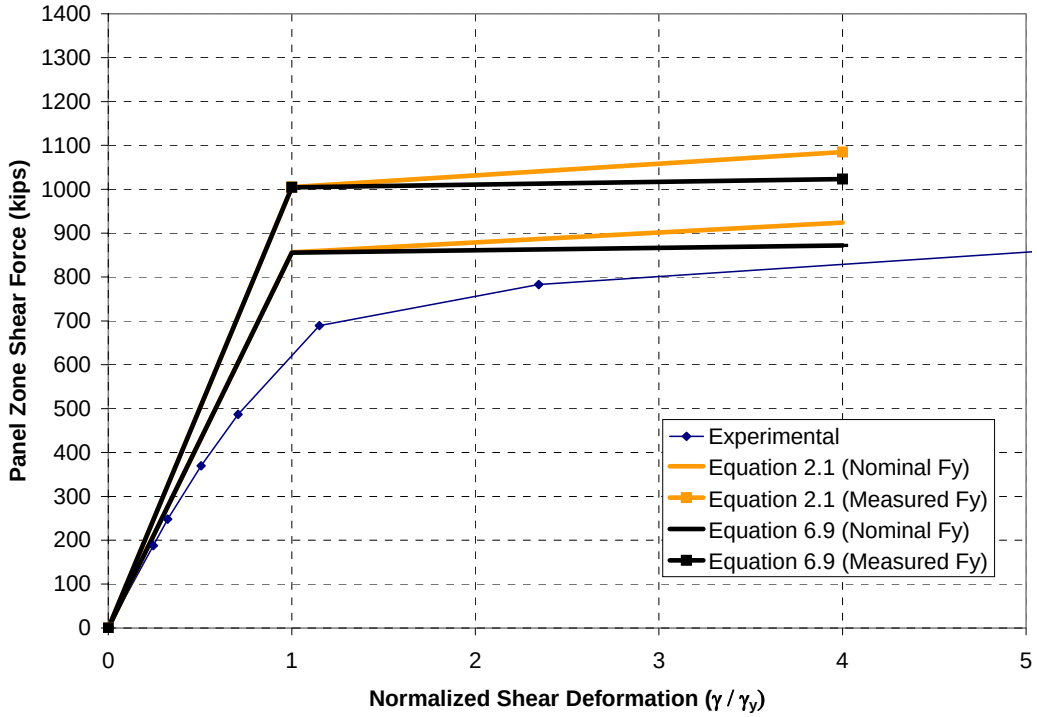


Figure 6.73: Comparison of Experimental Panel Zone Behavior to AISC (1997) and Equation 6.9, CR5

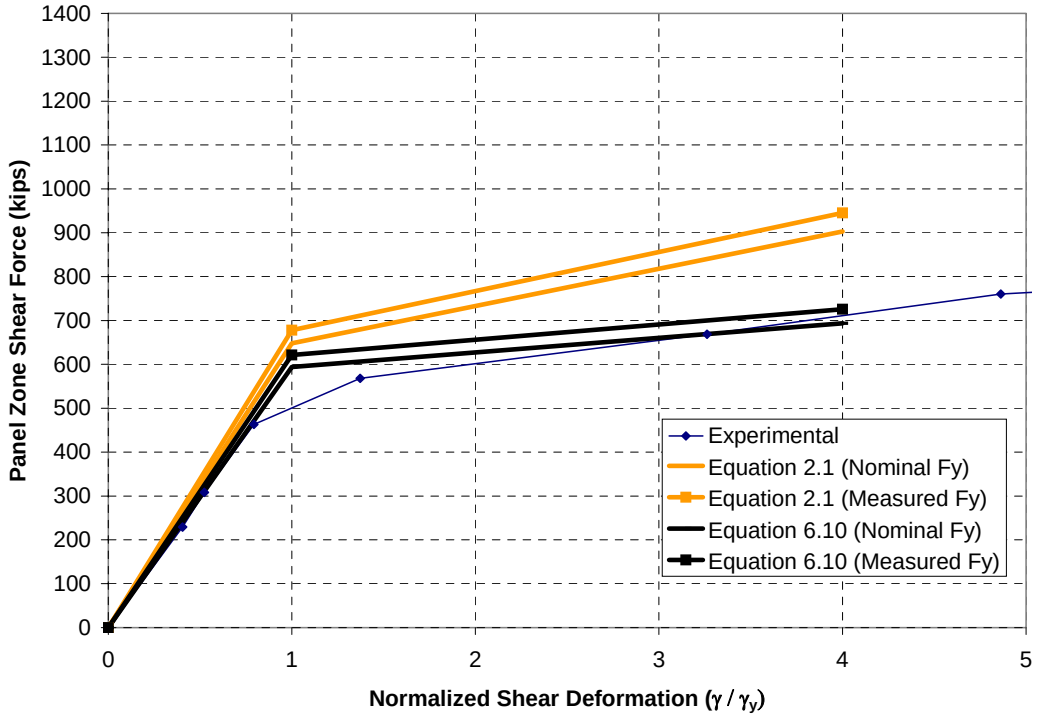


Figure 6.74: Comparison of Experimental Panel Zone Behavior to AISC (1997) and Modified Fielding and Huang Model (Equation 6.10), CR1

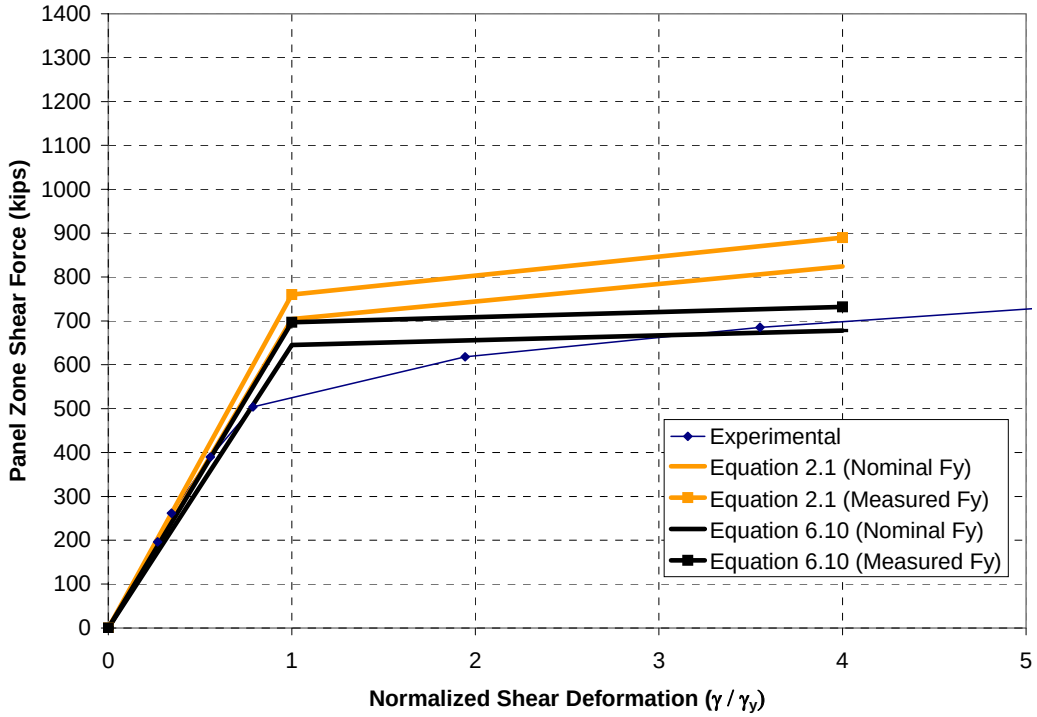


Figure 6.75: Comparison of Experimental Panel Zone Behavior to AISC (1997) and Modified Fielding and Huang Model (Equation 6.10), CR2

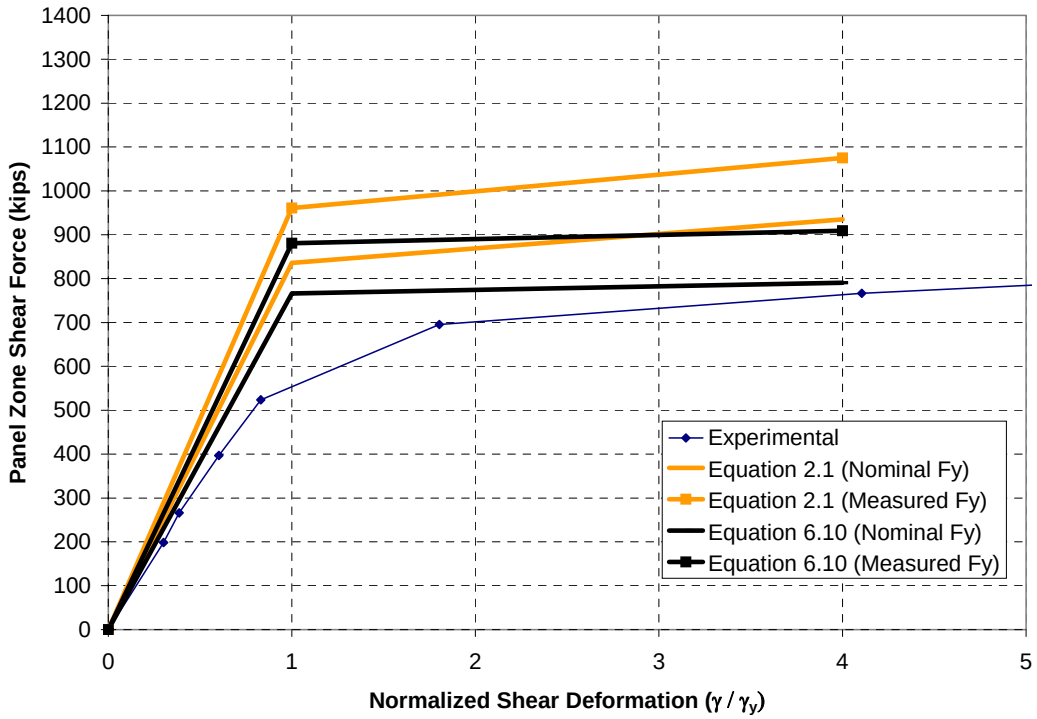


Figure 6.76: Comparison of Experimental Panel Zone Behavior to AISC (1997) and Modified Fielding and Huang Model (Equation 6.10), CR3

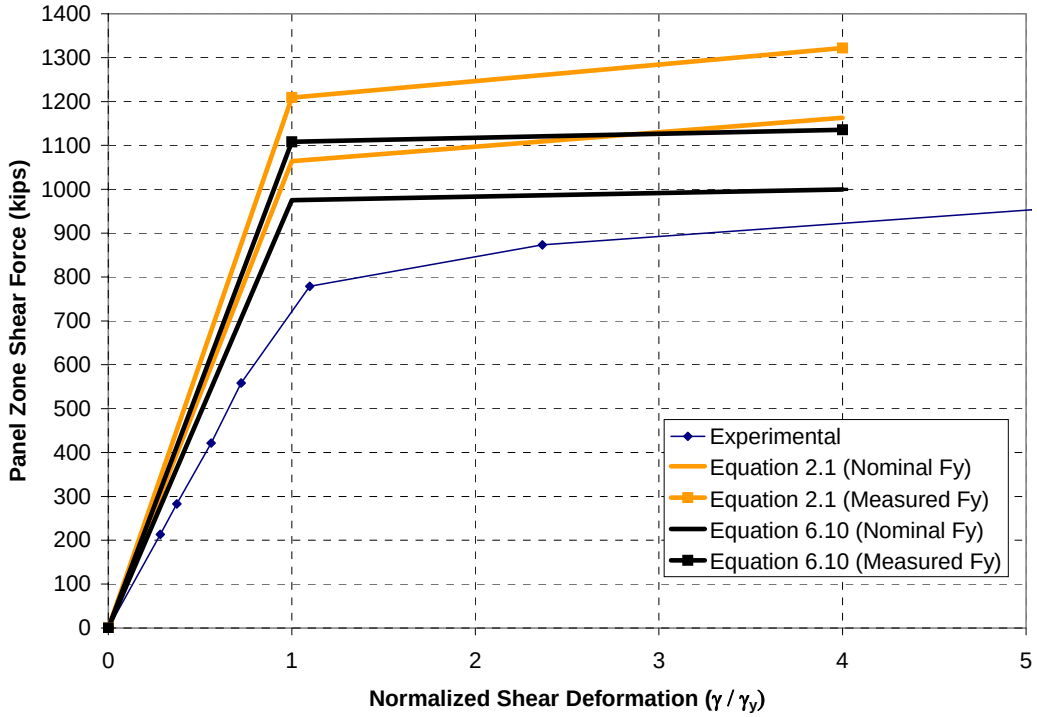


Figure 6.77: Comparison of Experimental Panel Zone Behavior to AISC (1997) and Modified Fielding and Huang Model (Equation 6.10), CR4R

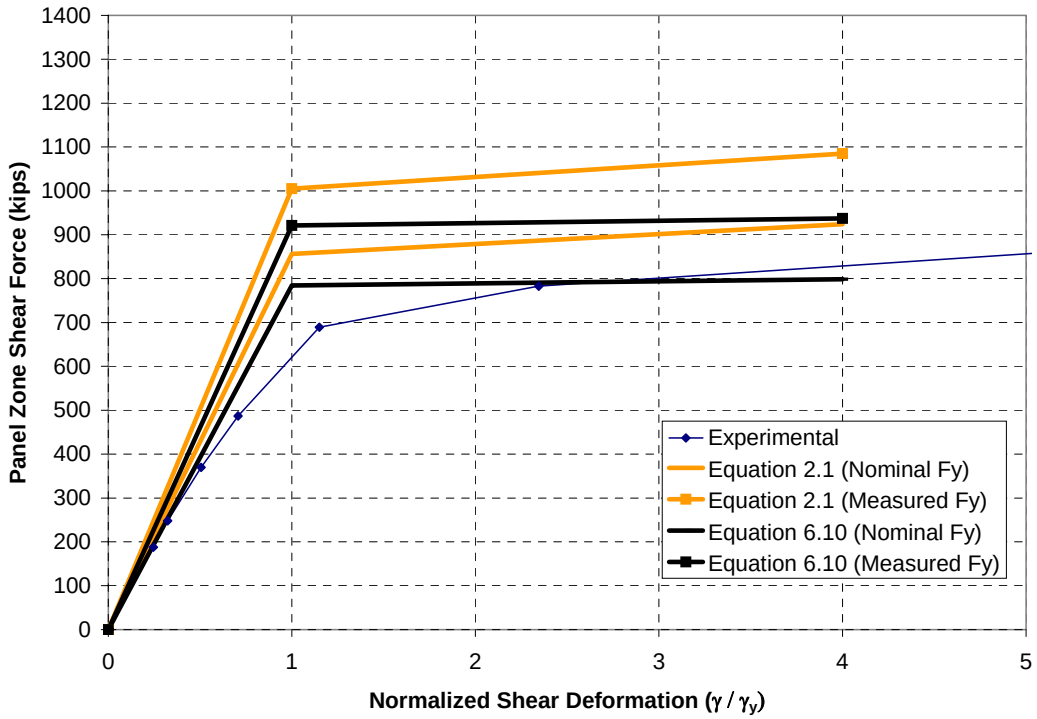


Figure 6.78: Comparison of Experimental Panel Zone Behavior to AISC (1997) and Modified Fielding and Huang Model (Equation 6.10), CR5

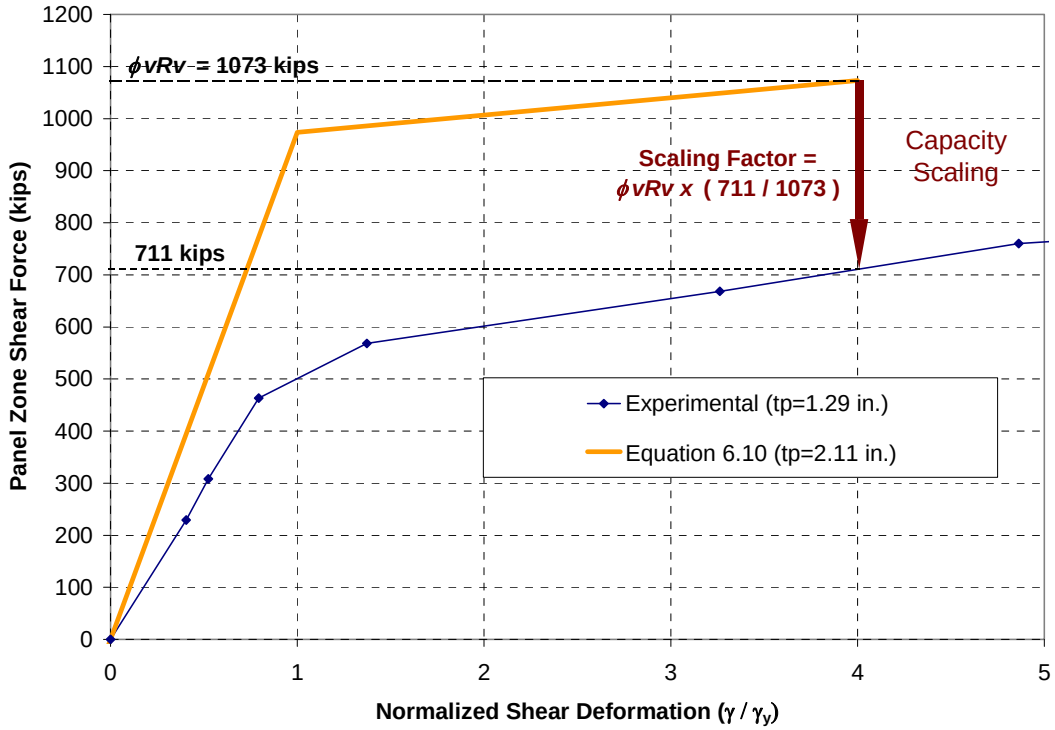


Figure 6.79: Schematic Explanation for Scaling of Panel Zone Capacity, Specimen CR1

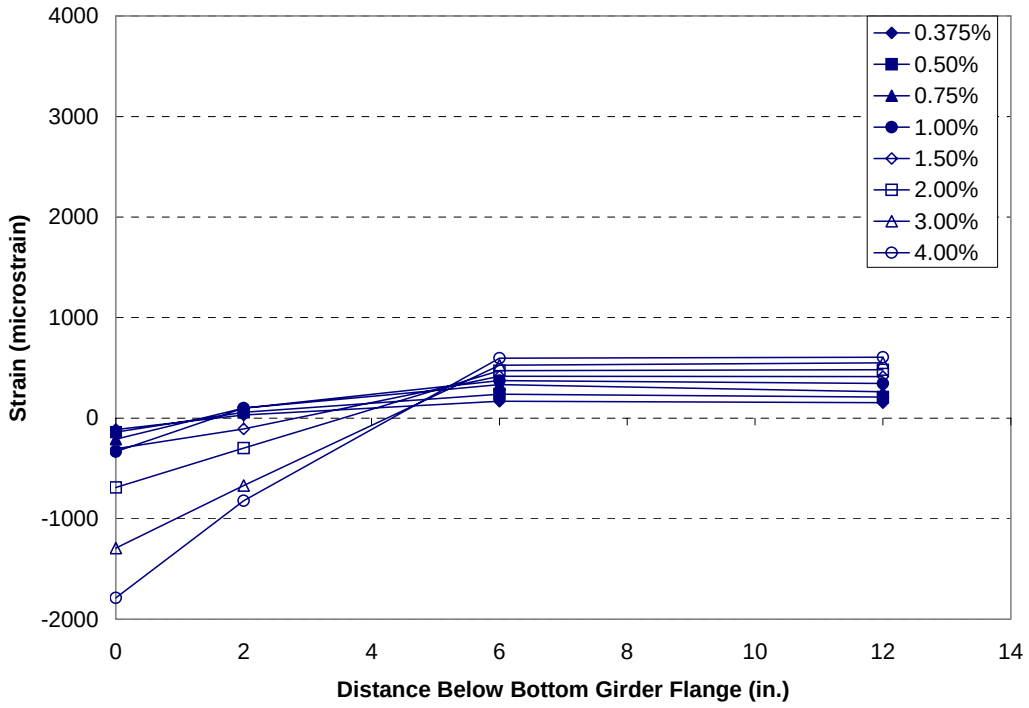


Figure 6.80: Longitudinal Strain on Inside Face of CR1 Column Flange Near Web (Bottom Girder Flange in Tension)

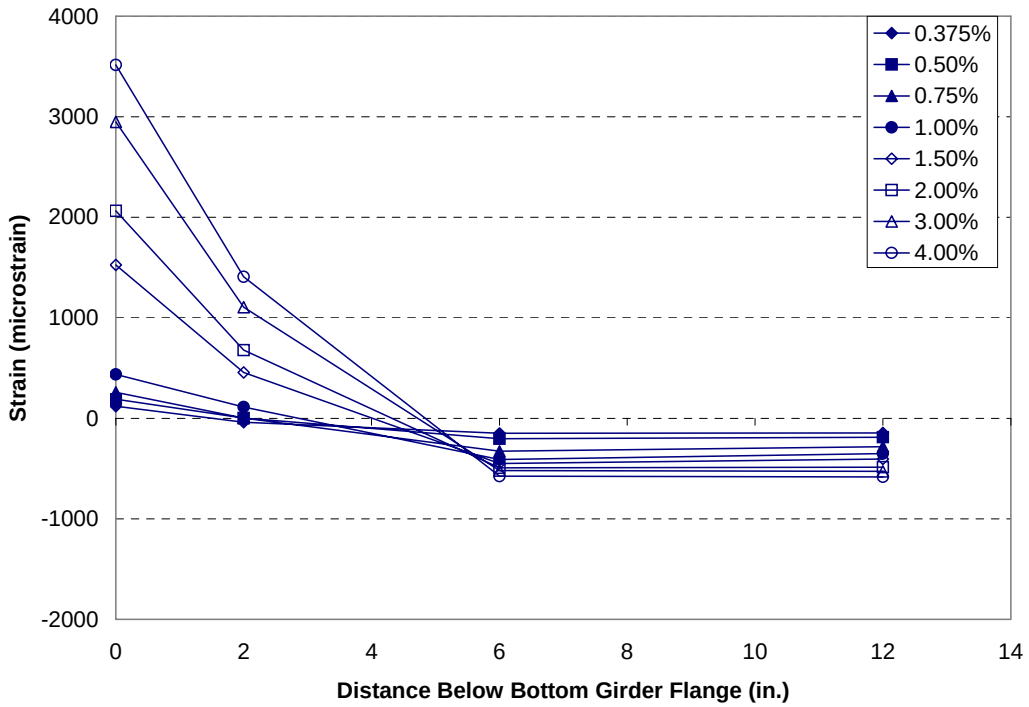


Figure 6.81: Longitudinal Strain on Inside Face of CR1 Column Flange Near Web (Bottom Girder Flange in Compression)

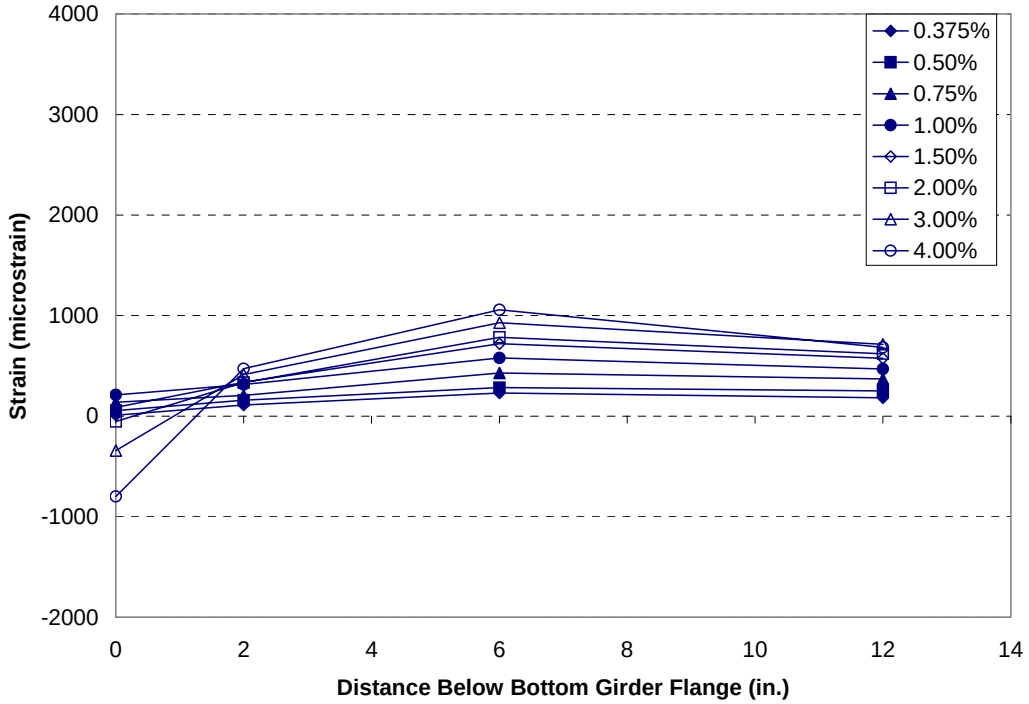


Figure 6.82: Longitudinal Strain on Inside Face of CR2 Column Flange Near Web (Bottom Girder Flange in Tension)

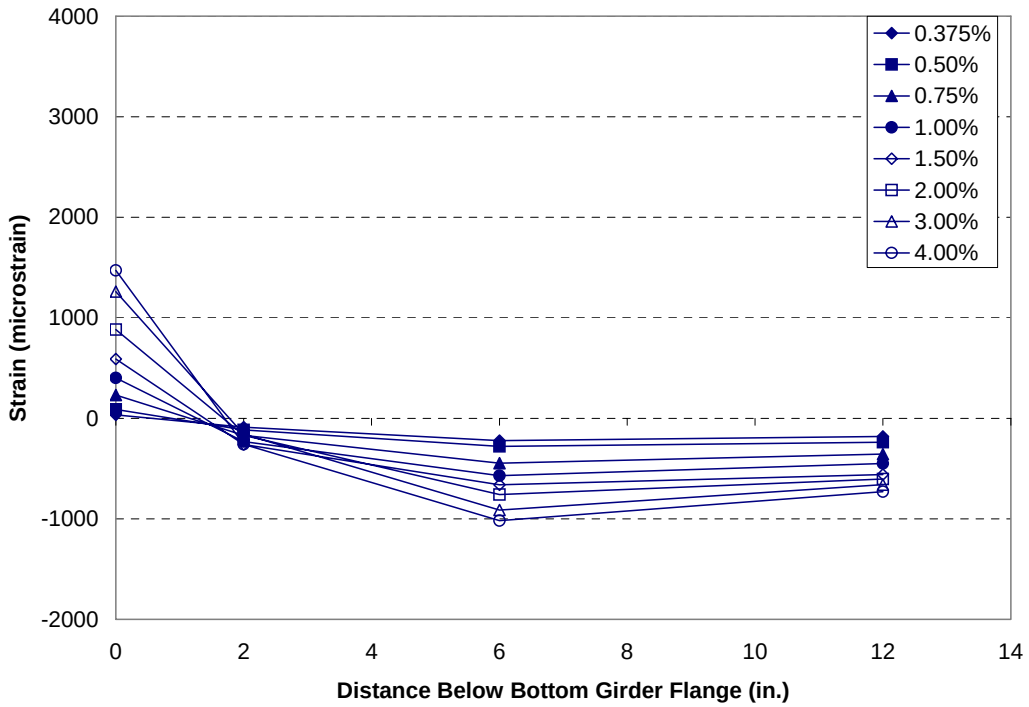


Figure 6.83: Longitudinal Strain on Inside Face of CR2 Column Flange Near Web (Bottom Girder Flange in Compression)

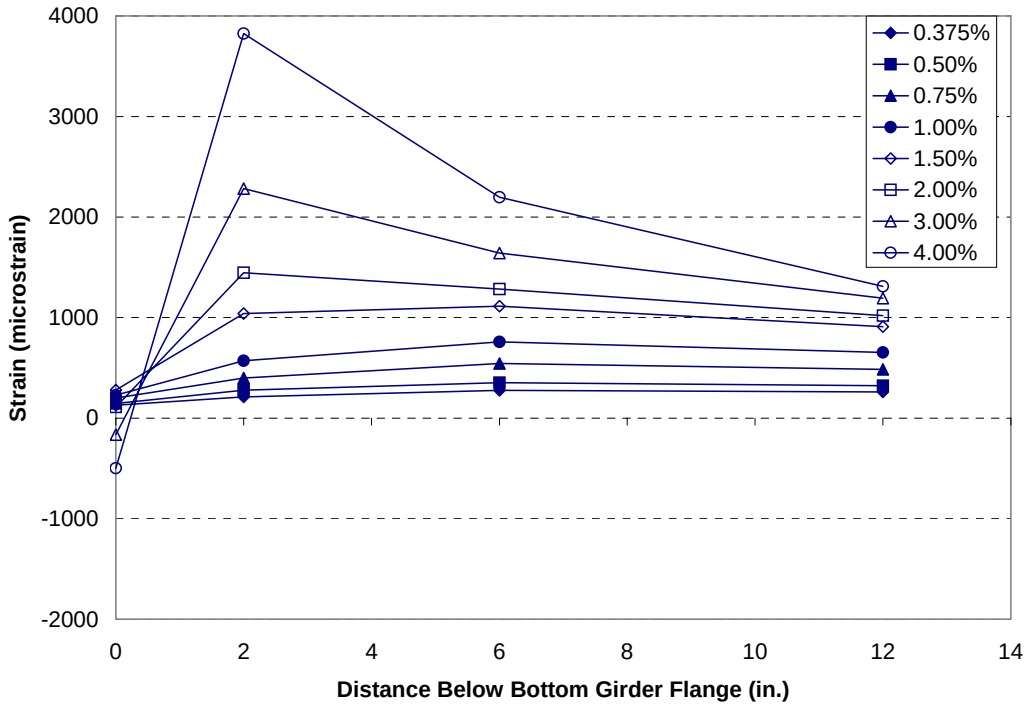


Figure 6.84: Longitudinal Strain on Inside Face of CR5 Column Flange Near Web (Bottom Girder Flange in Tension)

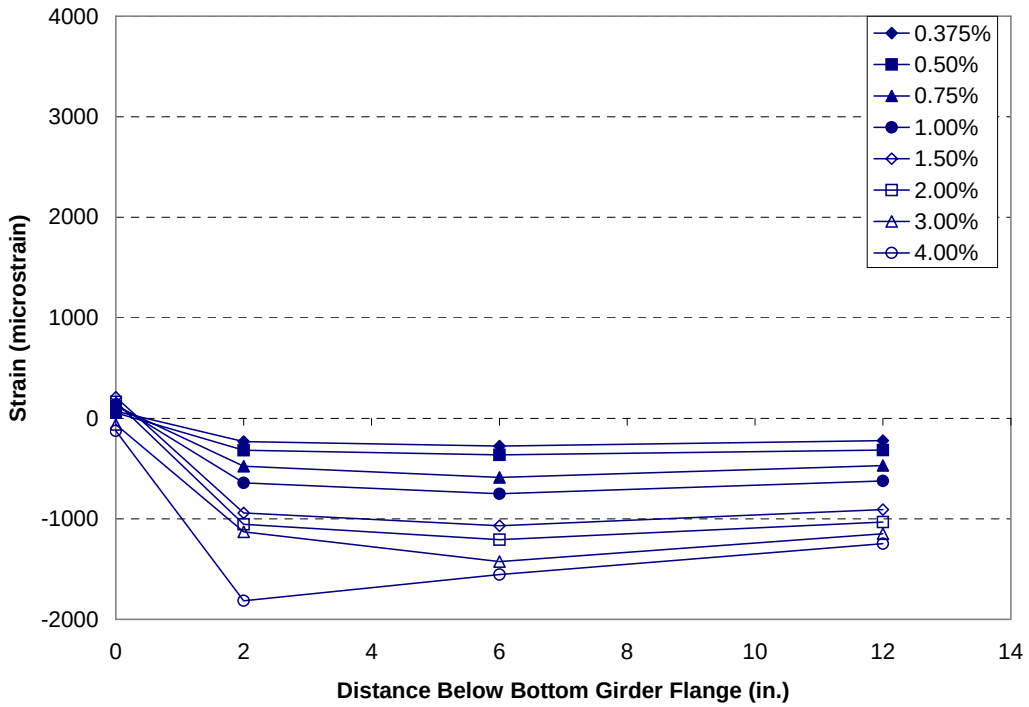


Figure 6.85: Longitudinal Strain on Inside Face of CR5 Column Flange Near Web (Bottom Girder Flange in Compression)

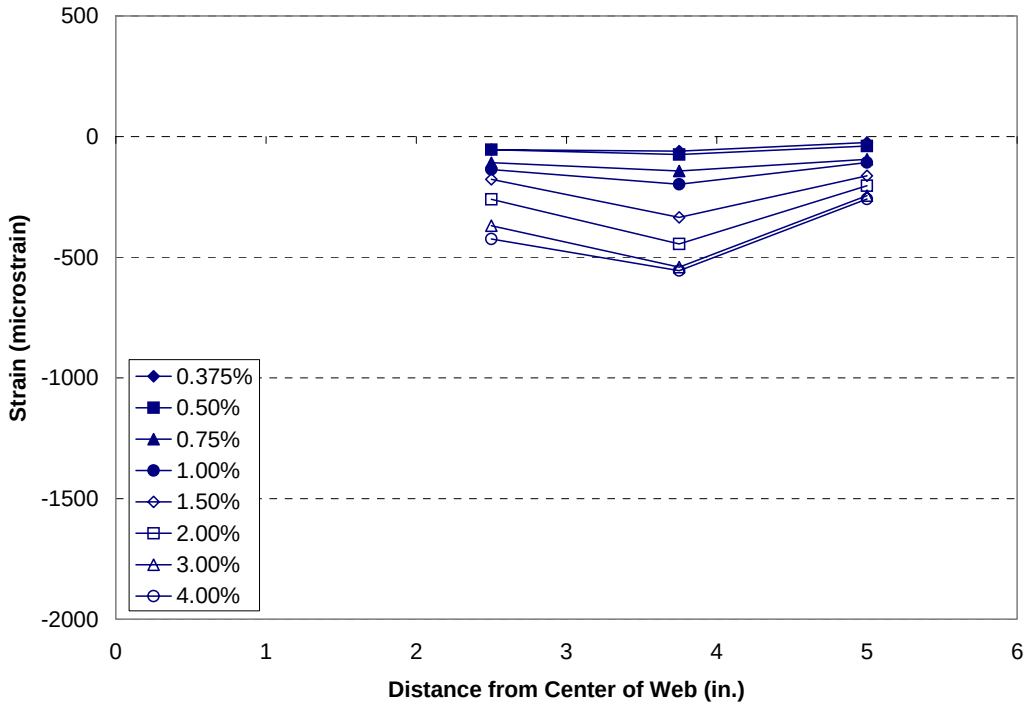


Figure 6.86: Transverse Strain on Inside Face of CR1 Column Flange at Location of Bottom Girder Flange (Bottom Girder Flange in Tension)

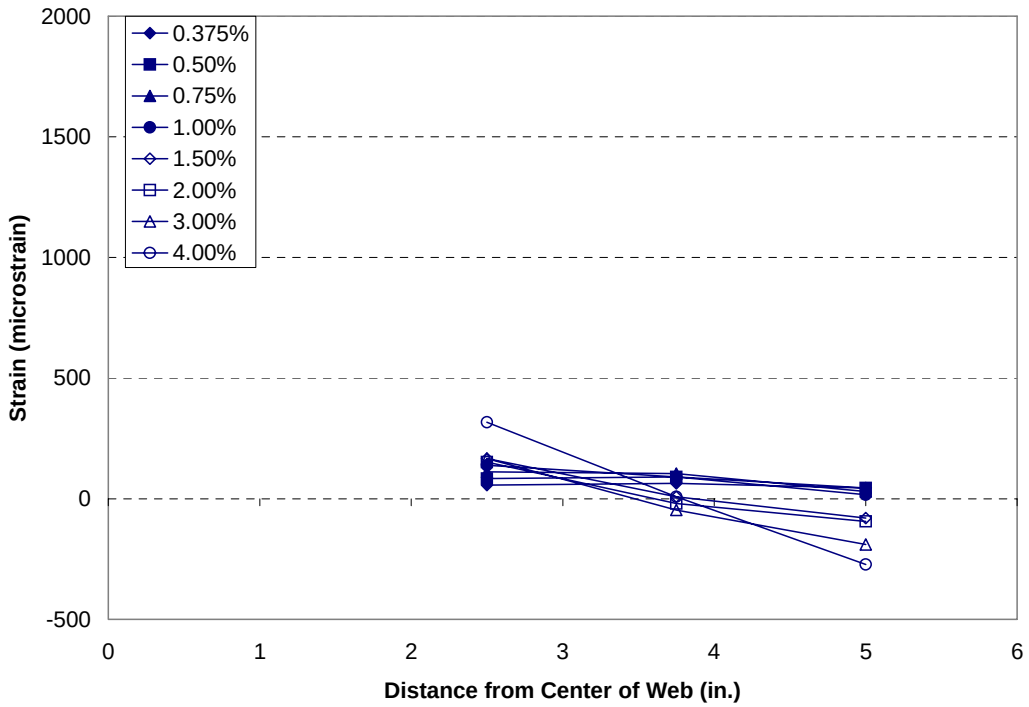


Figure 6.87: Transverse Strain on Inside Face of CR1 Column Flange at Location of Bottom Girder Flange (Bottom Girder Flange in Compression)

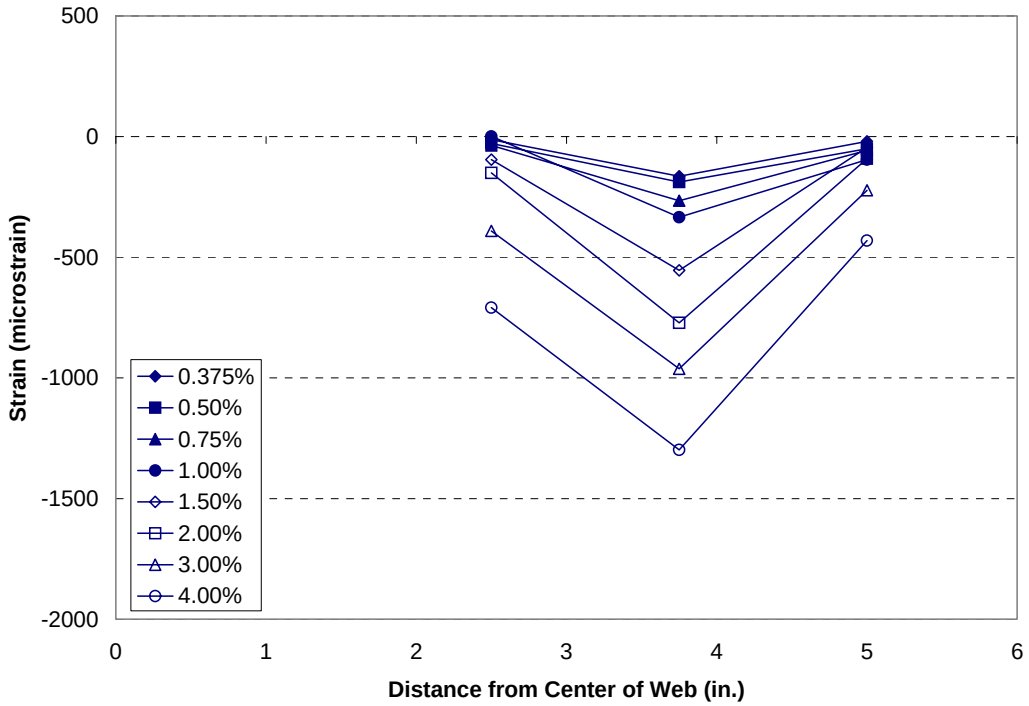


Figure 6.88: Transverse Strain on Inside Face of CR2 Column Flange at Location of Bottom Girder Flange (Bottom Girder Flange in Tension)

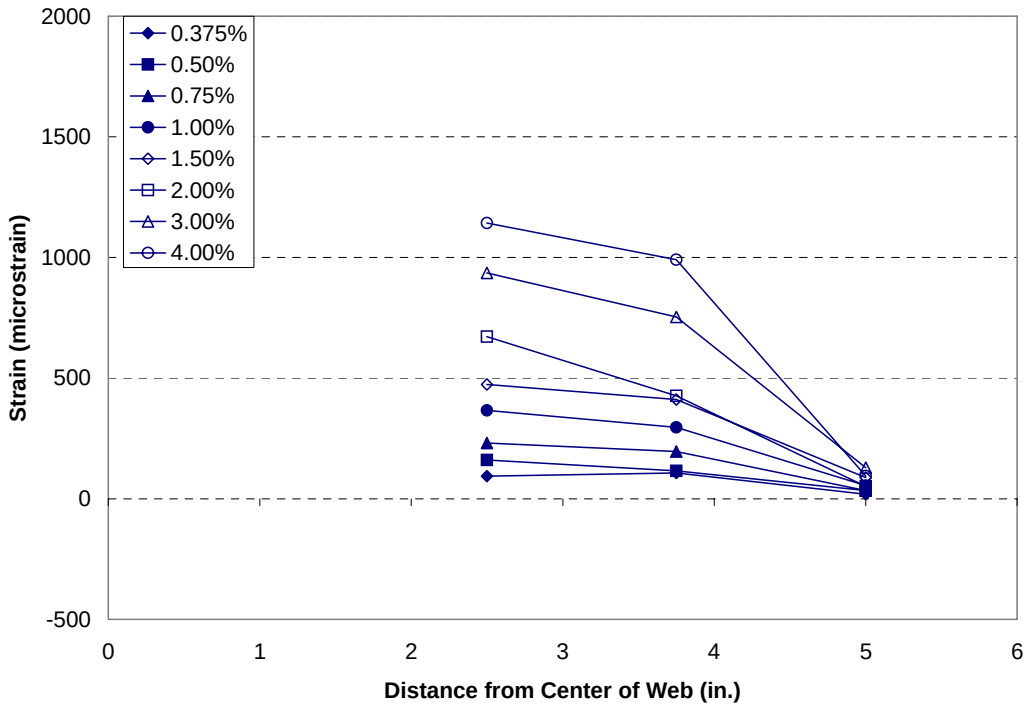


Figure 6.89: Transverse Strain on Inside Face of CR2 Column Flange at Location of Bottom Girder Flange (Bottom Girder Flange in Compression)

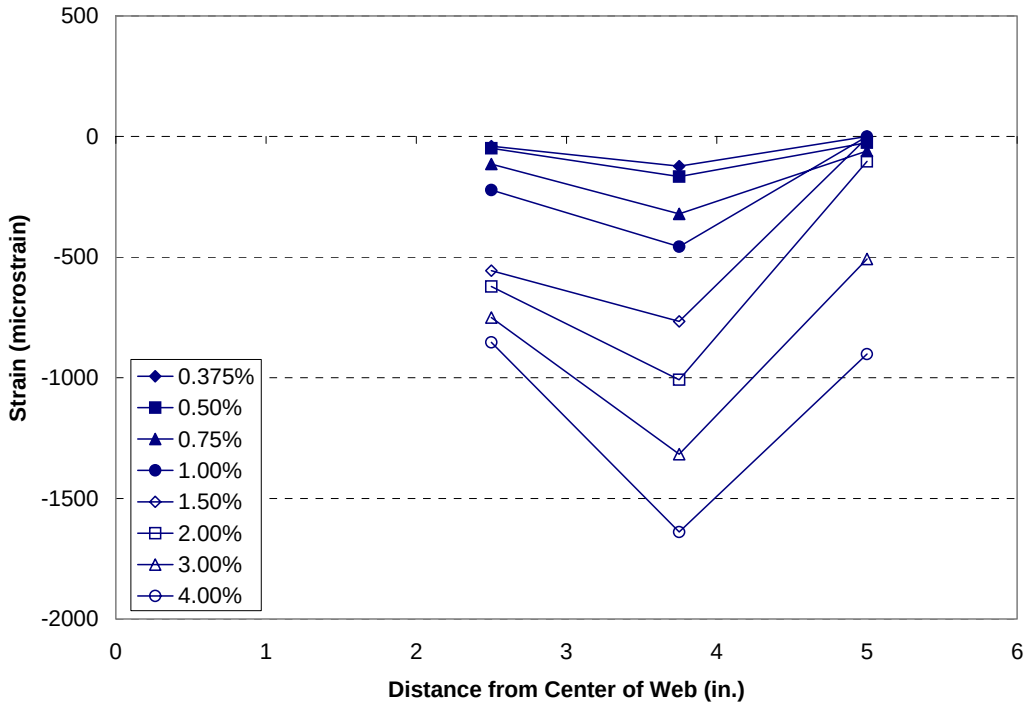


Figure 6.90: Transverse Strain on Inside Face of CR5 Column Flange at Location of Bottom Girder Flange (Bottom Girder Flange in Tension)

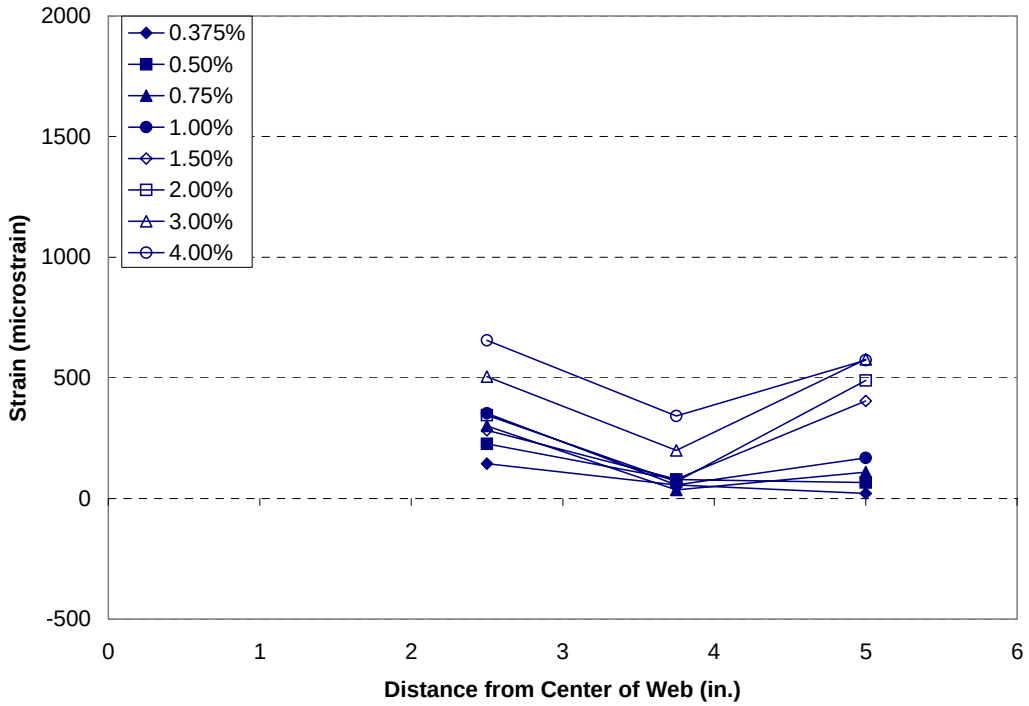


Figure 6.91: Transverse Strain on Inside Face of CR5 Column Flange at Location of Bottom Girder Flange (Bottom Girder Flange in Compression)

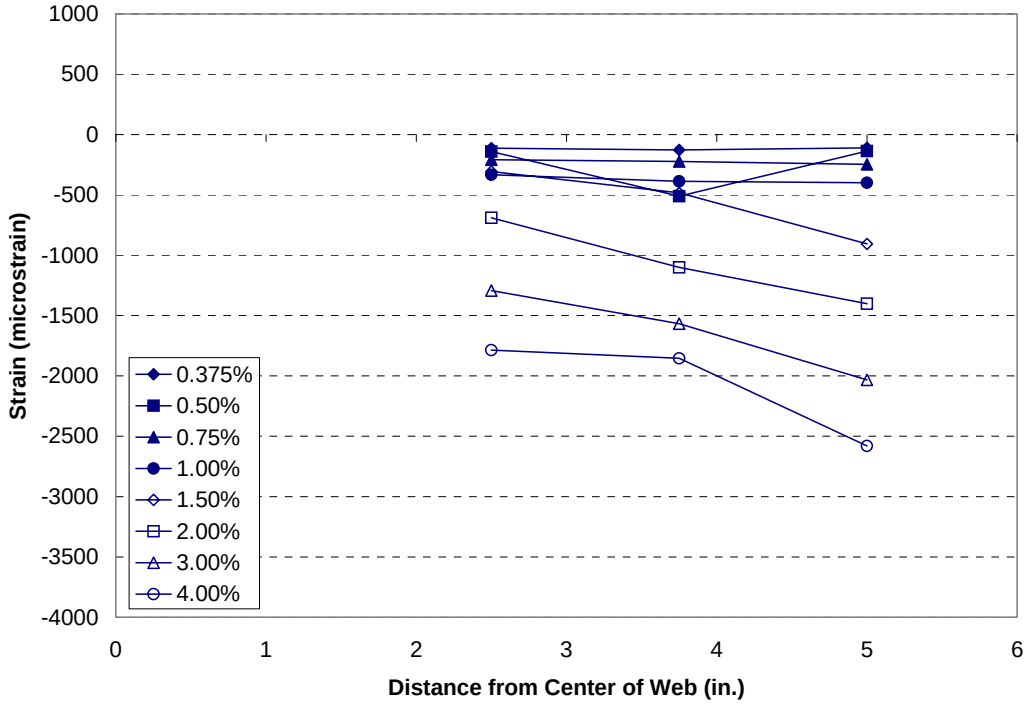


Figure 6.92: Longitudinal Strain in Transverse Direction on Inside Face of CR1 Column Flange (Bottom Girder Flange in Tension)

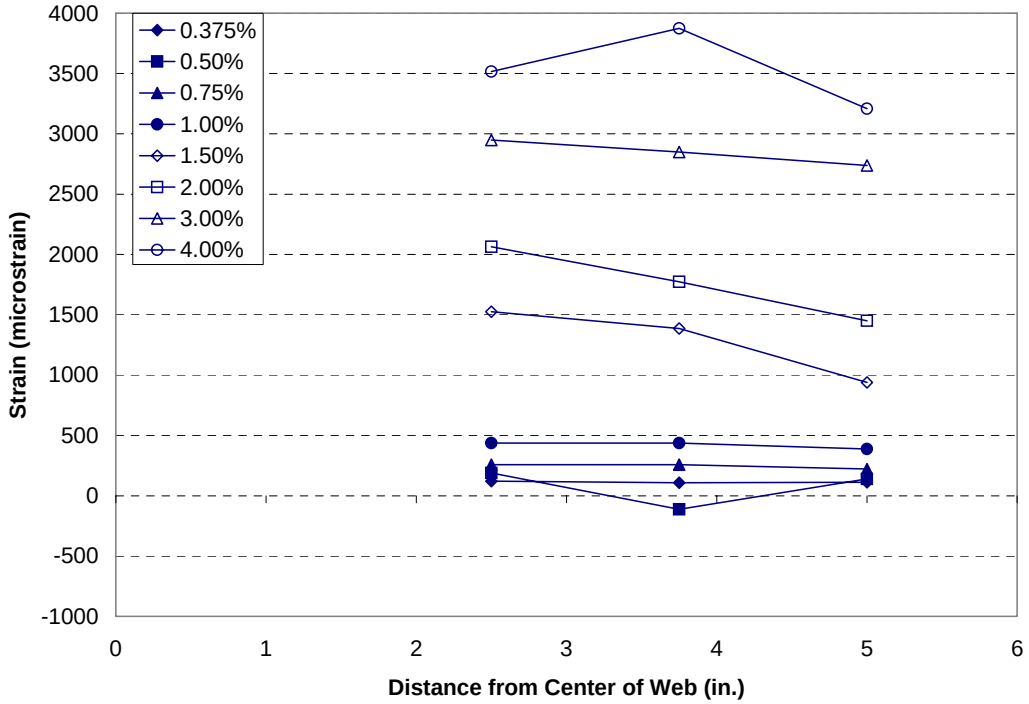


Figure 6.93: Longitudinal Strain in Transverse Direction on Inside Face of CR1 Column Flange (Bottom Girder Flange in Compression)

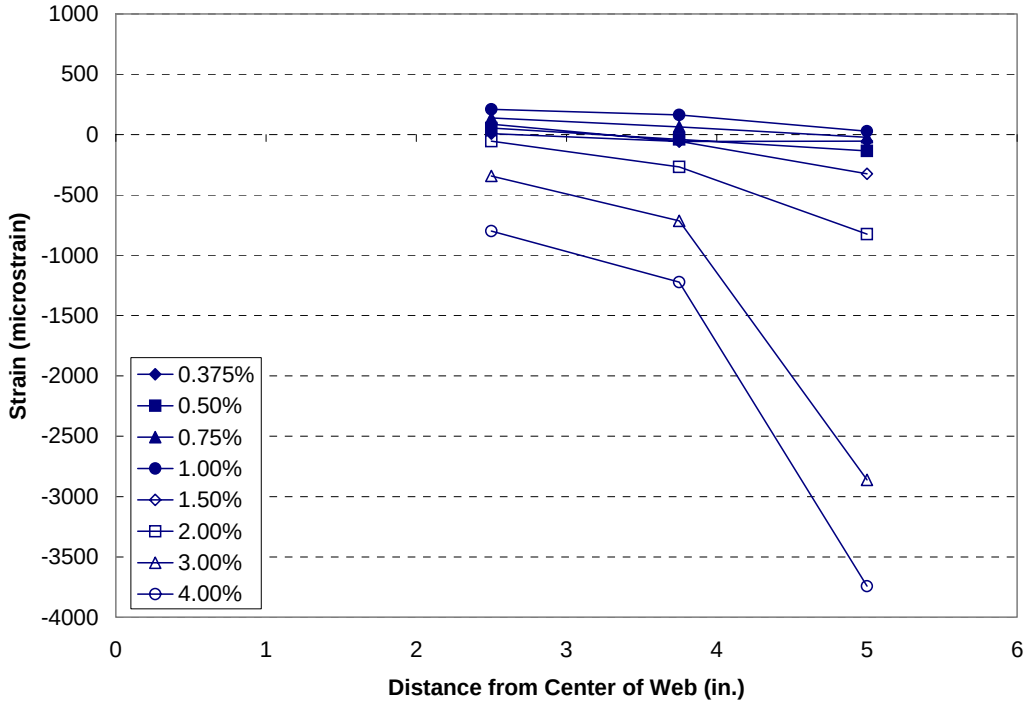


Figure 6.94: Longitudinal Strain in Transverse Direction on Inside Face of CR2 Column Flange (Bottom Girder Flange in Tension)

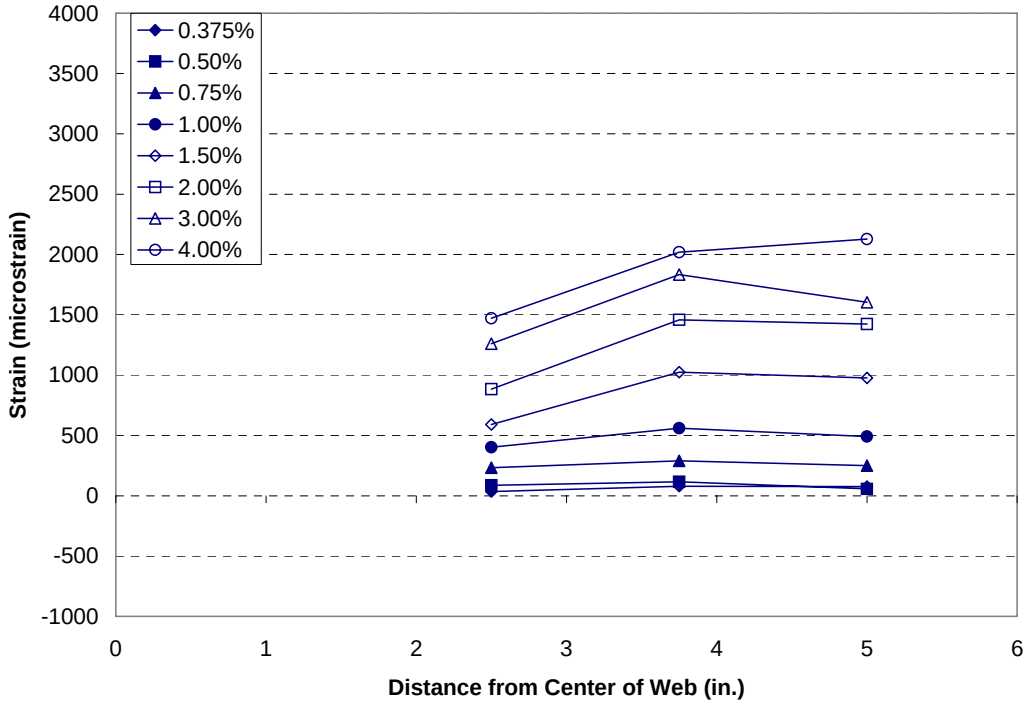


Figure 6.95: Longitudinal Strain in Transverse Direction on Inside Face of CR2 Column Flange (Bottom Girder Flange in Compression)

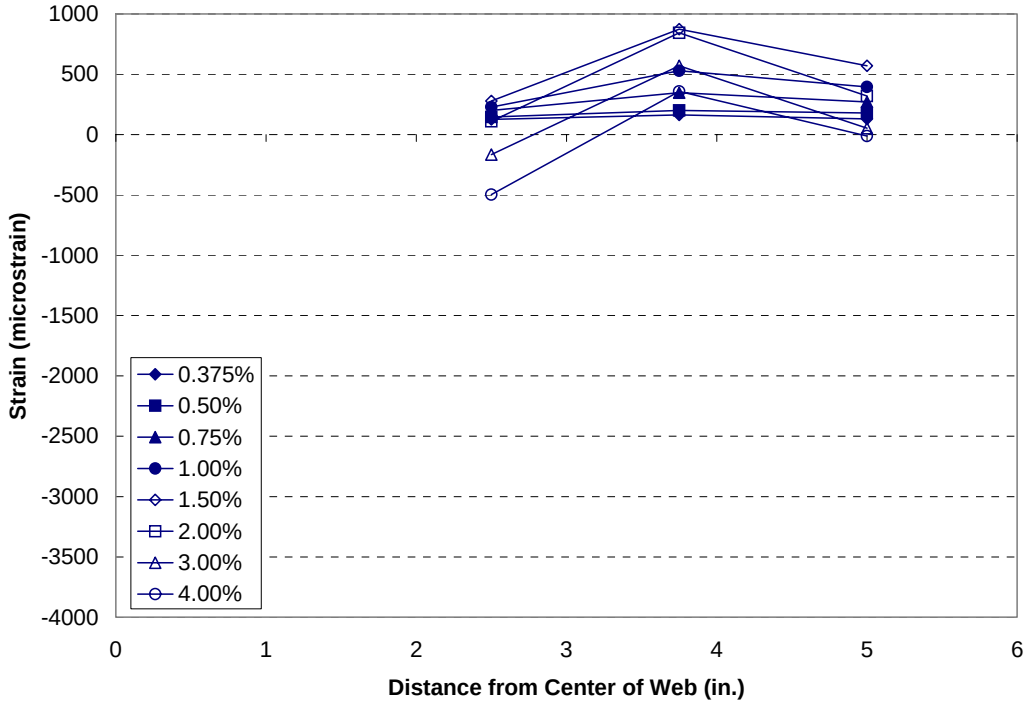


Figure 6.96: Longitudinal Strain in Transverse Direction on Inside Face of CR5 Column Flange (Bottom Girder Flange in Tension)

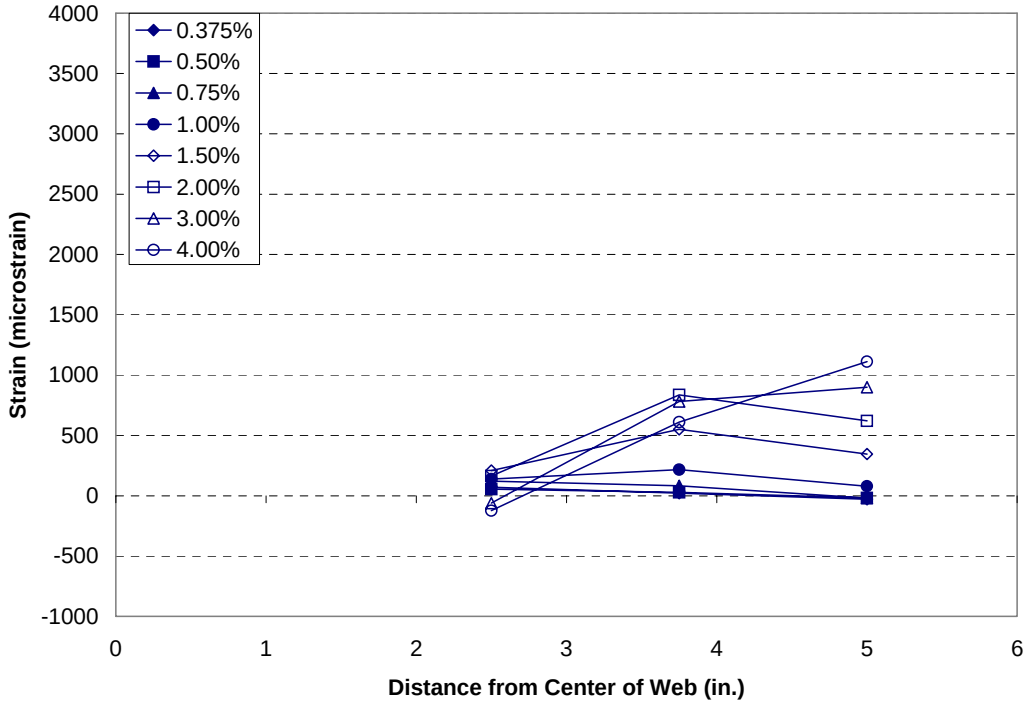


Figure 6.97: Longitudinal Strain in Transverse Direction on Inside Face of CR5 Column Flange (Bottom Girder Flange in Compression)

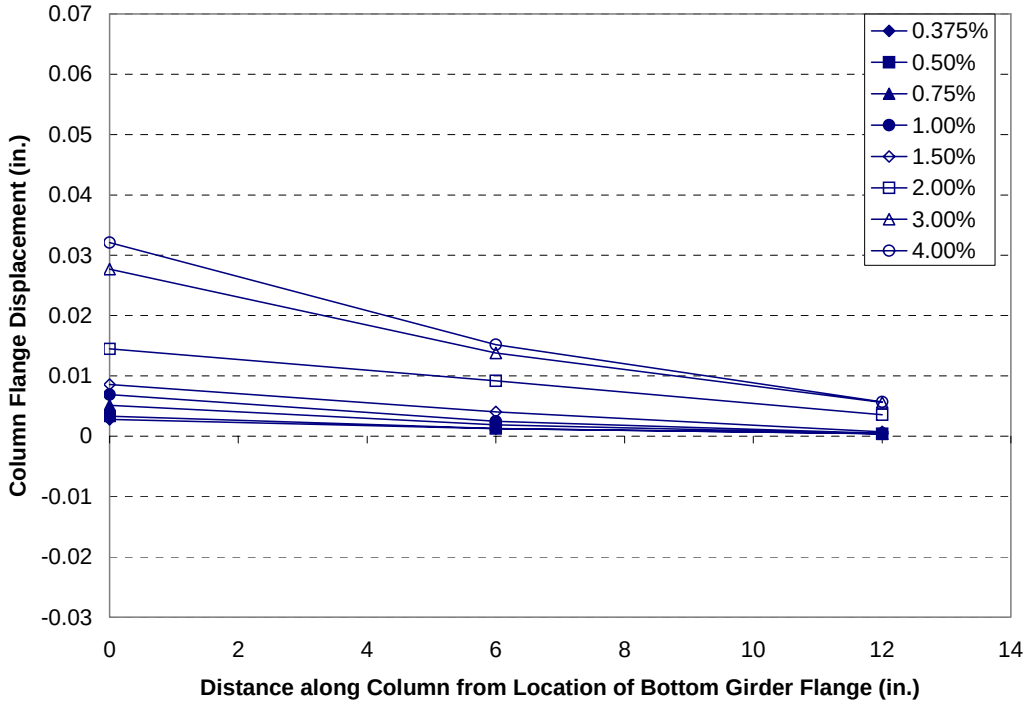


Figure 6.98: Specimen CR1 Column Flange Displacement Along Column Length (Bottom Girder Flange in Tension)

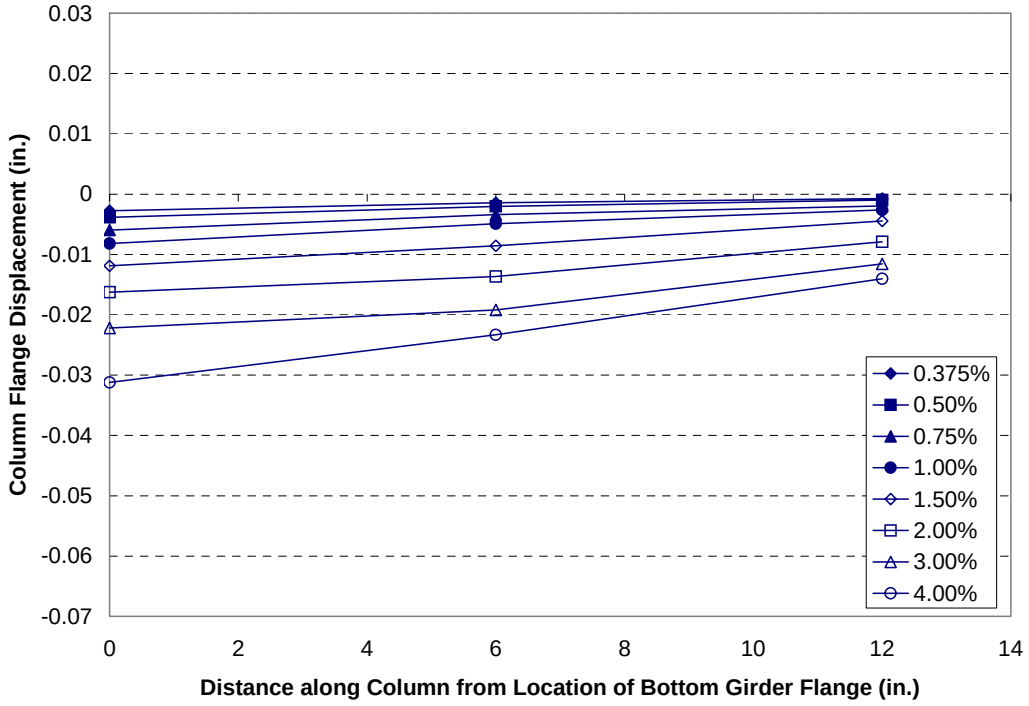


Figure 6.99: Specimen CR1 Column Flange Displacement Along Column Length (Bottom Girder Flange in Compression)

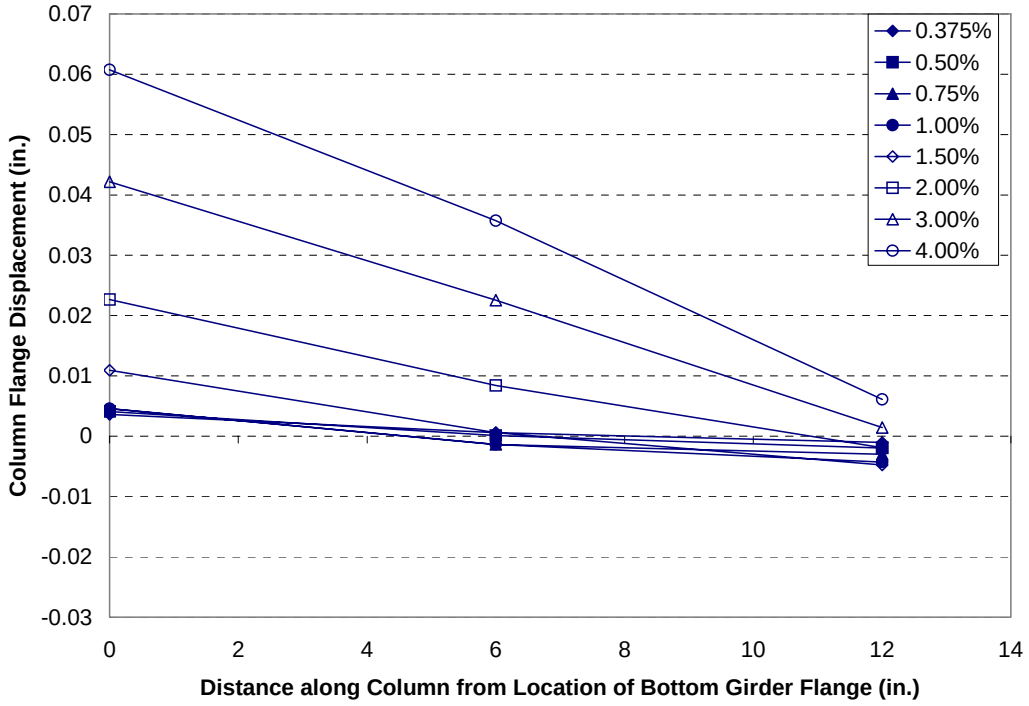


Figure 6.100: Specimen CR5 Column Flange Displacement Along Column Length (Bottom Girder Flange in Tension)

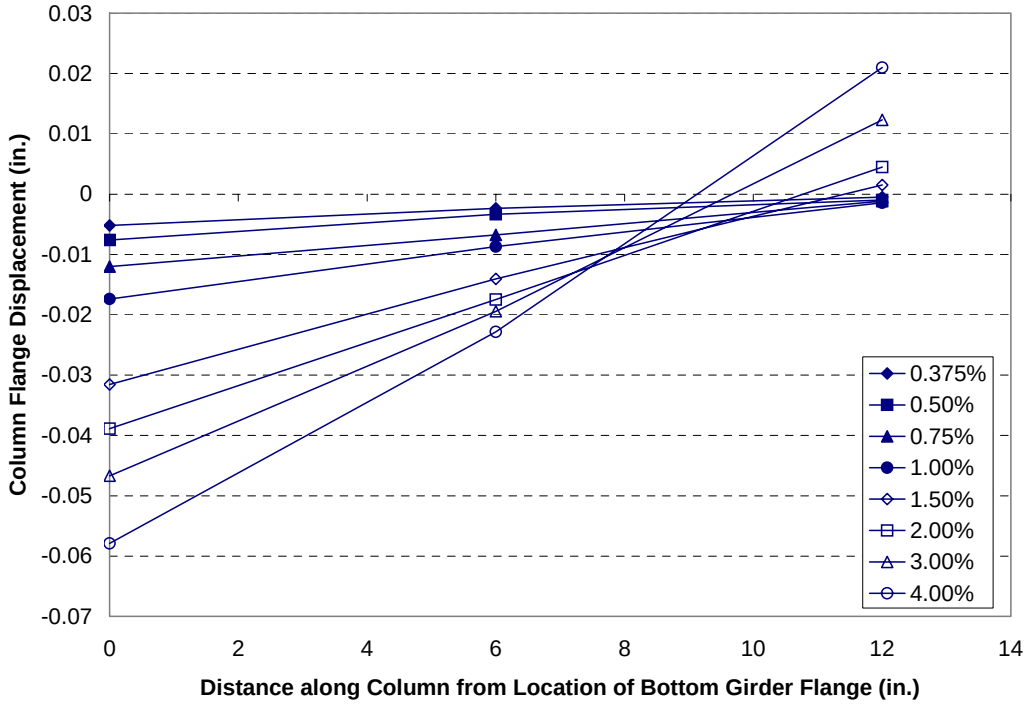


Figure 6.101: Specimen CR5 Column Flange Displacement Along Column Length (Bottom Girder Flange in Compression)

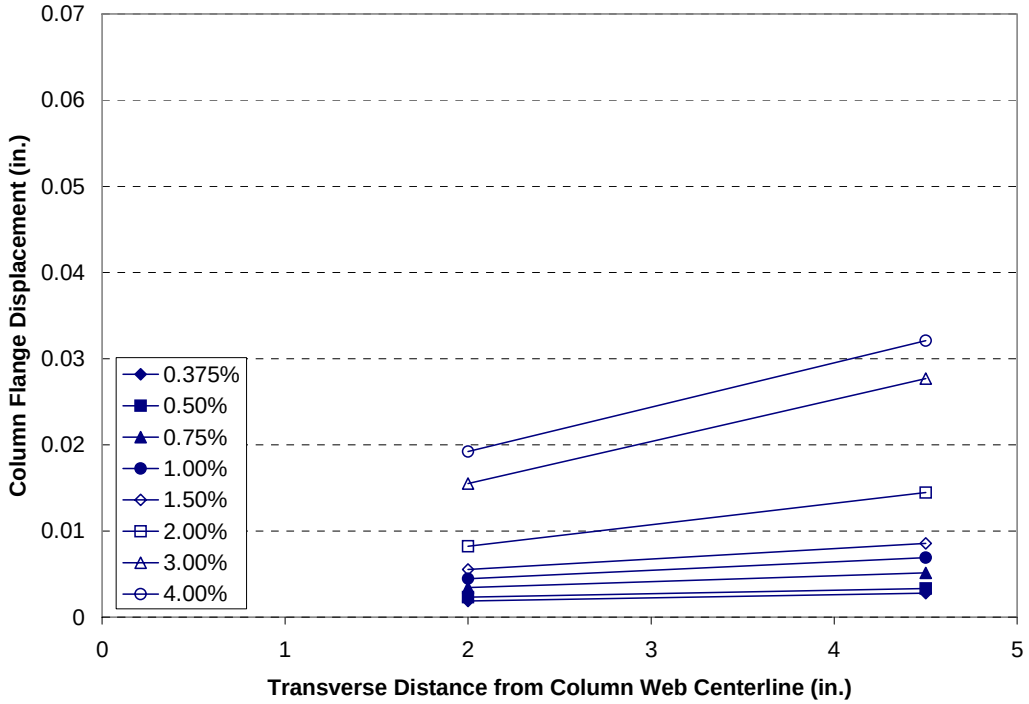


Figure 6.102: Specimen CR1 Column Flange Displacement Transverse to Column Length (Bottom Girder Flange in Tension)

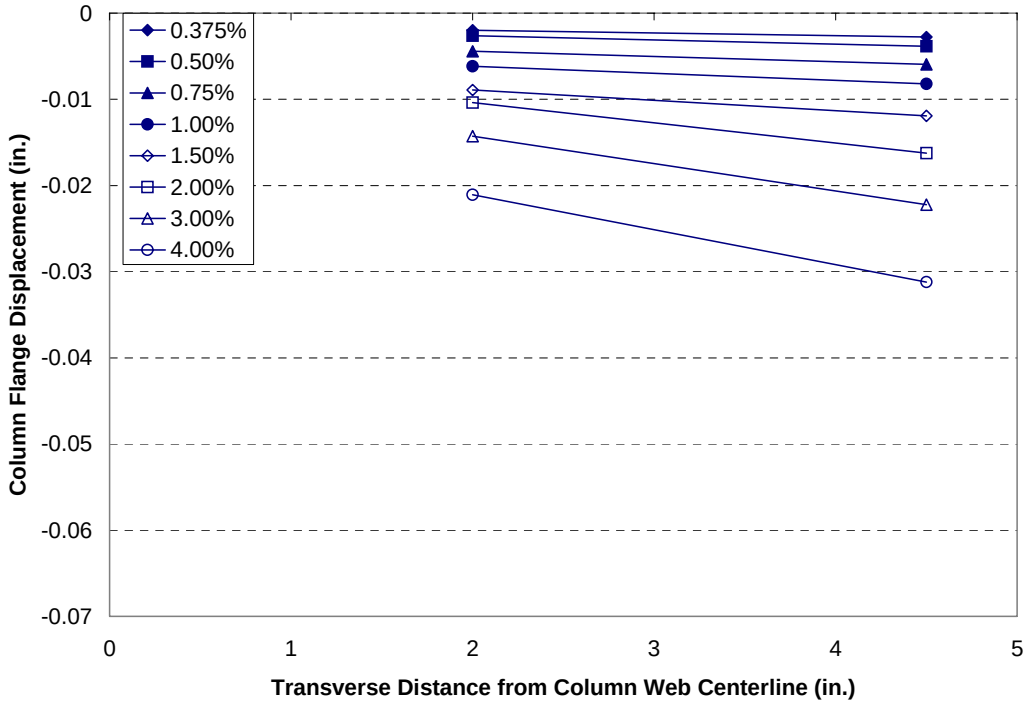


Figure 6.103: Specimen CR1 Column Flange Displacement Transverse to Column Length (Bottom Girder Flange in Compression)

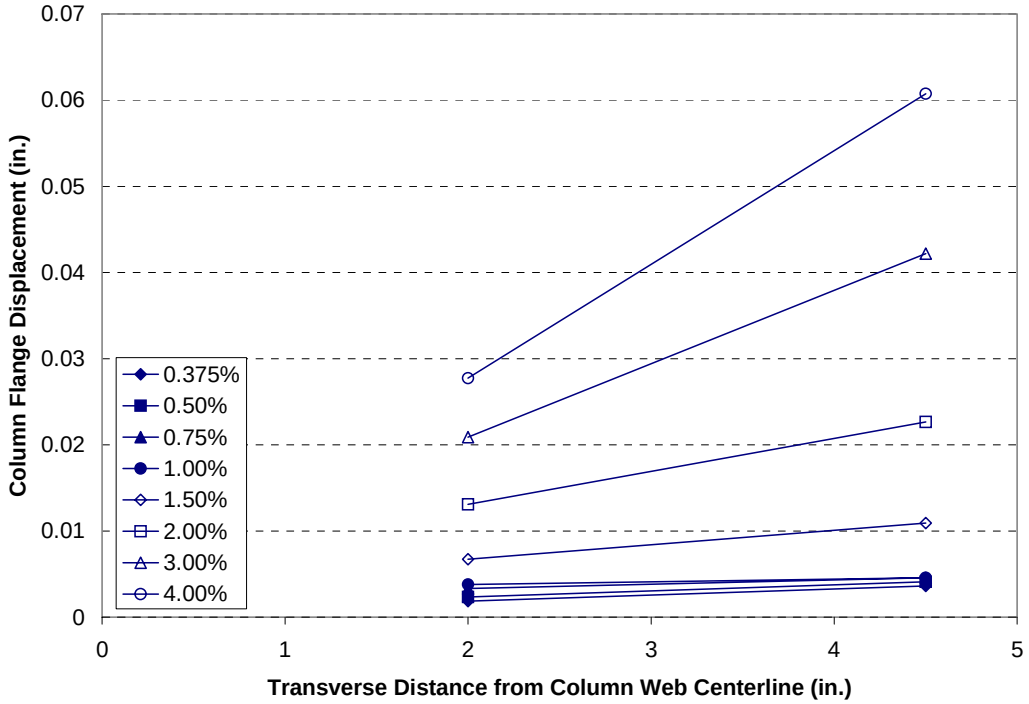


Figure 6.104: Specimen CR5 Column Flange Displacement Transverse to Column Length (Bottom Girder Flange in Tension)

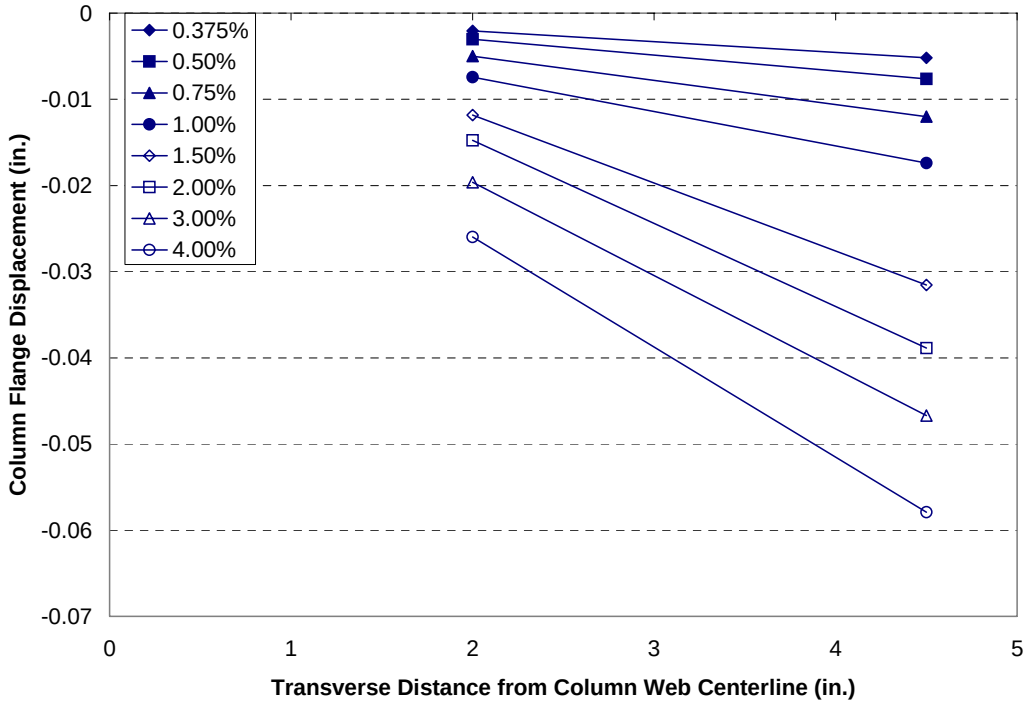


Figure 6.105: Specimen CR5 Column Flange Displacement Transverse to Column Length (Bottom Girder Flange in Compression)

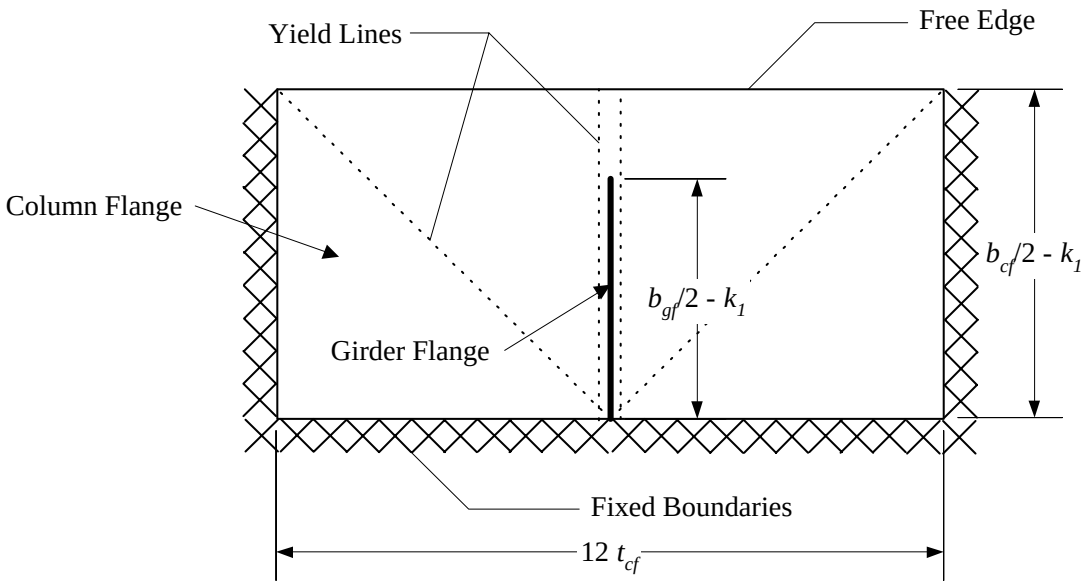


Figure 6.106: Assumed Yield Line Pattern in Column Flange Due to LFB

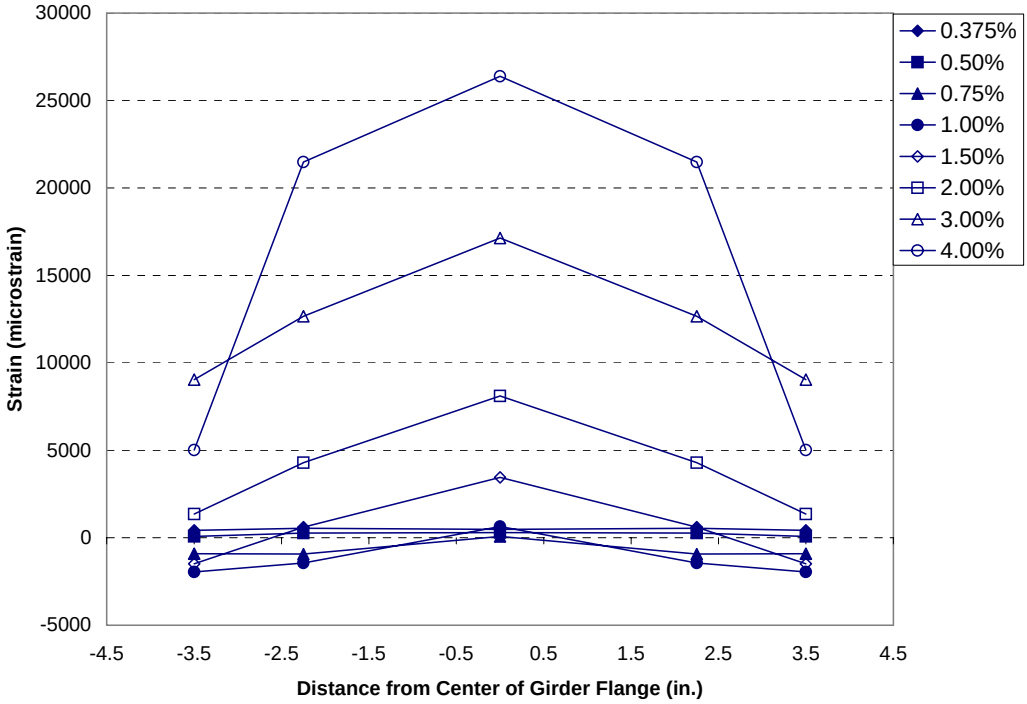


Figure 6.107: Longitudinal Strain on Specimen CR1 West Girder Top Flange near Column Flange (Girder Flange in Tension)

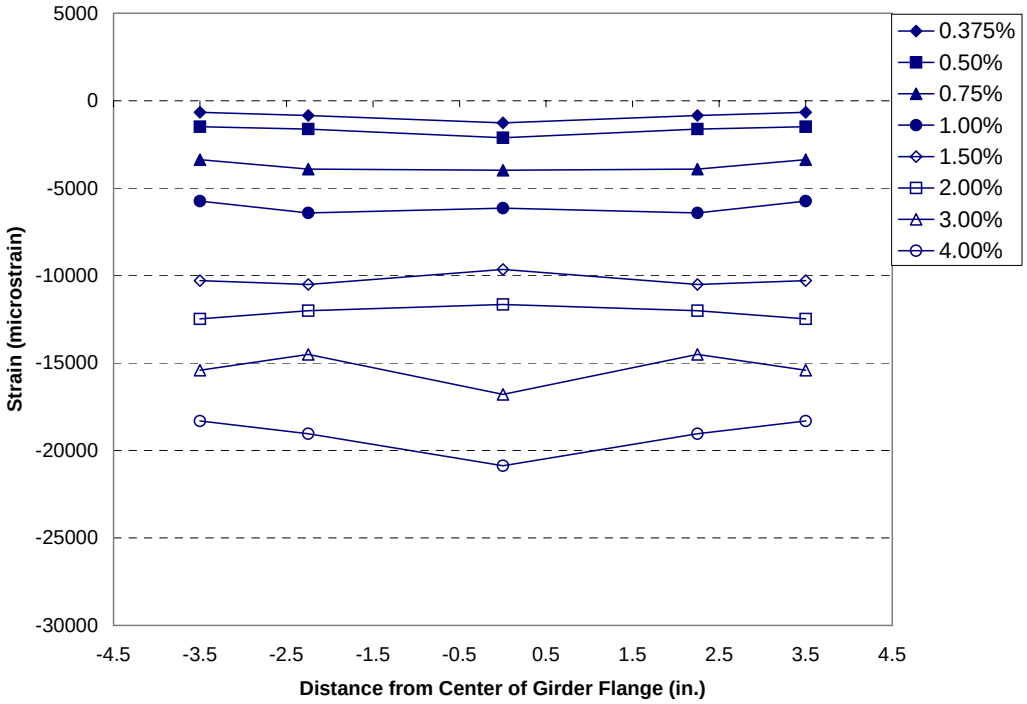


Figure 6.108: Longitudinal Strain on Specimen CR1 West Girder Top Flange near Column Flange (Girder Flange in Compression)

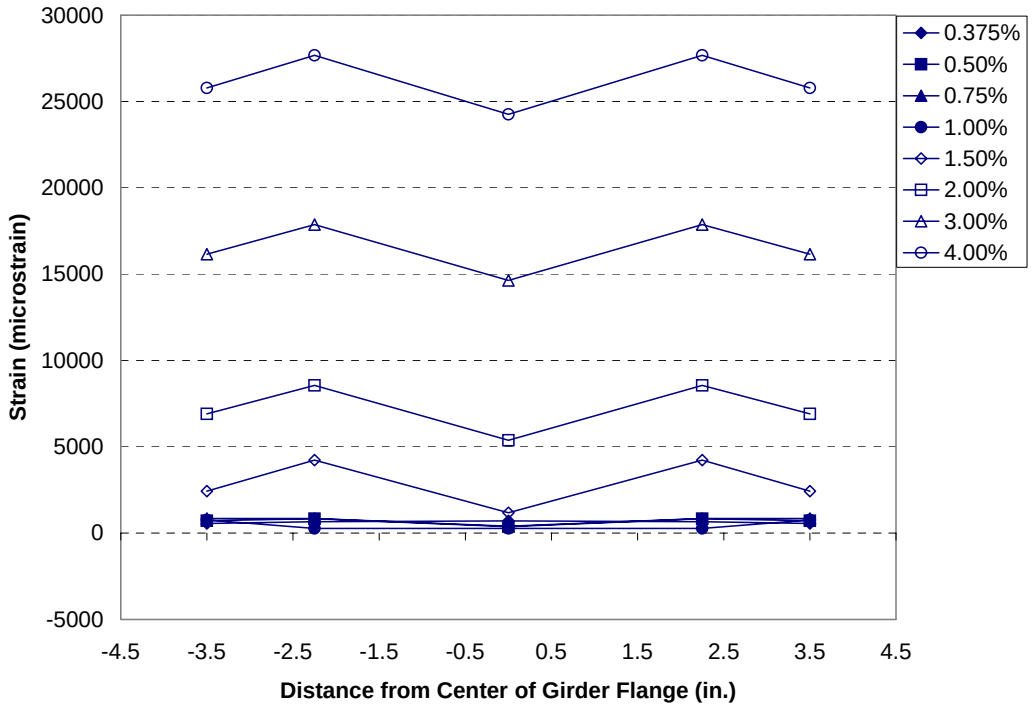


Figure 6.109: Longitudinal Strain on Specimen CR2 West Girder Top Flange near Column Flange (Girder Flange in Tension)

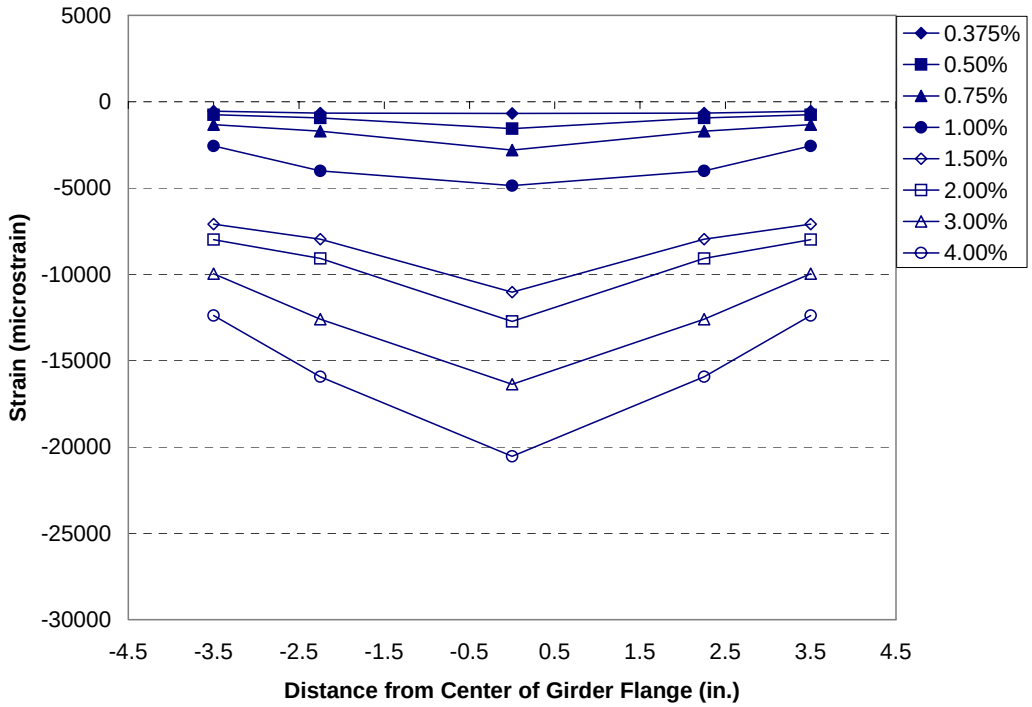


Figure 6.110: Longitudinal Strain on Specimen CR2 West Girder Top Flange near Column Flange (Girder Flange in Compression)

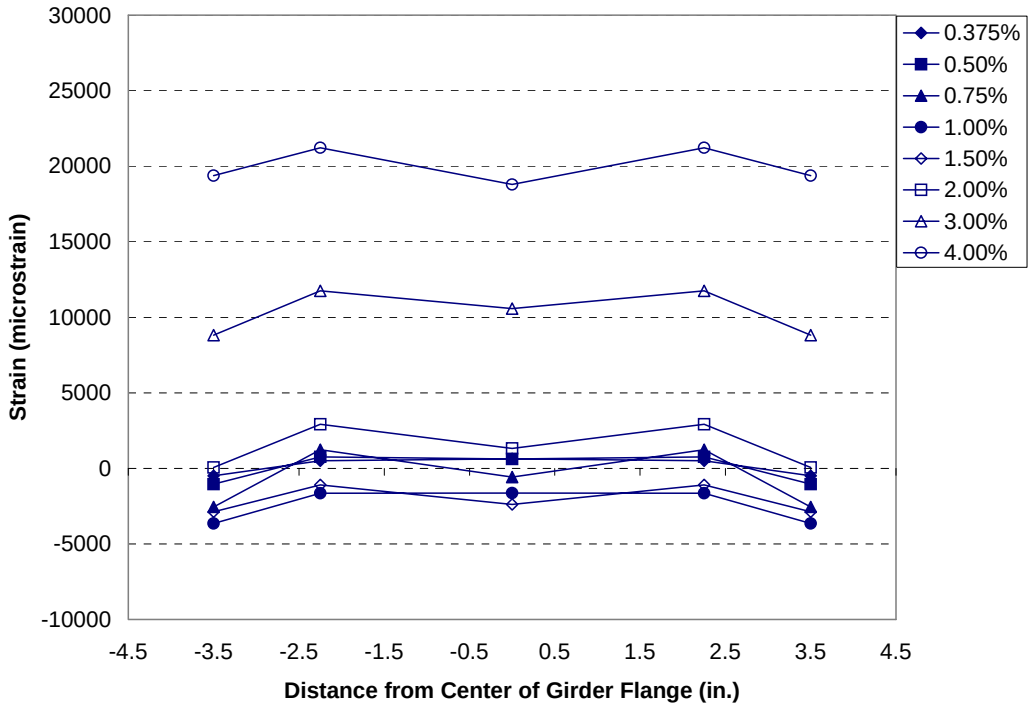


Figure 6.111: Longitudinal Strain on Specimen CR3 West Girder Top Flange near Column Flange (Girder Flange in Tension)

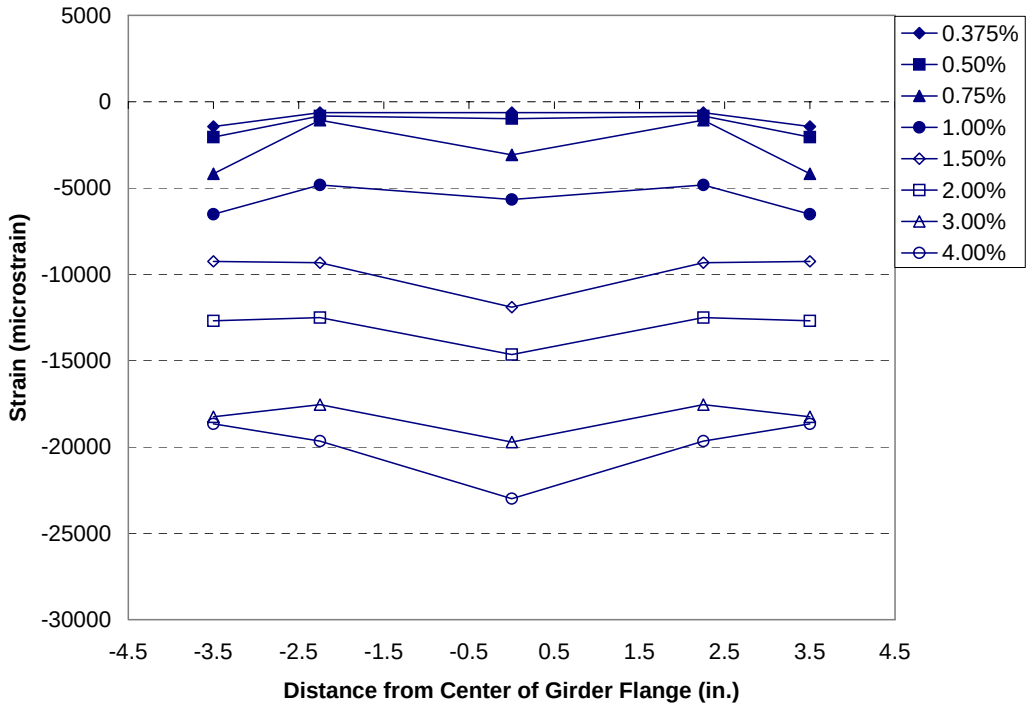


Figure 6.112: Longitudinal Strain on Specimen CR3 West Girder Top Flange near Column Flange (Girder Flange in Compression)

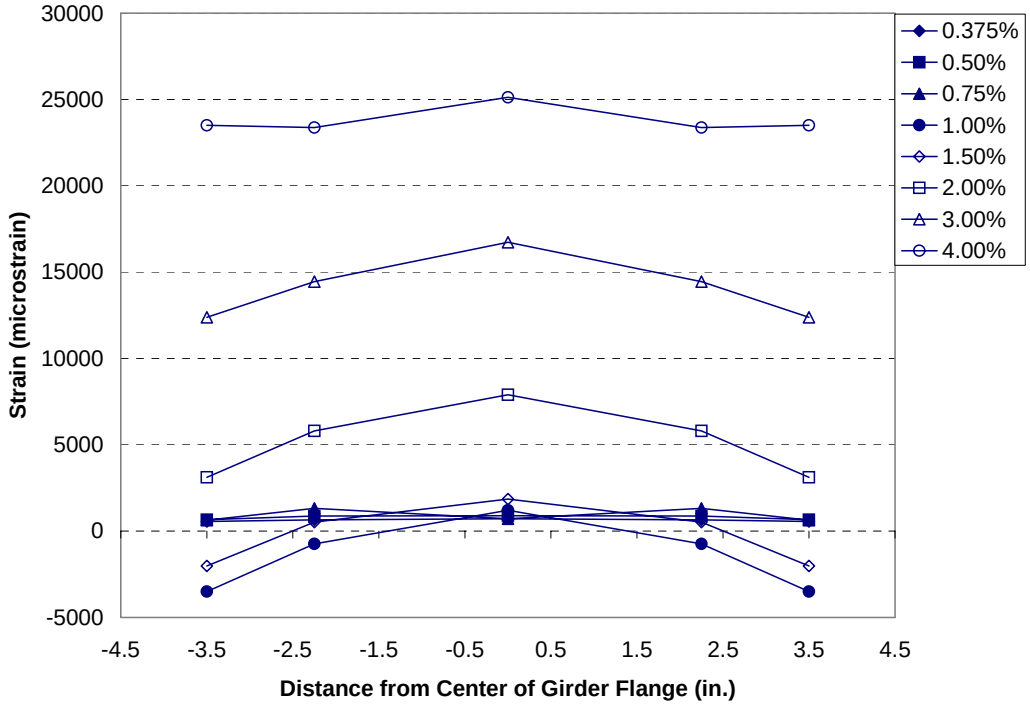


Figure 6.113: Longitudinal Strain on Specimen CR4R West Girder Top Flange near Column Flange (Girder Flange in Tension)

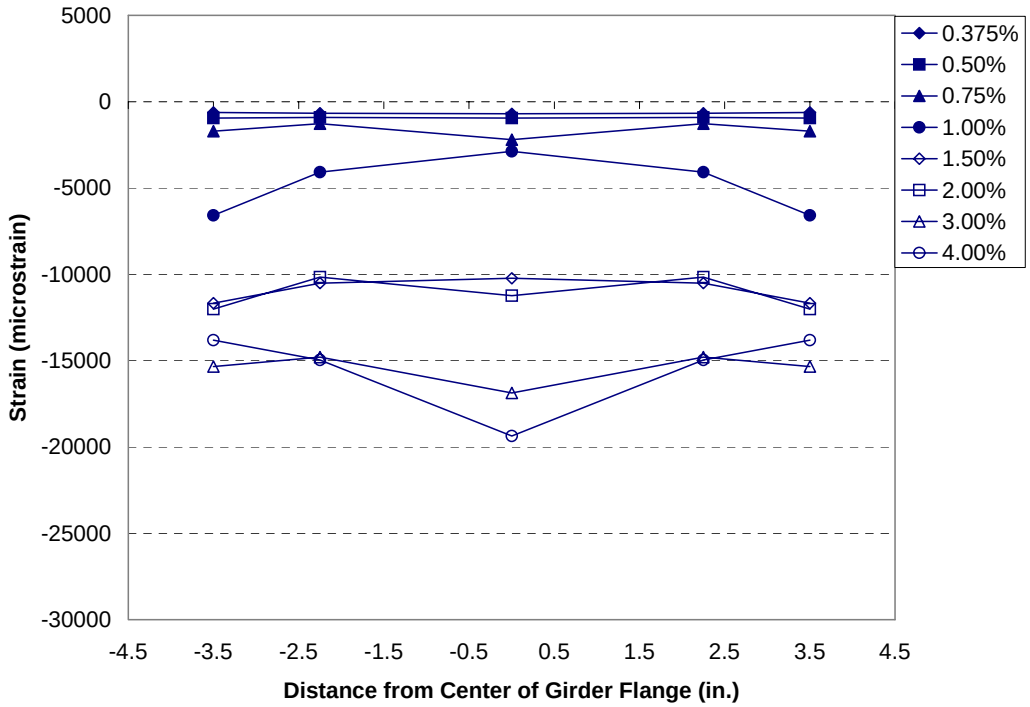


Figure 6.114: Longitudinal Strain on Specimen CR4R West Girder Top Flange near Column Flange (Girder Flange in Compression)

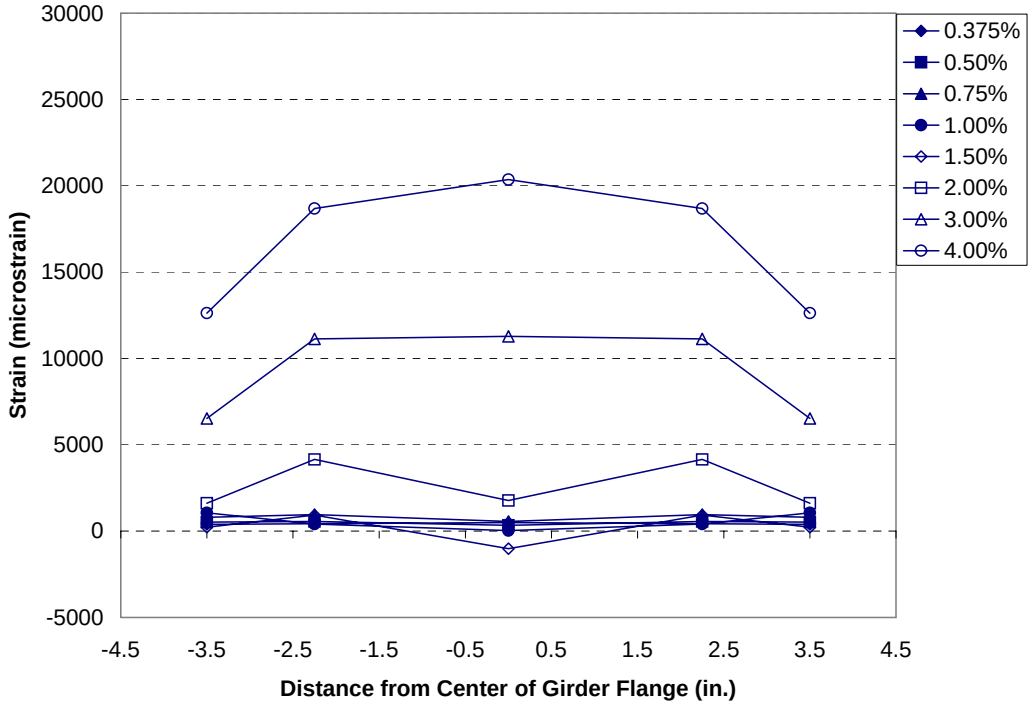


Figure 6.115: Longitudinal Strain on Specimen CR5 West Girder Top Flange near Column Flange (Girder Flange in Tension)

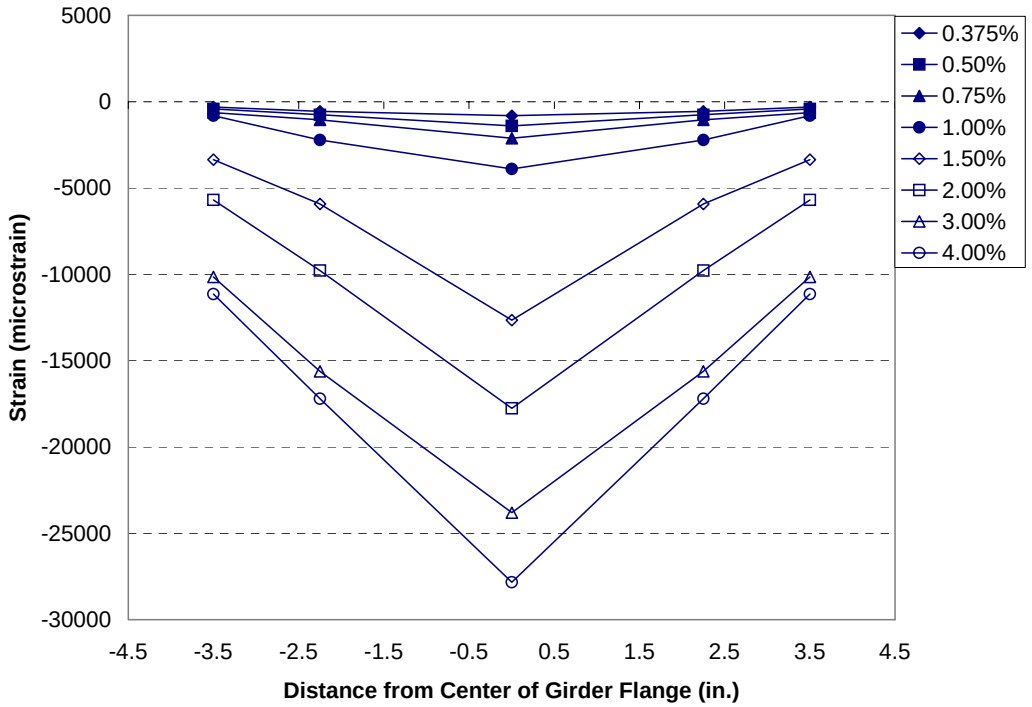


Figure 6.116: Longitudinal Strain on Specimen CR5 West Girder Top Flange near Column Flange (Girder Flange in Compression)

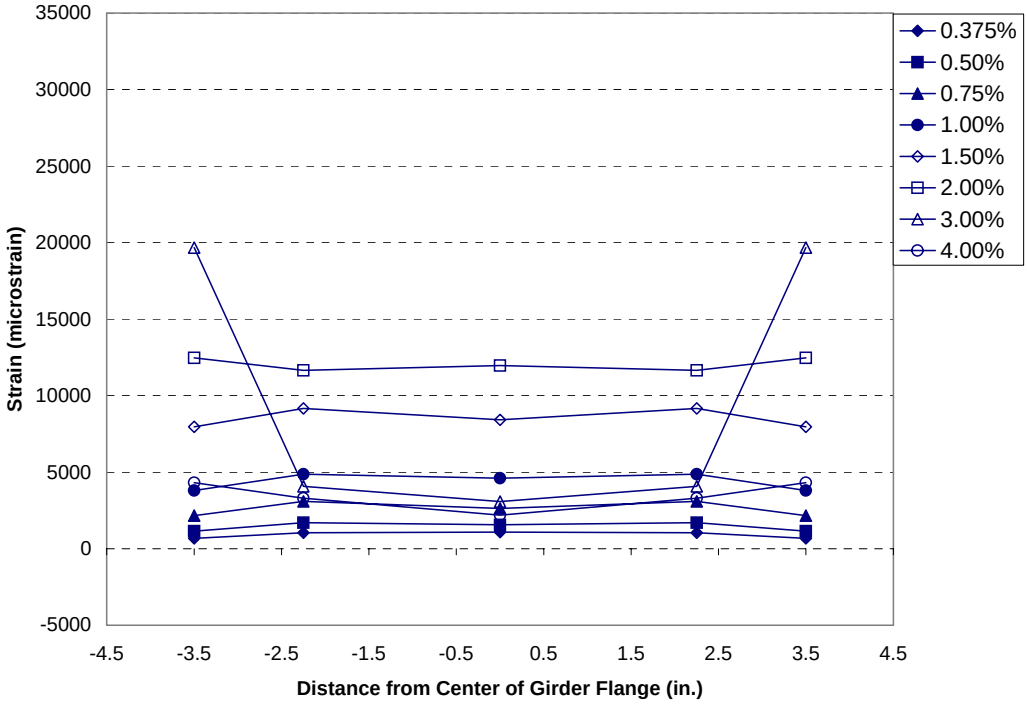


Figure 6.117: Longitudinal Strain on Specimen CR1 East Girder Bottom Flange near Column Flange (Girder Flange in Tension)

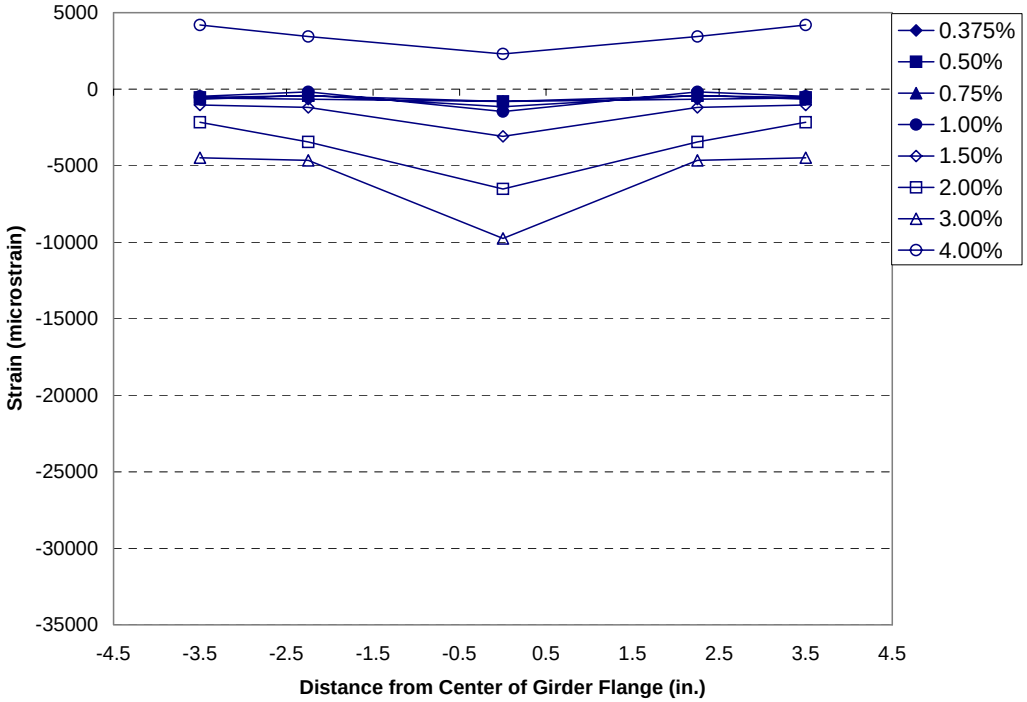


Figure 6.118: Longitudinal Strain on Specimen CR1 East Girder Bottom Flange near Column Flange (Girder Flange in Compression)

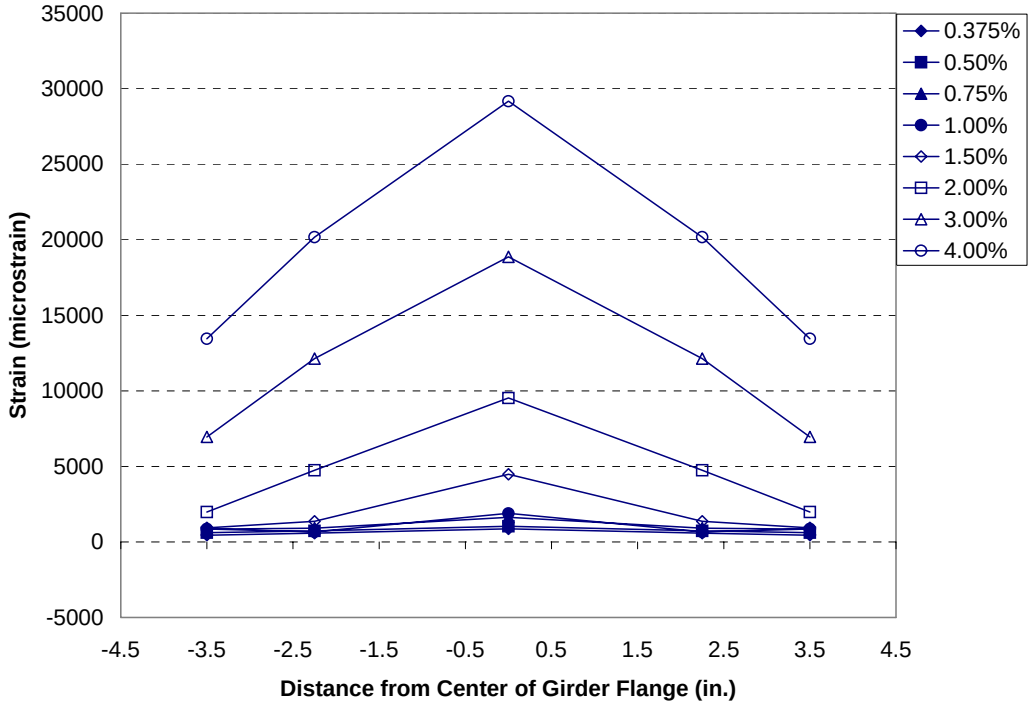


Figure 6.119: Longitudinal Strain on Specimen CR2 East Girder Bottom Flange near Column Flange (Girder Flange in Tension)

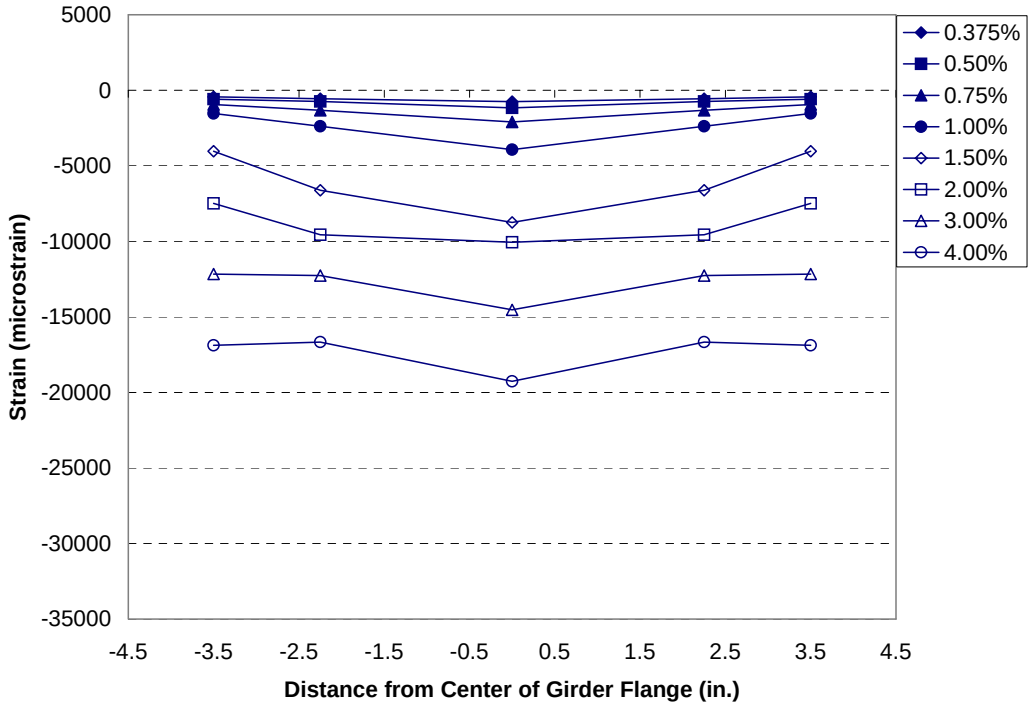


Figure 6.120: Longitudinal Strain on Specimen CR2 East Girder Bottom Flange near Column Flange (Girder Flange in Compression)

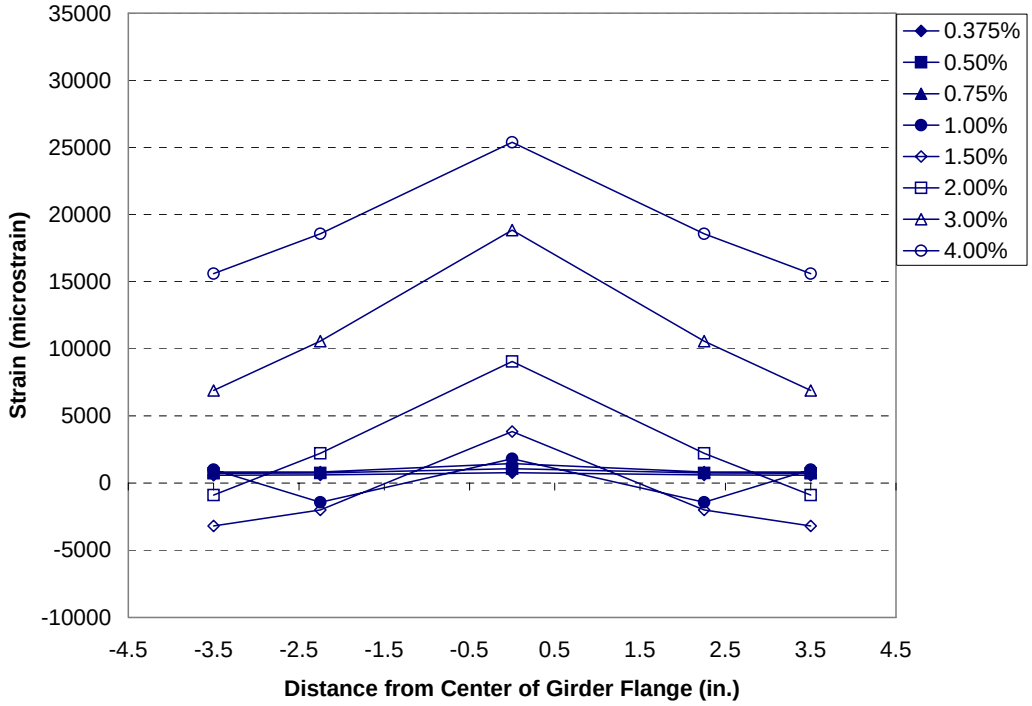


Figure 6.121: Longitudinal Strain on Specimen CR3 East Girder Bottom Flange near Column Flange (Girder Flange in Tension)

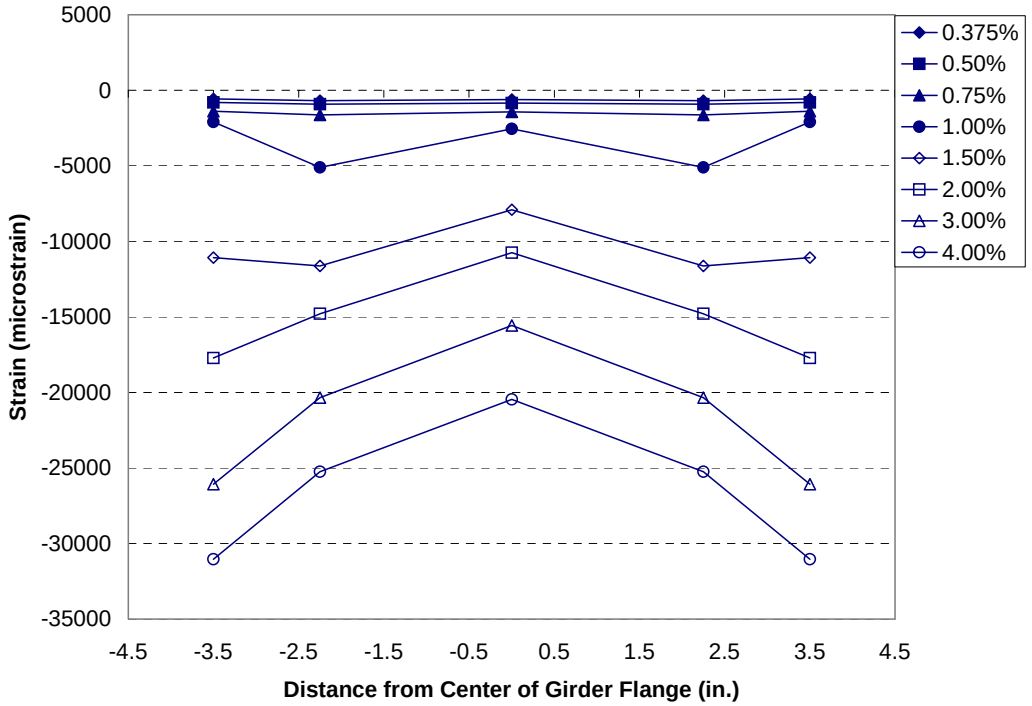


Figure 6.122: Longitudinal Strain on Specimen CR3 East Girder Bottom Flange near Column Flange (Girder Flange in Compression)

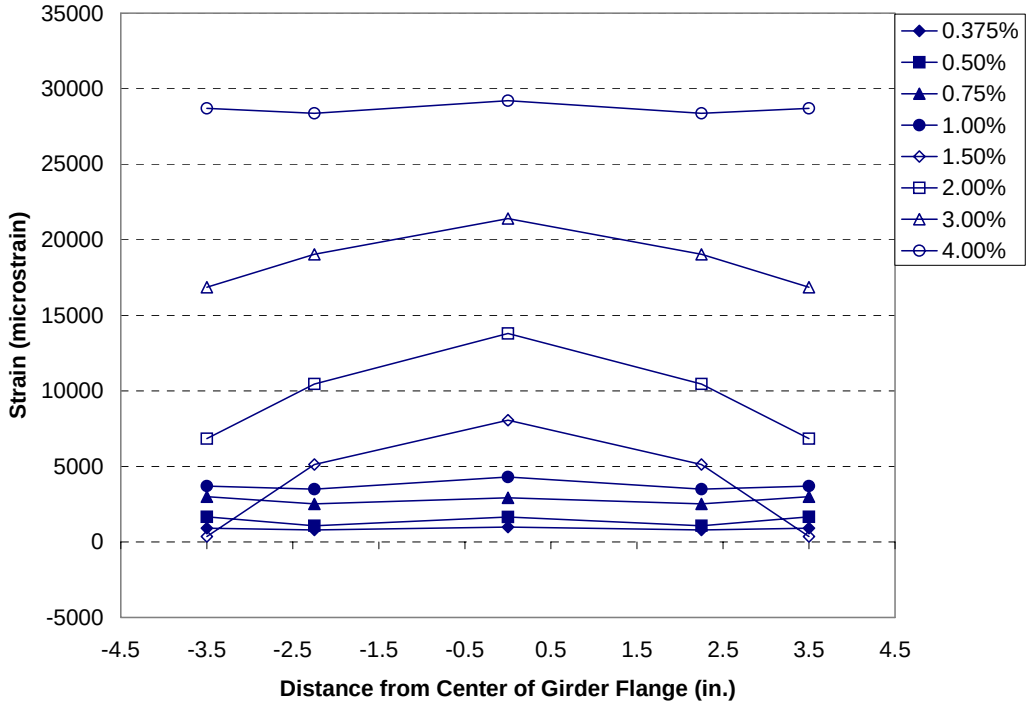


Figure 6.123: Longitudinal Strain on Specimen CR4R East Girder Bottom Flange near Column Flange (Girder Flange in Tension)

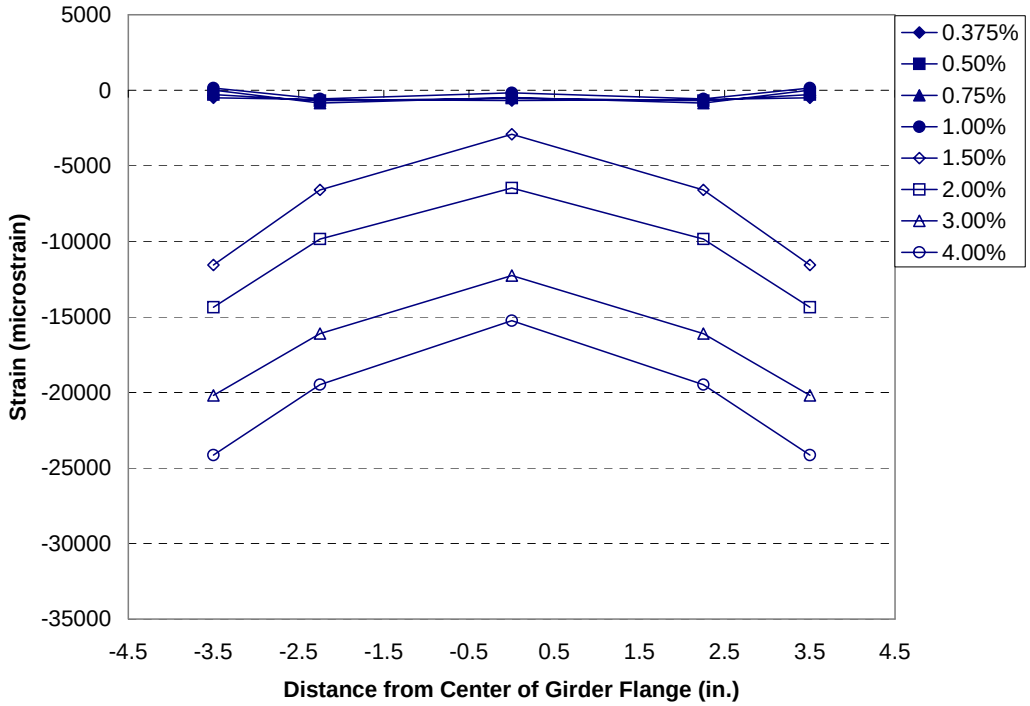


Figure 6.124: Longitudinal Strain on Specimen CR4R East Girder Bottom Flange near Column Flange (Girder Flange in Compression)

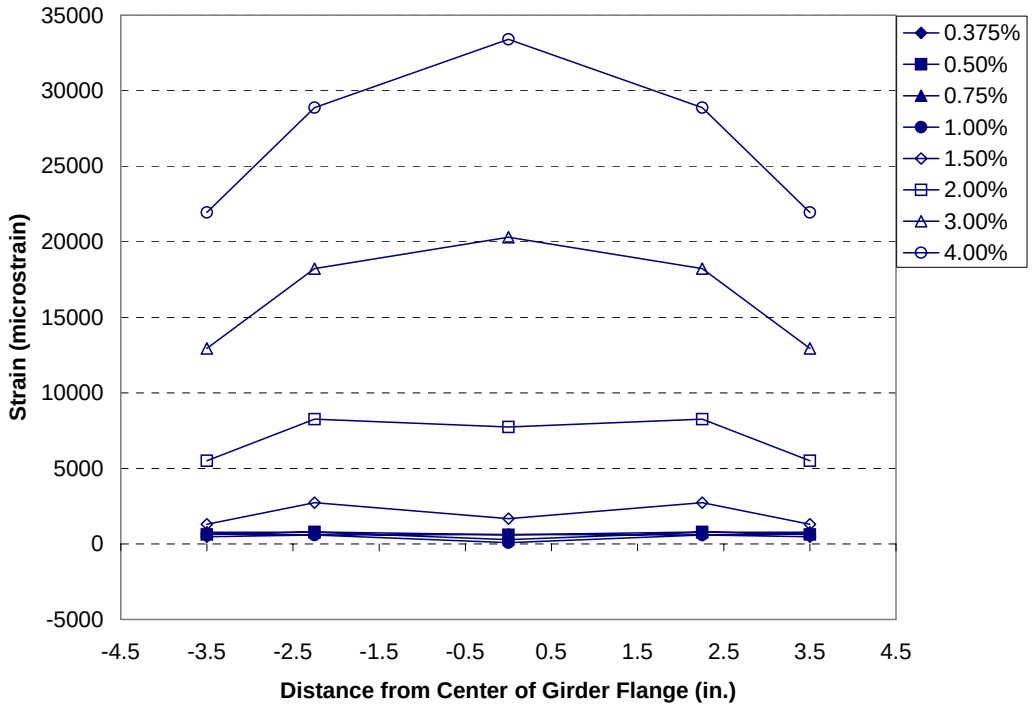


Figure 6.125: Longitudinal Strain on Specimen CR5 East Girder Bottom Flange near Column Flange (Girder Flange in Tension)

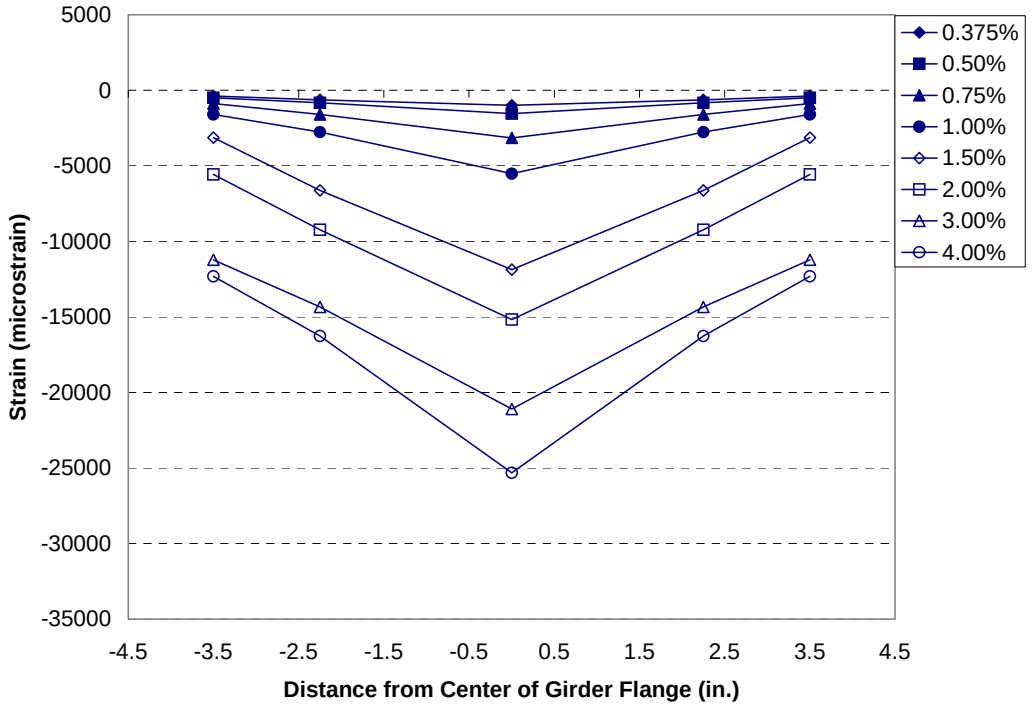


Figure 6.126: Longitudinal Strain on Specimen CR5 East Girder Bottom Flange near Column Flange (Girder Flange in Compression)

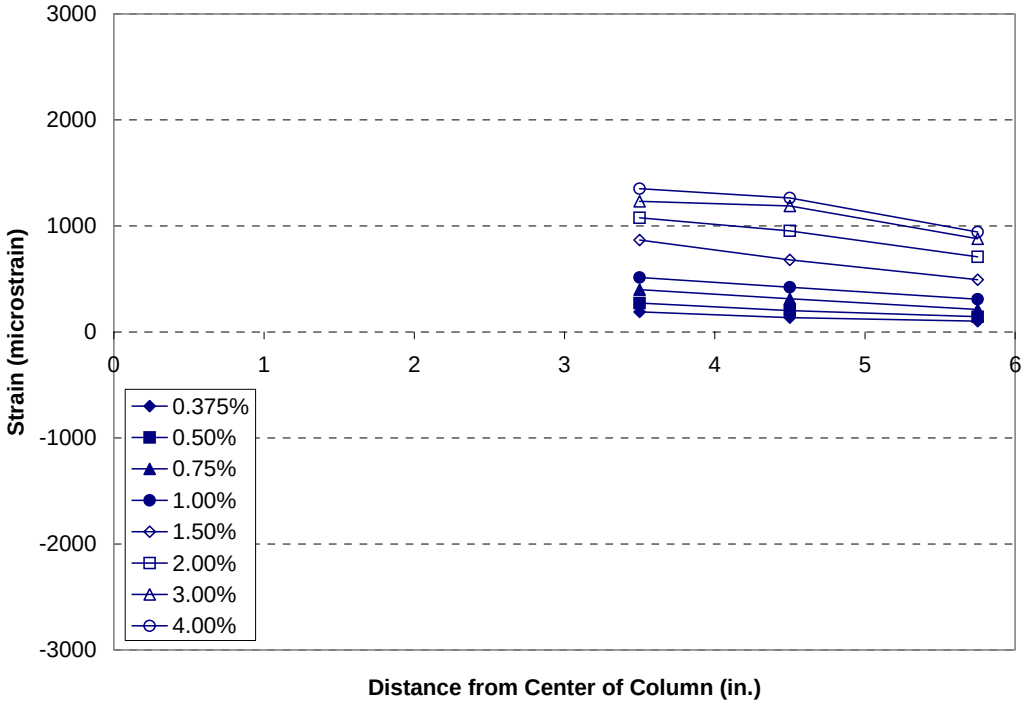


Figure 6.127: Strain Distribution (Strains CP3 to CP1) in Specimen CR3 Continuity Plate (East Top Flange in Tension)

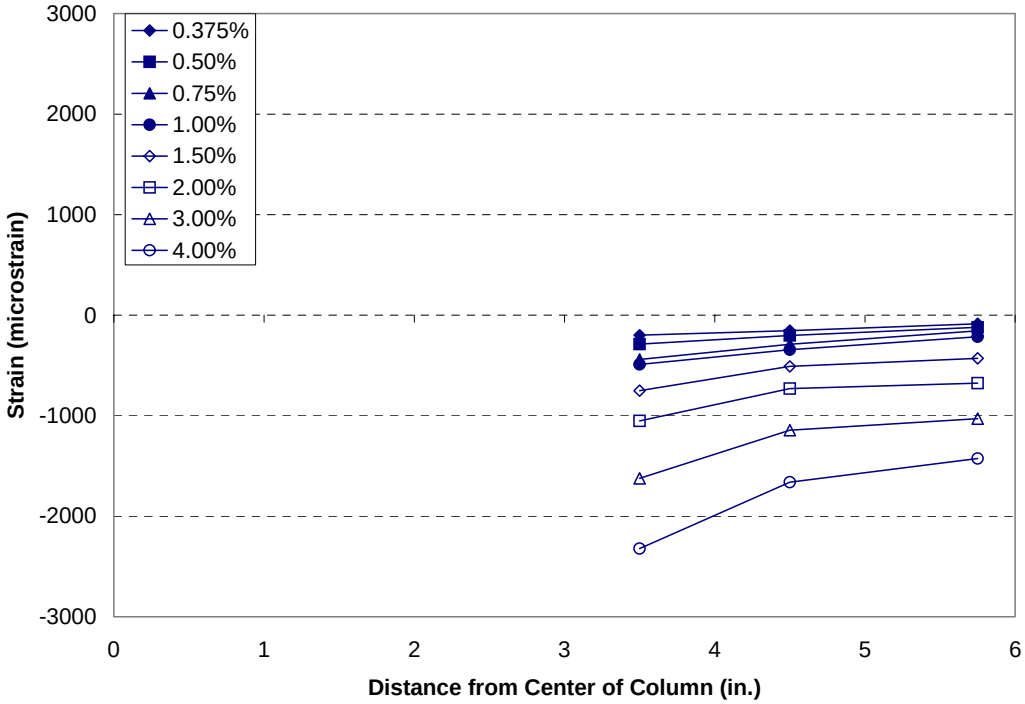


Figure 6.128: Strain Distribution (Strains CP3 to CP1) in Specimen CR3 Continuity Plate (East Top Flange in Compression)

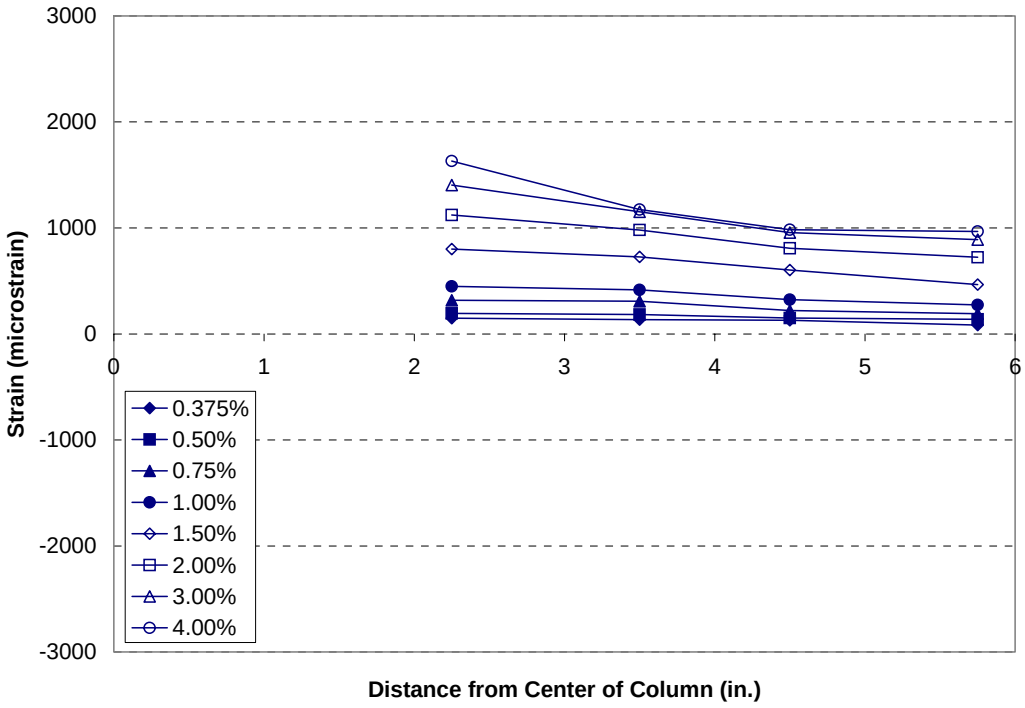


Figure 6.129: Strain Distribution (Strains CP7 to CP4) in Specimen CR3 Continuity Plate (East Top Flange in Tension)

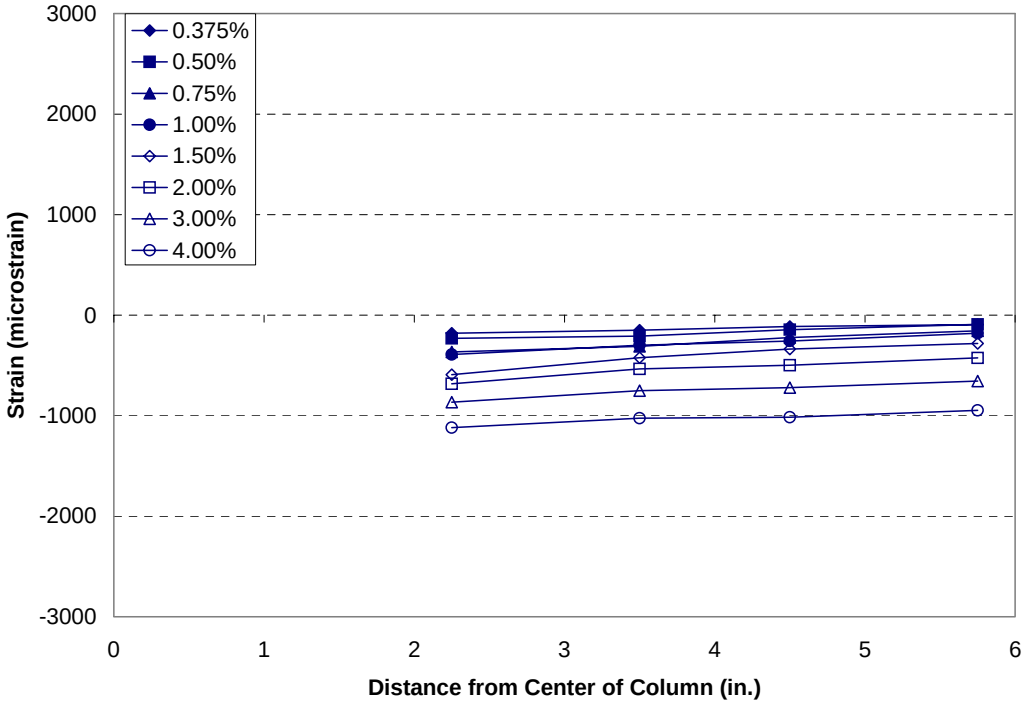


Figure 6.130: Strain Distribution (Strains CP7 to CP4) in Specimen CR3 Continuity Plate (East Top Flange in Compression)

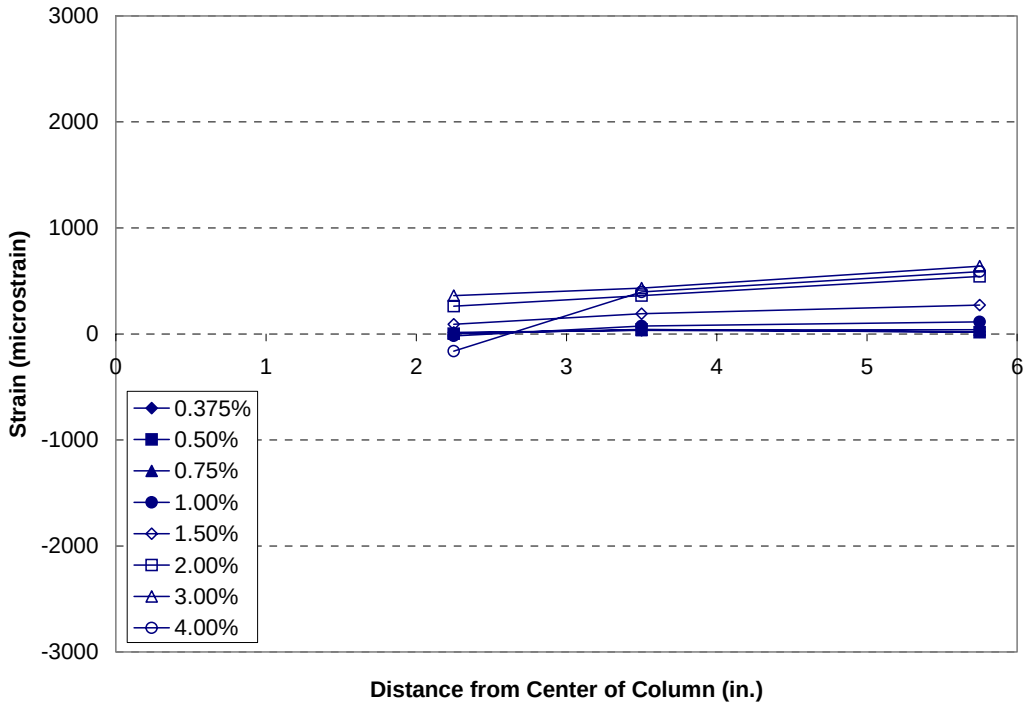


Figure 6.131: Strain Distribution (Strains CP10 to CP8) in Specimen CR3 Continuity Plate (East Top Flange in Tension)

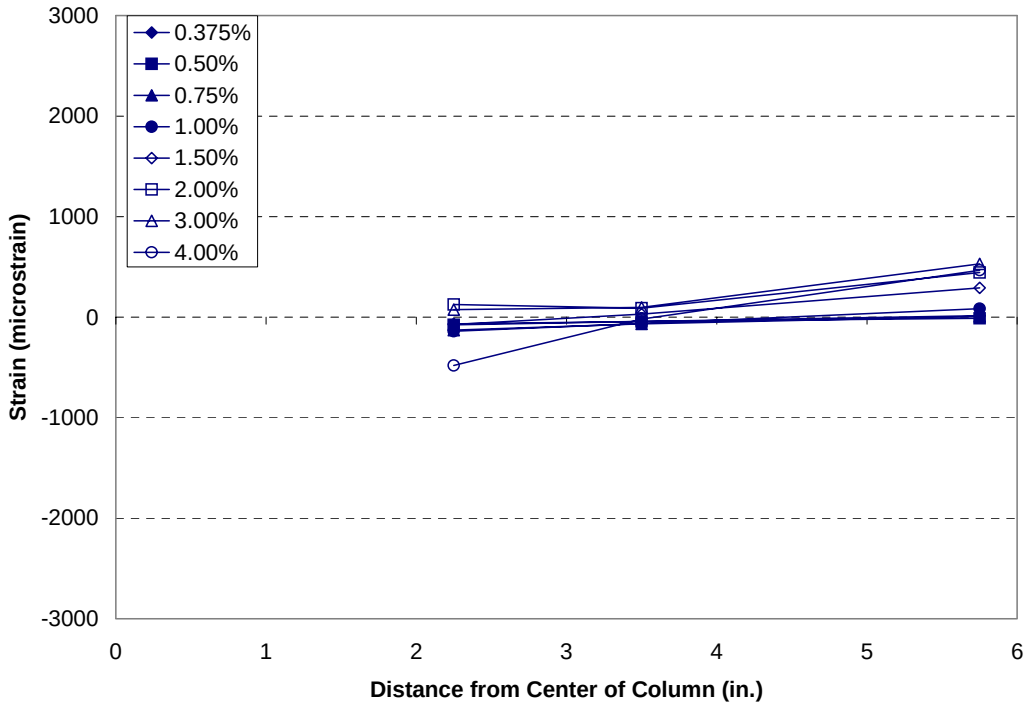


Figure 6.132: Strain Distribution (Strains CP10 to CP8) in Specimen CR3 Continuity Plate (East Top Flange in Compression)

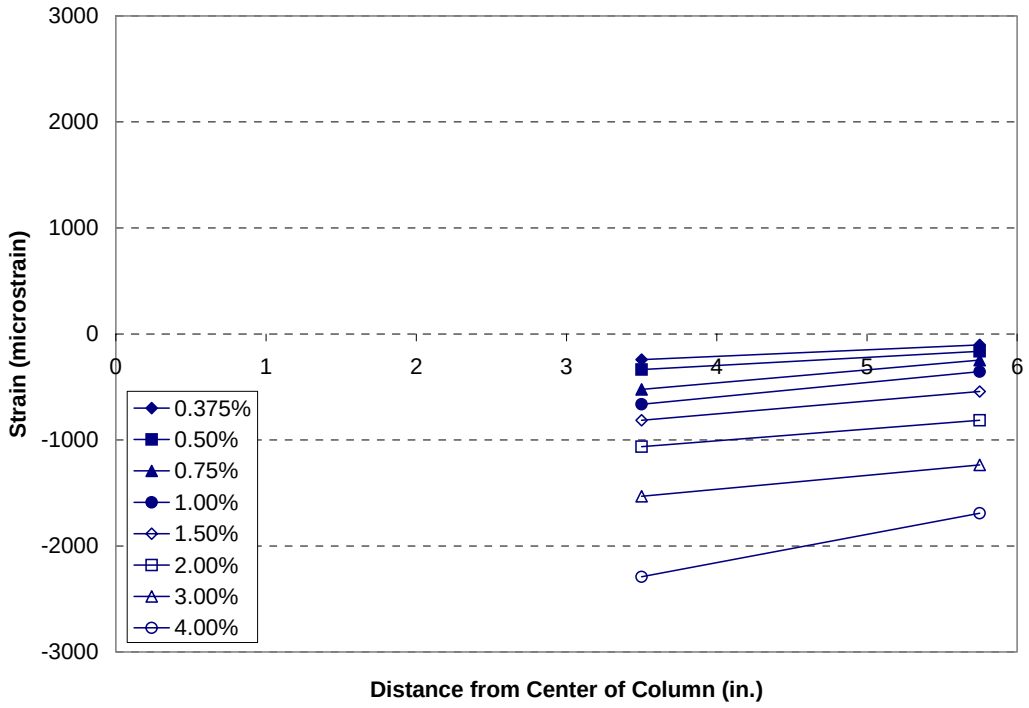


Figure 6.133: Strain Distribution (Strains CP12 to CP11) in Specimen CR3 Continuity Plate (East Top Flange in Tension)

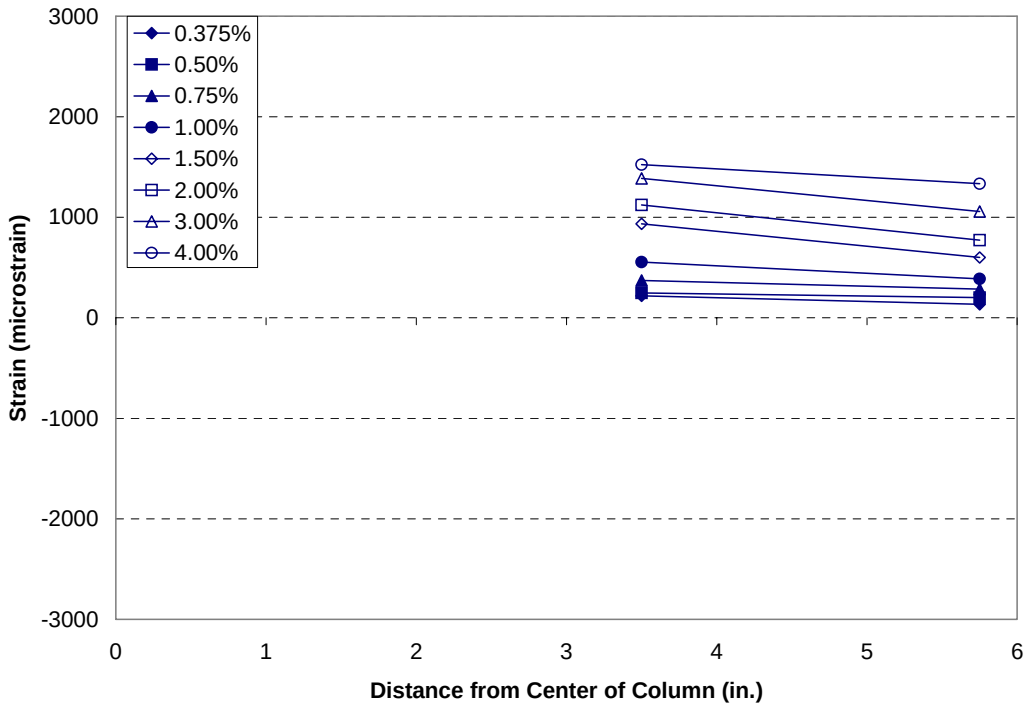


Figure 6.134: Strain Distribution (Strains CP12 to CP11) in Specimen CR3 Continuity Plate (East Top Flange in Compression)

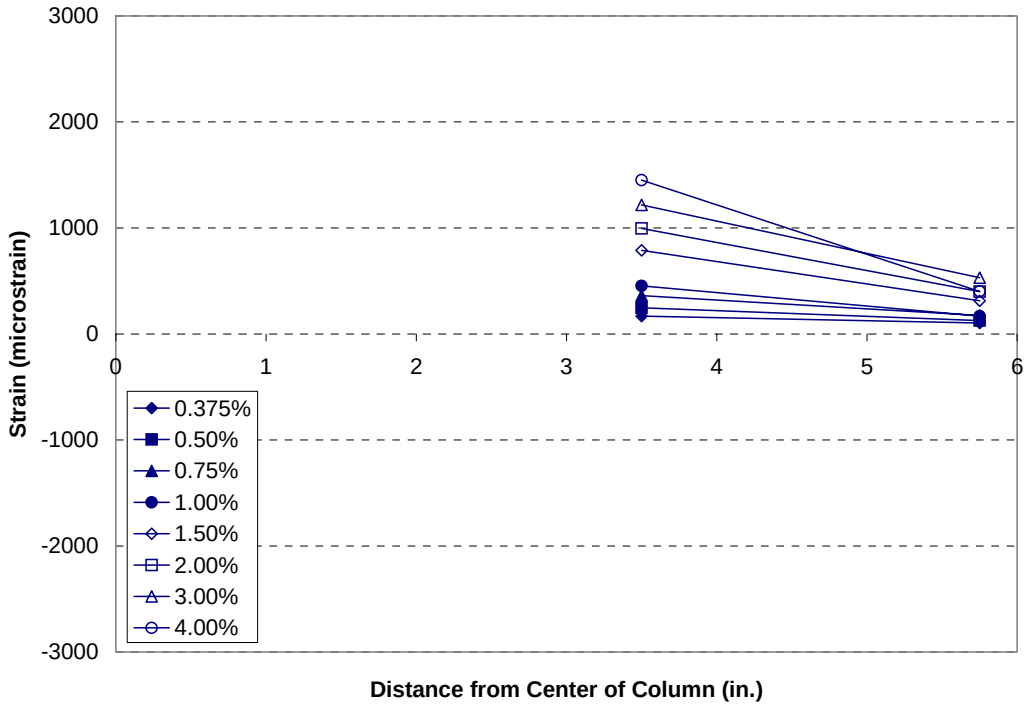


Figure 6.135: Strain Distribution (Strains CP13 to CP14) in Specimen CR3 Continuity Plate (East Top Flange in Tension)

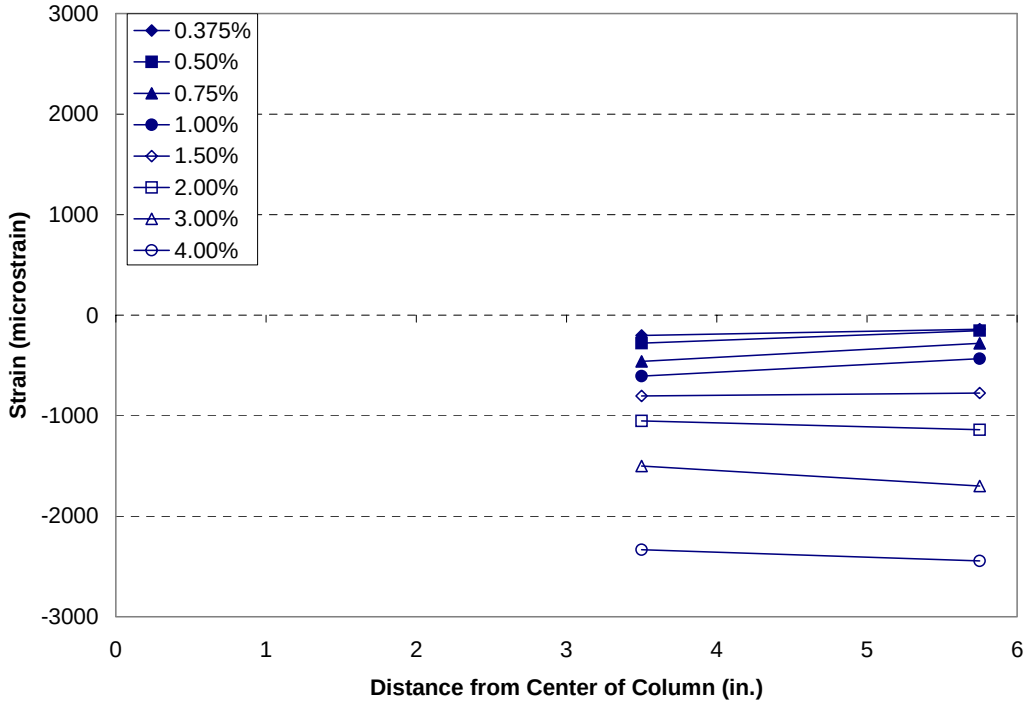


Figure 6.136: Strain Distribution (Strains CP13 to CP14) in Specimen CR3 Continuity Plate (East Top Flange in Compression)

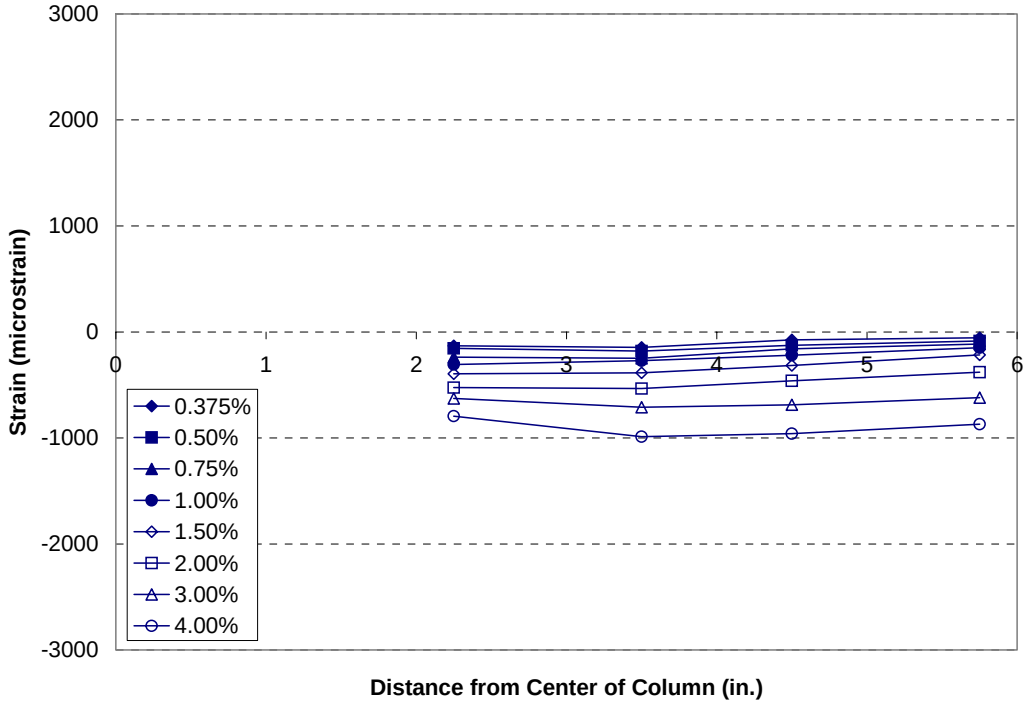


Figure 6.137: Strain Distribution (Strains CP15 to CP18) in Specimen CR3 Continuity Plate (East Top Flange in Tension)

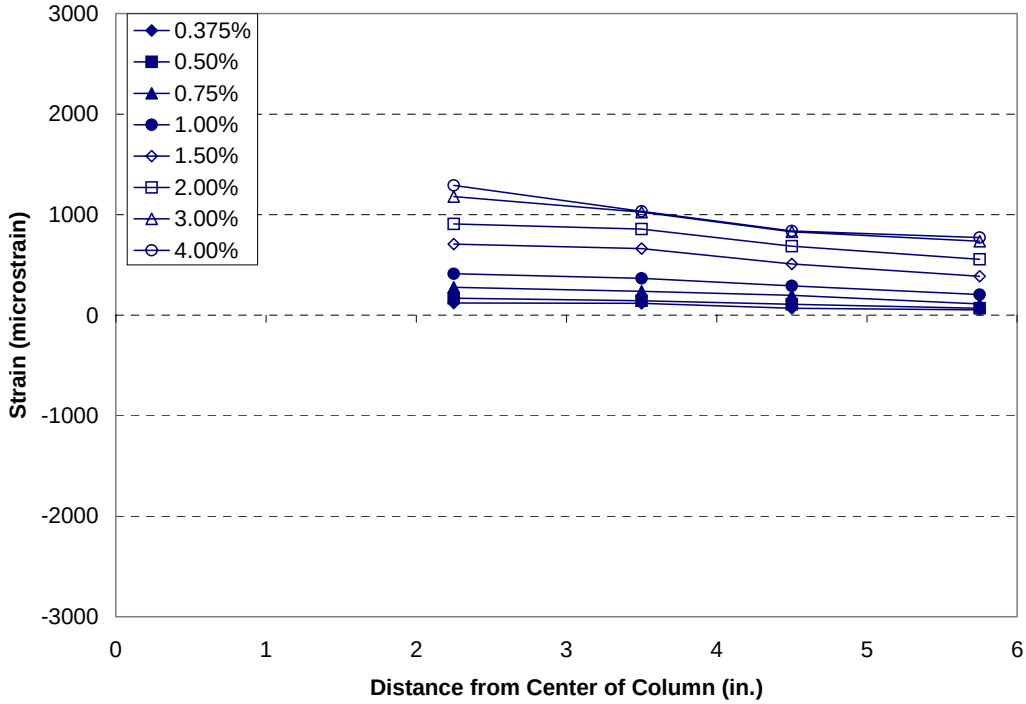


Figure 6.138: Strain Distribution (Strains CP15 to CP18) in Specimen CR3 Continuity Plate (East Top Flange in Compression)

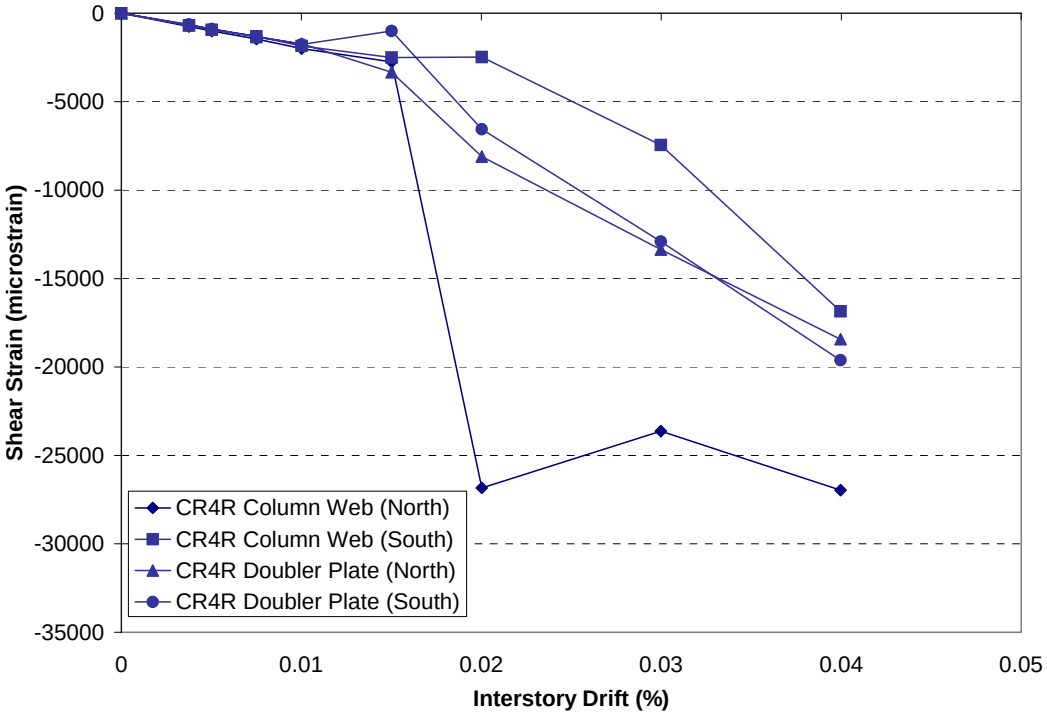


Figure 6.139: Shear Strain Variation in Specimen CR4R Panel Zone (East Bottom Flange in Tension)

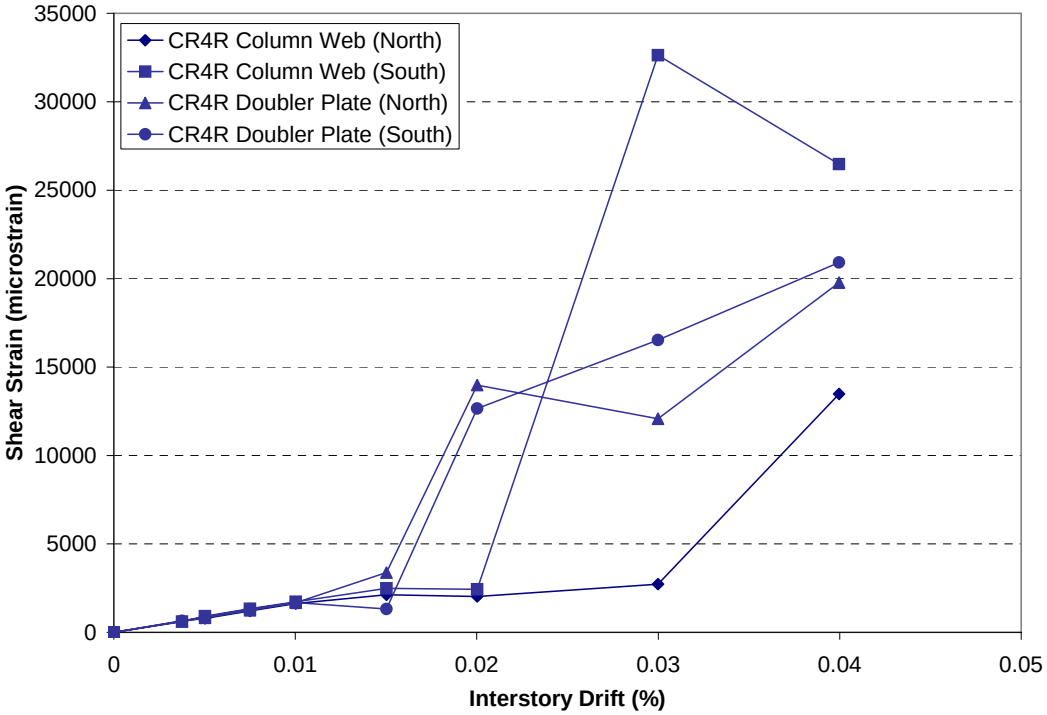


Figure 6.140: Shear Strain Variations in Specimen CR4R Panel Zone (East Bottom Flange in Compression)

Chapter 7

Summary and Conclusions

7.1 Research Summary

This report summarizes the findings of research that is part of an AISC-sponsored project to reassess the non-seismic and seismic design provisions for column stiffening, and to study the performance of new alternatives for stiffener detailing. The other components of this project are documented in Prochnow et al. (2000a, 2000b), Ye et al. (2000), Dexter et al. (2001), and Hajjar et al. (2002).

A total of six cruciform girder-to-column joint subassemblages were fabricated and tested in this project. Five joint subassemblages were originally designed and fabricated for an investigation into the provisions for detailing of column stiffening. However, due to premature brittle girder fracturing in Specimen CR4, a cruciform specimen with similar detailing (i.e., Specimen CR4R) was fabricated and tested. The panel zone (PZ) and local flange bending (LFB) provisions given by AISC (1993, 1997, 1999a, 2001) were the limit states targeted in this study, with the local web yielding (LWY) limit state being investigated primarily in the corroborating research (Prochnow et al., 2000a, 2002b; Ye et al., 2000; Dexter et al., 2001; Hajjar et al., 2002). The doubler plate and continuity plate details provided on the specimens were selected to avoid welding in the potentially low-toughness k-area of column sections, and to provide economical alternatives to the traditional groove-welded stiffeners.

A literature review was conducted to document the background of the current panel zone design equations contained in the AISC Seismic Provisions (1997). The history of these design provisions was presented, followed by a collection of opinions and recommendations related to panel zone and doubler plate design from various

researchers. The trend towards stronger panel zones and conservatism in design following the Northridge earthquake was noted.

A parametric study of stiffening requirements was undertaken to identify potential test configurations for the cruciform specimens. The final specimen matrix was selected after consideration of several factors, including the significant parameters related to the stiffener design, and correlation with past research, including the pull-plate testing by Prochnow et al. (2000a) and finite element research by Ye et al. (2000). The original five cruciform specimens feature a range of column sizes and stiffening details to investigate the panel zone and LFB provisions, as well as to evaluate the performance of the various column stiffener details.

Specimen CR1 featured an unstiffened W14x283 column to investigate the panel zone provisions for columns with thick flanges (i.e., those with large predicted post-yield strengths), and the cyclic LFB behavior. This test developed significant plastic rotation, the majority coming as a result of panel zone shear deformation. Specimen CR1 exhibited minimal local flange bending deformation in the column. Failure of Specimen CR1 consisted of a low-cycle fatigue rupture in East girder bottom flange. As was typical of the failure mode of every specimen (other than CR4), low cycle fatigue cracks formed at the girder-flange-side toe of the girder flange-to-column weld and grew increasingly deep until the flanges fractured. This specimen completed 14 cycles at 4.0% interstory drift without significant strength degradation.

Specimen CR2 represented a moderate-sized interior connection with a single-sided doubler plate. Verification of the LFB criterion outlined in the 1992 AISC Seismic Provisions (AISC, 1992), e.g., Equations 2.9 and 2.13, was the primary objective. This specimen requires continuity plates as per AISC (1992). The test results, however, confirmed that the current AISC LFB provisions are adequate and conservative when using Equation 2.13 for assessing the seismic demand on the column flange, and that continuity plates are not always necessary in steel moment-resisting connections. Specimen CR2 exhibited local flange bending deformation in the column flange, but it was less than the proposed limit of 1/8 inch out-of-plane displacement. The maximum total plastic rotation in this connection was similar to that of Specimen CR1, and the

plastic rotation was also dominated by panel zone shear deformation. This specimen completed 16 cycles at 4.0% interstory drift without significant strength degradation. Failure of Specimen CR2 consisted of a low-cycle fatigue rupture in West girder top flange.

Specimen CR3 represented a moderate-sized interior connection with both doubler plates and continuity plates. It was primarily intended to show the applicability of fillet-welded 1/2 in. thick continuity plates (equal to approximately half of the girder flange thickness) in steel moment-resisting connections. The panel zone strength provided was similar to Specimen CR1. The amount of maximum total plastic rotation in Specimen CR3 was also similar to those of Specimens CR1 and CR2, and was also dominated by panel zone shear deformation. This specimen completed 14 cycles at 4.0% interstory drift without significant strength degradation. Failure of Specimen CR3 consisted of a low-cycle fatigue rupture in East girder bottom flange.

Specimen CR4 featured a W14x176 column stiffened with an offset doubler plate detail. This detail was intended to stiffen both the column web and column flanges, thereby acting as both doubler plates and continuity plates. This test was stopped during the 2.0% interstory drift cycles following brittle fracture of three out of four of the girder flange-to-column flange complete joint penetration welds, and the specimen exhibited limited plastic deformation. Initial cracking at 1.0% drift was captured by strain gage data, and the first visible indications of cracking were evident in the 1.5% interstory drift cycles. The premature failure did not allow the performance of the stiffener detail to be evaluated.

An examination of the weld fractures experienced by Specimen CR4 was conducted to understand and explain the occurrence of the failures. Specimen CR4 was unintentionally prepared with very low toughness weld metal, an average of 2.0 ft-lbs at 0°F and 2.3 ft-lbs at 70°F. In contrast, the FEMA guidelines (FEMA, 2000e), require 20 ft-lbs at 0°F and 40 ft-lbs at 70°F. This was the only test that did not satisfy the connection prequalification requirement of completing two cycles at 4.0% interstory drift without significant strength degradation.

Due to the premature brittle fracturing in Specimen CR4, an additional specimen with similar detailing (i.e., Specimen CR4R) was fabricated, and notch tough weld metal was used for the girder flange groove welds of Specimens CR2, CR3, CR4R, and CR5. The provided panel zone strength of Specimen CR4R satisfied the current AISC Seismic Provisions (1997, 2001). This specimen completed 12 cycles at 4.0% interstory drift without significant strength degradation. The better performance of this test relative to Specimen CR4 indicates the importance of weld toughness in connection performance.

Failure of Specimen CR4R consisted of a low-cycle fatigue rupture in the East girder top flange. Due to the stronger panel zone, as compared with the other specimens, relatively small panel zone shear deformation was observed even though the amount of maximum total plastic rotation in Specimen CR4R was similar to those of Specimens CR1, CR2, and CR3. Specimen CR4R was subjected to 12 cycles at 4% drift before experiencing significant strength degradation. Specimen CR4R performed almost as well as specimens CR1, CR2, and CR3, which were subjected to 14, 16, and 14 cycles before significant strength degradation, respectively. Because of the small sample size, it cannot be determined whether there is any significance to the variation in the number of cycles in the range from 12 to 16 cycles, so it is assumed that these specimens performed equally well.

These specimens had a full range of column stiffening details and yet all performed comparably. Specimen CR1 had no stiffening at all. Specimen CR2 had no continuity plates [although they were required to satisfy seismic demand criteria as per AISC (1992)] and featured an innovative doubler plate detail, with a single-sided doubler plate in which a square cut (rather than beveled) doubler plate rested on the column fillets, slightly offset from the column web, and was fillet-welded to the column flanges. Specimen CR3 also featured this doubler plate detail, but had two doubler-plates as well as continuity plates, although these were only half the thickness of the girder flange and were fillet-welded to the column flanges and the doubler plates. Present seismic design criteria require continuity plates having the full thickness of the girder flange and that are groove-welded connections to the column flanges. Finally, Specimen CR4R included the offset doubler plate detail.

The fact that Specimens CR2 and CR3 performed equally well indicates that the present seismic demand criteria for continuity plates are somewhat conservative. The fact that Specimen CR3 performed well also indicates that if continuity plates are used, it is not necessary to use full thickness continuity plates that are groove welded to the column flanges. Also, the comparable performance of Specimen CR4R relative to Specimen CR3 shows that the box detail is equally effective as continuity plates in providing column flange bending resistance. These findings were also indicated by the pull-plate tests and corroborating finite element analyses for monotonic loading (Prochnow et al., 2000a, 2000b; Ye et al., 2000; Dexter et al., 2001; Hajjar et al., 2002), and it is now verified that cyclic loading does not affect these conclusions.

The fact that thinner continuity plates are recommended also means that smaller fillet welds are required to attach the continuity plates to the column, as compared to using thicker continuity plates. For example, only 3/8 inch fillet welds were required for Specimen CR3. The smaller welds pose a much less significant risk of causing k-line cracking.

These specimens also featured innovative doubler plate details, while Specimen CR1 had no doubler plate at all. Yet these variations had no significant impact on the performance of the connections in these tests. Therefore it cannot be concluded that any of these details are advantageous, and the most economical details should be recommended. This was also supported by the results of the pull-plate tests and corroborating finite element analyses (Prochnow et al., 2000a, 2000b; Ye et al., 2000; Dexter et al., 2001; Hajjar et al., 2002).

Specimen CR5 represents the smallest column section tested (W14x145), and it included fillet-welded doubler plates and no continuity plates. It was primarily intended to investigate the panel zone provisions for columns with thin flanges, and to evaluate the AISC LFB provisions for seismic design (Equations 2.9 and 2.13) as well as non-seismic design (Equations 2.9 and 2.12). The panel zone strength was again similar to Specimen CR1. Specimen CR5 exhibited significant local flange bending deformation in the column, however the deformation was less that the proposed limit of 1/8 inch. This specimen completed 6 cycles at 4.0% interstory drift without significant strength

degradation. Failure of Specimen CR1 consisted of a low-cycle fatigue rupture in West girder top flange.

Specimen CR5 was the most substantially underdesigned cruciform specimen with respect to local flange bending – the resistance-to-demand ratio was only 0.84 for non-seismic demand as per AISC (1993, 1999a), and it equaled to 0.47 for seismic demand as per AISC (1992). Specimen CR5 completed the SAC loading history (SAC, 1997) with more than two cycles at 4.0% interstory drift; therefore it is possible that the non-seismic demand criteria are sufficient even for seismic loading, although there is not enough evidence to support this conclusion.

Although the performance of Specimen CR5 was adequate, the number of cycles before significant strength degradation in this specimen was distinctly fewer than for the other specimens (except Specimen CR4). This relate to having an adverse effect of the small column or the lack of continuity plates. On the other hand, it cannot be concluded that this distinction is significant because it is not known how much variability is expected for low-cycle fatigue failures such as these.

The fact that these low-cycle fatigue failures are not significantly affected by the column stiffening seems inconsistent with finite element analyses showing an increase in stress or strain concentrations in the girder flange-to-column welds associated with excessively weak panel zones or insufficient continuity plates (El-Tawil et al., 1998; Ricles et al., 2000). However, a majority of these analyses have been monotonic, i.e. the cyclic reversal of the load was not modeled. The effect of any stress and strain concentrations is likely to be diminished by plastic shakedown within the high concentration regions.

The stress and strain concentrations exhibited in these monotonic analyses may be significant when it comes to brittle fracture, which usually occurs in the first few plastic cycles. However, provided the welds and base metal have sufficient toughness, brittle fracture is avoided and the failure mode becomes low-cycle fatigue after numerous cycles of plastic rotation. The important performance parameter becomes the number of cycles at a particular level of plastic rotation.

Specimen CR5 was analogous to the pull-plate test 2-LFB in Prochnow et al. (2000a, 2000) and Hajjar et al. (2002). These two different types of tests exhibited similar column flange displacement, and similarities in the strain distributions. These findings support the use of pull-plate tests to investigate local flange bending and other localized phenomena.

An analysis of the results of these six tests was conducted to better understand panel zone behavior and local column flange bending under cyclic large connection deformation. The panel zone behavior of each specimen was compared with predictions of the current AISC (1997, 2001) seismic panel zone provisions and with a model (Equation 6.10) modified from that proposed by Fielding and Huang (1971). In order to provide a panel zone design capacity corresponding to the experimental results from this research, as well as when comparing to panel zone strength results from past research, the panel zone strength equation of AISC (1997, 2001) in general needs to be scaled down. For this purpose, a new methodology was introduced for scaling down the panel zone design strength as well as the corresponding panel zone demand. The LFB behavior of Specimens CR1, CR2, and CR5 was also analyzed and compared to the results and recommendations from Prochnow et al. (2000a). The effects of different column stiffening details on the strain distributions in the longitudinal direction in the girder flanges was assessed as well.

7.2 Conclusions and Recommendations

Based on the experimental results of six full-scale interior steel moment-resisting connections, classified as Welded Unreinforced Flange-Welded Web (WUF-W) connections as per FEMA (2000a), and which include several new alternatives for column stiffener details, several conclusions and recommendations are made below. Conclusions regarding the non-seismic behavior of column stiffeners may be found in Prochnow et al. (2000a, 2000b) and Hajjar et al. (2002).

7.2.1 Conclusions

1. When properly detailed and welded with notch-tough filler metal, the Welded Unreinforced Flange-Welded Web (WUF-W) moment connections can perform adequately under large quasi-static cyclic loads even though relatively weak panel zone strengths are chosen, as compared with the AISC (1997) panel zone provisions. Specimens CR1, CR2, CR3, CR4R, and CR5 completed the SAC loading history up to 4.0% interstory drift cycles without noticeable strength degradation. After completing the two cycles at 4.0% interstory drift required by the SAC protocol, an additional 12 (CR1), 14 (CR2), 12 (CR3), 10 (CR4R), and 4 (CR5) cycles, respectively, were applied to the specimens before significant strength degradations were noted. The primary failure mode of these five specimens was Low-Cycle Fatigue (LCF) crack growth and eventual rupture of one or more girder flanges.

2. Achieving a required minimum Charpy V-Notch (CVN) toughness in the complete joint penetration (CJP) girder flange-to-column flange welds is critical for good connection performance. Specimen CR4 was unintentionally prepared with very low CVN weld metal, much lower than the FEMA guidelines' requirement. This was the only test that did not satisfy the connection prequalification requirement of completing two cycles at 4.0% interstory drift without significant strength degradation.

3. Application of the four new alternative column stiffener details (i.e., fillet-welded doubler plate; fillet-welded doubler plates and fillet-welded 1/2 in. thick continuity plates; groove welded offset doubler plates; and fillet-welded doubler plates that were backside-beveled) in steel moment-resisting connections was successfully verified. No cracks or distortion was observed in the welds connecting these stiffeners to column flanges before their girder flange rupturing. Additionally, no cracking occurred in the k-area of the column in these four column-stiffened specimens.

4. The measured maximum column flange deformation due to the concentrated girder flange force in the unstiffened specimens ranged from 26% of the assumed yield mechanism limit of 1/8 in. flange deformation in the case of Specimen CR1, to 49% of the 1/8 in. limit in the case of Specimen CR5. Specimen CR5 was the most substantially underdesigned specimen for local flange bending – the resistance-to-demand ratio was only 0.84 for non-seismic demand as per AISC (1993, 1999a), and it equaled to 0.47 for seismic demand as per AISC (1992). Specimen CR5 met the requirements for two cycles at 4.0% drift; therefore it is possible that the non-seismic demand criteria are sufficient even for seismic loading. At a minimum, the test results imply that, under the application of the corresponding seismic demand (AISC, 1992; FEMA, 2000a), the AISC LFB strength equation (AISC 1993, 1999a) is adequate and conservative.

5. Continuity plates may not be necessary in many steel moment connections, and design provisions similar to those in AISC (1992) or FEMA (2000a) permitting the design, or lack of inclusion, of continuity plates, are recommended for reintroduction into the AISC Seismic Provisions (note however that further research may be warranted to investigate the behavior of deep columns for the limit state of local flange bending). Specimens CR1, CR2, CR4R, and CR5, none of which had continuity plates (although Specimen CR4R included the offset doubler plate detail), showed very ductile connection behavior even though only Specimen CR1 met the seismic requirements of AISC (1992) and FEMA (2000a) with respect to continuity plates for the limit state of local flange bending. While continuity plates reduced the strain gradients in the girder flanges, the results from this research show that for a wide range of column sections and doubler plate detailing, strain gradients and strain magnitudes well above the yield strain did not prohibit the specimens from achieving the connection prequalification requirement of completing two cycles at 4.0% interstory drift without significant strength degradation. This was even the case for one specimen that had notch toughness in the weld metal that was significantly below the FEMA guidelines'

requirement. If continuity plates are required, fillet-welded continuity plates that were approximately half of the girder flange thickness performed well. The offset doubler plate detail can also function effectively as continuity plates while simultaneously serving as web doubler plates.

6. The effect of the column stiffening on the local flange deformation and the performance of the groove weld was similar in the cruciform and pull-plate tests performed in this research, and was corroborated well by the finite element analyses (Prochnow et al., 2000a, 2000b; Ye et al., 2000; Dexter et al., 2001; Hajjar et al., 2002). In view of the relative economy of pull-plate tests, they proved to be reasonable test specimens for investigation of local flange bending and other localized phenomena when the focus was on non-seismic response.

7. The modified access hole (see Figure 3.13) chosen for this experimental study showed very good performance under large repeated cyclic connection deformations. In the five specimens that failed by LCF, no low-cycle fatigue cracking occurred at the toes of these modified access holes prior to significant LCF cracking elsewhere in the connection.

8. Within this limited number of tests conducted in this research, correlation between the panel zone strength and fracturing of the shear tab welded to the column flange at its top and bottom edges was not observed. Instead, fracturing in the shear tab edges seems to be more directly affected by local buckling and/or low-cycle fatigue cracking in the girder flanges under large connection deformations. It should be noted that local buckling in the bottom girder flange, for instance, might increase the inelastic demand in the top girder flange, which may affect the shear tab edge.

9. In all the five successful tests, the seismic performance of the panel zones was stable and ductile. The analyses of the panel zone elastic and inelastic behavior

indicated significant energy dissipation in this region for Specimens CR1, CR2, and CR3. Relatively mild energy dissipation was observed in Specimens CR4R and CR5 even though the measured maximum amount of the connection total plastic rotation was similar in all cases. The smaller panel zone energy dissipation in these two specimens were mostly caused by the design of a stronger panel zone in the case of Specimen CR4R, and by the larger column flange yielding around each girder flange in the case of Specimen CR5.

10. The panel zone strength equation included in AISC (1997) was evaluated based on the five successful test results, as well as on a comparison with the 44 past experimental tests. This equation was found to significantly overpredict the panel zone strength at both the point of nominal yielding of the panel zone (i.e., achieving a panel zone shear strain of γ_y) and, for columns with relatively thick flanges, in the post-elastic range up to a panel zone shear deformation level of $4\gamma_y$.

11. An alternate model estimating the panel zone post-elastic stiffness was developed from a newly assumed panel zone behavior at its ultimate state, and modified based on the five experimental results so as to more accurately capture the post-yield panel zone strength at $4\gamma_y$ than does the current AISC (1997) equation. Based on a comparison with 49 past experimental results, including the five successful specimens of this research, a modified Fielding and Huang model (Equation 6.10) was found to be more accurate in its prediction of the panel zone strength of W14 and larger columns, and was shown to be somewhat conservative for smaller columns. A resistance factor of approximately 0.85 was computed for use with this panel zone strength equation. However, an assessment of the appropriate corresponding seismic demand would be warranted before adopting this equation.

12. In order to provide a more accurate assessment of panel zone strength corresponding to the panel zone behavior seen in the experiments in this research,

the panel zone strength equation for the design of steel moment-resisting connections needs to be scaled down. For this purpose, a new methodology, which properly scales the corresponding panel zone design demand as well as the panel zone strength, was introduced. This methodology may be used to evaluate a selected panel zone equation (e.g., Equation 2.1 or Equation 6.10) based on past experimental results, and can provide an appropriate demand for a selected panel zone strength resulting.

7.2.2 Recommendations for Future Research

1. It is possible that continuity plates are not necessary in a much wider range of connections than are presently believed. The seismic demand in particular appears to be conservative. More tests should be performed on a wider range of specimens without continuity plates to further verify this possibility.

2. It is possible that it is not necessary to size fillet welds to fully develop the continuity plates or doubler plates. These plates cannot exhibit deformation incompatible with the underlying column. More tests with underdesigned fillet welds should be performed to investigate this possibility.

3. The proposed panel zone strength model (i.e., the modified Fielding and Huang model) given by Equation 6.10 should be further evaluated as an alternative to the current design equations included in AISC (1993, 1997, 1999a, 2001). An analysis of past test data indicates that Equation 6.10 better predicts the shear strength of panel zones at a design deformation of $4\gamma_y$, particularly for columns with thick flanges. A further scaling down of Equation 6.10 may also be warranted for achieving a more accurate assessment of yielding in the panel zone. For columns with thinner flanges, the panel zone strength given in AISC (1997), Equation 2.1, is appropriate, if it is first scaled down appropriately. Thus, further research on these strength equations is warranted. In addition, when computing

required panel zone thicknesses for seismic demands, Equation 6.10 results in thicker panel zones than both AISC (1997) and FEMA (2000a). Thus, further consideration should be given to an appropriate demand for the use in assessing panel zone strength using Equation 6.10. Similarly, if the panel zone thicknesses resulting from AISC (1997) are deemed adequate, then the corresponding seismic demand should also be scaled down if Equation 6.14 or a scaled-down strength from AISC (1997) is adopted.

4. Weld toughness criteria should be reconsidered, accounting for the inherent variability in CVN toughness measurements. Further research should thus be conducted to characterize the statistical toughness distributions of several common electrode classifications used in seismic construction (e.g., E70T-6, E70TG-K2, and E71T-8). Tests should be conducted under a wide range of welding parameters, conditions, and equipment. Future welding consumable recommendations for seismic construction should take into account more comprehensively the resulting statistical variability of the particular electrodes.

Appendix A

Calculation of Specimen Deformation and Rotation Quantities

This appendix describes the procedures used to calculate the various specimen rotation and deformation quantities. The quantities of interest include interstory drift, total connection plastic rotation (which includes the contributions from the girders and panel zone), girder rotation (total and plastic), panel zone deformation (total and plastic), girder plastic rotation relative to the column centerline, and panel zone plastic rotation relative to the column centerline. Results from the sections that follow are discussed in Chapter 5 as they relate to specimen performance.

A.1 Rotation and Deformation from Displacement Data

The LVDTs placed on the girders and in the panel zone were used to determine the total girder rotation of the plastic hinge region and the total panel zone shear deformation, respectively. Refer to Figure 4.18 for the placement of the LVDTs. Actuator stroke data was used to calculate the interstory drift of the connections. As presented in Section 4.2, the interstory drift levels were specified in the loading protocol used during testing (SAC, 1997). Girder moments were calculated using the actuator load data as the load multiplied by the girder length to the column face.

The interstory drift was calculated from the girder tip displacement data as:

$$\theta = \frac{\Delta_{tip}}{\left(L_g + {}^{d_c}\!/_{2}\right)} \tag{4.1}$$

where:

θ = interstory drift angle

Δ_{tip} = actuator tip displacement

L_g = girder length between loading point and column face

d_c = column depth

The girder lengths, L_g, were 131.63 in., 132.26 in., 132.39 in., 132.39 in., and 132.61 in. for Specimens CR1, CR2, CR3, CR4 (and CR4R), and CR5, respectively. The quantity ($L_g + d_c/2$) is a constant 140 in. for all specimens. The load vs. stroke data (see Figures A.1 through A.12) was used to generate moment vs. interstory drift plots for the East and West connections of all specimens. Figures A.13 through A.24 show the moment vs. interstory drift behavior of all specimens.

The total girder rotation relative to the column in the plastic hinge region was calculated from LVDTs placed on the top and bottom flanges of the specimen girders. Figure A.25 illustrates calculation of the girder rotation from the LVDT displacements. Referring to Figure A.25, the girder rotation was calculated as:

$$\theta_g = \frac{|\Delta_T| + |\Delta_B|}{d'} \tag{A.1}$$

where:

θ_g = total rotation of the girder plastic hinge region

Δ_T = horizontal displacement of top flange LVDT

Δ_B = horizontal displacement of bottom flange LVDT

d' = depth between top and bottom flange LVDTs

The value of d' for the East and West girders of Specimens CR1 and CR4 was 27.4375 in. For the other specimens, 29.5 in. was used for the value of d'. Figures A.26 through A.37 illustrate the moment vs. girder rotation behavior of all specimens.

The total panel zone shear deformation was calculated from two diagonal LVDTs placed in the panel zone (see Figure 4.18). Referring to Figure A.38, the shear deformation of the panel zone was calculated as (from Krawinkler et al., 1971):

$$\gamma_{pz} = \frac{|\Delta_1| + |\Delta_2|}{2} \frac{\sqrt{b'^2 + h'^2}}{b'h'} \tag{A.2}$$

where:

γ_{pz} = average total panel zone shear deformation

Δ_1, Δ_2 = displacement of diagonal LVDTs

b' = width of panel zone between LVDT connection points

h' = height of panel zone between LVDT connection points

The values of (*b'*, *h'*) for Specimens CR1, CR2, CR3, CR4, CR4R, and CR5 were (10.0 in., 22.0 in.), (8.0 in., 22.5 in.), (8.0 in., 16.75 in.), (10.0 in., 22.0 in.), (9.0 in., 22.0 in.), and (8.5 in., 23.0in.), respectively. The values of (*b'*, *h'*) are slightly different each other because of different column stiffening detail and location of strain gauges. Figures A.39 and A.44 illustrate the total moment vs. panel zone shear deformation behavior for all specimens. The total moment was calculated as the sum of the individual girder moments.

A.2 Calculated Plastic Rotation and Deformation Quantities

Using the total rotation and deformation quantities calculated in Section A.1, the connection plastic rotation, plastic rotation of the girders, and plastic deformation of the panel zones were determined by subtracting the elastic components of all quantities. In the case of total connection plastic rotation, the elastic components were determined by a regression analysis of the elastic behavior. For girder and panel zone plastic deformations, the elastic components were calculated using assumed models from mechanics of materials.

The plastic connection rotation of the specimen was determined by subtracting the elastic component from the total interstory drift at each load step. The elastic slope was determined from a regression analysis of the elastic portion of the load vs. interstory drift data. The first half-cycle at 0.375% drift was used. The resulting slopes were 863,000 kip-in/rad for Specimen CR1, 746,000 kip-in/rad for Specimen CR2, 765,000 kip-in/rad for Specimen CR3, 810,000 kip-in/rad for Specimen CR4, 800,000 kip-in/rad for Specimen CR4R, and 715,000 kip-in/rad for Specimen CR5. These slopes were used to

calculate an elastic drift component at each load step. Figures A.45 through A.56 show the resulting connection plastic rotations, $\theta_{p,conn}$, for the East and West connections of all specimens. These plastic rotations include contributions from the girders, columns, and panel zones.

The plastic girder-to-column rotation, $\theta_{p,g}$, was determined by subtracting the calculated rotation due to elastic flexural deformation within the assumed plastic hinge region, L_h, from the total girder rotation given by Equation A.1. The length of the plastic hinge was assumed equal to half the girder depth, or approximately 12 in. The elastic girder rotation in the hinge region was calculated as (from Hajjar et al., 1998b):

$$\theta_{e,g} = \frac{PL_h\left(2L_g - L_h\right)}{2EI_g} \tag{A.3}$$

where:

$\theta_{e,g}$ = elastic rotation of girder plastic hinge region

P = applied girder tip load

E = Young's modulus of steel

I_g = girder moment of inertia = 2700 in^4

Figures A.57 through A.68 illustrate the resulting plastic girder rotation measured relative to the column face.

The plastic shear deformation of the panel zone, $\gamma_{p,pz}$, was determined by subtracting the calculated elastic component of deformation from the total deformation calculated by Equation A.2. For purposes of elastic shear deformation computation, the panel zone was treated as a body in pure shear. The elastic deformation of the panel zone was calculated as:

$$\gamma_{e,pz} = \frac{P_{tot}\left(L_g \big/ d_g - L_g \big/ L_c\right)}{GA_{cw}} \tag{A.4}$$

where:

$\gamma_{e,pz}$ = elastic panel zone deformation

P_{tot} = total girder tip loads (East and West girders)

d_g = girder depth

L_c = column length between pin centerlines

G = shear modulus of elasticity

A_{cw} = column web area = $d_c t_{cw}$

Figures A.69 and A.74 show the moment vs. plastic panel zone shear deformation behavior for all test specimens.

A.3 Plastic Rotations Relative to the Column Centerline

The plastic rotations and deformations reported in Figures A.57 through A.74 are not directly comparable quantities. The plastic girder rotations are measured relative to the column face instead of the column centerline, and the plastic shear deformations of the panel zones are not converted into an equivalent rotation. In this section, the data of Figures A.57 through A.74 are converted to plastic rotations relative to the column centerlines, such that the rotation values can be directly compared.

The plastic girder rotations were converted to rotations relative to the column centerline by scaling the results by the ratio of the girder length, L_g, to the distance to the column centerline. This is expressed as:

$$\theta_{p,g}^{CL} = \theta_{p,g}\left(\frac{L_g}{L_g + d_c/2}\right) \tag{A.5}$$

where:

$\theta_{p,g}^{CL}$ = plastic girder-to-column rotation relative to the column centerline

Figures A.75 through A.86 show the plastic girder rotation behavior as computed by Equation A.5.

The plastic panel zone shear deformations were converted to plastic shear rotations using a procedure from Leon (1983). The expression is given as:

$$\theta_{p,pz}^{CL} = \frac{1}{\left(L_g + d_c/2\right)}\left[\frac{\gamma_{p,pz} L_g \left(L_c - d_g\right)}{L_c} - \frac{\gamma_{p,pz} d_g d_c}{2L_c}\right] \tag{A.6}$$

where:

$\theta_{p,pz}^{CL}$ = plastic panel zone rotation relative to the column centerline

The terms in brackets represent the girder tip deflection due to plastic panel zone deformation, which is then converted to a plastic rotation by the first term of Equation A.6. Figures A.87 and A.92 illustrate the plastic panel zone rotations for all specimens as computed by Equation A.6.

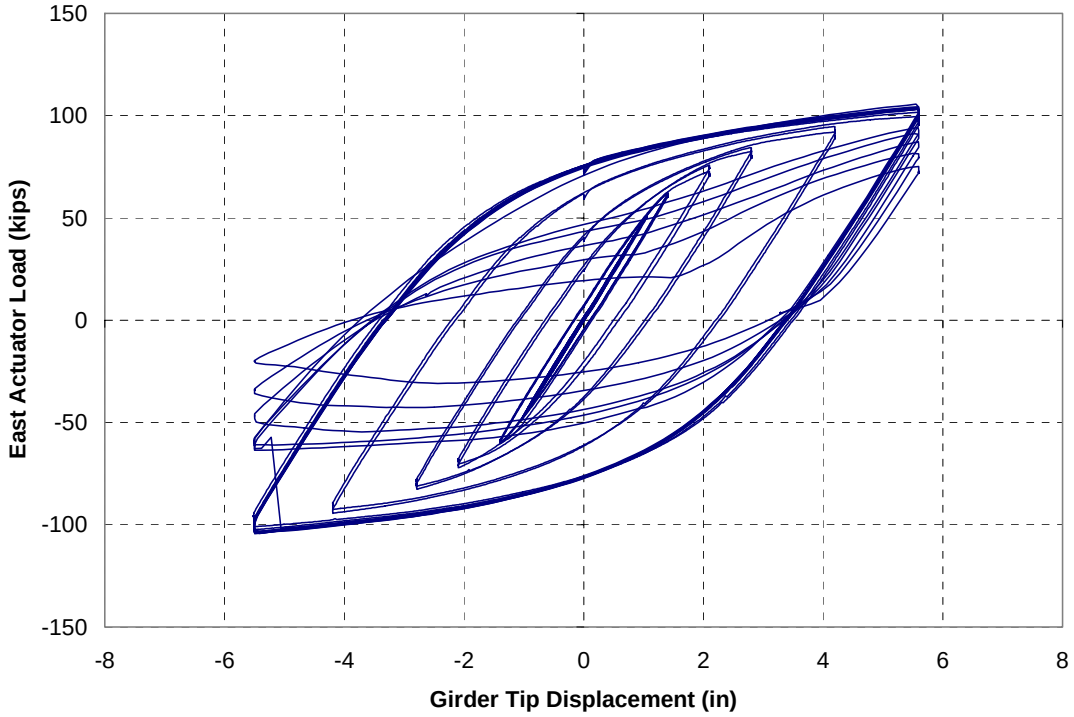


Figure A.1: Load vs. Stroke for East Girder, CR1

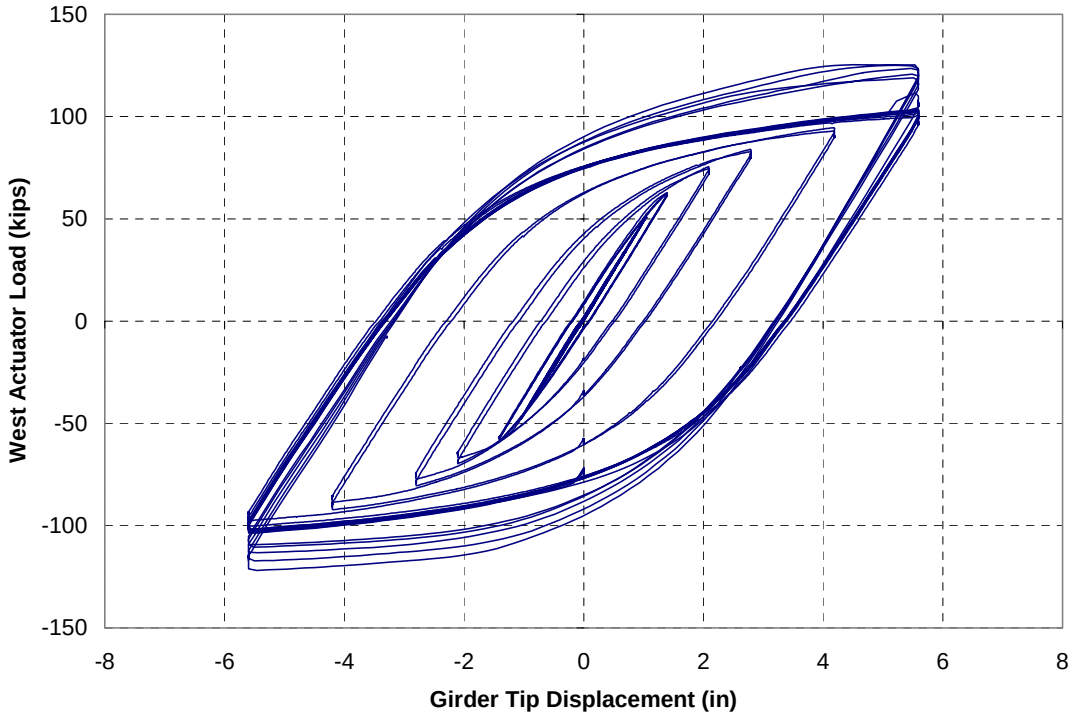


Figure A.2: Load vs. Stroke for West Girder, CR1

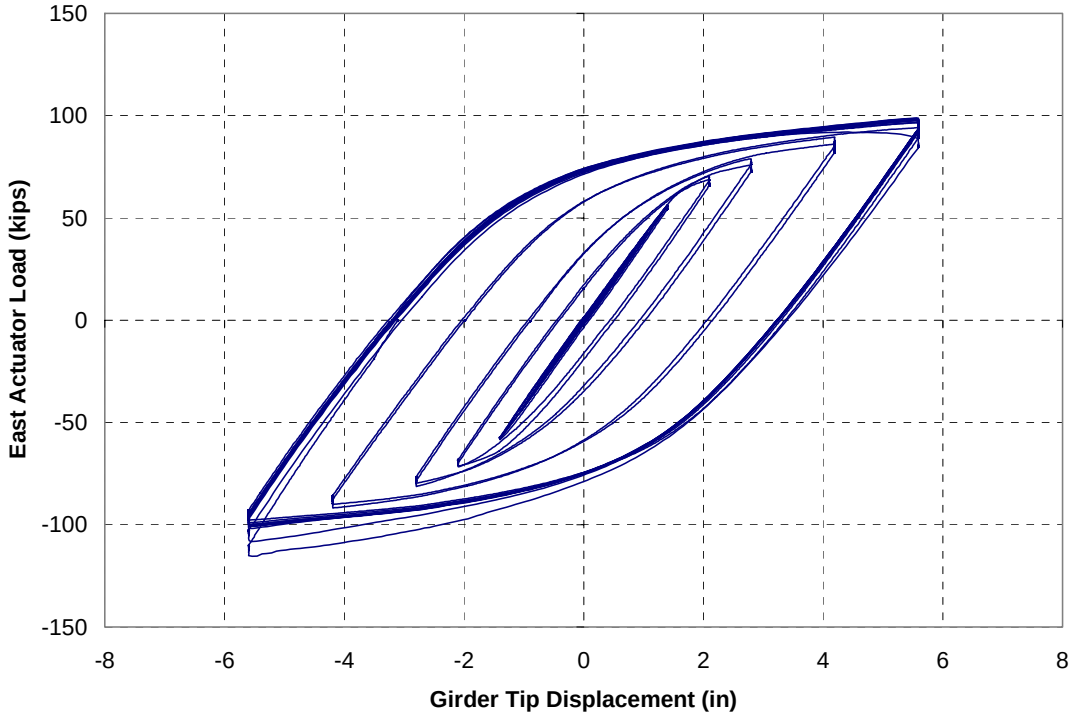


Figure A.3: Load vs. Stroke for East Girder, CR2

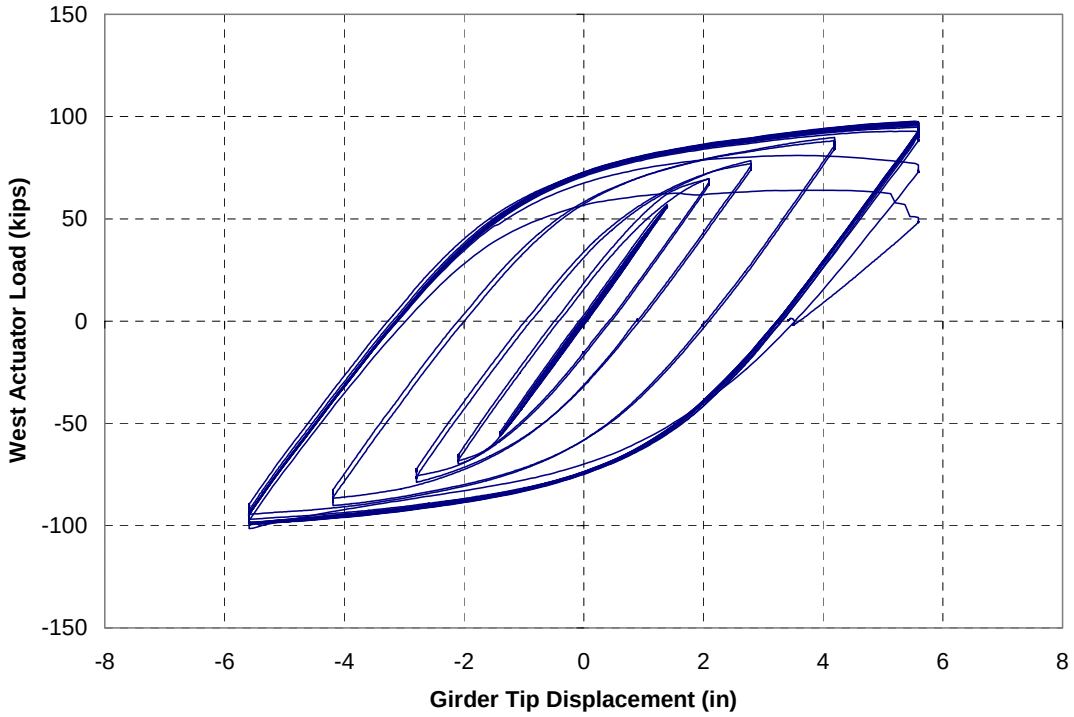


Figure A.4: Load vs. Stroke for West Girder, CR2

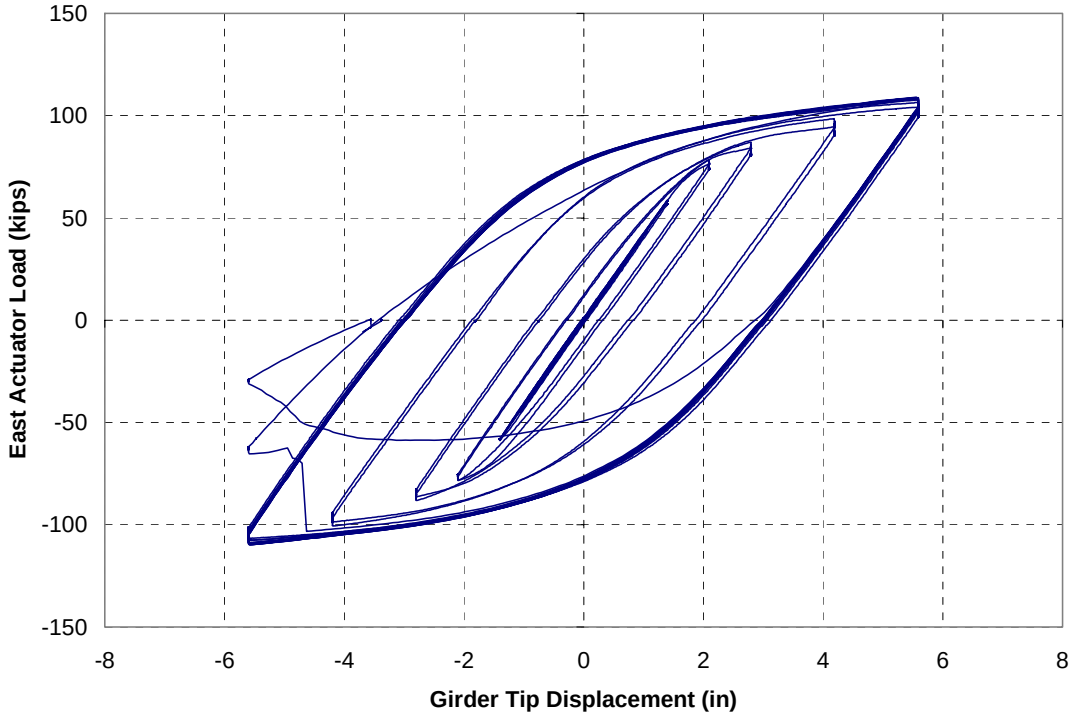


Figure A.5: Load vs. Stroke for East Girder, CR3

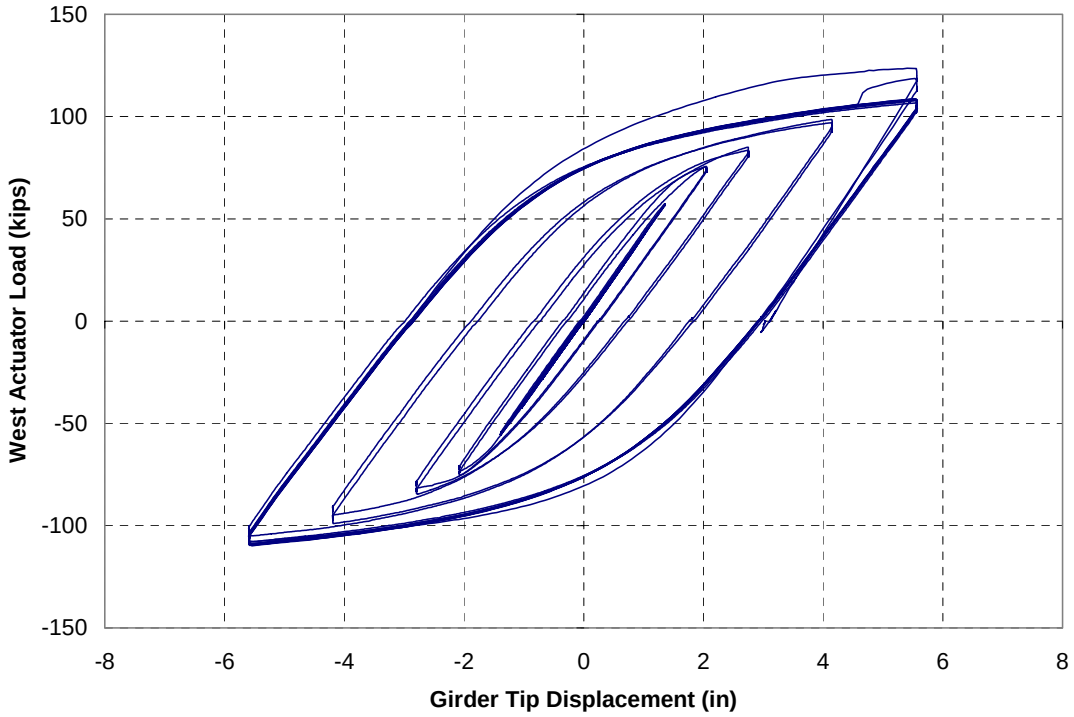


Figure A.6: Load vs. Stroke for West Girder, CR3

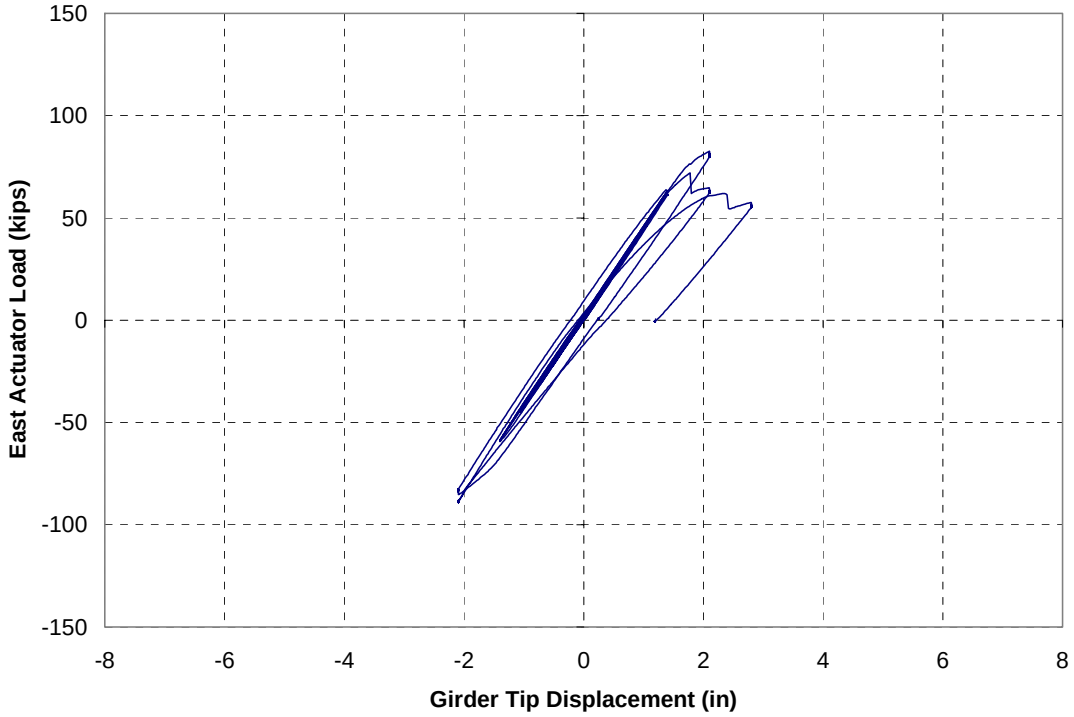


Figure A.7: Load vs. Stroke for East Girder, CR4

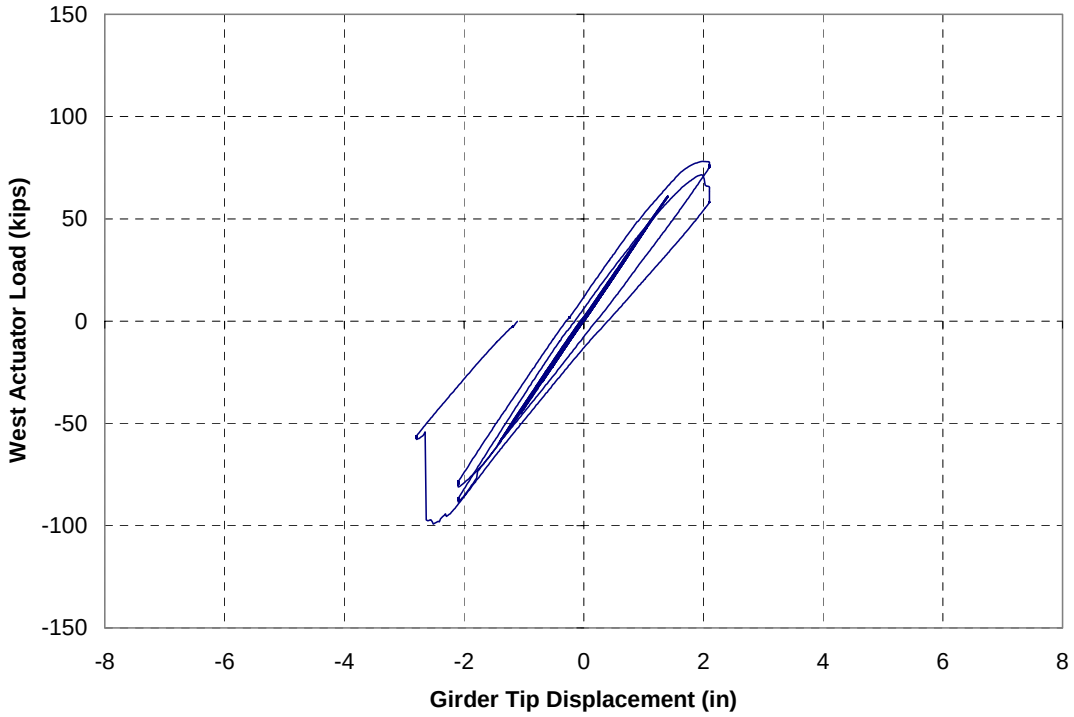


Figure A.8: Load vs. Stroke for West Girder, CR4

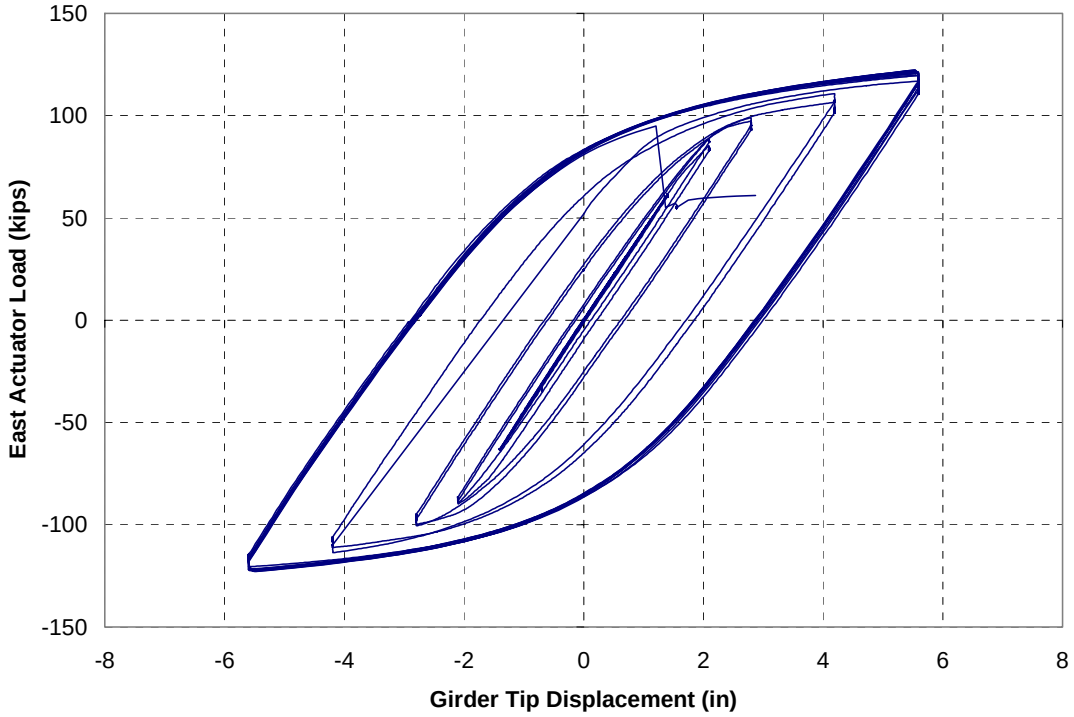


Figure A.9: Load vs. Stroke for East Girder, CR4R

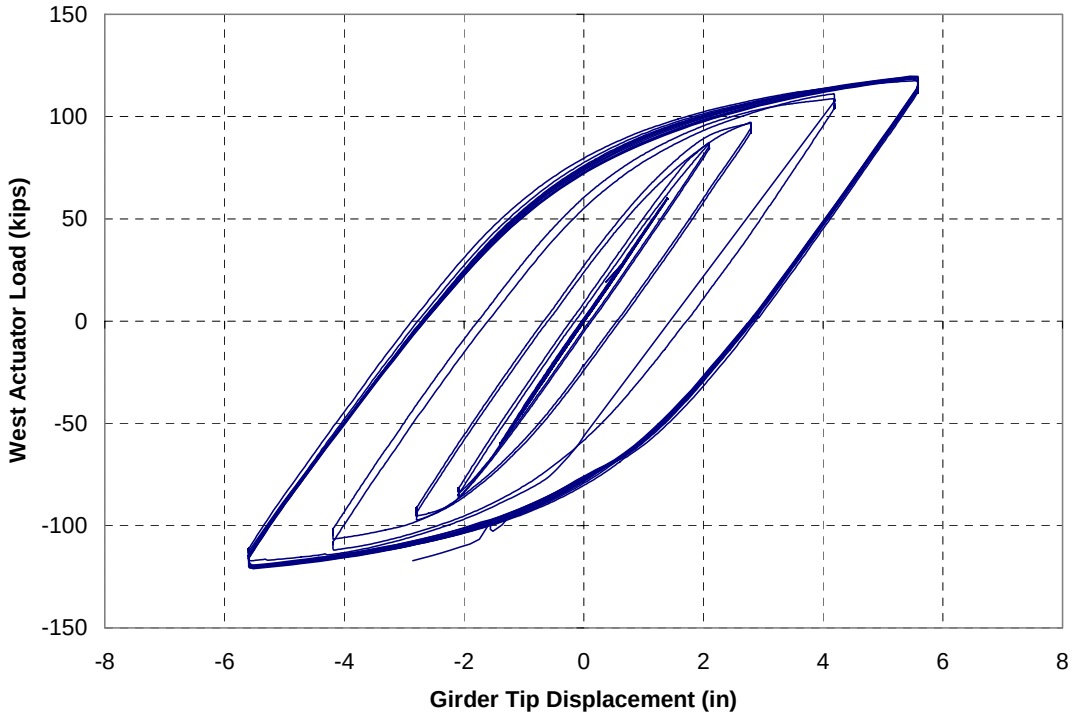


Figure A.10: Load vs. Stroke for West Girder, CR4R

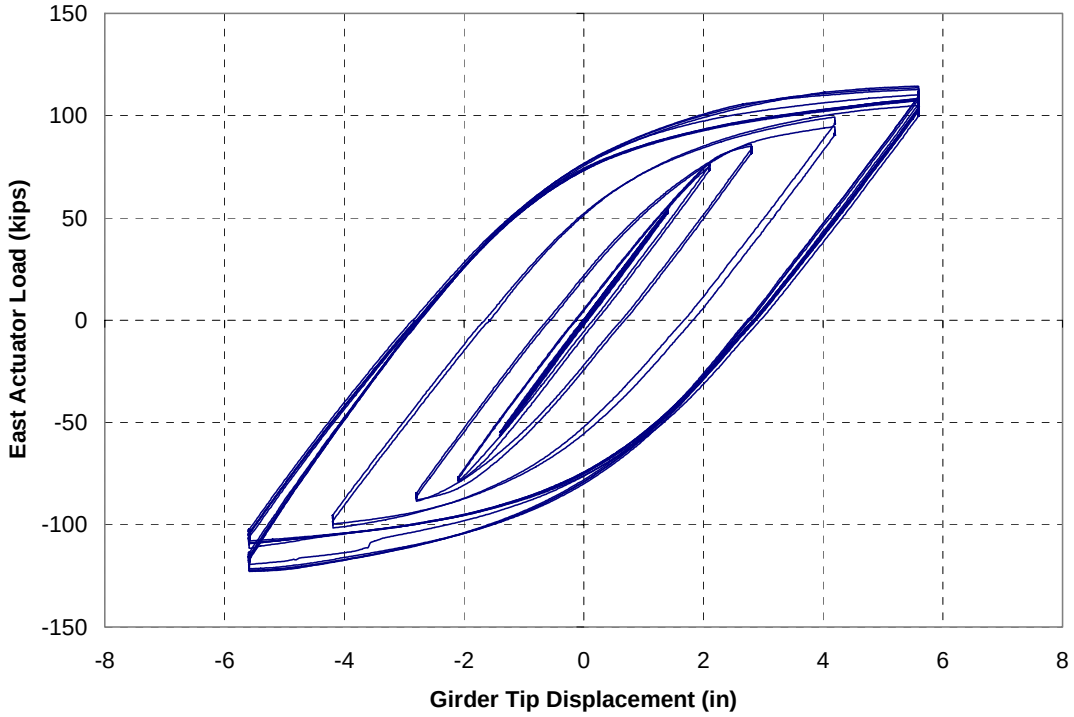


Figure A.11: Load vs. Stroke for East Girder, CR5

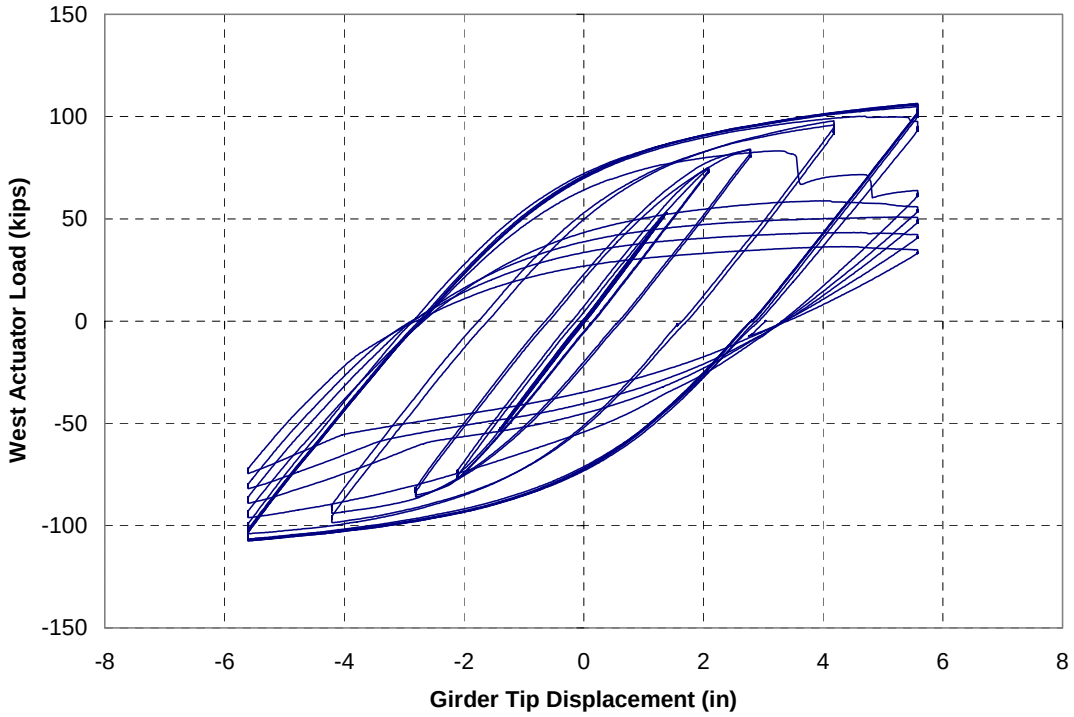


Figure A.12: Load vs. Stroke for West Girder, CR5

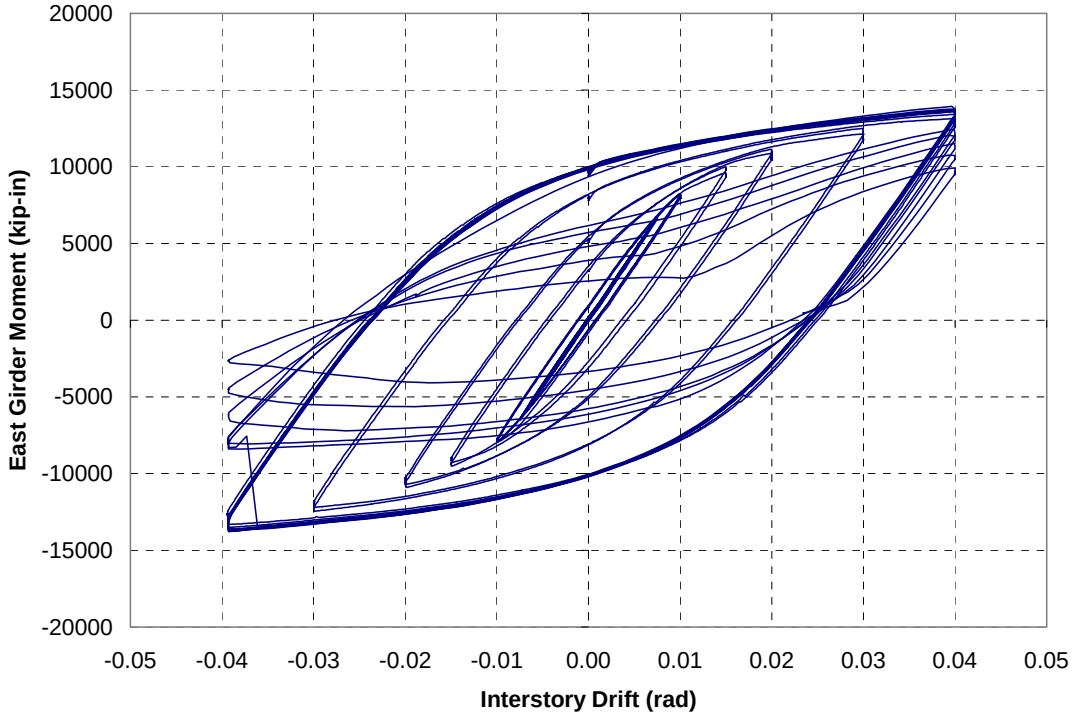


Figure A.13: Moment vs. Interstory Drift for East Girder, CR1

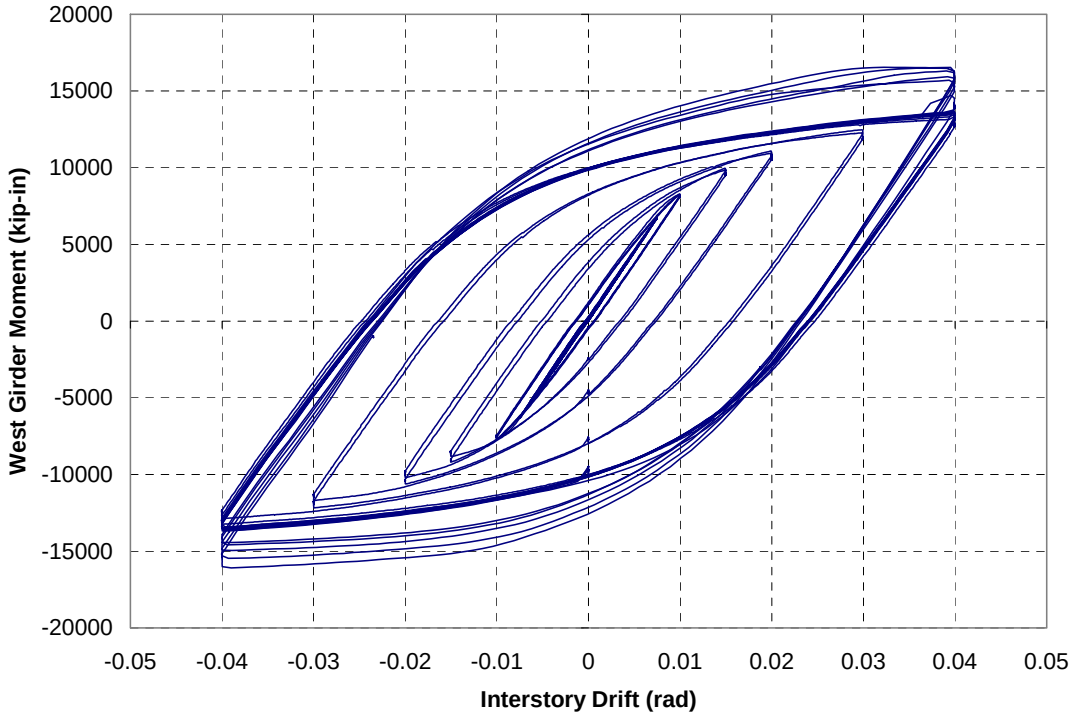


Figure A.14: Moment vs. Interstory Drift for West Girder, CR1

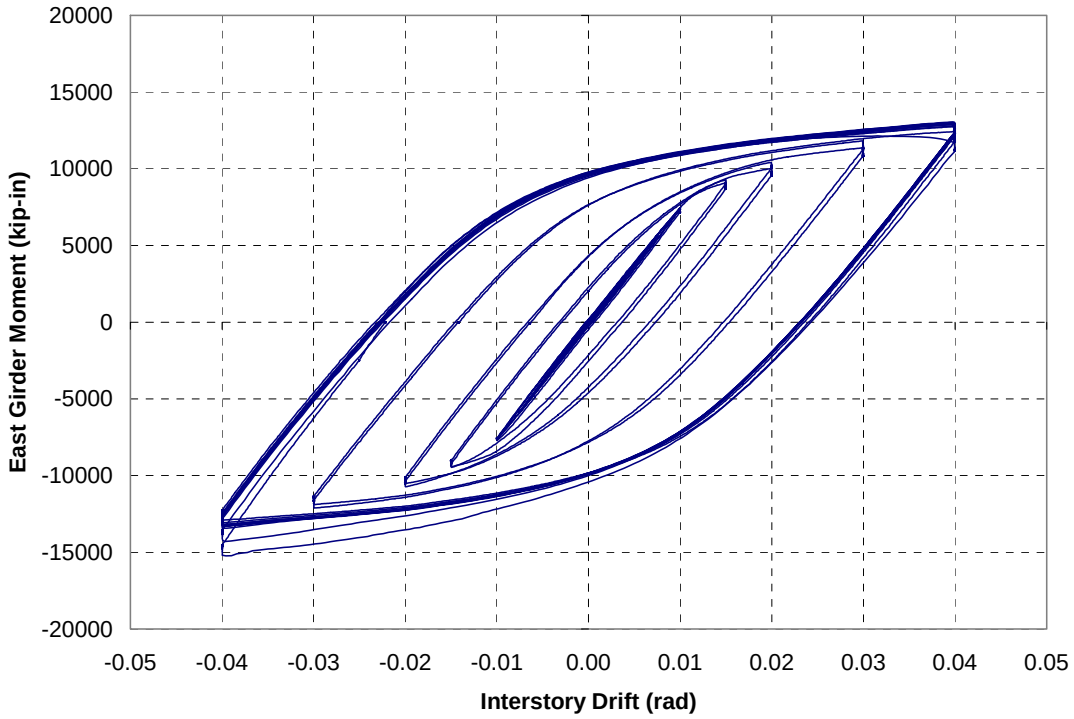


Figure A.15: Moment vs. Interstory Drift for East Girder, CR2

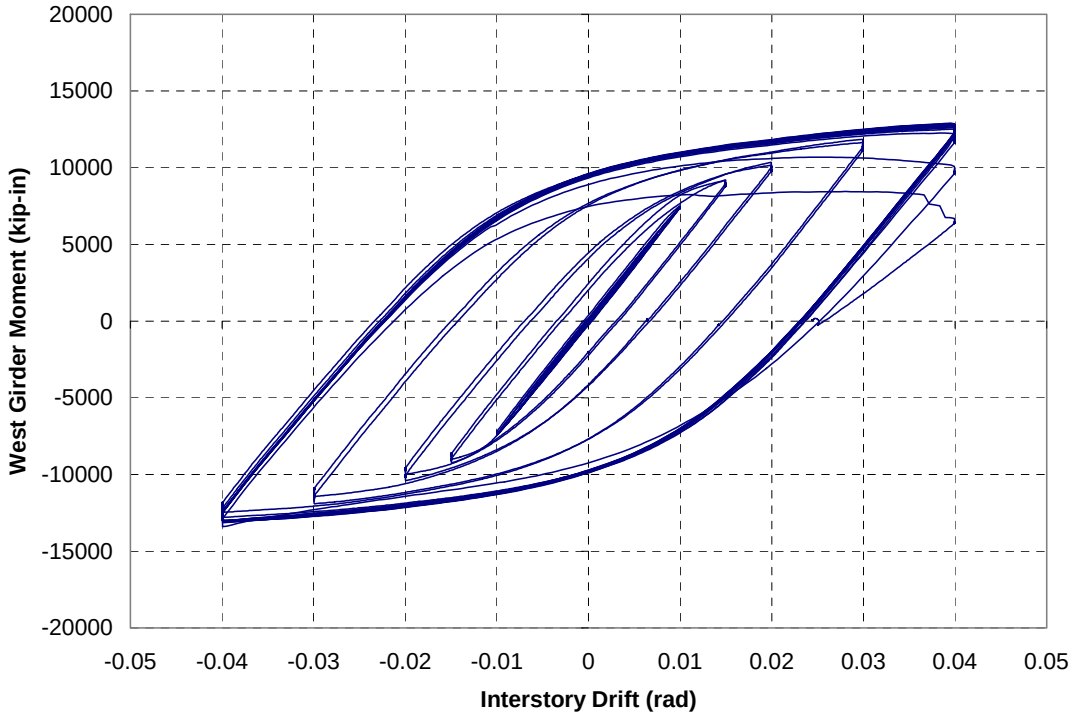


Figure A.16: Moment vs. Interstory Drift for West Girder, CR2

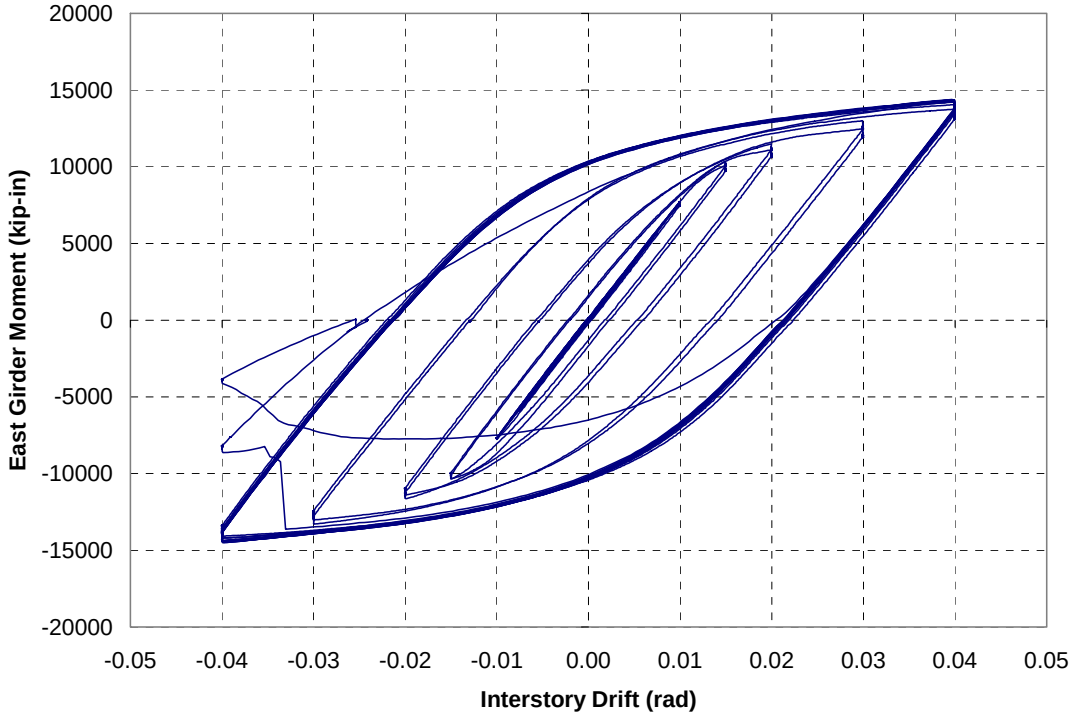


Figure A.17: Moment vs. Interstory Drift for East Girder, CR3

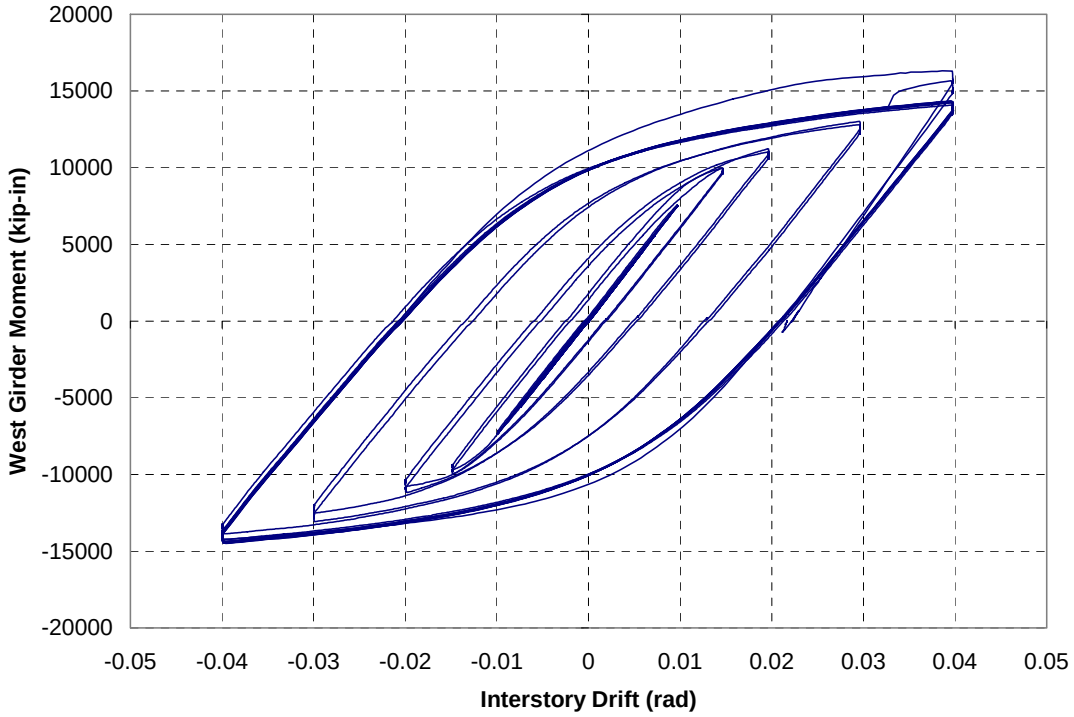


Figure A.18: Moment vs. Interstory Drift for West Girder, CR3

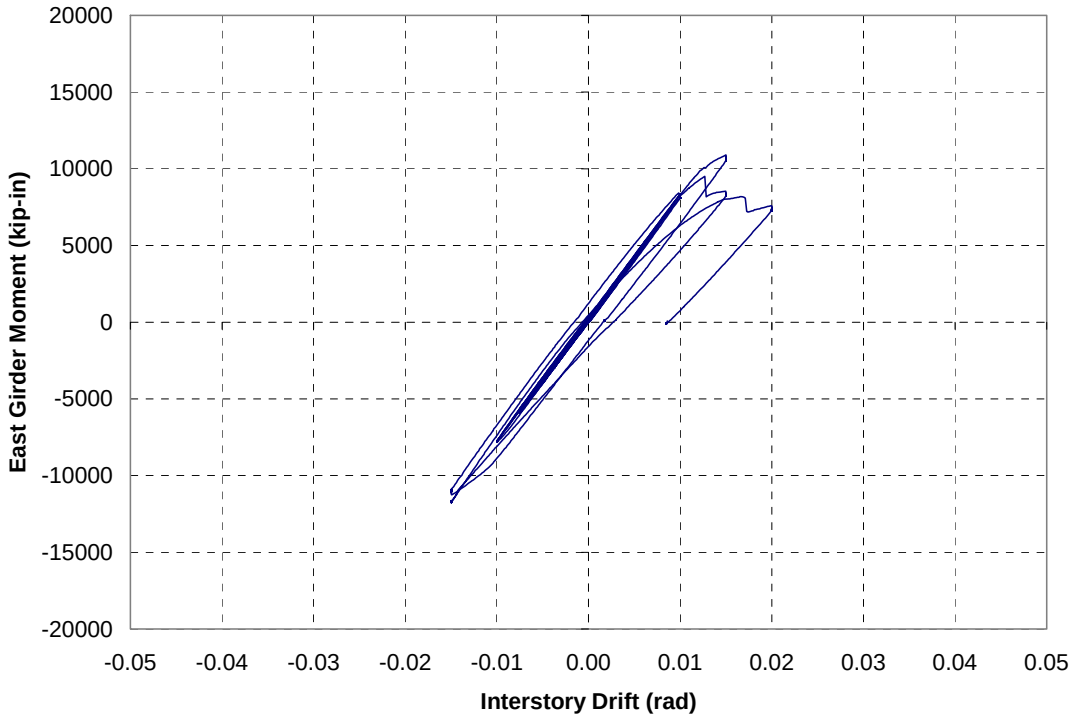


Figure A.19: Moment vs. Interstory Drift for East Girder, CR4

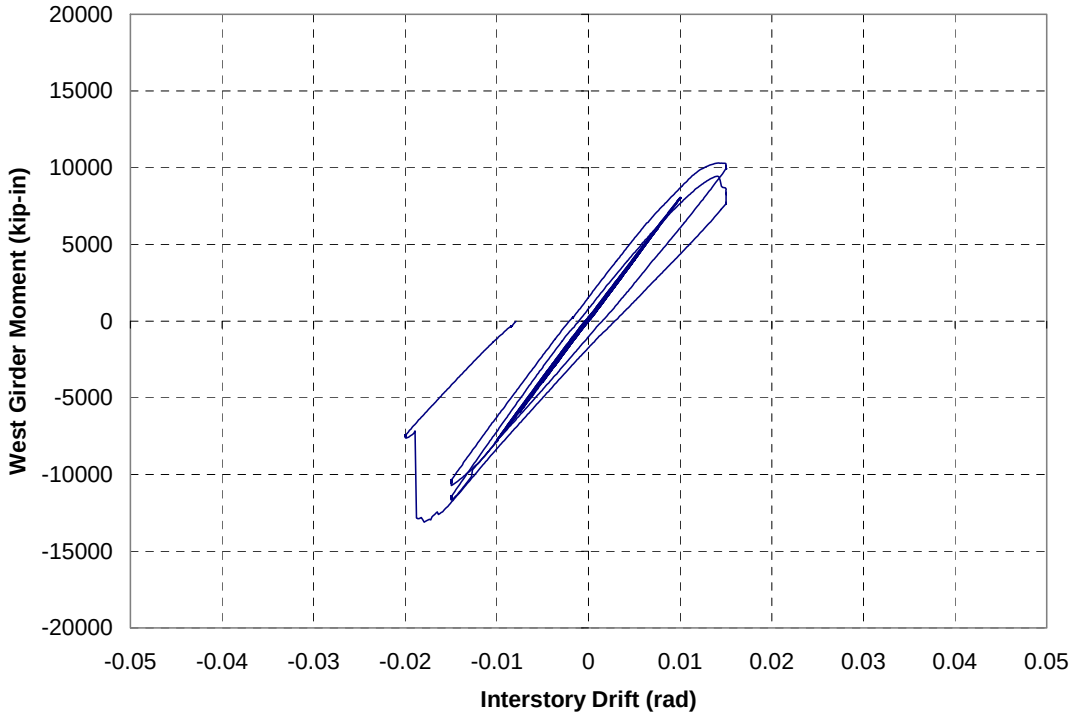


Figure A.20: Moment vs. Interstory Drift for West Girder, CR4

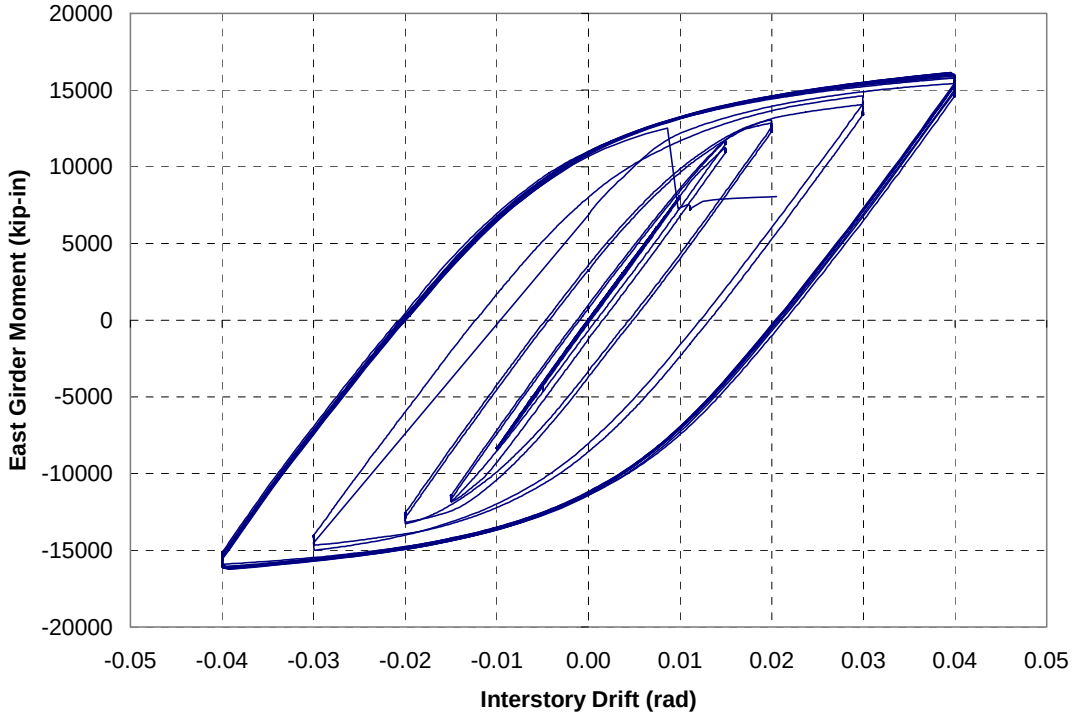


Figure A.21: Moment vs. Interstory Drift for East Girder, CR4R

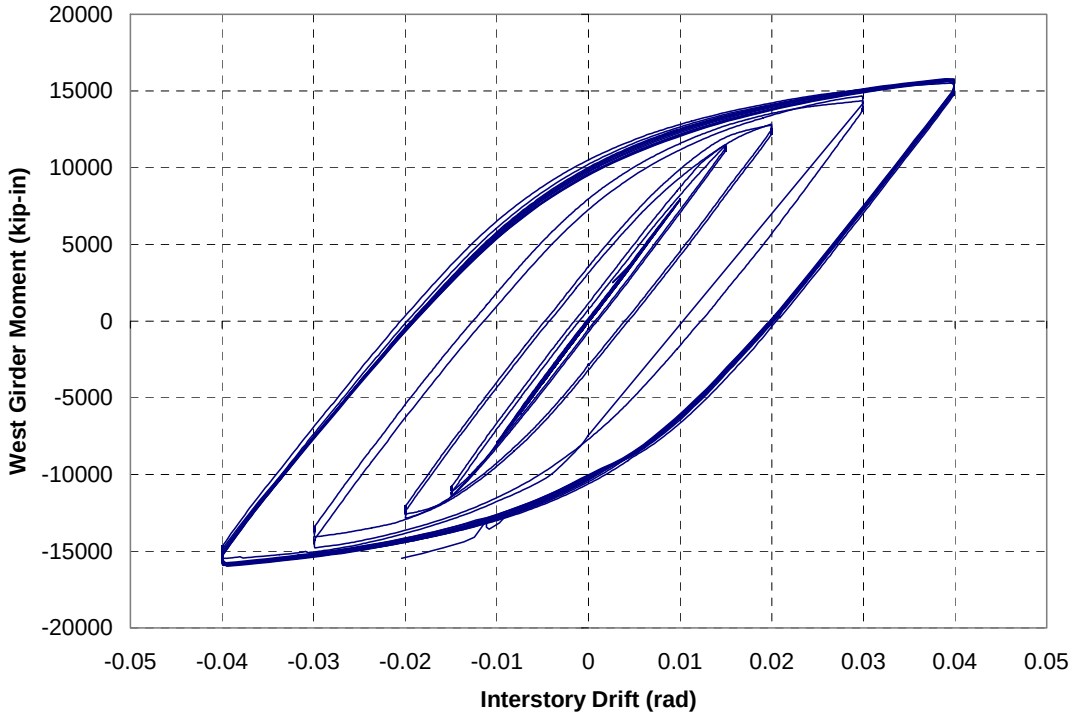


Figure A.22: Moment vs. Interstory Drift for West Girder, CR4R

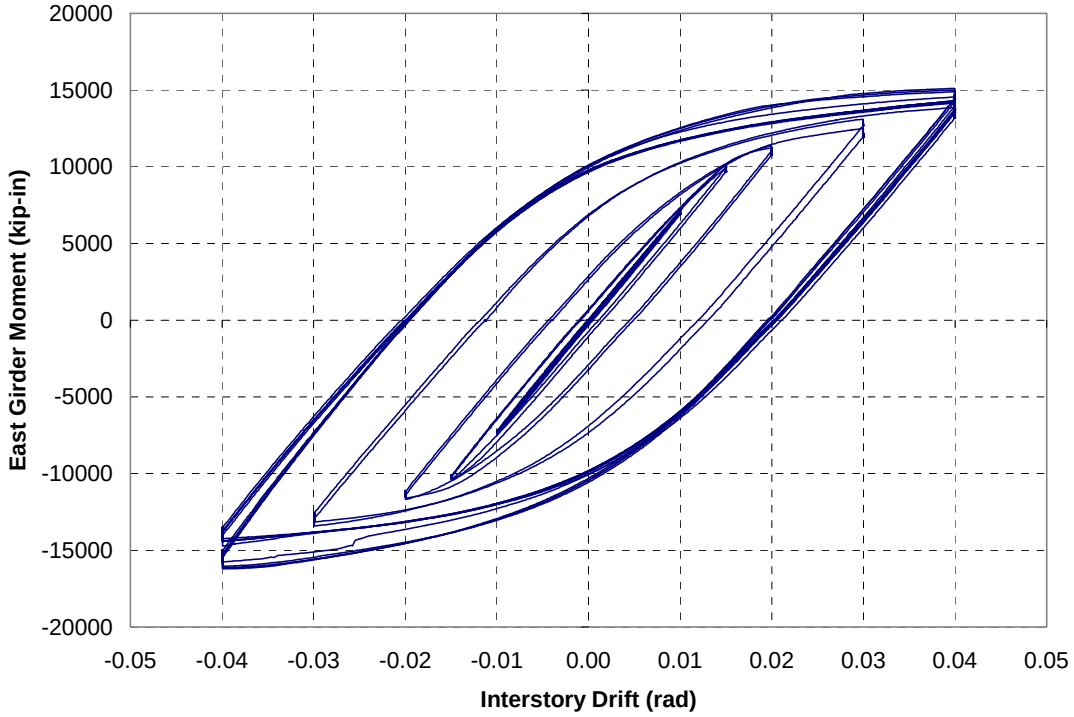


Figure A.23: Moment vs. Interstory Drift for East Girder, CR5

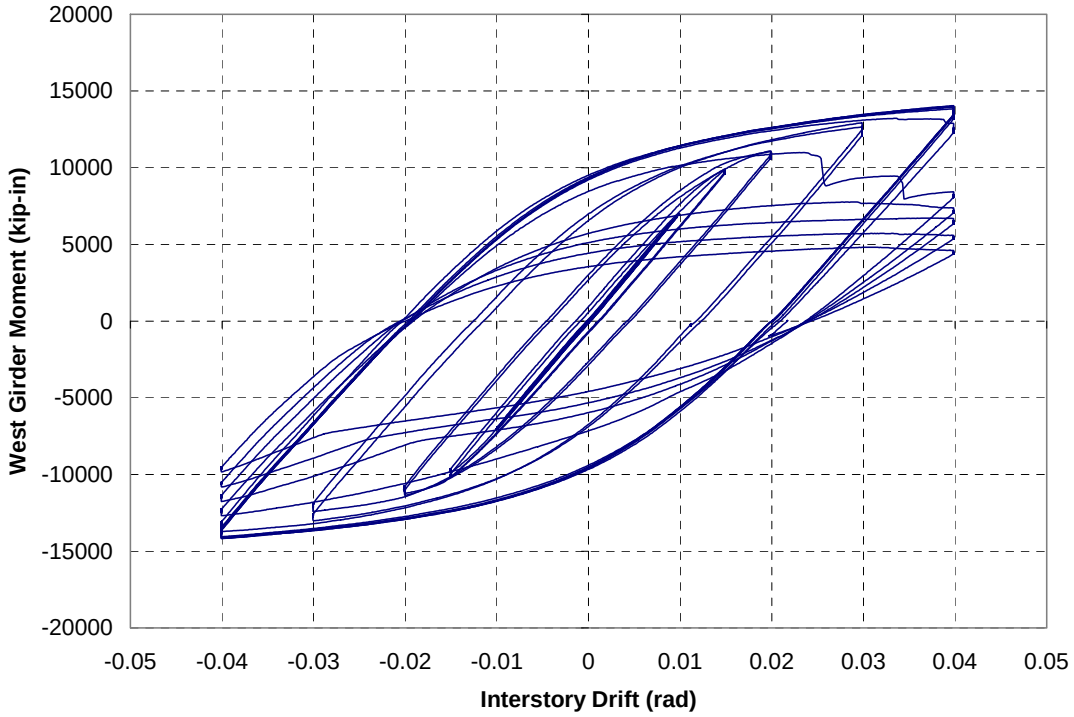


Figure A.24: Moment vs. Interstory Drift for West Girder, CR5

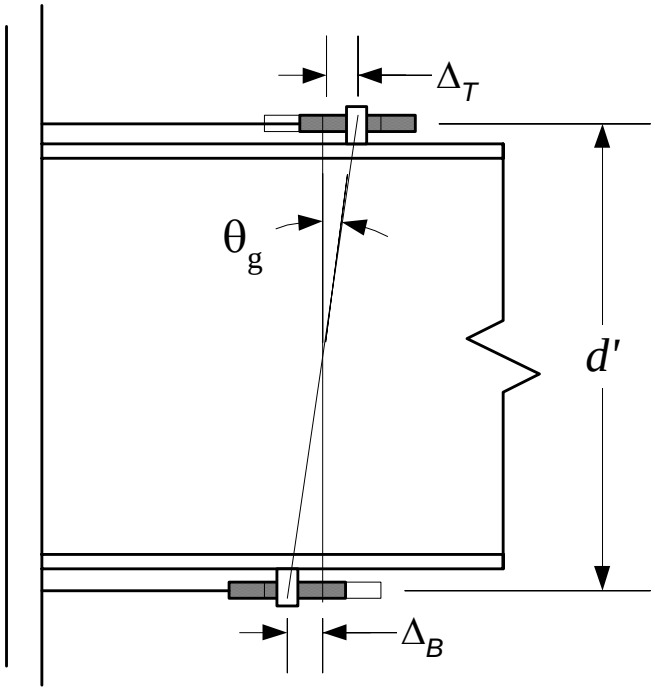


Figure A.25: Illustration of Girder LVDT Placement and Measurement of Rotation

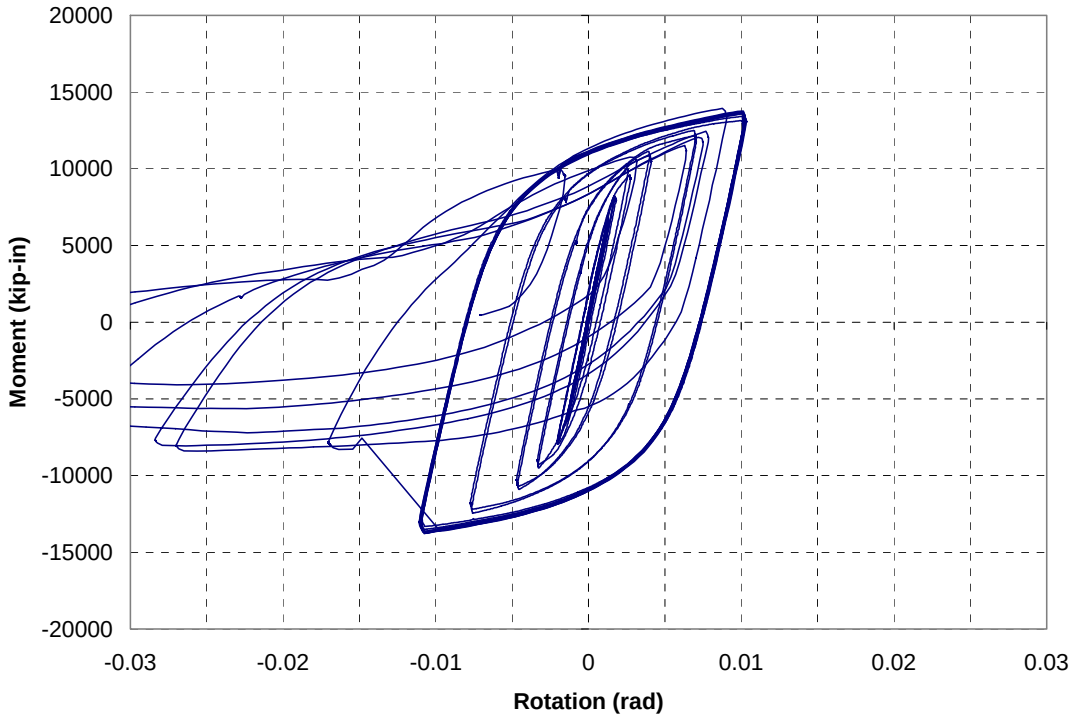


Figure A.26(a): East Girder Total Rotation, CR1

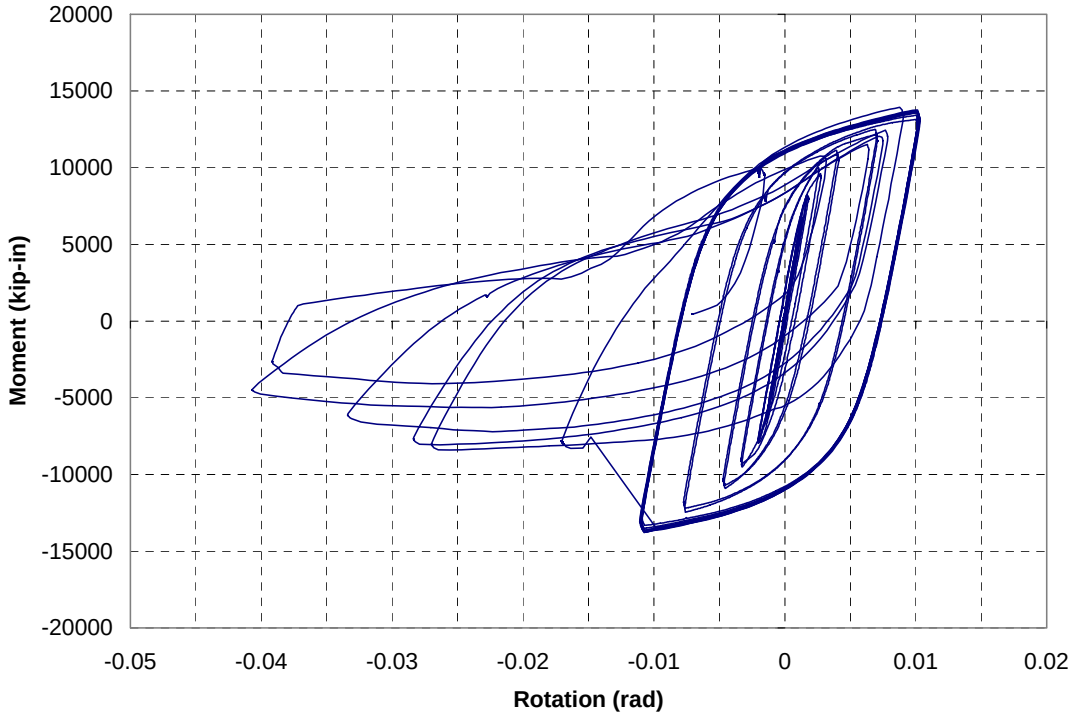


Figure A.26(b): East Girder Total Rotation, CR1 (Re-scaled)

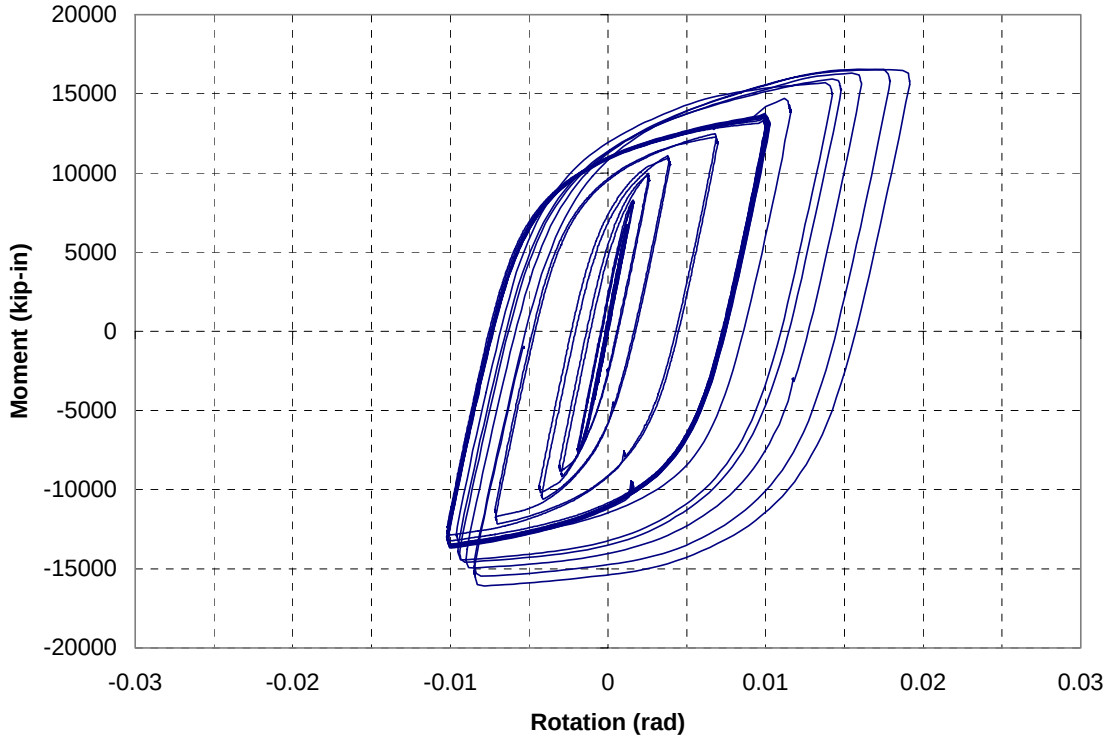


Figure A.27: West Girder Total Rotation, CR1

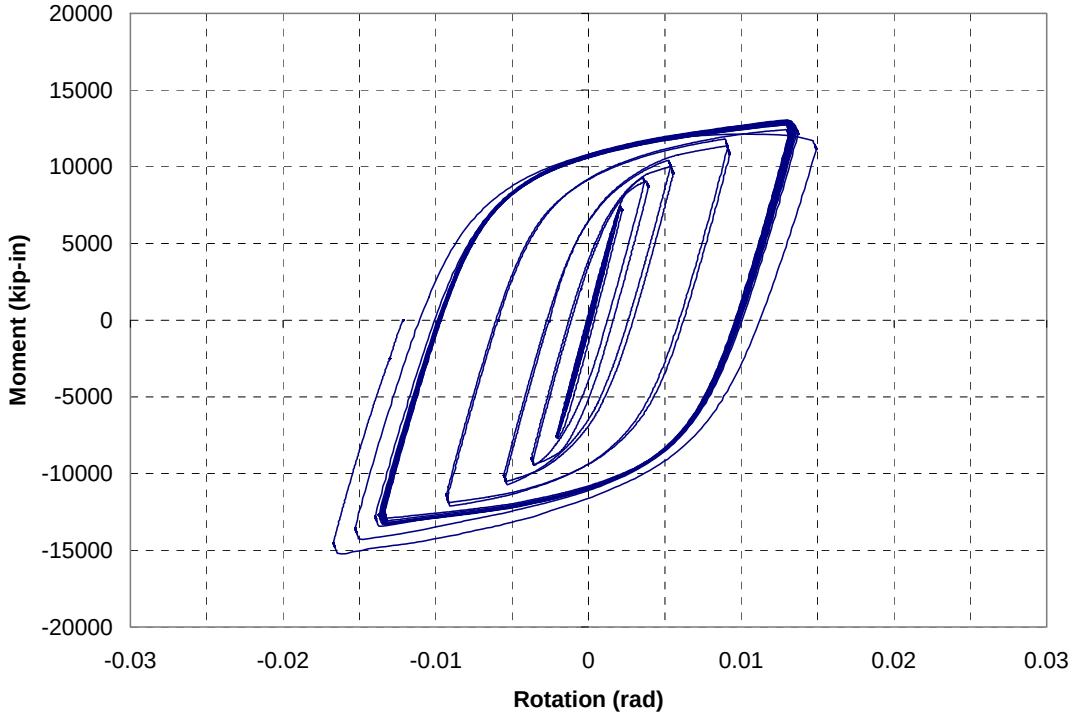


Figure A.28: East Girder Total Rotation, CR2

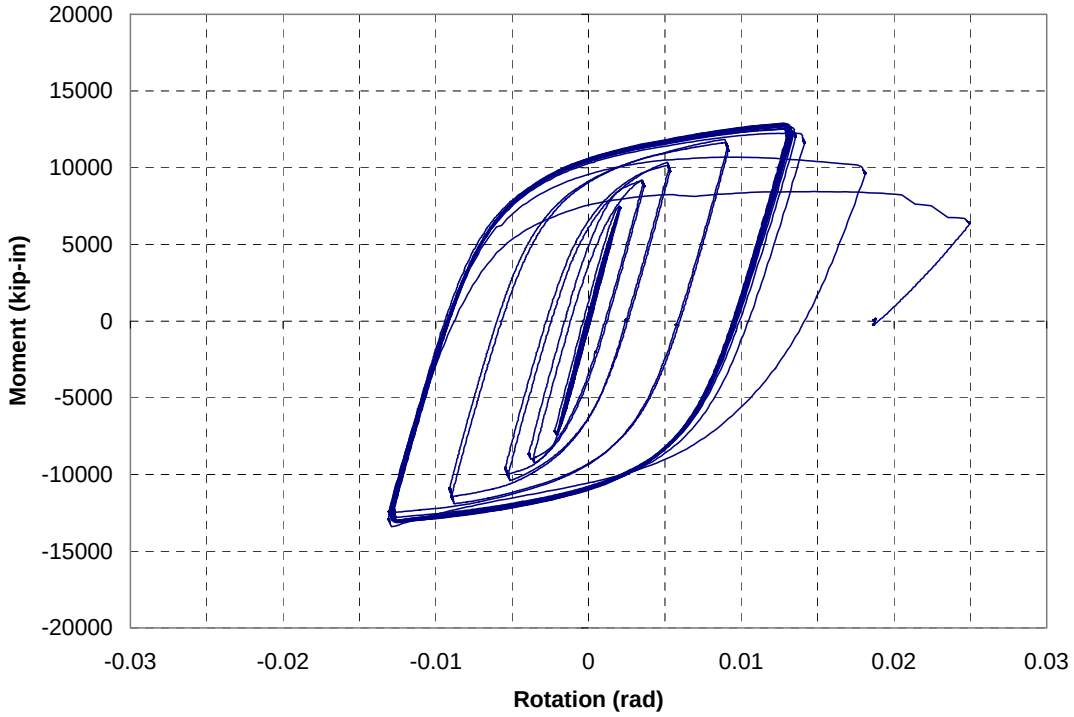


Figure A.29: West Girder Total Rotation, CR2

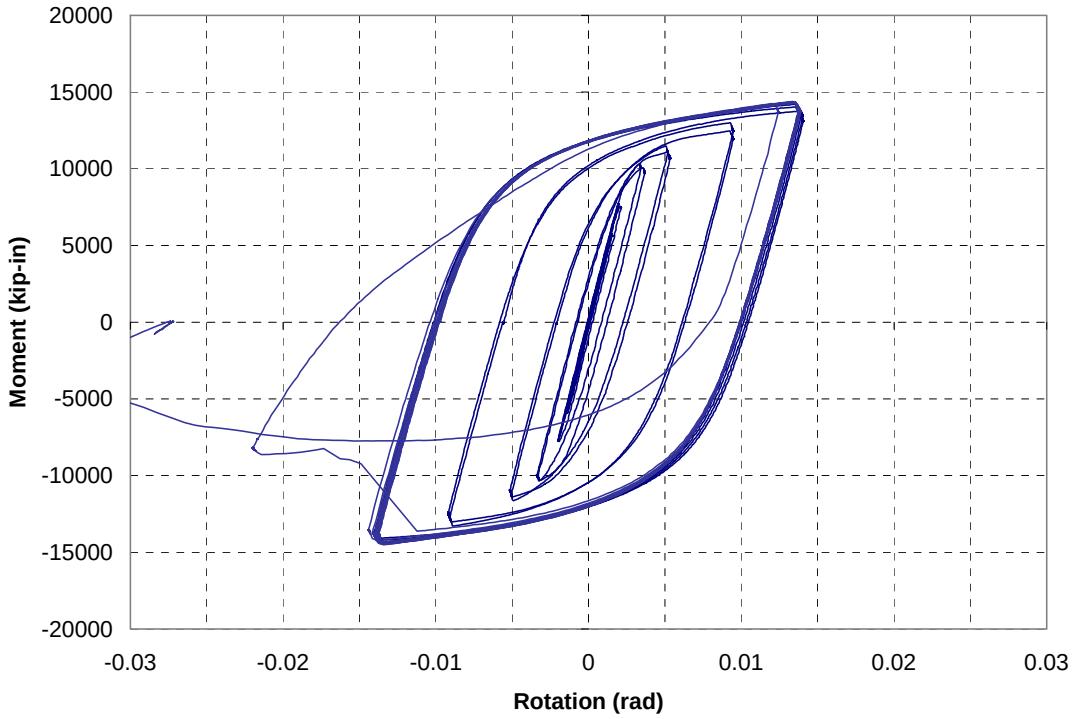


Figure A.30(a): East Girder Total Rotation, CR3

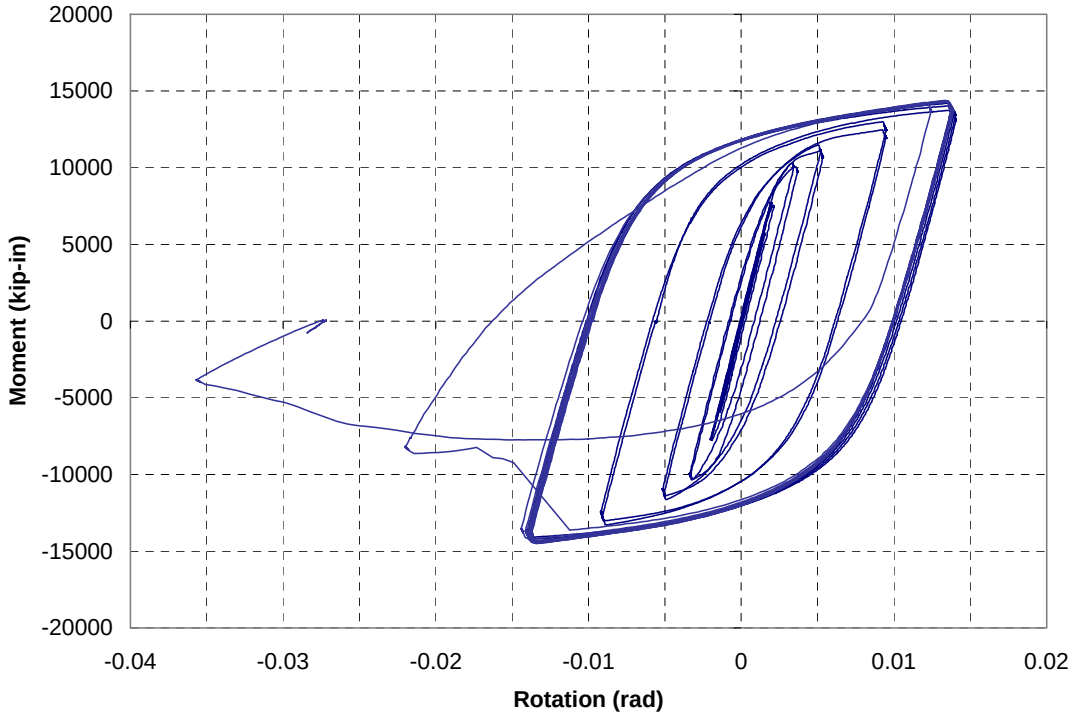


Figure A.30(b): East Girder Total Rotation, CR3 (Re-scaled)

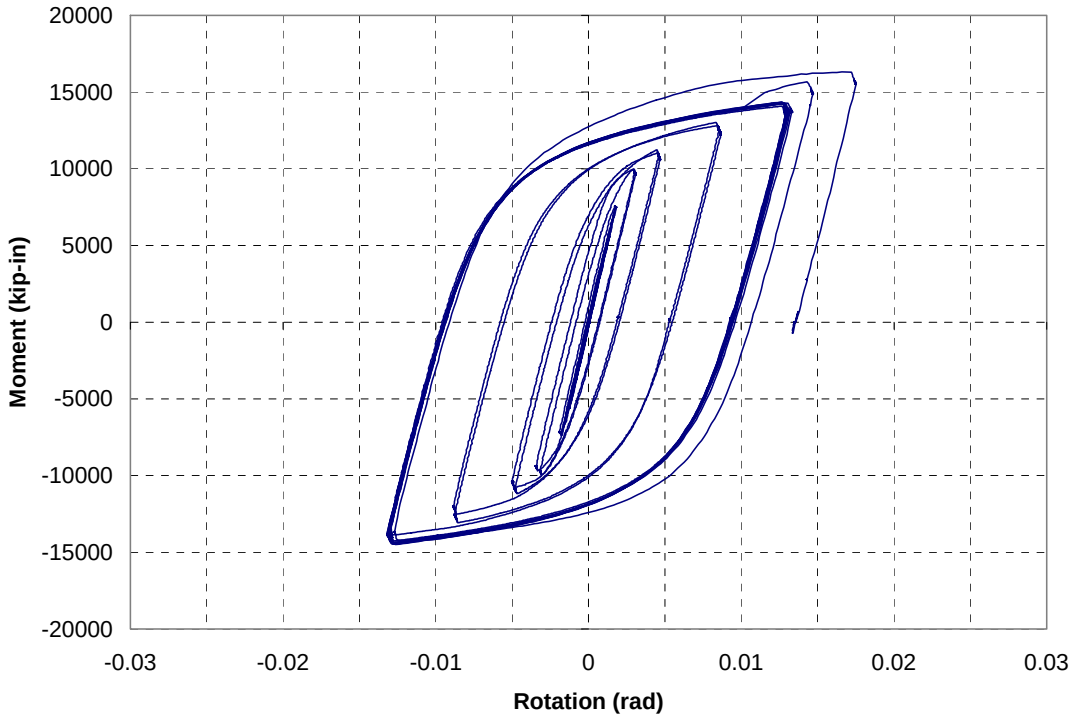


Figure A.31: West Girder Total Rotation, CR3

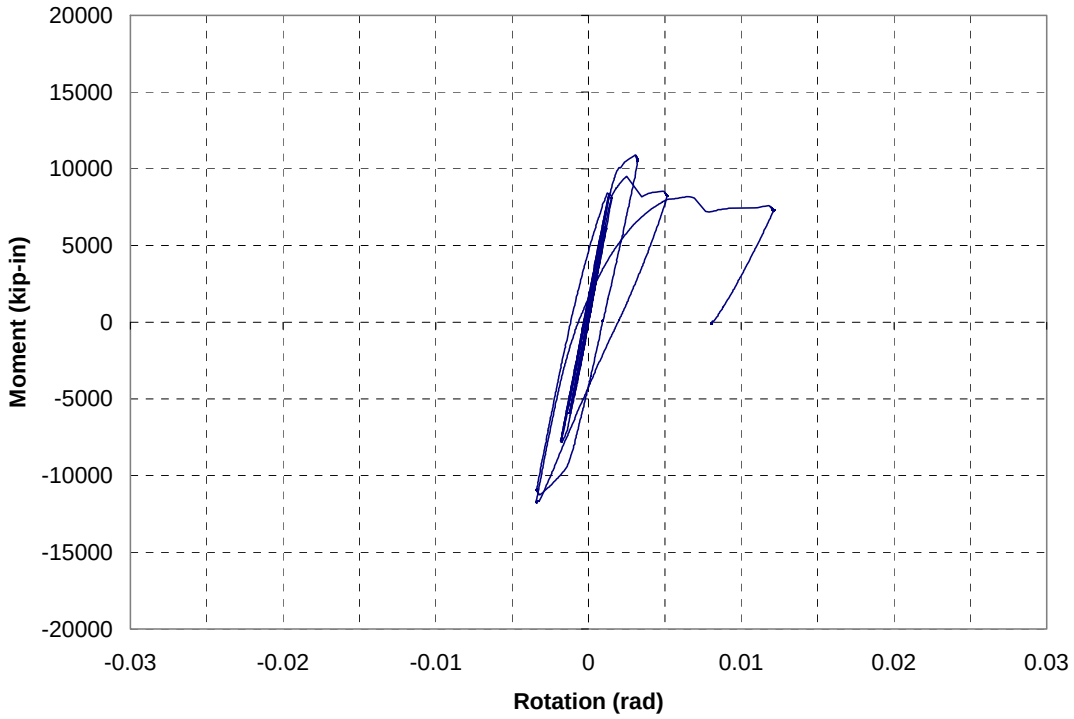


Figure A.32: East Girder Total Rotation, CR4

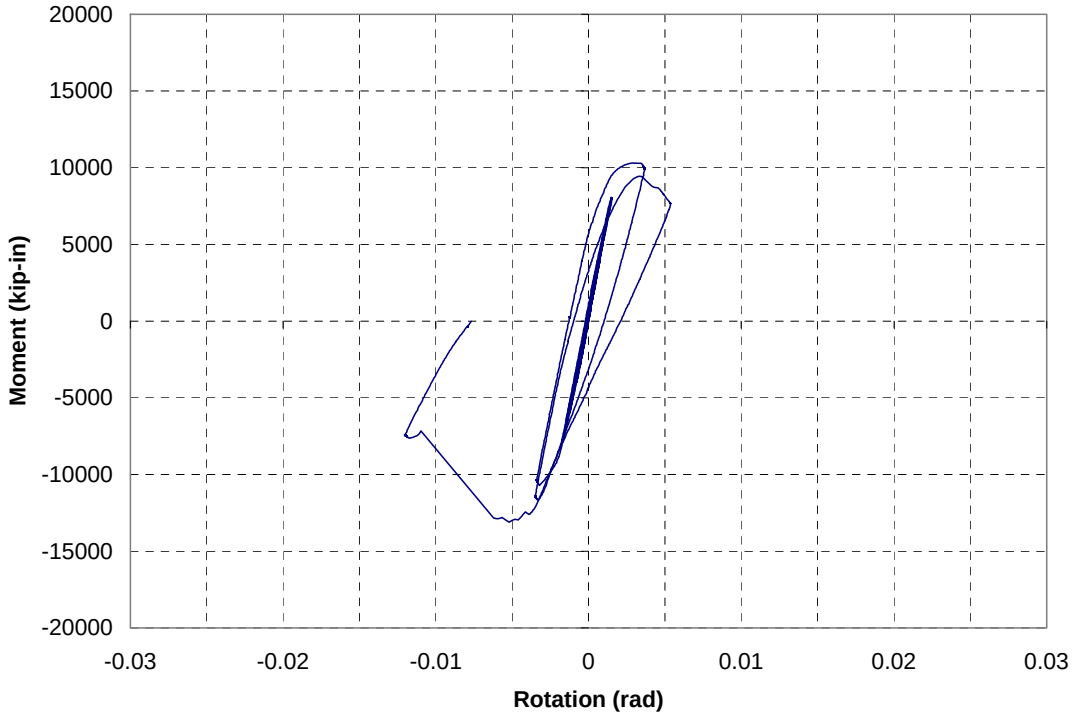


Figure A.33: West Girder Total Rotation, CR4

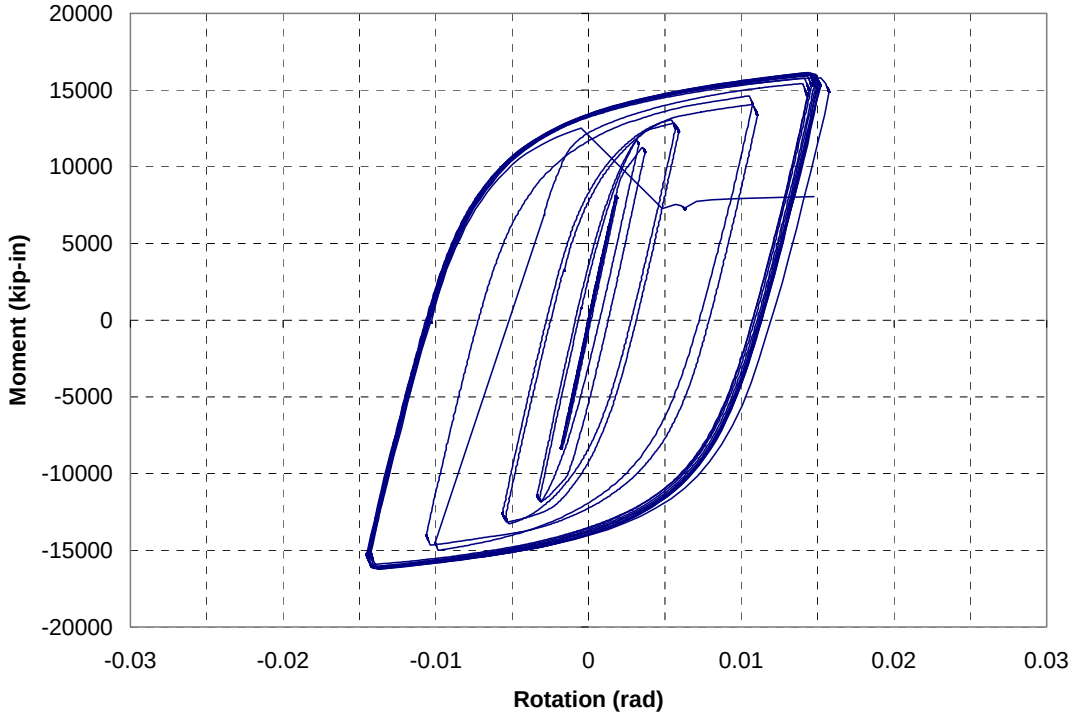


Figure A.34: East Girder Total Rotation, CR4R

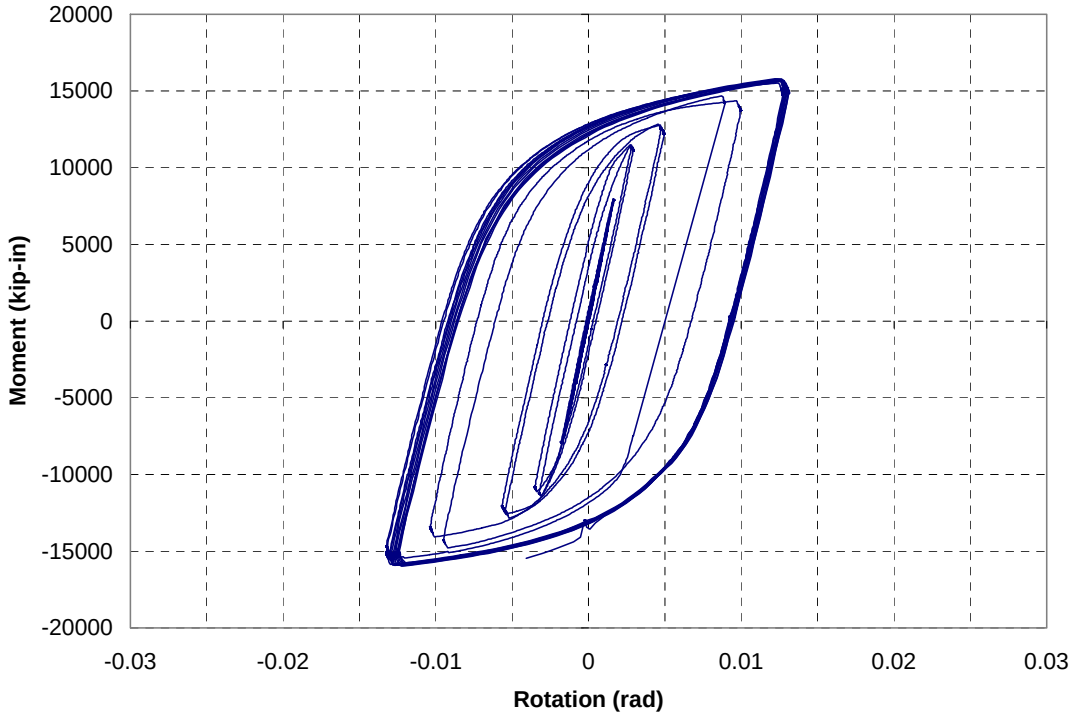


Figure A.35: West Girder Total Rotation, CR4R

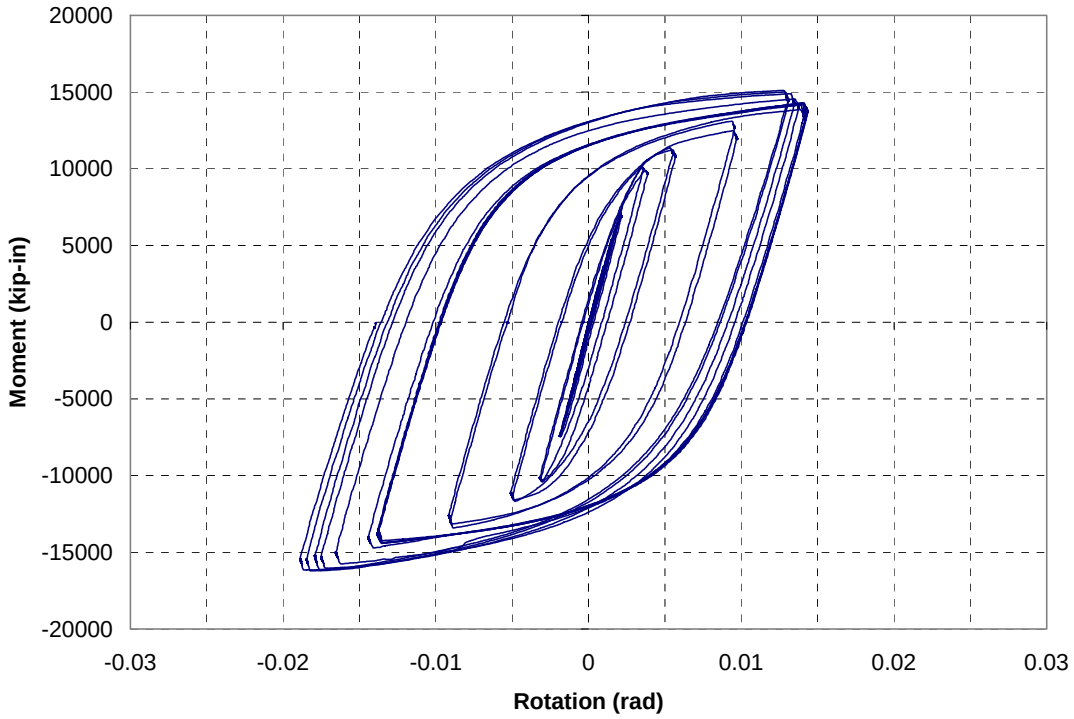


Figure A.36: East Girder Total Rotation, CR5

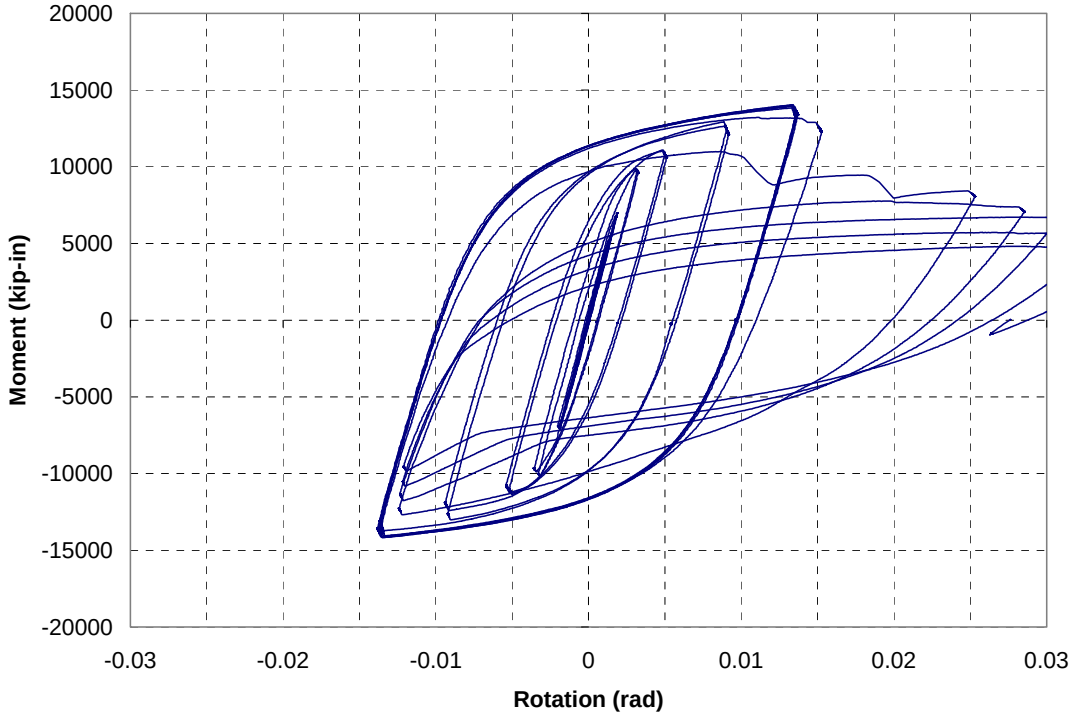


Figure A.37(a): West Girder Total Rotation, CR5

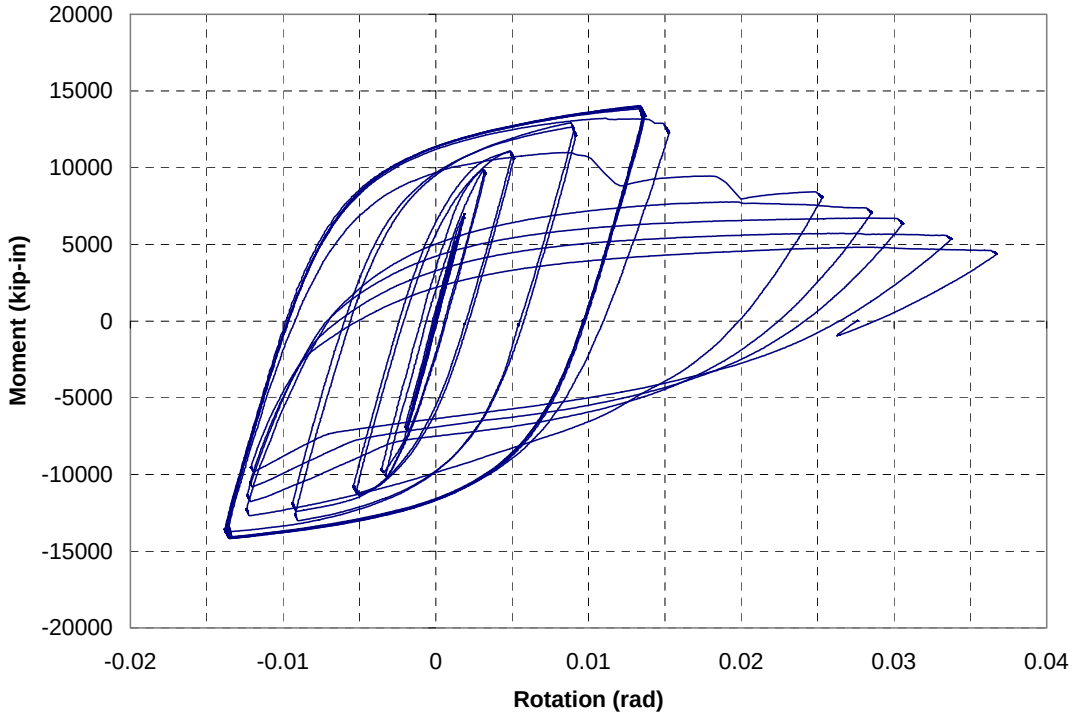


Figure A.37(b): West Girder Total Rotation, CR5 (Re-scaled)

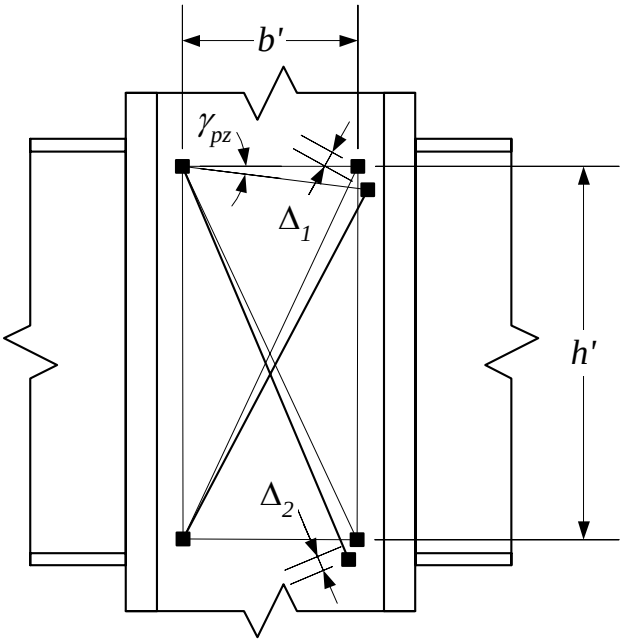


Figure A.38: Illustration of Panel Zone Shear Deformation Measurement [after (Krawinkler et al., 1971)]

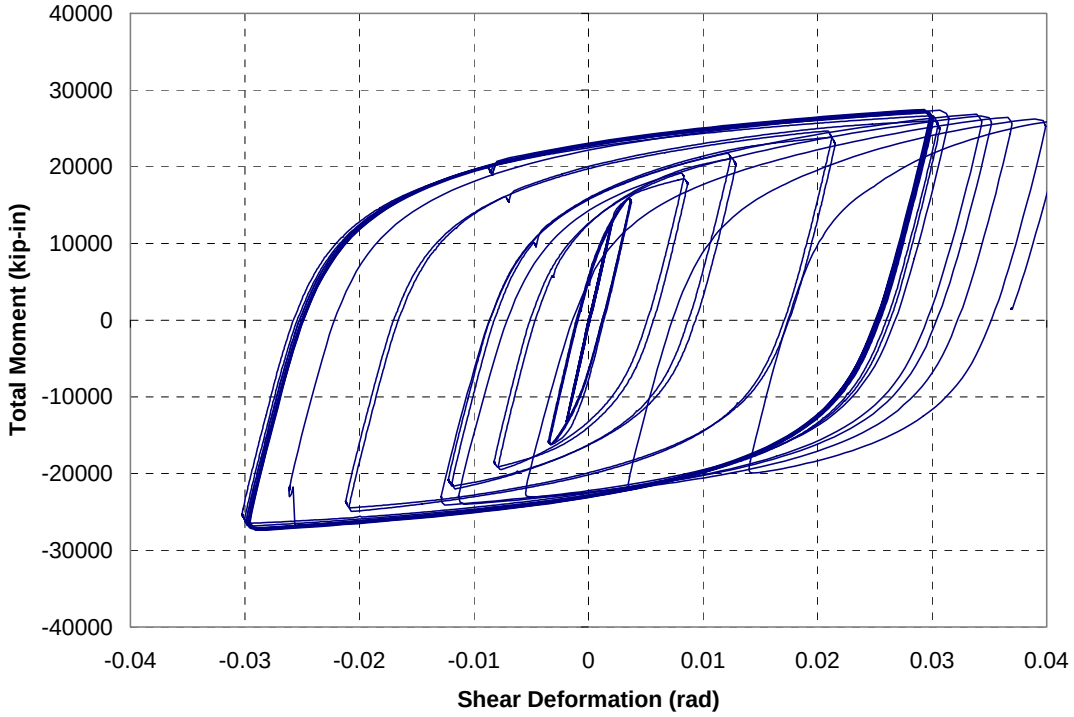


Figure A.39(a): Panel Zone Total Shear Deformation, CR1

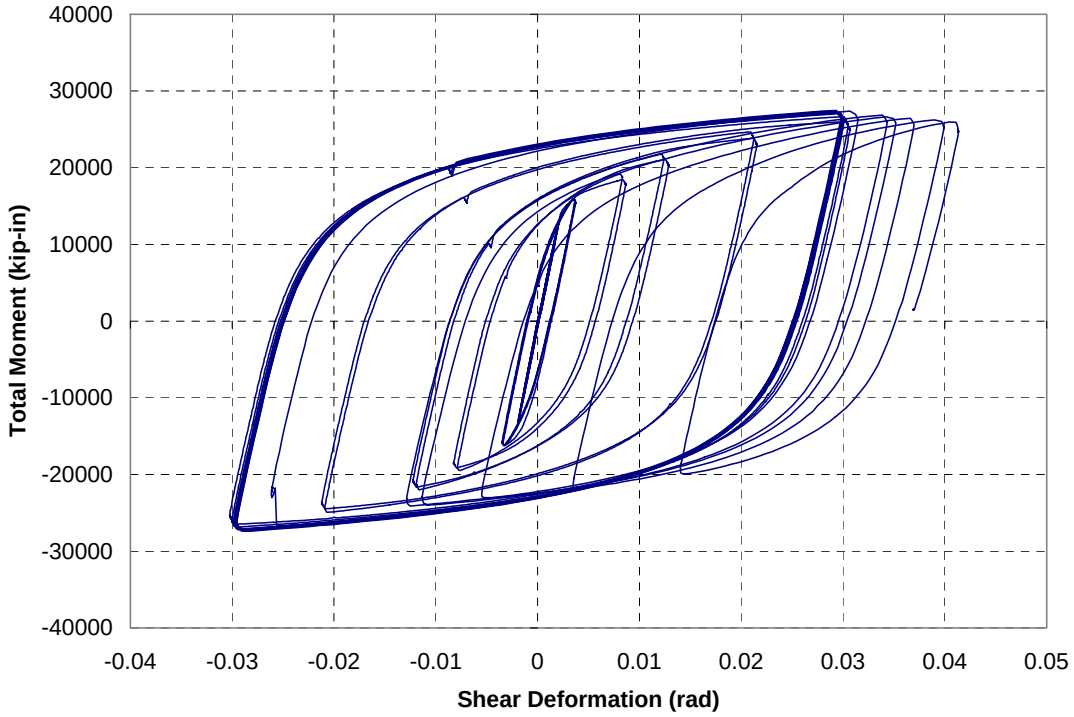


Figure A.39(b): Panel Zone Total Shear Deformation, CR1 (Re-scaled)

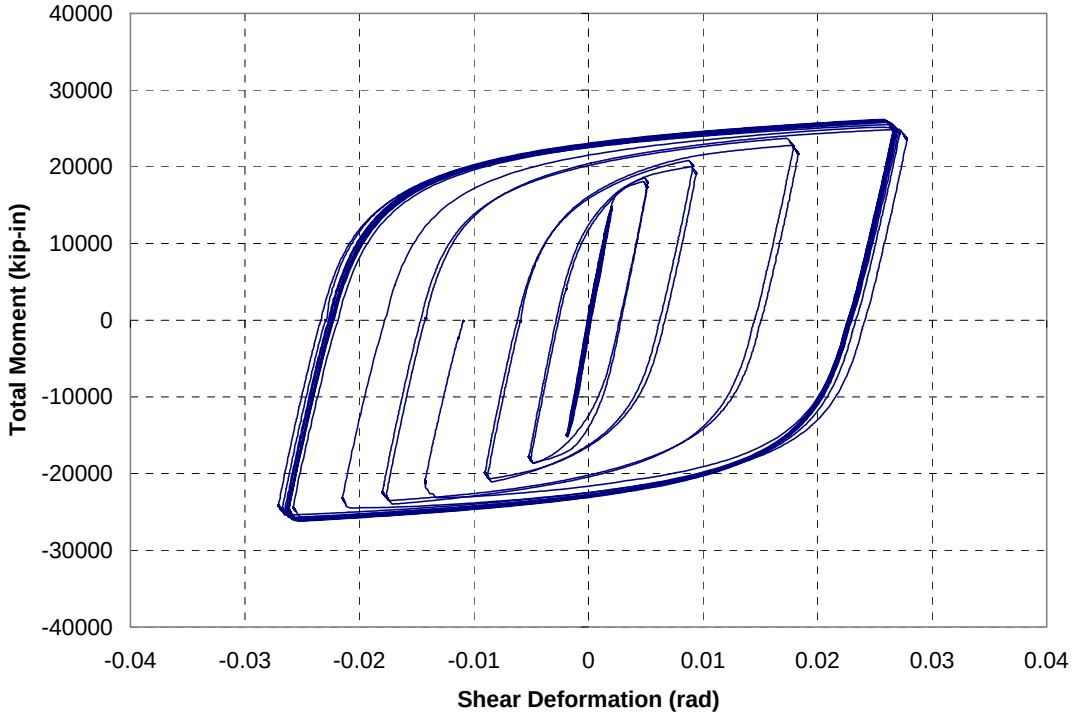


Figure A.40: Panel Zone Total Shear Deformation, CR2

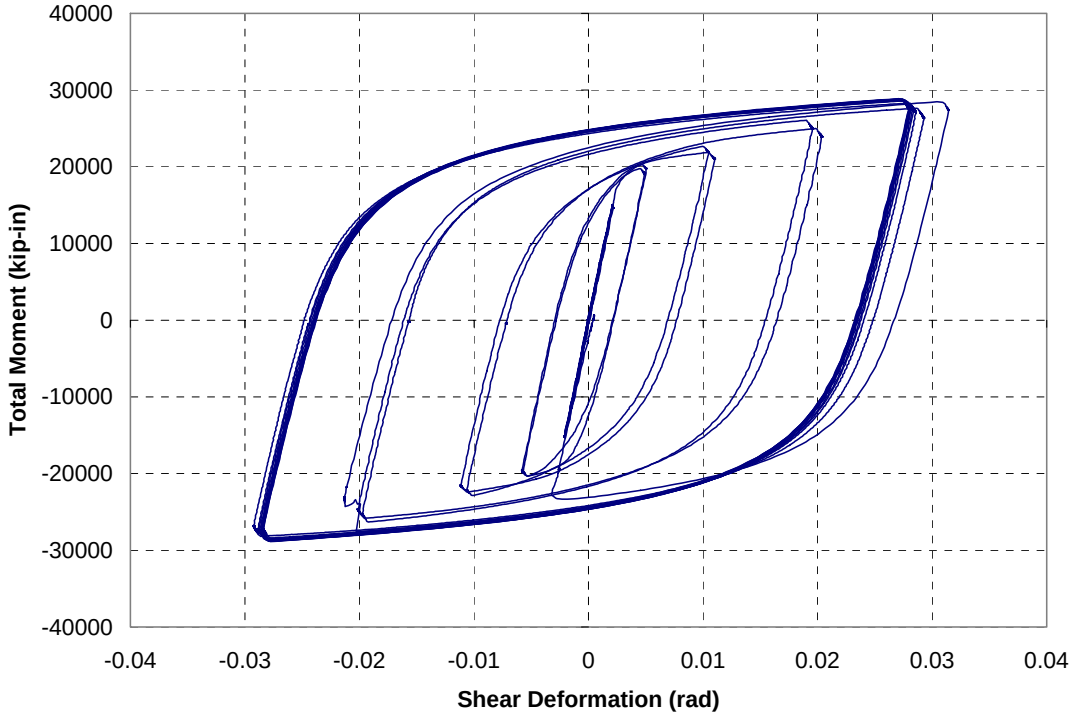


Figure A.41: Panel Zone Total Shear Deformation, CR3

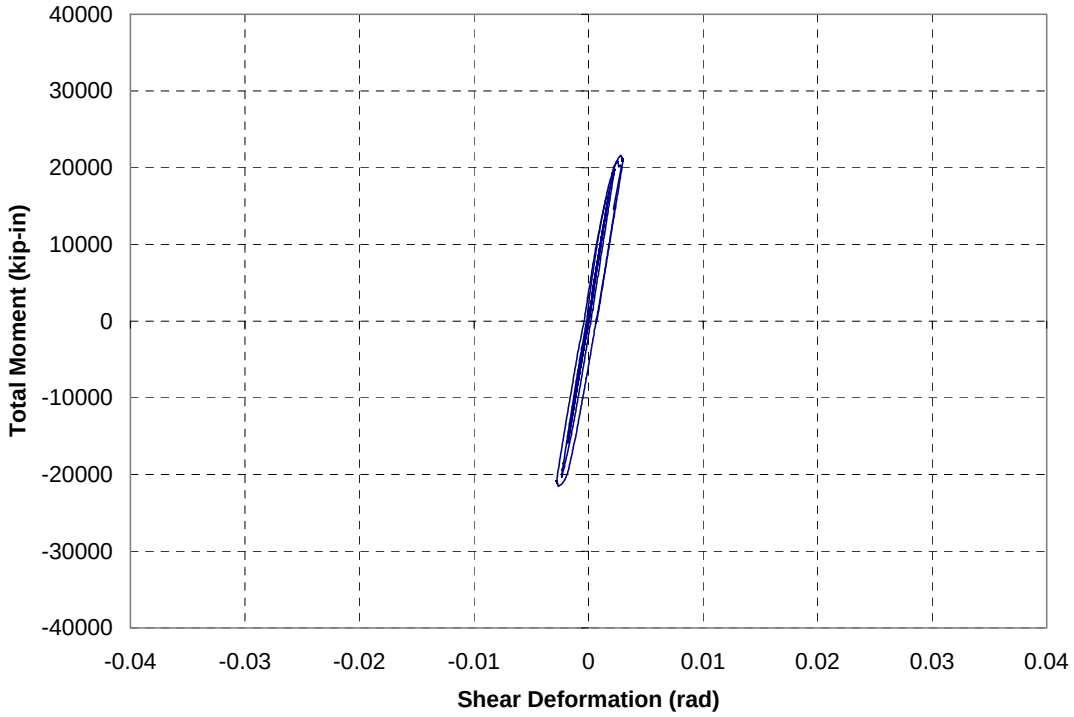


Figure A.42: Panel Zone Total Shear Deformation, CR4

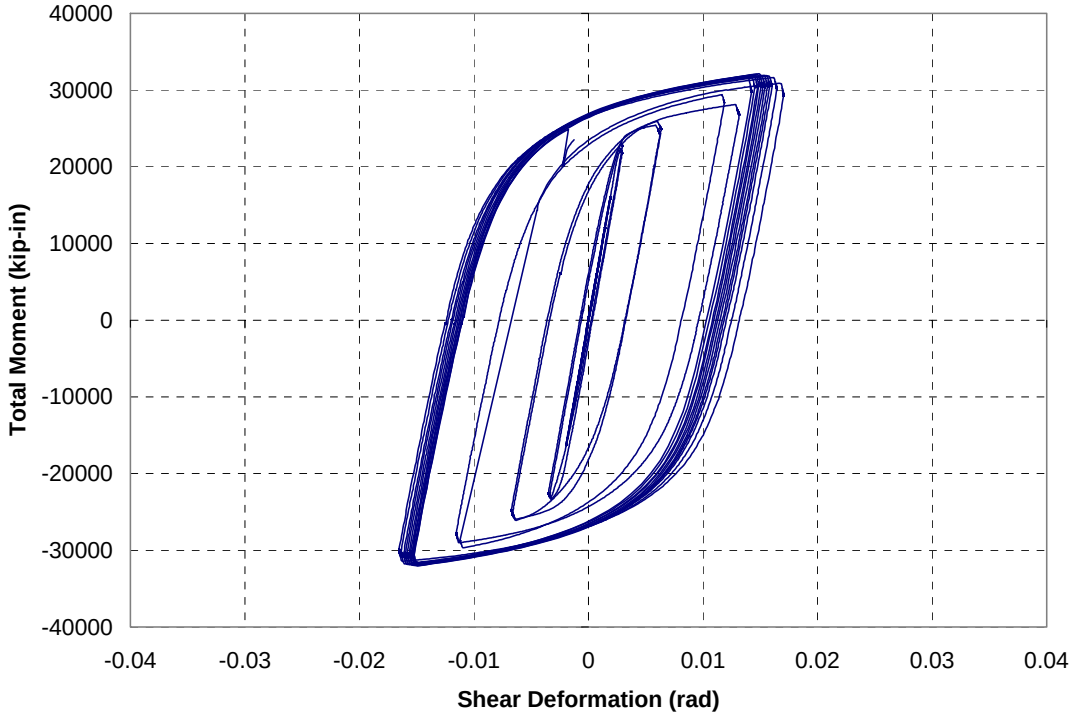


Figure A.43: Panel Zone Total Shear Deformation, CR4R

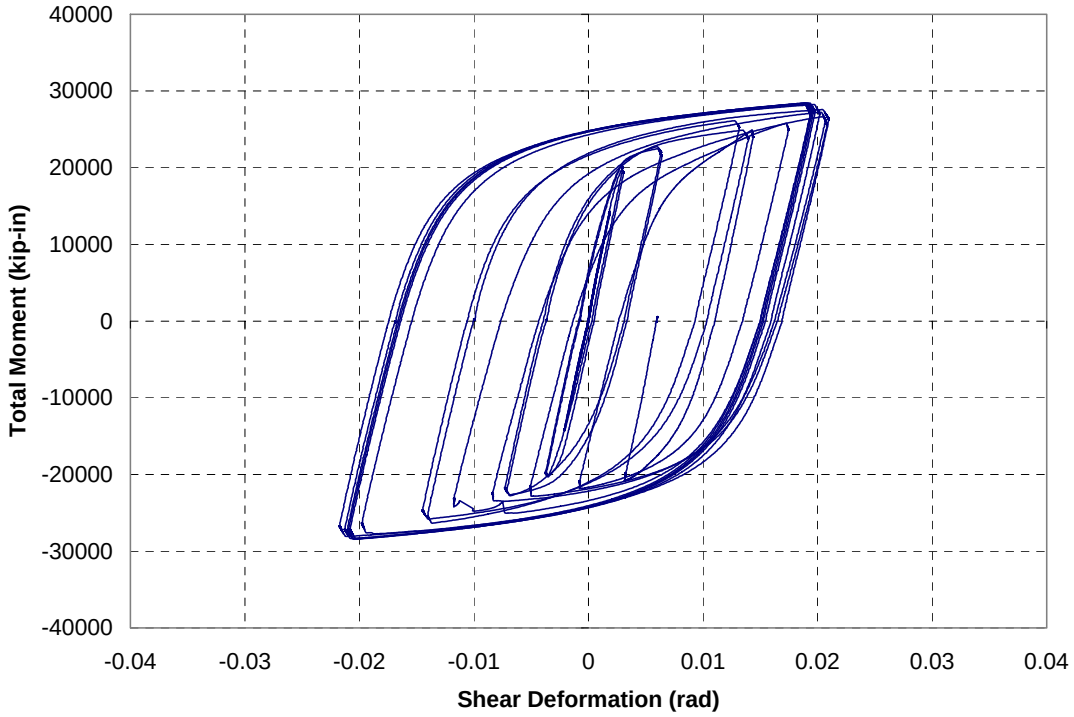


Figure A.44: Panel Zone Total Shear Deformation, CR5

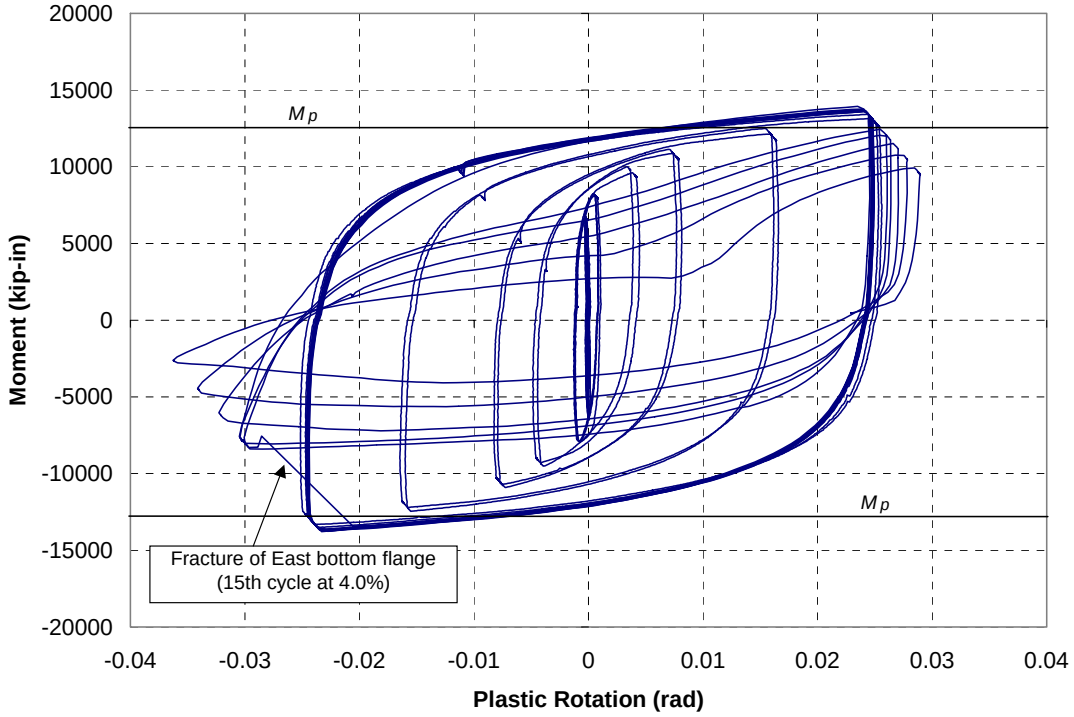


Figure A.45: Total Plastic Rotation of East Connection, CR1

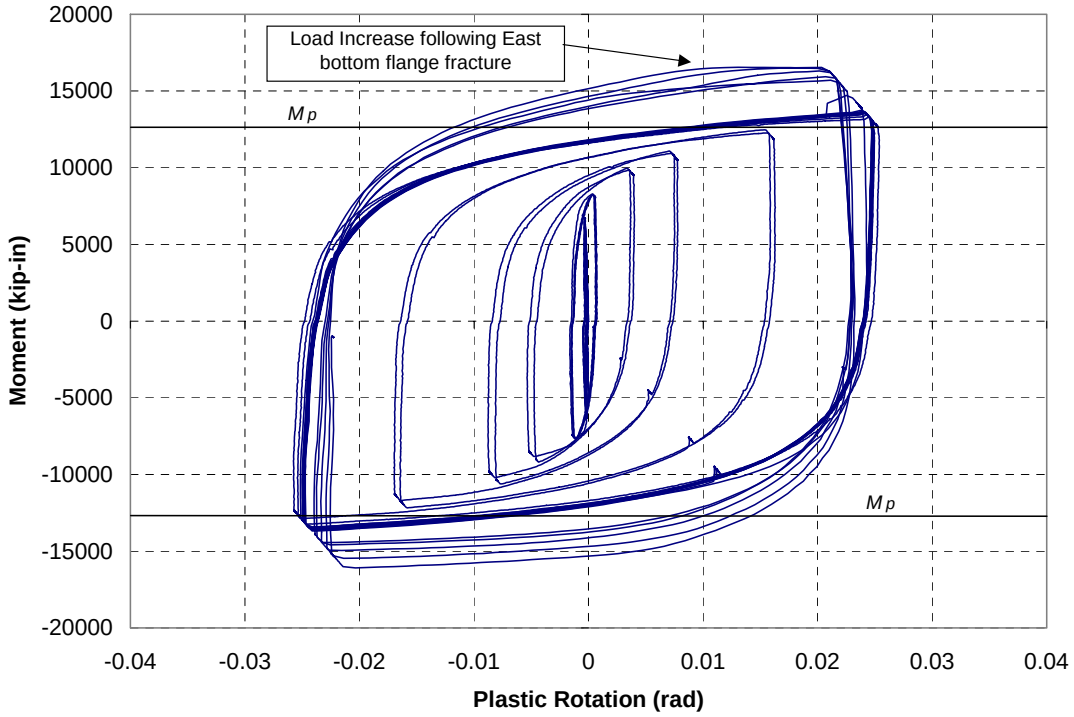


Figure A.46: Total Plastic Rotation of West Connection, CR1

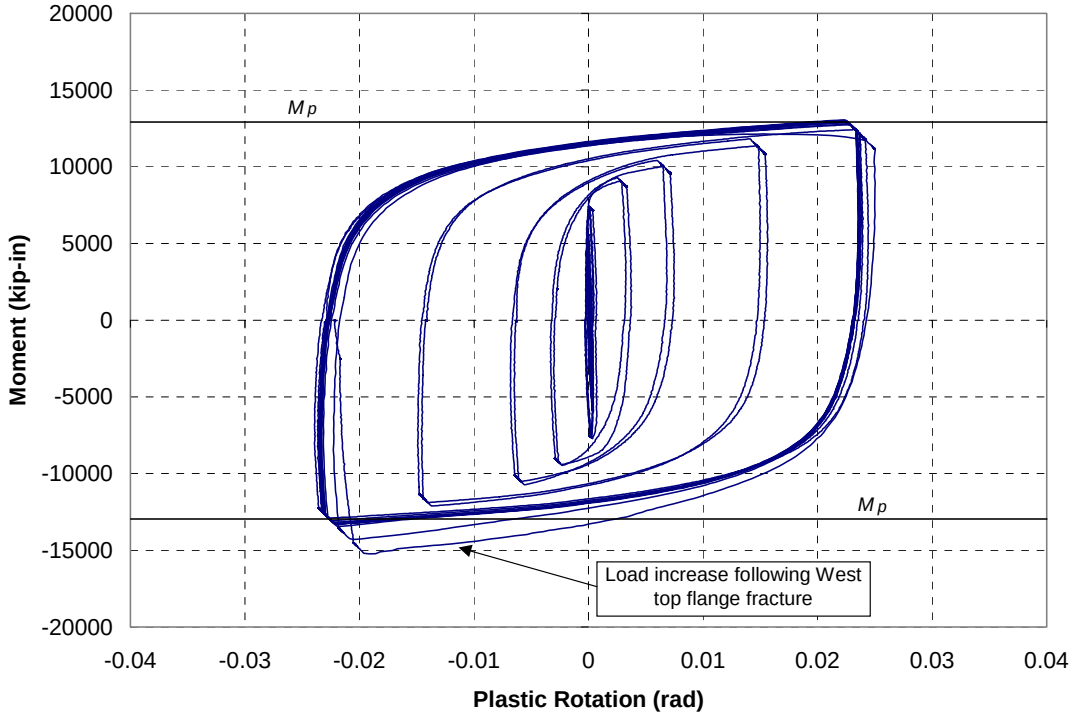


Figure A.47: Total Plastic Rotation of East Connection, CR2

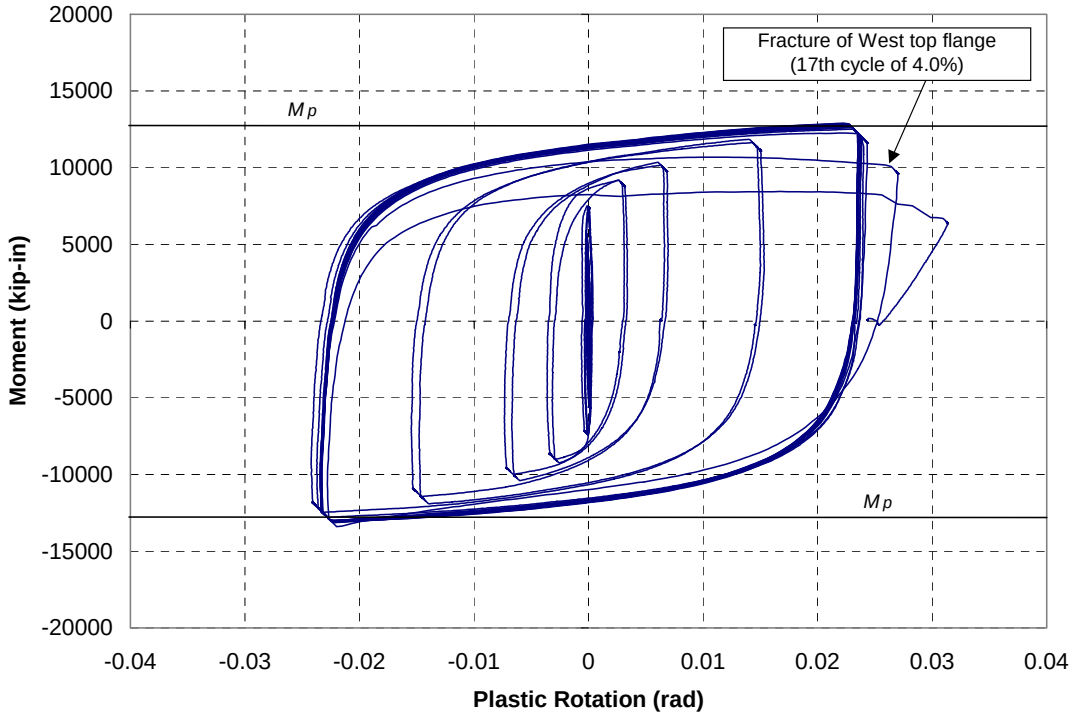


Figure A.48: Total Plastic Rotation of West Connection, CR2

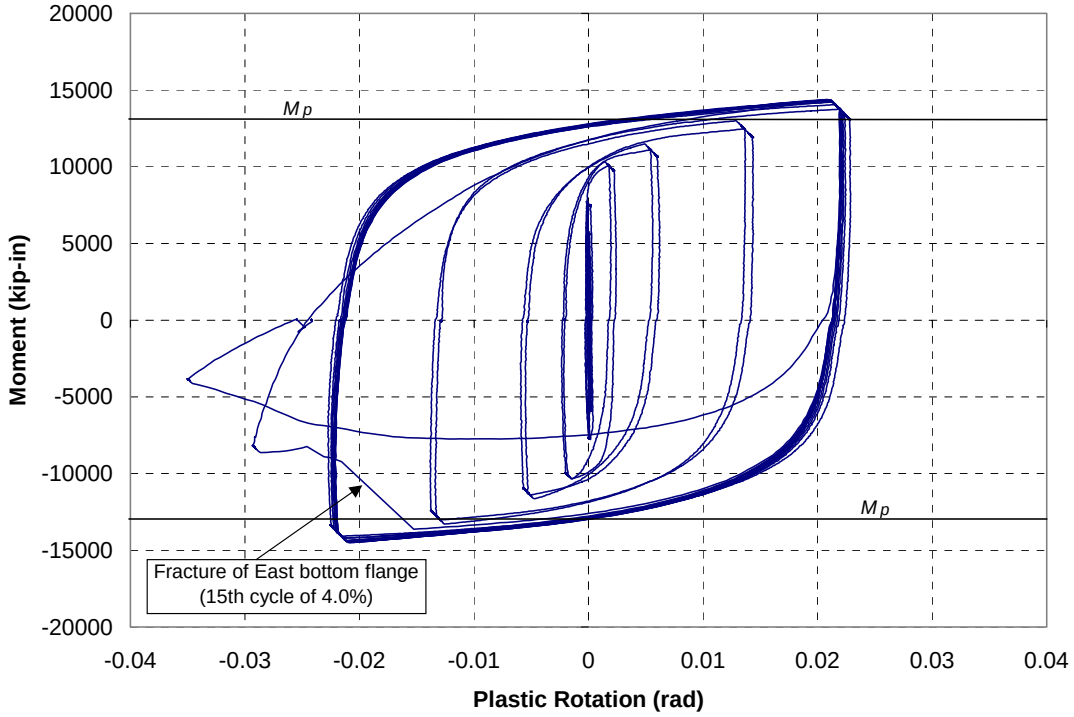


Figure A.49: Total Plastic Rotation of East Girder, CR3

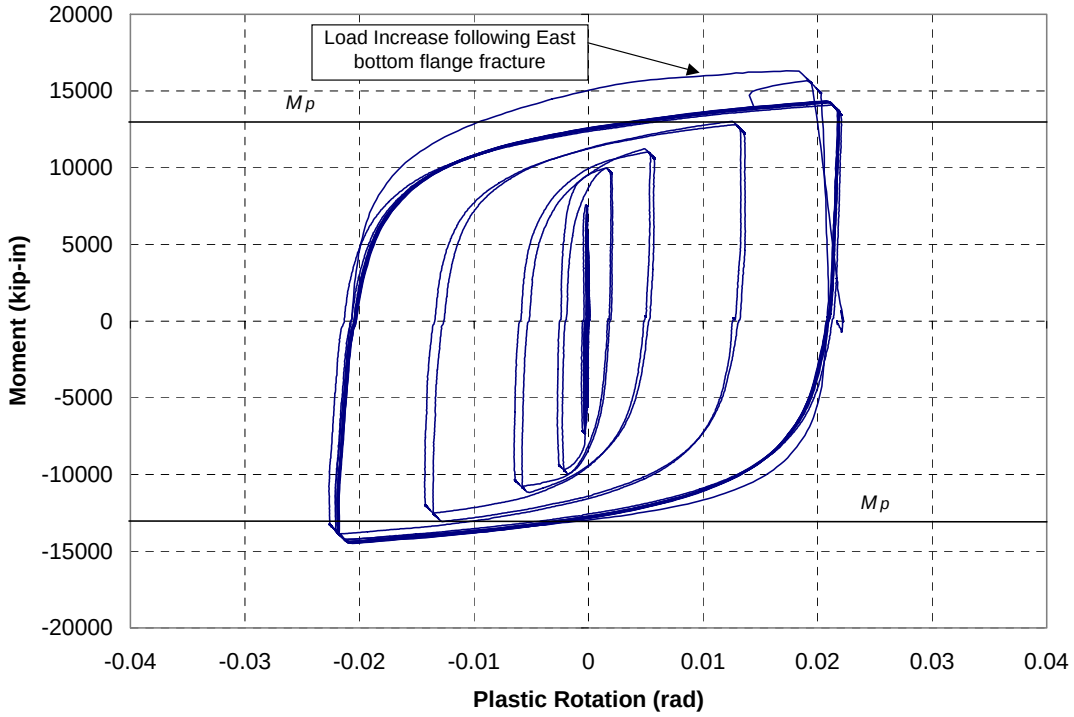


Figure A.50: Total Plastic Rotation of West Girder, CR3

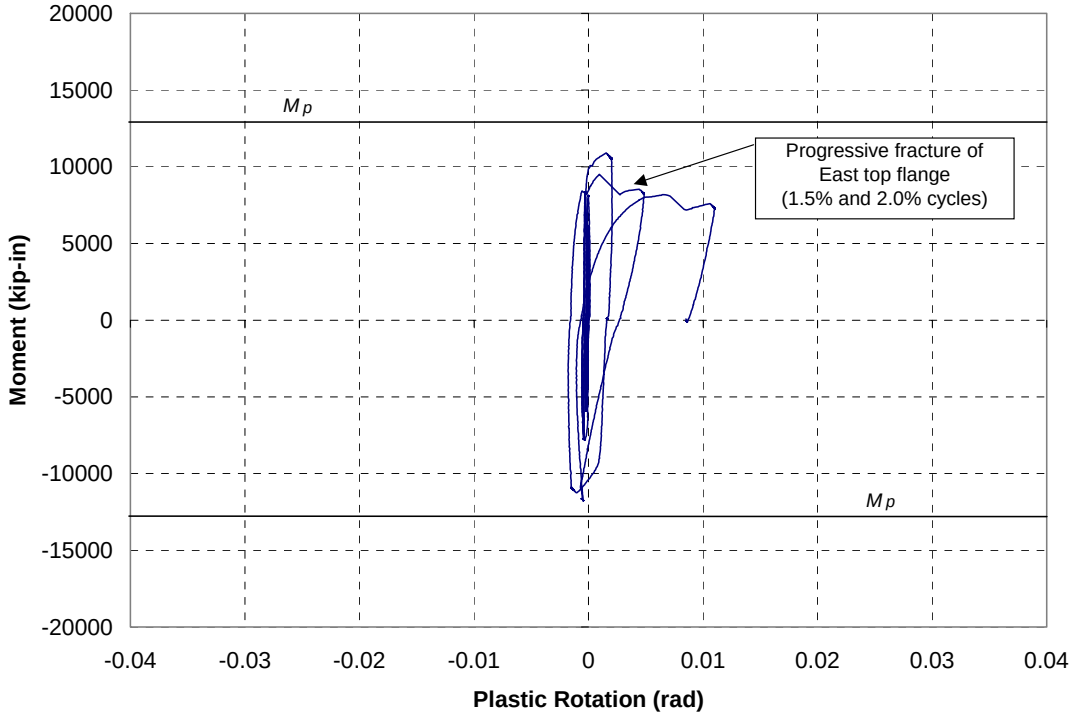


Figure A.51: Total Plastic Rotation of East Connection, CR4

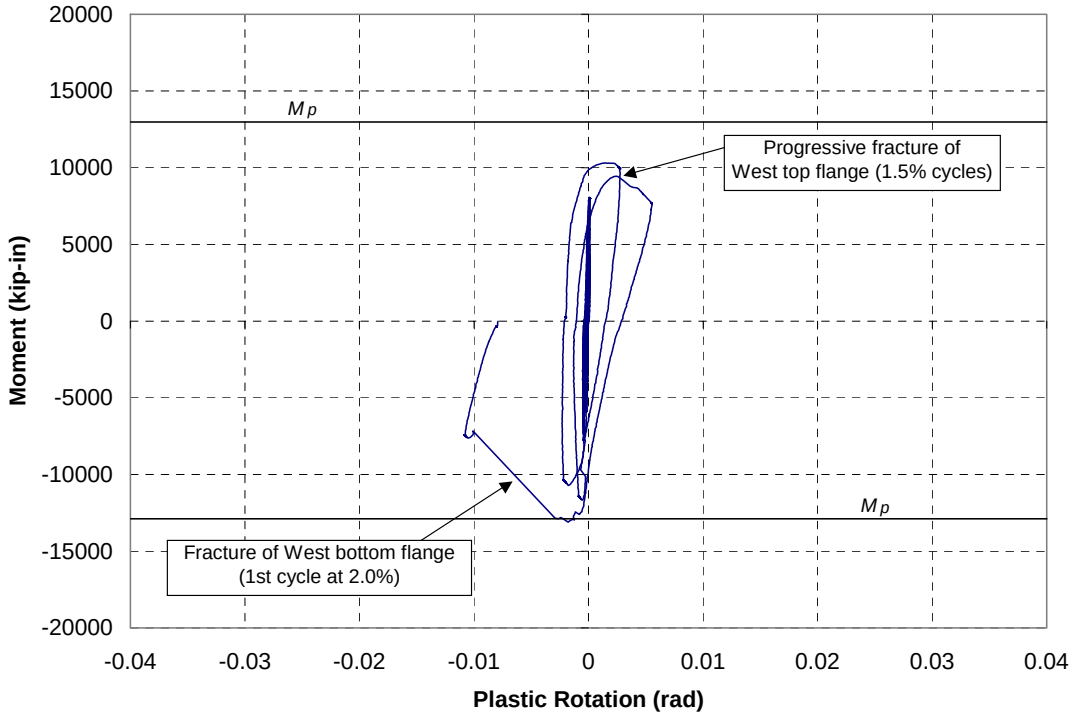


Figure A.52: Total Plastic Rotation of West Connection, CR4

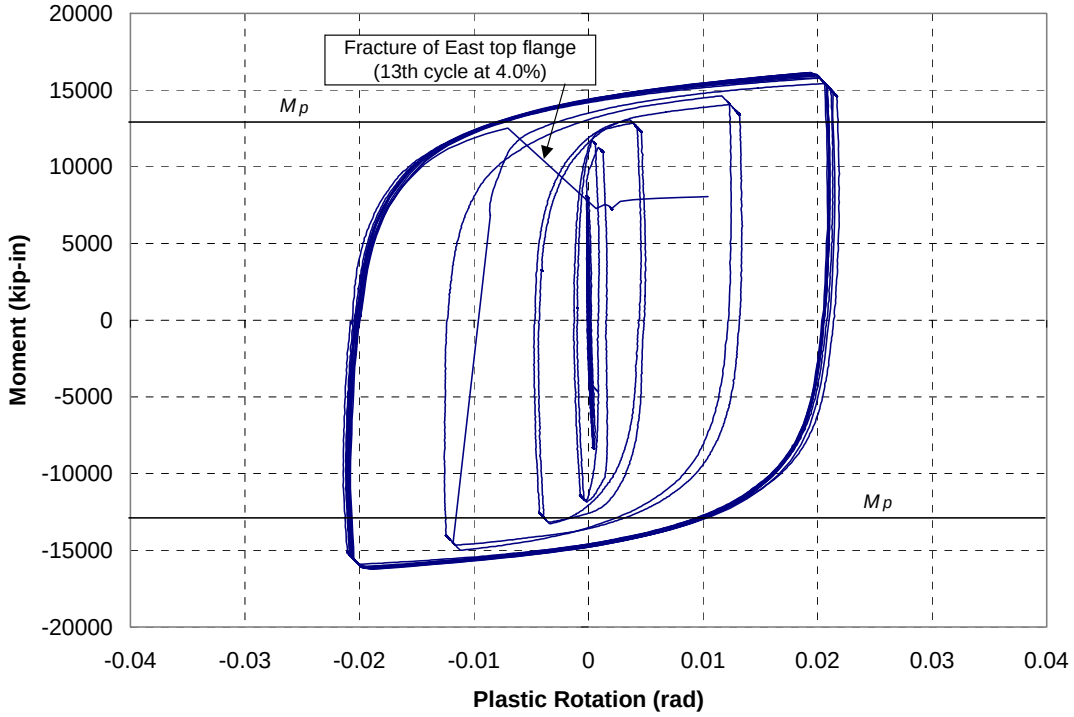


Figure A.53: Total Plastic Rotation of East Connection, CR4R

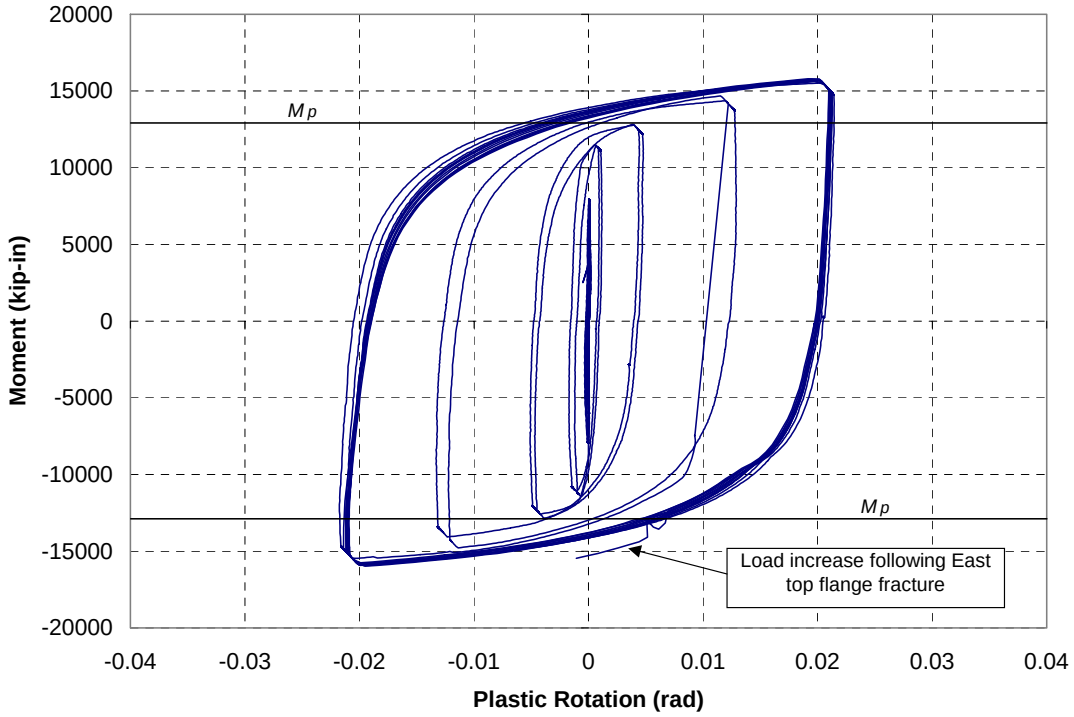


Figure A.54: Total Plastic Rotation of West Connection, CR4R

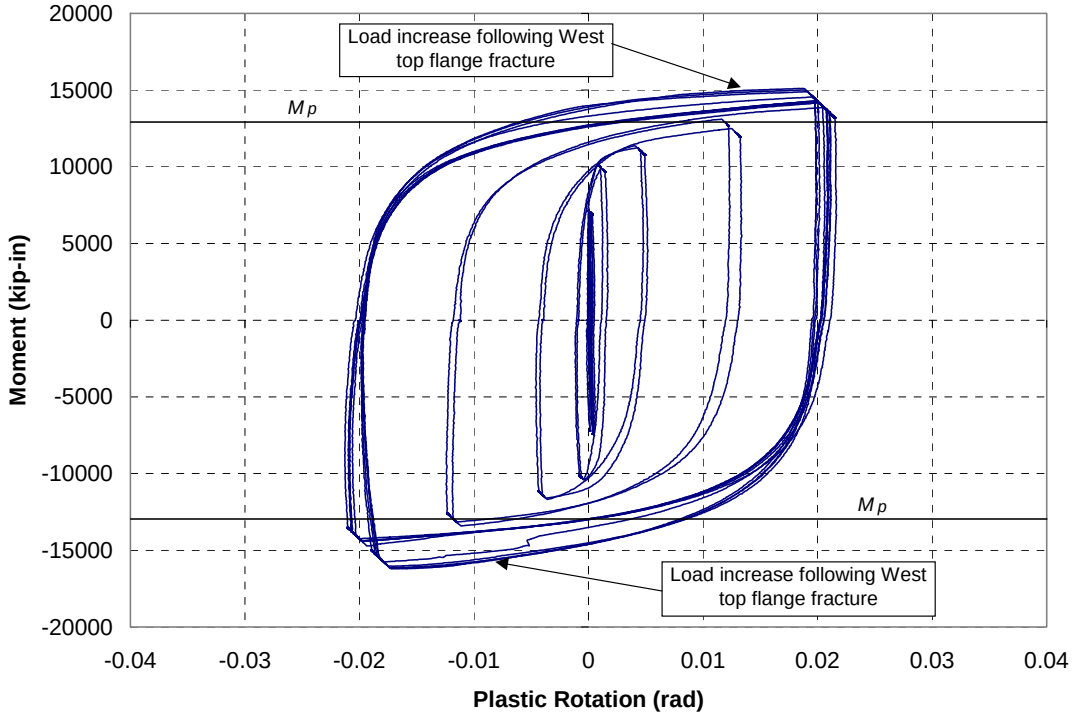


Figure A.55: Total Plastic Rotation of East Connection, CR5

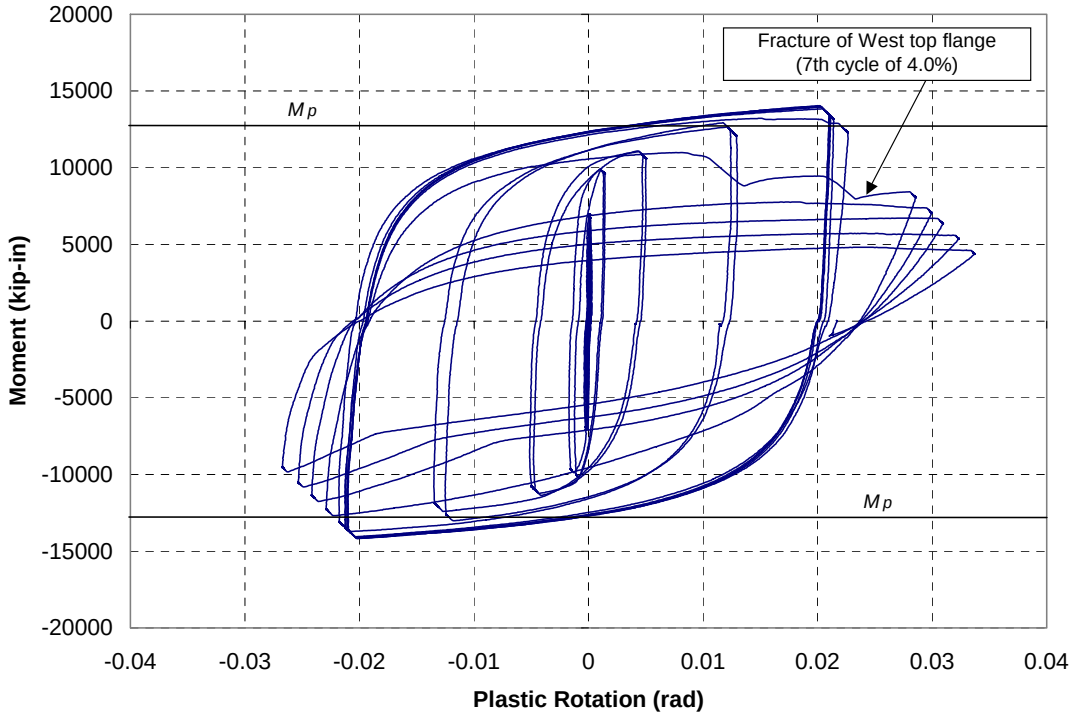


Figure A.56: Total Plastic Rotation of West Connection, CR5

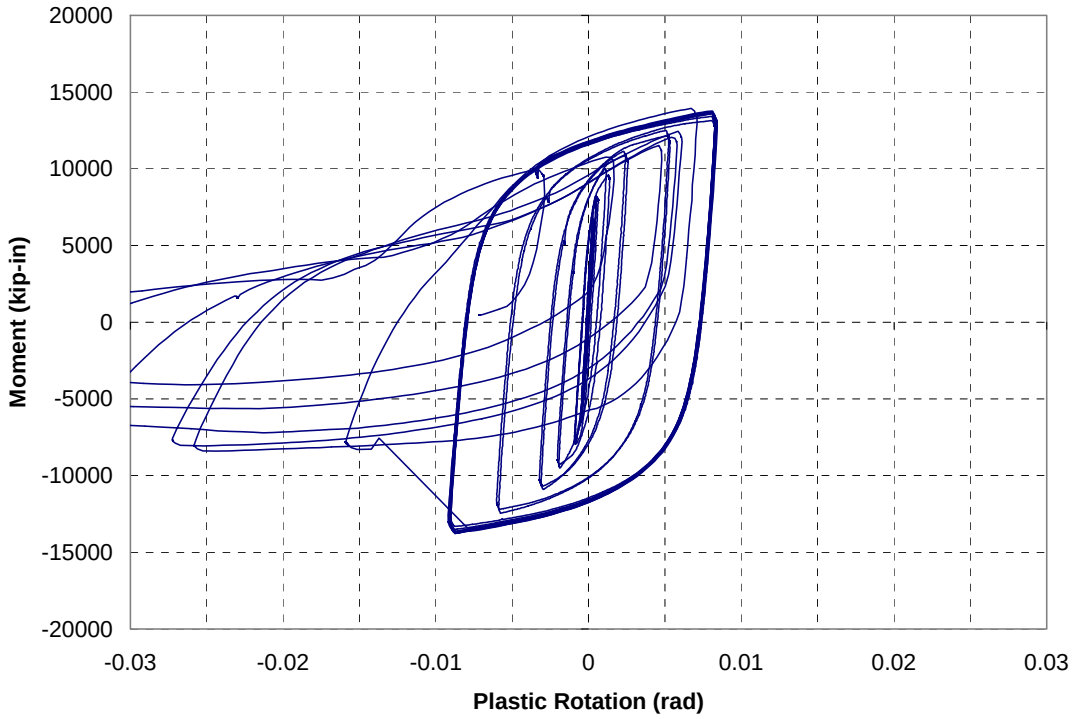


Figure A.57(a): East Girder Plastic Rotation, CR1

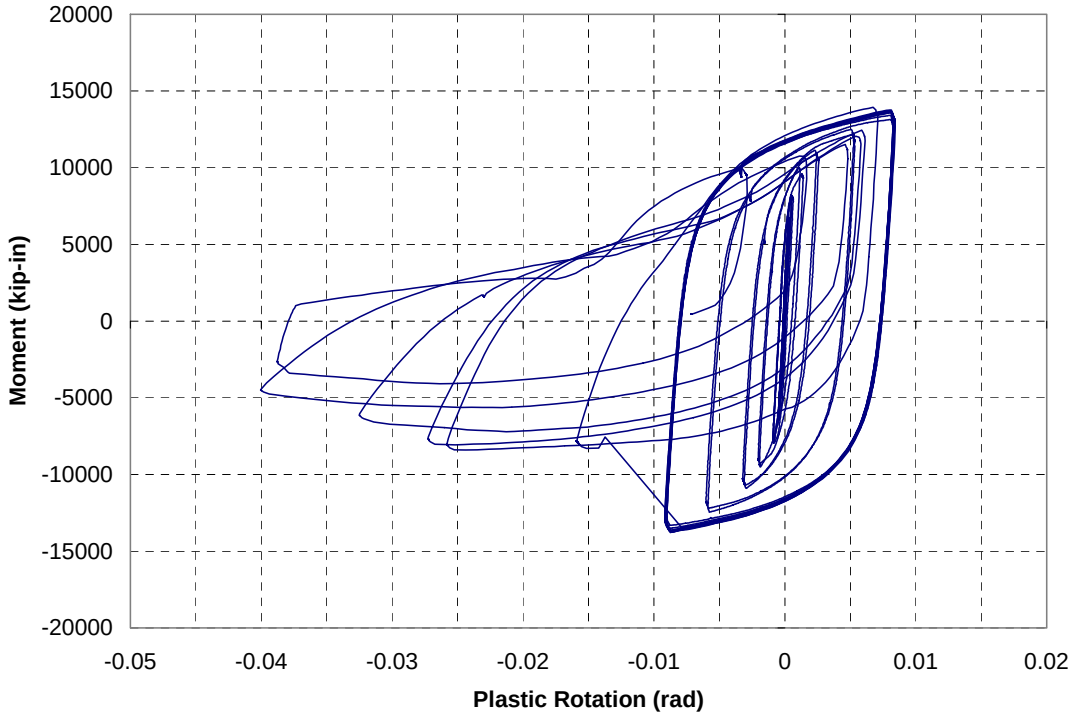


Figure A.57(b): East Girder Plastic Rotation, CR1 (Re-scaled)

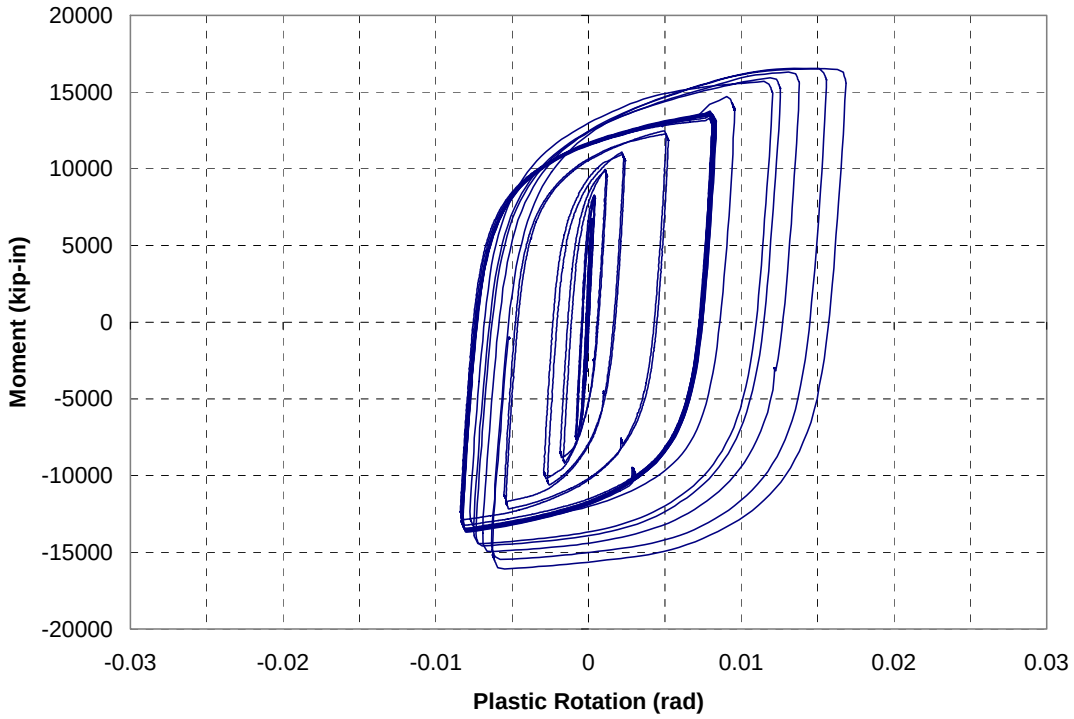


Figure A.58: West Girder Plastic Rotation, CR1

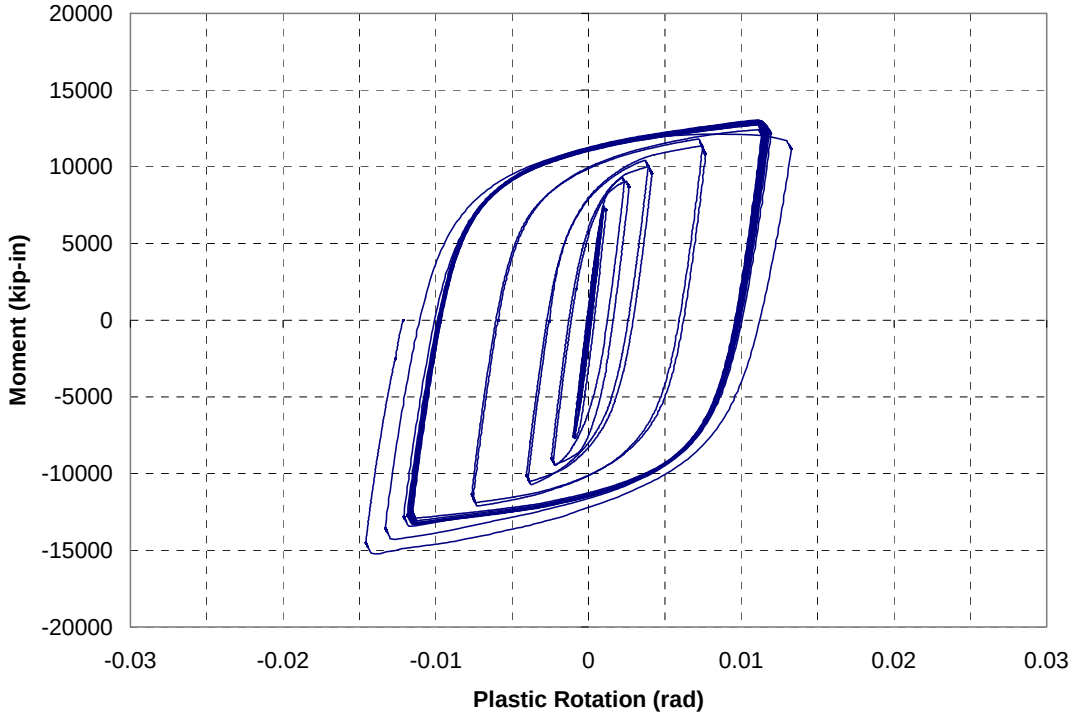


Figure A.59: East Girder Plastic Rotation, CR2

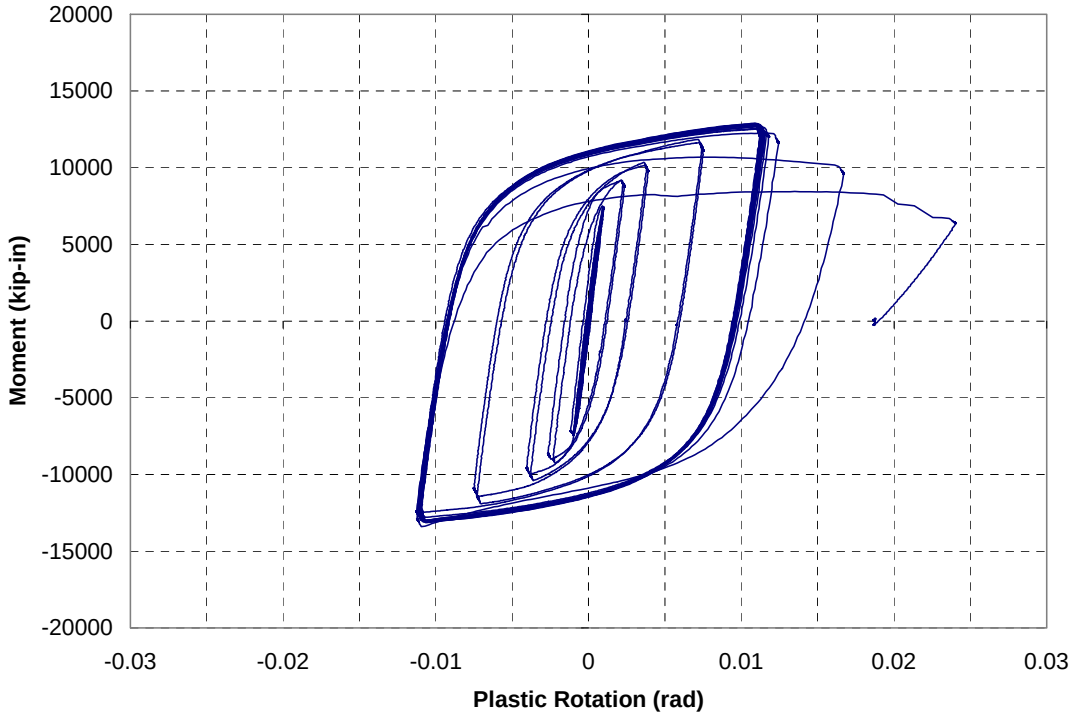


Figure A.60: West Girder Plastic Rotation, CR2

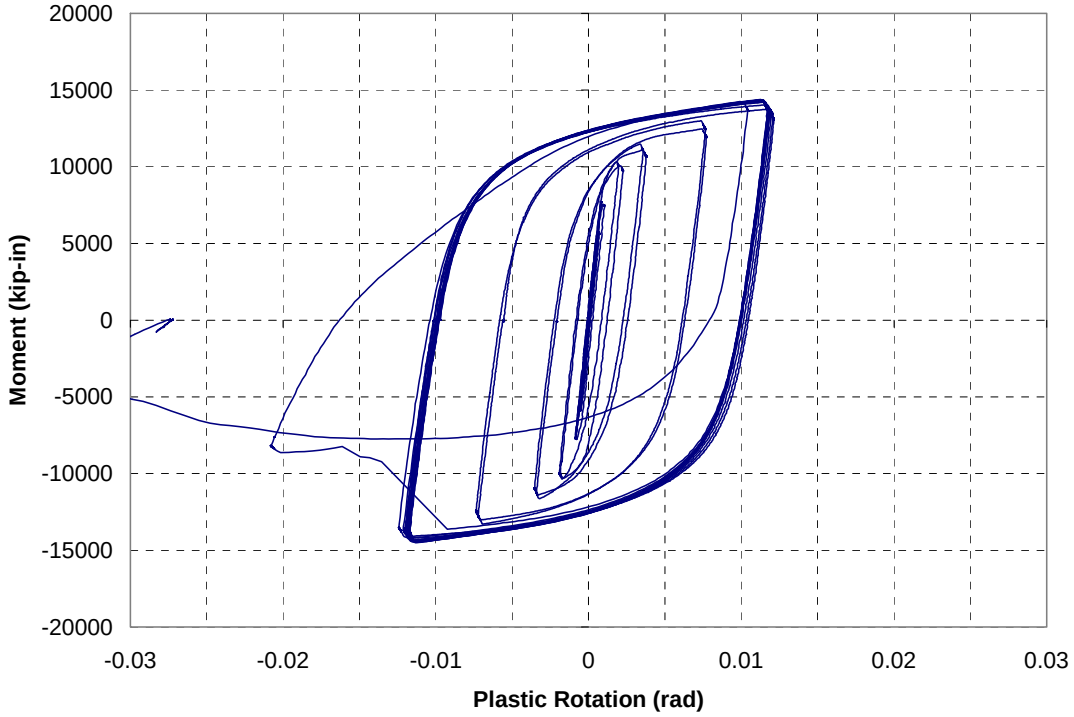


Figure A.61(a): East Girder Plastic Rotation, CR3

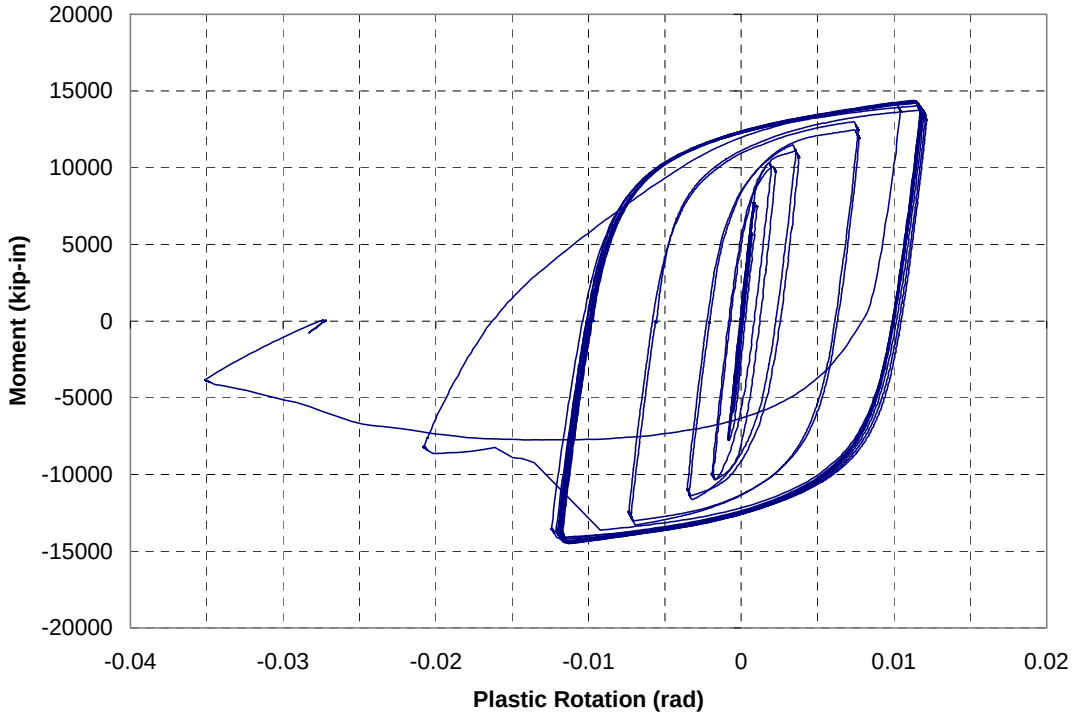


Figure A.61(b): East Girder Plastic Rotation, CR3 (Re-scaled)

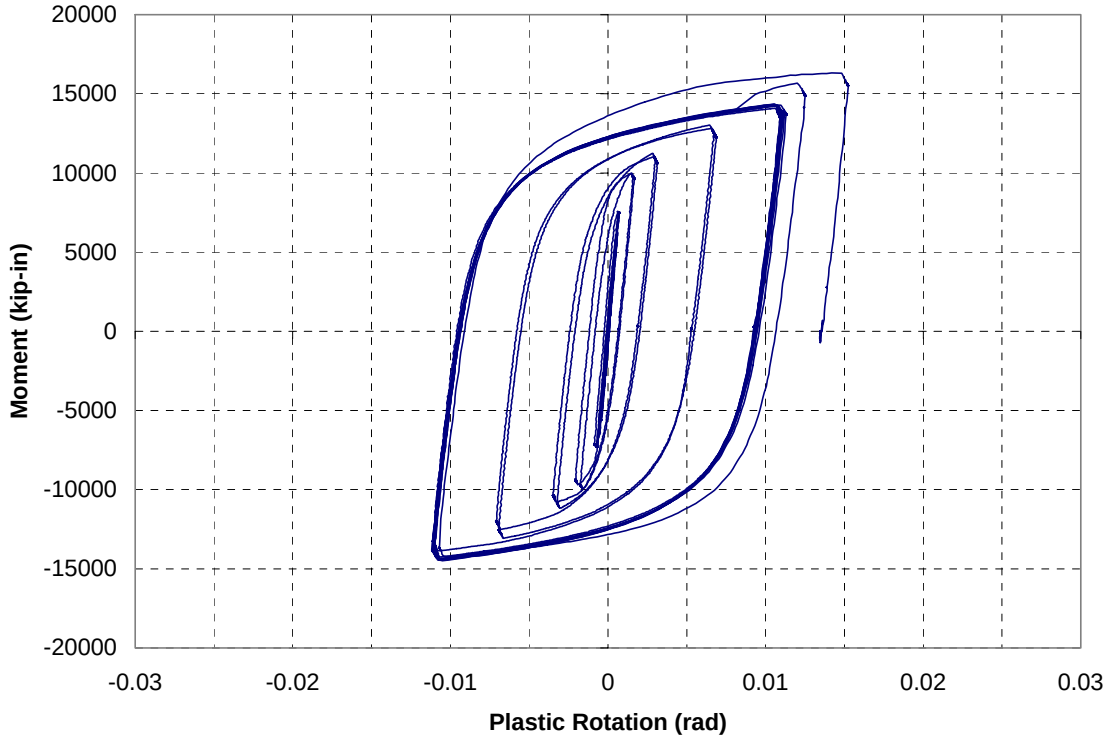


Figure A.62: West Girder Plastic Rotation, CR3

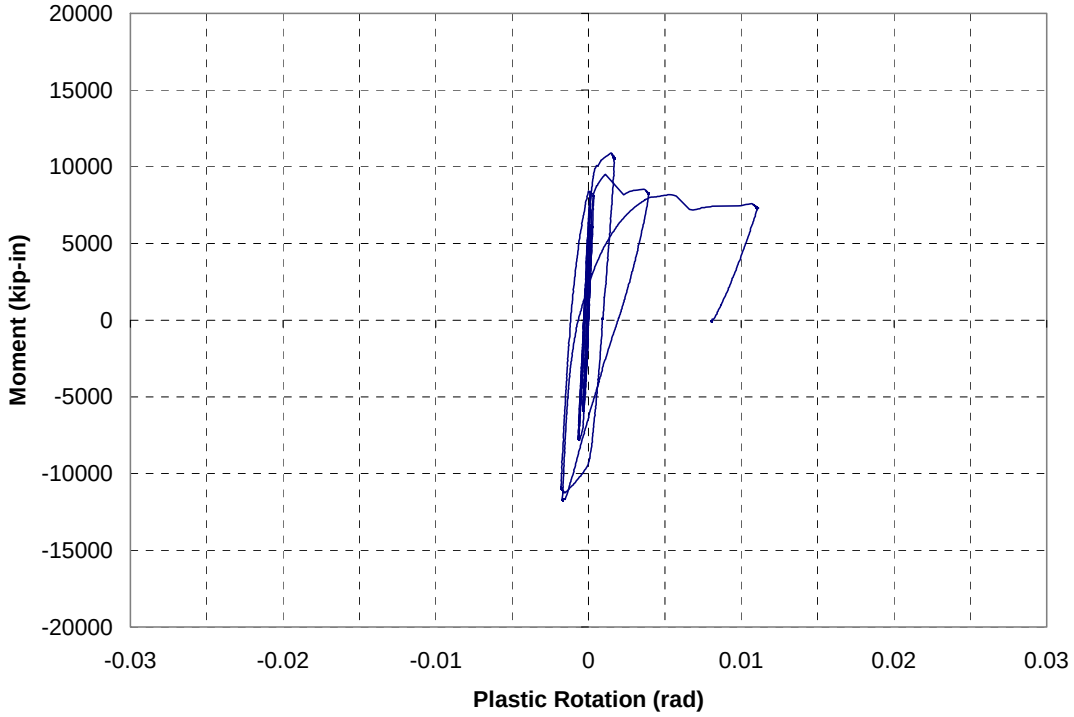


Figure A. 63: East Girder Plastic Rotation, CR4

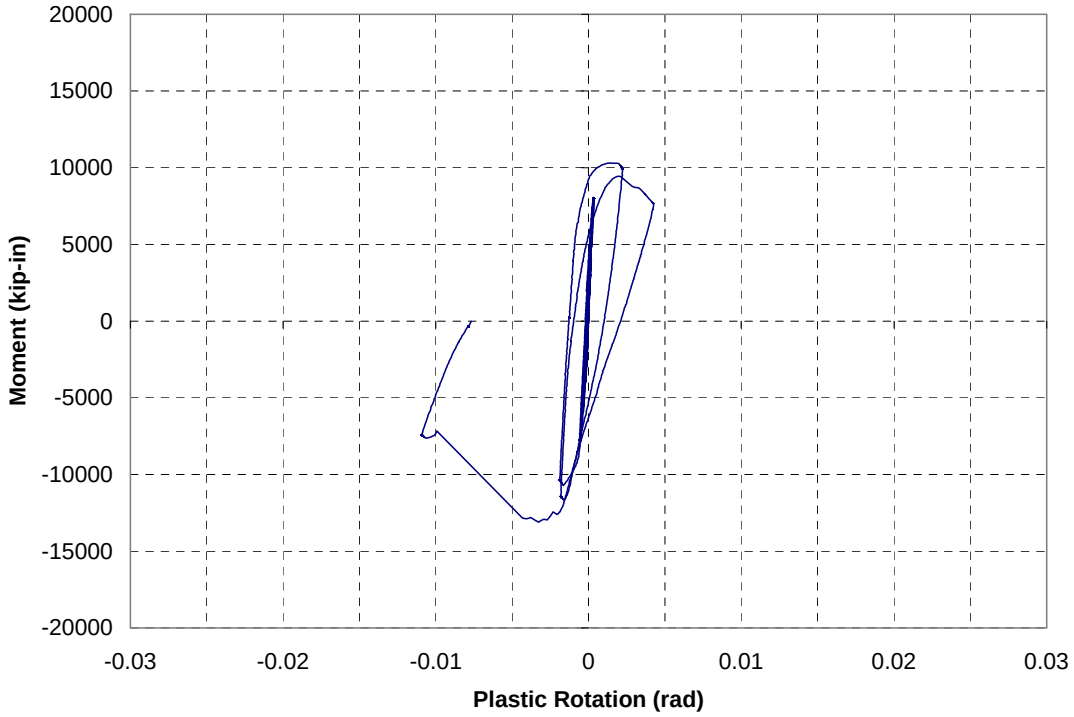


Figure A.64: West Girder Plastic Rotation, CR4

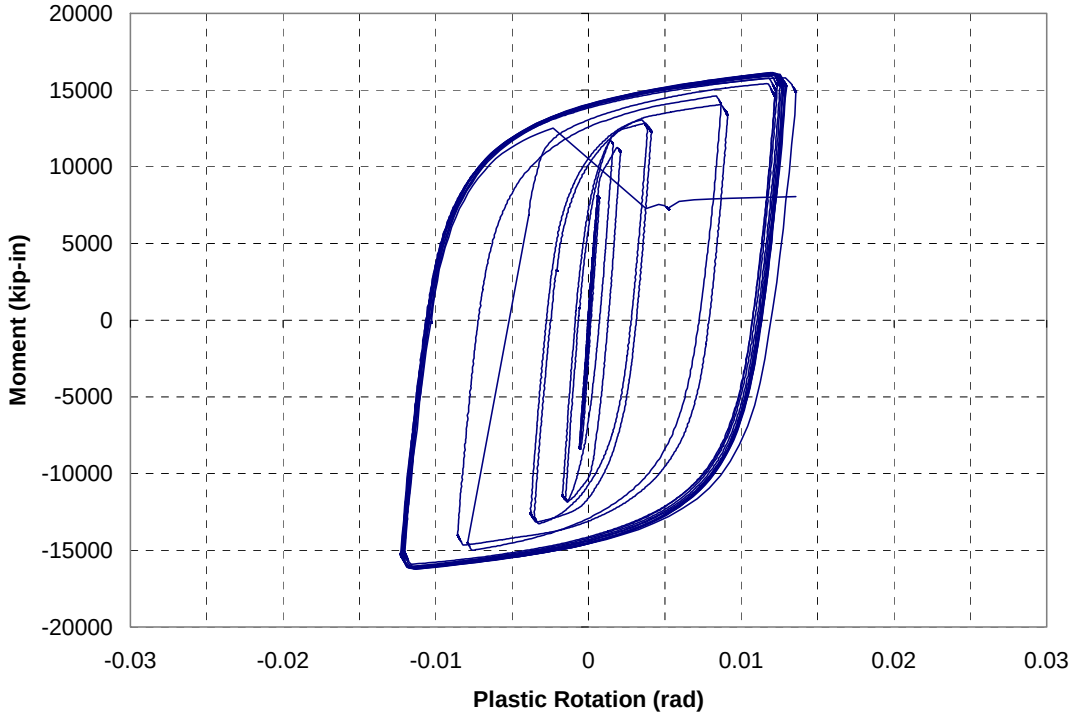


Figure A.65: East Girder Plastic Rotation, CR4R

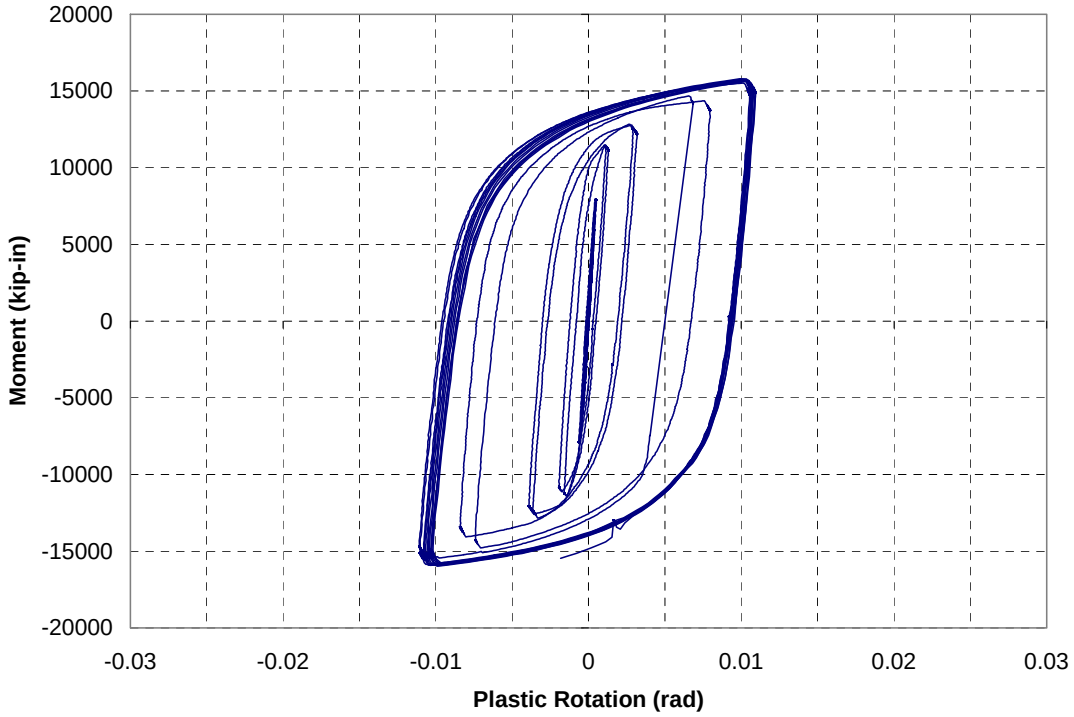


Figure A.66: West Girder Plastic Rotation, CR4R

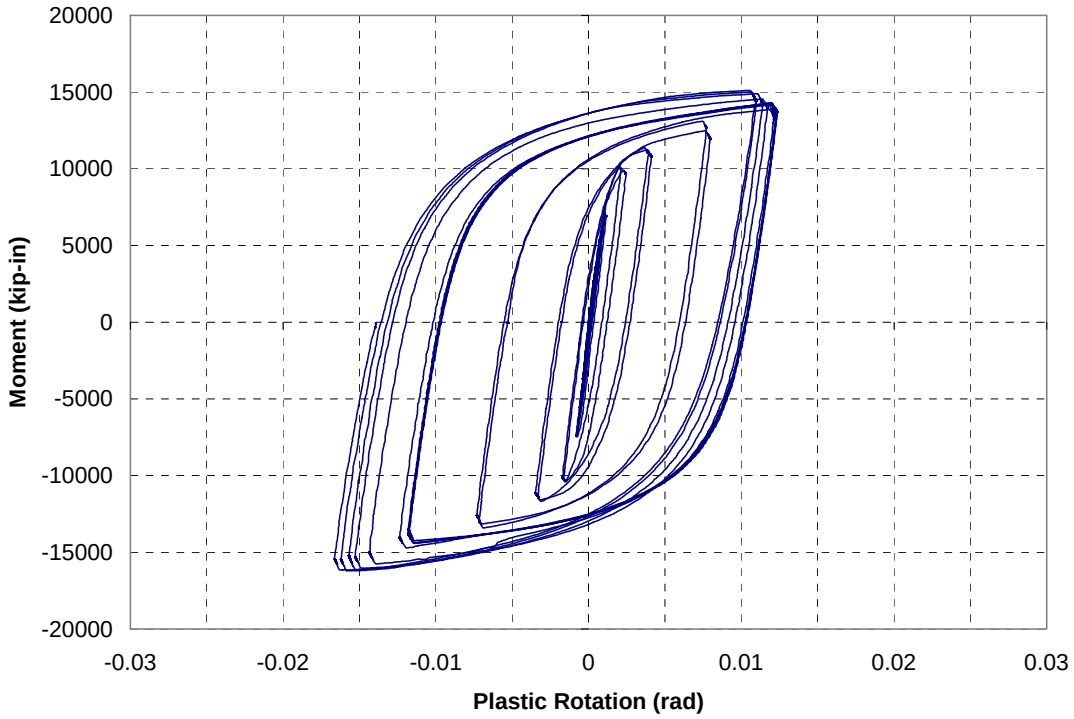


Figure A.67: East Girder Plastic Rotation, CR5

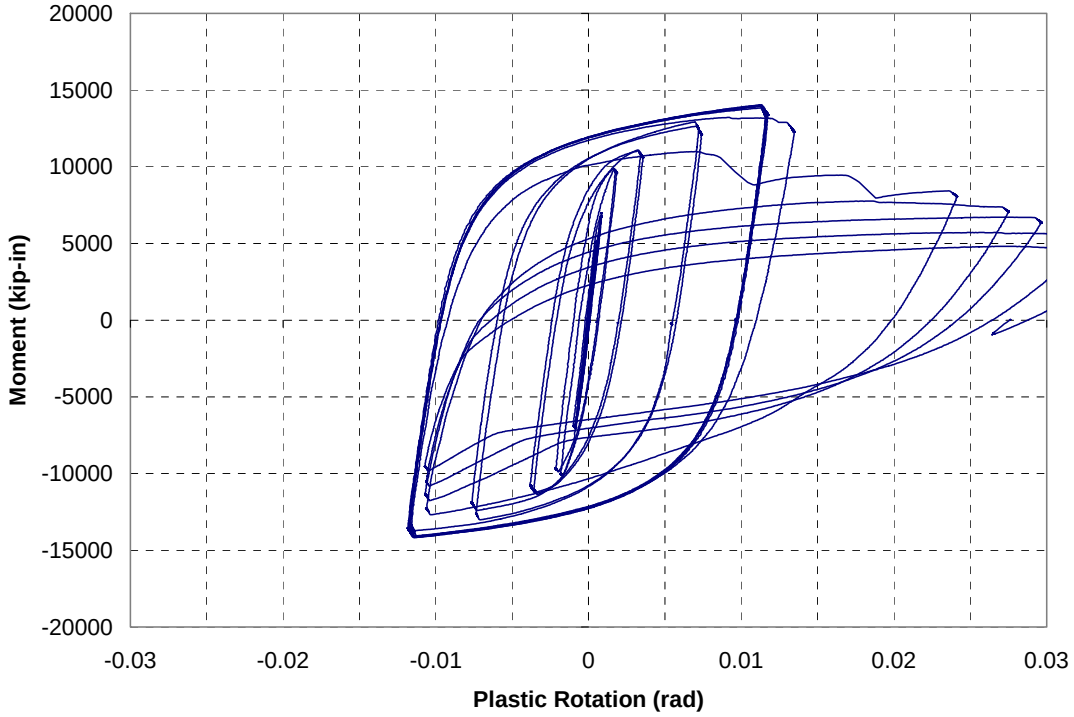


Figure A.68(a): West Girder Plastic Rotation, CR5

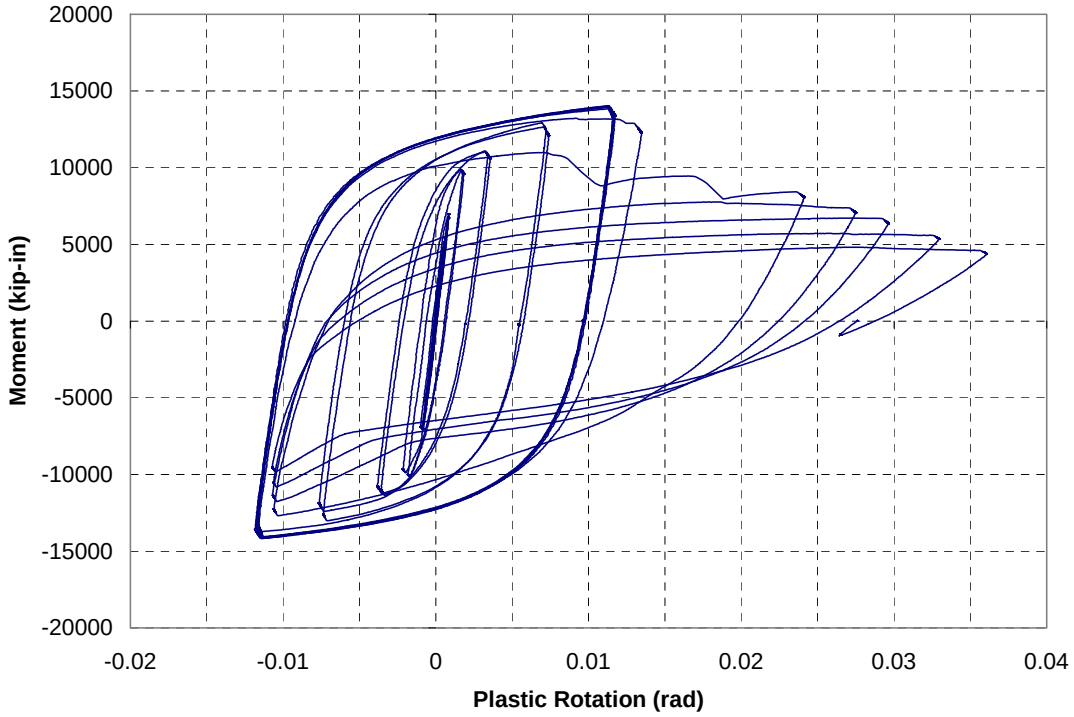


Figure A.68(b): West Girder Plastic Rotation, CR5 (Re-scaled)

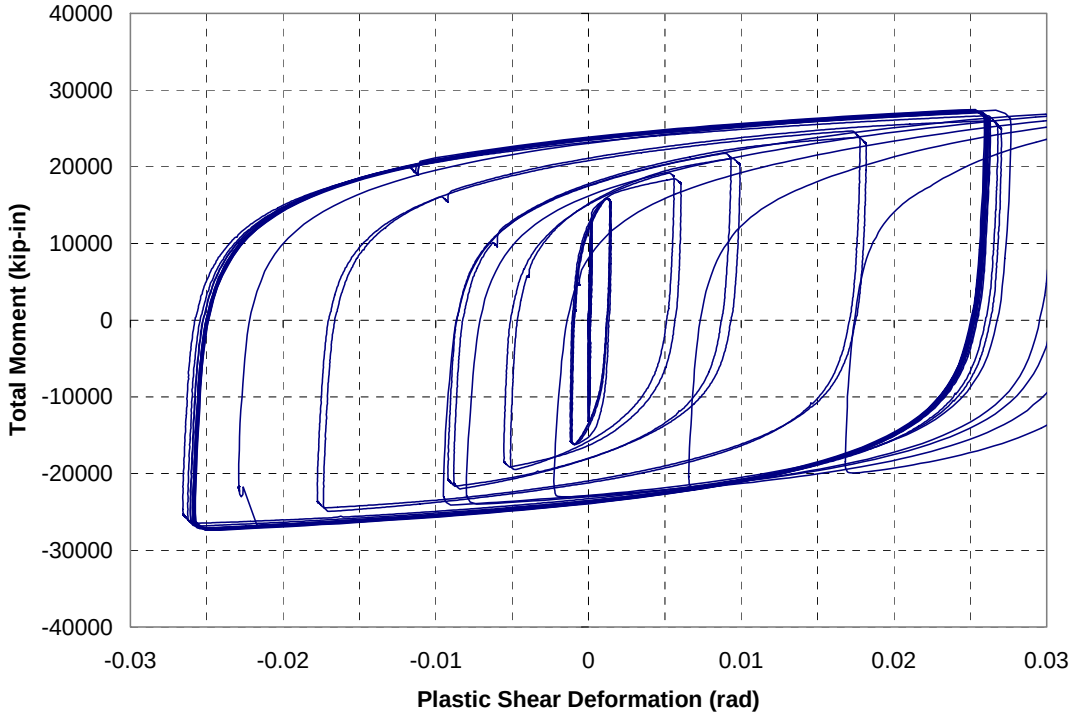


Figure A.69(a): Panel Zone Plastic Shear Deformation, CR1

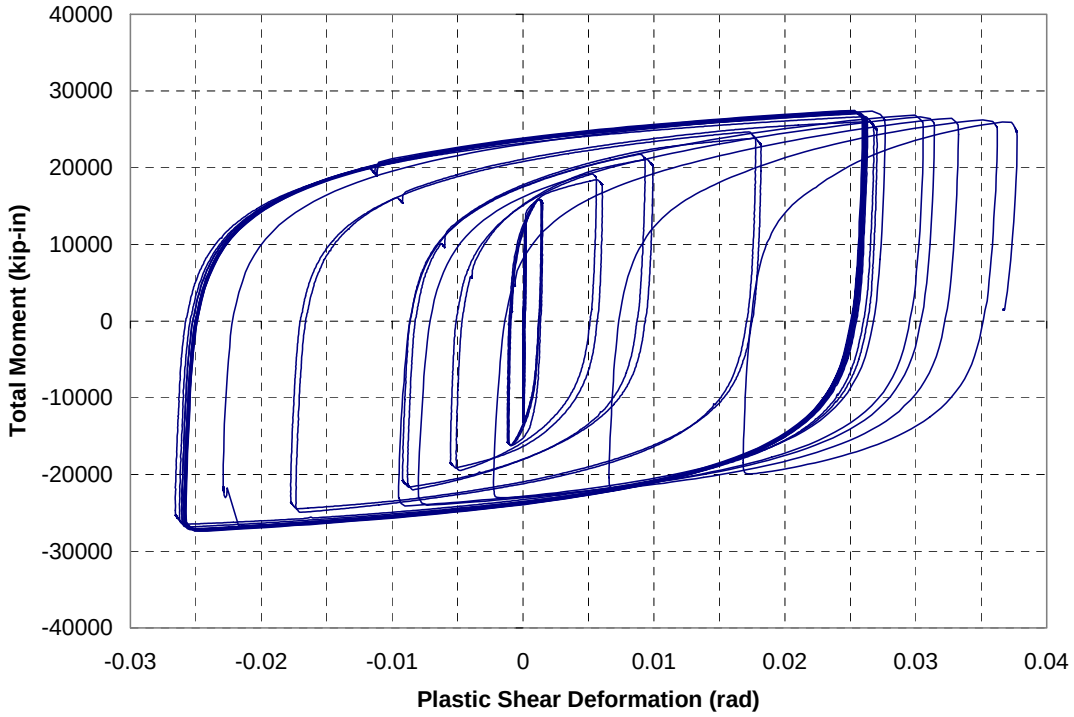


Figure A.69(b): Panel Zone Plastic Shear Deformation, CR1 (Re-scaled)

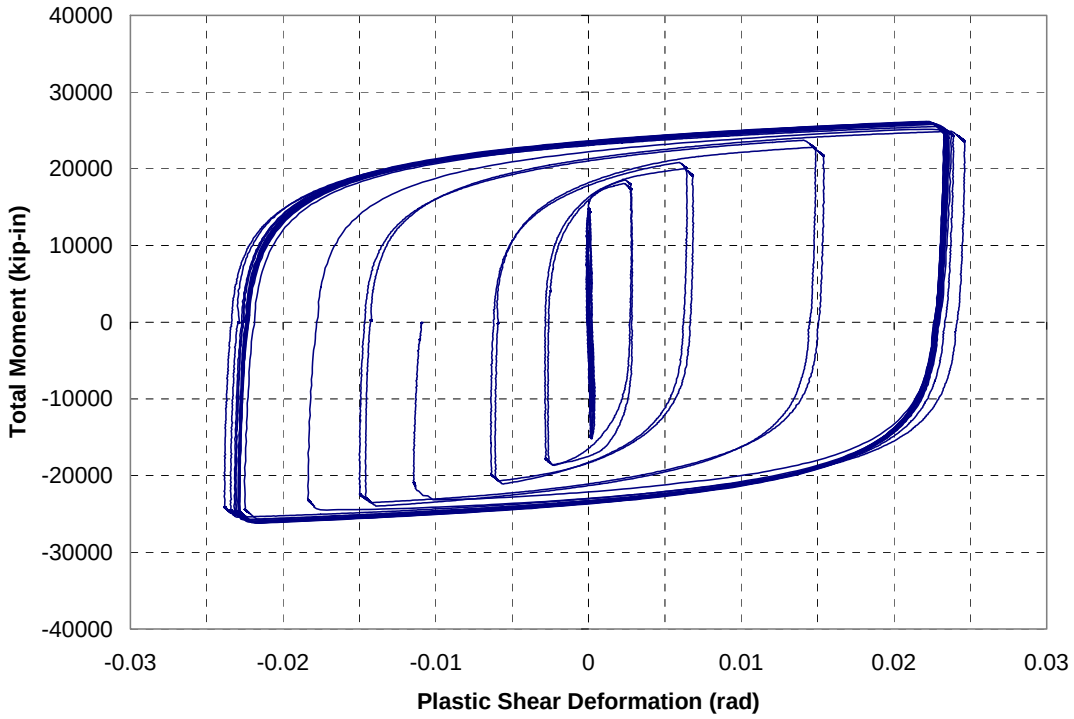


Figure A.70: Panel Zone Plastic Shear Deformation, CR2

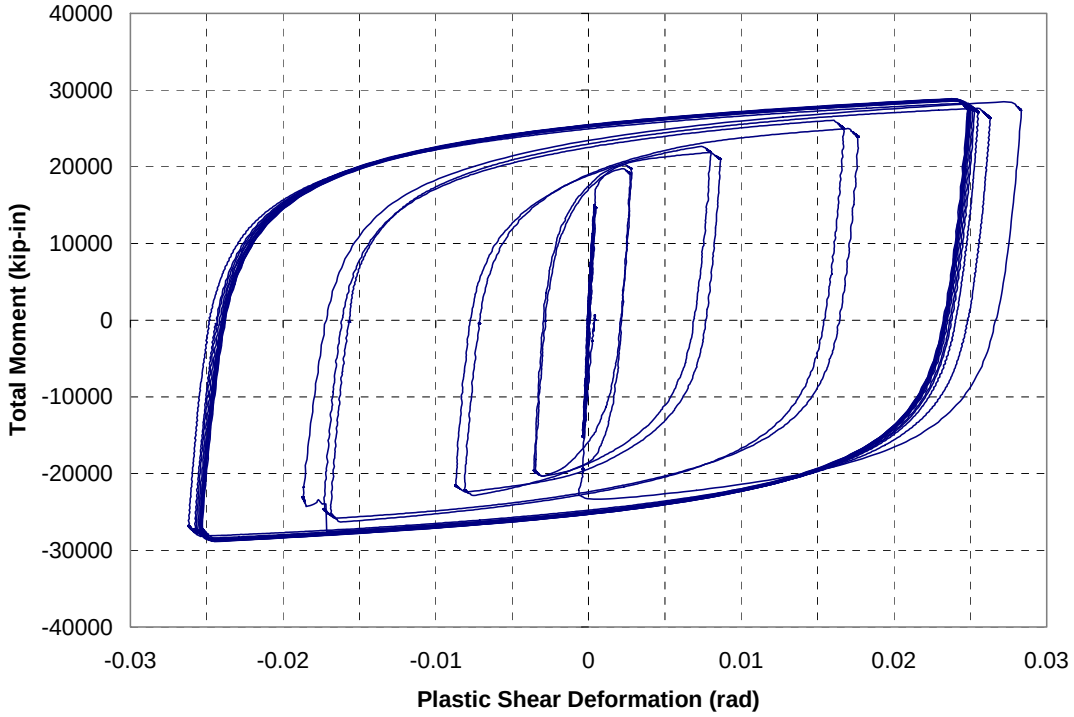


Figure A.71: Panel Zone Plastic Shear Deformation, CR3

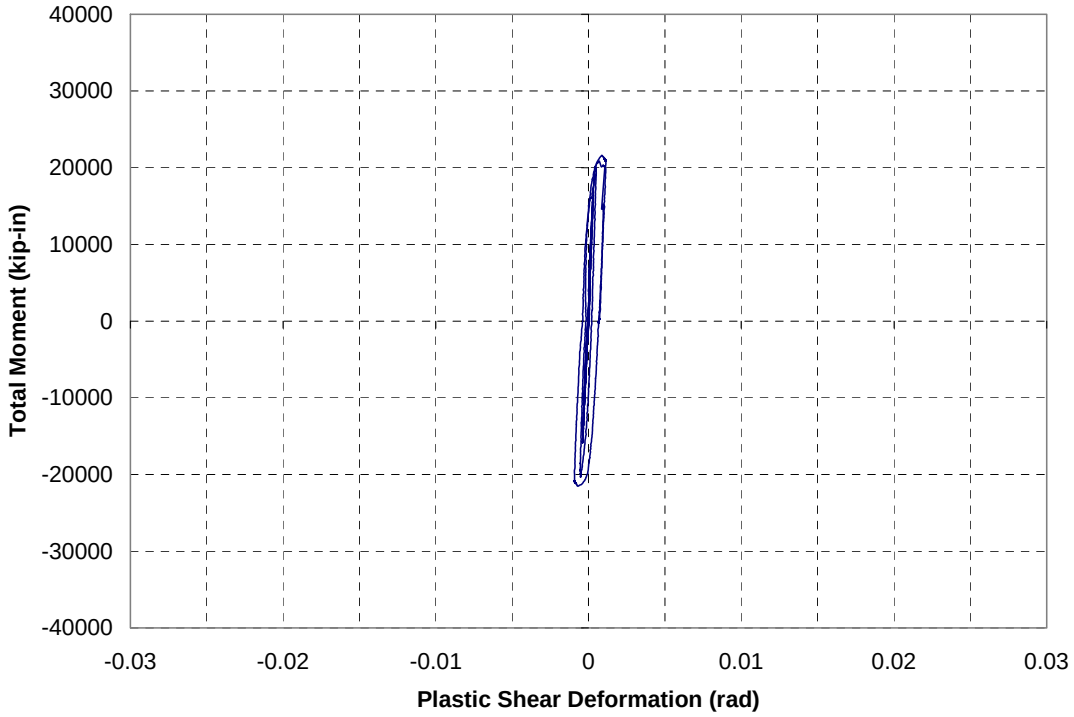


Figure A.72: Panel Zone Plastic Shear Deformation, CR4

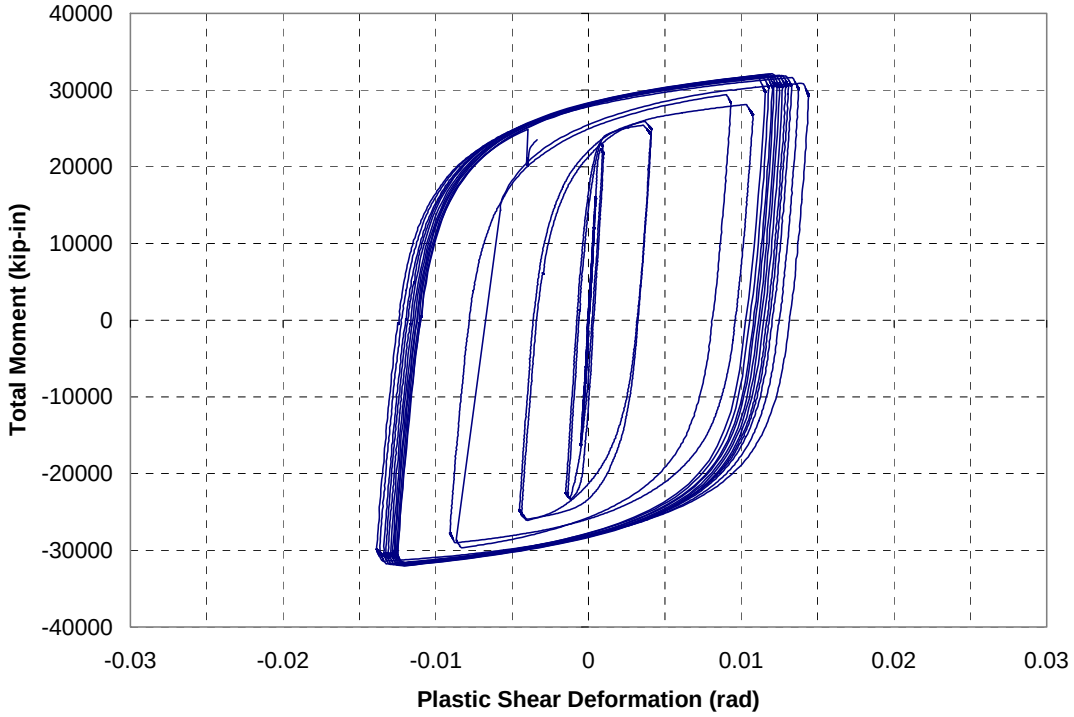


Figure A.73: Panel Zone Plastic Shear Deformation, CR4R

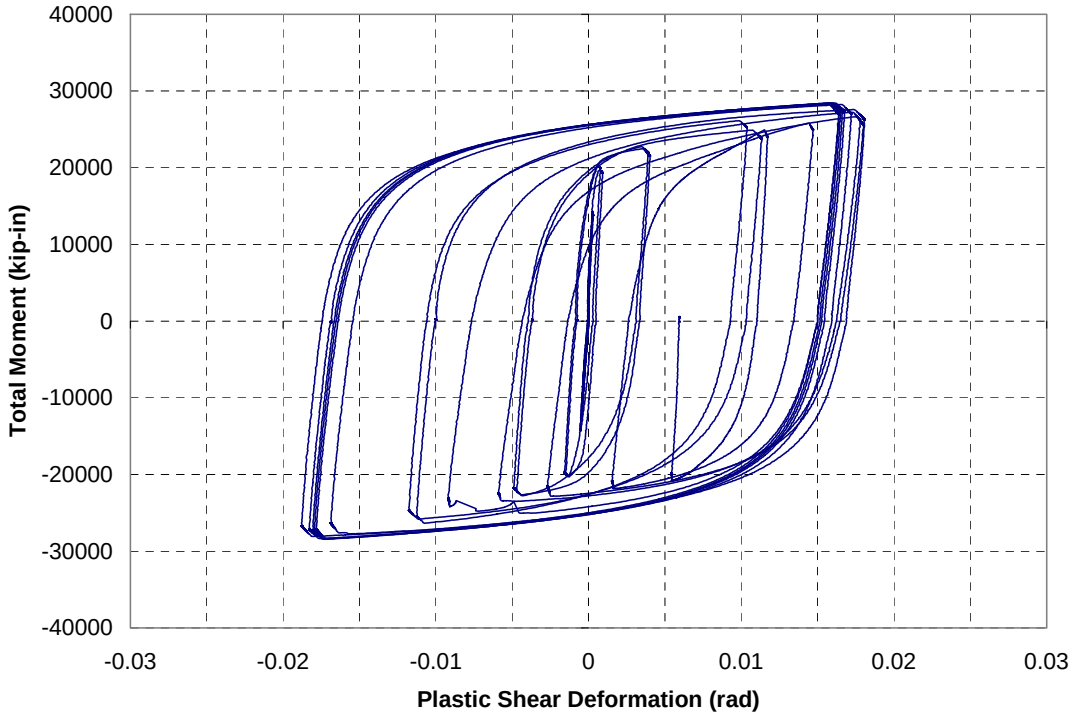


Figure A.74: Panel Zone Plastic Shear Deformation, CR5

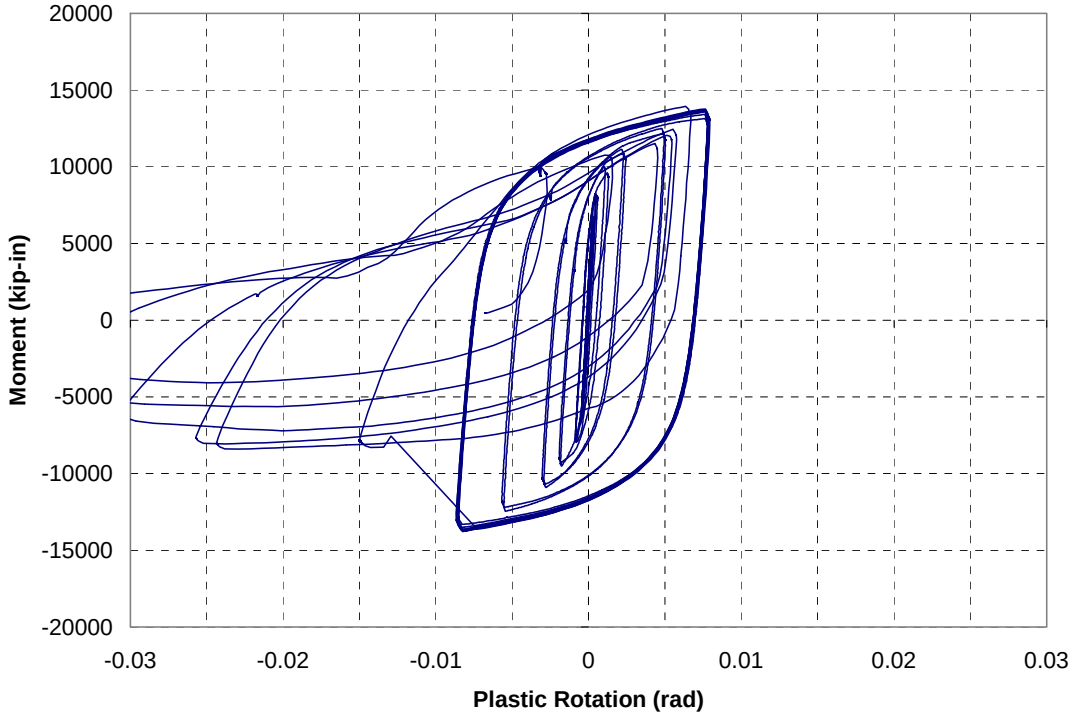


Figure A.75(a): East Girder Plastic Rotation Relative to Column Centerline, CR1

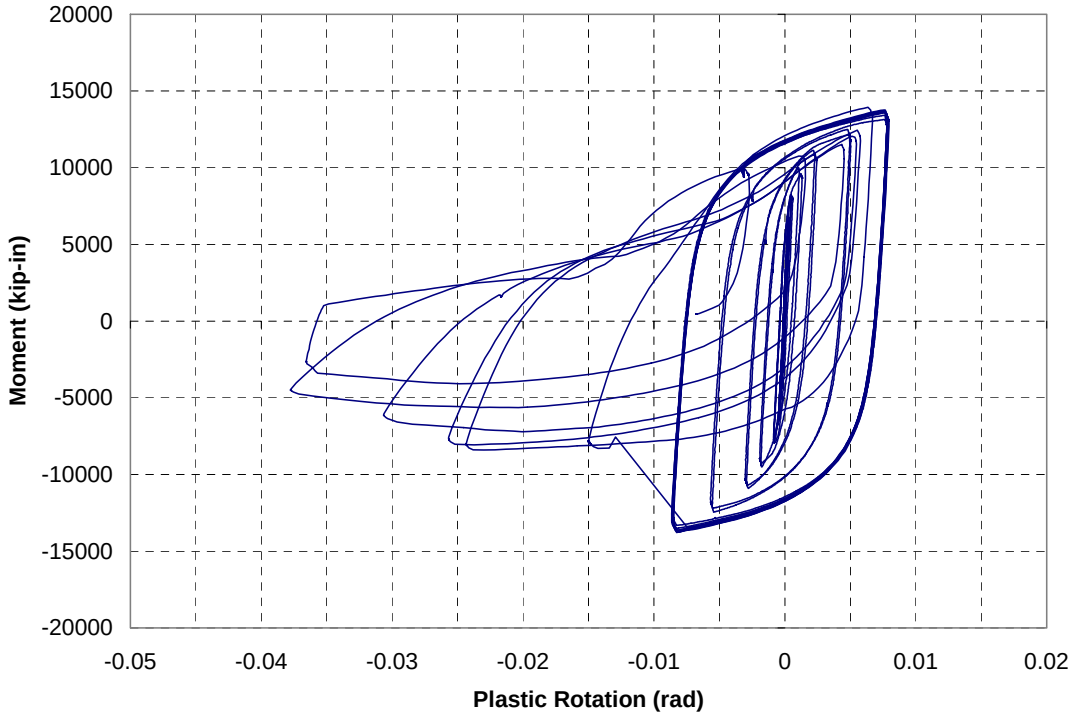


Figure A.75(b): East Girder Plastic Rotation Relative to Column Centerline, CR1 (Re-scaled)

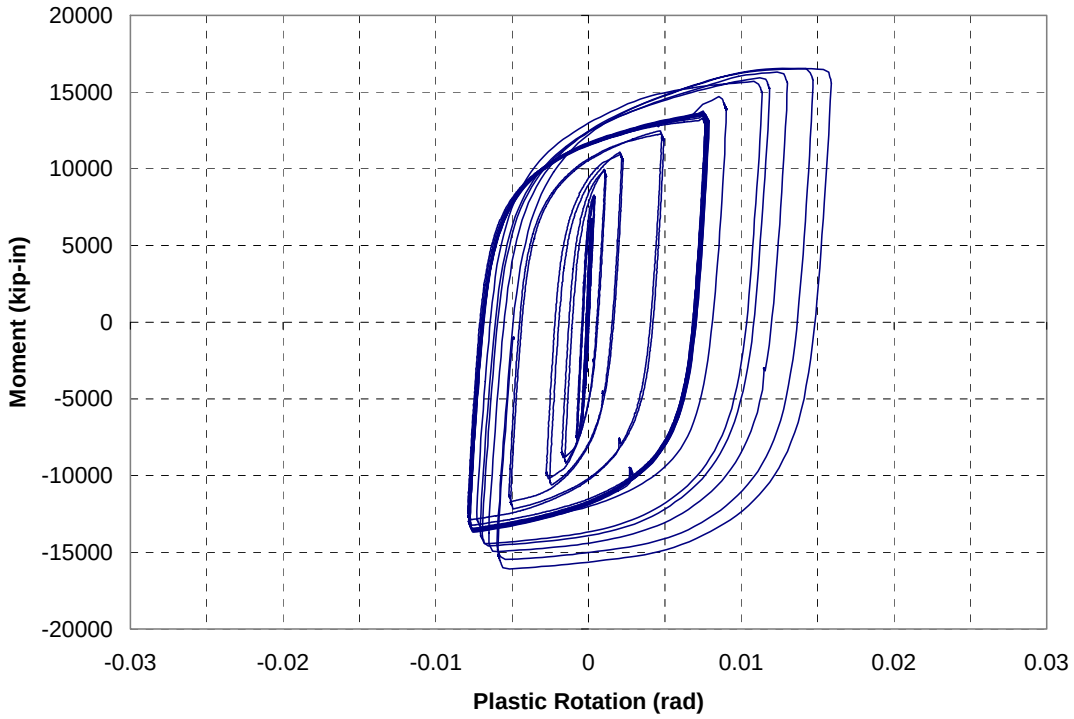


Figure A.76: West Girder Plastic Rotation Relative to Column Centerline, CR1

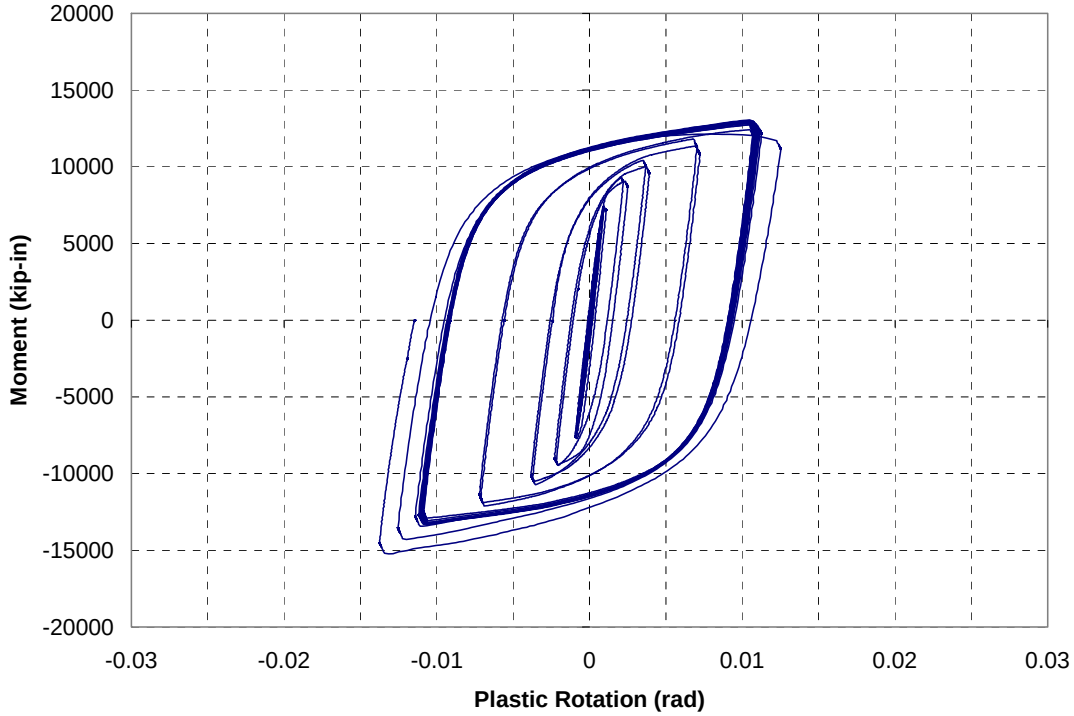


Figure A.77: East Girder Plastic Rotation Relative to Column Centerline, CR2

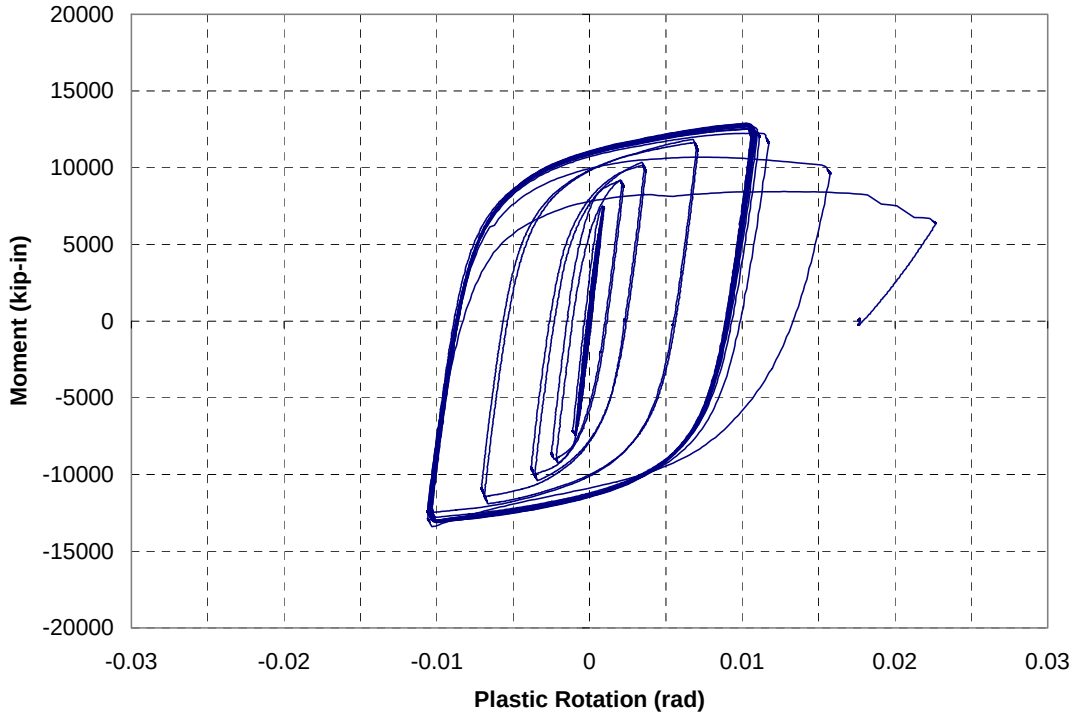


Figure A.78: West Girder Plastic Rotation Relative to Column Centerline, CR2

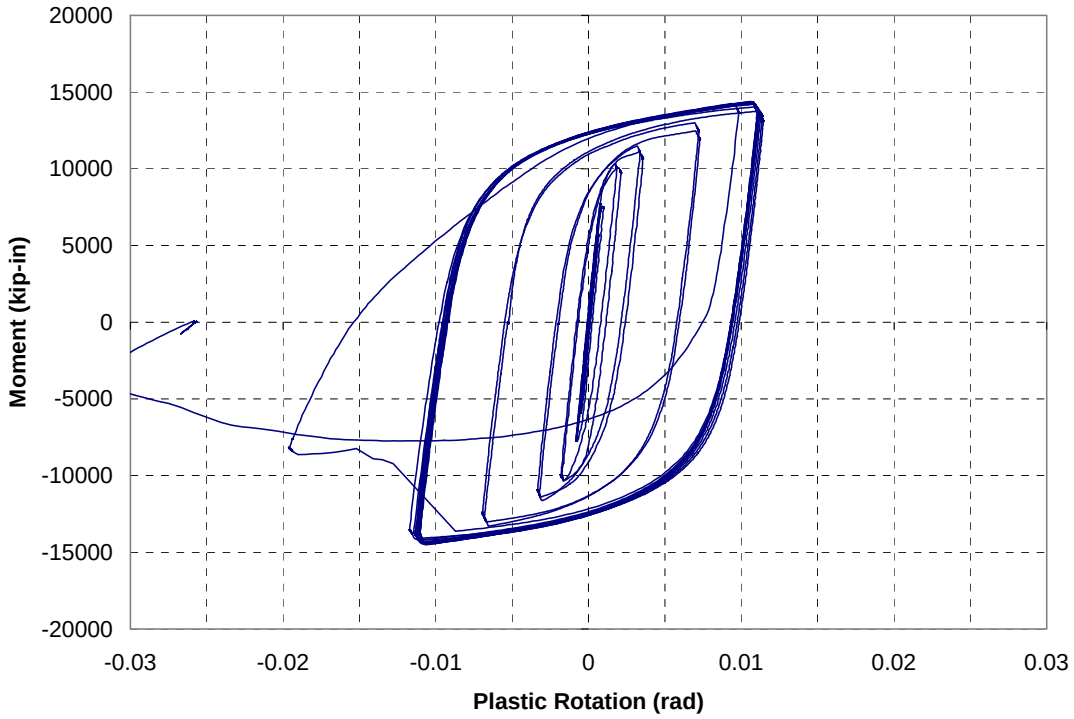


Figure A.79(a): East Girder Plastic Rotation Relative to Column Centerline, CR3

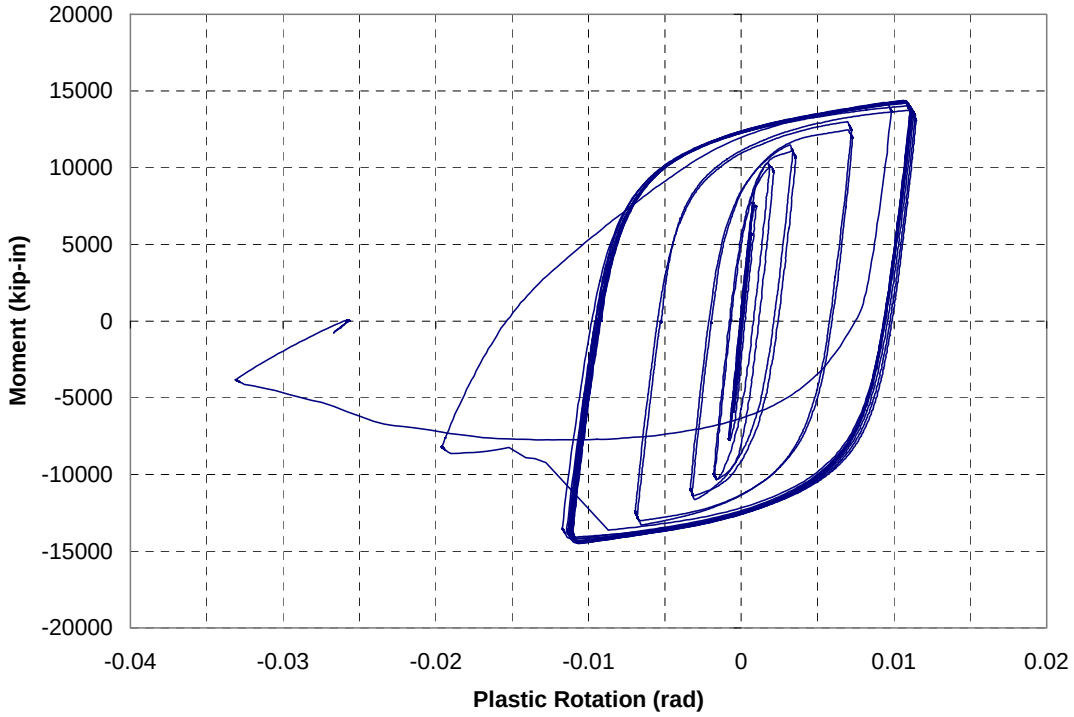


Figure A.79(b): East Girder Plastic Rotation Relative to Column Centerline, CR3 (Re-scaled)

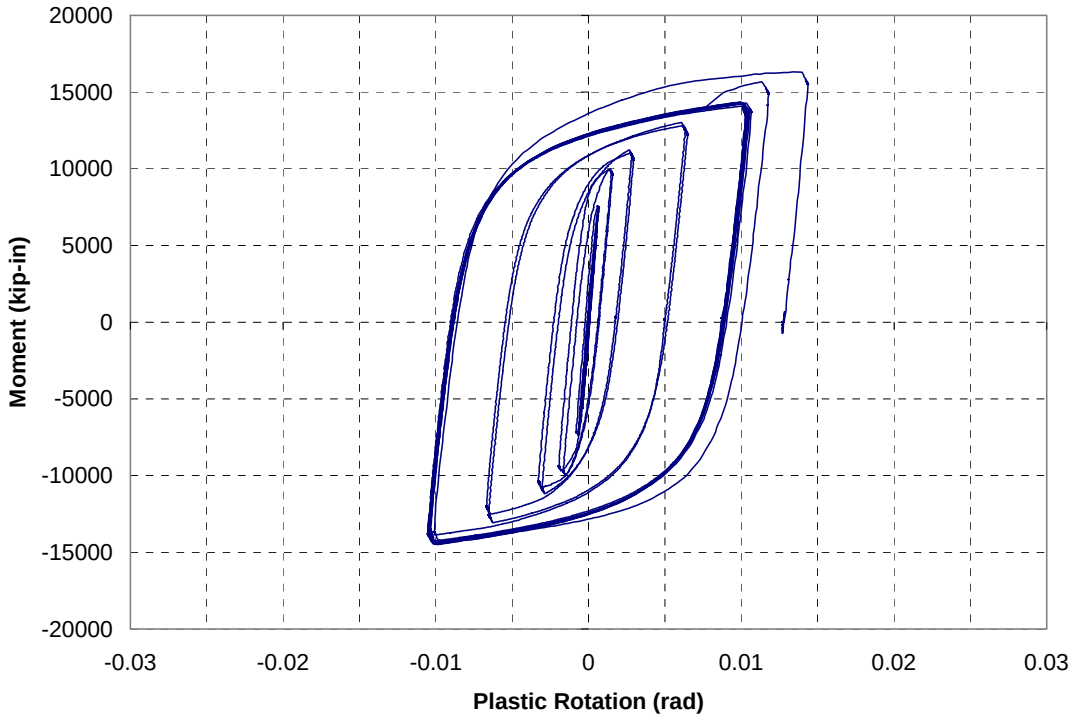


Figure A.80: West Girder Plastic Rotation Relative to Column Centerline, CR3

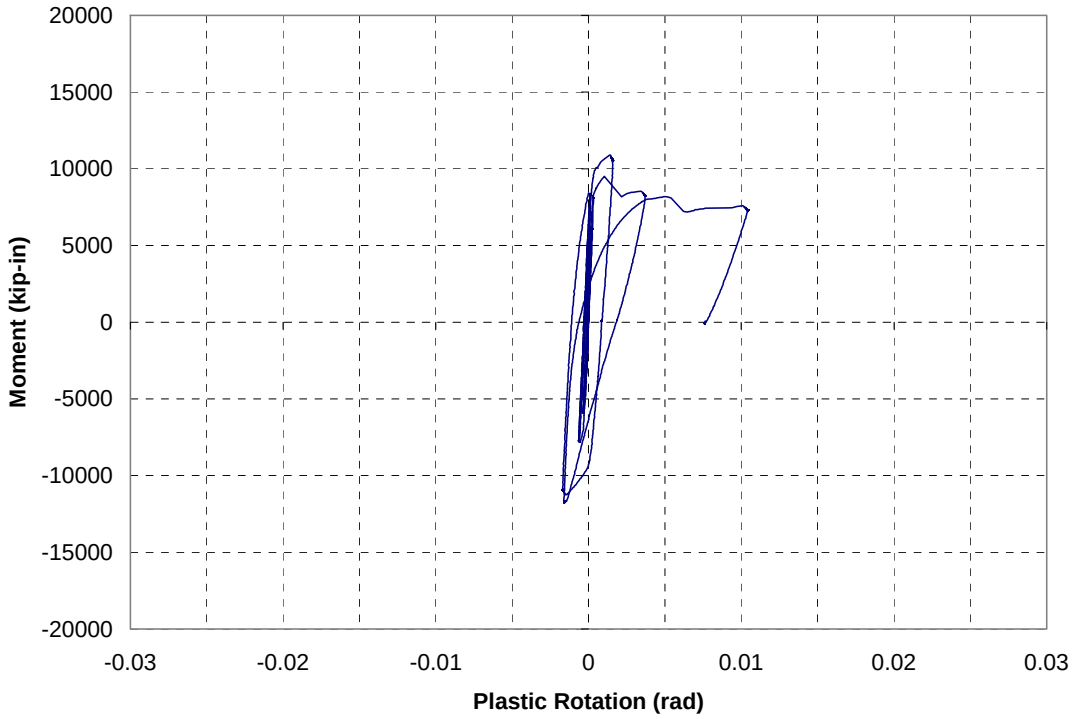


Figure A.81: East Girder Plastic Rotation Relative to Column Centerline, CR4

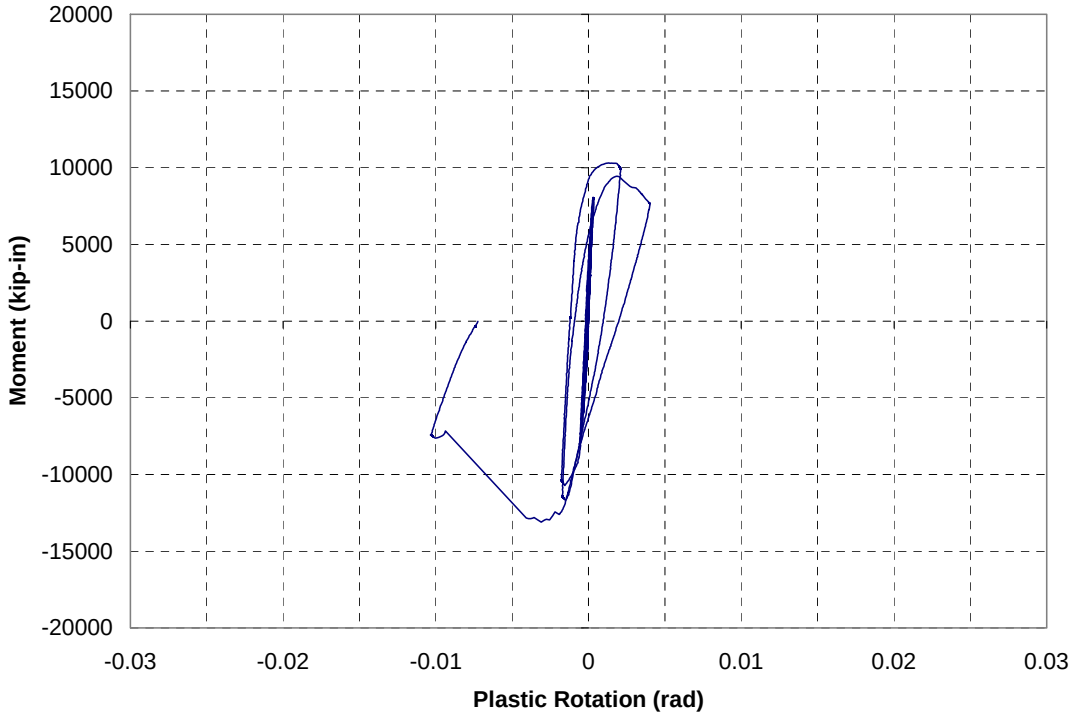


Figure A.82: West Girder Plastic Rotation Relative to Column Centerline, CR4

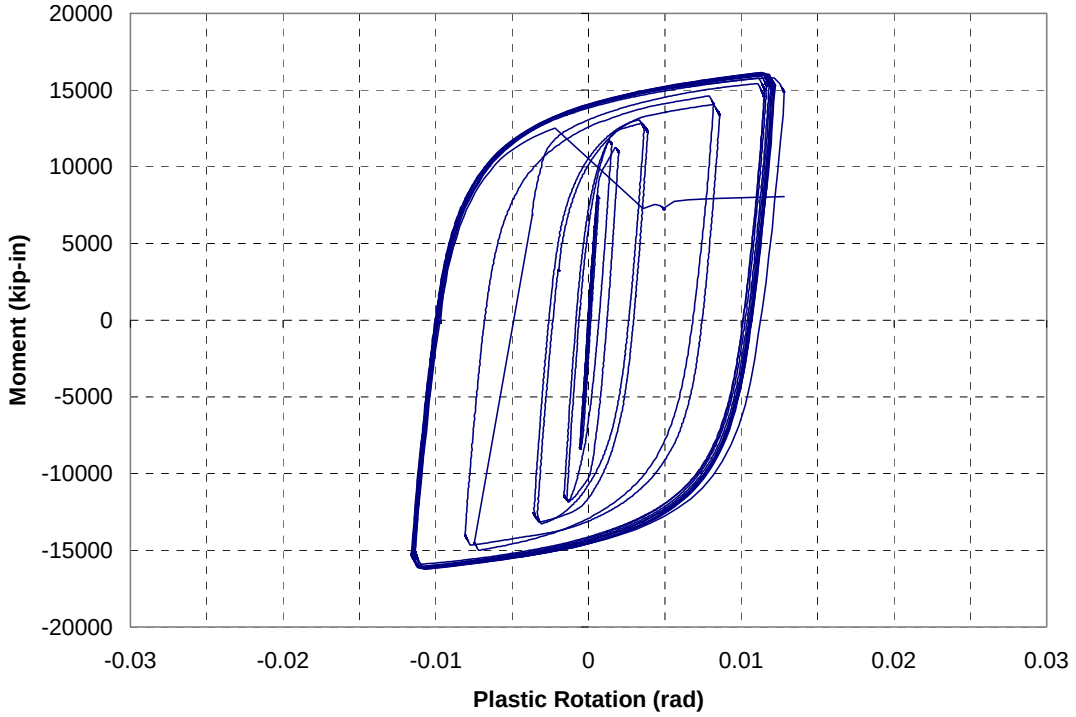


Figure A.83: East Girder Plastic Rotation Relative to Column Centerline, CR4R

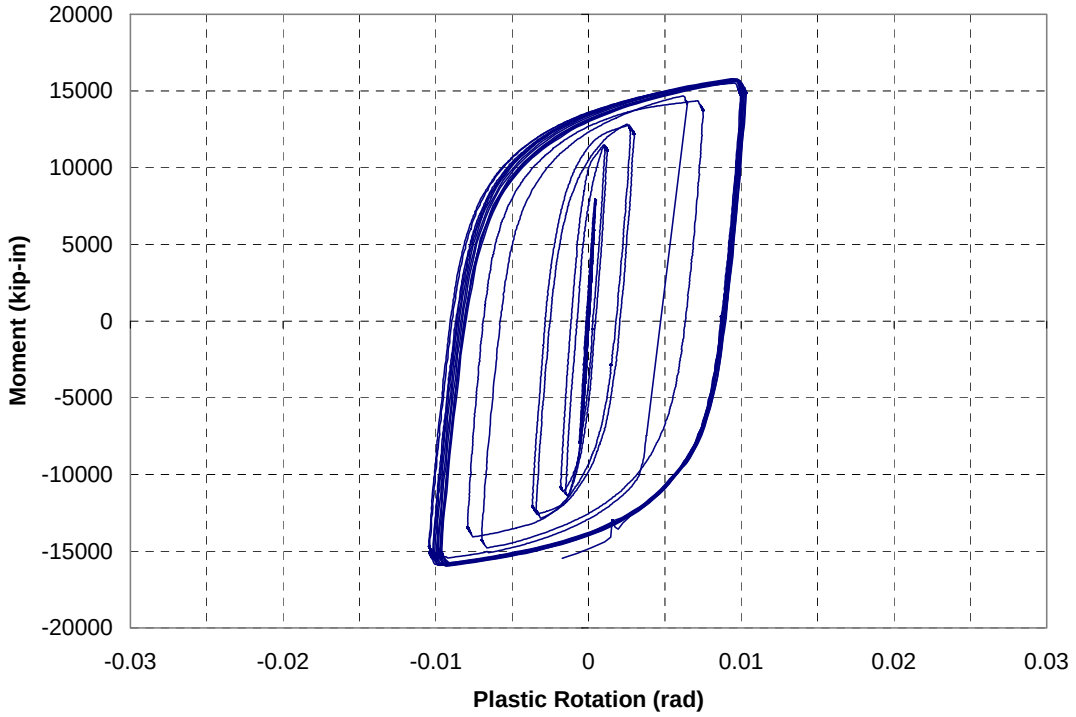


Figure A.84: West Girder Plastic Rotation Relative to Column Centerline, CR4R

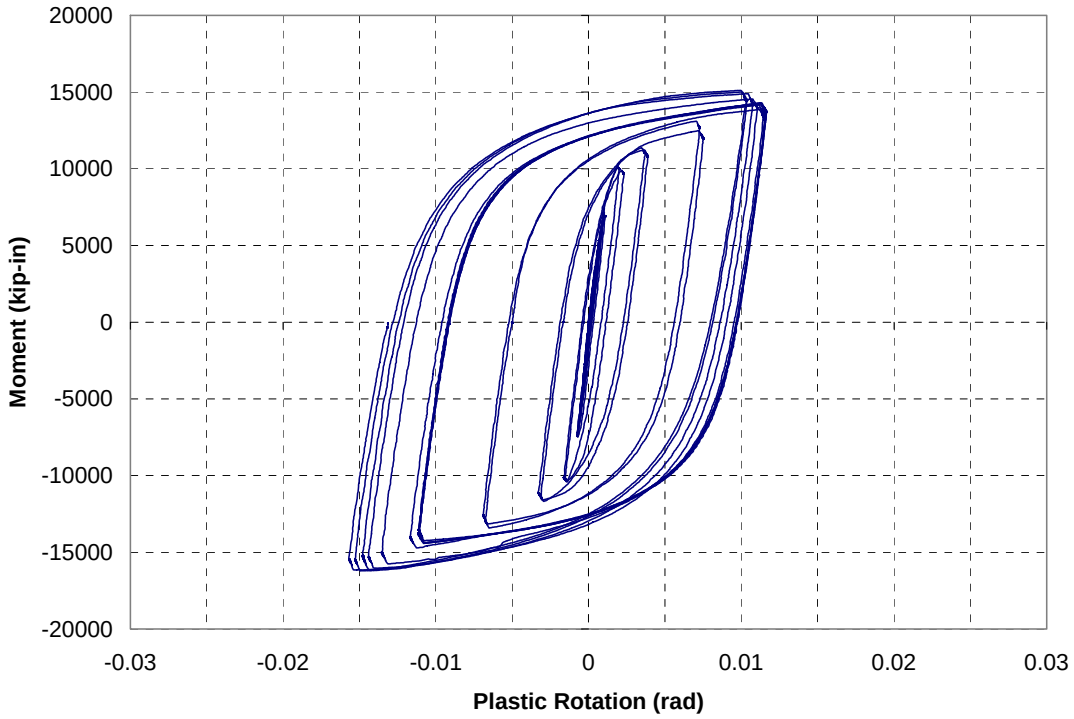


Figure A.85: East Girder Plastic Rotation Relative to Column Centerline, CR5

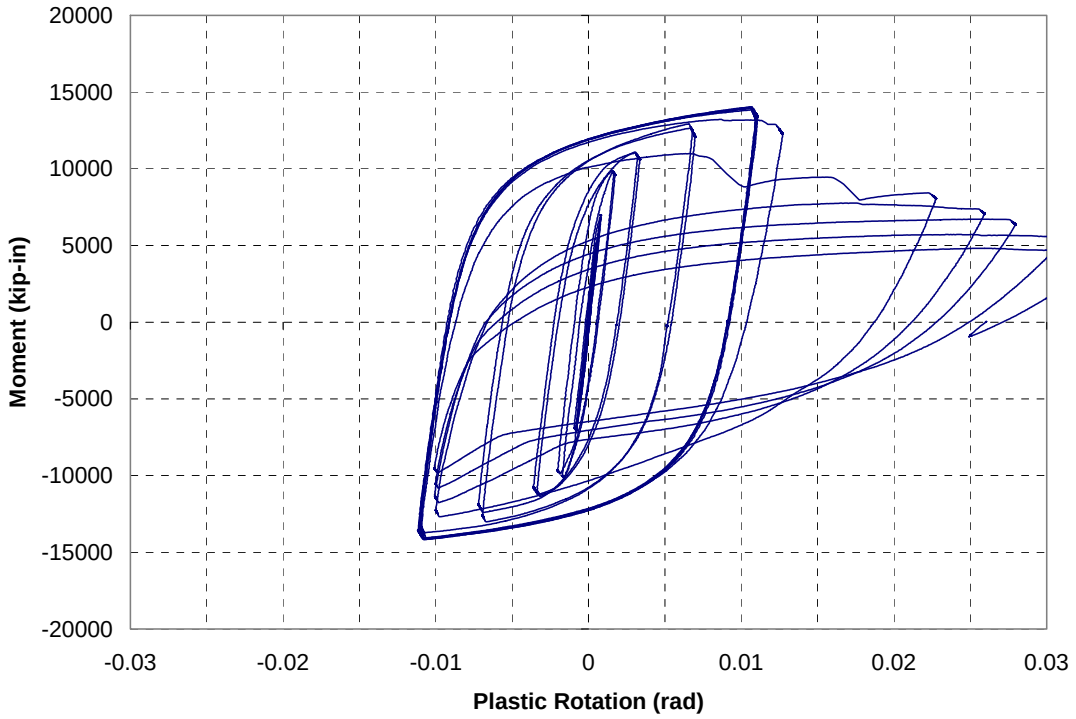


Figure A.86(a): West Girder Plastic Rotation Relative to Column Centerline, CR5

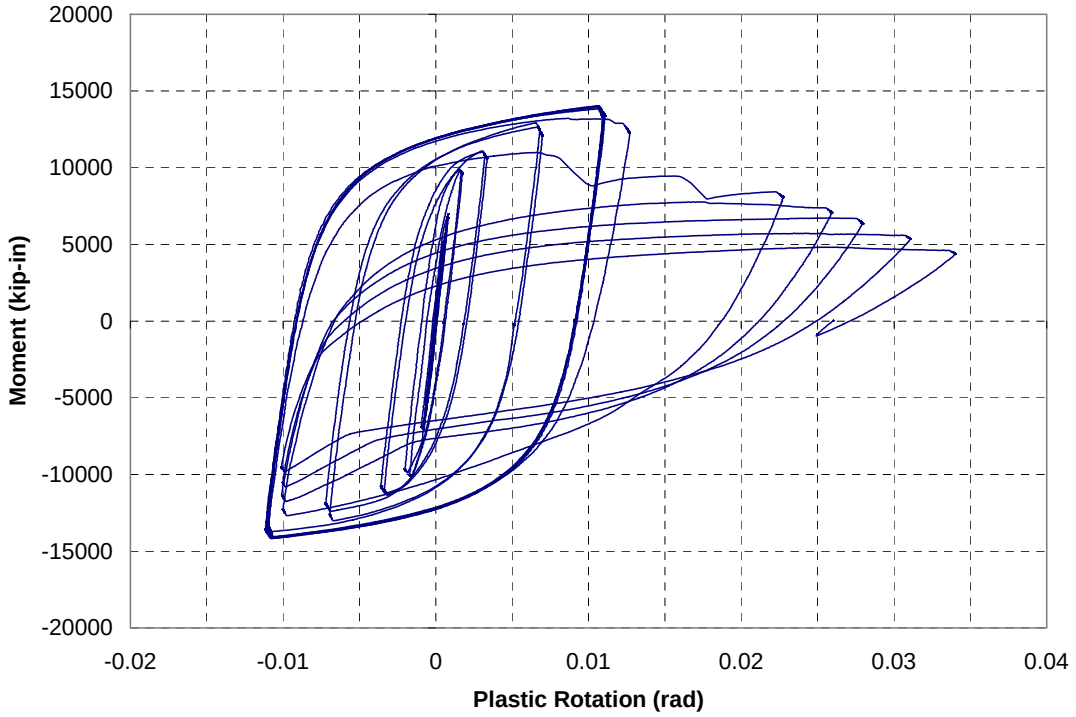


Figure A.86(b): West Girder Plastic Rotation Relative to Column Centerline, CR5 (Re-scaled)

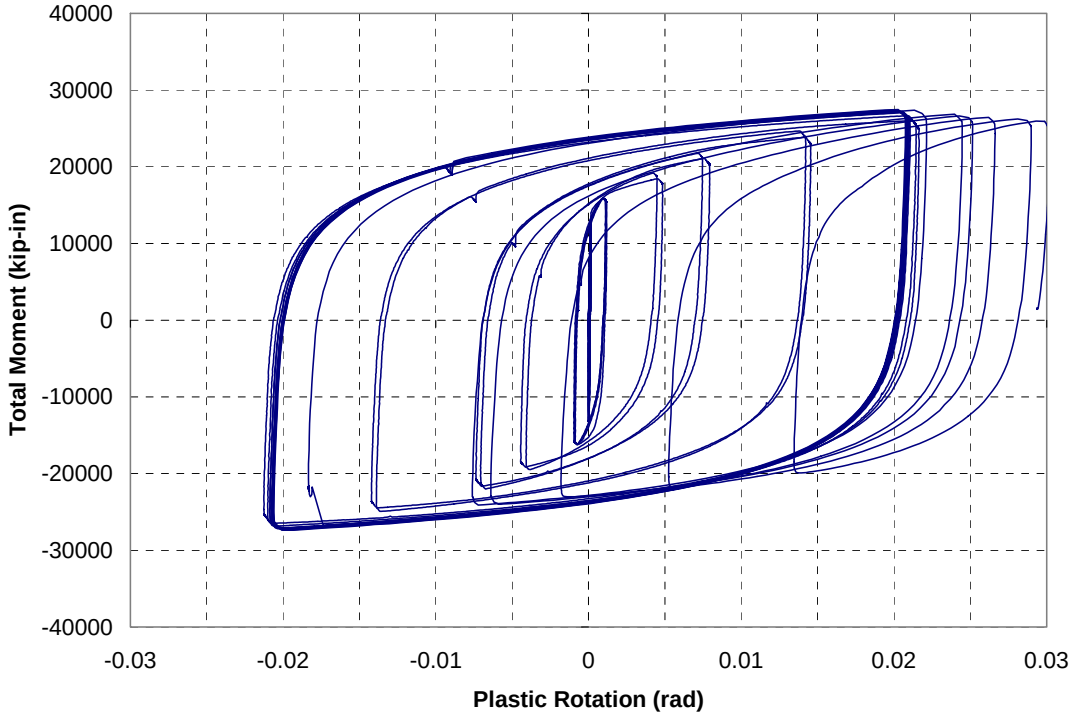


Figure A.87(a): Panel Zone Plastic Rotation Relative to Column Centerline, CR1

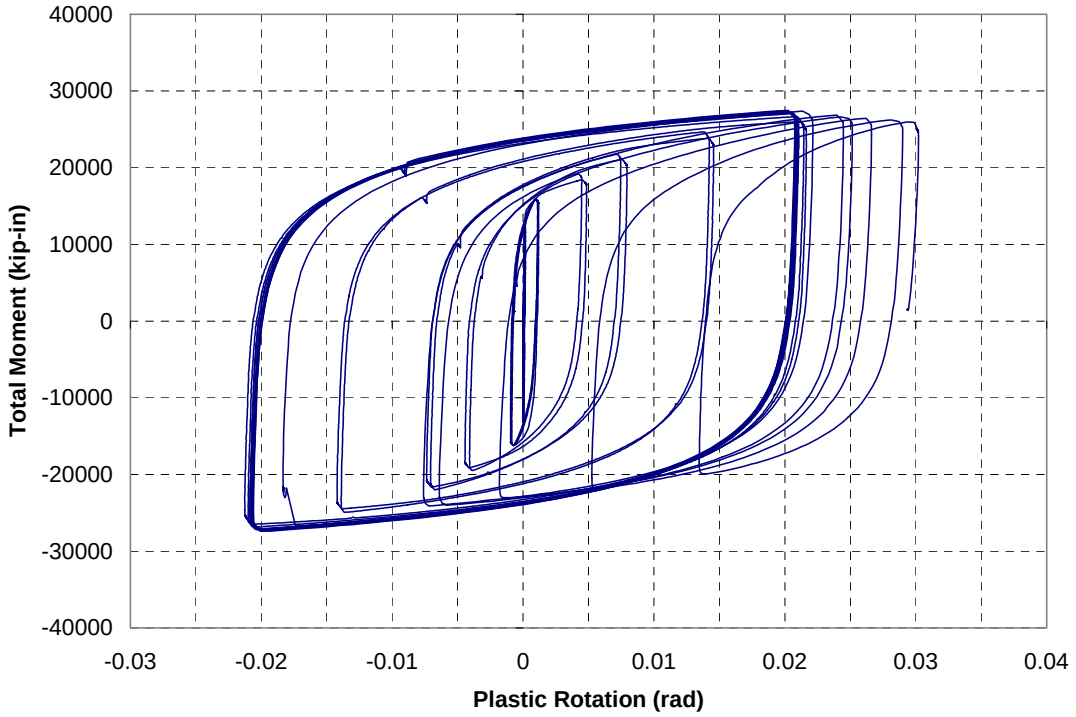


Figure A.87(b): Panel Zone Plastic Rotation Relative to Column Centerline, CR1 (Re-scaled)

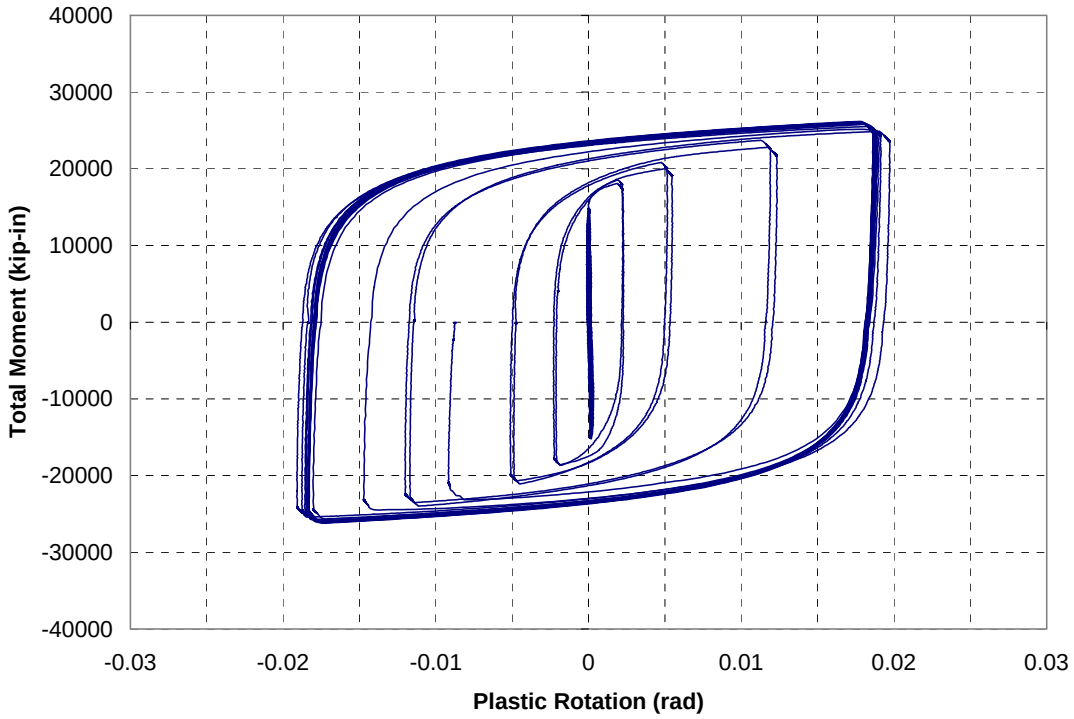


Figure A.88: Panel Zone Plastic Rotation Relative to Column Centerline, CR2

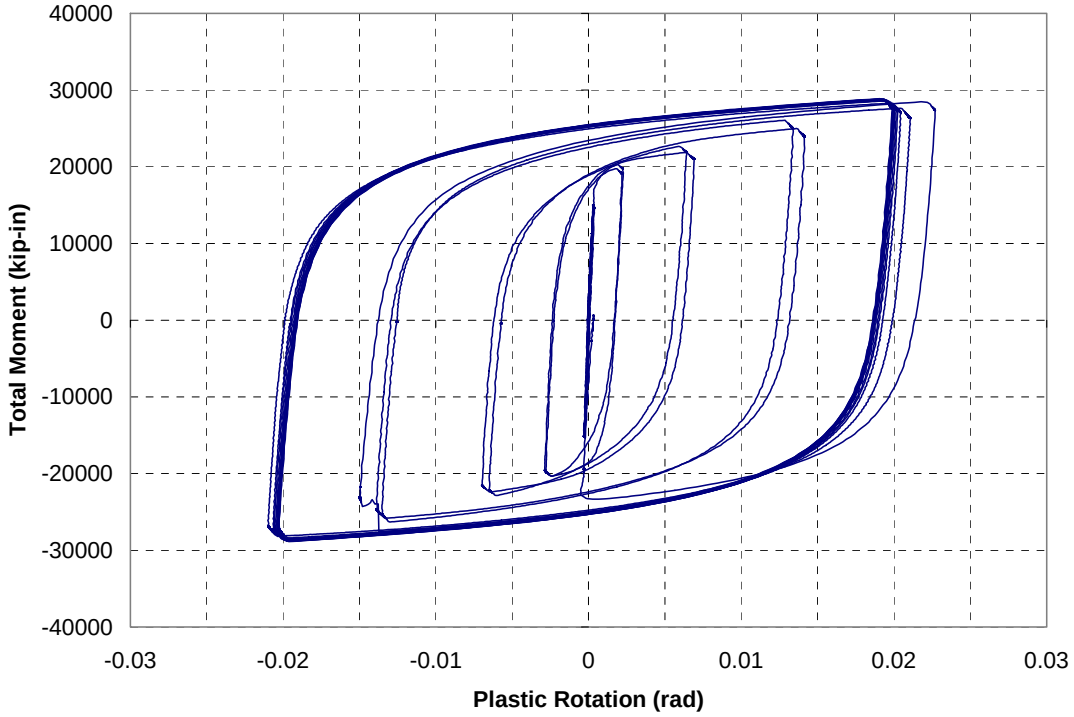


Figure A.89: Panel Zone Plastic Rotation Relative to Column Centerline, CR3

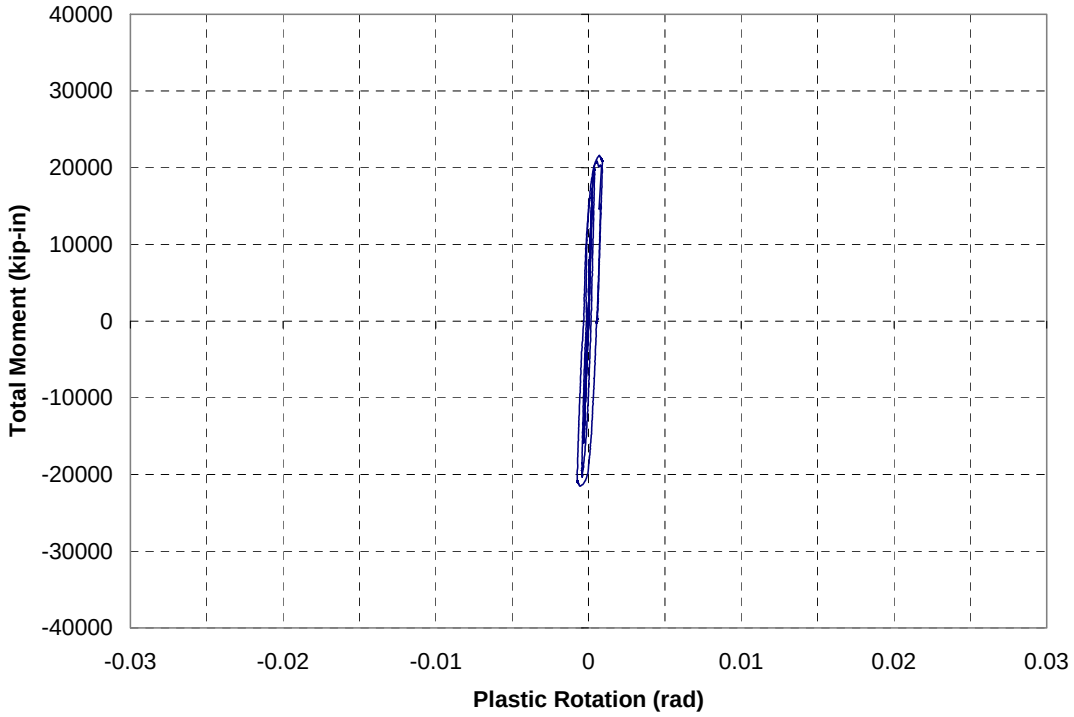


Figure A.90: Panel Zone Plastic Rotation Relative to Column Centerline, CR4

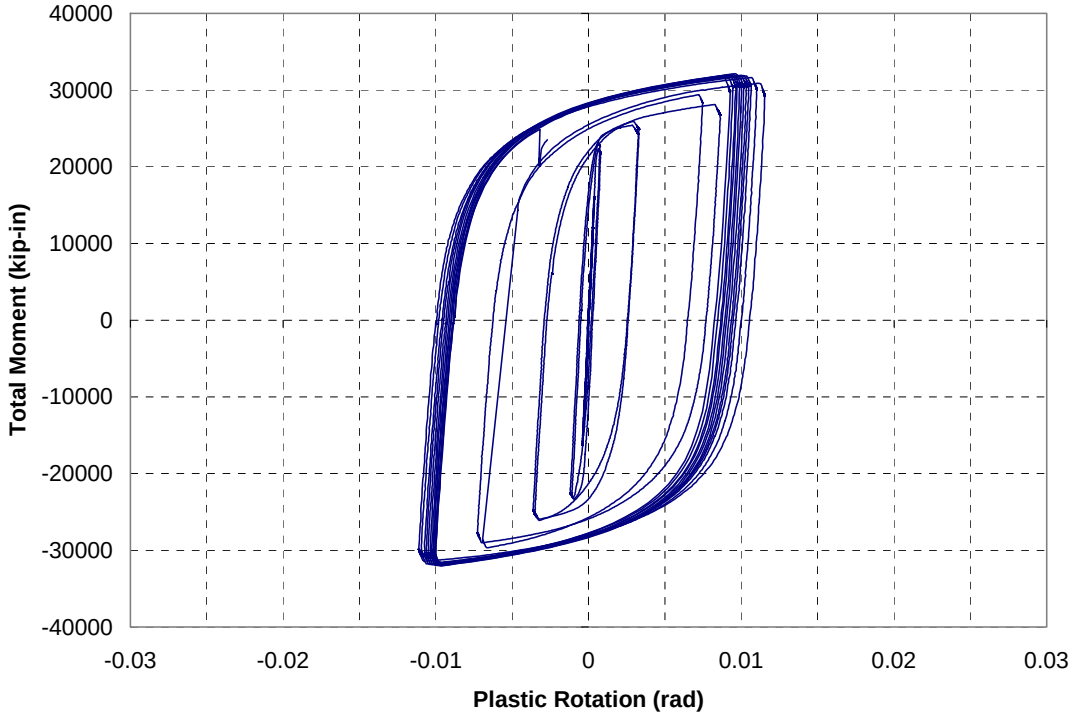


Figure A.91: Panel Zone Plastic Rotation Relative to Column Centerline, CR4R

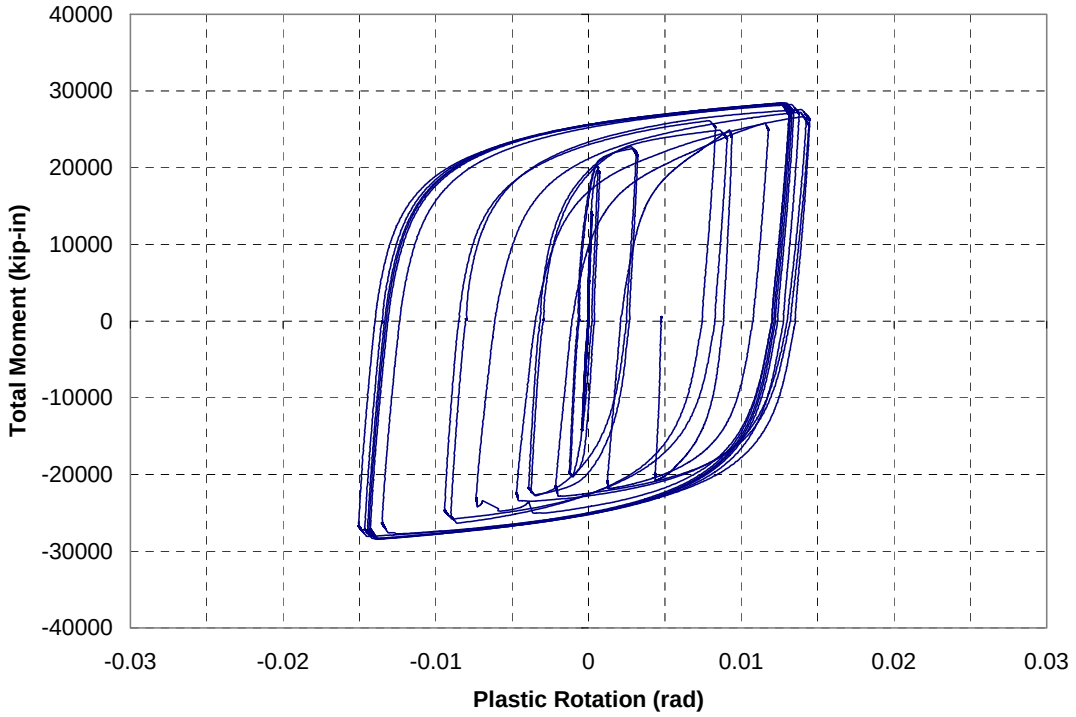


Figure A.92: Panel Zone Plastic Rotation Relative to Column Centerline, CR5

Appendix B

Failure Analysis of Specimen CR4

As a result of the weld failures occurring in Specimen CR4, a forensic investigation was conducted to determine the causes of the unexpected fractures. Brittle weld fracture was not an anticipated failure mode for the specimens, as notch-tough E70T-6 weld consumables were used for the flange welds. This material is recommended by SAC for new seismic construction (FEMA, 2000d), and was successfully used in the pull-plate experiments (Prochnow et al., 2000a), although different wire diameters and production lots were used for the cruciform and pull-plate tests. The SAC specified minimum Charpy V-Notch toughness (CVN) criteria is 20 ft-lb at 0°F and 40 ft-lb at 70°F. A study for SAC by Johnson (FEMA, 2000d) showed that the tested lots of E70T-6 generally met these toughness levels. The welds deposited for the pull-plate tests achieved CVN levels of 19.0 ft-lb at 0°F and 63.7 ft-lb at 70°F. This toughness was sufficient to prevent weld failure even when column flange separations exceeded ¼ in., and pull-plate strains near the weld exceeded 5.0%.

Strain histories in the girder flanges allow the progression of the cracking to be documented. Sudden drops in strain near the weld toes indicate likely crack propagation as load is shed from the cracked area and redistributed. Figure B.1 shows the strain in the East girder top flange during the 1.0% drift cycles. Refer to Figure 4.13 for the locations of the referenced strain gages. The first indication of cracking in Specimen CR4 is shown in Figure B.1, gage *ne_7gf_h*, located in the center of the flange, during the second cycle at 1.0% interstory drift. The lack of a strain drop in any other gage indicated the crack was localized in the center of the flange at this point. No global load drop was measured at this stage. The next indication of cracking occurred during the third cycle at 1.0% in the West girder top flange (see Figure B.2). In this case, all four

strain gages across the flange showed a strain drop, indicating a crack across most or all of the flange width. Again, no measurable load drop was noted. Neither bottom flange exhibited any indications of cracking at this drift level.

Girder loads during the 1.0% drift cycles corresponded to average moments of approximately 8,000 kip-in., or 63% of the nominal plastic moment capacity (M_p = 12,700 kip-in). Comparison with the nominal yield moment of the W24x94 girder, equal to 11,100 kip-in, indicates elastic behavior in the girders at this deformation level. The global load vs. deformation behavior remained essentially linear through these drift cycles. Calculated extreme fiber girder stresses of 36 ksi at the face of the column are associated with the moment of 8,000 kip-in. measured during the 1.0% cycles. While some minor localized yielding is indicated by the strain data of Figures B.1 and B.2, strains in the welds due to applied loads at this drift level were likely elastic, as the yield strength and cross-section of the welds is larger than the flange base metal. The localized yielding can be explained by high tensile welding residual stresses in the region of the strain gages. These self-equilibrating residual stresses in the welds and base metal result in an early onset of localized yielding and stress redistribution under the applied loads. Thus, fracture of the welds likely initiated at applied stresses at or below the 50.6 ksi yield strength of the girder flanges and the nominal 58 ksi yield strength of the welds.

Propagation of the fractures during the 1.5% and 2.0% drift cycles is shown by the strain data of Figures B.3 through B.5. Note that the bottom flange of the West girder fractured suddenly, giving no indication of cracking prior to complete fracture. The bottom flange of the East girder did not fracture. The somewhat different behavior of the bottom flanges relative to the top flanges may have been caused by removal of the bottom flange backing bars and placement of reinforcing fillet welds. This process can remove many weld discontinuities associated with the root pass of the CJP welds. Final fracture of the West top flange occurred during the second cycle at 1.5% drift, while the East top flange and West bottom flange were completely severed during the first cycle at 2.0% drift.

A typical fracture surface is shown in Figure B.6 after removal from the girder flange. The corresponding surface on the face of the column is shown in Figure B.7.

Figure B.8 shows a closer view of typical fracture surface details. The blocky, planar nature of the surface is typical of a cleavage fracture. Brittle behavior is often characterized by cleavage, which consists of fracture planes through the grains of the material (Fisher et al., 1997). Cleavage fractures generally occur in the presence of very little ductility. This is consistent with the loads and associated stresses at first cracking discussed above.

Ductile behavior, on the other hand, is characterized by a fibrous fracture surface appearance. The mechanism of ductile fracture is the initiation, growth and coalescence of voids within the steel on a microscopic scale (Fisher et al., 1997). A ductile fracture surface usually has a smooth, silky appearance, as opposed to the shiny, faceted appearance of cleavage fractures. A large amount of plasticity is also usually associated with ductile fracture behavior. Clearly this was not the case with the fractures of Specimen CR4.

Following removal from the girder flanges, the fracture surfaces were sectioned for polishing and etching of the weld cross-sections and further analysis of the surfaces. Two weld macro-sections were cut from each of the three fractures to examine the bead sizes, heat affected zones (HAZ), and fusion of the welds. The remaining sections of the fractures were prepared for analysis by a scanning electron microscope (SEM). Figure B.9 shows the typical sectioning of one fracture. The single unfractured flange weld (the East girder bottom flange) was removed from Specimen CR4 for CVN and chemical analyses. An unfractured flange weld from Specimen CR1 was also removed for a comparison of properties. Both specimens were welded with the same spool of E70T-6 consumable.

Figures B.10 through B.12 show weld macro-sections taken from each of the three fractured welds. All three sections reveal a large-grained weld bead structure. The sections from the top flanges (Figures B.10 and B.11) also have reinforcing fillet welds placed on the beam side of the backing bar. This weld is not required by the SAC WUF-W design guidelines (FEMA, 2000a), but was placed by the welder in addition to the required reinforcing fillet weld between the backer and column. These welds were made with an E71T-8 electrode. Note the contrast in grain structure between the two

types of weld. The bead sizes and stagger were checked against AWS D1.1-2000 requirements (AWS, 2000), and were found to be in compliance. The size of the HAZ is within typical values, and the fusion appears adequate. Note the small lack of fusion (LOF) defects between the weld passes in Figure B.11. Small LOF defects such as these are common in welded construction, however, and are not an indication of poor welding. One notable feature of the E70T-6 bead structure is the minimal grain refinement. Grain refinement occurs when subsequent weld passes remelt and reheat the prior pass. This form of heat treatment can improve the local notch toughness of the refined region (Miller, 1997). Aside from the coarse-grained structure, however, the weld macro-sections did not exhibit any atypical or unacceptable features.

Figure B.13 shows a macro-section taken from the unfractured East bottom flange of Specimen CR4. The features of this section do not reveal any visual differences in weld structure between the fractured and unfractured welds of this test. A macro-section was also cut from Specimen CR1 for comparison. It is shown in Figure B.14. The features of this macro-section are similar to those taken from CR4. One main difference is an increase in grain refinement in the CR1 weld. The HAZ is also slightly larger in the case of the CR1 macro. The bead sizes and fusion all appear similar to the fractured welds of Specimen CR4, however. Note the low cycle fatigue (LCF) crack that had initiated at the toe of the CJP weld in the CR1 macro, and the LOF and slag inclusion between the backing bar and root pass (see Figure B.14). Both macro-sections shown in Figures B.13 and B.14 were taken near the center of the respective welds.

The fracture surfaces were further analyzed visually and using an SEM to identify the typical weld discontinuities present and to confirm the brittle nature of the failures. Several LOF defects and slag inclusions were discovered on the surfaces, but ultrasonic testing of the welds prior to testing had not discovered any rejectable indications using AWS D1.1-2000 ultrasonic inspection criteria for cyclically loaded structures (AWS, 2000). Most discontinuities visible on the fracture surfaces were small and typical of welded moment frame construction. Using the radiographic inspection acceptance criteria contained in AWS (2000), however, a few visible discontinuities would be classified as rejectable. The failure analysis conducted by Barsom et al. (2001) has also

discovered the presence of numerous cracks within the fractured welds. They are believed to be a result of hydrogen-assisted cracking. Figures B.15 through B.17 show typical surface features of the welds. Figure B.15 shows an LOF defect and slag inclusions at one edge of the West girder top flange weld. Figure B.16 shows slag inclusions along the backing bar of the West girder top flange. Figure B.17 shows an LOF defect at the center of the West bottom flange weld, above the reinforcing fillet weld. This is a typical LOF location, as it is directly below the access hole where the weld passes must be stopped and started. These weld discontinuities are further discussed below in the context of a basic fracture mechanics analysis of the welds.

An SEM was used to look more closely at the fractured surfaces. All scanning electron microscopy was conducted in the Institute of Technology Characterization Facility at the University of Minnesota. The typical fracture surfaces of the welds revealed their brittle nature on the microscopic level. Figures B.18 and B.19 show the typical cleavage appearance of the E70T-6 weld fractures. To contrast, Figure B.20 is an SEM image from one of the fractured reinforcing fillet welds placed with E71T-8 electrodes. These reinforcing welds exhibited the void growth and coalescence typical of ductile failure. All images are at the same magnification of 5000x. This provided confirmation that all E70T-6 weld fractures were brittle in nature.

In addition to the examinations of the fracture surfaces, material investigations were also conducted. Results of the CVN testing of Specimens CR1 and CR4 are presented in Table B.1. An independent material testing facility conducted all CVN testing. The CVN values of approximately 2 ft-lbs are on the lower bound of any measured toughnesses. Measured toughness of the E70T-4 welds often used prior to the Northridge earthquake typically ranged between 5 and 20 ft-lbs at room temperature (Fisher et al., 1997).

It should be noted that the samples removed from the specimens were strained during testing, and were not standard AWS test plate CVN samples. The effect of pre-strain on weld CVNs is not documented, but it is believed to reduce toughness to some extent. It is well known that the toughness of rolled sections decreases with prestrain (Kaufmann et al., 2001), but no similar studies have been performed on prestrained weld

samples. To obtain an estimate of the effect of strain on weld toughness, Charpy samples were cut from one of the pull-plate specimens tested by Prochnow et al. (2000a). These welds were also E70T-6, but were made using a different diameter electrode (0.068" as opposed to 5/64" used for the cruciform tests). Table B.2 compares the toughnesses determined from the unstrained AWS test plate to those from the strained pull-plate specimen. The same spool of wire used for both the test plate and the pull-plate specimens. Note that the toughness of the strained samples was actually higher than the test plate CVNs at both temperatures. This indicates that factors other than prestrain have a more significant effect on weld toughness. Thus, while there may have been some reduction in toughness during testing of Specimens CR1 and CR4, it is very unlikely that the degradation was such that the welds would have met the SAC minimum toughness requirements (FEMA, 2000a) prior to testing.

Linear Elastic Fracture Mechanics (LEFM) may be used to analyze fractures when plasticity is limited. Basic LEFM involves a comparison of an applied stress-intensity factor at a crack location, K, to the resistance of the material, K_c. If the applied stress intensity exceeds the material resistance, fracture is predicted. This methodology was first developed by Irwin (1957) following World War II. The applied stress-intensity factor is related to the applied stress, crack size, and crack geometry. The basic formula is (Barsom and Rolfe, 1987):

$$K = F_c F_s F_w F_g \sigma \sqrt{\pi a} \tag{B.1}$$

where:

F_c = crack shape factor

F_s = free-surface factor = 1.12 for a surface crack, 1.0 for a buried crack

F_w = finite-width correction factor

F_g = stress-gradient factor = 1.0 for uniform stress

σ = nominal stress on gross section remote from the crack

a = characteristic crack size

The correction factors are used to modify the theoretical stress-intensity solutions for typical crack geometries. They have values generally on the order of 1.0. For surface

cracks, the characteristic crack size is equal to the depth of the crack. For buried cracks, the total crack depth is twice the characteristic value (i.e., a is equal to half the crack depth). The stress-intensity factor has units of ksi-√in or MPa-√m.

The material resistance, or critical stress-intensity factor, is related to the toughness of the material and is often correlated to CVN toughness using the following empirical relationship (Barsom and Rolfe, 1987):

$$K_d = 12.2\sqrt{CVN} \tag{B.2}$$

where:

K_d = dynamic fracture toughness (units of ksi-√in)

CVN = Charpy toughness (units of ft-lbs)

This empirical correlation is valid only for lower-shelf toughness behavior (i.e., brittle materials) and represents the material resistance under the very high strain rates associated with CVN testing. If used as an estimate of K_c, Equation B.2 yields a conservative estimate of the material resistance at a given temperature because of the strain rate effects. Much lower strain rates are encountered during earthquakes and quasi-static testing of beam-column connections. Under these lower strain rates, the brittle-to-ductile CVN transition curve shifts to lower temperatures. Because the observed fractures were brittle, however, it is reasonable to assume the weld material exhibited lower-shelf behavior at the tested strain rates. Thus, Equation B.2 should provide an acceptable estimate of K_c for Specimen CR4.

Two types of flaws common in welded moment frame construction are now analyzed using the procedure outlined above. These are center cracks and buried penny-shaped cracks. The center crack solution can be used to analyze the effects of the backing bar notch and weld root discontinuities on a top flange CJP weld with a reinforcing fillet weld under the backer. Figure B.21 illustrates the application of the LEFM idealization to a backing bar notch (Fisher et al., 1997). Assuming uniform tensile stress (F_g = 1.0), Equation B.1 reduces to:

$$K = F_w \sigma \sqrt{\pi a} \tag{B.3}$$

where:

F_w = finite width correction = $\sqrt{\sec \frac{\pi a}{2W}}$ (B.4)

W = half the width of the idealized plate (see Figure B.21)

Equation B.4 is known as the secant or Fedderson approximation of the finite width correction factor. The free-surface factor, F_s, is taken as 1.0 in this case because the top and bottom edges of the crack are contained within the welds. The crack shape factor, F_c, is also 1.0 because the crack is continuous across the width of the flange. While the assumption of uniform stress and the geometry of Figure B.21 is a rough approximation, the validity of the solution given by Equation B.3 for this application has been verified by fatigue crack growth rate tests (Fisher et al., 1997).

The buried, penny-shaped (circular) crack solution is applicable to a wide range of buried discontinuities within a weld (Fisher et al., 1997). For this case, Equation B.1 becomes:

$$K = F_c \sigma \sqrt{\pi a} \tag{B.5}$$

where:

$F_c = 2/\pi \approx 0.64$ for a penny-shaped crack

a = radius of the circular crack

For typical buried flaws that are small in comparison to the flange width (e.g., $a/W < 0.1$), F_w can be taken as 1.0. The free-surface factor, F_s, is 1.0 for buried flaws, and again assuming uniform stress, F_g is taken as 1.0. An elliptical crack shape correction factor formula can be used for non-circular flaws, but 0.64 will always be conservative because it is the lower bound of the crack shape correction factor (Fisher et al., 1997).

Using 2 ft-lbs as the weld toughness from the CVN tests of Specimen CR4, Equation B.2 yields an estimate of K_c equal to 17 ksi-√in. For the top flange welds, assuming no root flaws or weld root penetration, $2a$ is equal to the backing thickness of

0.375 in. and 2*W* is approximately 1.0 in. based on the size of the reinforcing fillet weld (see Figure B.21). The finite width correction factor (Equation B.4) then becomes 1.1, and assuming a stress equal to the yield stress of the girder flanges (50 ksi), Equation B.3 predicts an applied stress intensity factor of 42 ksi-√in at yielding of the girder flanges. This is substantially greater than the estimated resistance of 17 ksi-√in. Thus, fracture of the top flange welds due to the presence of the backing bar notch alone is predicted at applied stresses below 50 ksi. This is consistent with the initiation of the observed fractures at a moment below the yield moment of the girders.

For the bottom flange welds, the LOF defect at the center of the West bottom flange weld (Figure B.17) is treated as a penny-shaped crack. The maximum dimension of this discontinuity is approximately 0.5 in.; thus the radius *a* is taken as 0.25 in. Assuming stresses at yield, Equation B.5 yields 28 ksi-√in as an estimate of the applied stress-intensity factor. This is also larger than the estimated resistance of 17 ksi-√in and fracture of the welds is again predicted at flange stresses below 50 ksi.

For comparison, Equation B.2 predicts a critical stress-intensity factor of 54 ksi-√in for Specimen CR1 (using 19.3 ft-lbs of toughness at room temperature). This is larger than the predicted applied stress-intensity factors for both the center crack and penny-shaped crack solutions. Thus, the welds of Specimen CR1 would be predicted to tolerate discontinuities similar to those discovered in the welds of Specimen CR4 without fracture to stress levels beyond yield.

Because the weld toughness of Specimen CR4 was so low, a detailed investigation of the location of fracture initiation is not required. Typical discontinuities of acceptable size as per AWS D1.1-2000 (AWS, 2000) are likely to cause fracture when only 2 ft-lbs of toughness is provided in the weld. Maximum tolerable flaw sizes can be calculated by replacing K with K_c in Equations B.3 and B.5, and solving for the corresponding critical flaw size, a. Using 17 ksi-√in for K_c, Equation B.3 yields a value of 0.037 in. for the critical flaw size. The finite width correction, F_w, was conservatively taken as 1.0. This critical size represents the maximum depth before fracture is predicted of a crack continuous across the flange width, and is much smaller than the thickness of any typical backing bars (e.g., such as those left in place at the top girder flanges in the

WUF-W connection). Again using 17 ksi-√in for K_c, Equation B.5 yields 0.090 in. for the critical flaw size, a. This is equivalent to a buried circular crack with a critical diameter of 0.18 in. In both cases the stress was assumed equal to 50 ksi.

The radiographic inspection acceptance criteria for cyclically loaded structures contained in AWS D1.1-2000 were used to compare the calculated critical flaw sizes to the allowable sizes as per AWS (2000). Radiographic criteria are useful for this purpose because maximum flaw sizes are directly specified. In contrast, ultrasonic criteria are presented in terms of a defect rating in decibels, which cannot be directly correlated to an observed discontinuity size. For a 7/8 in. groove weld, the maximum dimension of any permitted discontinuity is 0.28 in. (AWS, 2000). This is significantly larger than the critical crack diameter of 0.18 in. calculated using Equation B.5. Thus, acceptable discontinuities as per AWS (2000) are predicted to cause fracture in the welds of Specimen CR4.

In addition to the CVN testing of the welds, chemical analyses of the welds of Specimens CR1 and CR4 were performed. Table B.3 presents the chemistries of the flange welds and also shows typical data from the producer. The lot of 5/64" diameter E70T-6 wire used for the two specimens was produced in 1999. The table reveals that the chemistry of the welds is similar to the producer's data from this year. Thus, it does not appear that an anomalous lot of E70T-6 was to blame, although it was impossible to draw any firm conclusions since the electrode in question was all consumed, precluding further evaluation. Note, however, the differences in chemistry between the 5/64" data from 1999 and the other selected data from the producer. The manganese content reported for the 1999 5/64" wire is approximately half that reported for both the 3/32" wire from 1999 and the 5/64" wire from 2000. It was confirmed that the chemistry of the 5/64" diameter E70T-6 was adjusted at some point in 1999 to more closely match the 3/32" diameter composition (Miller, 2001). It is unclear what, if any, effect this different chemical composition has on the typical toughness of welds produced from this electrode. The welds produced for the AWS Certificate of Conformance testing using the 5/64" diameter E70T-6 from 1999 met the minimum toughness requirement of 20 ft-lbs at -20°F (Lincoln Electric Co., 1999).

Finally, the equipment settings and Welding Procedure Specifications (WPS) were reviewed in an attempt to explain the low toughness measured in both Specimens CR1 and CR4. The WPSs were supplied by the fabricator and were based on recommended parameters from the wire manufacturer. A check of the recommended parameters confirmed that the WPS was appropriate for the E70T-6 consumable used for the flange welds.

Table B.4 compares the settings from the WPS to the ranges recorded during welding of the test specimens. All values recorded for Specimen CR1 were within the allowable 10% variation from the WPS. The recorded wire feed speed (WFS) and voltage for Specimen CR4 was within range, however the amperage was low. WFS is preferred over amperage for the monitoring of constant voltage welding procedures because amperage for a given WFS can vary depending on several other parameters such as polarity, electrode diameter, electrode type, and electrode extension (Blodgett et al., 1999). Note that different equipment was used for the welding of the two specimens. The welder and spool of E70T-6 were the same for both.

The cause of the low amperage recorded for Specimen CR4 is not definitively known, but several possibilities exist. First, one or more of the readouts may have been incorrect if, for example, the equipment was not properly calibrated. A second potential explanation is that the WFS may have been incorrectly set at a lower value. This is a possibility, as the wire feed unit had both a low- and high-range setting. If set on low-range, the desired WFS of 380 ipm would have actually been 190 ipm. Finally, very large electrode stickouts (ESO), incorrect polarity settings, or incorrect mode settings (i.e., constant current as opposed to constant voltage) could have affected the welding parameters. However, the effects of these settings are such that it is very unlikely they would have a substantial effect on amperage. Tentative conclusions point to the WFS range setting as the most likely explanation of the low amperage recorded during welding of Specimen CR4 (Miller, 2001). The observed voltage and amperage ranges from Table B.2 have been reproduced using a WFS of 190 ipm (Miller, 2001).

Even accounting for these potential procedural differences, there is still no firm explanation for the low toughness measured in both tests. The amperage differences may

well explain the toughness differences at 70°F, but not the fact that neither specimen met the SAC minimum toughness requirements of 20 ft-lbs at 0°F and 40 ft-lbs at 70°F. Recall that Specimen CR1 was welded within all WPS parameters and still did not meet the minimum toughness requirements at either temperature. No definitive conclusions explaining the low toughness of the welds of both specimens can be made from the investigation reported herein.

Following is a summary of the results of the investigation into the failure of Specimen CR4. The weld fractures were brittle in nature and occurred as a result of low-toughness welds. Measured CVNs of the E70T-6 weld metal were similar to values recorded for E70T-4 welds following the Northridge earthquake. Examinations of the fracture surfaces did not reveal any atypical defects. Basic LEFM calculations predict the fractures of Specimen CR4 based on the CVN data, and both the observed and allowable (AWS, 2000) weld discontinuities. Had the SAC minimum specified toughness (FEMA, 2000a) been provided, the welds would almost certainly not have failed in a brittle manner in the presence of the observed discontinuities. There is no indication that the box doubler plate detail contributed to the fractures. The procedural differences (e.g., recorded amperages) between Specimens CR1 and CR4 may explain the room temperature toughness difference, but the reasons for the overall unacceptable toughness of the welds of both tests are unclear. Weld chemistries from the two specimens were consistent with typical data from the producer, casting some doubt on the possibility of a bad lot of wire as the explanation. Further investigations were conducted by Barsom et al. (2001).

Based on these results, further evaluation of the present weld toughness criteria is suggested. It is believed that the SAC requirements (FEMA, 2000a) for minimum toughness are adequate, provided they can be consistently met. The acceptable results of Specimen CR1, despite toughness below the specified minimums, are encouraging in this regard. Toughness is an inherently variable material property, particularly in a non-homogeneous material such as a weld. For this reason, the toughness requirements should be treated as a lower-bound value and not an average. This can be accomplished

either through strict quality assurance, or specification of welding consumables that have lower-bound toughness consistently above the SAC minimums (FEMA, 2000a).

The former is the approach required by the SAC Recommended Specifications and Quality Assurance Guidelines (FEMA, 2000e). These Recommended Specifications require toughness testing on each production lot of the specified filler metal. However, upon approval of the engineer, this requirement may be waived and the consumable manufacturer's certification testing may be used to verify the material's suitability (FEMA, 2000e). This testing need only be conducted once per year on a single production lot of the particular electrode. As described above, the 5/64" diameter E70T-6 produced in 1999 had been certified by the manufacturer as meeting the minimum 20 ft-lbs at -20°F (Lincoln Electric Co., 1999) required by the AWS certification test (AWS, 1995). Alternatively, specification of higher toughness consumables (e.g., E71T-8) that consistently meet minimum requirements may be a more reliable means of insuring welds of sufficient toughness.

Table B.1: Comparison of Measured and Required CVN Toughness From Cruciform Tests

CVN Test Temp.	Specimen CR1	Specimen CR4	Required*
0°F	2.7 ft-lb	2.0 ft-lb	20 ft-lb
70°F	19.3 ft-lb	2.3 ft-lb	40 ft-lb

*Required CVN toughness from SAC recommended guidelines (FEMA, 2000a)

Table B.2: Comparison of AWS Test Plate and Strained Pull-Plate Specimen CVNs

CVN Test Temp.	AWS Test Plate	P-P Specimen	Required*
0°F	19.0 ft-lb	38.7 ft-lb	20 ft-lb
70°F	63.7 ft-lb	66.0 ft-lb	40 ft-lb

*Required CVN toughness from SAC recommended guidelines (FEMA, 2000a)

Table B.3: E70T-6 Weld Chemistry From Specimens CR1 and CR4, and Consumable Producer's Typical Data

Component	Specimen CR1	Specimen CR4	5/64 in. 1999*	3/32 in. 1999*	5/64 in. 2000*
C (%)	0.065	0.078	0.06	0.08	0.07
Mn (%)	0.71	0.62	0.62	1.26	1.63
P (%)	0.005	0.005	0.005	0.012	0.009
S (%)	0.007	0.005	0.005	0.005	0.003
Si (%)	0.20	0.26	0.21	0.23	0.27
Ni (%)	0.01	0.01	0.01	0.02	0.02
Cr (%)	0.03	0.03	0.04	0.03	0.03
Mo (%)	0.02	0.02	0.03	<0.01	0.02
Cu (%)	0.05	0.04	0.02	0.02	0.02
Al (%)	0.90	1.03	0.81	1.19	0.97
V (%)	<0.01	<0.01	<0.01	<0.01	<0.01
Ti (%)	0.13	0.18	NR	NR	NR
N (%)	0.045	0.026	NR	NR	NR

*Data from wire manufacturer's annual AWS Certificate of Conformance reports

Table B.4: Welding Parameters From Specimens CR1 and CR4

Parameter	CR1	CR4	WPS/Recommended
Voltage (V)	28.5 – 29.5	29.0 – 30.0	28
Wire feed speed (ipm)	~380	~380	380
Amperage (A)	430 – 460	330 – 380	480
Est. heat input (kJ/in)**	52 – 77	41 – 62	30 – 80*

*Recommended heat input from FEMA (2000d)
**Based on recommended travel speed range of 10 – 15 ipm

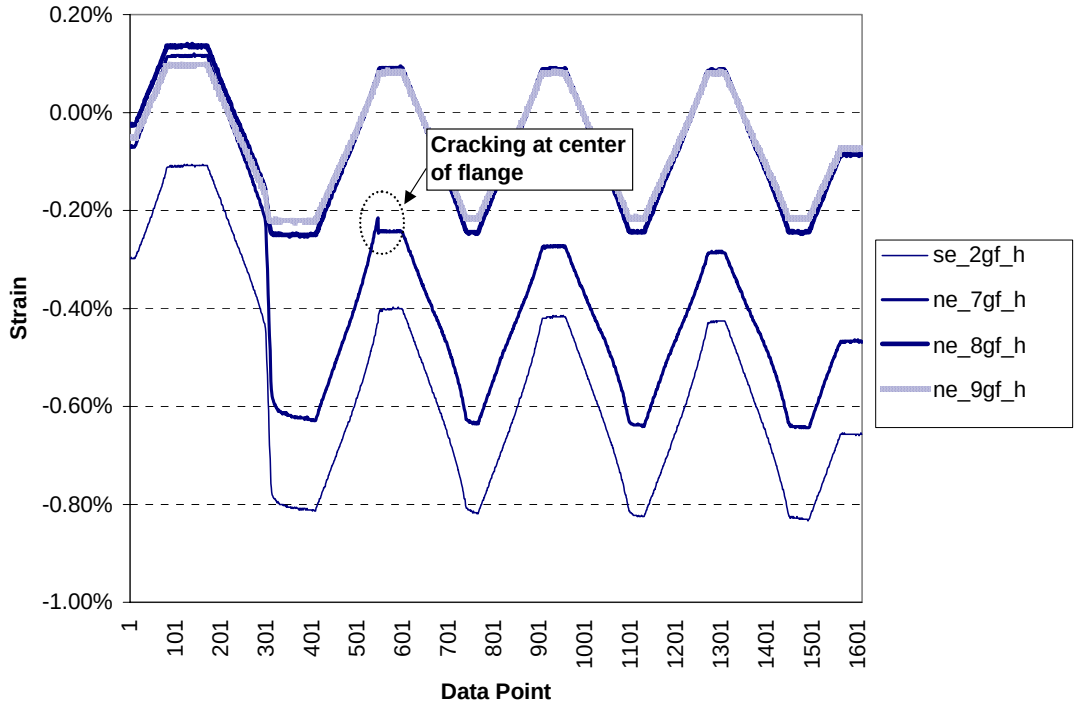


Figure B.1: Strain History of CR4 East Top Flange During 1.0% Drift Cycles

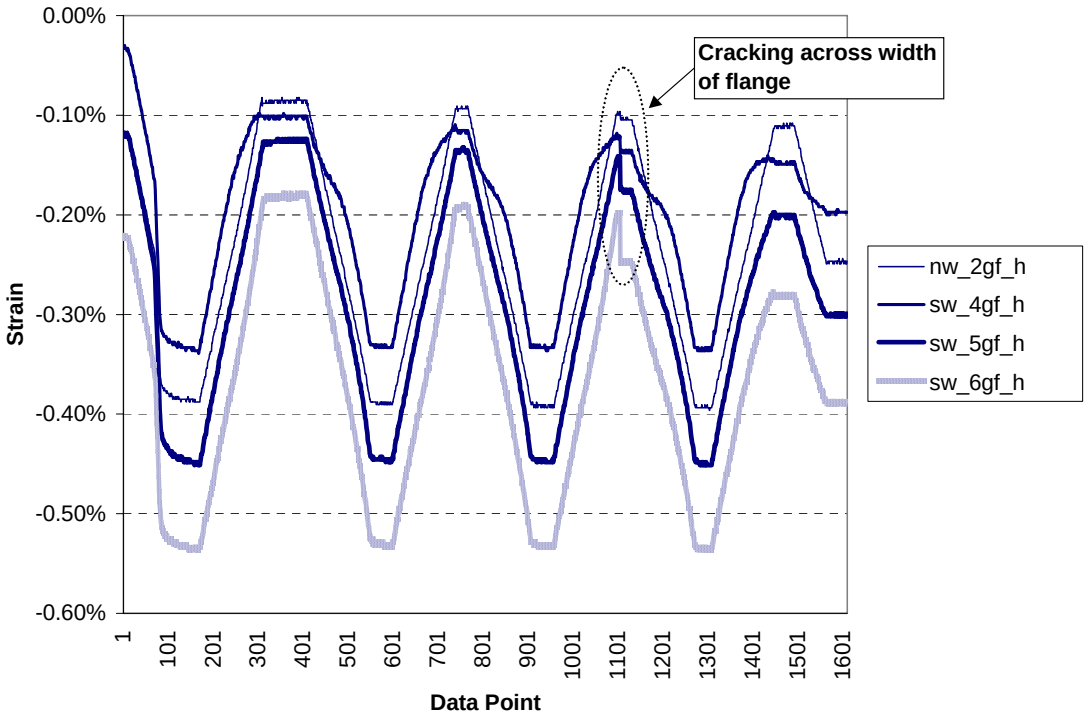


Figure B.2: Strain History of CR4 West Top Flange During 1.0% Drift Cycles

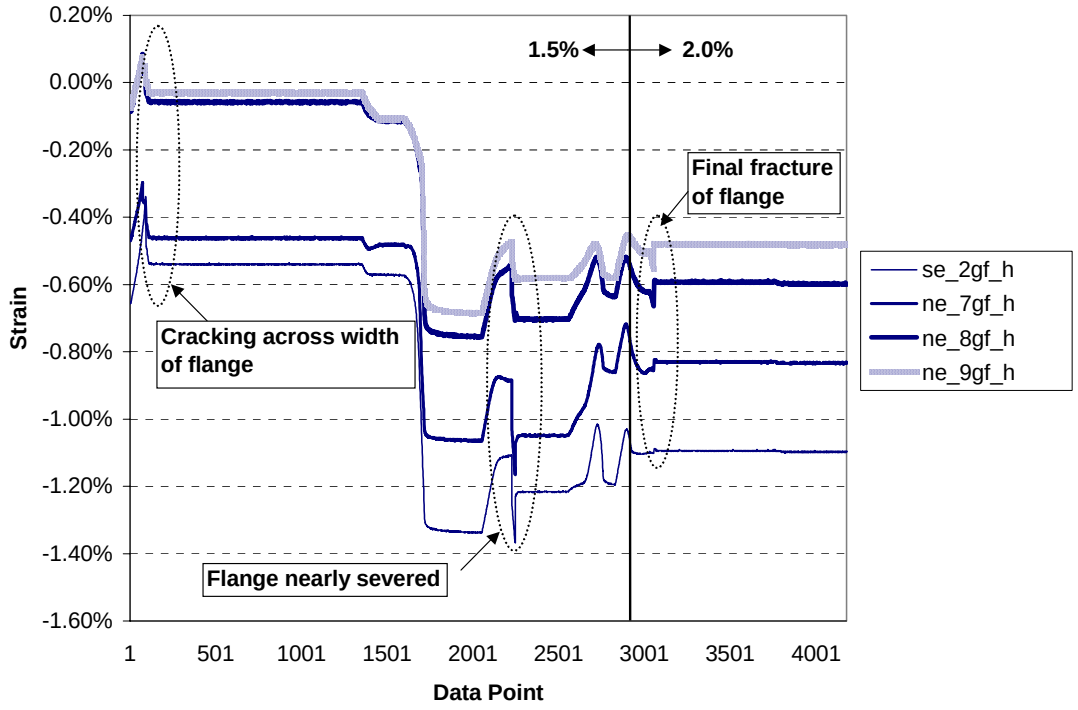


Figure B.3: Strain History of CR4 East Top Flange During 1.5%, 2.0% Cycles

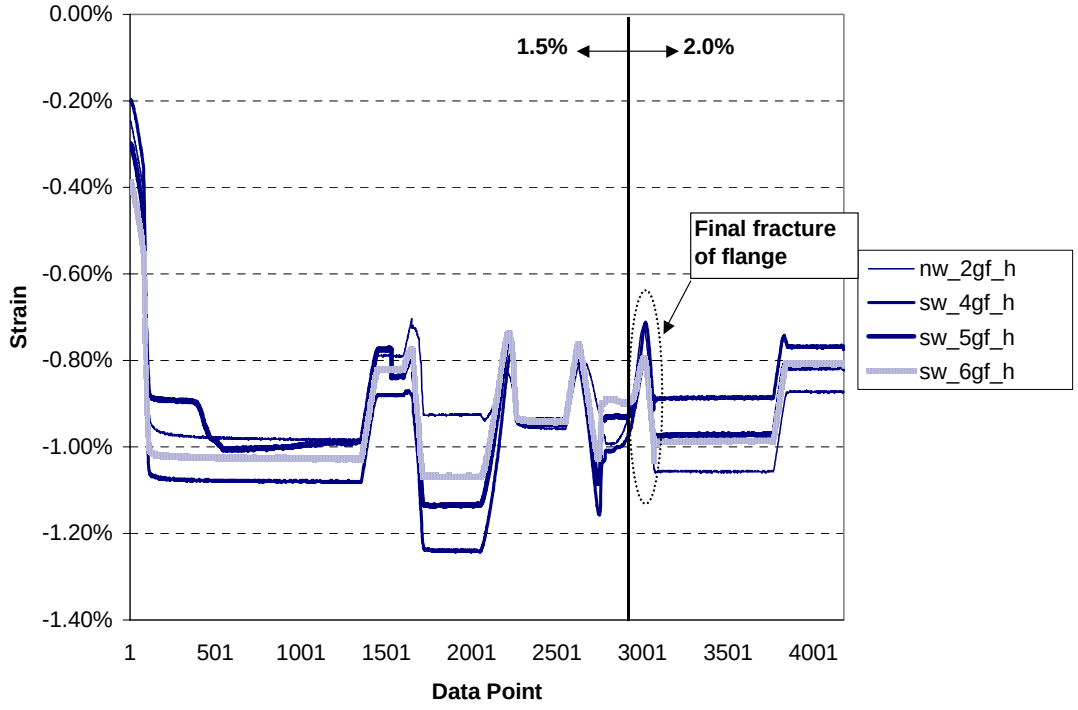


Figure B.4: Strain History of CR4 West Top Flange During 1.5%, 2.0% Cycles

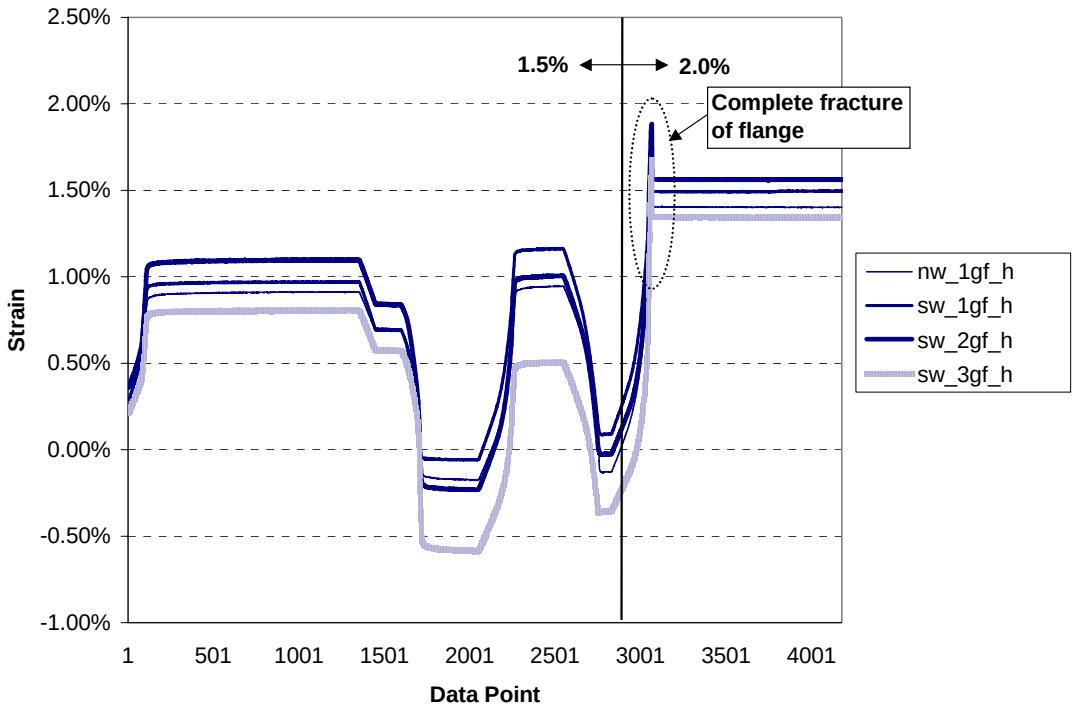


Figure B.5: Strain History of CR4 West Bottom Flange During 1.5%, 2.0% Cycles



Figure B.6: West Top Flange Fracture Surface From Specimen CR4



Figure B.7: West Top Flange Fracture Surface at Column Face from Specimen CR4



Figure B.8: Close-up View of Specimen CR4 Fracture Surface Features Near Center of Flange

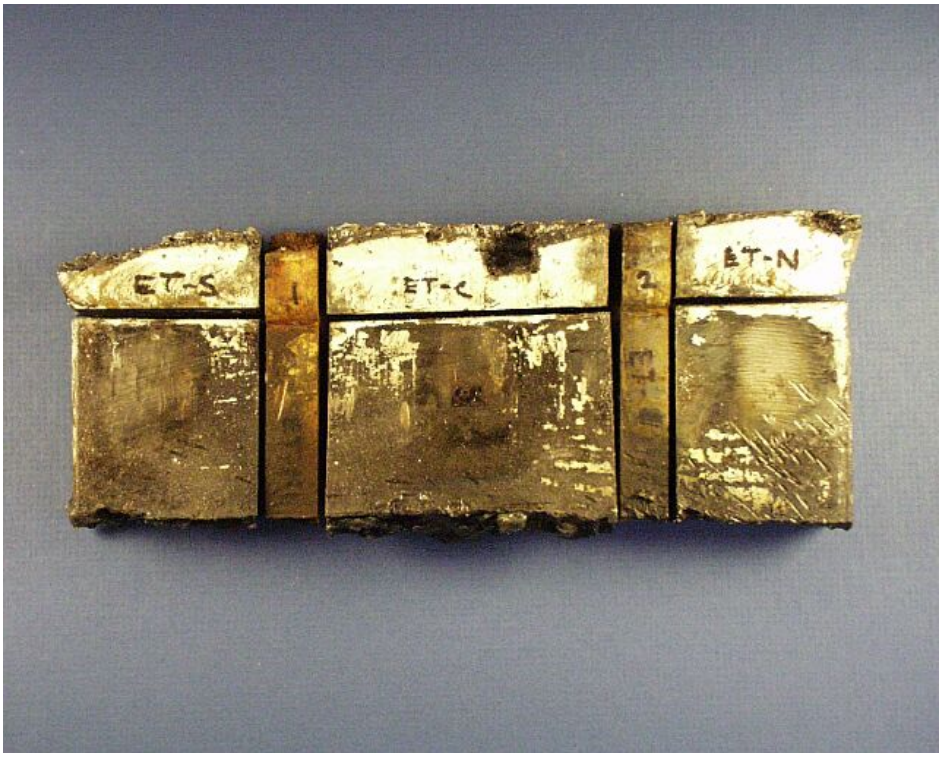


Figure B.9: Typical Sectioning of Fracture Surfaces for Investigation

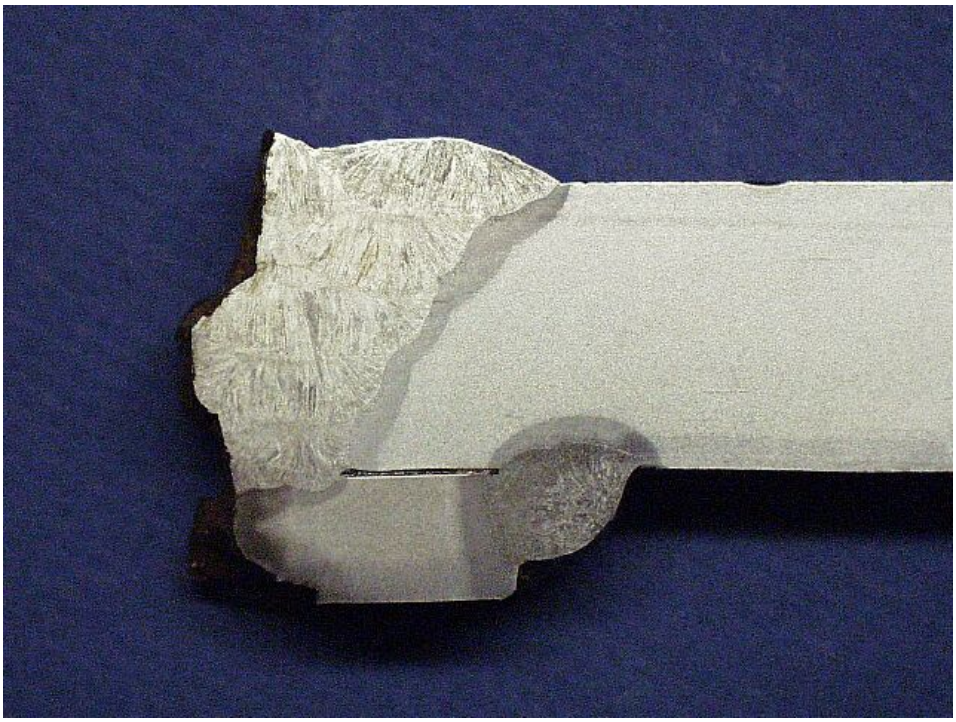


Figure B.10: Fractured Weld Section From East Top Flange of Specimen CR4



Figure B.11: Fractured Weld Section From West Top Flange of Specimen CR4

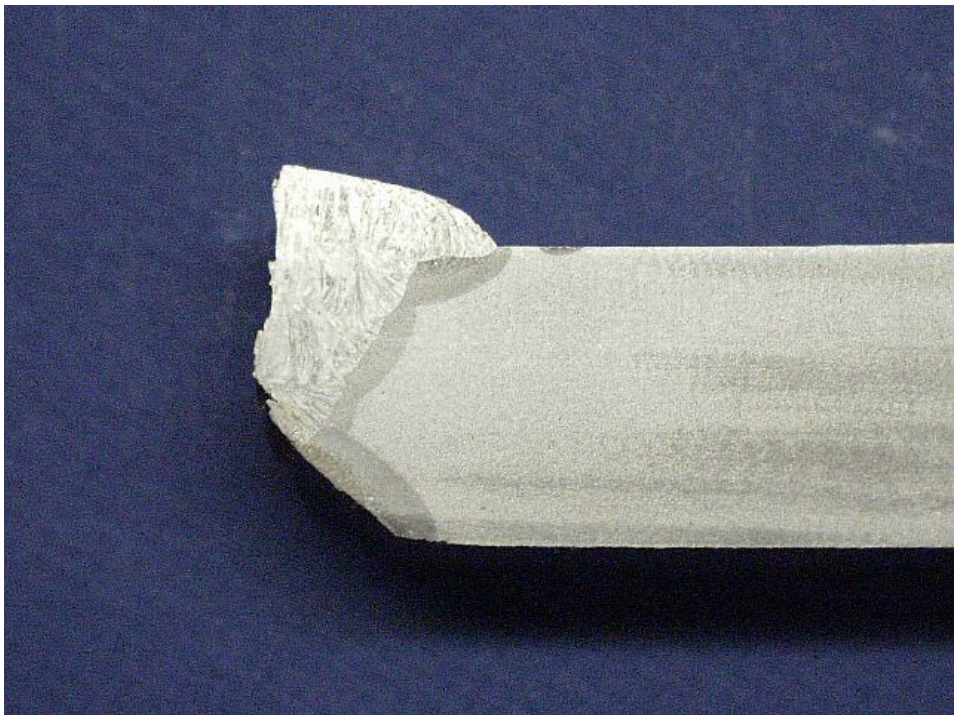


Figure B.12: Fractured Weld Section From West Bottom Flange of Specimen CR4

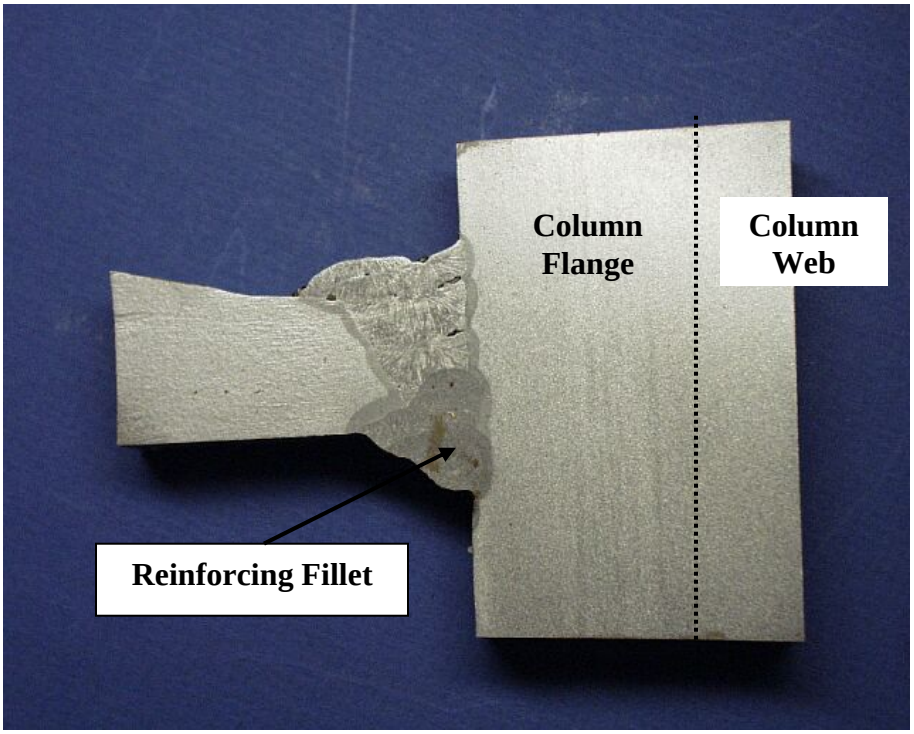


Figure B.13: Weld Section From East Bottom Flange of Specimen CR4

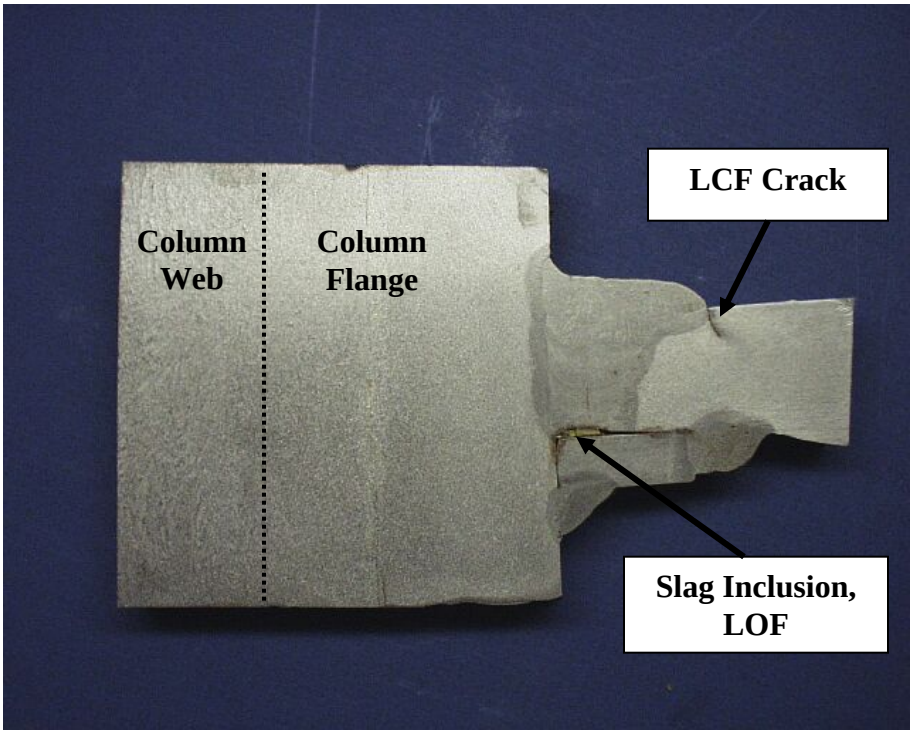


Figure B.14: Weld Section From Top Flange of Specimen CR1

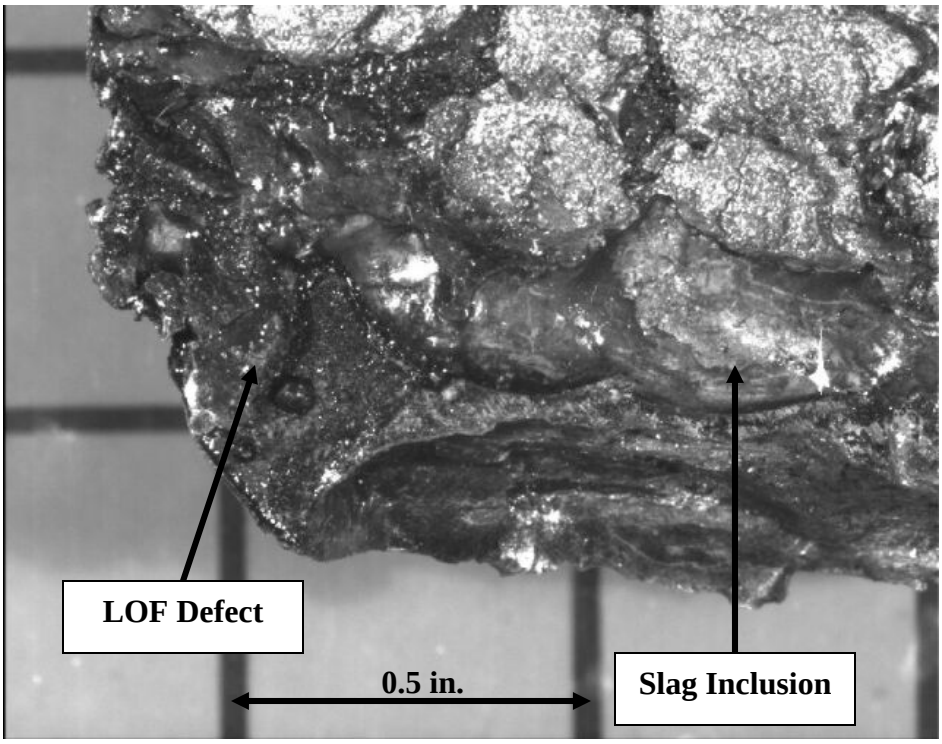


Figure B.15: LOF and Slag Inclusions in Specimen CR4 West Top Flange

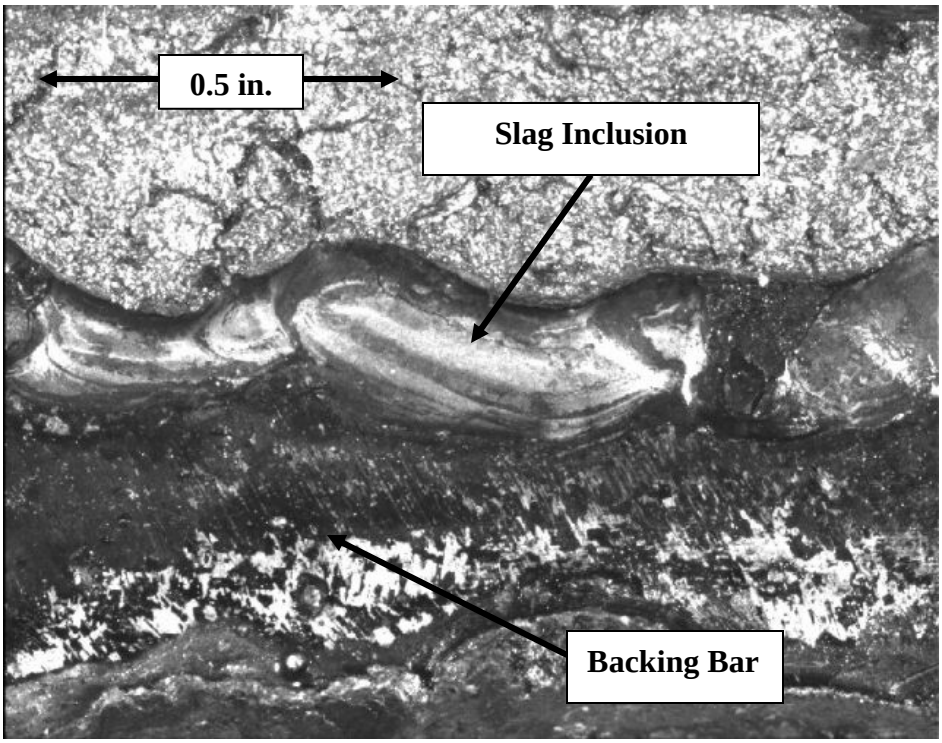


Figure B.16: Slag Inclusions Above Backing Bar in Specimen CR4 West Top Flange

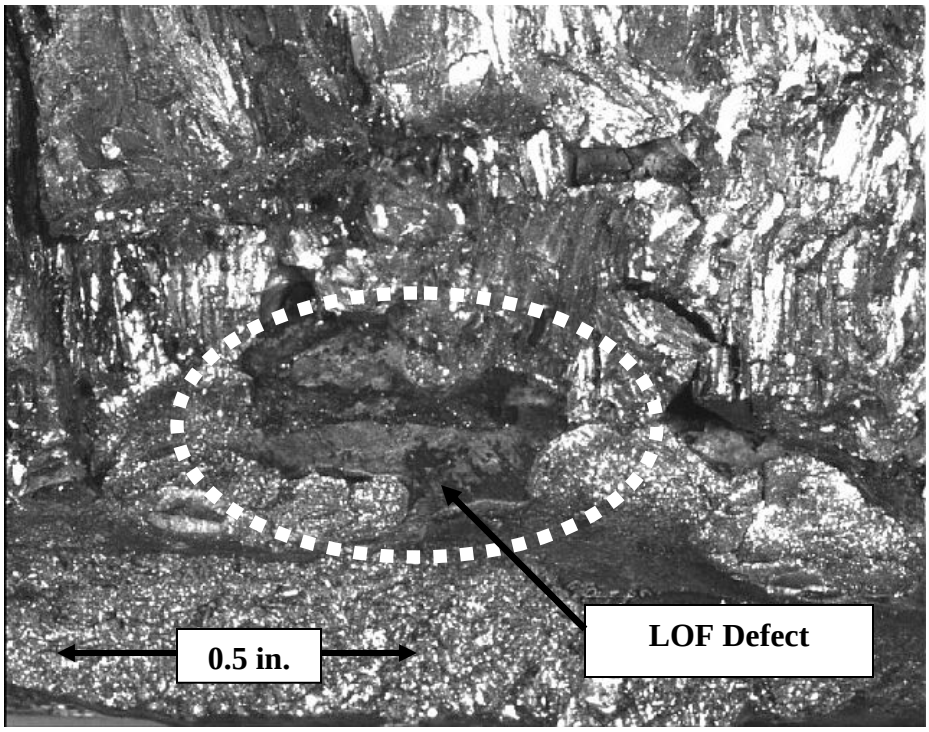


Figure B.17: LOF in Center of Specimen CR4 West Bottom Flange

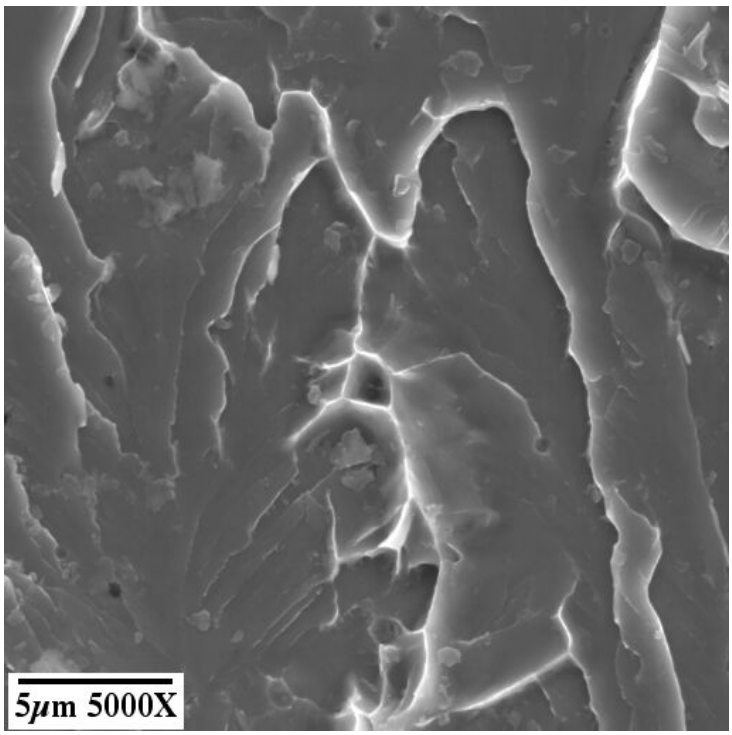


Figure B.18: SEM Photo Showing Cleavage Planes on Fracture Surface of Specimen CR4

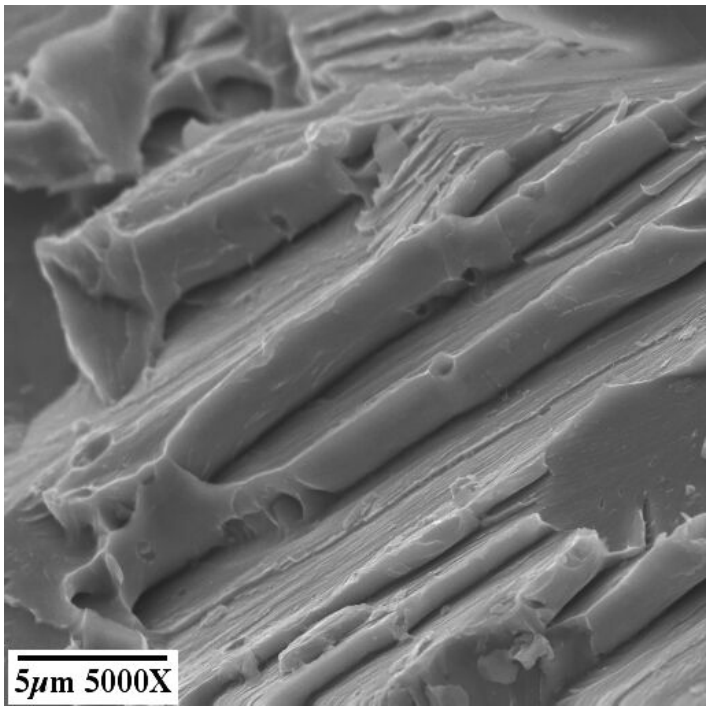


Figure B.19: SEM Photo Showing Brittle Cleavage Behavior of Welds of Specimen CR4

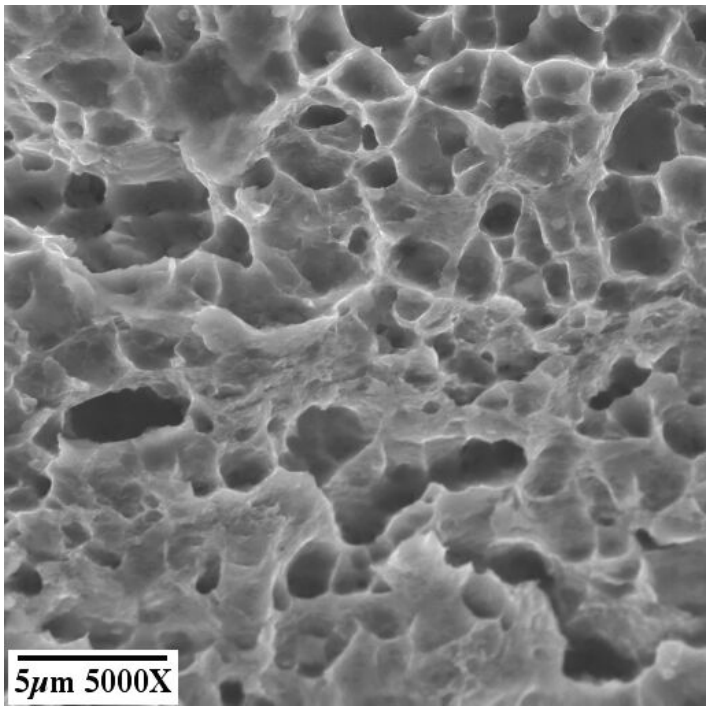


Figure B.20: SEM Photo Showing Ductile Fracture of E71T-8 Fillet Welds of Specimen CR4

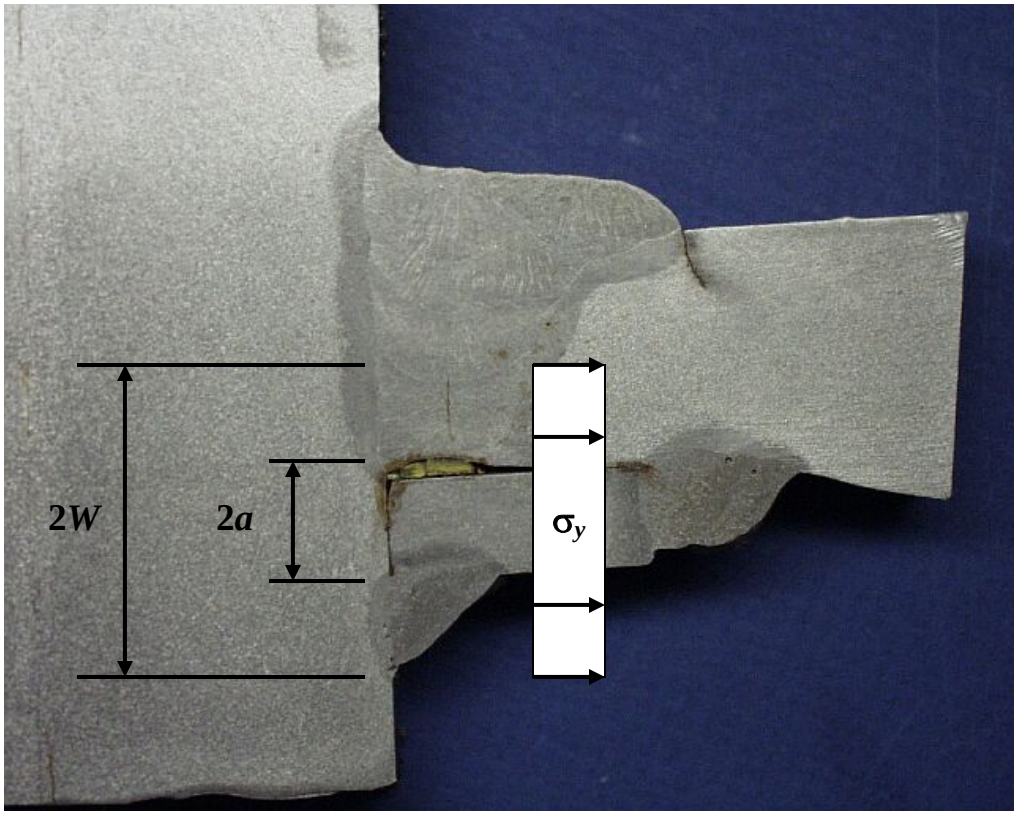


Figure B.21: Illustration of LEFM Application to Backing Bar Notch

References

American Institute of Steel Construction (AISC) (1959). *A Manual for Architects, Engineers, and Fabricators of Buildings and Other Steel Structures*, Fifth ed., AISC, New York, New York.

AISC (1978). *Manual of Steel Construction – Allowable Stress Design*, Eighth ed., AISC, New York, New York.

AISC (1992). "Seismic Provisions for Structural Steel Buildings," AISC, Chicago, Illinois.

AISC (1993). *Load and Resistance Factor Design Specification for Structural Steel Buildings*, Second ed., AISC, Chicago, Illinois.

AISC (1995). *Load and Resistance Factor Design Manual for Structural Steel Buildings*, Second ed., AISC, Chicago, Illinois.

AISC (1997). "Seismic Provisions for Structural Steel Buildings," AISC, Chicago, Illinois.

AISC (1999a). *Load and Resistance Factor Design Specification for Structural Steel Buildings*, Third ed., AISC, Chicago, Illinois.

AISC (1999b). "Seismic Provisions for Structural Steel Buildings (1997) Supplement No. 1," AISC, Chicago, Illinois.

AISC (1999c). *Stiffening of Wide-Flange Columns at Moment Connections: Wind and Seismic Applications*, Steel Design Guide Series 13, AISC, Chicago, Illinois.

AISC (2001). "Seismic Provisions for Structural Steel Buildings (1997) Supplement No. 2," AISC, Chicago, Illinois.

AISC Dimension Advisory (2001). "Changes to T, k and k_1 Dimensions for W-Shapes," February 14, 2001, AISC, Chicago, Illinois.

AISC k-line Advisory (1997). "AISC Advisory Statement on Mechanical Properties Near the Fillet of Wide Flange Shapes and Interim Recommendations January 10, 1997," *Modern Steel Construction*, February, p. 18.

American Society of Civil Engineers (ASCE) (1995). "Minimum Design Loads for Buildings and Other Structures," ANSI/ASCE 7-95, ASCE, Reston, Virginia.

American Society for Testing and Materials (ASTM) (1994a). "ASTM E8-94a: Standard Test Methods for Tension Testing of Metallic Materials," ASTM, Conshohocken, Pennsylvania.

ASTM (1994b). "ASTM E23-94a: Standard Test Methods for Notched Bar Impact Testing of Metallic Materials," ASTM, Conshohocken, Pennsylvania.

ASTM (1997). "ASTM A370-97a: Standard Test Methods and Definitions for Mechanical Testing of Steel Products," ASTM, Conshohocken, Pennsylvania.

ASTM (1998a). "ASTM A992/A992M: Standard Specification for Steel for Structural Shapes For Use in Building Framing," ASTM, Conshohocken, Pennsylvania.

ASTM (1998b). "ASTM A6/A6M: Standard Specification for General Requirements for Rolled Structural Steel Bars, Plates, Shapes, and Sheet Piling," ASTM, Conshohocken, Pennsylvania.

Applied Technology Council (ATC) (1992). "Guidelines for Cyclic Seismic Testing of Components of Steel Structures," ATC-24, ATC, Redwood City, California.

American Welding Society (AWS) (1995). "Specification for Carbon Steel Electrodes for Flux Cored Arc Welding," AWS A5.20-95, AWS, Miami, Florida.

AWS (2000). "Structural Welding Code – Steel," AWS D1.1-2000, AWS, Miami, Florida.

Barsom, J. M., and Rolfe, S. T. (1987). "Fracture and Fatigue Control in Structures – Applications of Fracture Mechanics," Second ed., Prentice-Hall, Englewood Cliffs, New Jersey.

Barsom, J. M., and James V. Pellegrino (2001). "Failure Analysis of a Welded Moment-Resisting Interior Connection," Report to AISC, Barsom Consulting, Ltd., Pittsburgh, PA.

Bartlett, F. M., Dexter, R. J., Graeser, M. D., Jelinek, J. J., Schmidt, B. J., and Galambos, T. V. (2001). "Updating Standard Shape Material Properties Database for Design and Reliability, " *Engineering Journal*, AISC, submitted for publication.

Becker, R. (1975). "Panel Zone Effect on the Strength and Stiffness of Steel Rigid Frames," *Engineering Journal,* AISC, Vol. 12, No. 1, pp. 19-29.

Bertero, V. V., Popov, E. P., and Krawinkler, H. (1972). "Beam-Column Subassemblages Under Repeated Loading," *Journal of the Structural Division*, ASCE, Vol. 98, No. ST5, pp. 1137-1159.

Bertero, V. V., Krawinkler, H., and Popov, E. P. (1973). "Further Studies on Seismic Behavior of Steel Beam-Column Subassemblages," Report No. EERC-73/27, Earthquake Engineering Research Center, University of California, Berkeley, California.

Bjorhovde, R., Goland, L. J., and Benac, D. J. (1999). "Tests of Full-Scale Beam-to-Column Connections," Southwest Research Institute, San Antonio, Texas.

Blodgett, O. W., Funderburk, R. S., Miller, D. K., and Quintana, M. A. (1999). "Fabricators' and Erectors' Guide to Welded Steel Construction," James F. Lincoln Arc Welding Foundation, Cleveland, Ohio.

Bruneau, M., Uang, C., and Wittaker, A. (1998). "Ductile Design of Steel Structures," McGraw-Hill, New York, New York.

Carter, C. J. (1999). "Column Economy Considering Stiffening Requirements," *Structural Engineering in the 21st Century*, Proceedings of the ASCE Structures Congress, Avent, R. R. and Alawady, M. (eds.), New Orleans, Louisiana, April 18-21, 1999, ASCE, Reston, Virginia, pp. 552-555.

Chi, W.-M., Deierlein, G. G., Ingraffea, A. (2000). "Fracture Toughness Demands in Welded Beam-Column Moment Connections," *Journal of Structural Engineering*, ASCE, Vol. 126, No. 1, pp. 88-97.

Choi, J.-H., Stojadinovic, B., and Goel, S. C. (2000). "Development of Free Flange Moment Connection," Report No. UMCEE 00-15, Department of Civil and Environmental Engineering, University of Michigan, Ann Arbor, Michigan.

Dexter, R. J. and Melendrez, M. I. (2000). "Through-Thickness Properties of Column Flanges in Welded Moment Connections," *Journal of Structural Engineering*, ASCE, Vol. 126, No. 1, pp. 24-31.

Dexter, R. J. (2000). "Structural Shape Material Property Survey," Final Report to Structural Structural Shape Producer's Council, University of Minnesota, Minneapolis, Minnesota.

Dexter, R. J., Hajjar, J. F., Prochnow, S. D., Graeser, M. D., Galambos, T. V., and Cotton, S. C. (2001). "Evaluation of the Design Requirements for Column Stiffeners and Doublers and the Variation in Properties of A992 Shapes," Proceedings of the North American Steel Construction Conference, Fort Lauderdale, Florida, May 9-12, 2001, AISC, Chicago, Illinois, pp. 14-1 – 14-21.

El-Tawil, S., Mikesell, T., Vidarsson, E., and Kunnath, S. (1998). "Strength and Ductility of FR Welded-Bolted Connections," Report No. SAC/BD-98/01, Applied Technology Council, Redwood City, California.

El-Tawil, S., Vidarsson, E., Mikesell, T., and Kunnath, S. (1999). "Inelastic Behavior and Design of Steel Panel Zones," *Journal of Structural Engineering*, ASCE, Vol. 125, No. 2, pp. 183-193.

Federal Emergency Management Agency (FEMA) (1995a). "Steel Moment Frame Structures: Interim Guidelines," Report No. FEMA 267 (SAC-95-02), SAC Joint Venture, Sacramento, California.

FEMA (1995b). "Steel Moment Frame Structures: Background Reports," Report No. FEMA 288 (SAC-95-09), SAC Joint Venture, Sacramento, California.

FEMA (1997a). "Interim Guidelines Advisory No. 1," Report No. FEMA 267A (SAC-96-03), SAC Joint Venture, Sacramento, California.

FEMA (1997b). "Connection Test Summaries," Report No. FEMA 289 (SAC-96-02), SAC Joint Venture, Sacramento, California.

FEMA (2000a). "Recommended Seismic Design Criteria for New Moment-Resisting Steel Frame Structures," Report No. FEMA 350, SAC Joint Venture, Sacramento, California.

FEMA (2000b). "State of the Art Report on Connection Performance," Report No. FEMA 335D, SAC Joint Venture, Sacramento, California.

FEMA (2000c). "State of the Art Report on Base Metals and Fracture," Report No. FEMA 355A, SAC Joint Venture, Sacramento, California.

FEMA (2000d). "State of the Art Report on Joining and Inspection," Report No. FEMA 355B, SAC Joint Venture, Sacramento, California.

FEMA (2000e). "Recommended Specifications and Quality Assurance Guidelines for Steel Moment-Frame Construction for Seismic Applications," Report No. FEMA 353, SAC Joint Venture, Sacramento, California.

Fielding, D. J., and Huang, J. S. (1971). "Shear in Steel Beam-to-Column Connections," *Welding Journal*, AWS, Vol. 50, No. 7, Research Supplement, pp. 313-326.

Fisher, J. W., Dexter, R. J., and Kaufmann, E. J. (1997). "Fracture Mechanics of Welded Structural Steel Connections," Report No. FEMA 288 (SAC 95-09), SAC Joint Venture, Sacramento, California, pp. 3-1 – 3-30.

Ghobarah, A., Korol, R. M., and Osman, A. (1992). "Cyclic Behavior of Extended End-Plate Joints," *Journal of Structural Engineering*, ASCE, Vol. 118, No. 5, pp.1333-1353.

Graham, J. D., Sherbourne, A. N., Khabbaz, R. N., and Jensen, C. D. (1960). "Welded Interior Beam-to-Column Connections," Welding Research Council, Bulletin No. 63, pp. 1-28.

Hajjar, J. F., Leon, R. T., Gustafson, M. A., and Shield, C. K. (1998a). "Seismic Response of Composite Moment-Resisting Connections. II: Behavior," *Journal of Structural Engineering*, ASCE, Vol. 124, No. 8, pp. 877-885.

Hajjar, J. F., Leon, R. T., Gustafson, M. A., and Shield, C. K. (1998b). "Full-Scale Cyclic Experiments of Composite Moment-Resisting Frame Connections," Report No. ST 98-02, Department of Civil Engineering, University of Minnesota, Minneapolis, Minnesota.

Hajjar, J. F., Dexter, R. J., Ojard, S. D., Ye, Y., and Cotton, S. C. (2002). "Continuity Plate Detailing for Steel Moment-Resisting Connections," *Engineering Journal*, AISC, submitted for publication.

Irwin, G. R. (1957). "Analysis of Stresses and Strains Near the End of a Crack Traversing a Plate," *Journal of Applied Mechanics*, ASME, Vol. 24, pp. 361-364.
Iwankiw, N. (1999). Personal communication, June 24, 1999.

Kaufmann, E. J., Xue, M., Lu, L. W., and Fisher, J. W. (1996). "Achieving Ductile Behavior of Moment Connections – Part I," *Modern Steel Construction*, Vol. 36, No. 1, pp. 30-39.

Kaufmann, E. J., Metrovich, B., Pense, A. W., and Fisher, J. W. (2001). "Effect of Manufacturing Process on k-Area Properties and Service Performance," Proceedings of the North American Steel Construction Conference, Fort Lauderdale, Florida, May 9-12, 2001, AISC, Chicago, Illinois, pp. 17-1 – 17-24.

Kawano, A., (1984). "Inelastic Behavior of Low-Rise Steel Frame Based on a Weak Beam-to-Column Connection Philosophy to Earthquake Motion," Proceedings of the Eighth World Conference on Earthquake Engineering, San Francisco, California, Vol. 4, pp. 519-526.

Krawinkler, H. (1978). "Shear in Beam-Column Joints in Seismic Design of Steel Frames," *Engineering Journal*, AISC, Vol. 15, No. 3, pp. 82-91.

Krawinkler, H., Bertero, V. V., and Popov, E. P. (1971). "Inelastic Behavior of Steel Beam-to-Column Subassemblages," Report No. EERC-71/7, Earthquake Engineering Research Center, University of California, Berkeley, California.

Krawinkler, H., Bertero, V. V., and Popov, E. P. (1975). "Shear Behavior of Steel Frame Joints," *Journal of the Structural Division,* ASCE, Vol. 101, No. ST11, pp. 2317-2335.

Lee, S., and Lu, L. (1989). "Cyclic Tests of Full-Scale Composite Joint Subassemblages," *Journal of Structural Engineering,* ASCE, Vol. 115, No. 8, pp. 1977-1998.

Lee, K.-H., Goel, S. C., and Stojadinovic, B. (1997). "Boundary Effects in Welded Steel Moment Connections," Report No. UMCEE 97-20, Department of Civil and Environmental Engineering, University of Michigan, Ann Arbor, Michigan.

Lee, K.-H., Stojadinovic, B., Goel, S. C., Margarian, A. G., Choi, J., Wongkaew, A., Reyher, B. P., and Lee D.-Y. (2000). "Parametric Tests on Unreinforced Connections," Report No. SAC/BD-00/01, SAC Joint Venture, Sacramento, California.

Leon, R. T. (1983). "The Influence of Floor Members on the Behavior of Reinforced Concrete Beam-Column Joints Subjected to Severe Cyclic Loading." University of Texas at Austin, Austin, Texas.

Leon, R. T., Hajjar, J. F., and Gustafson, M. A. (1998). "Seismic Response of Composite Moment-Resisting Connections. I: Performance," *Journal of Structural Engineering,* ASCE, Vol. 124, No. 8, pp. 868-876.

Lincoln Electric Co. (1999). Certificate of Conformance for Innershield NR-305 (E70T-6), Lincoln Electric Co., Cleveland, Ohio, August 6, 1999.

Mao, C., Ricles, J. M., Lu, L.-W., and Fisher, J. W. (2001). "Effect of Local Details on Ductility of Welded Moment Connections," *Journal of Structural Engineering,* ASCE, Vol. 127, No. 9, pp. 1036-1044.

Miller, D. K. (1997). "Welding of Seismically Resistant Steel Structures," Report No. FEMA 288 (SAC 95-09), SAC Joint Venture, Sacramento, California, pp. 2-1 – 2-124.

Miller, D. K. (2001). Personal communication to R. J. Dexter, June 15, 2001.

National Earthquake Hazards Reduction Program (NEHRP) (1994). *Recommended Provisions for Seismic Regulations for New Buildings and Other Structures,* Report No. FEMA 223, Building Seismic Safety Council, Washington, D.C.

NEHRP (1997). *Recommended Provisions for Seismic Regulations for New Buildings and Other Structures,* Report No. FEMA 302, Building Seismic Safety Council, Washington, D.C.

Peters, J. W., and Driscoll, G. C. (1968). "A Study of the Behavior of Beam-to-Column Connections," Report No. 333.2, Fritz Engineering Laboratory, Lehigh University, Bethlehem, Pennsylvania.

Popov, E. P. (1999). Personal communication to J. F. Hajjar, March 24, 1999.

Popov, E. P., Amin, N. R., Louie, J. J. C., and Stephen, R. M. (1986). "Cyclic Behavior of Large Beam-Column Assemblies," *Engineering Journal*, AISC, Vol. 23, No. 1, pp. 9-23.

Popov, E. P. (1987). "Panel Zone Flexibility in Seismic Moment Joints," *Journal of Constructional Steel Research*, Vol. 8, pp. 91-118.

Prochnow, S. D., Dexter, R. J., Hajjar, J. F., Ye, Y., and Cotton, S. C. (2000a). "Local Flange Bending and Local Web Yielding Limit States in Steel Moment-Resisting Connections," Report No. ST-00-4, Department of Civil Engineering, University of Minnesota, Minneapolis, Minnesota.

Prochnow, S. D., Ye, Y., Dexter, R. J., Hajjar, J. F., and Cotton, S. C. (2000b). "Local Flange Bending and Local Web Yielding Limit States in Steel Moment-Resisting Connections," Connections in Steel Structures IV, Roanoke, Virginia, October 22-24, 2000.

Ricles, J. M., Mao, C., Kaufmann, E. J., Lu, L.-W., and Fisher, J. W. (2000a). "Development and Evaluation of Improved Details for Ductile Welded Unreinforced Flange Connections," SAC BD 00-24, SAC Joint Venture, Sacramento, California.

Ricles, J. M., Mao, C., Lu, L., and Fisher, J. W. (2000b), "Ductility Analysis of Welded Unreinforced Beam-to-Column Moment Connections," *Proceedings of U.S.-Japan Workshop on Seismic Fracture Issues in Steel Structures*, San Francisco, California.

Ricles, J. M., Mao, C., Lu, L., and Fisher, J. W. (2002). "Inelastic Cyclic Testing of Welded Unreinforced Moment Connections," *Journal of Structural Engineering*, ASCE, Vol. 128, No. 4, pp. 429-440.

Roeder, C. W., and Foutch, D. A. (1996). "Experimental Results for Seismic Resistant Steel Moment Frame Connections," *Journal of Structural Engineering*, ASCE, Vol. 122, No. 6, pp. 581-588.

Roeder, C. W. (1997). "An Evaluation of Cracking Observed in Steel Moment Frames," Proceedings of the ASCE Structures Congress, Kempner, L., Brown, C. (eds.), Portland, Oregon, April 13-16, 1997, ASCE, New York, New York, pp. 767-771.

Roeder, C. W. (2000). "Connection Performance State of the Art Report," University of Washington, Seattle, Washington.

Roeder, C. W. (2002a). "General Issues Influencing Connection Performance," *Journal of Structural Engineering*, ASCE, Vol. 128, No. 4, pp. 420-428.

Roeder, C. W. (2002b). "Connection Performance for Seismic Design of Steel Moment Frame," *Journal of Structural Engineering*, ASCE, Vol. 128, No. 4, pp. 517-525.

SAC Joint Venture (SAC) (1996). "Technical Report: Experimental Investigations of Beam-Column Subassemblages," Report No. SAC-96-01, SAC Joint Venture, Sacramento, California.

SAC (1997). "Protocol for Fabrication, Inspection, Testing, and Documentation of Beam-Column Connection Tests and Other Experimental Specimens," Report No. SAC/BD-97/02, SAC Joint Venture, Sacramento, California.

Schneider, S. P., Roeder, C. W., and Carpenter, J. E. (1993). "Seismic Behavior of Moment-Resisting Steel Frames: Experimental Study," *Journal of Structural Engineering*, ASCE, Vol. 119, No. 6, pp. 1885-1902.

Structural Engineers Association of California (SEAOC) (1988). *Recommended Lateral Force Requirements*, Fourth ed., Seismology Committee, SEAOC, San Francisco, California.

Sherbourne, A. N., and Jensen, C. D. (1957). "Direct Welded Beam Column Connections," Report. No. 233.12, Fritz Laboratory, Lehigh University, Bethlehem, Pennsylvania.

Stojadinovic, B., Goel, S. C., Lee, K.-H., Margarian, A. G., and Choi, J.-H. (2000). "Parametric Tests on Unreinforced Steel Moment Connections," *Journal of Structural Engineering*, ASCE, Vol. 126, No. 1, pp. 40-49.

Structural Stability Research Council (SSRC) Task Group (1998). "SSRC Technical Memorandum No. 7: Tension Testing," SSRC, Bethlehem, Pennsylvania.

Tide, R. H. R. (2000). "Evaluation of Steel Properties and Cracking in 'k' –area of W Shapes," *Engineering Structures*, Vol. 22, No. 2, pp. 128-134.

Troup, E. W. (1999). "Effective Contract and Shop Drawings for Structural Steel," Proceedings of the AISC National Steel Construction Conference, Toronto, Ontario, May 19-21, 1999, AISC, Chicago, Illinois, pp. 37-1 – 37-15.

Tsai, K. C., and Popov, E. P. (1988). "Steel Beam-Column Joints in Seismic Moment Resisting Frames," Report No. UCB/EERC-88/19, Earthquake Engineering Research Center, University of California, Berkeley, California.

Tsai, K. C., Wu, S., and Popov, E. P. (1995). "Experimental Performance of Seismic Steel Beam-Column Moment Joints," *Journal of Structural Engineering*, ASCE, Vol. 121, No. 6, pp. 925-931.

Uniform Building Code (UBC) (1988). *Uniform Building Code*. International Conference of Building Officials, Whittier, California.

Webster, D. (2000). "Report on the Change in Model Material Properties Used for ABAQUS Finite Element Analysis," Department of Civil Engineering, University of Minnesota, Minneapolis, Minnesota.

Xue, M., Kaufmann, E. J., Lu, L.-W., and Fisher, J. W. (1996). "Achieving Ductile Behavior of Moment Connections – Part II," *Modern Steel Construction*, Vol. 36, No. 6, pp. 38-42.

Ye, Y., Hajjar, J. F., Dexter, R. D., Prochnow, S. C., Cotton, S. C. (2000). "Nonlinear Analysis of Continuity Plate and Doubler Plate Details in Steel Moment Frame Connections," Report No. ST-00-3, Department of Civil Engineering, University of Minnesota, Minneapolis, Minnesota.

Yee, R. K., Paterson, S. R., and Egan, G. R. (1998). "Engineering Evaluations of Column Continuity Plate Detail Design and Welding Issues in Welded Steel Moment Frame Connections," Welding for Seismic Zones in New Zealand, Aptech Engineering Services, Inc., Sunnyvale, California.